NASA TECHNICAL MEMORANDUM

NASA TM X-3377

NASA TM X-3377

FOR EARLY DOMESTIC DISSEMINATION

Because of its significant early commercial potential, this information, which has been developed under a U. S. Government program, is being disseminated within the United States in advance of general publication. This information may be duplicated and used by the recipient with the express limitation that it not be published. Release of this information to other domestic parties by the recipient shall be made subject to these limitations. Foreign release may be made only with prior NASA approval and appropriate export licenses. This legend shall be marked on any reproduction of this information in whole or in part.

Date for general release March 1978

DISTRIBUTION STATEMENT A
Approved for public release;
Distribution Unlimited

THIRD CONFERENCE ON FIBROUS COMPOSITES IN FLIGHT VEHICLE DESIGN

Part I

Held at
Williamsburg, Virginia
November 4-6, 1975

19960503 043

NATIONAL AERONAUTICS AND SPACE ADMINISTRATION • WASHINGTON, D. C. • APRIL 1976

DISCLAIMER NOTICE

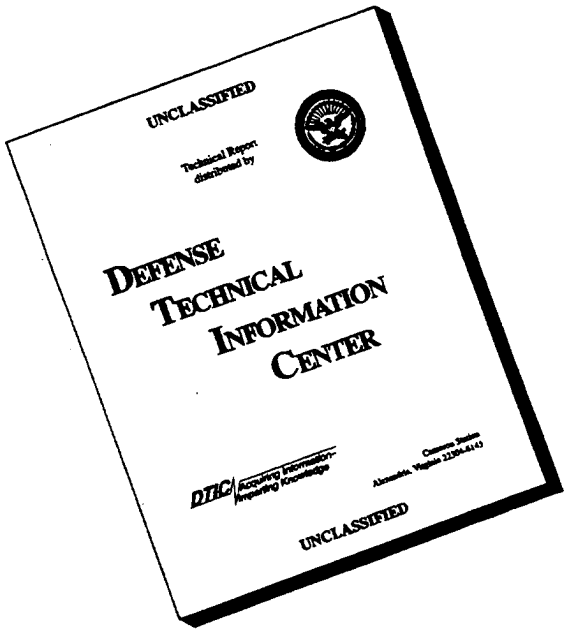

THIS DOCUMENT IS BEST QUALITY AVAILABLE. THE COPY FURNISHED TO DTIC CONTAINED A SIGNIFICANT NUMBER OF PAGES WHICH DO NOT REPRODUCE LEGIBLY.

1. Report No.	2. Government Accession No.	3. Recipient's Catalog No.
NASA TM X-337/		

4. Title and Subtitle	5. Report Date
THIRD CONFERENCE ON FIBROUS COMPOSITES IN FLIGHT VEHICLE DESIGN - PART I	April 1976
	6. Performing Organization Code
7. Author(s)	8. Performing Organization Report No. L-10640
	10. Work Unit No. 505-02-41
9. Performing Organization Name and Address: NASA Langley Research Center, Hampton, Va. 23665	11. Contract or Grant No.
	13. Type of Report and Period Covered: Technical Memorandum
12. Sponsoring Agency Name and Address: National Aeronautics and Space Administration and U.S. Air Force	14. Sponsoring Agency Code

15. Supplementary Notes

Held at Williamsburg, Va., November 4-6, 1975.

16. Abstract

The National Aeronautics and Space Administration and the United States Air Force sponsored a 3-day conference November 4-6, 1975, to focus national attention on the use of fibrous composite materials in the design of flight vehicle structures and the important impact the use of such materials will have on future vehicle systems.

Significant milestones have been achieved in composite structures design, test, and flight operations for a wide spectrum of aircraft, space vehicle, and civil sector applications. The continuing growth of the data base for material properties, design procedures, environmental exposure effects, manufacturing procedures, and flight service reliability has increased the level of acceptability and confidence necessary for widespread, routine composite applications. By including composites as baseline design materials, significant payoffs can be expected in terms of reduced structural weight fractions, longer structural life, reduced fuel consumption, reduced structural complexity, and reduced manufacturing cost.

Technical papers are presented which describe work performed by the Government and Industry. The topics covered include recent flight test work on composite components, unique design concepts and hardware, specialized applications, operational experience, certification and design criteria, and significant contributions to the design technology base.

17. Key Words (Suggested by Author(s))	18. Distribution Statement
Composites Materials Structural design Reliability	FEDD Distribution Subject Category 24

19. Security Classif. (of this report)	20. Security Classif. (of this page)	21. No. of Pages	22. Price*
Unclassified	Unclassified	496	$12.00

*For sale by Regional Dissemination Center (see STAR, vol. 12, issue 16, or subsequent issues).

CONTENTS

Part I

KEYNOTE ADDRESS 1
George G. Deutsch

SESSION IA - CURRENT COMPONENT DESIGN EFFORTS

Chairman: Frank D. Cherry
Air Force Flight Dynamics Laboratory

FLIGHT SERVICE PROGRAM FOR AN ADVANCED COMPOSITE FIN FOR A WIDE-BODY COMMERCIAL JET 9
Robert L. Vaughn and Arthur M. James

THE REALIZATION OF COST AND WEIGHT SAVINGS BY THE APPLICATION OF ADVANCED COMPOSITES TO THE B-1 VERTICAL STABILIZER 33
D. E. Parker, W. L. O'Brien, and W. R. Johnston

DESIGN, FABRICATION AND TEST OF THE B-1 COMPOSITE HORIZONTAL STABILIZER 51
Walter Ludwig, Herman Erbacher, and Joseph Visconti

DEVELOPMENT OF AN ADVANCED COMPOSITE RUDDER FOR FLIGHT SERVICE ON THE DC-10 71
George M. Lehman

DEVELOPMENT OF CONCEPTUAL HARDWARE FOR THE LIGHTWEIGHT FIGHTER 93
R. Roberts

SIMPLIFIED LOW COST ADVANCED COMPOSITE FUSELAGE STRUCTURE FOR FIGHTER AIRCRAFT 95
Lee Bernhardt

SESSION IB - CURRENT COMPONENT DESIGN EFFORTS

Chairman: R. S. Berrisford
Army Air Mobility R&D Laboratory

SHUTTLE ORBITER - GRAPHITE/EPOXY PAYLOAD BAY DOORS 115
D. Garcia and C. E. Halstead

B-1 COMPOSITES WEAPONS BAY DOOR 131
Leslie M. Lackman and Dean S. Klivans

DEVELOPMENT OF AN A-7D ADVANCED COMPOSITE OUTER WING FOR PRODUCTION AND IN-SERVICE EXPERIENCE 143
C. R. Foreman and C. Tanis

DEVELOPMENT AND TEST OF A GRAPHITE/EPOXY WINGBOX 165
G. C. Krumweide and E. E. Spier

MILITARY AIRCRAFT FLIGHT COMPONENT DEVELOPMENT. 191
W. R. Royston

LOW COST COMPOSITE AIRFRAME STRUCTURES 225
Melvin J. Rich and Raymond L. Foye

COST REDUCTION WITH COMPOSITES IN B-1 SLATS 243
W. Andrew Pitman

DESIGN, FABRICATION AND TEST FOR AN F-14A GRAPHITE/EPOXY MAIN LANDING GEAR STRUT DOOR 259
R. Carlson, G. Lubin, and A. Cowles

A THERMALLY INERT CYLINDRICAL TRUSS CONCEPT 275
Paul T. Nelson and Michael H. Krim

GENERAL COLLAPSE AND JOINT ANALYSIS OF A LAUNCH VEHICLE GRAPHITE/EPOXY CONICAL ADAPTER 305
E. E. Spier and G. D. Heller

SESSION IC - CURRENT COMPONENT DESIGN EFFORTS

Chairman: Eldon E. Mathauser
NASA Langley Research Center

COMPOSITE NACELLE STRUCTURES - DC-9 NOSE COWL 335
Robert A. Elkin

COMPOSITE NACELLE STRUCTURES - B-1 ENGINE NACELLE RAMP 349
Norman O. Brink

H-3 HELICOPTER COMPOSITE MAIN ROTOR BLADE DEVELOPMENT PROGRAM 363
D. J. Ianniello and J. B. Sainsbury-Carter

SESSION II - OPERATIONS ENVIRONMENT EXPERIENCE

Chairman: Eldon E. Mathauser
NASA Langley Research Center

TIME-TEMPERATURE-STRESS CAPABILITIES OF COMPOSITE MATERIALS FOR ADVANCED SUPERSONIC TECHNOLOGY APPLICATIONS 383
J. Haskins and J. Kerr

MOISTURE - AN ASSESSMENT OF ITS IMPACT ON DESIGN OF RESIN BASED ADVANCED COMPOSITES 405
Charles D. Shirrell, John C. Halpin, and Charles E. Browning

FLIGHT SERVICE EVALUATION OF KEVLAR-49/EPOXY COMPOSITE PANELS IN WIDE-BODIED COMMERCIAL TRANSPORT AIRCRAFT 427
Robert H. Stone and H. Benson Dexter

PROGRESS REPORT OF THE NASA GRAPHITE SPOILER FLIGHT SERVICE PROGRAM 441
Robert L. Stoecklin and Richard A. Pride

ENVIRONMENTAL EXPOSURES OF ADVANCED COMPOSITES FOR AIRCRAFT APPLICATIONS 455
Richard A. Pride and Marvin B. Dow

THE AIR FORCE IN-SERVICE ADVANCED COMPOSITE EVALUATION PROGRAM 471
T. Bennett

ADVANCED COMPOSITE FAN BLADE FLIGHT EVALUATION PROGRAM 473
Matthew H. Chopin

Part II*

SESSION III - DESIGN CRITERIA AND RELIABILITY

Chairman: Philip A. Parmley
Air Force Flight Dynamics Laboratory

APPLICATION OF THE AIR FORCE'S NEW STRUCTURAL REQUIREMENTS TO COMPOSITES 491
Gary K. Waggoner

CERTIFICATION REQUIREMENTS FOR CIVIL COMPOSITE COMMERCIAL AIRFRAME STRUCTURES 501
James E. Dougherty, Jr.

FAIL-SAFE DESIGN AND RELIABILITY IN COMPOSITE COMMERCIAL AIRCRAFT STRUCTURE 513
Dale S. Warren

FAIL-SAFE DESIGN AND RELIABILITY IN COMPOSITE COMMERCIAL AIRCRAFT STRUCTURE 523
Robert E. Watson

LIFE ASSURANCE TECHNOLOGY 533
J. Halpin and M. Waddoups

STATISTICAL DESIGN CRITERIA 535
B. Walter Rosen

DESIGN, FABRICATION, AND FLIGHT SERVICE EVALUATION OF COMPOSITE-REINFORCED C-130 CENTER WING 547
W. E. Harvill and H. Benson Dexter

SESSION IVA - DESIGN TECHNOLOGY BASE

Chairman: Michael F. Card
NASA Langley Research Center

BOLTED JOINT STATIC STRENGTH MODEL FOR COMPOSITE MATERIALS 563
James R. Eisenmann

DESIGN OF THE B-1 COMPOSITE HORIZONTAL STABILIZER ROOT JOINT 603
B. Whitman, P. Shyprykevich, and J. Whiteside

CURRENT LANGLEY RESEARCH CENTER STUDIES ON BUCKLING AND LOW-VELOCITY IMPACT OF COMPOSITE PANELS 633
Martin M. Mikulas, Jr., Harold G. Bush, and Marvin D. Rhodes

*Sessions III and IV are presented under separate cover.

ADVANCED COMPOSITE TORQUE BOX OPTIMIZATION 665
Donald Y. Konishi, George Hayase, and Jonas Surdenas

AN AEROELASTIC TAILORING STUDY OF A HIGH ASPECT RATIO WING 687
Kenneth E. Griffin

ADVANCED DESIGN COMPOSITE AIRCRAFT 711
R. N. Hadcock

A HYBRID COMPOSITE FUSELAGE DESIGN WITH INTEGRAL CRACK ARRESTERS 737
S. L. Huang and T. E. Hess

SESSION IVB - DESIGN TECHNOLOGY BASE

Chairman: Edward J. McQuillen
Naval Air Development Center

BATTLE DAMAGE TOLERANT WING STRUCTURAL DEVELOPMENT 759
Ken deBooy

LIFE ASSURANCE OF COMPOSITE STRUCTURES 779
R. V. Wolff and D. J. Wilkins

ON PROCESS ZONE INTERACTIONS IN THE WEAROUT PROCESS 803
M. Waddoups, J. Halpin, and G. Lemon

FATIGUE OF NOTCHED COMPOSITES 805
P. V. McLaughlin, Jr., S. V. Kulkarni, S. N. Huang,
and B. Walter Rosen

FRACTURE BEHAVIOR OF NOTCHED COMPOSITE LAMINATES 829
James M. Whitney and Ran Y. Kim

SUPER-HYBRID COMPOSITES - AN EMERGING STRUCTURAL MATERIAL 851
C. C. Chamis, R. F. Lark, and T. L. Sullivan

ADVANCED COMPOSITES IN BURD II 879
Edward Crawley and John Wendell

KEYNOTE ADDRESS

by

George C. Deutsch

Director
Materials and Structures Division
Office of Aeronautics and Space Technology
NASA Headquarters
Washington, D.C.

First, I would like to extend Dr. Lovelace's greetings and best wishes for a successful conference. As your program indicates, he was originally scheduled to be your keynote speaker. Unfortunately, he is testifying in Congress this morning and in our scheme of things within the federal government, that has a very high priority indeed. I know he was looking forward to being here with you and is very disappointed at not being able to make it.

In my introductory remarks I will try to give a somewhat more general view of composites than is covered in the more detailed papers that you will be hearing and to raise some questions which I feel are urgently in need of answers. Perhaps you can keep these questions in the back of your mind while you listen to the wide variety of excellent presentations that I see in your program.

As I looked over your program, I was particularly struck by what appears to me to be the rather remarkable transition that advanced composites have made in the past decade - and indeed in the past several years since your last meeting. We no longer get together to discuss our efforts to achieve high strength or stiffness-to-weight ratios and we no longer feel it necessary to prove that advanced composites are, in fact, in many respects superior to the alloys that we hope they will replace. Your program indicates to me that you apparently feel confident that this superiority is now well understood and that it is just a question of time until advanced composites will take their rightful place in the inventory of materials from which designers can draw.

We no longer concentrate on how to make components from fibers and resins - instead we assume, certainly justifiably, that components can be made and we discuss the characteristics of the airframe, engine, and spacecraft components that have been fabricated and that we are now testing. We are still groping for that never attainable idea of optimized components and in this groping I note that you are very much in tune with the times with your much needed emphasis on low cost production.

So it appears to me that we have come a long way and this highly partisan group, at least, regards composites pretty much as an accepted, technologically ready achievement which will, like other new materials, find its proper role in the aircraft and spacecraft of the future. Many of the papers in this conference appear to me to be exploring just what is this proper role. Reports are being made on component demonstration programs for a wide variety of applications to military and civil airframes, engine components, and spacecraft structures.

It also appears to me that your program indicates that there is a growing number of component demonstrations. I think these are much needed and I think now is the time to conduct them. Let me mention just a few of these programs. I will use NASA examples because I am naturally most familiar with these. In addition to the secondary structure components that NASA has reported in the past, we have initiated a primary structure tail program, we hope to very shortly initiate a new program for a full span civil aircraft wing some 80 feet long, and are seriously considering initiating a program on a major fuselage section. It is our belief that these major pieces of primary structure are "clinchers" which will convincingly demonstrate the utility and advantages - particularly fuel savings of advanced composites for the airframes of civil aircraft. The Air Force, Army, and Navy have similar programs to similarly demonstrate major primary structural components for bombers, fighters, and helicopters.

Composites for engines, both the cold and hot ends, appear to be lagging somewhat. However, for the cold

end we, in NASA, are working in an interdependent way with the services to demonstrate the superiority of composites for fan stage and compressor components in turbofan engines. With regards to the hot end of the engine, composites appear to be about at the stage where the ambient temperature composites were four or five years ago.

Thus the National program, as I see it, consists of an extensive effort to apply composites in the ambient temperature regime, coupled with smaller programs to extend the utility of composites to both the 600°-800°F range and ultimately to the over 2000°F range for turbines.

This conference is, of course, concerned with the composites for use at ambient temperatures. Looking over the large and growing program that is being reported at this conference, one can easily be lulled into feeling that our work in advanced composites is in its final stages. One can get the feeling that final demonstrations are still needed but that after they are completed, the new materials will be eagerly grasped by designers. I would like to suggest that this is not at all the case - and that we still have a hard and arduous road ahead of us. To encourage you to think about the road blocks on the path still ahead, I would like to pose and then briefly discuss several questions. These are:

1. How can we assure that the large quantity of low cost and uniformly high quality fibers and resins that we will require if composite components are routinely incorporated into production aircraft will be available?

2. Our flight experience to date has been largely with very conservatively designed and lightly stressed components and has not really been adequate to uncover the unexpected problems that are inevitably revealed during the early usage of any new materials. Do we in fact have the technological background so that as these problems arise they can be understood and quickly resolved?

3. All of the flight programs that you will hear described during the next three days are programs that have been initiated and largely paid for by research and development groups in government and industry. In the early phases of the evolution of a new material - especially one that is as radically different as are advanced composites, this is inevitably the case. Nevertheless, it is my conviction that composites have not really arrived and will bog down unless the project offices within the government and the production divisions of commercial aircraft producers are more extensively involved than is presently the case, and are seriously planning for their routine use. How do we progress from the point of nearly total research and development initiatives to one of largely user initiated activities?

Let me discuss these questions in turn. First the question of assuring the supply of fibers and resins. When I talk to the large chemical companies that are the large fiber and resin producers, I find that they are very cautious about the aerospace market. They are used to thinking of profitable markets as being measured in millions of pounds of product and neither they nor I can see this developing in the foreseeable future in aerospace. I, therefore, feel that it is incumbent on each of us to do what we can to foster the nonaerospace uses of advanced composites - and unless we do this we will not achieve the uniformly high quality and low cost fibers and resins that will assure the cost effective use of composites. We are all familiar with the gradually increasing use of composites in sporting goods - tennis rackets, golf clubs, skis, and fishing rods. These markets are certainly very helpful in increasing the demand for fibers and resins and I believe they helped make last year a milestone year for advanced composites. It is my understanding that during the last year, for the first time, the use of advanced composites in nonaerospace applications exceeded that of the aerospace applications. I regard this as an exceedingly promising development, but the use of advanced composites in sporting goods will simply not achieve the tonnage required in the time required and we must expand our horizons. The automotive and truck industries, the

machine tool industry, the optical industry, and the construction industry all appear to me to offer promising market potentials and I believe we, in the aerospace industry, for purely selfish reasons have a strong incentive to encourage and assist in exploitation of composites by these users. It might turn out that these nonaerospace uses could be profitable financial ventures as well.

Next I would like to discuss the adequacy - or perhaps the inadequacy - of our understanding of the basic science and technology to meet the needs that we will encounter as these materials are used more and more, and as production specialists become more and more interested in them. Probably the most frequently asked question by those curious and highly important people who, unlike us, are not enthusiasts for advanced composites, the systems decision makers, has to do with the durability of these no longer so new materials. They are afraid to wholeheartedly embrace these materials because while they see the many advantages that your papers will so carefully document they do not fully understand nor are we able to assure them of their behavior in the presence of moisture, brine, and the other environmental factors that inevitably will be encountered. They don't have a good picture of how and under what conditions advanced composites fracture, or how they behave in the presence of cracks and other defects. They don't feel very confident with the inspection procedures that we use - particularly those where we adhesively bond composites to metallic parts. They don't feel confident about the long time chemical stability of composites - and in view of the fact that they are not designing airplanes for up to twenty years of service life, this is a highly important consideration. All of these questions are valid and legitimate and we will have to provide answers to make us and the users comfortable with the composites that we anticipate they will elect for the next generation of aerospace vehicles.

It seems to me that we have been derelict in not devoting enough attention to these factors and while I can understand the trends in our program and the need we

feel to get composites into flight service programs, I think we should seek to reestablish a better balance in our programs and increase our research and technology activity. I certainly do not have the magic number that would specify what percentage of the effort in advanced composites should be devoted to this basic understanding. But I feel that our program has gotten out of balance and we no longer have a science and technology program that is commensurate with and appropriate to the growing component demonstration and use programs that you will hear about in the next few days.

I would now like to turn to the final and most elusive question - that is, what is - or perhaps should be - the proper role from here on out of research and development groups in continuing evolution of advanced composites. Traditionally, with many new materials, the R&D groups have carried the materials through demonstration programs to clearly demonstrate their advantages and to show that they are technologically ready for application. We are of course doing this in the case of composites and perhaps because of the radically different nature of these materials more extensive demonstration programs are required than for, for example, a new alloy system. The user groups - both military and commercial - on the other hand, have applied the technology to their own products and have traditionally developed the production techniques for their particular needs. In addition, they have borne the cost of the capitalization of production facilities. In other words, they have paid for the evolution of the hard tooling required and have borne the costs that are involved in moving down the learning curve. This, it seems to me, is the traditional differentiation between the R&D groups and the user groups. I think in the case of composites, this differentiation is very much blurred. There are many reasons for this - the fact that fewer systems are being built, the fact that we are treating radically new materials, and several others - and therefore, it seems to me that the research and development groups must, for some time to come, continue their development programs until designers develop a greater conviction that the materials are ready to be used in a cost effective way. On the other hand, it is also very clear to me that it is incumbent upon the user groups to immediately

consider how they might use composite structures to improve the performance of their products and to actively plan for this usage. I realize that the line differentiating these two areas of activity is not clear and it is certainly hard to draw. Nevertheless, it is my strong conviction that the user groups, whether they be military project offices or civil aircraft divisions of aerospace companies, are not devoting the attention to composites that these materials warrant. I realize that industry is not in the best of financial times but it seems to me that if we, as a nation, are to retain our share of the world's civil aircraft market and the superiority of our military aircraft, we must continuously improve our products. In the final analysis, the research and development activity only assists in this and the key decisions must be made by the users. It is my belief that the users are not adequately considering this question and it is my conviction that we should do everything we can to insure that this situation is reversed.

It has been my purpose in these introductory remarks to raise questions that are of concern to decision makers in both government and industry and perhaps to somewhat broaden your outlook as you listen to the many excellent technical papers that I see listed on your program. I really feel that your conference could be more productive if papers were listened to with these questions in mind and if, in addition to technical excellency, they could be judged in terms of the contributions they are making to answering what I have tried to state as fundamentally important issues. I am looking forward to hearing these technical papers and to participating in your activities over the next three days.

FLIGHT SERVICE PROGRAM FOR AN ADVANCED COMPOSITE FIN FOR A WIDE-BODY COMMERCIAL JET

By Robert L. Vaughn and Arthur M. James
Lockheed-California Company

SUMMARY

A team comprised of Lockheed-California, Lockheed-Georgia, and Rockwell International has been awarded a contract by NASA for the first flight-service program of an advanced composite material primary structural component of a commercial aircraft, the structural box of the Lockheed L-1011 vertical fin. The fin box has a span of twenty-five (25) feet, a root chord of nine (9) feet, and a planform area of one hundred fifty (150) square feet. A weight saving of twenty-five (25) percent of the current metal box design is anticipated with over eighty (80) percent by weight of the redesigned box being made with composite material. Program plans are discussed in detail including a description of candidate structural configurations, test programs, and flight-service evaluation procedures.

INTRODUCTION

The objective of this program is the development and flight demonstration of an advanced composite empennage component, manufactured in a production environment, at costs competitive with those of its metal counterpart, and at a weight saving of at least twenty (20) percent. The empennage component selected to achieve these objectives is the vertical fin box of the L-1011 aircraft. The box structure extends from the fuselage production joint to the tip rib and includes the front and rear spars, see Figure 1.

Lockheed will design, develop, fabricate, and test one advanced composite vertical fin structural box and then fabricate and deliver two complete vertical fin assemblies, installed on L-1011 aircraft, for evaluation in commercial service for five (5) years.

The duration of this program is one hundred six (106) months with completion scheduled for March 1984. The program is organized in five overlapping phases: Phase I - Engineering Development (5 months); Phase II - Detail Design (21 months); Phase III - Fabrication (24 months); Phase IV - Ground Tests (7 months); and Phase V - Flight Service Evaluation (5 years). A calendar of all major program events is shown on the Program Master Schedule in Figure 2.

The Lockheed-California Company (Calac) has teamed with the Lockheed-Georgia Company (Gelac) and the Los Angeles Aircraft Division of Rockwell International (LAAD) in the development of the advanced composite vertical fin (ACVF). Team member responsibilities are shown in Figure 3. Calac, as prime contractor, has overall program responsibility and will design and fabricate the covers, conduct the full-scale ground tests, install the flight articles, and evaluate service experience; Gelac will design and fabricate the front, rear, and auxiliary spars, and assemble the component at their plant in Meridian, Mississippi, where the present L-1011 vertical fins are assembled; and LAAD will design and fabricate all ribs.

During Phase I various design options such as stiffened covers and sandwich covers will be evaluated to arrive at a configuration which will offer the highest potential for satisfying the program objectives. The preferred configuration will be selected approximately ninety (90) days after go-ahead. Material screening tests will be performed to select an advanced composite material system; preliminary weight and cost analysis will be made, targets established, and tracking plans developed. Plans for subsequent phases will also be developed in this phase. These include FAA certification, ancillary test program, quality control, and structural integrity control.

Phase II covers the main engineering effort. Detail design, analysis, and development testing will be accomplished. Limited production tooling will be designed and fabricated and plans for the fabrication of the full-scale components will be written. Phase III provides for the fabrication of the full-scale ground test component and the two components to be used for flight service evaluation. Fabrication of the flight service articles will not begin until after tests on the full-scale ground test component have started. During fabrication, actual costs will be documented, and components weighed to develop the weight update for the assembled structures.

Ground tests will be conducted on a full-scale vertical fin box beam structure mounted on a fuselage afterbody structure during Phase IV. The test plan will include spectrum fatigue tests to two (2) lifetimes, ultimate load, fail-safe, and residual strength tests. Repair techniques and procedures established for in-service maintenance and inspection will be employed throughout these tests. Phase V provides for the installation of two ACVF's on commercial aircraft for flight service evaluation for a period of five (5) years. Inspection procedures and inspection intervals will be established in conjunction with the participating airlines. Prior to delivery and introduction into regular service, each aircraft will be processed through normal predelivery and other check flights as required by Engineering and the FAA.

CURRENT ALUMINUM DESIGN

An exploded view of the existing metallic vertical fin of the L-1011 is shown in Figure 4. The figure shows details of the existing structure and indicates which parts will be redesigned using composite materials. The vertical fin covers are attached to the fuselage afterbody structure through a double shear butt joint. The vertical fin box beam is constructed of 7075-T6 aluminum

alloy skin and stringers supported by 17 ribs and two spar assemblies built-up from aluminum sheets and extrusions. Five of the ribs are solid web type, ten are truss ribs, and the remaining two consist of a combination of truss and web design.

The five segmented leading edge assemblies are constructed of clad 7075-T6 aluminum skins, stiffened by aluminum sheet metal ribs. De-icing is not required in the leading edge.

The vertical fin trailing edge consists of the trailing edge surfaces providing faired surfaces between the box rear spar and the rudder leading edge, the trailing edge support structure, and the rudder hinge support fittings. Hinged panels on the fin trailing edge provide access to the rudder hydraulic control system and to the six hinges. A flush VOR antenna is installed in the removable fin tip.

Access is provided for inspection of the interior structure box through access holes located in the front and rear spars and through an access hole in the afterbody bulkhead at the fin interface.

ADVANCED COMPOSITE DESIGN CONCEPTS

Extensive preliminary design studies are being conducted to develop advanced composite design concepts which demonstrate superior cost, weight, and risk performance over conventional metallic structures. A broad spectrum of cover configurations and compatible substructure elements is being explored. The various concepts being evaluated are illustrated in Figure 5 and range from highly optimized configurations requiring a minimum of material to simplified production forms of lower structural efficiency. From these studies, it appears that two designs, namely, a hat stiffened cover and a sandwich cover configuration offer the highest potential for satisfying program objectives. For either concept, the composite component is defined as the main structural box of the vertical fin; it includes the front and rear spars, left and right covers, and all ribs. The tip closure rib, all hinge and actuator fittings, and the auxiliary spar are retained in the metal configurations.

Hat Stiffened Cover Design Concept

Preliminary weight, cost, and structural analyses of various concepts have been performed and the most promising options combined to produce the hat stiffened box configuration shown in Figure 6. Both covers feature hat-section stiffeners located at approximately 6.0-inches spacing parallel to the rear beam. These stiffeners utilize 0°, $\pm 45^{\circ}$ graphite/epoxy. The stiffener shape was selected for adaptability to automated production techniques (pultrusions). The stiffeners are sized to provide adequate column stability and for bending due to surface pressures. At the lower end of each cover, the stiffeners transition into a simple flat plate to mate with the existing fuselage-to-cover bolted joint. The cover skins utilize a combination of both graphite/epoxy and Kevlar 49 material with sizes and ply orientations selected to match

the strength and stiffness requirements of the current vertical fin. The distribution of area between spar caps and covers at the fin root is dictated by a requirement to maintain the same load distributions between the vertical fin and fuselage as that in the existing metallic structure. This requirement ensures structural compatibility with the fuselage reaction structure.

The substructure consists of ten (10) full ribs, one partial rib, and continuous front and rear molded spars. Three distinctly different rib designs are utilized in this configuration. The three upper ribs feature a thin (1/8-in. to 3/16-in.) honeycomb sandwich, called "miniwich," stiffened web with integrally molded rib caps and cover attachment flanges. The seven remaining full-size ribs are truss ribs with graphite/epoxy molded caps and aluminum diagonals. The partial rib, which distributes the rudder actuator load, is a stiffened web design.

A segment of the fin box representing the box structure at the rear beam at a "miniwich" rib intersection has been fabricated and is shown in Figure 7. Typical details associated with the attachment of the rib, spar, and surfaces are reflected in this specimen. Each element of the component was fabricated by appropriate team members, i.e., the surfaces were fabricated by Calac, the rear spar by Gelac, and the rib by LAAD. Assembly was accomplished by Calac with all elements mating within the specified tolerances.

Sandwich Cover Design Concept

The honeycomb stiffened cover concept emerging as the best compromise of weight, cost, and structural efficiency is the continuous core design shown in Figure 8. It features transition from a sandwich to a flat plate at the fuselage joint to eliminate eccentricities normally associated with axial load transfer of honeycomb panel runouts. The skin concept selected, primarily for manufacturing simplicity, consists of graphite/epoxy precured sandwich skins bonded to continuous fiberglass honeycomb core. The core is potted at each rib station to provide added strength for the attachment of ribs to covers. The inner and outer skins of each cover have the same ply orientations and consist of 0° and $\pm 45^{\circ}$ plies to provide the strength and stiffness required.

The substructure used in the sandwich design concept is the same as that used in the hat stiffened cover concept, but the ribs are fastened directly to the covers through the rib caps, thereby eliminating the need for the integral clips required in the hat stiffened cover design.

The critical design detail associated with each concept being evaluated occurs at the attachment of the cover panels to the fuselage afterbody structure. This joint detail, the geometry of which is fixed, was evaluated by fabricating and testing representative joints for both the stiffened and sandwich cover concepts. The stiffened cover design was evaluated using an I-stiffener concept and a hat stiffener concept. For the I-stiffener and sandwich concepts, two specimens were evaluated, one using a 250°F cure resin system (E715), and one using a 350°F resin system (934). The skins were fabricated from a hybrid of T300 graphite and Kevlar 49, 281 cloth. The

stiffeners were all T300 graphite. One hat stiffener concept has been fabricated and tested utilizing T300/934 and a second one utilizing T300/5209 (260°F cure) will be tested shortly. The test specimens and test results are shown in Figure 9. As shown in this figure, all specimens exceeded design requirements.

Lightning protection will be provided in the fabrication of the ACVF. One method being considered for lightning protection is by providing a continuous single layer of an aluminum wire mesh cocured to the outside surface of each cover. Protection against corrosion of the wire mesh is achieved by providing a layer of Kevlar 49 as a barrier between the aluminum and graphite.

Cost/Weight Performance

The weight breakdown of material utilization for the hat stiffened and sandwich cover designs is shown in Figures 10 and 11, respectively. As shown in these figures, over eighty (80) percent of the box structure consists of composite material, with the hat stiffened cover concept being the lighter of the two. A comparison of the estimated costs and weights of the candidate design concepts with those of the aluminum baseline is shown in Figure 12. It indicates cost savings of 14.4% for the honeycomb sandwich cover design and 15.5% for the hat stiffened cover design based on the cumulative average cost for a production quantity of 250 aircraft.

It should be noted that these are comparative costs, not total costs for the entire vertical fin box. The comparison includes recurring production, quality assurance labor, and production materials. The auxiliary spar, upper closure rib, actuator and hinge rib fittings, and rib truss members are retained in their aluminum configurations. Weight savings are estimated to be 20.4% and 25.3%, respectively (see Figure 12).

Production costs for the candidate designs were determined from study of drawings and manufacturing plans. A list of operations to fabricate each part such as layup, cut, trim, bag, debulk, and cure, etc., was developed for each part. Numbers and orientation of plies were calculated and time standards applied. Assembly costs were estimated by developing an assembly sequence plan and estimating the time required for loading parts and drilling and installing fasteners. Appropriate realization factors for fabrication and assembly were applied to the time standards to calculate the production costs, resulting in an overall learning curve of 76 percent. A comparison of the number of parts and fasteners used in the existing metallic vertical fin with that anticipated for the candidate composite design is also shown in Figure 12. The reduction in parts and fasteners required for the composite designs is the primary reason for achieving reduced costs.

Currently, under Phase I - Preliminary Design, trade evaluations are being conducted to determine the optimum configuration for the ACVF. The two concepts discussed above are included in the matrix of configurations being evaluated. The results of the trade-off evaluation and the selection of the recommended configuration will be presented to NASA Langley at a Preliminary

Design Review (PDR) to be held on 12 November 1975. With NASA's concurrence, the selected configuration will be used in proceeding with the detail design and development activities.

CERTIFICATION PLAN

The development and certification of the Lockheed L-1011 airplane with the ACVF installed will be conducted in accordance with the requirements of applicable portions of the FAA governing documents and Lockheed documents. The applicable FAA documents include the following Federal Aviation Regulations (FAR):

FAR Part 21 - Certification Procedures for Products and Parts

FAR Part 25 - Airworthiness Standards - Transport Category Airplanes

The Lockheed documents include applicable L-1011 criteria and loads reports modified as required to reflect composite structure.

Lockheed intends to obtain certification of the ACVF installed on L-1011 aircraft early in 1979. Certification will be based on satisfying both static strength and fail-safe requirements and by demonstrating durability.

A certification plan has been submitted to the FAA for their consideration and approval. Significant elements of that plan include:

- Structural Integrity and Quality Control Plans
- Ancillary Tests
- Full-Scale ACVF Ground Tests
- Flutter Tests

A Structural Integrity Control Plan will be implemented to complement the fail-safe design of the ACVF. This plan will have many of the features of fracture control programs currently in use on metal aircraft structure. Emphasis is placed on tailoring the strength and durability assurance requirements on a part-by-part basis. This approach is in line with the overall policies that have resulted in safe and durable commercial aircraft in the past and will lead to successful introduction of primary composite structure into commercial airline service.

The Structural Integrity Control Plan will establish those actions that need to be applied in addition to those specified by the Quality Control Plan to ensure that strength and durability objectives are met. The plan will be responsive to special requirements that arise in individual parts or areas as a result of potential failure modes, damage tolerance and defect growth requirements, loadings and local configuration, inspectability and as a result of local sensitivities to manufacture and assembly. The Structural Integrity Control Plan will also develop any special in-service inspection requirements that may be required to ensure that strength objectives are met throughout service use. This part-by-part review and planning will ensure that design, strength, and durability objectives are met by an adequate and cost effective

plan which is particularly suited for the part or area where it is to be applied. While the structural integrity control may vary with each part/area, the major emphasis will be to provide evidence that the local structural integrity of each part produced is, in critical areas, equal to or in excess of the minimum required to obtain the strength and durability objectives as provided for in the design and within acceptable levels of variation from that demonstrated in the component and full-scale tests.

The Quality Control Plan will provide for the routine or generally applicable material, manufacture, and assembly controls.

Demonstration that static strength, durability, and fail-safe objectives are capable of being met for production hardware will be provided by component and full-scale tests and by related analyses. Demonstration that these objectives are met on each production composite vertical fin will be provided by implementing the Quality Control Plan and the Structural Integrity Control Plan.

The ancillary test program is designed to screen for material selection, develop design allowables, evaluate concepts, determine environmental effects, develop process and inspection specifications, and to substantiate design details. The test specimens will consist of coupons for materials and joint allowables data, elements of parts, and subcomponents of assemblies.

Subcomponent tests will include such items as full-scale ribs, spars, major joints and segments of surface panels. Sections of full-scale ribs and spars at various locations of the box beam will be tested. Major joints representative of spar-to-fuselage attachment, rudder hinge and actuator fittings, and surface panel-to-fuselage attachment will be tested for static strength and fatigue resistance. Large cover panel components will be tested to verify stability, interface loads between cover and ribs, and damage containment. Several of the larger components will be repaired and retested to verify repair techniques. The coverage of the box structure currently planned is shown in Figure 13. One significant test which will be accomplished will be conducted on a subcomponent consisting of a major portion of the box structure. This component will be fabricated from production tooling and consists of one hundred (100) inches of the rear spar and thirty-six (36) inches of the box chord and will include the fuselage/box joint.

All coupon and subcomponent fatigue testing will be for four (4) lifetimes and residual strength and static test to failure will follow fatigue testing. These static test results will be compared with the results of static tests on articles which are not fatigued to determine the degradation, if any. A sufficient number of static and fatigue coupon and subcomponent tests will be performed to determine the effect of environmental factors (temperature and humidity) on mechanical properties and behaviors.

Upon completion of the ancillary test program, the effects of environmental factors on mechanical properties and failure modes will have been defined and strength, durability, and damage tolerance of typical structure and design details will have been demonstrated. Information will also be available for

defining the degree to which the loads and/or cycles would have to be increased to provide for environmental effects in the ground test of the full-scale ACVF.

Ground tests will be conducted on a full-scale ACVF box beam structure mounted on a fuselage afterbody structure. Results of these tests will be used to verify structural integrity and to provide additional demonstration of durability. The test plan is summarized in Figure 14 and includes influence coefficient tests, spectrum fatigue test to two (2) lifetimes, ultimate load, fail-safe, and residual strength tests. Repair techniques and procedures established for in-service maintenance and inspection will be employed throughout these tests.

Instrumentation will provide strain, deflections, and load measurements. Data are acquired, recorded, and processed automatically. Quick-look plots of load vs. response will be provided during the test to minimize the risk of inadvertent premature failures. Test setup will consist of a multi-channel electro-hydraulic closed loop servo system as shown in Figure 15. Approximately fourteen (14) channels will be utilized to provide the required test loading. The system controls the action of the jacks in applying the test load and for monitoring of test data.

Following completion of the ground test program, a teardown inspection will be performed. Portions of the structure will be cut into material evaluation specimens from which fiber and resin content will be determined. Mechanical properties will be checked and a microanalysis conducted.

The flutter integrity of the composite configuration will be substantiated through a ground shake test and a limited flight flutter program. The flutter safety of the basic L-1011 vertical fin has been demonstrated by analysis, flutter model tests, and flight flutter tests. In view of the design criteria for stiffness of the ACVF, flight tests to demonstrate freedom from flutter can be very simple with the airplane flying a speed-altitude path corresponding to V_D; in-flight modes can be excited by rudder kicks. Accelerometers on the vertical fin can be used to record the response, which is expected to indicate ample damping of all in-flight modes.

FLIGHT SERVICE EVALUATION

Two flight service evaluation components will be installed on U.S. Flag commercial aircraft. Lockheed is currently negotiating with Delta, TWA, and EAL as possible participating airlines on this program. It is intended that the composite vertical fins will be installed in the normal assembly sequence, in lieu of the regular components. The regular metallic components will be crated and held until completion of the flight service evaluation period. The flight service evaluation is presently scheduled for a five (5) year period. At the completion of the flight service evaluation, the composite components will be removed and replaced by the metallic parts. The composite components will then be shipped to NASA Langley.

Aircraft in commercial service are normally inspected at regular intervals with intervals increasing as the aircraft accumulates flight hours at a rate of about three thousand (3,000) flight hours per year. An agreement will be negotiated with participating airlines to provide for satisfactory inspection procedures and intervals. Inspection of participating aircraft will be conducted no less frequently than on present aircraft.

At the completion of four (4) years of flight service, a flight service review will be conducted. Data presented will include results of all comprehensive inspections, a discussion of maintenance and repairs, proposed changes, and additions or deletions to establish maintenance and repair procedures. Based on this evaluation, the desirability of extending the flight service evaluation beyond five (5) years will be determined and recommendations presented. NASA intends to contract for one or more extensions of the flight service evaluation (in three-year increments) so long as the components have demonstrated to be flightworthy and useful flight service data are being obtained.

During the flight service evaluation, all labor and material costs associated with the maintenance and repair of the two flight components will be tracked and documented. These costs will be used to update the cost estimates projected during Phase I.

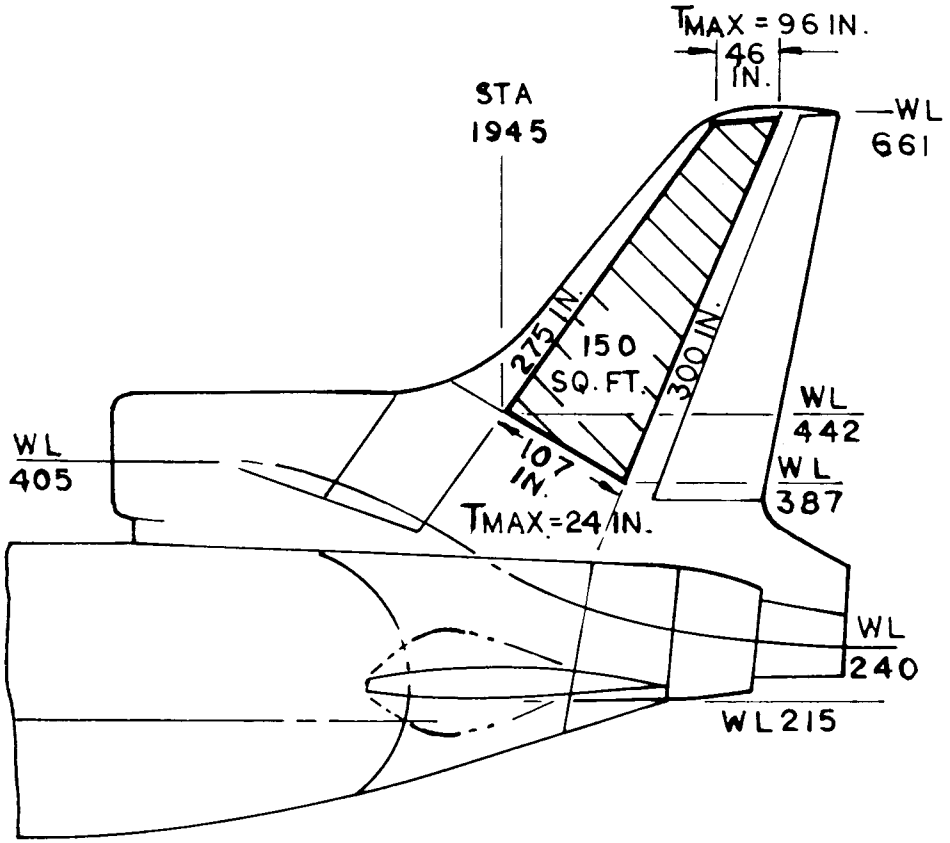

Figure 1. L-1011 Vertical Fin Box Basic Data and Orientation

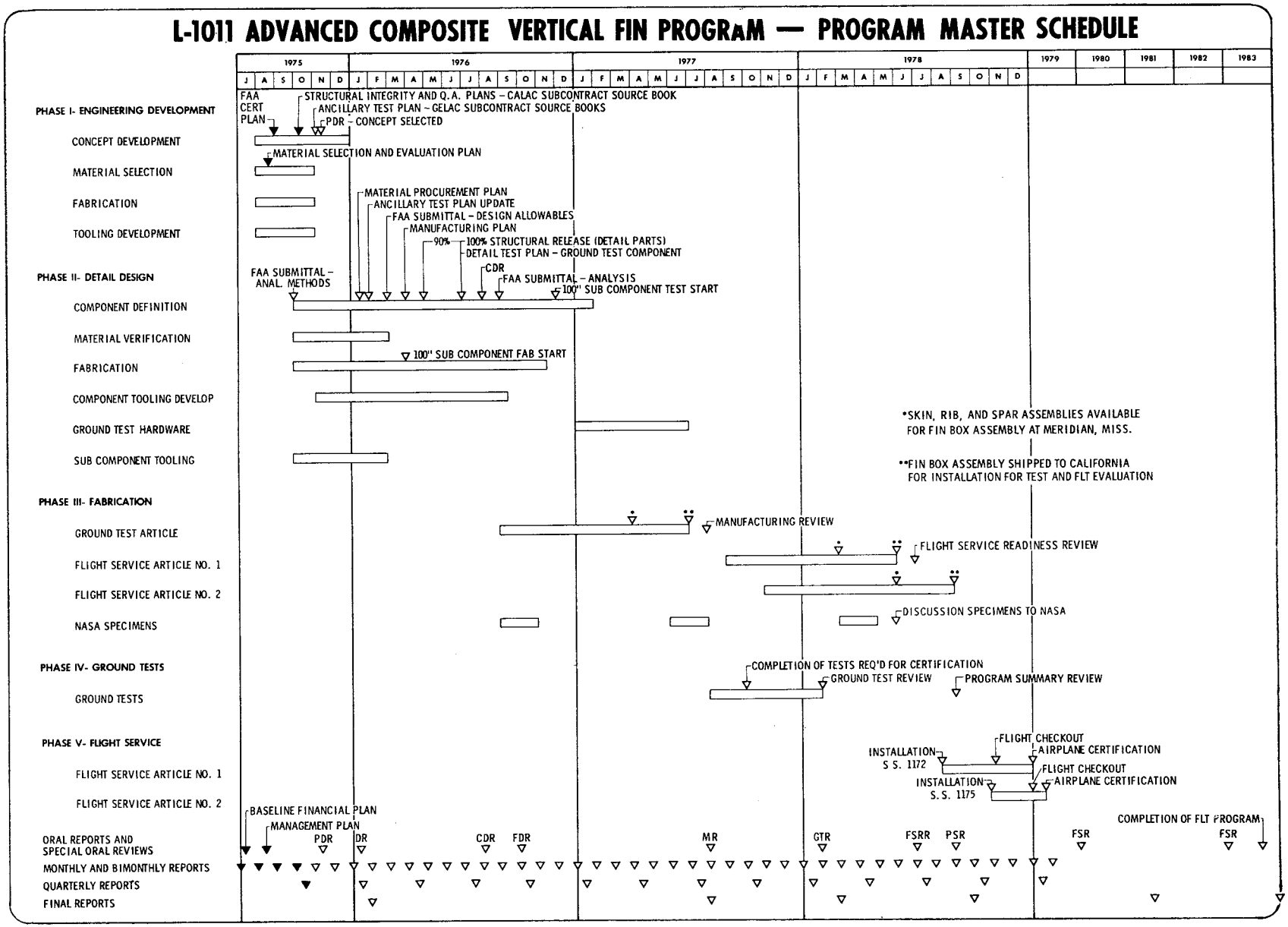

Figure 2. Program Master Schedule

	PHASE I ENGINEERING DEVELOPMENT	PHASE II DETAIL DESIGN	PHASE III FABRICATION	PHASE IV GROUND TESTS	PHASE V FLIGHT SERVICE
LOCKHEED- CALIFORNIA CO	PRELIMINARY DESIGN DESIGN DOCUMENTATION PROGRAM PLANS CONCEPT EVALUATION TESTS COST WEIGHT ESTIMATES 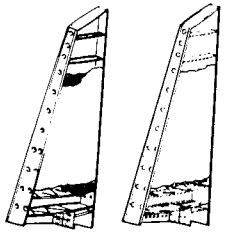	DESIGN AND ANALYSIS OF COVERS DESIGN AND FABRICATE TOOLING MANUFACTURING PLANS ANCILLARY TESTS GROUND TEST PLANS 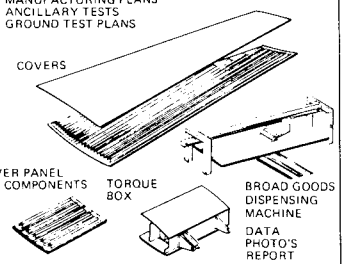 COVERS COVER PANEL SUB COMPONENTS TORQUE BOX BROAD GOODS DISPENSING MACHINE DATA PHOTO'S REPORT	FABRICATE COVERS SHIP TO MISSISSIPPI 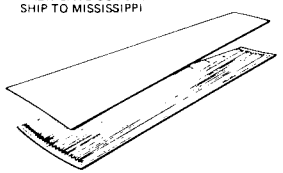 QUALITY CONTROL SPECIMENS 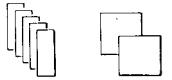 DATA PHOTO'S REPORT	GROUND TESTS VIBRATION, FATIGUE, ULTIMATE, FAIL SAFE, RESIDUAL STRENGTH 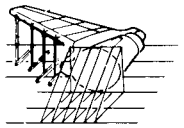 DATA PHOTO'S REPORT	FLIGHT TEST STORE METAL FINS PERIODIC INSPECTIONS 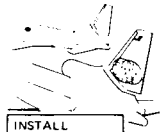 INSTALL METAL FINS SHIP COMPOSITE FINS TO NASA DATA PHOTO'S REPORT
LOCKHEED GEORGIA CO.	FURNISH PERSONNEL TO CALAC	DESIGN AND ANALYSIS OF SPARS DESIGN AND FABRICATE TOOLING MANUFACTURING PLANS ANCILLARY TESTS 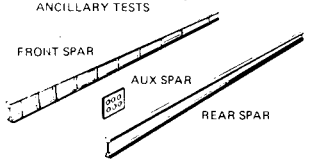 FRONT SPAR AUX SPAR REAR SPAR SPAR SUB COMPONENTS 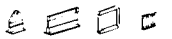 DATA PHOTO'S REPORT	FAB. SPARS ASSEMBLE BOX SHIP TO CALAC INSTRUMENT RIBS 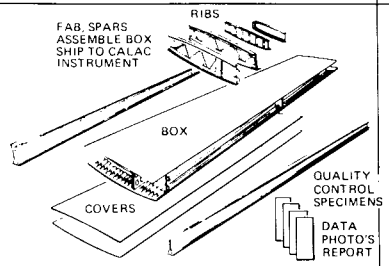 BOX QUALITY CONTROL SPECIMENS COVERS DATA PHOTO'S REPORT	WITNESS TESTING	NO EFFORT
LOS ANGELES AIRPLANE DIV./ ROCKWELL	FURNISH PERSONNEL TO CALAC	DESIGN AND ANALYSIS OF RIBS DESIGN AND FABRICATE TOOLING MANUFACTURING PLANS ANCILLARY TESTS 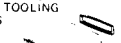 RIBS 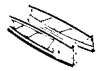 SUB COMPONENTS 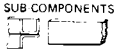 DATA PHOTO'S REPORT	FABRICATE RIBS SHIP TO MISSISSIPPI QUALITY CONTROL SPECIMENS RIBS DATA PHOTO'S REPORT	WITNESS TESTING	NO EFFORT
AIRLINES FAA	CONSULTING - LIAISON	CONSULTING ANALYSIS APPROVAL	LIAISON	LIAISON COMPONENT CERTIFICATION	FLIGHT EVALUATION L-1011 FLY 5 YEARS

Figure 3. Program Responsibilities

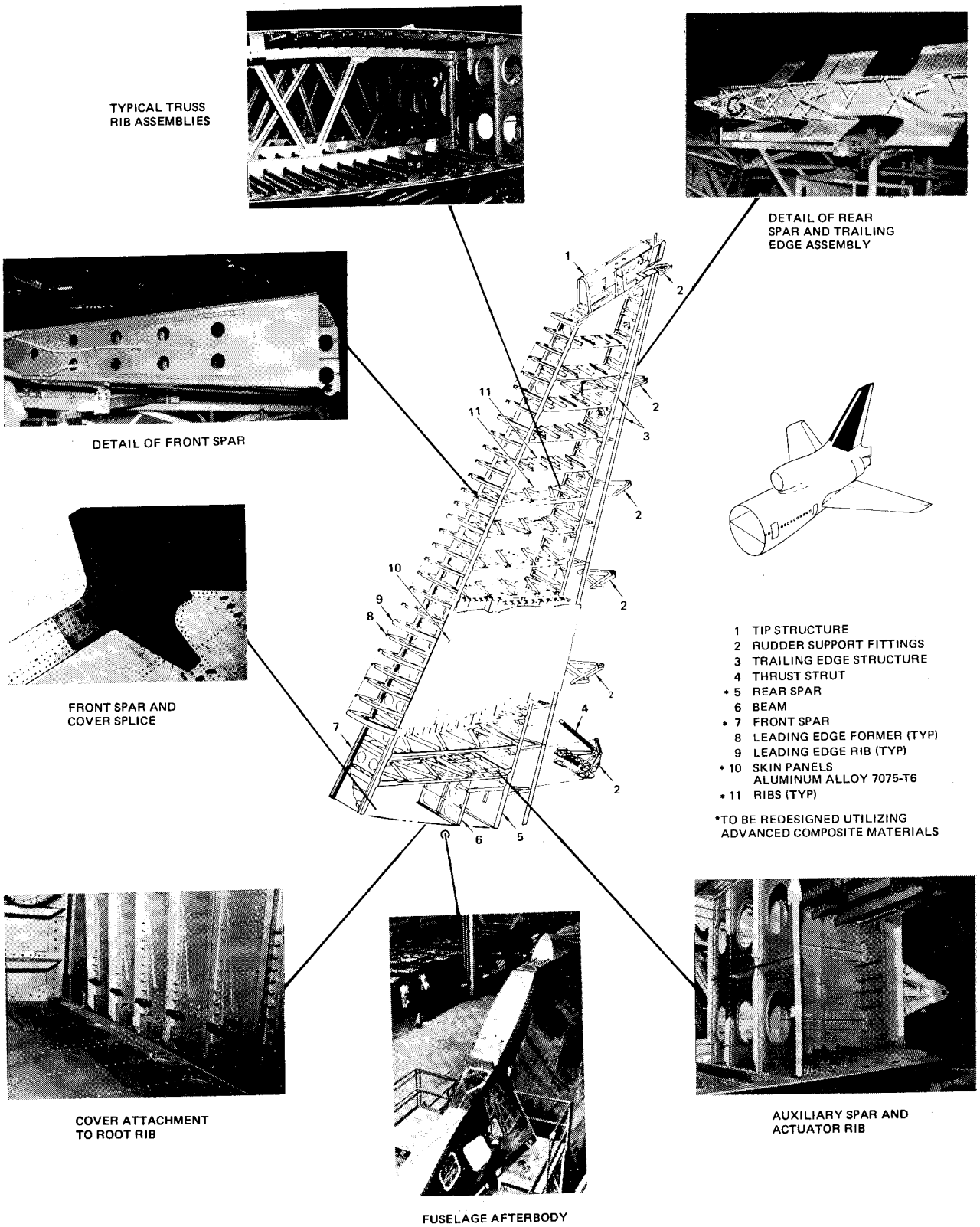

Figure 4. L-1011 Vertical Fin Box Structure

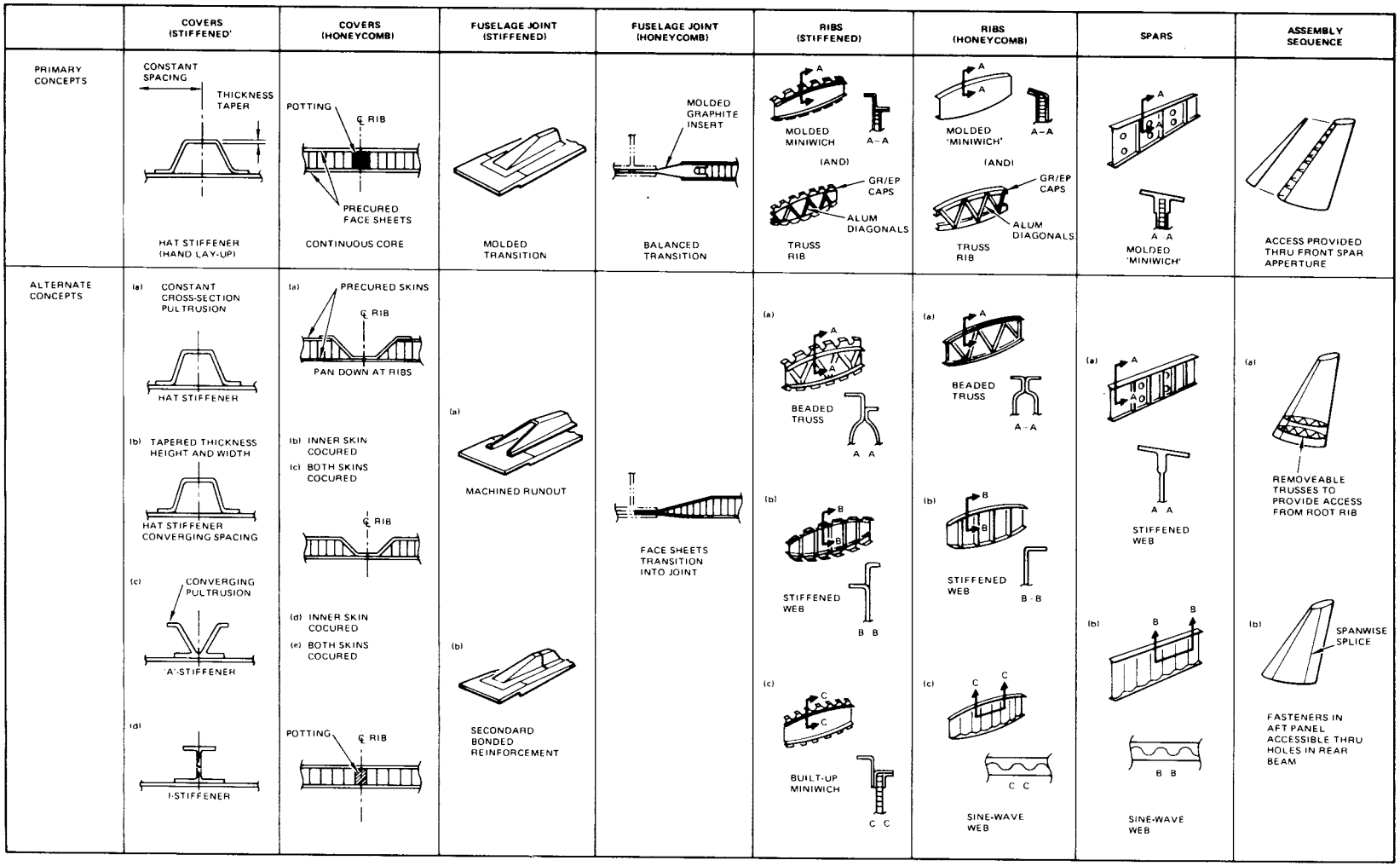

Figure 5. Concept Evaluation

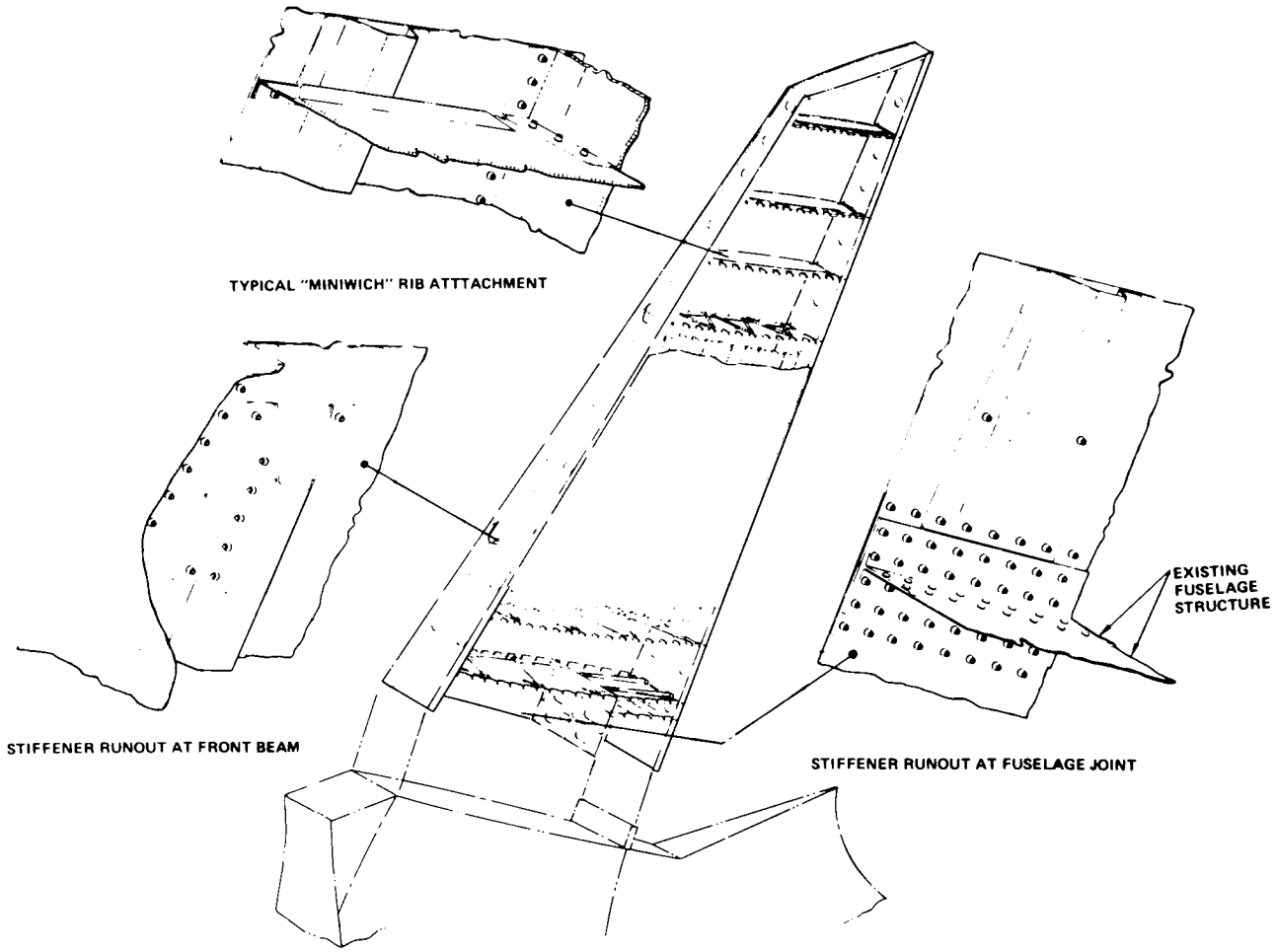

Figure 6. Hat Stiffened Cover Concept

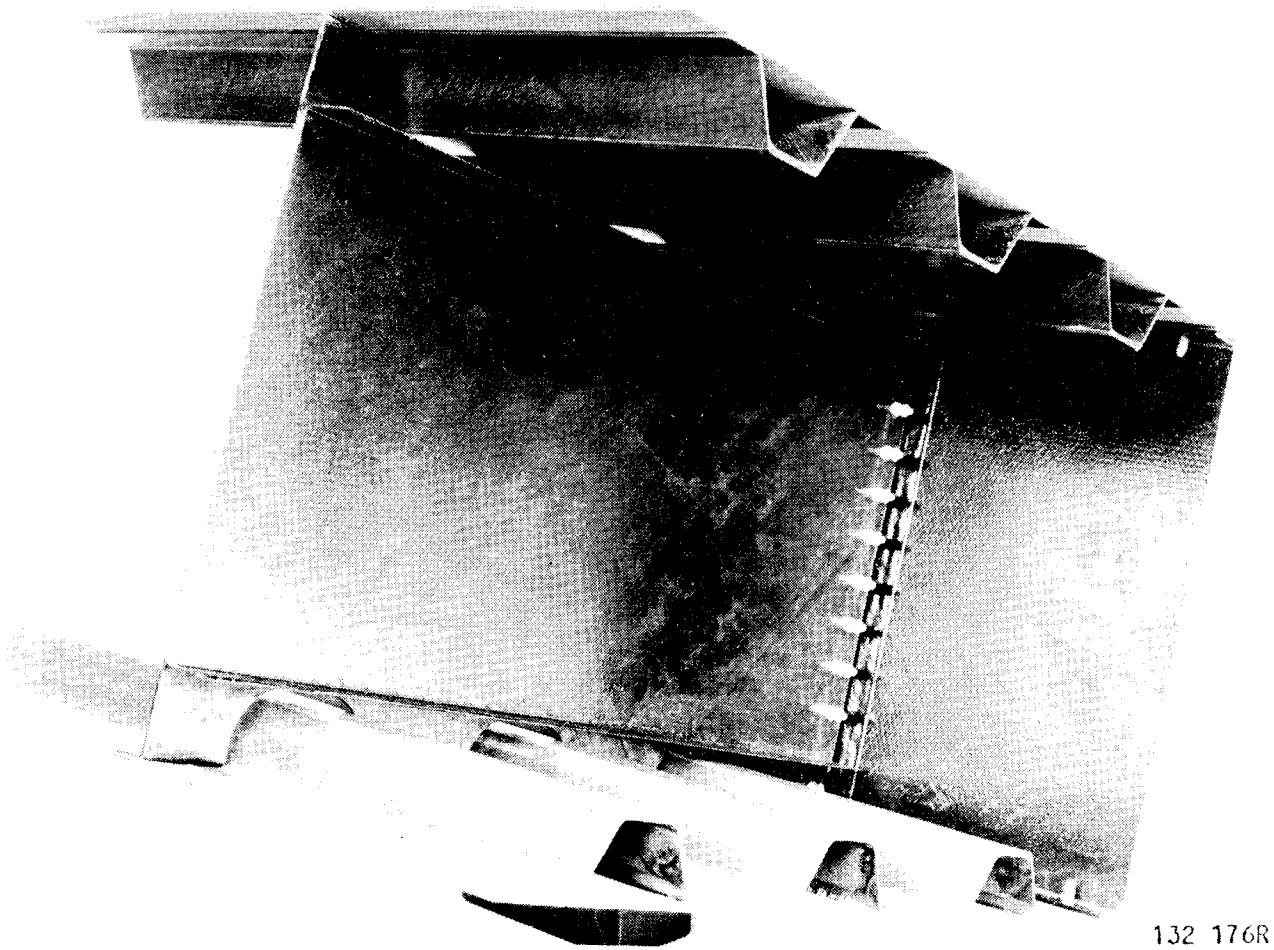

Figure 7. Hat Stiffened Cover Design Concept - Miniwich Spar and Rib

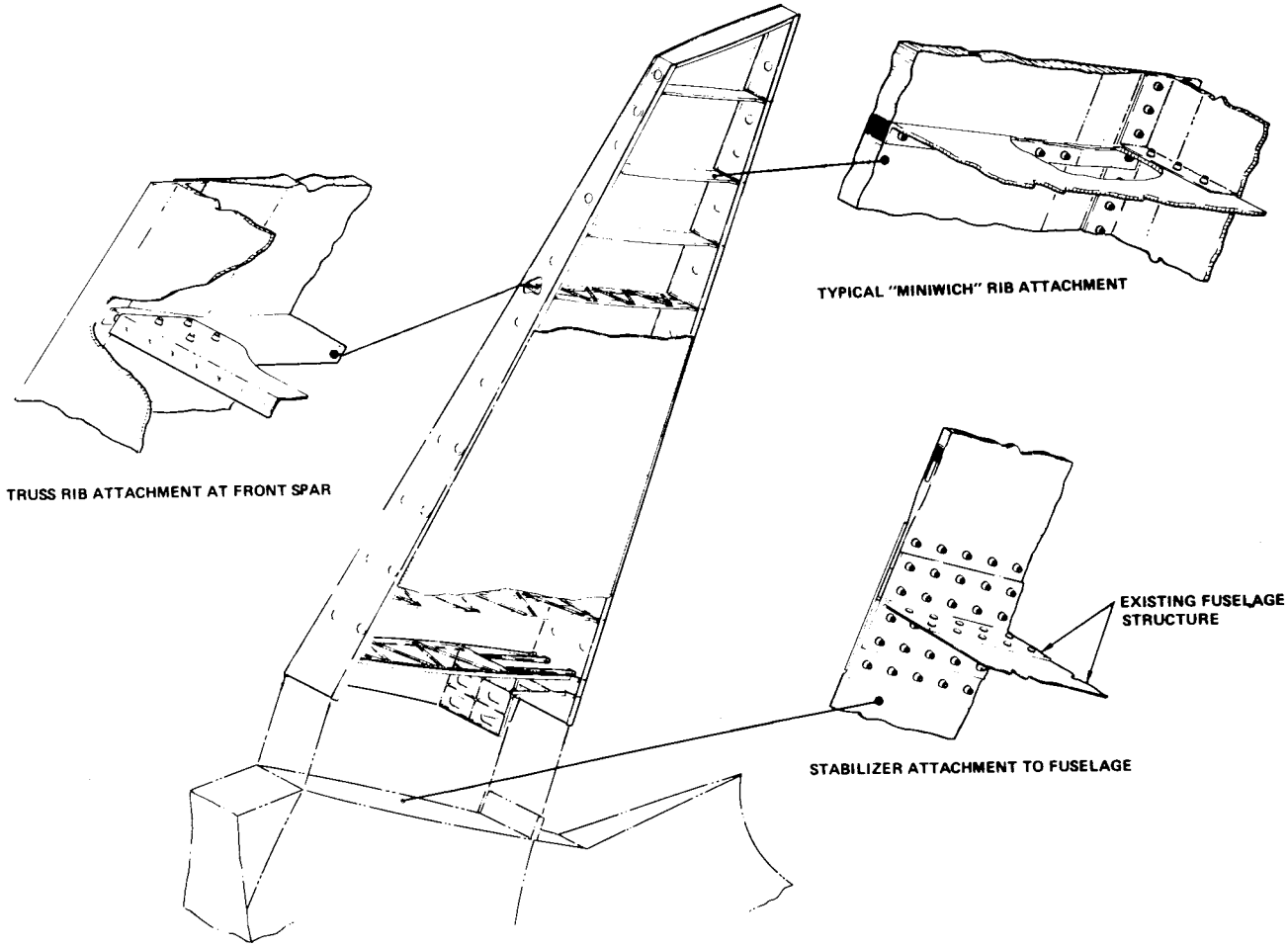

Figure 8. Honeycomb Cover Concept

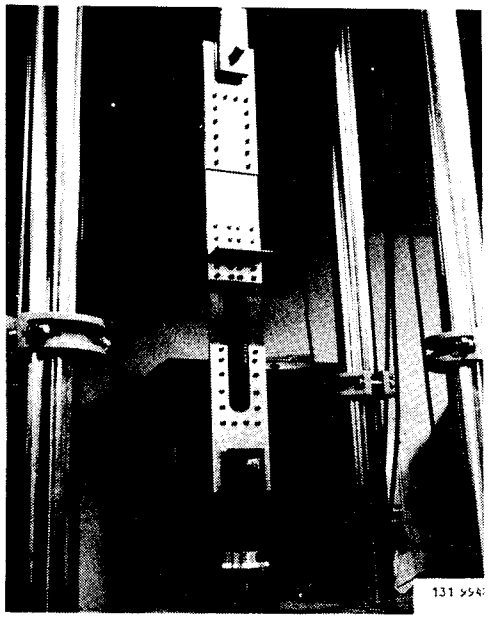

'I' STIFFENED COVER/FUSELAGE
JOINT SPECIMEN
(250°F CURE & 350°F CURE
SPECIMENS)

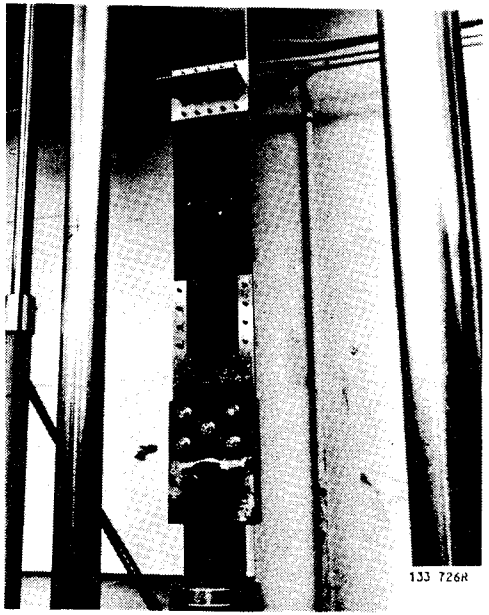

HAT STIFFENED COVER/FUSELAGE
JOINT SPECIMEN
(350°F CURE SPECIMEN)

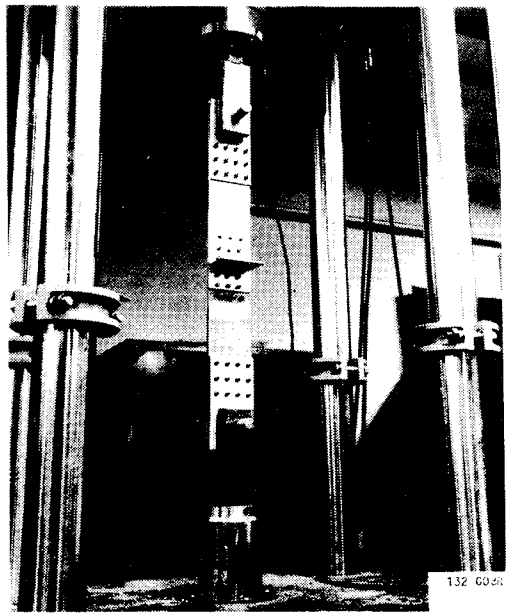

SANDWICH COVER/FUSELAGE
JOINT SPECIMEN
(250°F CURE & 350°F CURE
SPECIMENS)

TEST SPECIMEN	DESIGN LOAD-LB	SUSTAINED LOAD-LB
HAT STIFFENED COVER/FUS 350°F CURE	22,800	32,400
'I' STIFFENED COVER/FUS 250°F CURE	18,000	27,000
'I' STIFFENED COVER/FUS 350°F CURE	18,000	31,300
SANDWICH COVER/FUS 250°F CURE	18,000	25,600
SANDWICH COVER/FUS 350°F CURE	18,000	26,800

Figure 9. Fin Cover/Fuselage Joint Concept Tests

COMPONENT	HAT STIFFENED COVER DESIGN						
	STIFFENED COVER DESIGN LBS	Gr/Ep AND K/Ep	FIBER-GLASS CORE	ADHESIVE	FOAM	TOTAL COMPOSITE	NON COMPOSITE
COVERS	321.0	314.0	—	7.0	—	321.0	—
FRONT SPAR	60.4	54.4	2.0	3.0	~1.0	60.4	—
REAR SPAR	53.8	47.3	1.5	4.0	~1.0	53.8	—
ACTUATOR RIBS							
VSS 90.1	9.0	4.9	—	—	—	4.9	4.1
VSS 97.1	21.0	11.1	—	—	—	11.1	9.9
HINGE RIBS							
UPPER CLOSURE RIB	7.6	—	—	—	—	—	7.6
VSS 145.7	11.9	7.8	—	—	—	7.8	4.1
VSS 197.1	8.9	5.9	—	—	—	5.9	3.0
VSS 248.5	6.3	4.1	—	—	—	4.1	2.2
VSS 299.9	4.2	3.2	0.3	0.5	0.2	4.2	—
INTERMEDIATE RIBS							
VSS 121.9	14.0	9.1	—	—	—	9.1	4.9
VSS 172.0	10.3	6.7	—	—	—	6.7	3.6
VSS 223.3	7.5	4.9	—	—	—	4.9	2.6
VSS 274.2	5.2	3.5	0.4	0.7	0.6	5.2	—
VSS 334.2	3.0	2.0	0.2	0.4	0.4	3.0	—
LIGHTNING PROTECTION	12.0	—	—	—	—	—	12.0
STAB. ASSY HARDWARE	21.2	—	—	—	—	—	21.2
RIB AND SPAR FITTINGS (ALUM)	18.1	—	—	—	—	—	18.1
AUXIL SPAR	6.6	—	—	—	—	—	6.6
PROTECTIVE FINISH	9.6	—	—	—	—	—	9.6
DESIGN GROWTH ALLOWANCE	29.0	29.0	—	—	—	29.0	—
TOTALS	640.6	507.9	4.4	15.6	3.2	531.1	109.5
PERCENT OF TOTAL WEIGHT		79.2%				82.9%	17.1%
		CONSIST OF: 54% – 349 LB OF Gr 25% – 158 LB OF K 507 LB					

Figure 10. Weight Breakdown of Material Utilization

COMPONENT	SANDWICH COVER DESIGN						
	SANDWICH COVER DESIGN LBS	Gr/Ep AND K/Ep	FIBER-GLASS CORE	ADHESIVE	FOAM	TOTAL COMPOSITE	NON COMPOSITE
COVERS	371.0	227.0	76.0	32.0	36.0	371.0	—
FRONT SPAR	60.4	54.4	2.0	3.0	~1.0	60.4	—
REAR SPAR	53.8	47.3	1.5	4.0	~1.0	53.8	—
ACTUATOR RIBS							
VSS 90.1	9.0	4.9	—	—	—	4.9	4.1
VSS 97.1	21.0	11.1	—	—	—	11.1	9.9
HINGE RIBS							
UPPER CLOSURE RIB	7.6	—	—	—	—	—	7.6
VSS 145.7	10.2	6.6	—	—	—	6.6	3.6
VSS 197.1	7.7	5.0	—	—	—	5.0	2.7
VSS 248.5	5.4	3.5	—	—	—	3.5	1.9
VSS 299.9	3.6	2.6	0.3	0.5	0.2	3.6	—
INTERMEDIATE RIBS							
VSS 121.9	12.1	7.8	—	—	—	7.8	4.3
VSS 172.0	8.9	5.8	—	—	—	5.8	3.1
VSS 223.3	6.4	4.2	—	—	—	4.2	2.2
VSS 274.2	4.5	2.8	0.4	0.7	0.6	4.5	—
VSS 334.2	2.5	1.5	0.2	0.4	0.4	2.5	—
LIGHTNING PROTECTION	12.0	—	—	—	—	—	12.0
STAB. ASSY HARDWARE	21.2	—	—	—	—	—	21.2
RIB AND SPAR FITTINGS (ALUM)	18.1	—	—	—	—	—	18.1
AUXIL SPAR	6.6	—	—	—	—	—	6.6
PROTECTIVE FINISH	9.6	—	—	—	—	—	9.6
DESIGN GROWTH ALLOWANCE	30.9	30.9	—	—	—	30.9	—
TOTALS	682.5	415.4	80.4	40.6	39.2	575.6	106.9
PERCENT OF TOTAL WEIGHT		60.8%				84.3%	15.7%
		CONSIST OF: 49% – 335 LB OF Gr 12% – 80 LB OF K 415 LB					

Figure 11. Weight Breakdown of Material Utilization

	CURRENT METAL FIN	STIFFENED COVER DESIGN	SANDWICH COVER DESIGN
STABILIZER BOX WEIGHT	857.7 lbs.	640.6 lbs.	682.5 lbs.
WEIGHT SAVING	BASELINE	25.3%	20.4%
COMPOSITE UTILIZATION	–	82.9%	84.3%
PROJECTED COSTS CUM AVE @ 250	$62,909.	$53,139.	$53,828.
COST SAVING	BASELINE	15.5%	14.4%
PART COUNT:			
● ASSEMBLIES	23.	17. (74%)	17. (74%)
● PARTS	716.	231. (32%)	203. (28%)
● FASTENERS	40,871.	6,697. (16%)	5,647. (14%)

Figure 12. Comparisons to Metal Baseline

ITEM NO.	TESTS		TEST DESCRIPTION
	STATIC	FATIGUE	
(14) · (17)	✓	✓	MATERIAL VERIFICATION VARIOUS PLACES
(18)	✓	✓	SURF. SPAR ATTACH. SURF/RIB ATTACH.
(19)	–	✓	SPAR CAP JOINT
(20)	✓	–	SPAR BENDING RIB BENDING
(21)	✓	–	SPAR WEB SHEAR RIB WEB SHEAR
(22)	✓	–	SPAR WEB COMPRESSION RIB WEB COMPRESSION
(23)	✓	✓	FRONT SPAR JOINT
(24)	✓	–	RUDDER HINGE SUPPORT ACTUATOR/HINGE SUPPORT
(25)	✓	✓	SURFACE/FUSELAGE ATTACHMENT
(26)	✓	✓	STIFFENER RUNOUT
(27)	✓	–	SURFACE PANEL COMPRESSION
(28)	–	✓	SURFACE PANEL DAMAGE TOLERANCE
(29)	✓	–	FLAW EFFECT
(30)	✓	–	BOX BEAM

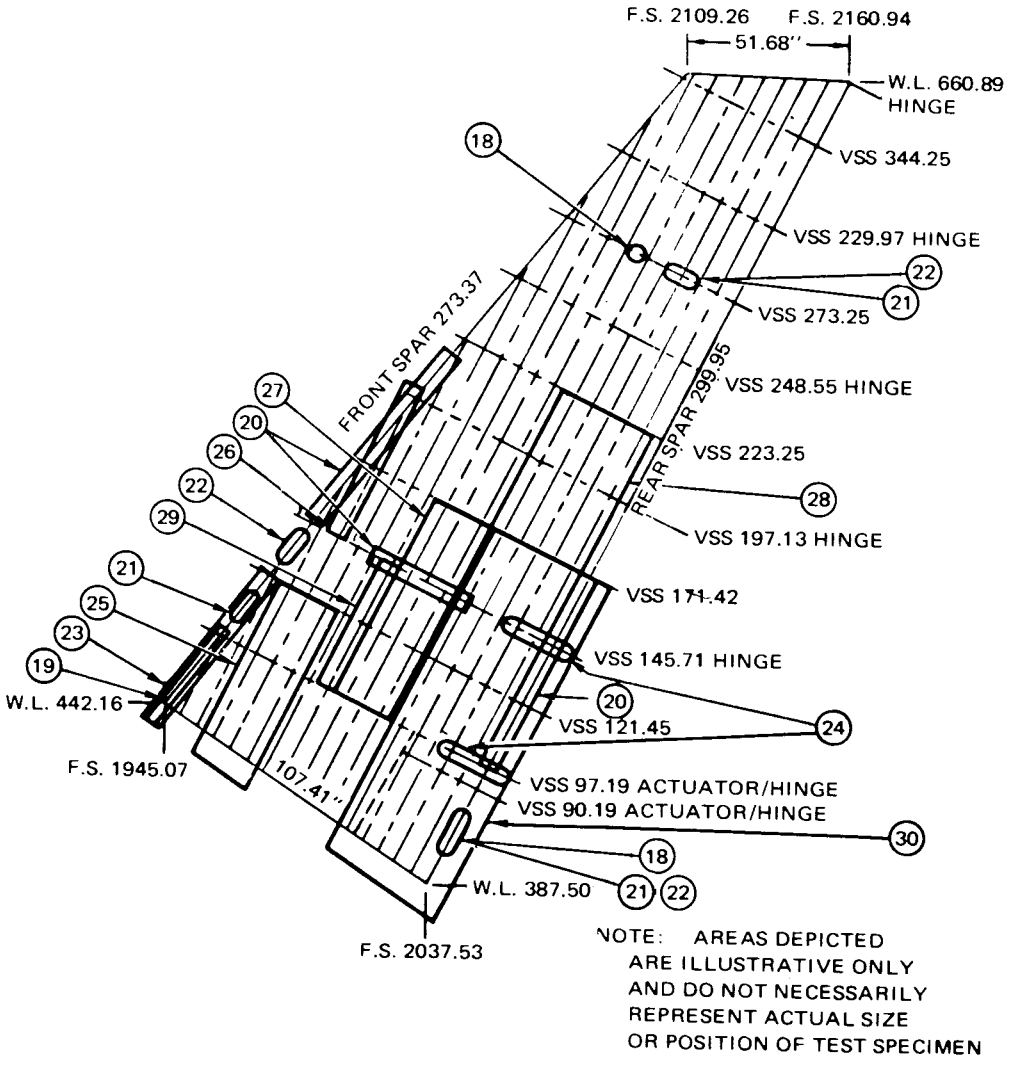

Figure 13. Ancillary Test Coverage

TEST SEQUENCE

- 5 INFLUENCE COEFFICIENT TESTS
- 2 LIFETIME FATIGUE TESTS*
- 2 ULTIMATE LOAD STATIC TESTS
- 3 DAMAGE TOLERANCE FAIL SAFE TESTS
- REPAIR DAMAGED AREAS
- ULTIMATE STRENGTH TESTS

*INSPECTION PER PLANNED IN SERVICE INSPECTION PROCEDURES

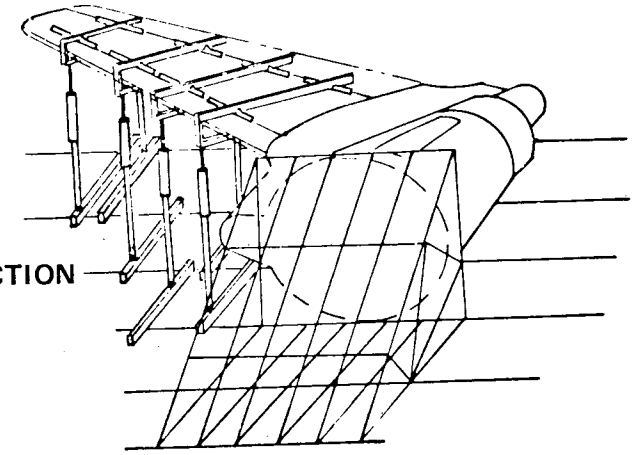

INSTRUMENTATION

- 275 STRAIN GAGES
- 11 DEFLECTION GAGES
- 14 LOAD CELLS

TEST ARRANGEMENT

- STABILIZER MOUNTED ON L-1011 FUSELAGE AFTERBODY SECTION
- LOADS APPLIED THROUGH COMPRESSION PADS ON FRONT AND REAR BEAM AND THROUGH RUDDER SUPPORT FITTINGS
- 14 CHANNEL SERVO CLOSED LOOP LOADING AND CONTROL SYSTEM

POST TEST INSPECTION

- NDI TECHNIQUES
- FAILURE ANALYSIS
- CUT SELECTED SECTIONS INTO MATERIAL SPECIMENS
- CHK FIBER AND RESIN CONTENT
- CONDUCT MICRO ANALYSIS
- CHK MECH. PROPERTIES

Figure 14. Ground Tests

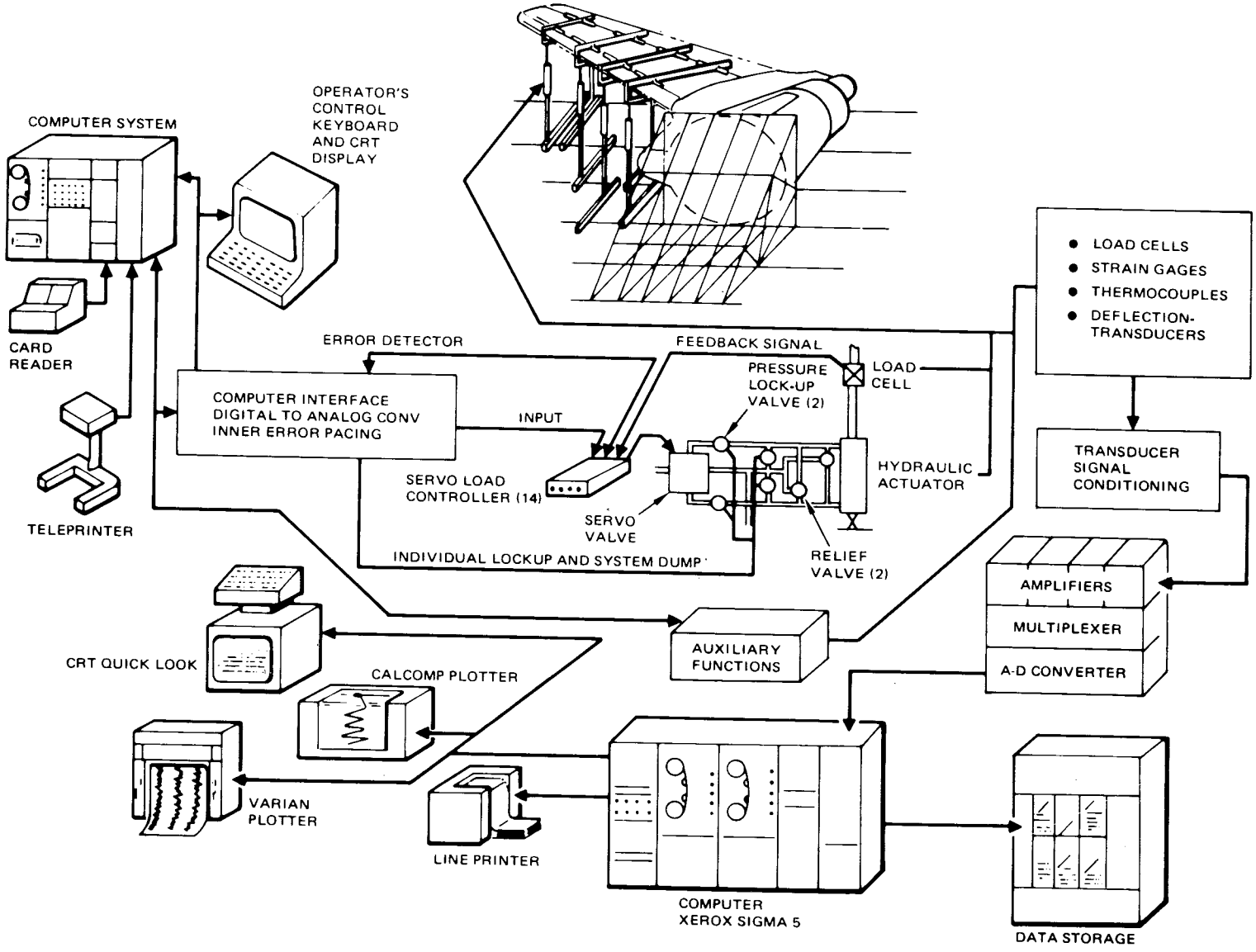

Figure 15. Schematic of Loading Control System

THE REALIZATION OF COST AND WEIGHT SAVINGS BY THE APPLICATION OF ADVANCED COMPOSITES TO THE B-1 VERTICAL STABILIZER

By D. E. Parker and W. L. O'Brien, Rockwell International,
and W. R. Johnston, Air Force Flight Dynamics Laboratory/FBB

SUMMARY

A solid technology base in advanced composite structures has been established which confirms that these materials can offer significant cost and weight savings to primary and secondary structures to which they are intelligently applied. The B-1 vertical stabilizer was one of several B-1 components selected by the Air Force Laboratories to provide a design option to the B-1 by using advanced composite materials.

INTRODUCTION

The development of boron and graphite fibers provided the potential for new aerospace materials having greatly improved properties. Past achievements in the metallurgical sciences resulted in new alloys which had combinations of lower weight and increased strength, or lower weight and increased modulus. These new alloys, although providing the designer with improved capabilities for certain requirements, often had other properties which reduced the scope of their apparent improvement. However, the new fibers indeed combined both high strength with high modulus providing the potential for stronger, lighter, stiffer materials, but the fibrous nature of these materials created the problem of application. This was solved by combining those fibers with matrix materials so that the resulting material may be reasonably formed to the required structural configuration with a minimum of large capital investment; then the material was processed (cured) to provide the required properties. The result we now call "advanced composites." These new materials also gave the designer a new parameter for design, that of actually designing the material to provide the strength and stiffness required by the design, thereby reducing the total weight. The matrix materials used have been primarily the epoxies, although there have been developments in both metal matrix and polyimides to extend the thermal properties over those of the epoxies.

Concurrent with the development of these materials has been the application of these materials to actual structure. The Air Force has conducted a series of advanced composite structural programs resulting in structural components of ever-increasing complexity. Most of the development programs have

been eminently successful. Some of the programs also resulted in hardware which was put into service to develop some level of flight experience. For the most part, that flight experience has resulted in positive results comparable to the baseline metal parts. Indeed, the developmental experience of the advanced composites has been positive enough to provide the basis for the production decision to use boron/epoxy for the torque box covers in the empennage of both the F-14 and F-15 systems.

This total experience provided the impetus for higher Headquarter's direction to the Air Force Laboratories to implement an advanced development program whose goals were the application of the advanced composite to an emerging weapon system, specifically the B-1. Response from the laboratories resulted in approval for development of both the horizontal and vertical stabilizers and some selected secondary structures (specifically a slat, flap, and avionics bay door) utilizing the advanced composites. These developments, by direction, are to result in fully interchangeable hardware providing the form, fit, and function of the baseline metal hardware. The design goal of this hardware is to be both lighter in weight and lower in cost than its metal counterparts.

The remainder of this paper reviews the effort directed toward the development of a low-cost, lightweight advanced composite vertical stabilizer for the possible application to the B-1 weapon system. This program received go-ahead in mid-October 1974, with the schedule for major milestones and task activity shown in figure 1. The objectives of the program are the design, development, and verification of an advanced composite vertical stabilizer torque box which reduces both weight and cost while meeting B-1 structural performance requirements (figure 2).

DEVELOPMENT OF A LOW-COST ADVANCED COMPOSITE VERTICAL STABILIZER FOR THE B-1 WEAPON SYSTEM

SCOPE

Selection of the B-1 vertical stabilizer as a candidate for redesign utilizing advanced composite material reflects advantages which extend beyond its value to the present B-1 weapon system in terms of cost and weight savings.

The vertical stabilizer design requires design solutions for interface problems with every type of system except the problems which would be associated with integral fuel. Figure 3 indicates that the number and type of interface requirements is very similar to what might be expected in a wing

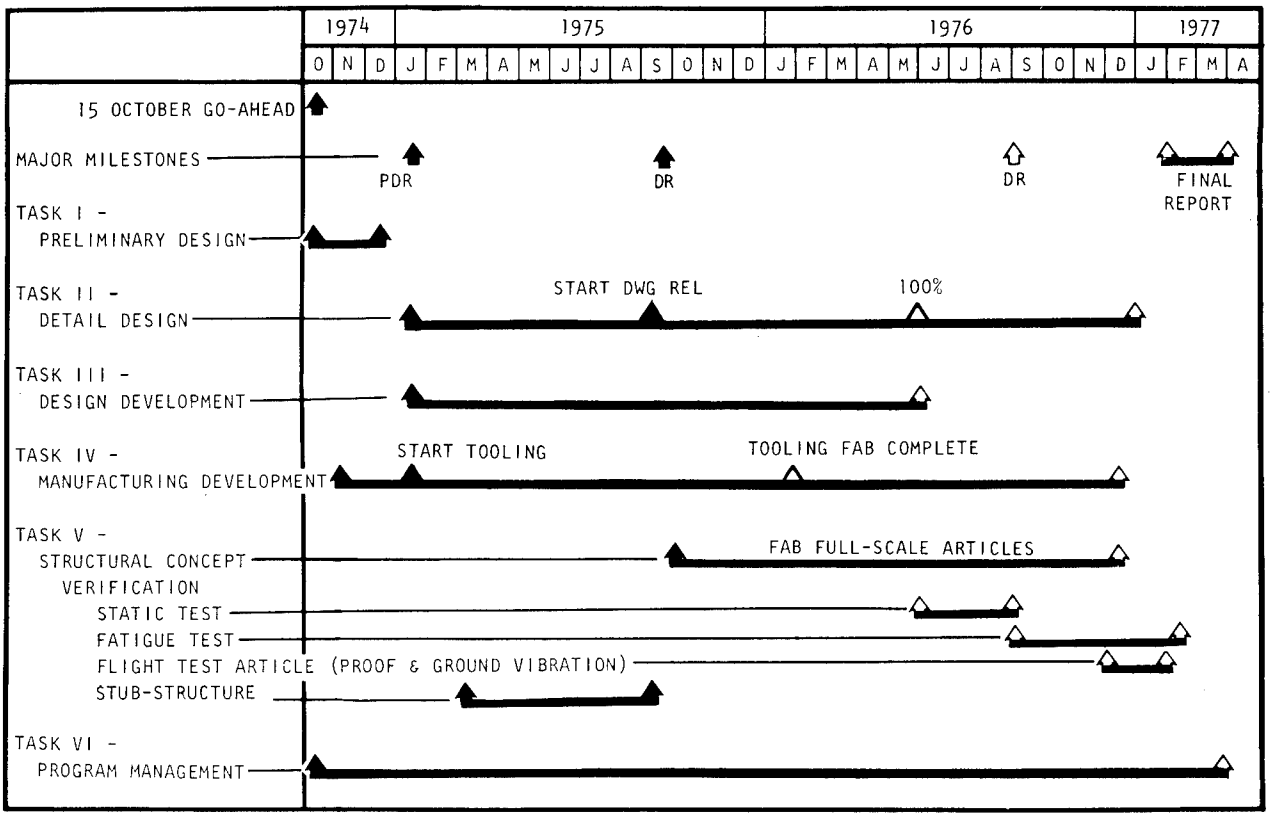

Figure 1.- Program schedule.

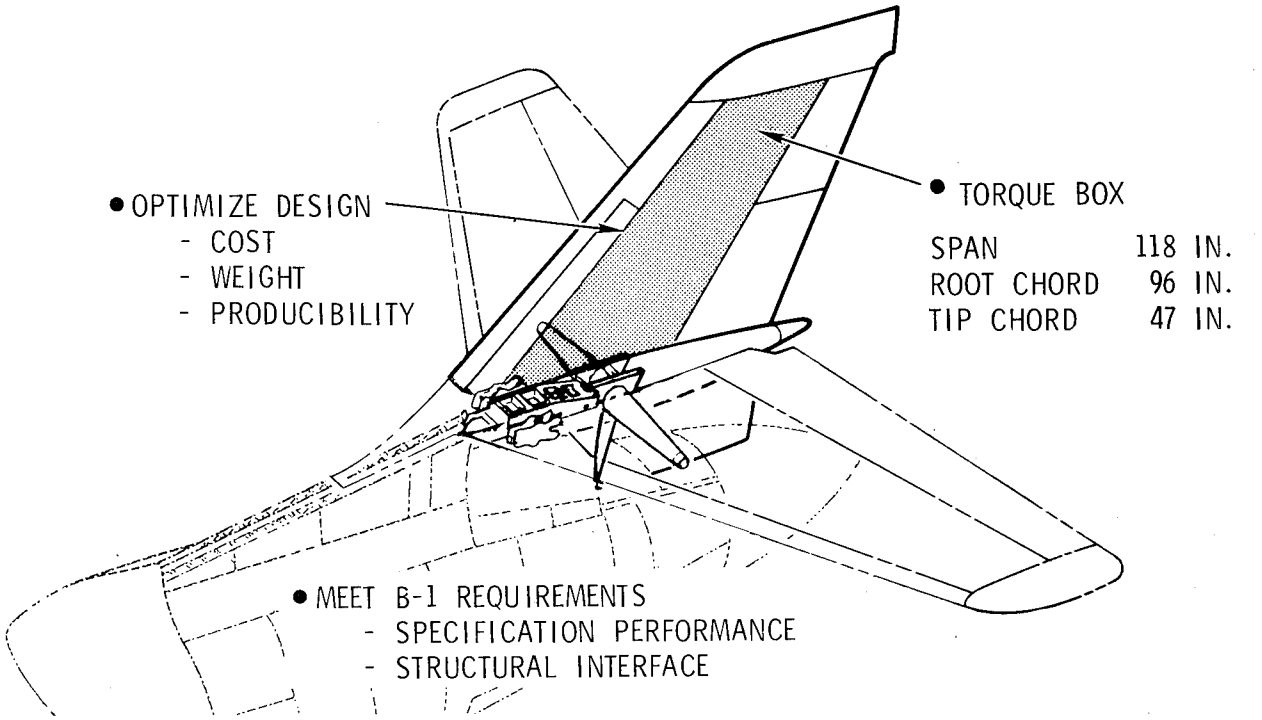

Figure 2.- Program objectives.

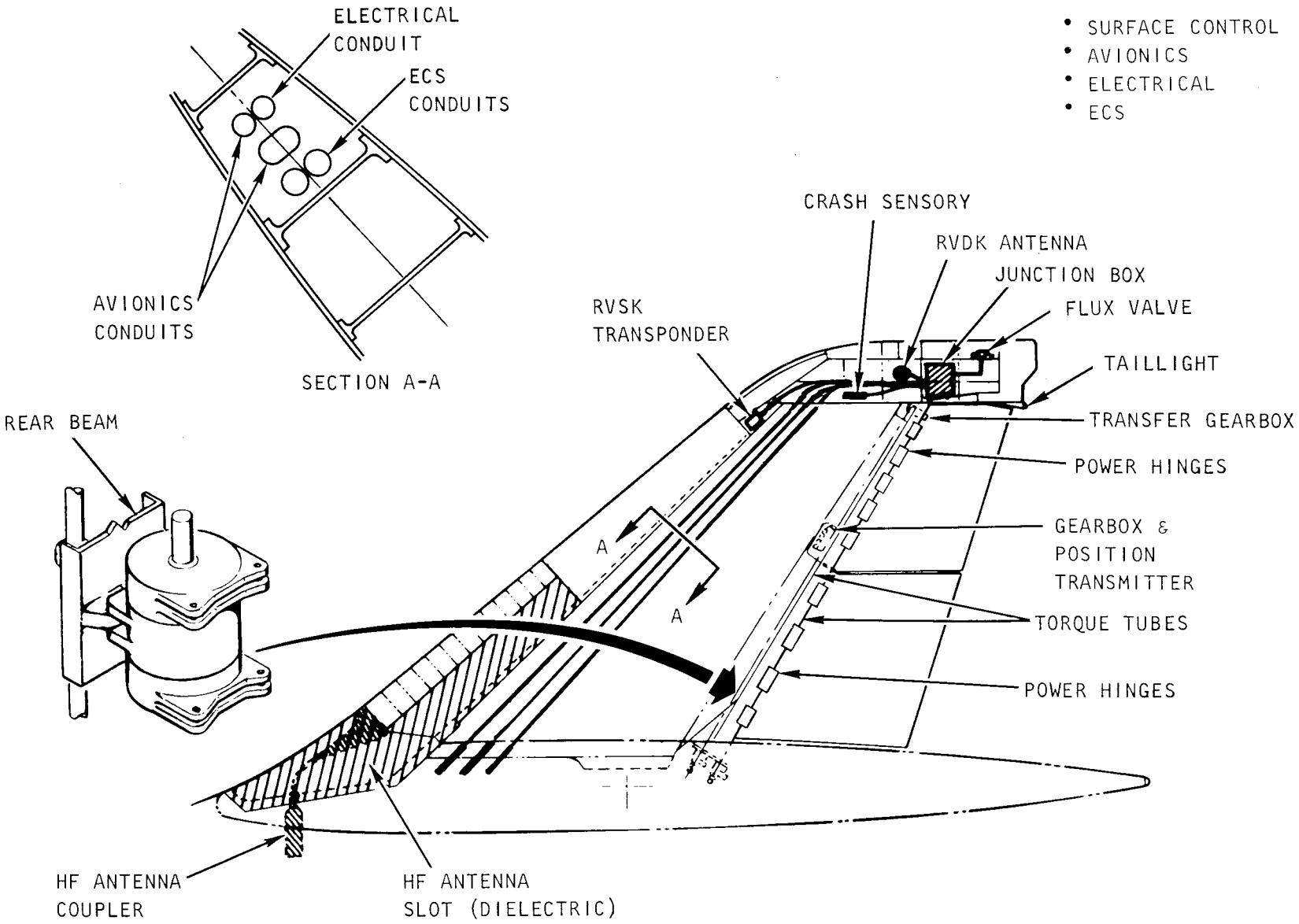

Figure 3.- System integration considerations.

design, particularly a low-aspect-ratio fighter-type wing. The experience gained through the flight testing of this surface transcends its immediate value to the B-1 program.

The vertical stabilizer consists of four major elements: the main torque box, the leading edge, the tip, and the upper two rudder segments (figure 4). The main box is being redesigned using advanced composite materials to provide both cost and weight savings of approximately 20 percent when compared to its metal counterpart. The existing leading edge, tip, and rudder components will be utilized with only minor revisions. The advanced composite torque box will retain, as closely as possible, the identical form, fit, and function of its metal counterpart. It is primarily designed by the stiffness requirements for flutter and aeroelastic stability and control (torsional stiffness GJ and bending stiffness EI). However, strength requirements, both static and fracture, govern the area near the root splice as well as at fastener and joint locations (figure 5). Interface requirements governing both hard point locations and loading distribution must be met in the areas where the torque box attaches to the fuselage, horizontal stabilizer actuator fairing, and rudders, as indicated in figure 6.

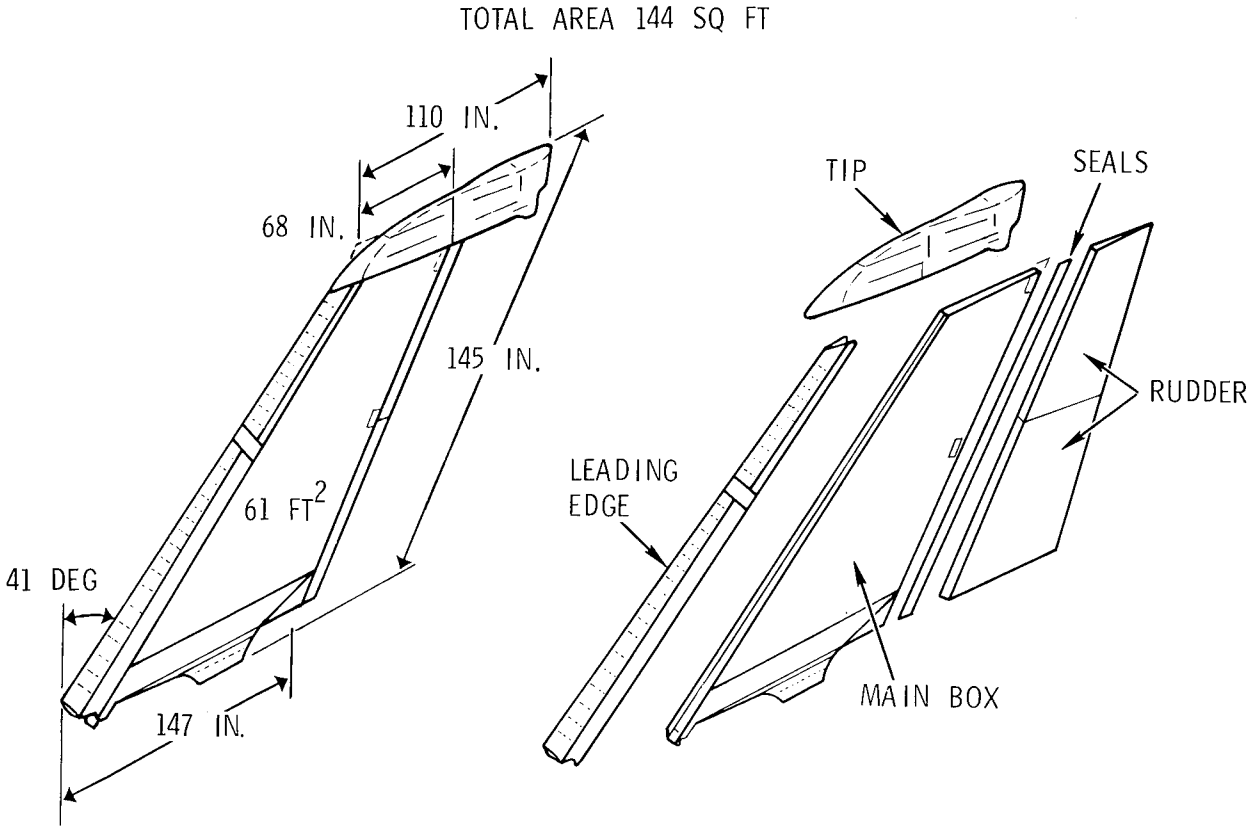

Figure 4.- Major components.

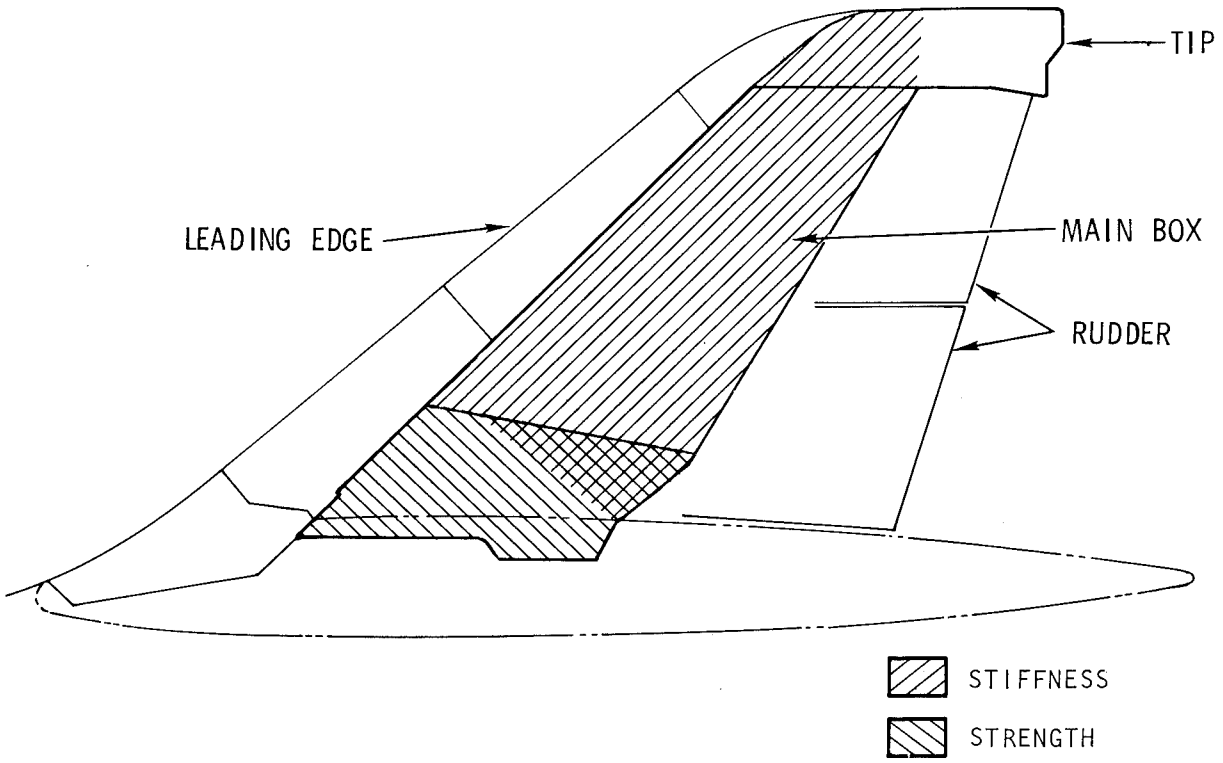

Figure 5.- Structural design criteria.

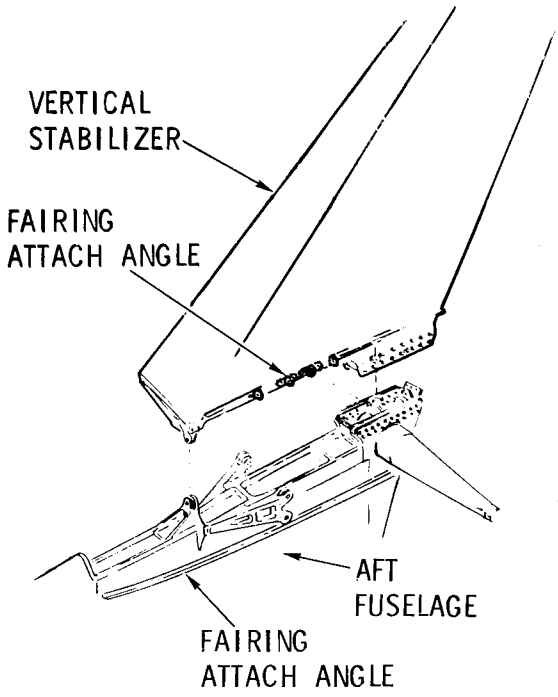

Figure 6.- Structural interface.

Metal Baseline Configuration

Figure 7 shows the current metal torque box consisting of aluminum machined covers supported by a conventional substructure. The substructure consists of a forged aluminum machined rear spar (or beam), a machined aluminum root rib (also a forging), a machined aluminum front spar, and machined or sheet metal intermediate and tip ribs. The intermediate spars are fabricated by welding the separately machined caps to the sine wave web as shown in figure 8. To minimize tooling costs and simplify the fabrication procedures, the spars were placed on element lines which then provided straight-line tapers and minimized the cap twist or swarf.

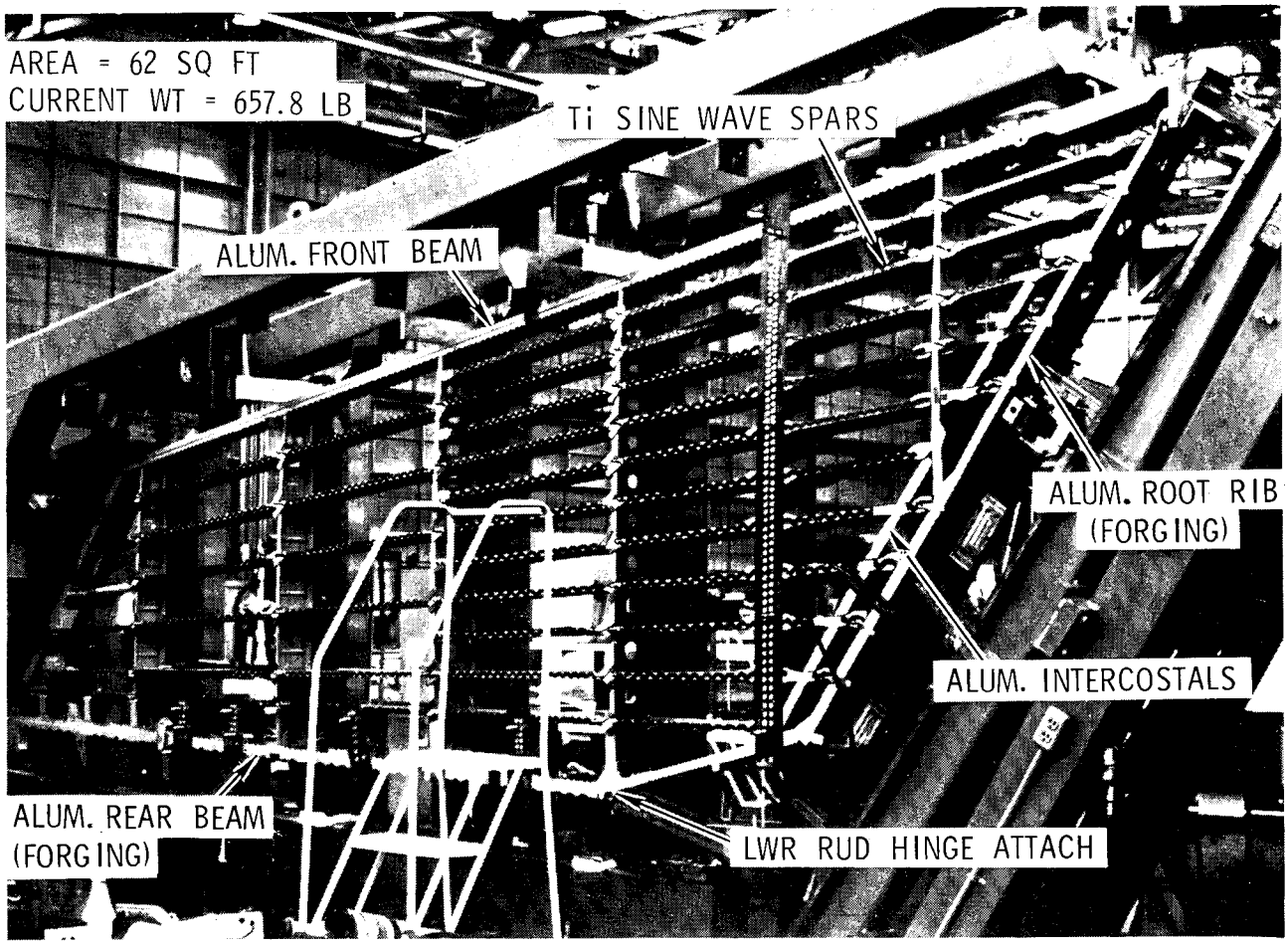

Figure 7.- B-1 metal vertical stabilizer main box.

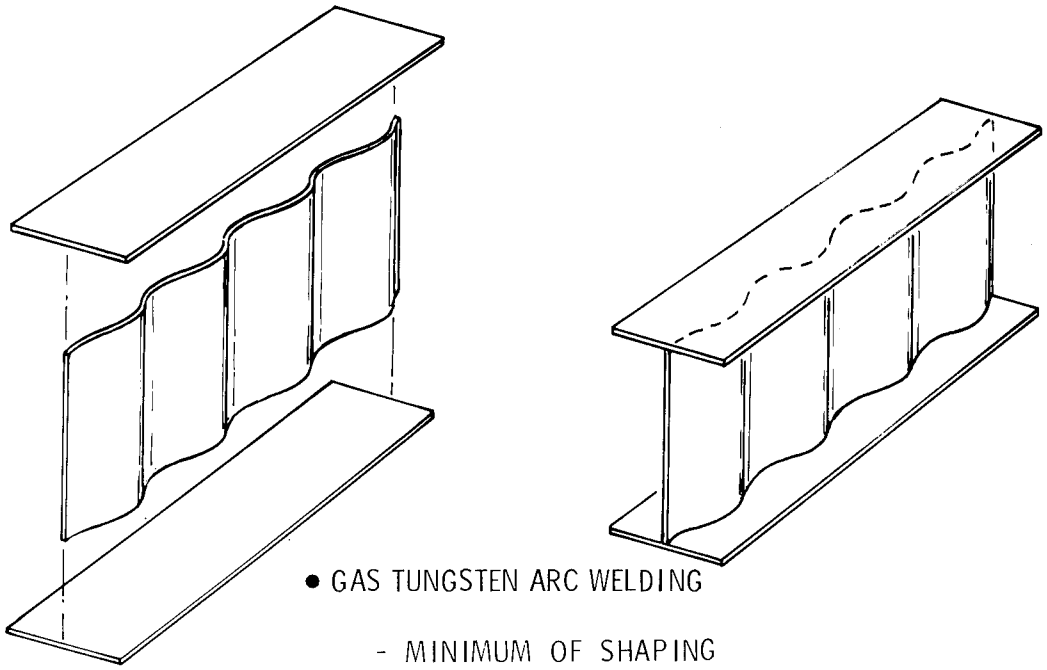

Figure 8. - Metal spar fabrication.

Composite Torque Box Design

Substructure. During the preliminary design task, various trade studies were conducted to optimize the cost and weight savings by comparing various elements fabricated from metal and advanced composites. The metal rear spar was retained since the machined aluminum design provided the most cost-effective approach when compared to two configurations of advanced composite spars being considered. One was a continuous spar with machined aluminum fittings; the other was an intermittent composite spar utilizing aluminum interconnect fittings. Figure 9 provides a comparison of the three concepts.

The sine wave configuration for the intermediate spars was retained because of its characteristic of high strength-to-weight ratio. Here we are able to take advantage of one of the more significant features of advanced composite material. As indicated in figure 10, a sine wave part is laid up in four segments or subassemblies, a right- and a left-hand web and two caps. Since these parts are formed from uncured material, forming to varying swarf angles or varying web heights poses no significant fabrication problem. Autoclave curing after forming provides a net molded part to final dimensions requiring a minimum of cleanup or preparation for final assembly.

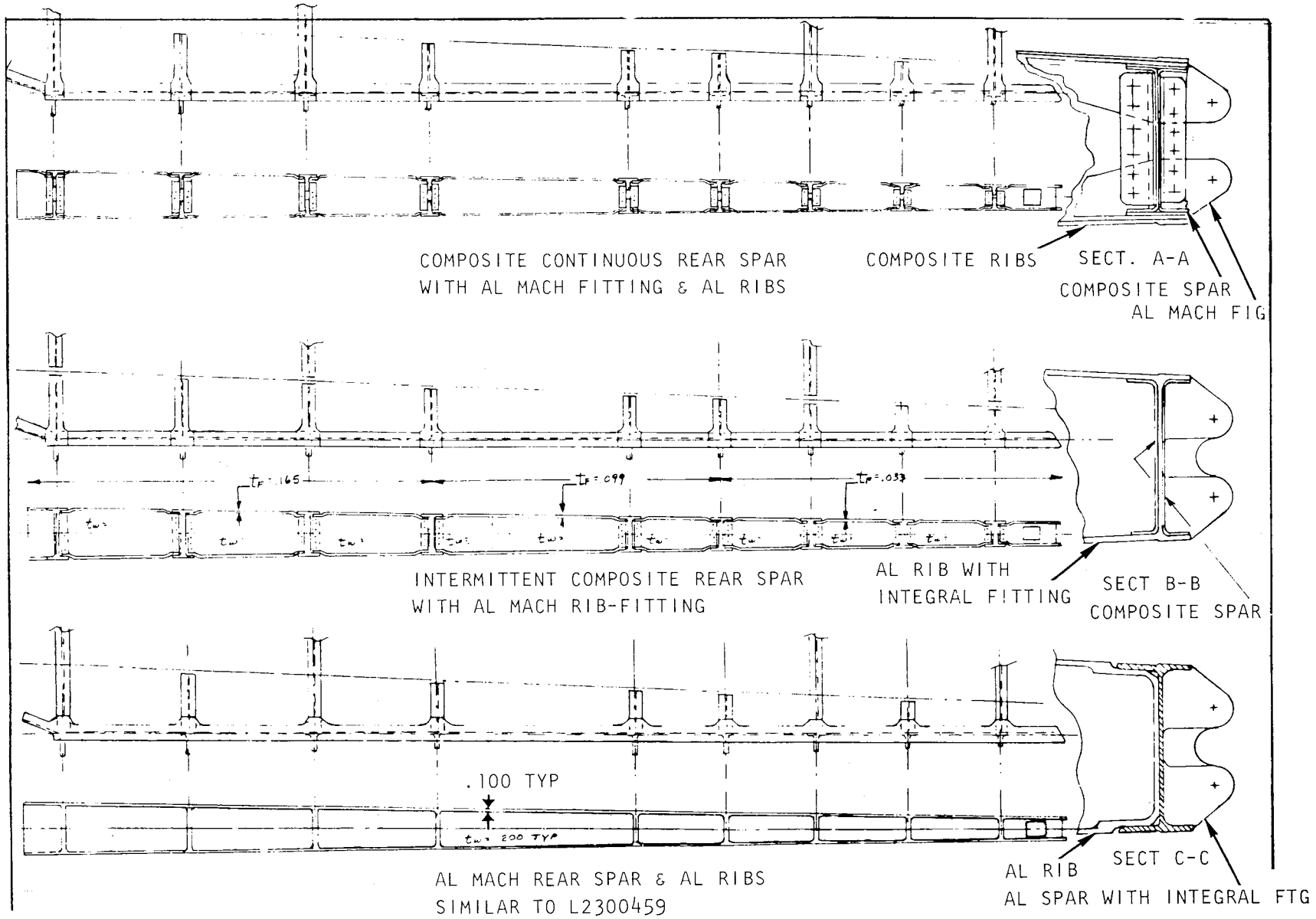

Figure 9.- Preliminary design trade study - rear spar and power hinge backup ribs.

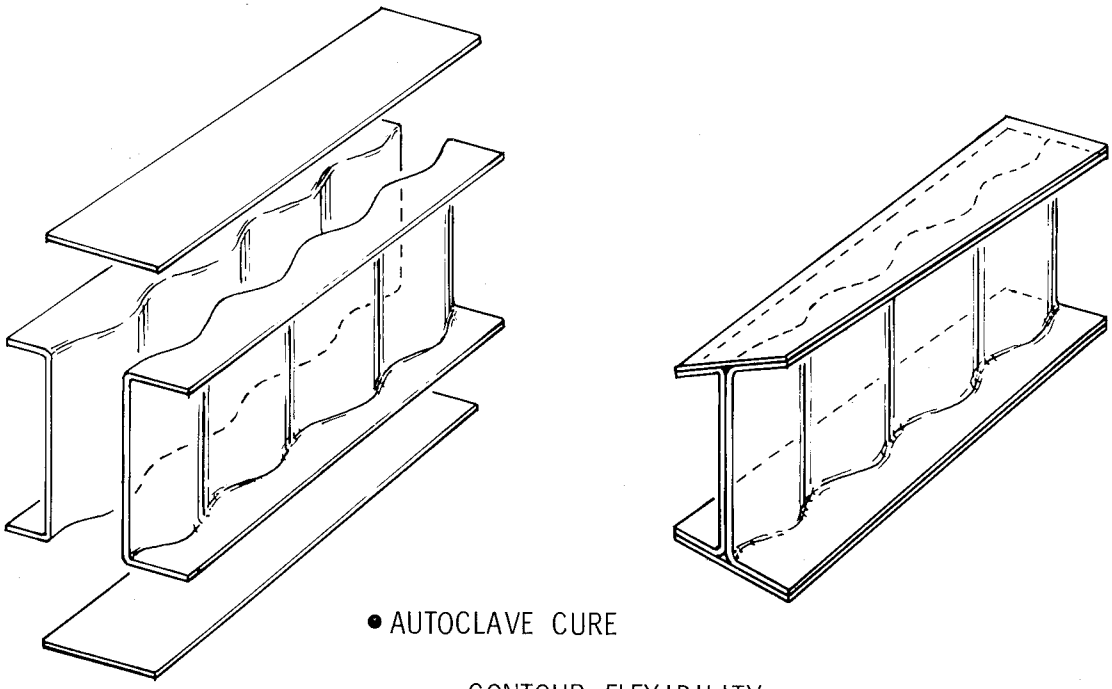

Figure 10. - Composite spar layup.

This flexibility of fabricating the sine wave spars from advanced composite material provides the capability of optimizing the substructure configuration to one of parallel spars. The most important advantage of the parallel spar arrangement is that the covers can now be more easily tailored to provide optimum load introduction into the root area and to meet the stiffness requirements of both flutter and aeroelasticity. Another advantage of the parallel spar configuration is the reduction in the lineal inches of spar required to support the cover.

This reduction of intermediate spars combined with elimination of a number of chordwise ribs has provided an overall simplification of the torque box which can be best expressed by the parts count summary listed in table I.

TABLE I.- PART COUNT

	Metal	Composite
Part count	80	59
Total length (in.)	2,271	1,824
Joints	150	118

A comparison of the two substructures is provided in figure 11.

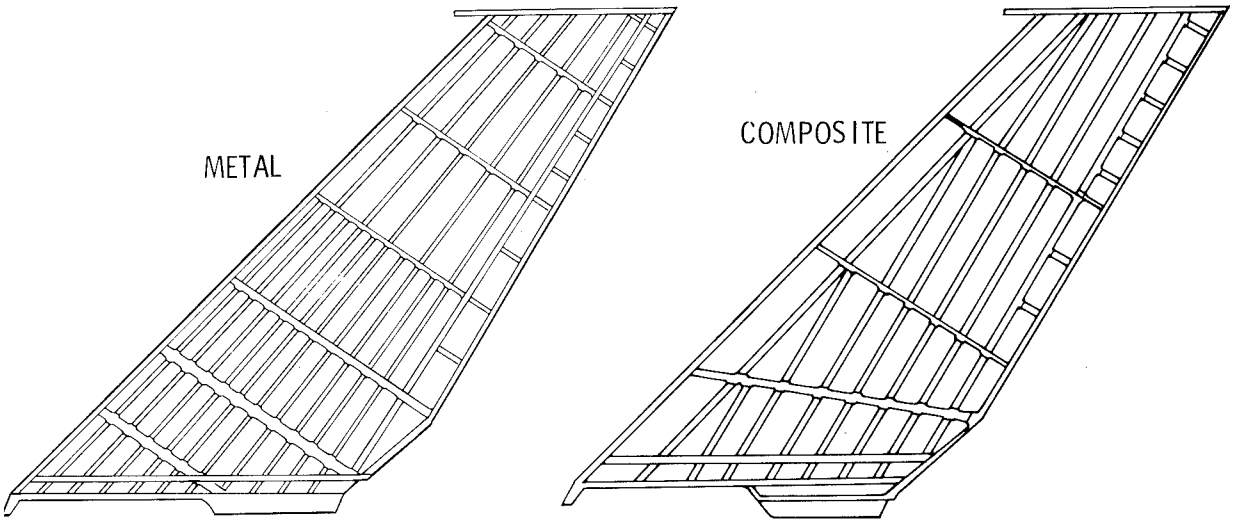

Figure 11. - Substructure comparison.

Cover. - During preliminary analysis, it was found that tailoring of the advanced composite covers could be accomplished in a manner that maintained the torsional stiffness (GJ) which primarily influences flutter stability, while reducing the bending stiffness (EI) to near strength requirements, and still meet the overall flutter speed margin. A comparison of the metal versus composite stiffness characteristics is given in figure 12. Because EI has been reduced while maintaining GJ, a weight savings of 24 pounds has been realized over a design which maintained the metal EI or GJ values.

One of the major trade studies performed during the early design phase was directed toward resolving the vertical stabilizer to the fuselage attachment. The bending moment tie between the metal vertical stabilizer and fuselage is achieved by bolting the monolithic aluminum alloy cover of the torque box to a steel fuselage fitting as shown in figure 6. The advanced composite is required to meet the same form, fit, and function requirements of its metal counterpart. In addition, the design must maintain a similar bolt load distribution chordwise along the joint. It first appeared that bolting the composite cover directly to the steel fuselage fitting offered the lightest and the lowest cost design, but due to the relative high loads and insufficient

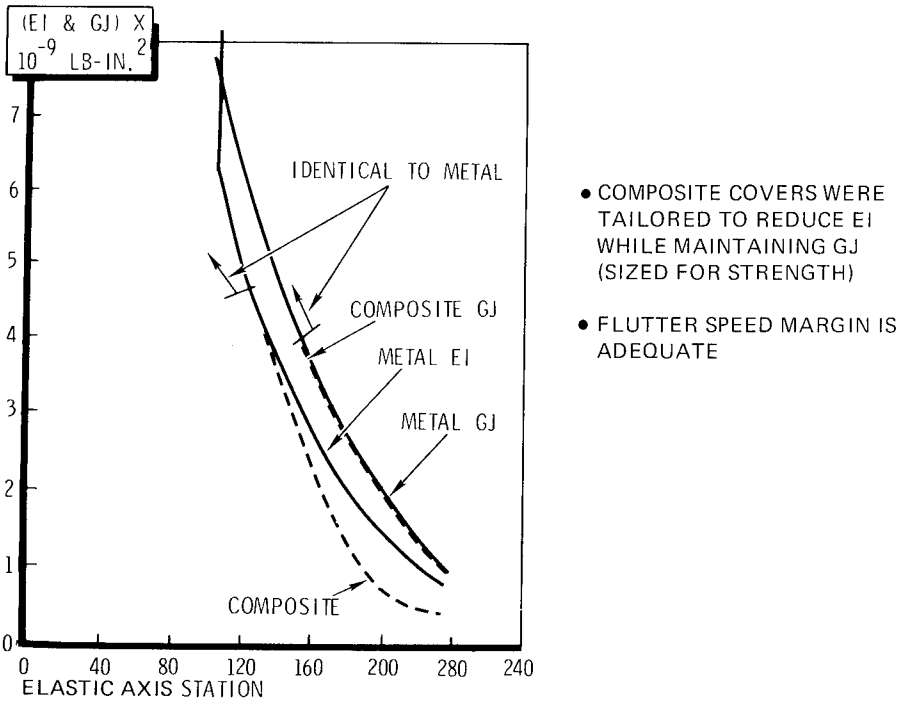

Figure 12.- Flutter considerations.

edge distance (2D) for shearout, alternate methods of attachment had to be considered. These studies included the following:

(1) Addition of titanium or steel shims to the laminate in the attachment area to increase the local properties of the composite

(2) Bonding the composite cover to an aluminum or titanium splice plate which would terminate as a blade

(3) Bolting the composite cover either through a single-shear or double-shear joint to an aluminum blade

The bonded type joints were discarded due to concern from the standpoint of reliability, inspectability, and fatigue, since very little historical data exist on bonded adhesive primary joints subject to relatively high load, extreme environmental conditions, and long usage.

The design finally selected was a single-shear bolted-on aluminum plate arrangement. Had a complete redesign of the vertical-to-fuselage attachment been permitted, an additional 20 to 25 pounds in weight savings could have been realized, indicating the application of advanced composite during the preliminary design phase can realize even greater weight savings.

The design which has evolved to date is shown in figure 13.

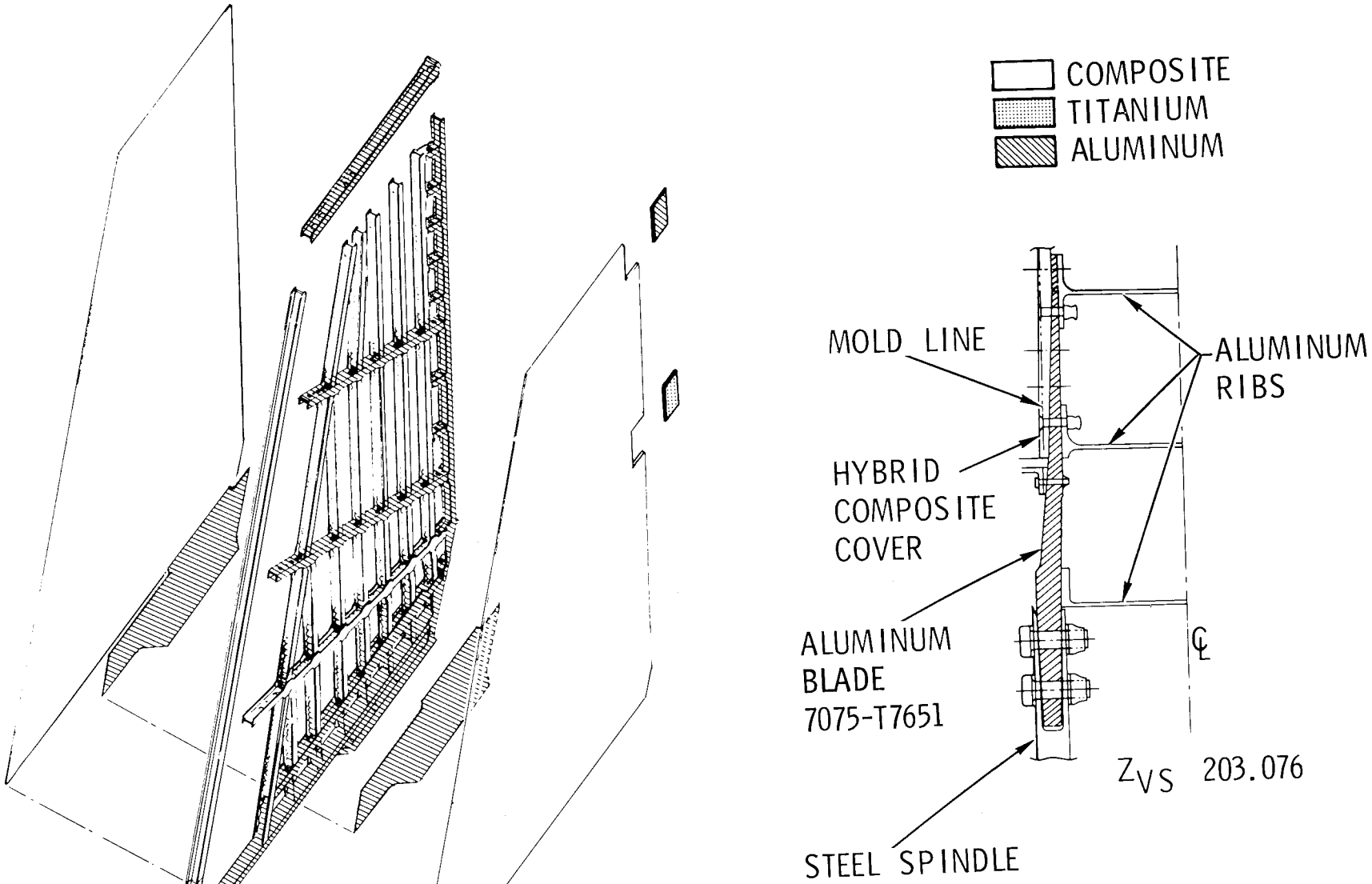

Figure 13.-Current configuration.

The design consists of parallel composite sine wave spars; a composite front spar with a machined aluminum fitting at the lower shear attach; machined aluminum root rib, kick rib, and tip rib; machined aluminum rear spar; and a combination of sheet metal upper intermediate ribs and an advanced composite sine wave canted rib. Trade studies are still under way to establish whether the upper intermediate ribs should be changed to an advanced composite material to further reduce weight. The covers consist of 48 plies of graphite/epoxy at the tip varying to 94 plies of graphite/epoxy and boron/epoxy in the blade transition area (boron/epoxy replaced the 0° graphite in the root area). The blade is machined of 7075 T7651 aluminum which is the same material used in the current metal cover. Table II provides a gross indication of the material mix in the torque box.

TABLE II. - MATERIAL DISTRIBUTION

Material	Percent of Torque Box Weight
Graphite/epoxy	56
Boron/epoxy	2
Metal	39
Miscellaneous	3

Weight and Cost Comparions. - Table III provides a comparison of the weight of the present metal stabilizer compared to the target weight saving for the advanced composite torque box.

TABLE III.– WEIGHT COMPARISON

Structure	Metal (lb)	Composite Target (lb)
Cover	413.8	312.0
Lightning strike protection		15.0
Front spar	30.6	24.0
Intermediate spars	54.8	40.0
Rear spar	26.3	25.0
Tip rib	4.0	4.0
Intermediate ribs	34.3	29.0
Root rib area	37.0	32.0
Fasteners and shim, etc	42.1	57.6*
Total torque box	657.5	538.6
Percent savings over metal		18.0

*Weight includes 14.6 pounds of avionics conduits.

Table IV indicates the projected cost savings over the metal vertical. It should be noted that the projected cost savings for the advanced composite torque box are based on production estimating techniques which have not been reviewed and accepted by the Air Force and are, therefore, only a preliminary estimate.

TABLE IV.– COST SAVINGS

Torque Box	Percent Savings Over Metal
Material dollars	17.9
Covers, fabrication	57.1 (increase)
Substructure, fabrication	26.2
Assembly	22.6
Subtotal	17.4
Leading edge, tip	Same
Tooling & engineering sustaining	Same
Total	12.9

Development Testing.– To provide early verification of the design concepts, a large subcomponent test structure has been designed, fabricated, and tested. The specimen (figures 14 and 15) is approximately 72 inches long, 18 inches wide, and 10 inches deep. The primary test objective was to verify the design of the root splice between the composite cover and the aluminum blade.

The test was highly successful, with failure occurring at 104 percent of the predicted value.

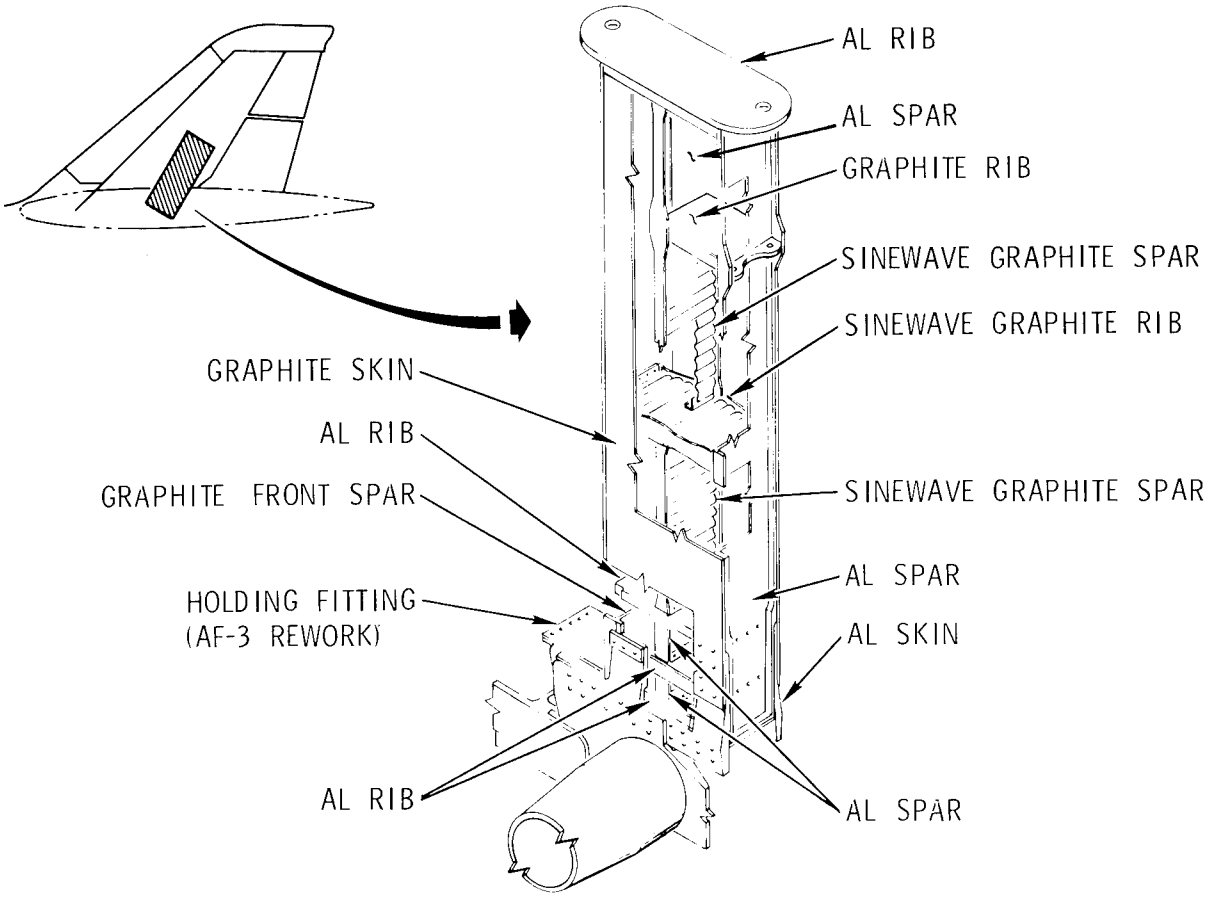

Figure 14.- Stub structure test specimen.

Figure 15.- Stub structure test setup.

CONCLUDING REMARKS

The design and testing activity to date has indicated that significant weight and cost savings can be realized by the proper application of advanced composite materials to primary aircraft structure. It is further evident that optimization techniques must recognize the structural properties of all materials (both conventional and advanced composite) to arrive at the optimum blend of materials to accomplish the task at hand. In addition, greater weight savings are potentially possible by the application of advanced composite technology during the preliminary design phase.

DESIGN, FABRICATION AND TEST OF THE B-1 COMPOSITE HORIZONTAL STABILIZER

By Walter Ludwig, Herman Erbacher and Joseph Visconti

Grumman Aerospace Corporation

SUMMARY

Grumman Aerospace Corporation, under contract to the U.S.A.F. Flight Dynamics Laboratory, is developing a horizontal stabilizer for the B-1 bomber that makes extensive use of graphite and boron epoxy materials. The composite stabilizer is estimated to save 14% in weight for the total structure with 20% weight saving for the composite box over the existing metal configuration. Cost savings of 17% are indicated in production. The design makes use of graphite epoxy sine wave spars and ribs and a combination of graphite and boron epoxy material in the covers. Over 1,000 coupons and elements have been tested to provide design data and verification of specific design features. Detailed processing procedures and a manufacturing plan have been prepared to permit fabrication of 2 shipsets of stabilizers. Static and fatigue tests on full scale stabilizers will be conducted during the first half of 1976. A shipset of stabilizers will be fabricated and made available in October of 1976 for flight test.

INTRODUCTION

The U.S.A.F. Materials Laboratory initiated the program with Grumman in July of 1973. The objective was to demonstrate that weight savings, reduced costs, improved damage tolerance and vehicle performance improvements could be obtained by applying composite design concepts to the B-1 horizontal stabilizer. The program plan used to develop the stabilizer is shown in Figure 1. The plan provides for the detail design of the stabilizer and the supporting specimens; the fabrication and test of the specimens; the development of the required manufacturing processes; detailed cost tracking of the individual composite parts and assembly operations used in the stabilizers; and the fabrication and test of two shipsets of full scale stabilizers. The left and right hand stabilizers of the first shipset are used for static and fatigue testing respectively while the second shipset will be proof tested and made ready for flight. The program extends over 42 months and ends in December of 1976.

The composite design that was developed is shown in Figure 2. The stabilizer is approximately 240 square feet in area with a root chord of 17 feet and a length of 30 feet. It is approximately 14 inches deep at the root. The stabilizer pivots about a shaft that extends out from the fuselage and is actuated by two hydraulic cylinders. The torque box structure was simplified from the existing metal design by reducing the number of parts and eliminating specific high cost composite items such as bonded sandwich construction and bonded metal splice plates and inserts. Drilling through boron epoxy and titanium was minimized. The composite design retained the location of the front and rear spars and tip rib and as a result, the existing leading edge, trailing edge and tip assemblies from the metal stabilizer were used with only minor changes. These assemblies are full depth honeycomb bonded structures. The bearing support fitting is similar to the one used in the metal stabilizer and is made from the same titanium forgings. The composite stabilizer mounting, actuation and handling is identical to that of the metal stabilizer.

The principal composite component of the stabilizer is the torque box, shown in Figure 3. The box consists of spars, ribs, covers and the bearing support fitting. The entire assembly is mechanically fastened using conventional aircraft fasteners; titanium Hi-Loks for the substructure and lower cover attachment and A286 Jo-Bolts for the upper cover attachment. The covers, which are the largest composite parts in the assembly are composed of graphite and boron epoxy. The graphite epoxy layers of the cover form the basic laminate while the boron epoxy layers are added to provide longitudinal stiffness and to aid in transferring the load between the covers and the bearing support fitting. The boron epoxy layers are in strips over the intermediate spars and are spread through the laminate in the area of the bearing support fitting. A typical section through the cover in the area of the spars is shown in Figure 4. A graphite epoxy strip is incorporated at each spar location such that all attachments to the substructure are through the strips. This concept minimizes the drilling costs and avoids the structural penalty associated with drilling the boron epoxy layers. Approximately 90% of the cover attachment holes are through graphite. The covers vary in thickness from 92 plies at the root to 36 plies at the outboard area.

The substructure is composed of graphite epoxy sine wave spars and ribs and flat web front and rear spars. The ribs are continuous while the spars are intercostal. This structural arrangement was necessitated by the high acoustical environment that the stabilizer must withstand. Figure 5 shows the details of a typical spar-rib intersection. The design minimizes the amount of reinforcement and the number of parts required at the joint and avoids drilling the boron-epoxy layers in the cover.

In addition to the composite parts, the torque box substructure contains three aluminum fittings at the hoist points and the Ti6-4 alloy bearing support fitting.

DESIGN

The design criteria imposed on the program comes from two sources, namely: (1) the B-1 Systems Definition Manual which is supplied to Grumman by the Rockwell International Corporation and, (2) Grumman's in-house design criteria for advanced composite materials. The former document contains all the applicable detailed air vehicle specifications and appropriate military specifications for the horizontal stabilizer. The Grumman design criteria has been developed from our past experience in designing with composite materials. The criteria includes filamentary controlled composites, laminate stacking sequence, ply drop off and non buckling structure up to ultimate load.

Design allowables for the program were taken either from existing documents (Air Force Design Guide or AFML-TR-72-232) or generated through coupon test programs. Approximately 1,000 test specimens have been tested on the program to obtain design allowables. In general when insufficient data was available to calculate "B" basis allowables, the average test data was multiplied by .8 to obtain an "S" basis allowable.

Internal loads were obtained by using a finite element analysis including the anisotropic properties of the composite materials. The flexibilities of the 130 bolts attaching the bearing support fitting to the cover were included in the model. The prime driver of the design exclusive of the pivot region was aeroelastic consideration. Several flutter analyses were conducted in conjunction with the design. The resultant EI and GJ curves compared to the metal stabilizer are shown in Figure 6. The final skin configuration is shown in Figure 7. In general the cover is stiffness designed outboard of X_{HS40} 105, stability critical from X_{HS40} 105 to X_{HS} 67 and strength critical at the attachments to the bearing support fitting.

An in-house study of orthotropic composite materials application to various spar web designs concluded that a circular arc configuration (sine wave) resulted in a minimum weight web for moderately loaded spars. The designs studied included plane, back-to-back bead stiffened and back-to-back sandwich stiffened shear webs. The sine wave web is the most efficient because the small radius results in a high allowable local buckling stress. The results indicate that for the moderate shear loading index (less than 1500 lb/in) associated with the majority of intermediate spars on the horizontal stabilizer, the A/S or T-300 type graphite-epoxy sine wave is the most structurally efficient.

The procedure for optimization of the spar web was formulated using the basic approach developed for isotropic webs loaded in pure shear. The procedure, as extended at Grumman, also covers the case of flexure-induced beam web crushing loads as normally encountered in aircraft flight service design. For full depth (cap-to-cap) circular arc beam webs, spanwise bending stresses are assumed negligible. The geometry and loading is shown in Figure 8.

The criterion for minimum weight for either the pure shear case or crushing load case is simultaneous occurrence of both local and general instability buckling modes of failure. For the shear load case, the optimum configuration occurs for an angle ϕ equal to 80 degrees. For the crushing load case, the optimum angle ϕ is 90 degrees. A compromise angle equal to 85 degrees was chosen since it is near optimum for each loading case while still allowing sufficient draft to remove subassemblies from their mold form. Analytical results for a typical minimum gage spar (0 - zero degree plies/ 2 - 90 degree plies/4 ± 45 degree plies) for the pure shear case is shown in Figure 9. Test results obtained during the manufacturing study phase on 5 inch deep minimum gage spars loaded in three point bending indicate the spar can sustain 1080 lb/in at room temperature. Shear failure occurred in the web along the ± 45 degree ply orientations. These results compare favorably with the analytically predicted failure of 1092 lb/in. A similar failure was obtained on a 10 inch deep spar at 260°F which failed in shear at 852 lb/in.

Other technical factors that influenced the selection and configuration of the sine wave spar include tension/compression support (otherwise referred to as foundation modulus) provided by the spar to preclude local wrinkling failure of the cover and the pull-through strength of fasteners in the cap of the spar.

A test program to evaluate these potential failure modes was conducted on minimum gage spars.

No problems were encountered in compression testing. Test crushing strength results equaled or slightly exceeded by ten percent analytical predictions while compression modulus at ultimate load was within 15% of predicted. During tension testing, problems were encountered with the NAS 1672-3L (3/16 inch dia. A-286 Jo-Bolt) fasteners for attaching the upper blind side cover to the stabilizer. The low pull-through strength of 125 lbs per fastener at 300°F test temperature is attributed to the small annulus on the upset collar of the fastener. In further tests using a 0.312 inch diameter washer under the upset collar no pull-through failures were observed. It should be noted that a 0.312 inch diameter washer is equal to the collar diameter of the 3/16 inch diameter titanium Hi-Loks used on the lower stabilizer cover. In the final design .020 inch thick 2024-T6 aluminum washers co-cured with the spar are used in combination with all Jo-Bolt fasteners. Additional tests were conducted on foundation modulus specimens with co-cured washers installed on the upper Jo-Bolt flange and a 3/16 inch diameter Hi-Lok fastener without a washer installed on the lower flange. A pull-through failure load of 444 lbs per fastener at a test temperature of 260°F was obtained. Pull through occurred on the Hi-Lok flange side. This capability is more than sufficient to satisfy the strength requirement of the stabilizer for the compression load with normal air load superposed.

The covers and substructure are assembled using titanium Hi-Loks with stainless steel collars in the lower cover and A-286 corrosion resistant Jo-Bolts in the upper cover. The cover is attached to the titanium support fitting with titanium bolts and stainless steel nuts.

To verify the design several large elements were fabricated and tested. The relationship of the elements to the structural box is shown in Figure 10. The results of some of the tests are shown in Figure 11. The longitudinal compression panel shown in Figure 12 consisted of a section of the cover located approximately one third of the span from the root. Supporting the cover was a representative section of the rear beam and 3 sine wave spars. The specimen failed at a longitudinal cover strain of 4600 microinches at 260°F (147 percent of design ultimate load). Failure originated in the substructure.

A series of environmental tests were conducted including corrosion, acoustic fatigue, thermal nuclear pulses and lightning strike.

The acoustic fatigue specimen is shown in Figure 13. It represented the areas of largest spar spacing in the stabilizer. The specimen withstood 191 hours of acoustic fatigue that varied from 152 to 167 db without any composite failures.

The lightning strike protection system is a 6 mil layer of flame sprayed aluminum covering approximately 50% of the surface area. A 3 foot by 4 foot panel was fabricated and tested to meet the basic requirements of MIL-B-5087B. The panel withstood strikes up to 200,000 amps sustaining only minor damage. Figure 14 shows the lightning strike panel after test.

FABRICATION

The composite stabilizer developed under the program makes use of several unique tooling concepts and manufacturing processes which include the following:

- o single cure cycle molding of the sine wave spars and ribs on metal reinforced silicone rubber tools
- o molding of 23 foot long channels that vary in height from $1\frac{1}{2}$ to 12 inches
- o application of aluminum flame spray coating to the covers for lightning strike protection
- o ultrasonic drilling and countersinking of boron and graphite epoxy laminates for holes up to $\frac{1}{2}$ inch in diameter

Three general types of composite parts are used in the fabrication of the stabilizer; namely, sine wave spars and ribs, flat web front and rear spars and covers. The procedures used for fabrication of these composite parts and for assembling the stabilizer are described in the paragraphs below.

Sine Wave Web Spars and Ribs

The sine wave web spars and ribs are fabricated using a single cure process on matched silicone rubber faced dies, see Figure 15. The layup is initially made in four parts: two channel halves and two cap sections. Fabrication of the channel halves is initiated by laying up graphite epoxy tape on mylar templates. The plies are transferred to the rubber tool, which has been prepared with a release system and web bleeder. The layup is then compacted and the flanges are formed by vacuum pressure.

The caps are fabricated by laying up plies of graphite epoxy tape on mylar templates. The plies are stacked and transferred to the channel halves during the assembly operation.

The assembly is initiated by clamping the channel halves together and filling the gap in the radius area with an epoxy casting compound. The caps are then installed and a bleeder system is applied. The entire assembly is then bagged and placed in the autoclave for curing. Following the curing operation the part is removed from the tool and the bleeder system is removed. The part is then post cured. Final trimming, inspection (dimensional, ultrasonic and radiographic) and weighing complete the fabrication and inspection cycle.

Flat Web Front and Rear Spars

Fabrication of the front and rear spars is accomplished by laminating two (2) channel sections and two (2) caps and then adhesive bonding them to form the I-beam-shaped spar structural section, see Figure 16. This approach reduces manufacturing risks associated with very long composite parts, since only half the web thickness is molded at a time. It also enhances NDT inspection of the structure, provides greater dimensional control, and reduces potential rework and rejection costs.

The fabrication cycle for each channel is initiated by laying up plies of graphite/epoxy tape on mylar templates. The plies are stacked and transferred to a steel male mold form. Vacuum and heat are applied to form the channel flanges to the mold form. After forming, a bleeder system is applied to the layup, and the entire assembly is inserted in a vacuum bag and cured in the autoclave. An oven post-curing operation, trimming, and dimensional, ultrasonic, and radiographic inspection complete the manufacturing/inspection cycle for each spar channel section. A completed spar is shown in Figure 17.

The spar caps are fabricated by laying up plies of graphite/epoxy tape on mylar templates. The plies are stacked on the tool and a bleeder system is applied prior to bagging the layup tool and curing in the autoclave. The caps are post-cured in an oven and are subjected to a dimensional/ultrasonic inspection similar to the channel sections.

Bonding of the channels and caps is accomplished using the steel mold forms. The parts are pre-assembled on the tool (with mylar adhesive isolation sandwiches on all surfaces to be bonded), cured, and disassembled to establish adhesive requirements. After completing this procedure, the channels and caps are prepared for the bonding operation by removing the peel ply and laying up the required amount of adhesive on the surfaces to be bonded. The parts are re-assembled on the tool, bagged, and autoclave-cured. After curing, the spar section is inspected (dimensional, ultrasonic and radiographic) and trimmed to final size. Weighing completes the manufacturing and inspection cycle.

Covers

The covers are molded on steel air passage tools as shown in Figure 18. Prior to layup, an aluminum flame spray coating is applied to the tool surface. This coating provides a lightning strike protection system for the stabilizer. The plies, both graphite and boron epoxy, are laid up on mylar templates and transferred to the tool. Approximately 585 templates are used to apply the 92 cover plies. The layup is periodically de-bulked in the autoclave to insure proper compaction. After all the plies have been stacked on the tool, a nylon peel ply, fiberglass anti-breakout drilling strips and the bleeder system are added. Steel caul plates are placed over the spar pads to ensure flatness. A contoured silicone rubber pressure pad and nylon vacuum bag are placed over the layup prior to autoclave cure. The cover is cured and post cured in a convection type autoclave. After cure the part is weighed and ultrasonically and dimensionally inspected. Final trimming of the cover is accomplished during the final assembly operation. A completed cover is shown in Figure 19.

Assembly

The entire stabilizer is assembled in a fixture as shown in Figure 20. The torque box is assembled first, followed by installation of the leading edge, trailing edge and tip cap assemblies.

The assembly of the torque box consists of installing the bearing support fitting, the front and rear spars and tip rib followed by installation of the remaining substructure details. The inboard end of the stabilizer substructure is installed first with a progressive buildup toward the outboard end. The covers are ultrasonically drilled in the hybrid inboard areas and then liquid shimmed to the substructure. The lower cover is permanently installed first followed by the upper cover installation. Approximately 3500 holes are drilled in each cover with approximately 400 located in the hybrid area. A maximum thickness of .030 inches of liquid shim is permitted between the covers and substructure. Assembly of the static stabilizer torque box is shown in Figure 21.

TEST

The qualification plan for the stabilizer includes full scale static and fatigue tests and element tests to evaluate the effects of temperature, moisture and real time loading.

The static article will be first used to measure structural influence coefficients. Three critical loading conditions will be applied of which two are at 260°F, and final is at room temperature. The stabilizer will be tested to failure in the final condition.

The fatigue article will be proof loaded to 110% of limit load both positive and negative. Two lives of accelerated fatigue will be applied followed by a room temperature residual strength test.

Environmental effects will be evaluated by testing both root joint splice elements and sine wave spars. The effects of moisture, temperature and quasi real time fatigue loading will be evaluated. The goal is to establish wear out rates and proof load levels for production stabilizers.

CONCLUDING REMARKS

At present the composite stabilizer design is complete and the fabrication effort is in progress. Delivery of the static stabilizer to test is scheduled for November 15, 1975, followed by the fatigue stabilizer on February 15, 1976. Preliminary evaluations indicate high confidence that the weight and cost targets established by the Air Force will be achieved. Figure 22 shows the estimated weight of the composite stabilizer and the current metal stabilizer. The composite design provides a savings of approximately 473 pounds per aircraft. With approximately 90% of the actual weights accounted for on the static and fatigue stabilizer, a weight of 48 pounds under the estimate is indicated. This data provides the confidence that the weight target for the composite stabilizer will be satisfied.

Figure 23 shows a comparison of projected production costs for the metal and composite horizontal stabilizer.

The use of composite materials permits a design that has 60% less substructure than the metal stabilizer. This reduction in substructure parts reduces the number of attachments by 46% and consequently reduces the assembly costs The reduction in substructure parts, attachments and assembly more than offsets the increased cost of the covers and produces a less expensive stabilizer.

Successful completion of the static and fatigue test will validate the design and provide the Air Force with a composite stabilizer that is both lighter and less expensive than its metal counterpart.

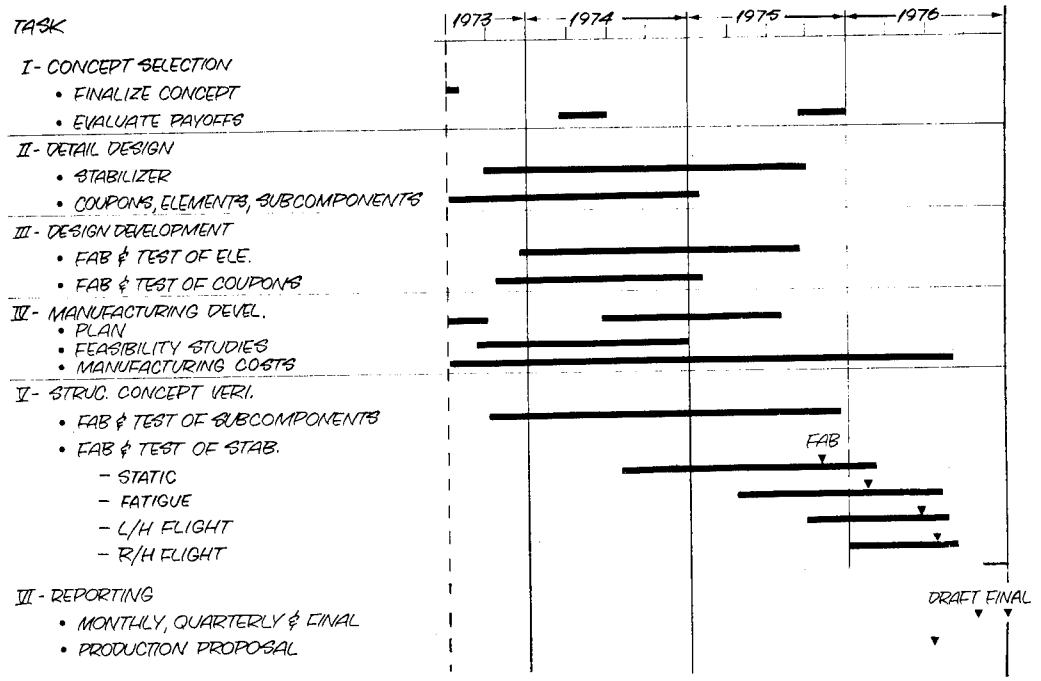

Figure 1.- 42-month program.

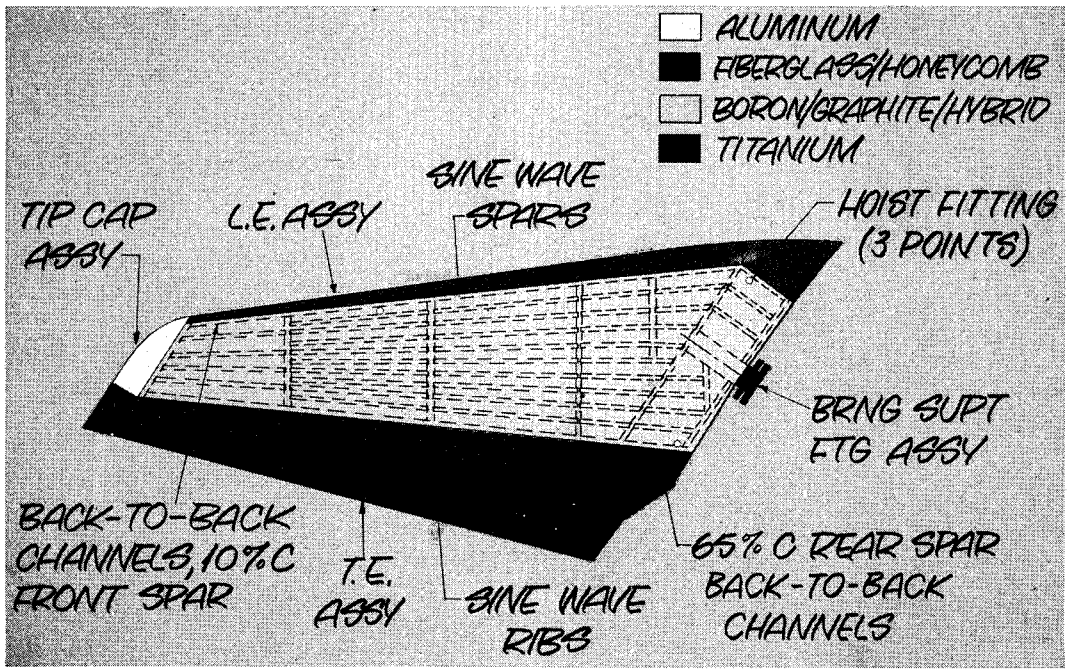

Figure 2.- Composite stabilizer.

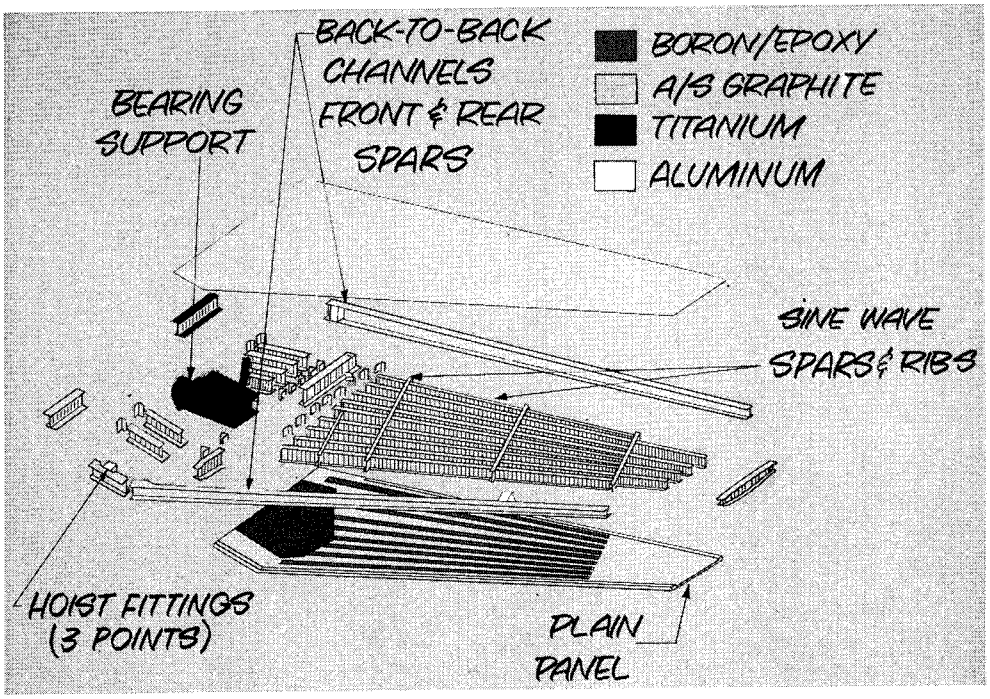

Figure 3.- Composite stabilizer torque box.

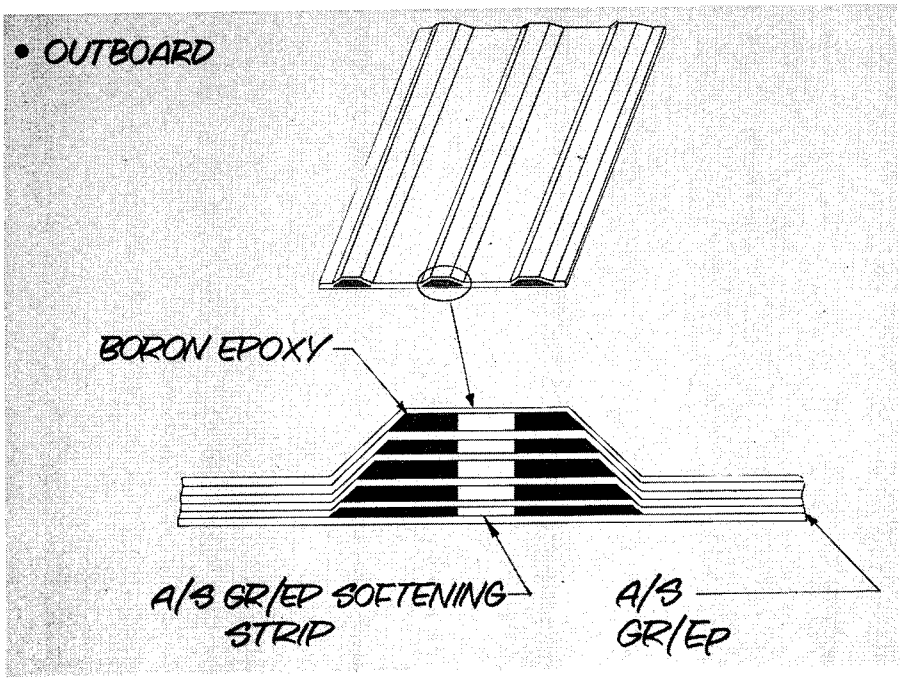

Figure 4.- Composite stabilizer cover details.

- CONTINUOUS RIBS
  - PERMITS SPLICING WITH MINIMUM REINFORCEMENT
  - PROVIDES A MORE ADVANTAGEOUS DESIGN DETAIL FOR ACOUSTIC FATIGUE

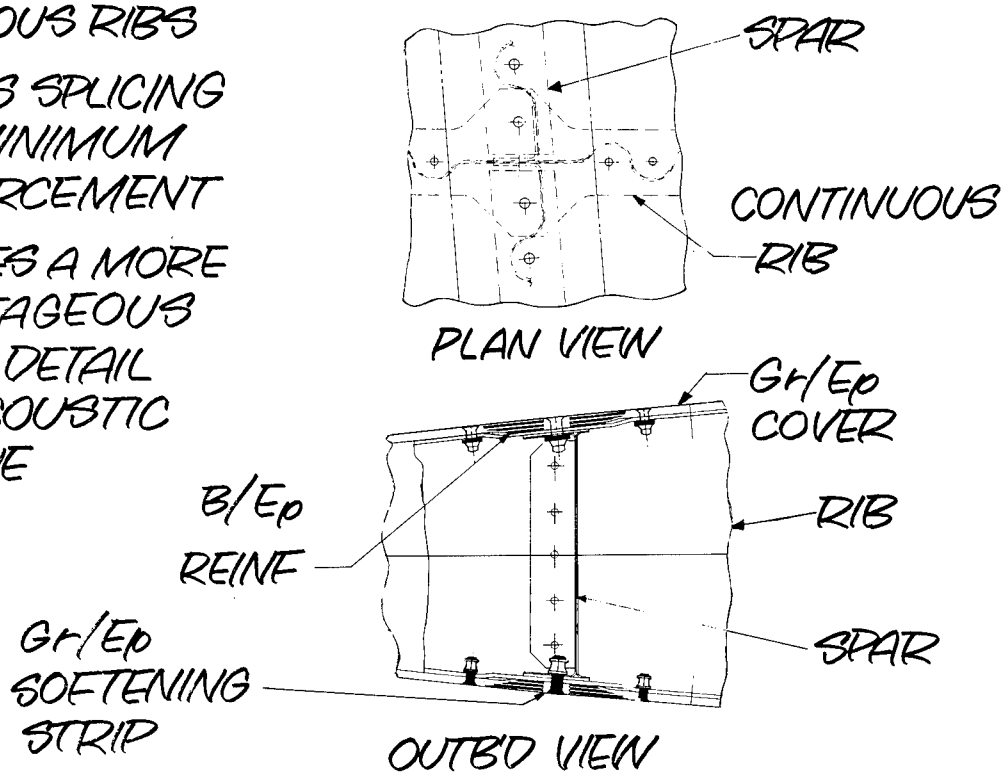

Figure 5.- Span-rib intersection.

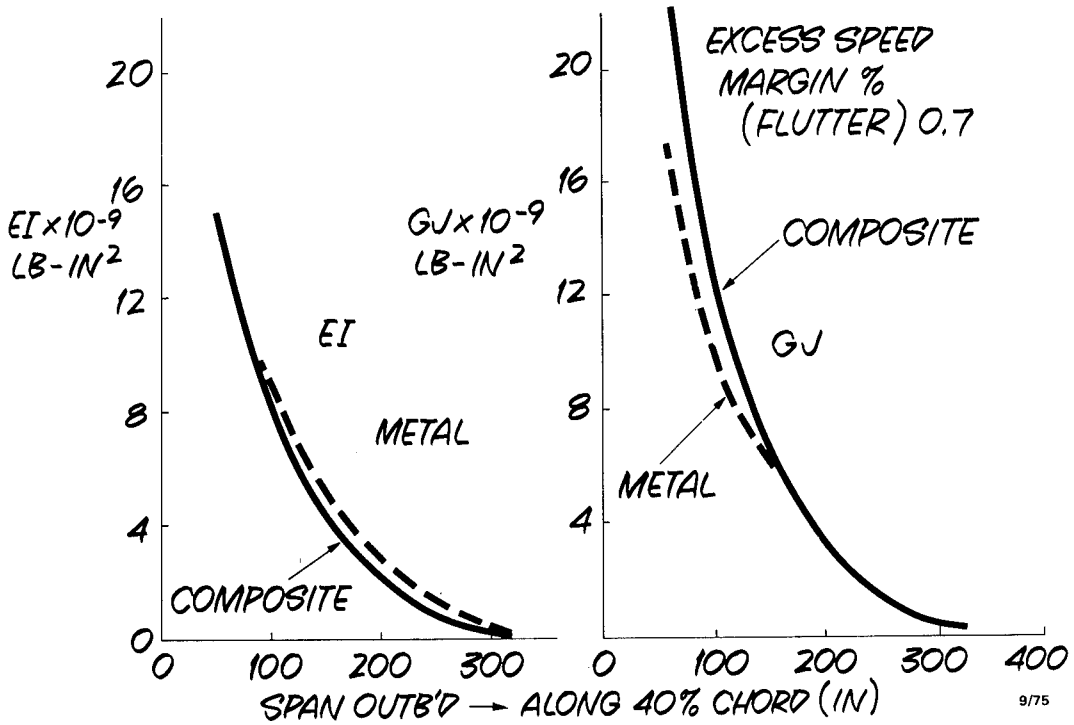

Figure 6.- EI and GJ composite versus metal stabilizer.

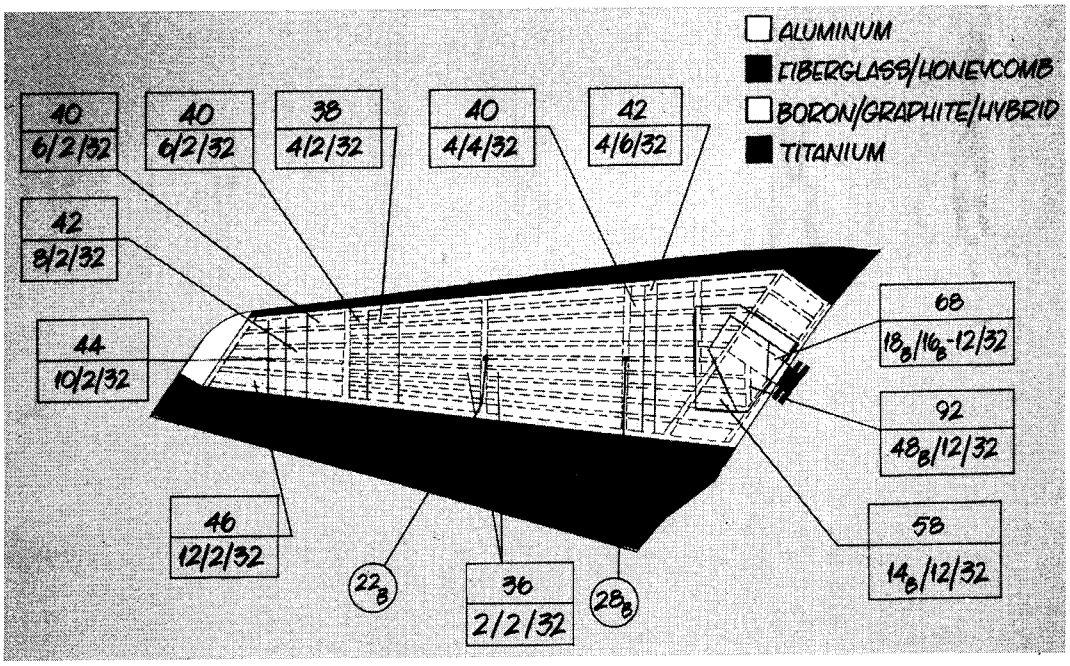

Figure 7.- Composite stabilizer.

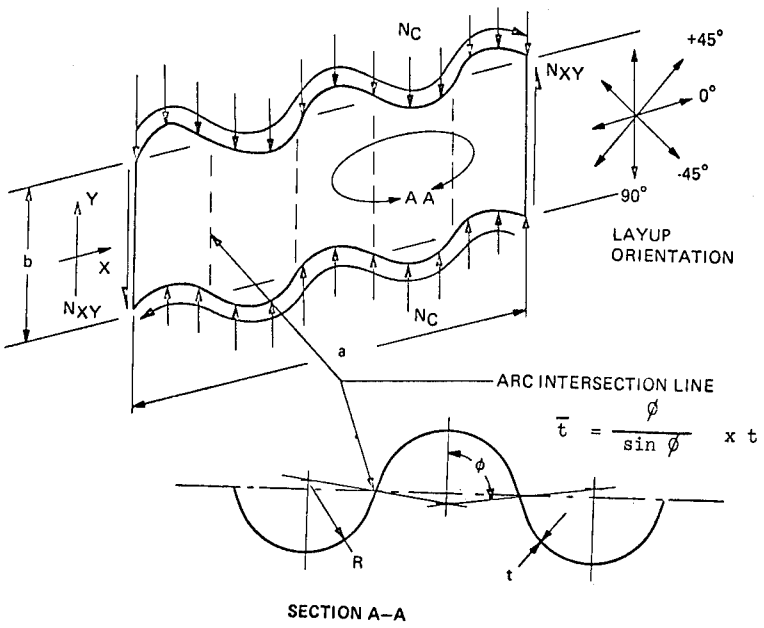

Figure 8.- Composite web geometry.

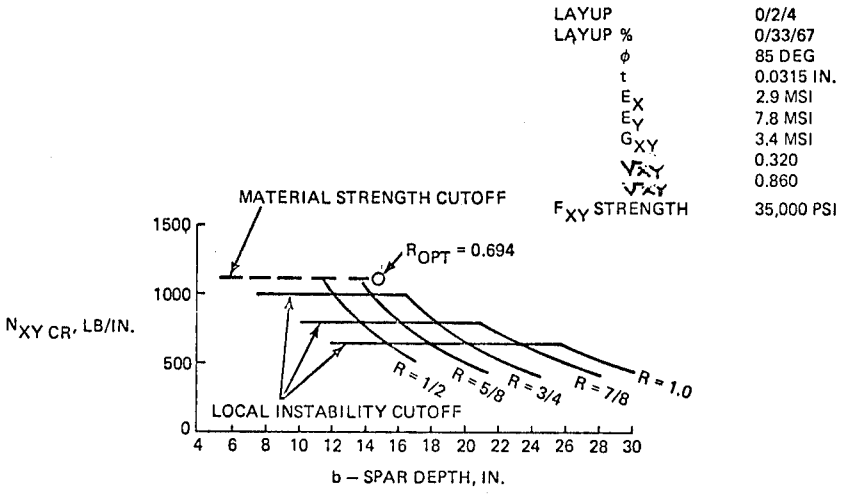

Figure 9.- Shear load case. Gr/Ep material - R.T.

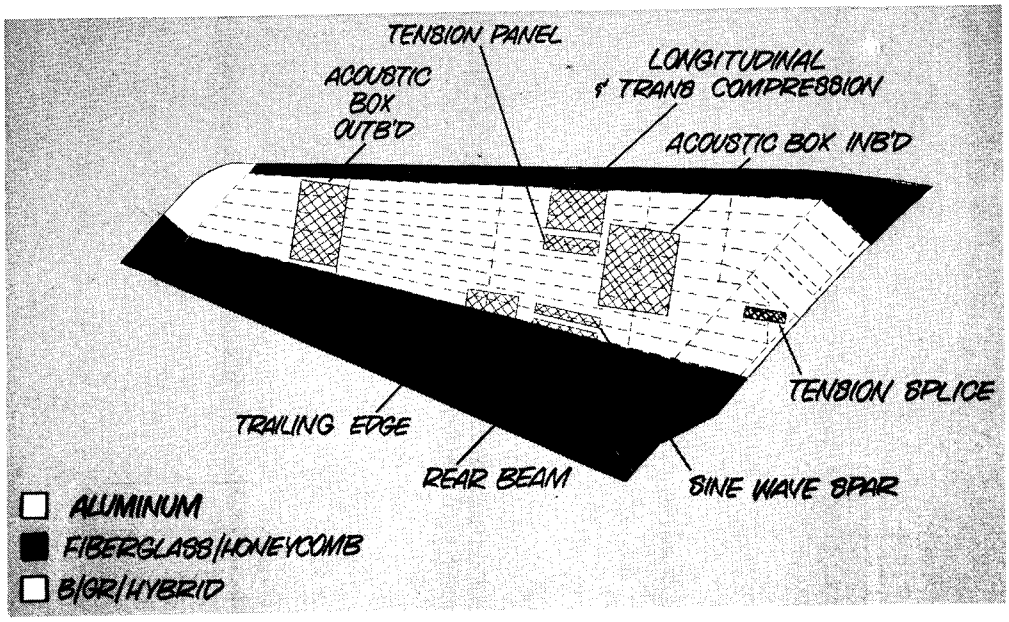

Figure 10.- Relationship of elements to structural box.

SPECIMEN	TEST TEMP, °F	FAILING LOAD	% DUL
• TENSION PANEL	300	87,500 LB	170
• TENSION SPLICE PANEL	RT	20,900 LB/IN.	136
• SINE WAVE SPAR	260	852 LB/IN.	135
• REAR BEAM	RT	1,850 LB/IN.*	130
• TRANSVERSE COMPRESSION	260	1,075 LB/IN.	150
• LONGITUDINAL COMPRESSION	260	270,000	147
• FOD BOX	RT	STATIC TEST AFTER 1/2 FATIGUE LIFE	170

* INITIAL BUCKLING

Figure 11.- Element test results.

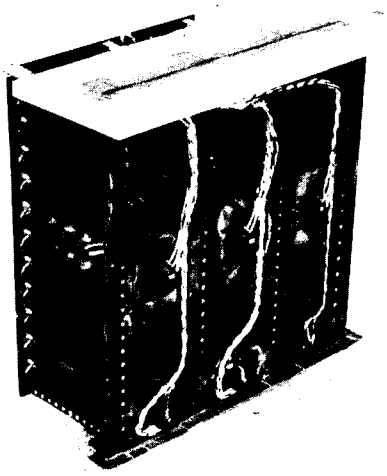

Figure 12.- Longitudinal compression panel.

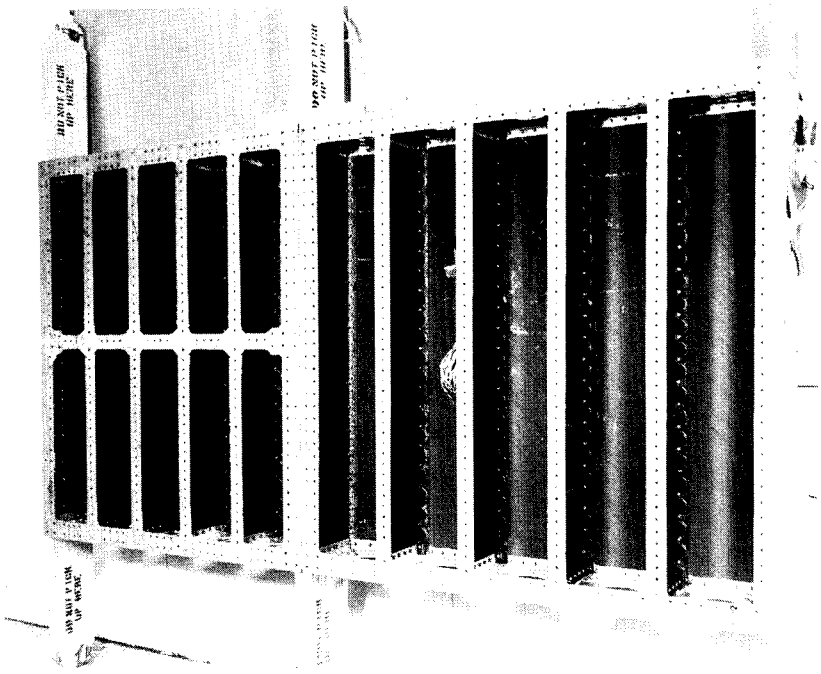

Figure 13.- Acoustic fatigue test specimen - upper cover removed.

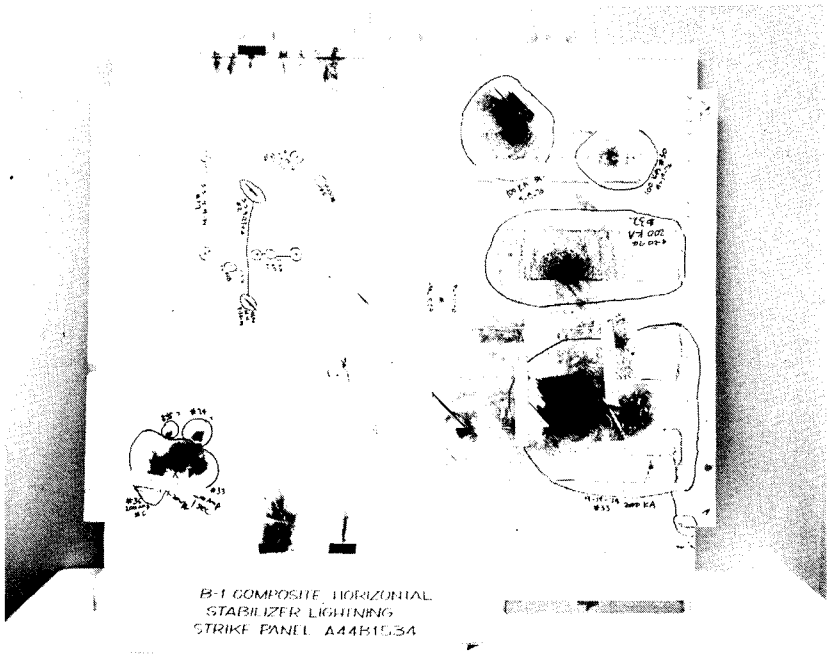

Figure 14.- Lightning strike panel.

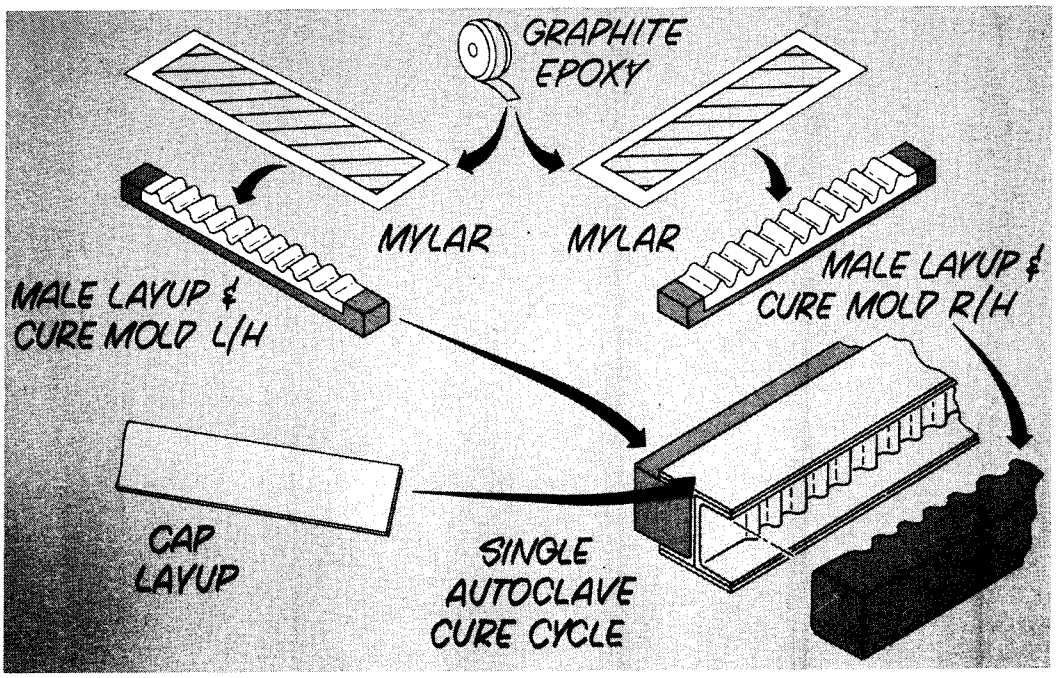

Figure 15.- Fabrication of sine wave spars/ribs.

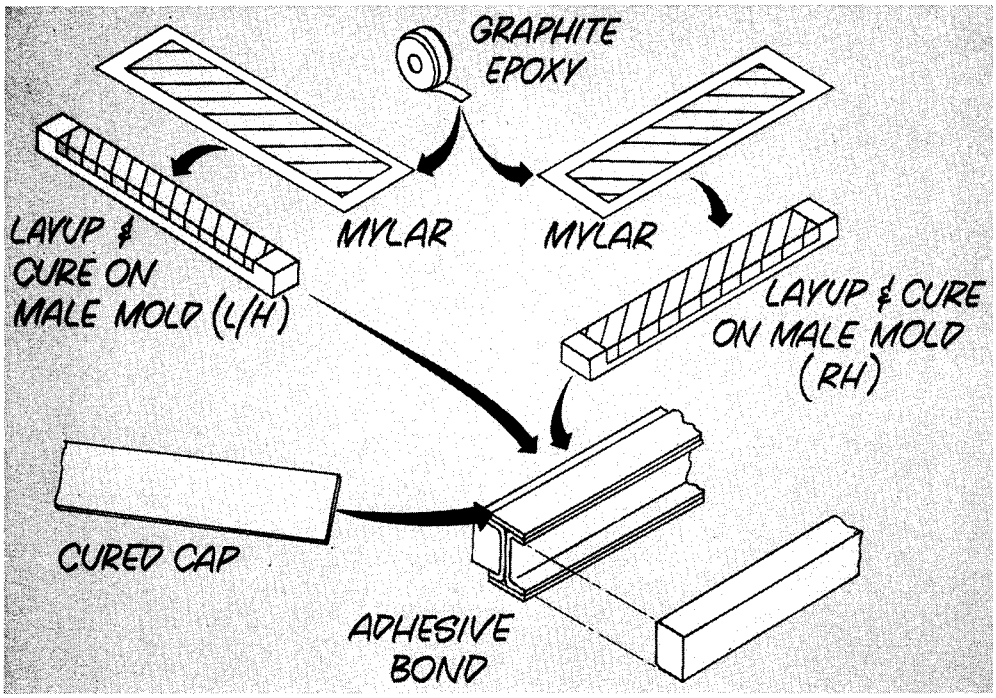

Figure 16.- Fabrication of front and rear spars.

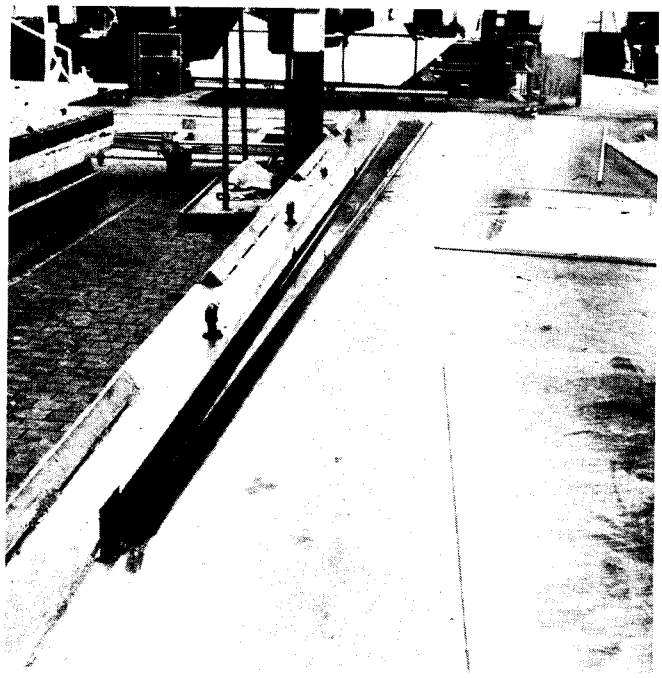

Figure 17.- Beam channel - prior to bonding.

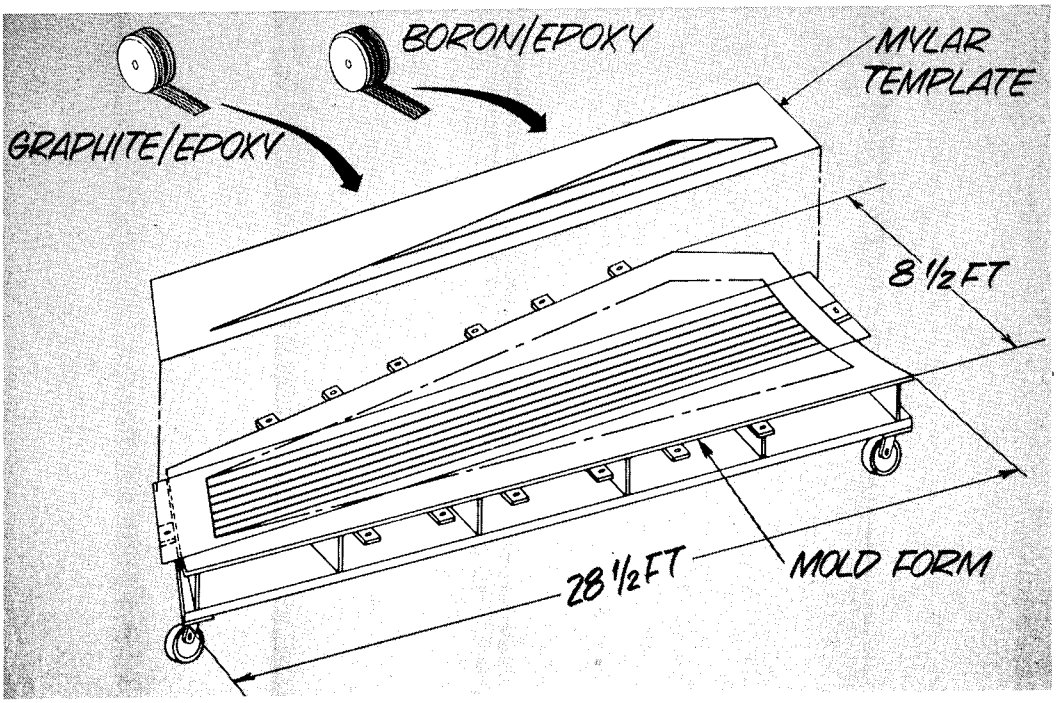

Figure 18.- Fabrication of stabilizer cover.

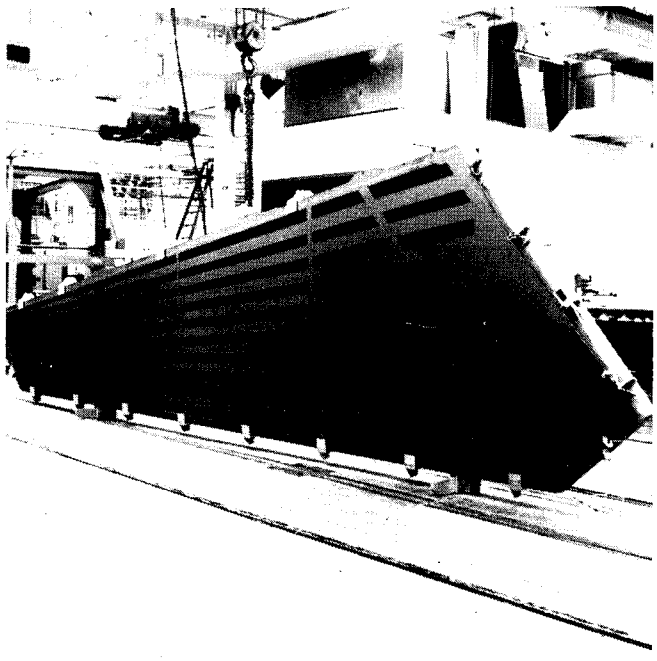

Figure 19.- Stabilizer cover - (in transport dolly).

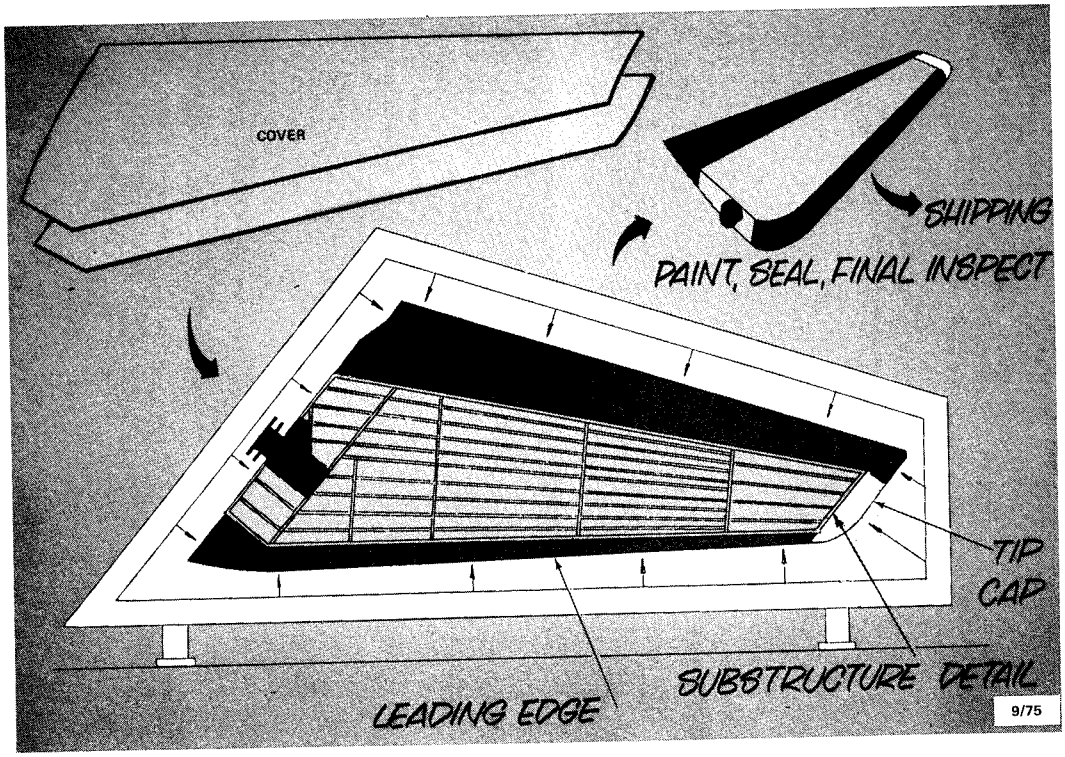

Figure 20.- Stabilizer assembly operation.

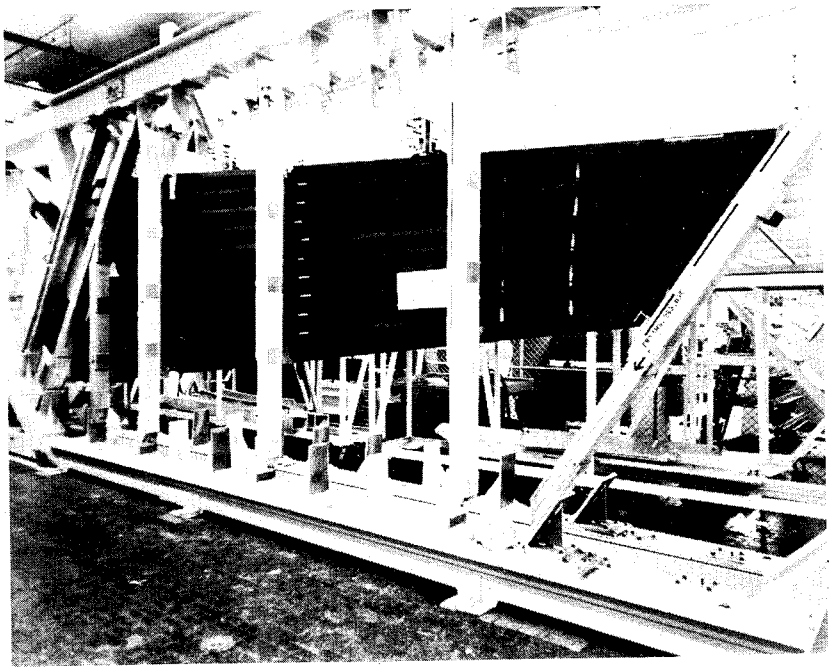

Figure 21.- Static stabilizer assembly - substructure and lower cover.

COMPONENT	METAL	COMPOSITE
COVERS	1687.6	1359.5*
FRONT & REAR SPARS	192.0	112.5
INTERMEDIATE SPARS	244.4	202.8
RIBS	153.1	113.7
MISC (SHIM & HOIST FITTING)	-	29.0
TOTAL BOX	2277.1	1817.5
LE, TE, TIP	575.5	575.5
SEAL (INBD)	46.3	15.4
FINISH	40.3	40.3
BEARING SUPPORT FITTING	376.0	395.0
TOTAL STABILIZER	3315.2	2843.7

- WEIGHT SAVING: 472.6 LB (14.3%)
- TARGET WEIGHT: 2856 LB

* INCLUDES SURFACE PROTECTION & FASTENERS

Figure 22.- Weight status (lb/shipset).

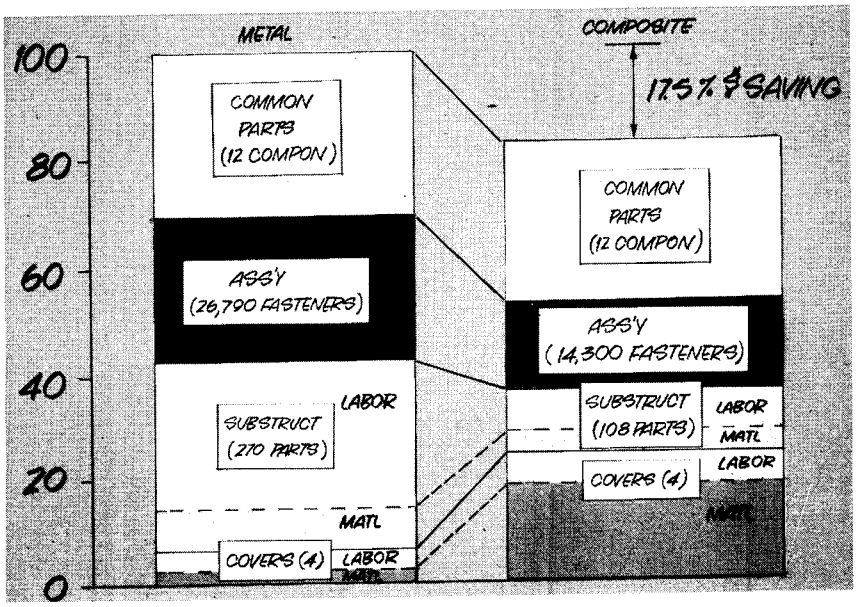

Figure 23.- Horizontal stabilizer production costs.

DEVELOPMENT OF AN ADVANCED COMPOSITE RUDDER FOR FLIGHT SERVICE ON THE DC-10

by

George M. Lehman

Douglas Aircraft Company
McDonnell Douglas Corporation

ABSTRACT

Design and manufacturing development of a graphite-epoxy rudder for the DC-10 commercial transport is discussed. An objective of the program is to develop a structure with significant weight saving and competitive cost in comparison with the existing metal design. The composite structure was designed and fabricated using a unique processing method in which the thermal expansion characteristics of rubber tooling mandrels were used to generate curing pressures during an oven cure cycle. This method eliminated the need for autoclave curing and secondary assembly bonding of the rudder structure. Development of the rudder is traced through construction and testing of a group of fabrication feasibility specimens and structural development components representing salient details of the structure. The ground test program is fully coordinated with the FAA and will result in certification of the rudder for passenger-carrying flights. Results of the structural and environmental tests are interpreted and detailed development of the rudder tooling and manufacturing process is described. Processing, tooling, and manufacturing problems encountered during initial fabrication of the graphite rudders are discussed and the results of corrective actions are described. The program will culminate with a monitored 5-year flight-service period for several graphite-epoxy rudders in the actual operating environment.

INTRODUCTION

Douglas Aircraft Company interest in advanced composites started in 1964 through participation in the Air Force Project Forecast in which the excellent structural potential of boron reinforced composites was first identified. This interest has continually grown since then through knowledge of and participation in the many advanced composite technology and structural applications programs conducted throughout the airframe industry.

In 1972, Douglas initiated an applications study on the DC-10 commercial transport to identify potential structural uses of Thornel 300/5208 graphite-epoxy materials. Several promising areas of application were identified and one of these, the upper-aft rudder, was selected for further design and development. The rudder was selected because of its excellent potential for weight reduction (being a mass-balanced surface) and because of its adaptability to a unique manufacturing approach, the thermal expansion molding process, under development in Douglas laboratories at that time.

In January 1974, a contract was negotiated with the NASA Langley Research Center to complete manufacturing development, structural qualification, and actual service exposure of the rudder. Primary objectives of the contract are to document manufacturing costs and to determine the response of the material system to the actual service environment.

The program has now progressed through engineering design, tooling and process development, and ground qualification testing. This paper presents the rationale for selection of the structural design concept, discusses problems encountered and solutions employed during scale-up of the tools and processes from small laboratory samples to full-size rudder proportions, and summarizes results of a series of design verification tests on critical details of the structure. Documentation of the test results is presently in progress as part of the FAA certification requirement. The graphite-epoxy rudders will enter flight service in mid-1976 when FAA certification is obtained.

DESIGN SYNTHESIS

The general arrangement of the DC-10 rudder system is shown in Figure 1. The rudder is divided into upper and lower rudder assemblies, each consisting of forward and aft rudders. The upper-aft rudder has a span of 158 inches and a planform area of approximately 34 square feet. Each of the aft rudders is driven by a mechanical linkage connected to the forward rudder assembly. When the forward rudder is deflected, the mechanical linkage causes the desired differential motion between forward and aft rudders.

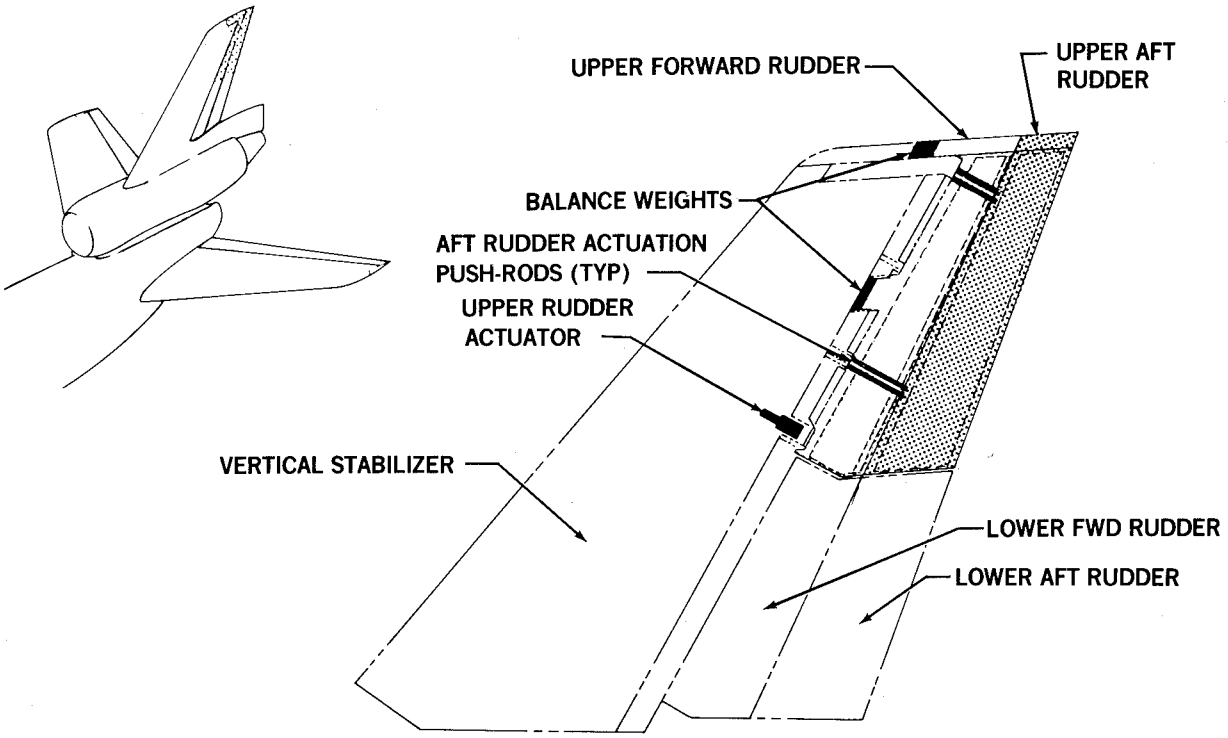

FIGURE 1. GENERAL ARRANGEMENT OF THE DC-10 RUDDER SYSTEM

In preliminary design stages, seven candidate structural design concepts of the upper-aft rudder were evaluated. These concepts are illustrated in Figure 2. Interest was initially centered on the honeycomb sandwich skin panel and full-depth honeycomb configurations, Figure 3, because of the fully stabilized skins and relative simplicity in terms of part numbers and assembly techniques.

As the design studies proceeded, two developments at Douglas broadened the range of interest to include additional structural configurations. The two developments included (1) success in the laboratory in producing graphite-epoxy parts using a unique new fabrication approach, the thermal expansion molding technique, and (2) a laboratory test indicating that skin buckling could be tolerated in the rudder design.

The fundamental elements of the thermal expansion molding technique are illustrated in Figure 4. The individual parts of the molding assembly were laid up in the "B" stage, densified, and trimmed to size on simple ancillary tools. The individual parts were then assembled in a curing tool which consisted of various metal and silicone rubber elements. The assembled tool was heated so that the thermal expansions of the rubber elements furnished the pressure required to consolidate the "B" stage parts into a cured laminate assembly. The heating cycle was controlled to provide the temperature and pressure phasing required to cure the laminate.

The thermal expansion molding technique was used to fabricate the shear panel shown in Figure 5. The overall size of the panel was 13.5 by 23.5 inches. The skin was a 6-ply layup (0/45/-45)S with a thickness of 0.034 inch. The panel stiffeners were spaced 4 inches on center to represent anticipated spacings in the rudder. The panel was first tested in fatigue to 4000 cycles of limit shear stress in a critical rudder design condition and then under static loads to failure. Shear loads were introduced to the panel through the pin-ended "picture frame" jig shown in Figure 5. The static load was applied in 2000-pound increments and visual observations for buckling deformations were made after each load

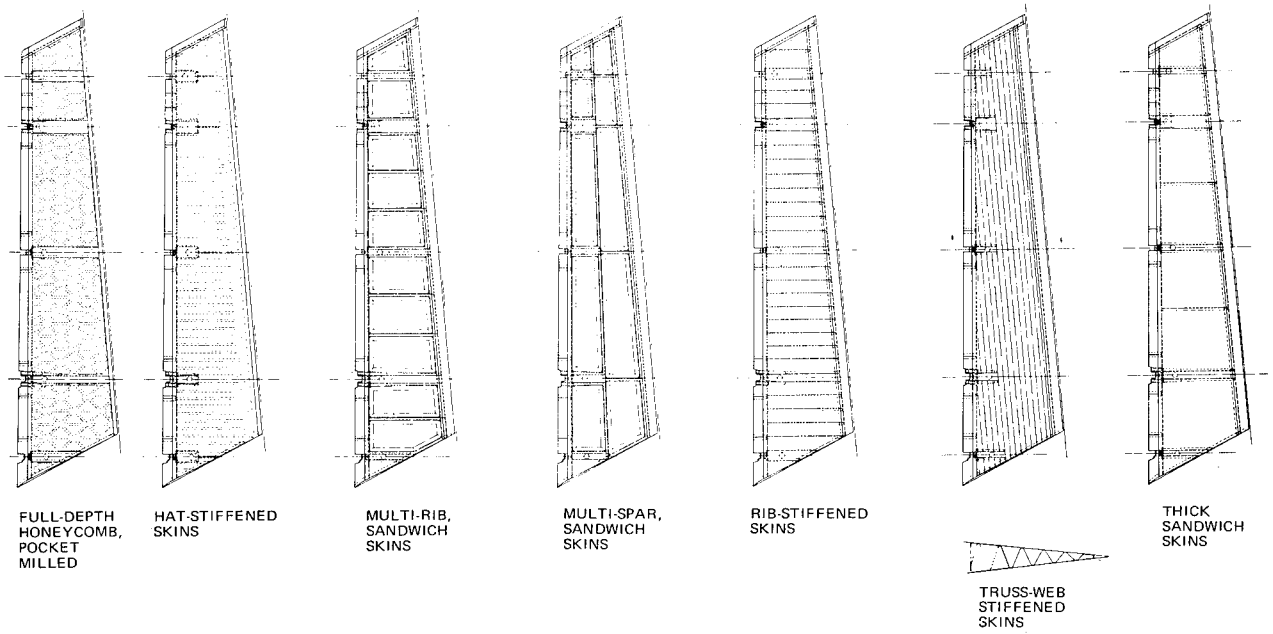

FIGURE 2. CANDIDATE STRUCTURAL CONFIGURATIONS FOR THE GRAPHITE-EPOXY RUDDER

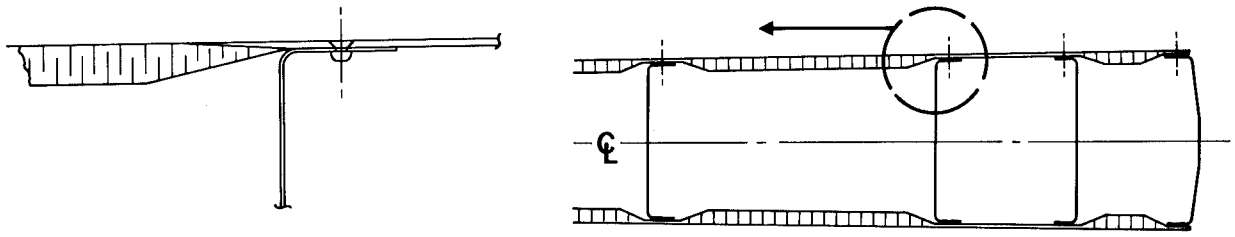

HONEYCOMB SANDWICH PANELS

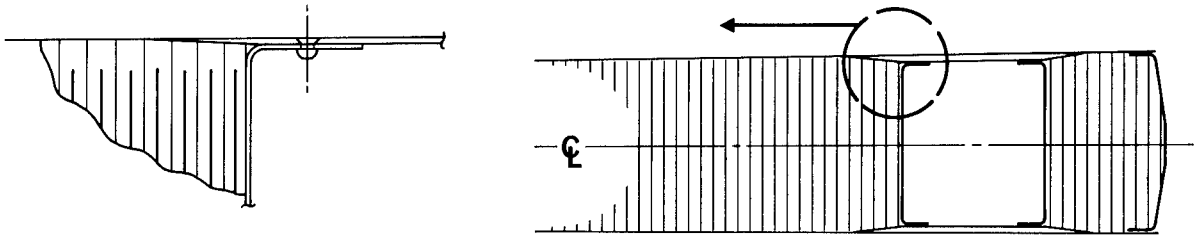

FULL-DEPTH HONEYCOMB

FIGURE 3. HONEYCOMB STRUCTURAL CONFIGURATIONS

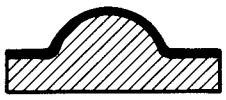

- LAYUP INDIVIDUAL PIECES ON ANCILLARY TOOLS
- DENSIFY
- TRIM TO SIZE
- STORE IN FREEZER

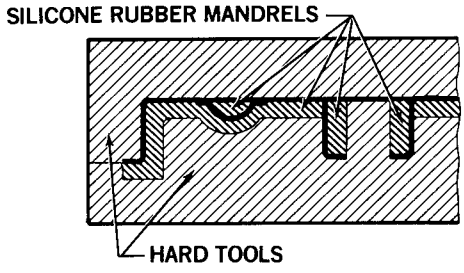

- ASSEMBLE PIECES IN CURE TOOL
- APPLY HEAT
- PRESSURE SUPPLIED BY EXPANSION OF SILICONE RUBBER WITHIN TOOL CAVITY
- NO BAGGING, BLEED-OFF OR ADHESIVE REQUIRED

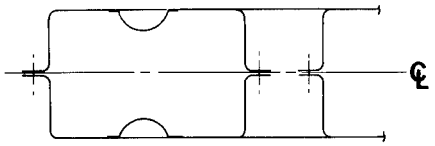

- JOIN RUDDER HALVES WITH ROOM-TEMPERATURE ADHESIVE AND FASTENERS

FIGURE 4. SCHEMATIC OF THERMAL EXPANSION MOLDING TECHNIQUE

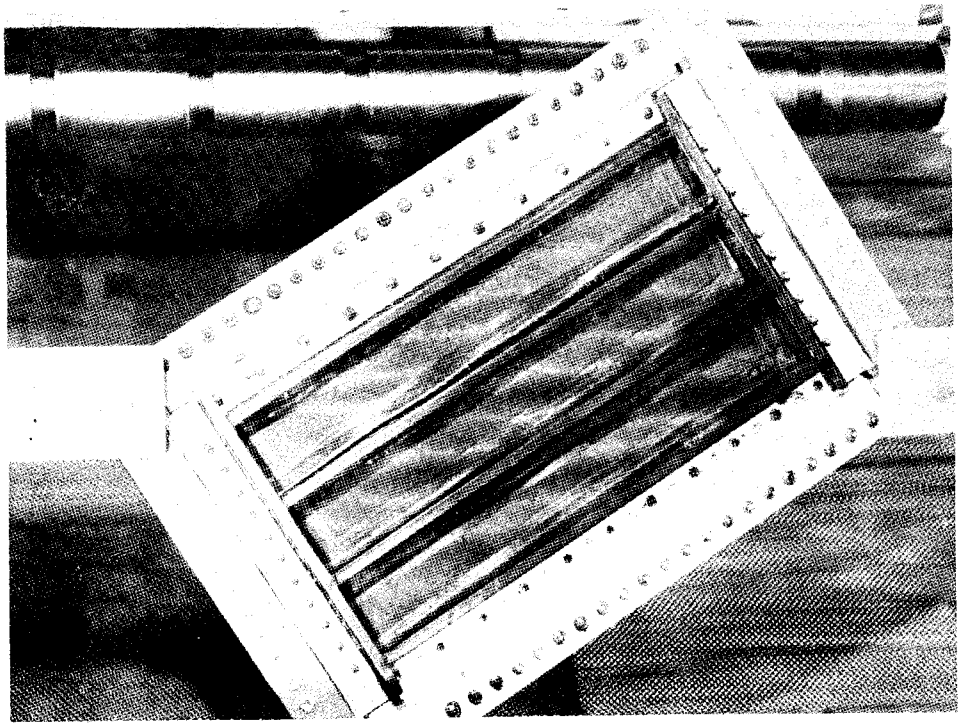

FIGURE 5. GRAPHITE-EPOXY SHEAR PANEL UNDER LOAD

application. Skin buckling was first observed at 10,000-pound load (11,300-psi shear stress in the skin panel). The buckle pattern became more fully developed with increasing loads, developing an ultimate shear stress of 26,550 psi at failure. These test results established the feasibility of permitting elastic buckling of skin panels in the graphite rudder design, so hat-stiffened and rib-stiffened rudder configurations, Figure 6, were added to the structural configurations of interest.

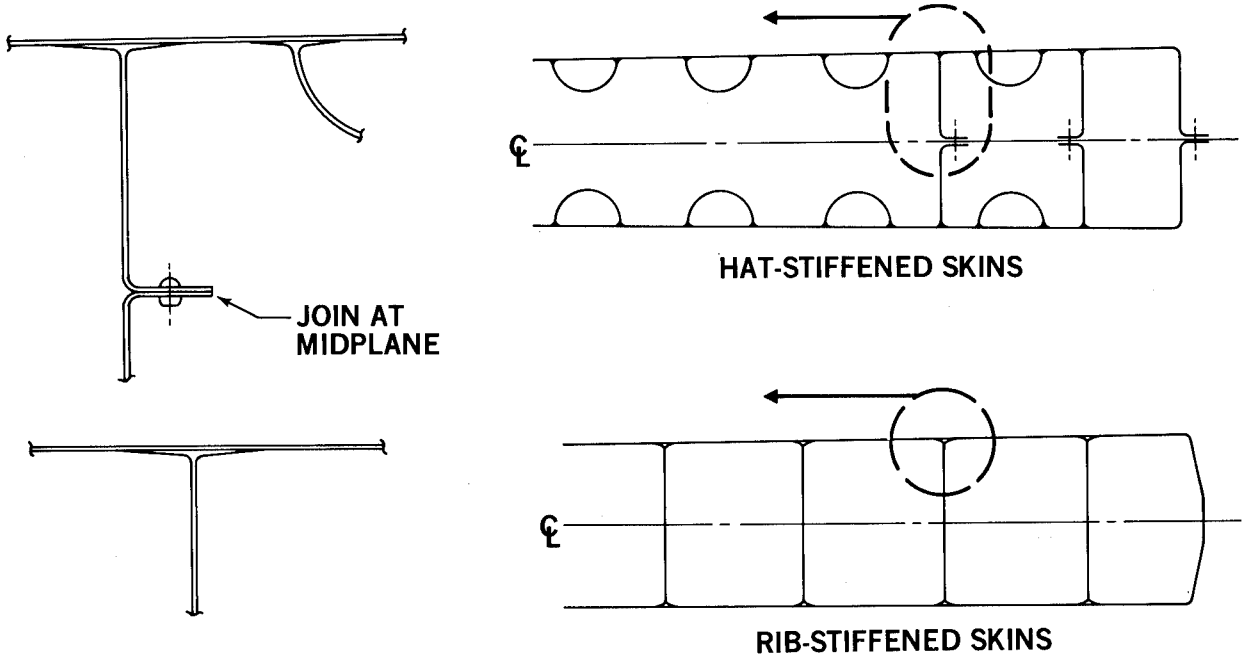

FIGURE 6. STIFFENED STRUCTURAL CONFIGURATIONS

The choice of structural configuration for the graphite-epoxy rudder was based on evaluation of relative weights and fabrication costs. On a weight basis, each configuration for the graphite structural box (with the exception of the full-depth honeycomb) indicated an average weight near 0.60 pound per square foot of wetted area. The full-depth honeycomb configuration was about 8 percent heavier because of the relatively large volume of honeycomb core material.

Relative costs were evaluated through consideration of part counts and preliminary evaluations of tooling and manufacturing operations required to produce the various structural concepts. The results of these evaluations are summarized in Tables 1 through 3.

On the basis of detailed part count (Table 1), the design concepts were initially ranked in the following order:

1. Full-depth honeycomb
2. Hat-stiffened skins
3. Honeycomb panels
4. Rib-stiffened skins.

However, further consideration to tooling requirements and manufacturing operations reordered the ranking significantly.

TABLE 1
DETAIL PARTS REQUIRED FOR VARIOUS DESIGN CONCEPTS

DETAIL PARTS IN GRAPHITE BOX STRUCTURE	DESIGN CONCEPT			
	HONEYCOMB PANELS	FULL-DEPTH HONEYCOMB	HAT-STIFFENED SKINS	RIB-STIFFENED SKINS
SKIN PANELS	4	2	4	2
HONEYCOMB CORE	14	6	0	0
SPARS	2	2	1	2
RIBS	14	12	24	32
TOTAL PARTS	34	22	29	36

TABLE 2

TOOLS REQUIRED FOR VARIOUS DESIGN CONCEPTS

TYPE	TOOLS	DESIGN CONCEPT			
		HONEYCOMB PANELS	FULL-DEPTH HONEYCOMB	HAT-STIFFENED SKINS	RIB-STIFFENED SKINS
SIMPLE TOOLS AND SHOP AIDS	CAUL PLATES	1	1	1	1
	FLAT PATTERN TEMPLATES	20	16	15	36
	FORM BLOCKS ("B" STAGE)	0	0	26	34
	APPLY TRIM AND DRILL TEMPLATES	2	2	2	2
FABRICATION AND ASSEMBLY TOOLS	HONEYCOMB MACHINING FIXTURES	14	6	0	0
	LAMINATING MOLDS	16	16	0	0
	HONEYCOMB BONDING FIXTURES	2	1	0	0
	ASSEMBLY BONDING FIXTURES	1	0	3	1
FINAL ASSEMBLY	ASSEMBLY JIG	1	1	1	1

TABLE 3

MANUFACTURING OPERATIONS REQUIRED FOR VARIOUS DESIGN CONCEPTS

SEQUENCE	MANUFACTURING OPERATION	DESIGN CONCEPT			
		HONEYCOMB PANELS	FULL-DEPTH HONEYCOMB	HAT-STIFFENED SKINS	RIB-STIFFENED SKINS
"B" STAGE	LAYUPS	7	5	6	5
	DENSIFICATION CYCLES	7	5	4	5
	CUT FLAT PATTERNS	20	14	29	34
	PREFORM DETAILS	18	14	27	34
FABRICATION AND SUBASSEMBLY	CURE DETAILS	18	16	3	1
	HONEYCOMB COCURE AND BOND	2	0	0	0
	BOND PREFIT	1	1	1	0
	SECONDARY BOND	1	1	1	0
FINAL ASSEMBLY	TRIM AND DRILL	1	1	1	1
	INSTALL FITTINGS AND EDGES	1	1	1	1

Evaluation of the tools required for the various rudder concepts was weighted with consideration of tool complexity as well as numbers required. The fabrication and assembly tools listed in Table 2 were considerably more expensive than simple tools and shop aids. The design concept ranking on the basis of potential tooling costs was therefore reordered:

1. Rib-stiffened skins

2. Hat-stiffened skins

3. Full-depth honeycomb

4. Honeycomb panels.

Manufacturing operations were similarly weighted with considerations of relative difficulty. The fabrication and subassembly operations listed in Table 3 were again more costly than those accomplished in the "B" stage. The design concept ranking on the basis of potential manufacturing costs was therefore in agreement with the tooling basis result.

Through formulation of the preliminary tooling and manufacturing plans, it became evident that the rib-stiffened rudder was essentially a one-step manufacturing operation. This approach eliminated repeated handling of the same details during sequential fabrication and subassembly operations, reduced the need for maintaining precision dimensions in fabricated details, and completely eliminated secondary bonding operations during assembly. A second look at the part count evaluation indicated that after one cure cycle the graphite-box part counts for the various concepts were as follows:

Honeycomb panels	– 34 parts
Full-depth honeycomb	– 22 parts
Hat-stiffened skins	– 17 parts
Rib-stiffened skins	– 1 part

The rib-stiffened design was therefore adopted as the configuration to be developed.

Detail design of the rib-stiffened structure was completed as shown in Figure 7. In addition to the one-piece graphite box (shown exploded in Figure 7), the rudder had demountable leading and trailing edge assemblies, tip assembly, and fittings. The leading and trailing edge assemblies and the tip assembly were primarily fiberglass-epoxy for electrical isolation of the graphite box. The trailing edge and tip assemblies were equipped with metal conductive straps (isolated from the graphite) for grounding direct lightning strikes to metal structure. The graphite box was also provided with a dielectric coating (an epoxy surfacer and polyurethane paint coat) to preclude swept-stroke lightning attachments. The hinge and drive station fittings were conventional aluminum alloy mechanically attached to the graphite.

The existing forward rudder A-frame hinge brackets were redesigned to accommodate the differential thermal deformations between the aluminum alloy forward rudder and the graphite aft rudder during the temperature excursion from 70°F to −65°F. This problem was resolved by providing the required vertical load reaction at a rigid center hinge bracket and by providing brackets which flex under loads

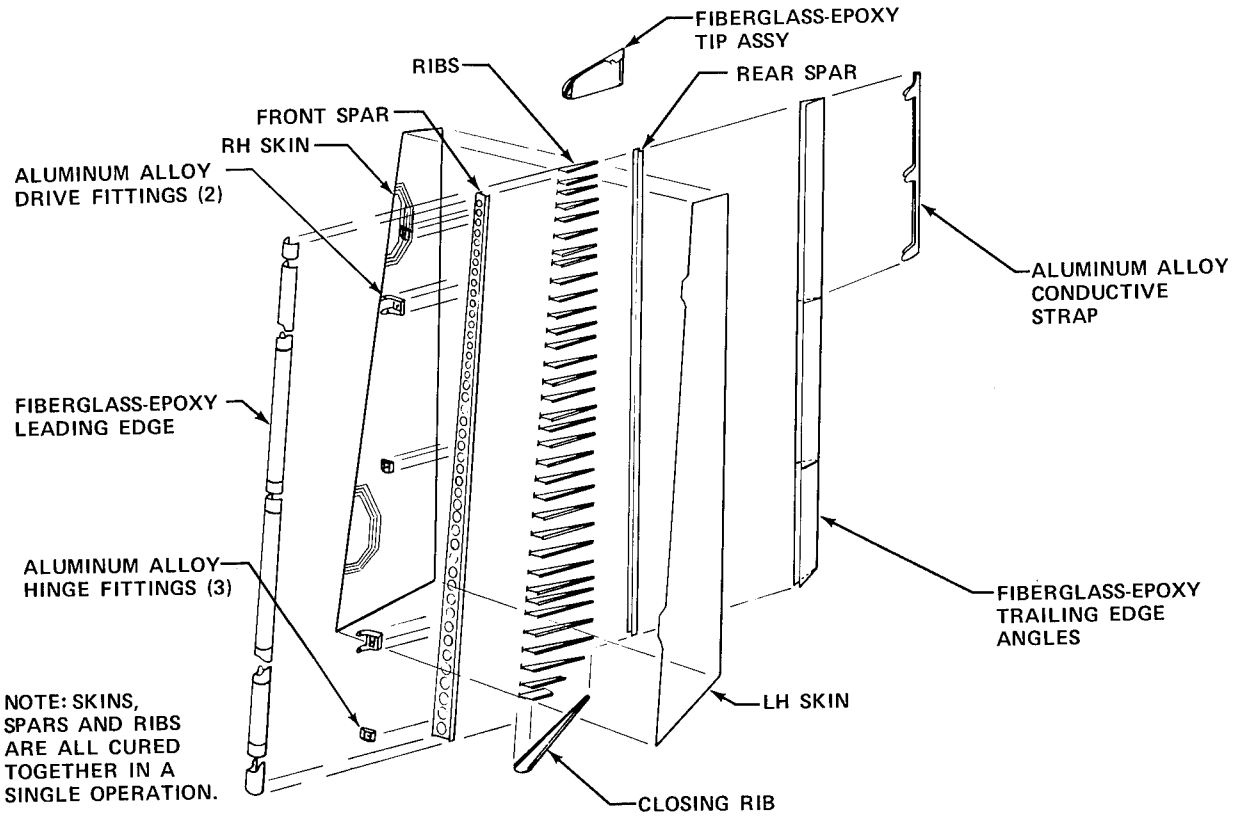

FIGURE 7. STRUCTURAL ARRANGEMENT FOR ADVANCED COMPOSITE RUDDER

parallel to the aft rudder hingeline at the other four hinge stations. All brackets were designed with dimensional free-play and rigidities normal to the hinge centerline equivalent to the production rudder to retain existing flutter margins.

The conventional metal rudder weighs 91.3 pounds. The graphite-epoxy rudder weighed 57.2 pounds, a weight reduction of 37 percent. The rudder is mass-balanced (the balance weight being mounted on the upper-forward rudder), so an additional 2.2 pounds could be removed from the balance weight for each pound of weight saved on the aft rudder (another 75 pounds). A total weight reduction of 109 pounds could be realized, a reduction of 120 percent of the weight of the metal structure being replaced. However, to meet the objectives of this program at minimum cost, the balance weight installation will not be reworked. The rudder assembly will, therefore, be conservatively over-balanced on aircraft with the graphite rudder installed.

TOOLING CONCEPT DEVELOPMENT

The tooling concept for the rib-stiffened box was a simple extension of the thermal expansion tooling concept (Figure 4). The hard tooling included all external lofted surfaces of the rudder and internal metal mandrels within each of the rib bays, see Figure 8.

Feasibility of the tooling concept was demonstrated through the fabrication of eight development components on the form mold die (FMD) shown in Figure 9. The side plates of the FMD (2-inch steel plates) were removed for clarity. The internal metal mandrels and the cast room temperature

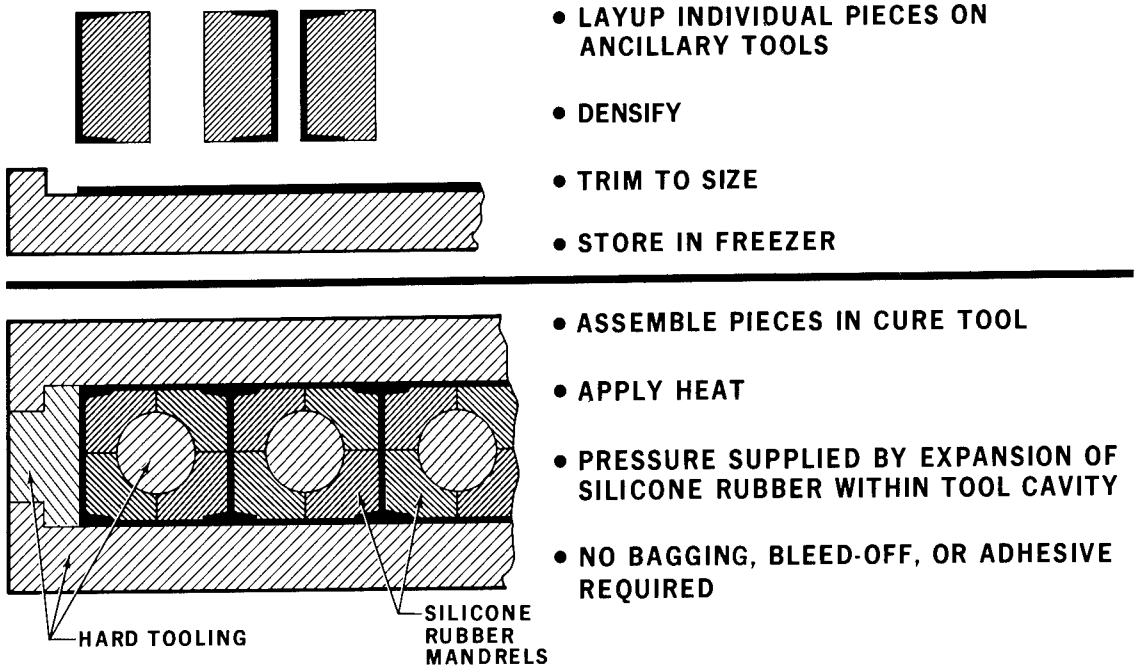

FIGURE 8. SCHEMATIC OF RUDDER TOOLING CONCEPT

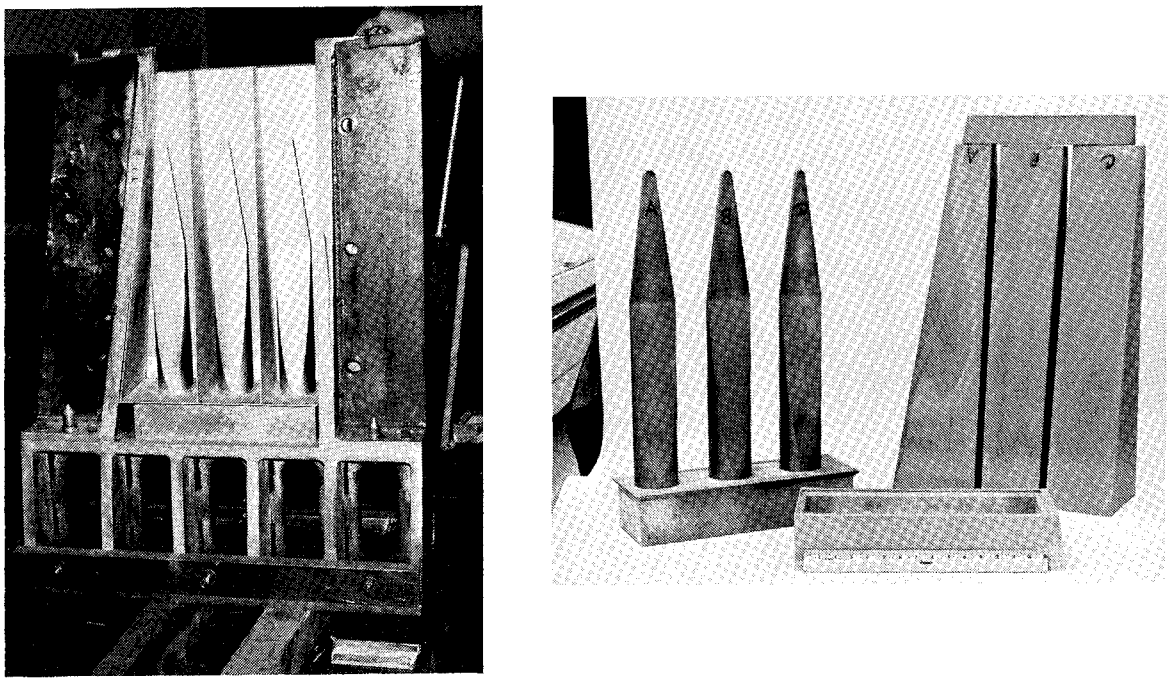

FIGURE 9. FEASIBILITY DEMONSTRATION TOOLING

vulcanizing (RTV) rubber mandrels are shown separately. The rubber mandrels were subsequently cut into segments for removal through the three holes in the front spar of the development component provided for the internal metal mandrels.

Four significant problems were encountered during fabrication of the development components. These problems are summarized in Table 4. During the first cure cycle, excessive pressures were developed in the Silastic "J" rubber mandrels (estimated at 1000 to 1500 psi) and two of the 1-inch-diameter tooling bolts retaining the side plates failed in tension. The heatup rate was also very slow due to the mass of the FMD.

The internal metal mandrels were redesigned and the rubber mandrels were recast (using Dapcocast 38-3) for the second cure cycle. The redesigned metal mandrels reduced the volume of rubber and incorporated internal electrical heaters which increased the heatup rate and reduced thermal gradients through the assembled tool and laminate during the cure cycle. In addition, the metal mandrels were a multipiece aluminum alloy rather than the 1-piece steel mandrel (Figure 9). The aluminum alloy promoted internal heat transfer and the multipiece construction facilitated mandrel removal.

A fiberglass subcomponent, shown in Figure 10, was successfully cured during the second cure cycle. However, considerable shrinkage of the rubber mandrels was discovered after their removal from the three rib bays. The mandrels shrunk approximately 1/4 inch on the chordal dimension of about two feet.

The third cure cycle was attempted using the rubber mandrels which shrunk during the second cycle. Although the laminates were satisfactorily cured, there was poor fiber collimation and regions of large resin accumulation because the undersized mandrels expanded too late during the cure cycle. In subsequent cure cycles, the shrinkage problem was resolved by including a coarse wire mesh screening within the pieces of cast rubber. The screening provided a mechanical restraint against shrinkage and the rubber mandrels were dimensionally stable thereafter.

TABLE 4
SUBCOMPONENT DEVELOPMENT PROBLEMS AND SOLUTIONS

CURE CYCLE	PROBLEMS	CAUSE	SOLUTION
1	ONE-INCH DIAMETER TOOLING BOLTS FAILED.	EXCESSIVE PRESSURE.	CHANGED RUBBER FORMULATION. REDUCED RUBBER VOLUME.
2	RUBBER MANDRELS SHRUNK.	CREEP BEHAVIOR UNDER CURING HEAT AND PRESSURE.	REMADE RUBBER MANDRELS WITH METAL INCLUSIONS TO STABILIZE DIMENSIONS.
3	POOR FIBER COLLIMATION AND LARGE ACCUMULATIONS OF RESIN.	LAMINATE CURED WITH INADEQUATE PRESSURE.	ADDED ELECTRICAL HEATERS WITHIN METAL MANDRELS FOR INSIDE-OUT HEATING.
4	RUBBER MANDRELS STUCK.	CURING HEAT AND PRESSURES.	ADDED TEFLON TAPE AT FAYING SURFACES.
5-8	NONE	–	–

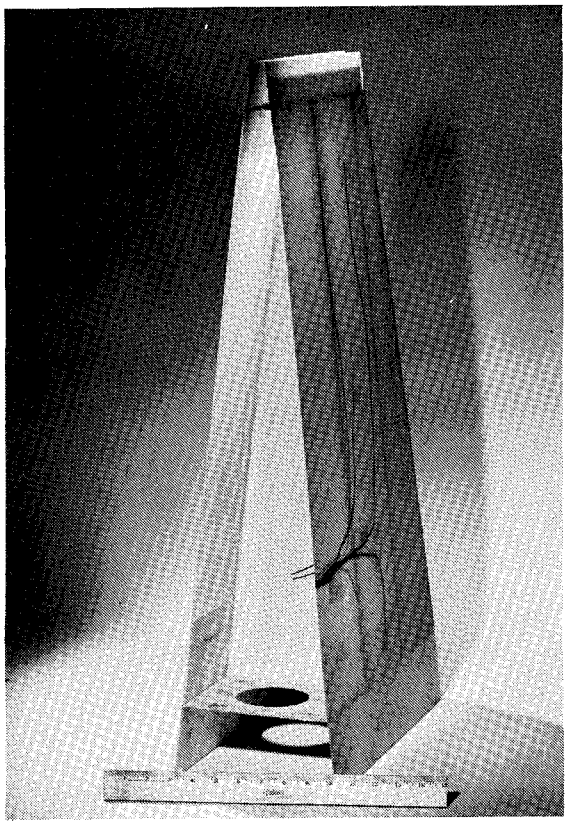

FIGURE 10. FEASIBILITY DEMONSTRATION FIBERGLASS SUBCOMPONENT

During fabrication of the first three subcomponents, removal of the rubber mandrel segments was particularly difficult. Although the mandrels were liberally sprayed with a release agent prior to assembly, the temperatures and pressures sustained during the cure cycles effectively bonded the rubber segments to each other, to the metal mandrels, and to the laminates. This problem was finally resolved by coating the segments with a 3-mil teflon tape at all appropriate faying surfaces.

Four additional subcomponents were fabricated after the metal mandrels were modified to incorporate internal heaters and the rubber mandrels were stabilized with metal screening and coated with teflon. No further problems were encountered and each of the four additional subcomponents was successfully completed.

Construction of full-scale rudder tooling was completed after successful fabrication of the eighth development component. Essential details of the full-scale rudder molding die are shown in Figure 11. The assembled steel tool weighed about 6 tons. It was mounted on tracks to facilitate moving it into and out of the curing oven.

Four graphite rudder boxes were cured during the full-scale proof-of-tooling phase. Significant problems encountered during cure of the first three boxes are summarized in Table 5. After curing the second unit shown in Figure 12, it was concluded that the rubber mandrels had been cast slightly oversize. Although the tooling bolts were carefully torqued, the mold could not be fully closed. The resulting gaps near the rear-spar flanges caused voided laminates in that locality and poor dimensional control. These problems were remedied by recasting the rubber mandrels.

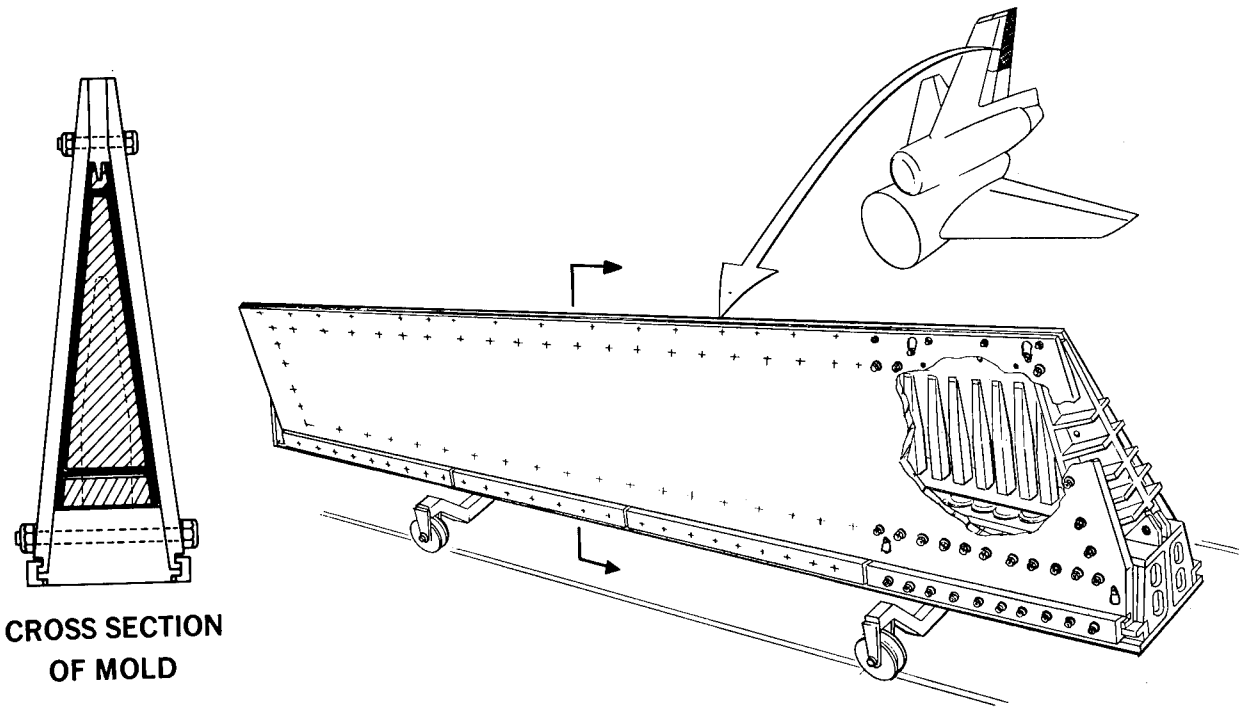

FIGURE 11. COMPOSITE RUDDER MOLDING DIE

TABLE 5

FULL-SCALE RUDDER DEVELOPMENT PROBLEMS AND SOLUTIONS

CURE CYCLE	PROBLEM	CAUSE	SOLUTION
1-2	VOIDED REGIONS NEAR REAR SPAR. POOR LATERAL DIMENSIONAL CONTROL.	UNABLE TO CLOSE MOLD BECAUSE OF OVERSIZED RUBBER MANDRELS.	RECAST RUBBER MANDRELS.
3	REGIONS OF SKIN CURED WITH INADEQUATE PRESSURE.	EXCESSIVE DENSIFICATION STAGING OF SKINS. DEVELOPED PRESSURE TOO LATE IN CURE CYCLE.	REDUCED DENSIFICATION CONDITIONS. EXPANDED RUBBER SOONER WITH INTERNAL HEAT.
1-3	LOCALIZED CRACKS IN FRONT SPAR.	INDUCED STRESSES DURING COOL-DOWN.	ADDED LOCAL LAYERS. IMPROVED PREFORM TECHNIQUE TO REMOVE ECCENTRICITIES.
4	NONE	–	–

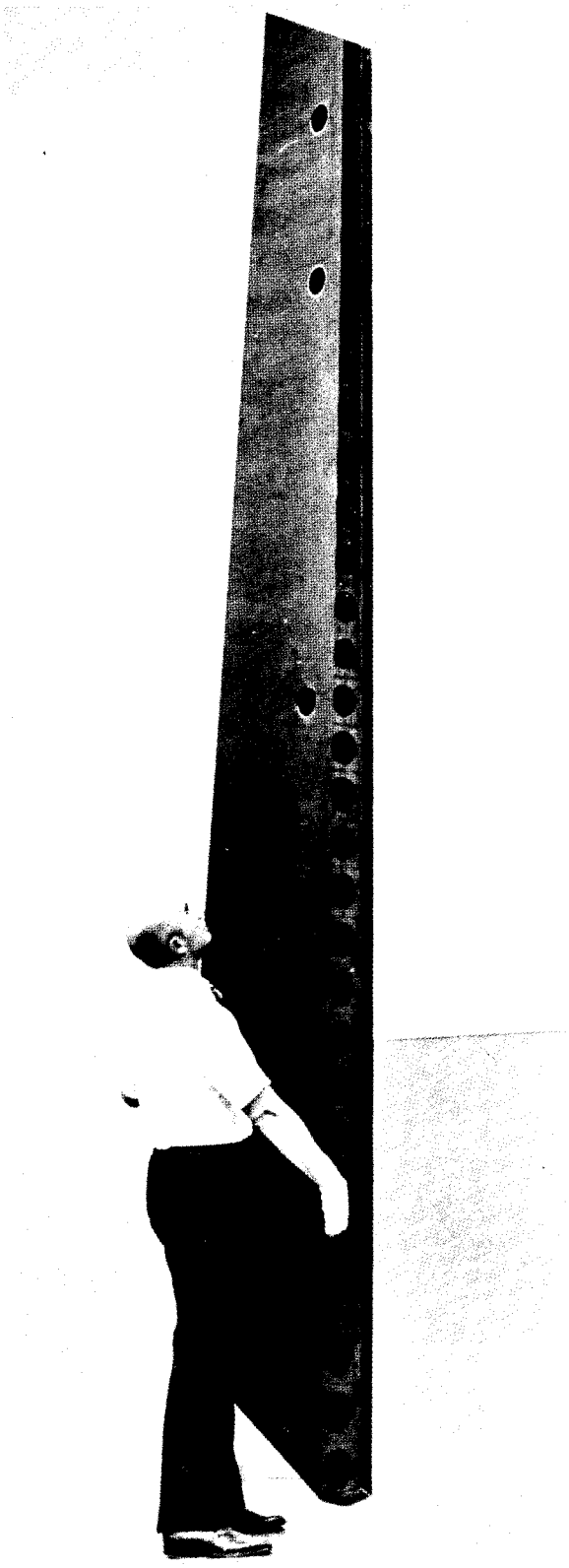

FIGURE 12. GRAPHITE-EPOXY RUDDER BOX ASSEMBLY

The mold was fully closed without difficulty for the third trial cure cycle and the cure was accomplished routinely. When the mold was opened, the laminate resin and void contents were very good and dimensions were within engineering tolerances. However, there were localized regions in the skin panel which had cured with inadequate pressure. Because the skin had been hard densified (about 2 hours at 250°F under vacuum pressure), it was concluded that the skins had cured prematurely before adequate pressure was developed by the expanding rubber. Densification of the laminates for the fourth graphite box was reduced (30 minutes in a 250°F oven under vacuum pressure) and the subsequent cure cycle was satisfactory.

The most difficult problem encountered during full-scale rudder development was the occurrence of localized cracks in the front-spar laminates. These cracks occurred to some extent in each of the first three graphite boxes. After analysis, it was concluded that the predominant cause was laminate deformations induced during cooldown of the mold after the cure cycle. The magnitude of these deformations is illustrated in Figure 13.

The stresses induced during cooldown were intensified by imperfect preforming of the spar laminates in the "B" stage. The spar laminates tended to develop small buckles at the critical cross sections and the resulting bending stresses were sufficient to initiate cracking.

The spar cracks were eliminated in the fourth graphite box unit by increasing the spar-web thickness in the critical region (24 plies rather than 16), preforming the spar details on accurate form blocks, and densifying the forward and aft parts of the spar as a single unit. On completion of quality control tests and inspection, the fourth graphite box unit was accepted for use in the ground test rudder assembly, Figure 14.

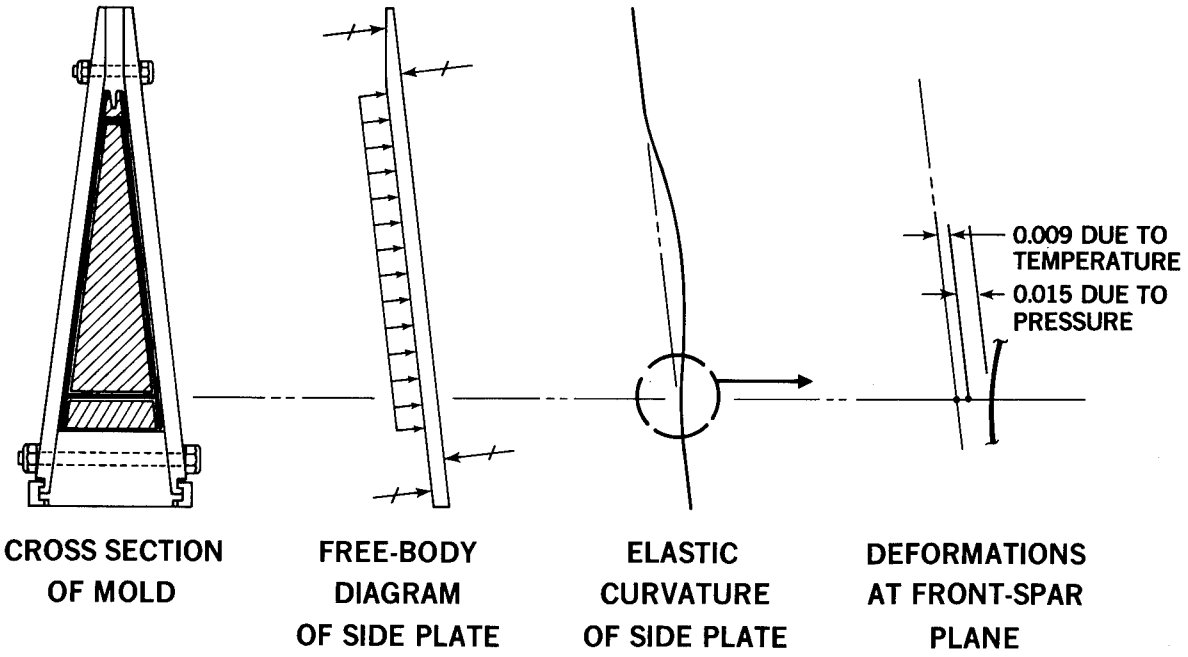

FIGURE 13. INDUCED DEFORMATIONS DURING COOL DOWN

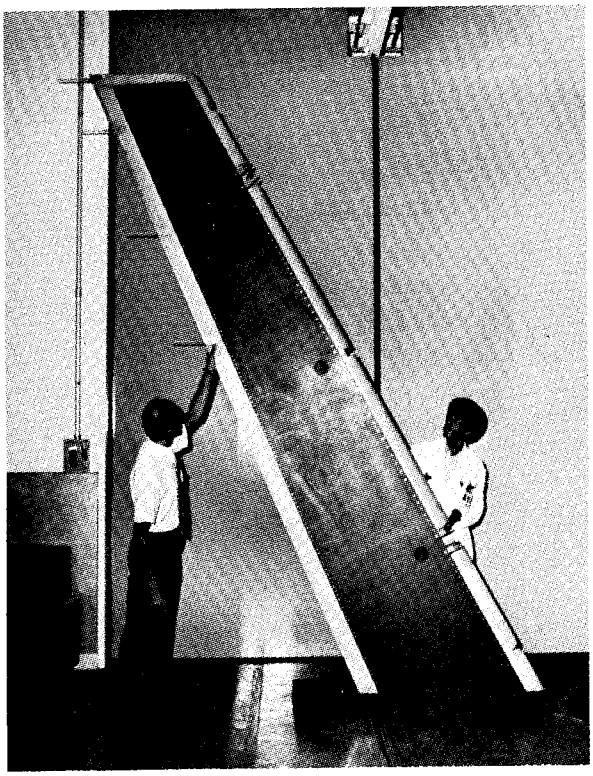

FIGURE 14. GROUND TEST RUDDER ASSEMBLY

DESIGN VERIFICATION TESTS

Engineering tests were conducted on a series of development components in conjunction with the tooling and process development work. The objective of these tests was to verify salient design features of the graphite rudder.

Spectrum fatigue testing was completed on a development component to verify fatigue strength of the graphite laminate and the mechanical fasteners at the hinge and actuator crank fitting attach points, see Figure 15. A simplified but conservative load spectrum was derived to permit testing on a Sonntag machine. Head failures were initially experienced with two types of 1/4-inch-diameter screws because of spurious bending stresses in the screw heads in conjunction with the stress concentrations caused by the screwdriver slots. The 1/4-inch-diameter screws were replaced with HLT336-10 pins (5/16-inch diameter) for increased bending strength at the head to shank interface. Some debonding and delaminating of the specimen was also experienced near the point of test load input, but the laminate was intact in the test section. After repair of the damage, the spectrum fatigue test was resumed and the specimen withstood three lifetimes of fatigue loads without difficulty. On completion of the spectrum loading, a residual static strength test was conducted. The test ultimate design load was 1900 pounds and the ultimate strength of the specimen was 3740 pounds, indicating a positive margin of safety of 96 percent for this loading mode. The fasteners failed in shear and the laminates were secondarily damaged at the bearing surfaces and under the bolt heads due to excessive deformations of the fasteners.

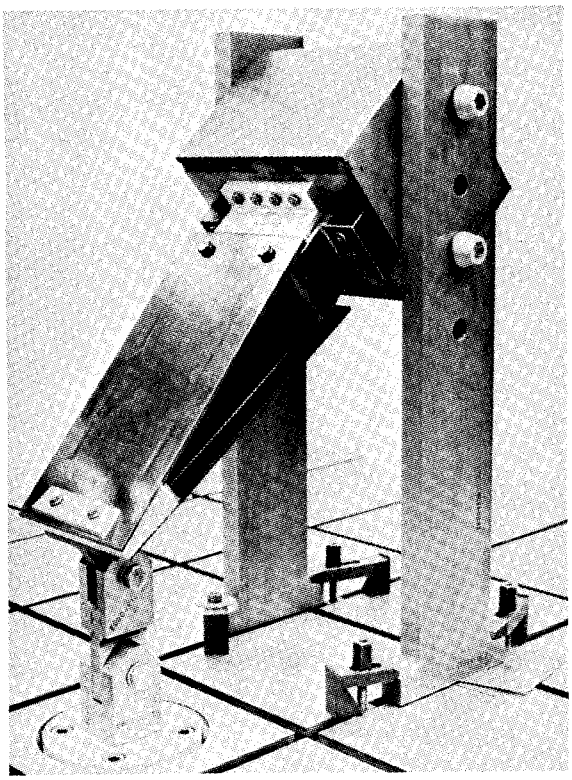

FIGURE 15. HINGE FITTING FASTENER FATIGUE TEST SETUP

Static tests were also completed on a spar component to verify design details in the vicinity of the hinge and actuator fittings as shown in Figure 16. Two separate test setups were used to simulate spar stresses, first at the lower drive station and then at the center hinge station. For the first test setup, the test ultimate design load was 1554 pounds and the ultimate strength of the specimen was 2770 pounds, indicating a positive margin of safety of 78 percent. For the second test setup, the test ultimate design load was 2099 pounds and the ultimate strength of the specimen was 5000 pounds, indicating a positive margin of safety of 140 percent. In each case, the specimen failed initially in a shear mode through a circular cutout in the shear web as shown in Figure 17.

Static tests were completed on a box component, Figure 18, to verify design concepts of the rudder in the vicinity of the critically loaded hinge and actuator fittings. Design details of the fitting attachments and supporting structures were substantiated under design load conditions and several fail-safe variations. The basic test setup is shown in Figure 19. The structural tests were conducted either in an "all well" configuration or in a "failed" configuration in which a single structural element, a drive rod or attach bolt, was intentionally omitted from the structure. In the "all well" configurations, ultimate design loads (150-percent design limit loads) were applied. In the "failed" configurations, design limit loads were applied in accordance with design criteria requirements. The test loads were successfully sustained in all cases. The final test was carried to ultimate strength (failure) of the graphite specimen. The specimen failed in the expected mode (rib-cap compression) at an applied stress of 19,000 psi. The calculated design ultimate stress was 15,500 psi in the critical rib-cap, so a positive margin of safety of 22 percent was indicated.

FIGURE 16. SPAR COMPONENT TEST SETUP

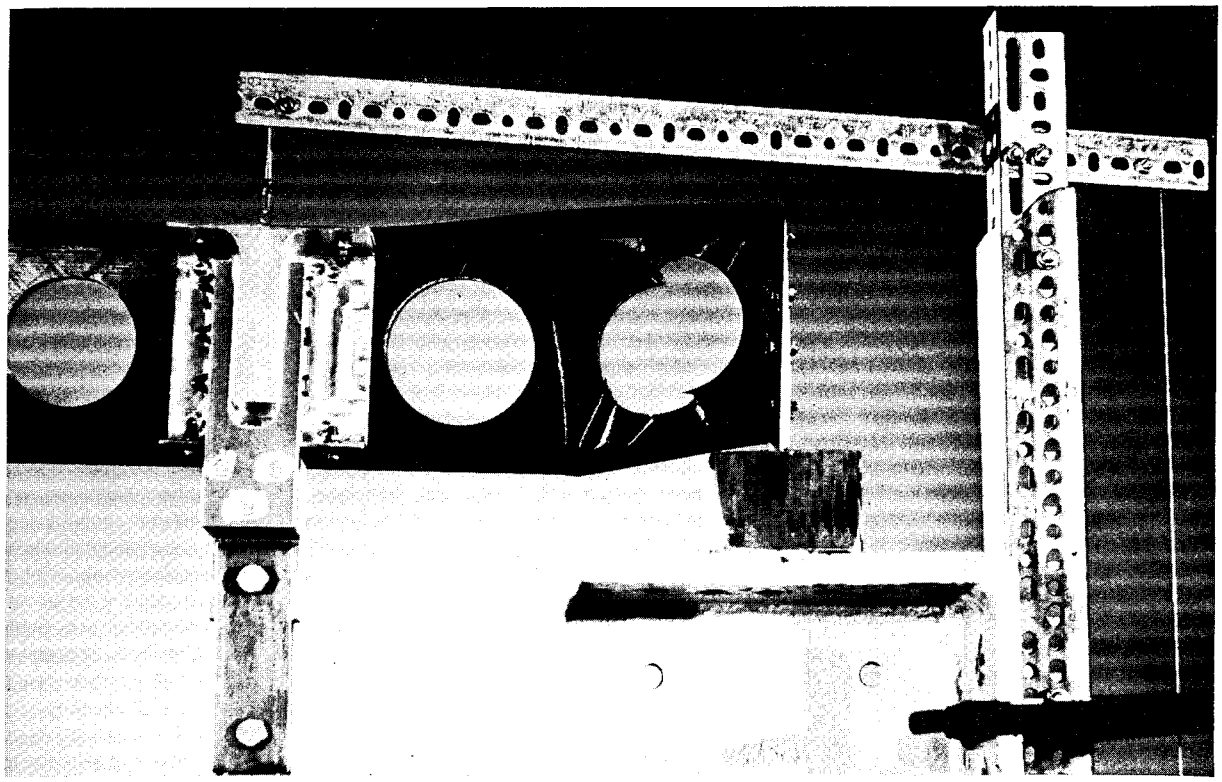

FIGURE 17. SPAR COMPONENT SHEAR WEB FAILURE

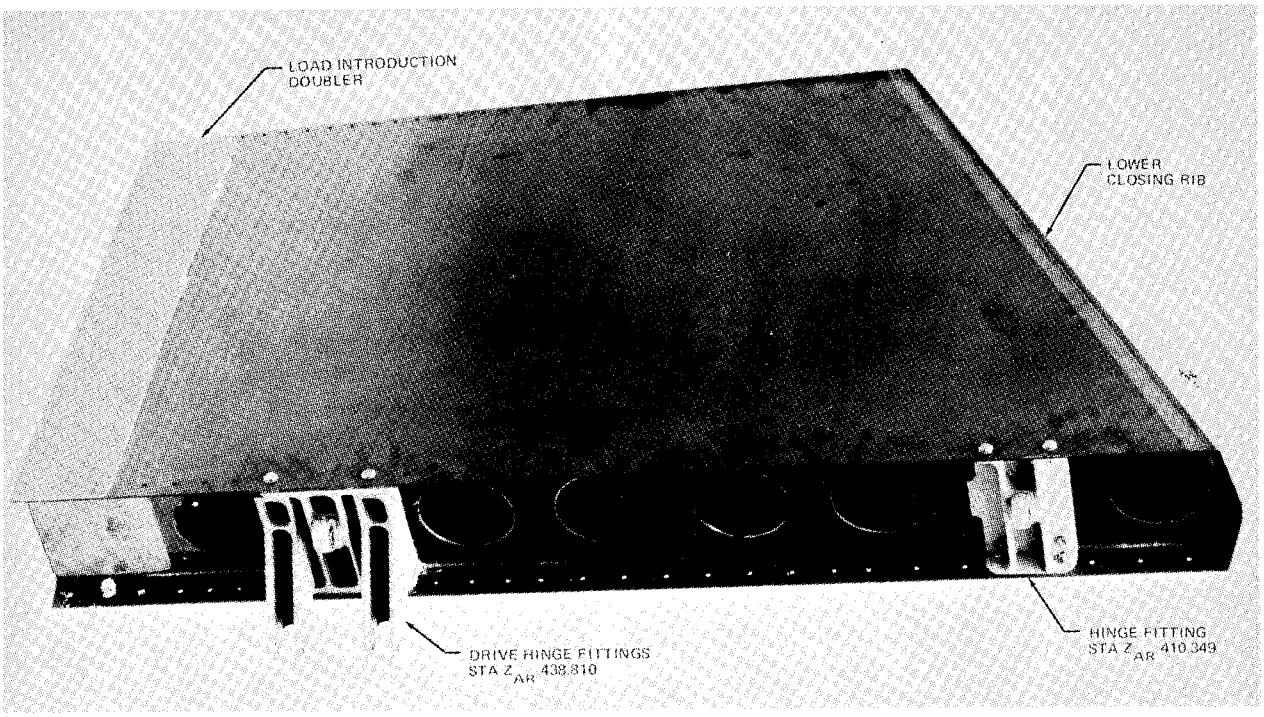

FIGURE 18. STATIC TEST BOX COMPONENT

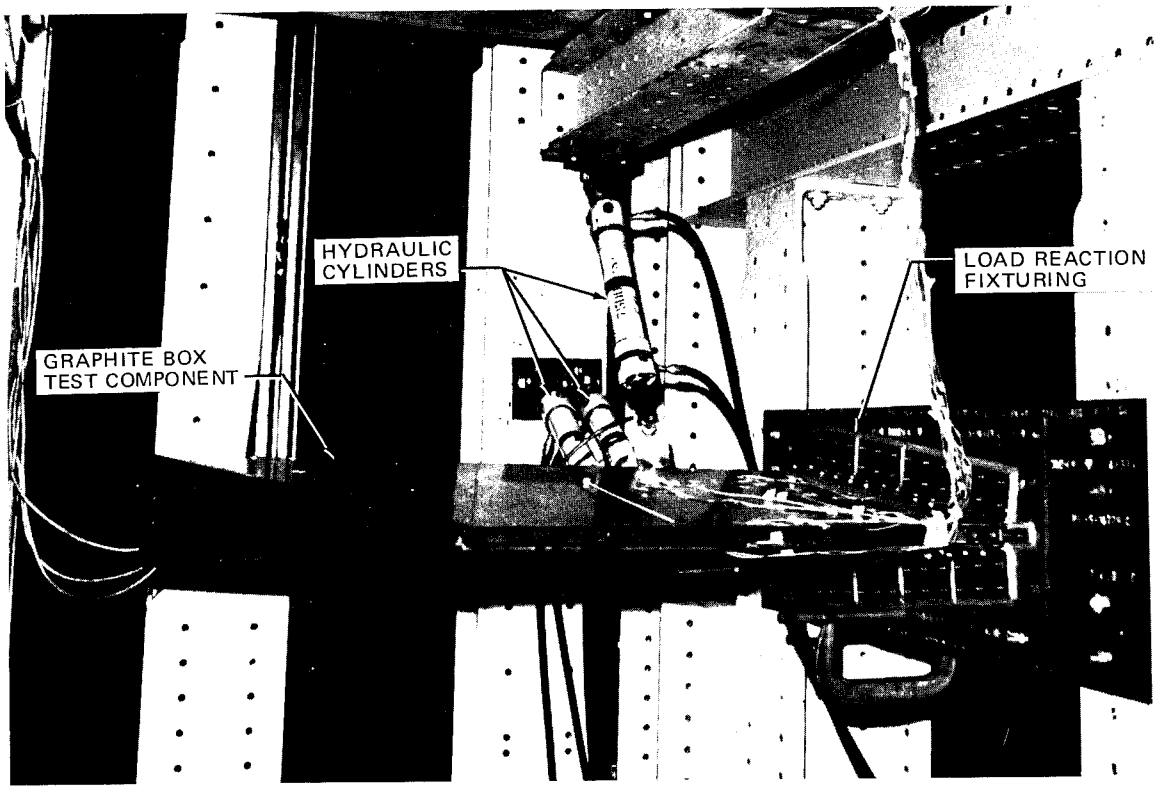

FIGURE 19. STATIC TEST BOX COMPONENT TEST SETUP

Vibration tests were completed on a 3-foot-long box component representing the upper end of the composite rudder. The component was mounted on a vibration test machine using production push-rods and attaching hardware as shown in Figure 20. A modal survey was first conducted and six channels of strain gages were installed to monitor stresses in the component at selected locations on the skin panels. A random vibration environment typifying in-service rudder conditions was applied to the component. The random vibration environment consisted of an 8.6g root-mean-square lateral acceleration over a frequency range of 350 to 1800 Hz. The duration of the random test was 46 hours, the time required to accumulate 100 million stress cycles, approximately three aircraft lifetimes, at 620 Hz, the vibration frequency producing maximum stress in the skin panels of the component. There was no significant damage to the component at the conclusion of testing.

The final design verification tests were conducted on the full-scale ground-test rudder. A typical test setup is shown in Figure 21. All critical flight loads were simulated, including loads induced from forward rudder bending and applied airloads. The rudder structure was substantiated under all critical ultimate stress conditions and fail-safe variations through a series of nine test sequences.

The tenth test sequence duplicated one of the ultimate stress conditions, but the applied loads were increased above ultimate in an attempt to determine the failure load and mode for the rudder. The load was increased to 430-percent design limit load without failure. At this point the test was suspended since the compression whiffletree system was near critical load conditions.

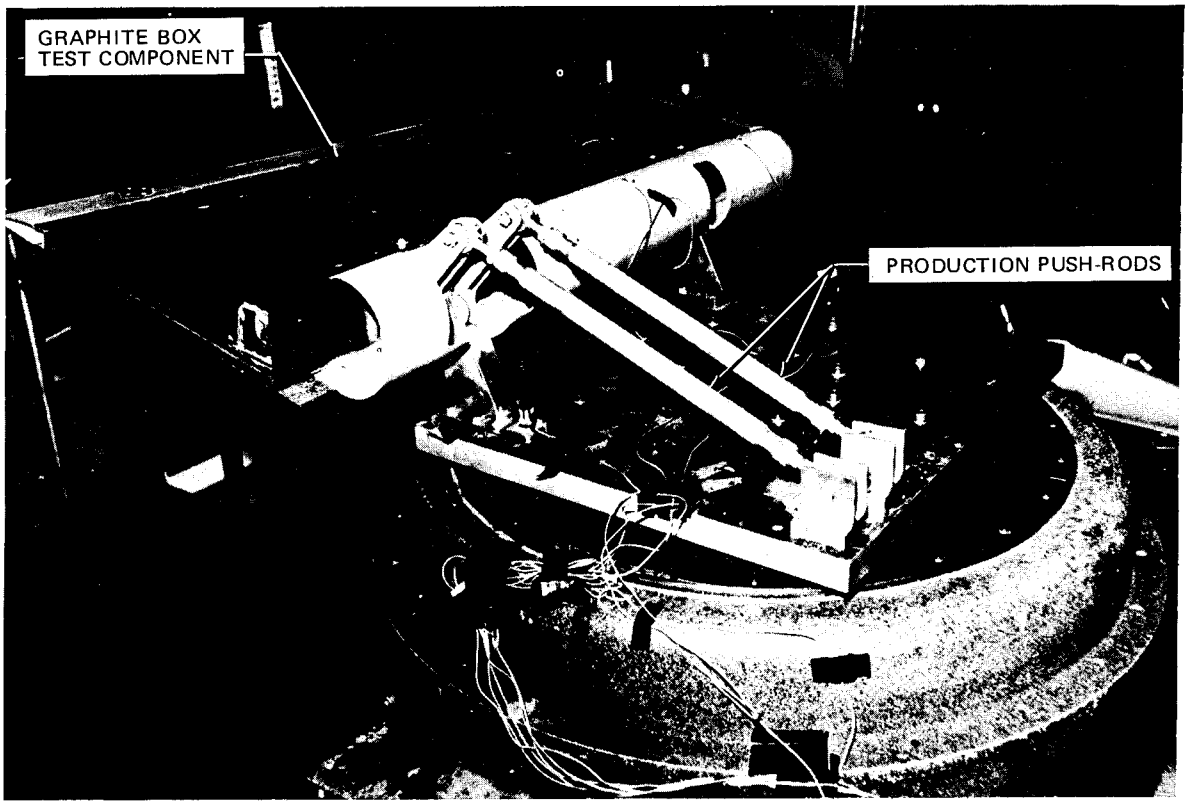

FIGURE 20. VIBRATION TEST BOX COMPONENT TEST SETUP

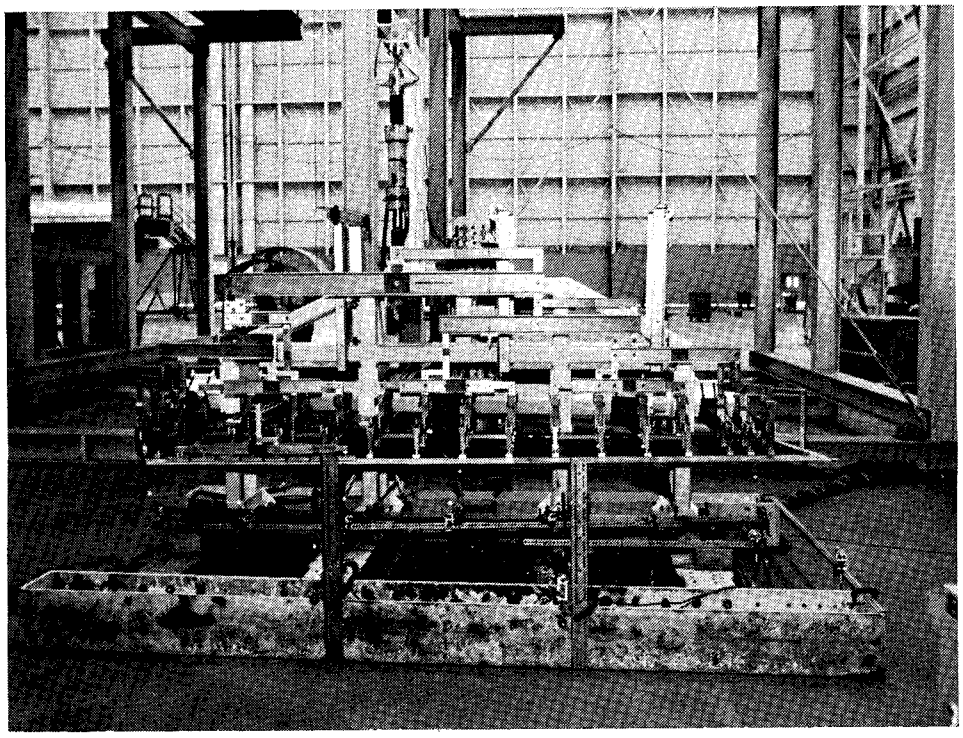

FIGURE 21. RUDDER GROUND TEST SETUP

CONCLUSIONS

An advanced composite rudder for the DC-10 has been designed and developed using a unique manufacturing approach. The rudder was extensively ground tested for strength verification of all critical details of the structural design concept.

The manufacturing approach utilized the thermal expansion characteristics of trapped rubber mandrels to generate curing pressures, thereby eliminating the need for autoclave curing and secondary bonding during consolidation of the structural box. Rubber mandrel development problems were solved by adjustments to the rubber formulation for control of curing pressures, metal screening inclusions to prevent shrinkage, and teflon coatings to prevent sticking. Process development required the incorporation of internal heaters to expand the rubber mandrels early in the cure cycle. Adjustments to the densification cycle of "B" state laminates were required to control resin flow and gelation during the cure cycle. Thermal stress cracks in the cured laminates were eliminated through care in preforming the "B" stage laminate details and through local reinforcement of critical sections.

Although strength levels attained in ground tests are substantially greater than design requirements, a 37-percent weight reduction was achieved. Ground test results are presently being documented for FAA certification and flight service is expected to begin in April 1976.

DEVELOPMENT OF CONCEPTUAL HARDWARE FOR THE LIGHTWEIGHT FIGHTER

By R. Roberts
General Dynamics

Paper not available for publication

SIMPLIFIED LOW COST

ADVANCED COMPOSITE FUSELAGE STRUCTURE

FOR

FIGHTER AIRCRAFT

By Lee Bernhardt

Northrop Corporation/Aircraft Division

SUMMARY

This paper presents the results of a Northrop Corporation Aircraft Division in-house program for the development of a low-cost advanced composite fuselage structure for fighter aircraft. This structural design study was conducted in parallel with an AFML-funded Northrop contract, "Low Cost Manufacturing Concepts of Advanced Composite Primary Aircraft Structures" (Ref. 1), referred to as "MANTEC". The program married these concepts with a simplified design to create a fully interchangeable, advanced composite forward fuselage for the Northrop YF-17 aircraft. The new fuselage is lower in cost and in weight than its metallic equivalent. An all-bonded honeycomb sandwich panel structure was utilized, employing three unique moment-carrying joints. The rationale for these joints, plus their test results are discussed. Estimated cost and weight reductions of 30% and 41% respectively were achieved through this design approach. A side effect was an increased utilization of the aircraft interior space, even though greater structural volume is inherent with sandwich construction. Further efficiencies are possible if standard approaches to structural arrangement and aircraft configuration are discarded in favor of a more truly monocoque design.

INTRODUCTION

Designing an aircraft primary structure of advanced composite materials, at acquisition costs competitive with aluminum is, at first glance, a formidable task. The material substitution approach of past designs cannot achieve this goal. No longer can the designer depend solely on the improved mechanical properties and increased specific stiffness of advanced composites and hope to produce a weight and cost-effective design. The old design parameters and value judgments are no longer necessarily valid. The fundamental question now asked of the designer is: "Is this the most economical design approach to achieve structural integrity and maintain a weight advantage?" The low-cost manufacturing concepts synergized

in the concurrent MANTEC program (Ref. 1) would do much to reduce the final cost of the structure under study. But, options were still available to the designer that were fully compatible with the MANTEC program and these had to be exercised to ensure a low final article cost. No amount of manufacturing expertise or innovation can transform an overly expensive design into a cost-competitive structure.

As this development program was conducted concurrently with MANTEC, a brief description of that program is in order. The MANTEC objectives were to develop and establish manufacturing methods in concert with simplified design approaches for the fabrication and assembly of advanced composite primary aircraft structures that would be cost-competitive with comparable advanced metallic structures.

The MANTEC program goal was the development of a cost-competitive graphite/epoxy YF-17 forward fuselage, utilizing a synergized low-cost manufacturing approach. The principal manufacturing methods utilized were cocuring, vacuum bag curing, reusable rubber bags, no-bleed, and ion graphing control of the curing cycle. Fabrication and testing of both coupons and representative structural elements of the forward fuselage were undertaken to determine the effects of these techniques on the composite's mechanical properties, dimensional stability, and their ease of application to construction of aircraft primary structures. Cost and weight analysis of the representative fuselage structural elements, a two-foot fuselage cross section, and a projected nineteen-foot-long forward fuselage component was completed, demonstrating the cost competitiveness of the developed synergized manufacturing method/simplified design approach.

The second phase of the MANTEC program will include the manufacture and test of three-dimensional joint components, point load introduction structure and a large structural component including the rear cockpit bulkhead. Phase II will demonstrate the scaled-up application of the Phase I two dimensional concepts to a large fuselage assembly.

DESIGN PHILOSOPHY

To achieve a minimum cost design, a basic design philosophy was adopted: simplicity and standardization. Theoretically optimum composite aircraft structure design approach ground rules were formulated to aid in achieving the low cost objective. The salient features of these design optimums are:

1. All composite panels are to be composed of symmetrical face sheets. This produces panels with minimal prestressing and warpage. The panels have less tolerance accumulation, thus reducing assembly fit-up problems. Symmetrical layup of panels also allows the curing of shown and opposite assemblies from neutral plies, and decreases the number of discrete parts and templates requiring traceability and identification.

2. Only 0°, ±45°, and 90° ply orientations are to be used; this reduces the complexity of the wet layup task and simplifies inspection.

3. All panel cutouts are to be cut after panel layup is complete and before cure. This allows the continuous panel plies to be neutral; only the completed panel will be shown or opposite. This production sequence greatly reduces the number of ply templates required for layup. The interior portions of these holes are retained in position in the layup and during cure; when cured they become process control test specimens.

4. All panel cutout edge reinforcement is to be standardized and independent of the face plies. This also allows the face sheet plies to be neutral hand parts, thereby reducing the number of templates required. A finite element analysis of this standardized reinforcement approach has been completed as part of a current in-house composite research program on reinforcing unloaded holes (Ref. 2).

5. All continuous structural panels, whether flat or curved, are to be manufactured as one-piece cocured structural assemblies. Maximum implementation of this rule assures a minimized piece count and its concomitant economies of manufacture.

6. All honeycomb core is to be of constant height; it can then be purchased from the vendor, and most in-house core machining eliminated.

7. All assembly joints are to be bonded joints. Mechanical fasteners for assembly purposes severely reduce the strength of the composite laminates. In the proposed design, use of mechanical fasteners has been limited to the attachment of removable panels, system component mounting, and attachment of metal fittings to the composite structure.

8. Maximum utilization will be made of the drapeability of composites to eliminate manufacturing tolerance accumulation. Where this is not possible, (i.e., the assembly of precured panels), foam adhesives are employed to absorb the tolerances.

These design optimums have but one primary objective— the maximum reduction in labor hours required to build a fuselage. While 100 percent application of these precepts is not possible, their maximum utilization will do much to lower the cost of the fuselage. The practical result of their application is a structure which, because of its basic simplicity, permits maximum dollar return from the synergistic manufacturing approach of the MANTEC program.

DESIGN REQUIREMENTS

As described earlier, the prototype YF-17 forward fuselage was the baseline structural component selected. This component was picked because it represented the most complex and structurally discontinuous portion of an Advanced Technology Air Superiority Fighter Aircraft. The composite forward fuselage would be a completely interchangeable "bolt-on" nose containing all of the systems of the metallic structure. The accessibility of the baseline structure was not to be compromised. The load and temperature spectra were to be identical. The stiffness and dynamic response of the structure had to be equal to or superior to the metallic structure. All this must, of course, be accomplished while minimizing both the weight and cost of the composite nose.

BASELINE DESCRIPTION

The YF-17 (Fig. 1) is a twin-engine fighter aircraft of modest wing sweep with a pronounced leading edge extension at the root, underwing engine air inlets, and twin vertical tails. There are two pylons and a missile launcher on each wing. The forward fuselage (the left-hand side of Figure 2) contains the usual control, avionics, hydraulics, environmental control systems, etc. It also contains the cockpit, nose landing gear, an M61 20mm gun with 500 rounds of ammunition, an inflight refueling receptacle, and a fuel tank containing 680 kilograms (1500 pounds) of fuel.

The structure is conventional, all aluminum longeron and frame, stressed skin construction. The principal longerons are at 10, 2, 4, and 8 o'clock. The frame spacing is approximately 19 cm (7.5 inches) on center. There are four major bulkheads functioning both as shear redistribution members and to provide pressure barriers for the gun bay cockpit and fuel tanks. The cockpit floor, fuel floor and the fore and aft upper cockpit decks complete the pressurized internal structure in the nose. Two fore and aft vertical webs form the nose gear well and support both the nose gear and cockpit floor. The nose also contains numerous decks and access doors. The majority of the latter are structural in nature. The metallic nose structure has a weight of 437 kilograms (963.6 pounds). The forward fuselage/center fuselage production break occurs at fuselage station 370.00; the bulkhead at this station is a portion of the center fuselage and is not included in the weight figure above.

ADVANCED COMPOSITE DESIGN DESCRIPTION

The right-hand side of Figure 2 shows the composite forward fuselage that resulted from this program. It is composed almost entirely of honeycomb sandwich panels. The structural planes remain unchanged from the baseline, with these exceptions: the aft cockpit bulkhead is no longer canted and the fuel tank side walls have been repositioned inboard from the fuselage mold line to eliminate the severe convolutions necessary to form the control cable tunnels running alongside the tank.

A bead-stiffened panel construction was investigated concurrently with the honeycomb design; it soon became apparent that its piece count was inherently greater than that of the honeycomb design. A design study conducted under the Northrop/AFM Advanced Composite Aircraft Conceptual Design Study Program indicated a 13 percent cost increase for a bead-stiffened panel design when compared to an equivalent honeycomb panel design (Ref. 3).

SYSTEM COMPATIBILITY

This design represents a functionally interchangeable low-cost composite forward fuselage. All aircraft systems are unchanged except for minor revisions in equipment support structure and systems routing caused by the relocation of mounting planes resulting from the increased thickness of the honeycomb sandwich structural elements of the forward fuselage. Systems rerouting has been necessary only where the panel cutouts needed to be regrouped to maintain structural integrity in the composite panels. No control system or mechanical components (i.e., nose gear, actuators, canopy mechanism, air conditioning units, etc.) have been revised.

DESIGN ADVANTAGES OF HONEYCOMB PANEL CONSTRUCTION

There are several distinct advantages to the honeycomb sandwich panel approach when designing in composites. When honeycomb panels are fabricated as cocured subassemblies, the core-face sheet fitup problems normally encountered in all metallic honeycomb panels are completely eliminated. The use of honeycomb stiffened panels largely eliminates the need for fuselage frames, deck beams and bulkhead stiffeners, resulting in an impressive piece count reduction and the elimination of many subassembly bonding operations. Additionally, since the honeycomb face sheet panels have, at most, half the ply count of a plain panel, the problems of resin content control and panel thickness variations are greatly reduced. Finally, the lack of definitive data on the effects of buckling on solid composite panels is not a design consideration in a nonbuckling honeycomb sandwich design.

The structure is composed of low-pressure and low-temperature cured Thornel 300/SP-288 graphite epoxy laminates unless otherwise specified. All core material will be aluminum alloy honeycomb coated with a corrosion preventive compound. FM-37 foam adhesive and/or FM-123 film adhesives are used in all adhesive bonding assembly operations.

Figure 3 depicts the final assembly sequence of the forward fuselage. This illustration, plus the piece count comparisons given in Figure 2, truly shows the reduction in complexity achievable with this simplified design approach. The resultant structure is devoid of mechanical fasteners for all primary structural joints. Fasteners are used only to attach removable structure or system components and mechanisms. The completed fuselage is,

in fact, a highly monolithic structure with a remarkable reduction in stress gradients as compared with conventional metallic structure.

As there is little of design interest in a simple honeycomb panel, a detailed structural description would be tedious and of little importance. Similarly, access requirements and system mounting provisions were accomplished in ways already familiar to the designer. Therefore, a detailed structural description is not included in this paper.

A design composed entirely of sandwich elements does, however, pose certain difficulties unique to honeycomb construction. These difficulties arise when attempting to join separate panel assemblies. The problem is particularly acute at the juncture of three noncoplanar details (e.g., a sidepanel-bulkhead-floor intersection).

Many joints, both rigid and pinned, were considered in an attempt to eliminate flatwise tension stresses. Obviously, the complete elimination of these stresses in the laminates was unlikely. Some relief was available through the use of mechanical fasteners in pinned joints of construction similar to that found in metallic honeycomb structure; this approach resulted in increased weight and complexity. It was also felt the presence of mechanical fasteners tended to reduce structural integrity and posed sealing problems in this region. It soon became apparent that few panel edge joints could be made to turn the corner while retaining their structural continuity. Significantly, more design hours were spent on joint design during this project than is customary with more conventional structural systems, whether metal or composite.

Three basic types of bonded joints were developed, the application of which is governed principally by the load intensity and mode experienced at the specific location. These three generic joints are all moment-carrying joints rather than the pin-ended joints common to metallic construction. They generally supply a direct load path between all face sheets in the constituent panels. With varying degrees of success, they effectively allow the full depth sandwich panel to "turn the corner", while keeping face sheet thicknesses and piece count minimized.

The stress levels and/or load intensities in these joints are also amenable to design alteration. By this, we mean changes in joint geometry or face sheet thickness can reduce stress levels or lower loads to produce a structurally acceptable joint. In most instances, these joints avoid load paths dependent on interlaminar or flatwise tension for strength.

Because of their uniqueness, the bulk of the design description will concern itself with design, structural behavior and testing of these joints.

COCKPIT CORNER JOINTS

The cockpit corner rigid joint (shown in Figure 4) is utilized in all pressurized areas of the nose with the exception of the fuel tank section.

The final joint configuration was selected for the following reasons. First, it is the simplest configuration of the many joints studied. Only one additional piece of honeycomb core per edge is required to complete this joint. Secondly, and perhaps most important, by varying the edge core density, and/or the interior and exterior corner radii, the designer has some control over the flatwise tension stresses without increasing the complexity and piece count of the joint. Finally, as this joint does not thin down the intersecting members, it results in less deflection under load than a pinned joint and is thus less susceptible to deflection induced peel stresses.

Figure 4 also shows the most critical loading mode (i.e., internal pressure) of a cockpit corner joint and a free body diagram of the resultant internal loads. The highest margin of safety existing in the joint is for normal tension (W_D). This is deliberate, as it is felt to be the mechanical property most subject to degradation with heat and moisture. It is readily apparent that all of the joint margins of safety can be increased by increasing face sheet thickness core density or corner radii.

The joint face sheets are composed of $90°/0°/90°/\pm45°$ laminates. The panel core is of 0.48 cm (0.187 in.) cell 72 kg/m^3 (4.5 lb/ft^3) density 5056 AL honeycomb core. The formed and machined corner core element is of increased density, it being 98 kg/m^3 (6.1 lb/ft^3). The precured internal tee is of $\pm45°/90°/\pm45°$ construction bonded to an extruded foam fillet. This tee is bonded to the bulkhead panel in a subassembly operation. The side panel and bulkhead are positioned in the assembly fixture with a layer of film adhesive between the tee and the side panel outer face sheet. The core corner elements and adhesives are put in place and the prepreg strips connecting the interior face sheets are applied. The resulting assembly is then bagged and cured.

Tests were conducted on an asymmetrical configuration with only one piece of formed core present. The other side of the joint (the unpressurized side) is a half-socket joint. Manufacturing difficulties were experienced in the fabrication of this joint and design changes were made to eliminate these problems. Increasing the corner radii of the interior tee and preforming the foam fillet allowed the vacuum bag pressure to be better transmitted to the interior of the joint, eliminating the voids experienced with the original design. Two asymmetrical joints, of the many produced, were free of voids and successfully withstood design loads, and test specimen strain gage readings corresponded well to the analytically predicted strains.

FOAM BONDED SOCKET JOINTS

The wheel well web socket joint in the cockpit floor (see Figure 5) is formed by an interruption of the panel core and lower face sheet. The side of this socket is formed of two precured angles cocured to the floor panel. This socket has been widened to allow for manufacturing tolerance buildup. A series of simple lap joint tests were conducted to ascertain the effect of gap variation and foam expansion on the strength of the foam bonds. These test results were used to set the tolerances permissible for the socket. The wheel well webs will be bonded, on final assembly, to the floor panel with adhesive foam. Foam adhesive (Reliabond 370B) is used to minimize the weight penalties incurred in joining panels where manufacturing tolerances produce gaps at the joint interfaces. Both panels are cured prior to assembly and are joined with foam-in-place adhesive. The socket-type joint employed eliminates most of the structural discontinuity, potting, and flatwise tension stresses normally encountered in tee joints of honeycomb panels where the panel is not pierced.

The socket-type joint is generally restricted, in this design, to joints where the continuous panel is subjected to modest in-plane bending loads.

Figure 5 also shows the principal loading mode, free body diagram and critical internal load table of the socket joint. It is obvious that the most critical stress is the tension stress developed between the inner face sheet flange of the tee cap and the tee leg face sheet. Some reduction in this stress is possible by increasing the cap core height. However, if moment joints, as previously described, are used at the cap edges, a condition met in this design, the in-plane bending moments experienced in this panel are considerably reduced from what are normally experienced in pin-ended panels, greatly expanding the utilization of this type of joint.

The socket joint test results are shown in Figure 6. The joints were subjected to various loading modes other than those experienced in the specific applications described. This was done to further define the "structural envelope" of the socket joint to increase the applications of this, the most simple joint devised in this program.

FUEL TANK JOINT DESIGN

A further development of the moment joint concept is the fuel tank corner joint shown in Figure 7. This design is employed at all right angle panel junctures in the fuel tank. The joint is essentially one-half of the cockpit corner joint, with the exterior face sheet corner radius increased to its maximum in relation to the interior radius (i.e., constant panel thickness around the corner). This is necessitated by the high 2.9×10^5 N/m^2 (42 psi) internal fuel pressures experienced during a 40g

crash condition. Extensive testing of this joint was conducted, as it is the most highly loaded panel joint in the nose.

It must be noted that the design depicted is not really an assembly joint as such, as the fuel tank is laid up as a one-piece five-sided box. The inner face sheet is laid up first on a bagged male plug. The preassembled core halves are then positioned on the tool and the outer face sheet laid up on the core. Proper tape orientation is impossible to maintain in the spherical corners, so formed graphite/epoxy cloth patches are used in this area. The face sheet laminate is of $0°/90°/0°/90°\pm45°$ stacking. The second 0° ply is actually not needed structurally, but its inclusion simplifies layup.

The completed tank layup is enclosed in a split female bonding fixture, vacuum applied to the silicone rubber bag and the male plug is removed. The thus fixtured assembly is ready for curing.

This joint underwent extensive testing, as it is the most highly loaded panel joint in the nose. These test results are shown in Figure 8. Failure modes and strains correlated well with the joint analysis. The lower failure loads of the autoclave cured specimens were attributable to the increased face sheet dimpling caused by the higher pressures experienced during cure.

COST AND WEIGHT ANALYSIS

Throughout both the design program and concurrent MANTEC (Ref. 1) program, weight and cost were continually monitored. Actual labor hours were compiled for all of the joint test specimens manufactured. Actual and calculated weights of these test specimens were compared. Similar cost and weight tracking was conducted during the fabrication of a two-foot cross section of the fuselage through the fuel tank area (see Figure 9).

The actual weight of the two-foot cross section proved to match the calculated weight within 0.5%. This was most gratifying, as it meant that the actual quantities of core potting compound and foam adhesives used matched the engineering drawing estimates, and the design's feared high sensitivity to weight gain from excess adhesive and potting failed to materialize.

With the cost and weight performance of the joint specimens and fuselage cross section in hand, an estimate of the entire forward fuselage cost and weight was made. Figure 10 shows the results of that effort. The 31% cost savings shows almost uniform reductions in material, recurring and non-recurring costs in comparison with the metallic baseline.

The weight reductions are equally impressive at 41%. The unitizing, rigidizing and simplifying of the structure produced similar synergistic effects, as did the MANTEC program's combination of low-cost manufacturing techniques. The monolithic nature of the structure makes it practically free of high stress gradients, and the structural elements are correspondingly uniform in thickness.

CONCLUSIONS

The program has successfully combined a simplified design approach with a variety of low-cost manufacturing approaches to produce an eminently viable forward fuselage which is both lighter and more economical than its metal counterpart. Deflection analysis indicates one-third the deflection of the metallic nose. Even though the structural volume is increased through the use of honeycomb sandwich construction, the usable interior volume is appreciably increased as the composite structure is practically as smooth and uncluttered on the inside as it is on the outside. Its monolithic nature greatly reduces the complexity, cost and weight of the fuel system. No fuel bladders are necessary, as the structure by its very nature is fuel tight and the fuel tanks are devoid of entrapped air. Systems routing is also simplified (e.g., no frames to pierce) and hand access is unimpeded by the usual structural clutter of conventional structure.

While the general results of the program have been most satisfactory, certain problem areas and constraints remain. Principal among the problem areas are longerons. Thick shapes in composites are to be avoided, as recurring labor costs increase directly with thickness in composites, which is not true in metal. It is doubtful that the longerons in the forward fuselage are cost competitive by themselves. Their use is forced on the designer because the baseline aircraft was originally configured in metal and the forward fuselage had to mate with a metalic center fuselage which contained mating longerons.

To fully maximize the economies of advanced composites, it is felt that a given vehicle must be configured mindful of the unique properties and requirements of advanced composites. Fuselage configurations approaching full monocoque palletized systems and ellipsoidal access doors are but two items to be considered for composite structures. If all-metal construction changed the shape of aircraft, it is not too much to assume that all composite construction will change more than just the color of aircraft.

It is felt that the structural concepts presented here may be advantageously applied to both center and aft fuselage structure. These design precepts, if not the design specifics, can be applied to wing and empennage structures. Current in-house design study efforts to this end are being conducted.

REFERENCES

1. D.L. Stansbarger, Et Al: Low Cost Manufacturing Concepts of Advanced Composite Primary Aircraft Structures. AFML-TR-75-145, September 1975.

2. N.M. Bhatia: Stress Concentration, Fracture Behavior, and Design Procedures for Advanced Composite Laminates with Reinforced Cutouts. NOR-74-345, Northrop Corp/Aircraft Division, Oct. 1975.

3. J.V. Noyes, Et Al: Advanced Composite Aircraft Conceptual Design Study, Interim Progress Report, Air Force Materials Laboratory, Air Force System Command, Wright Patterson Air Force Base, Ohio, dated 14 May through 13 October 1973, Contract No. F33615-73-C-5095, Project No. 6169CW.

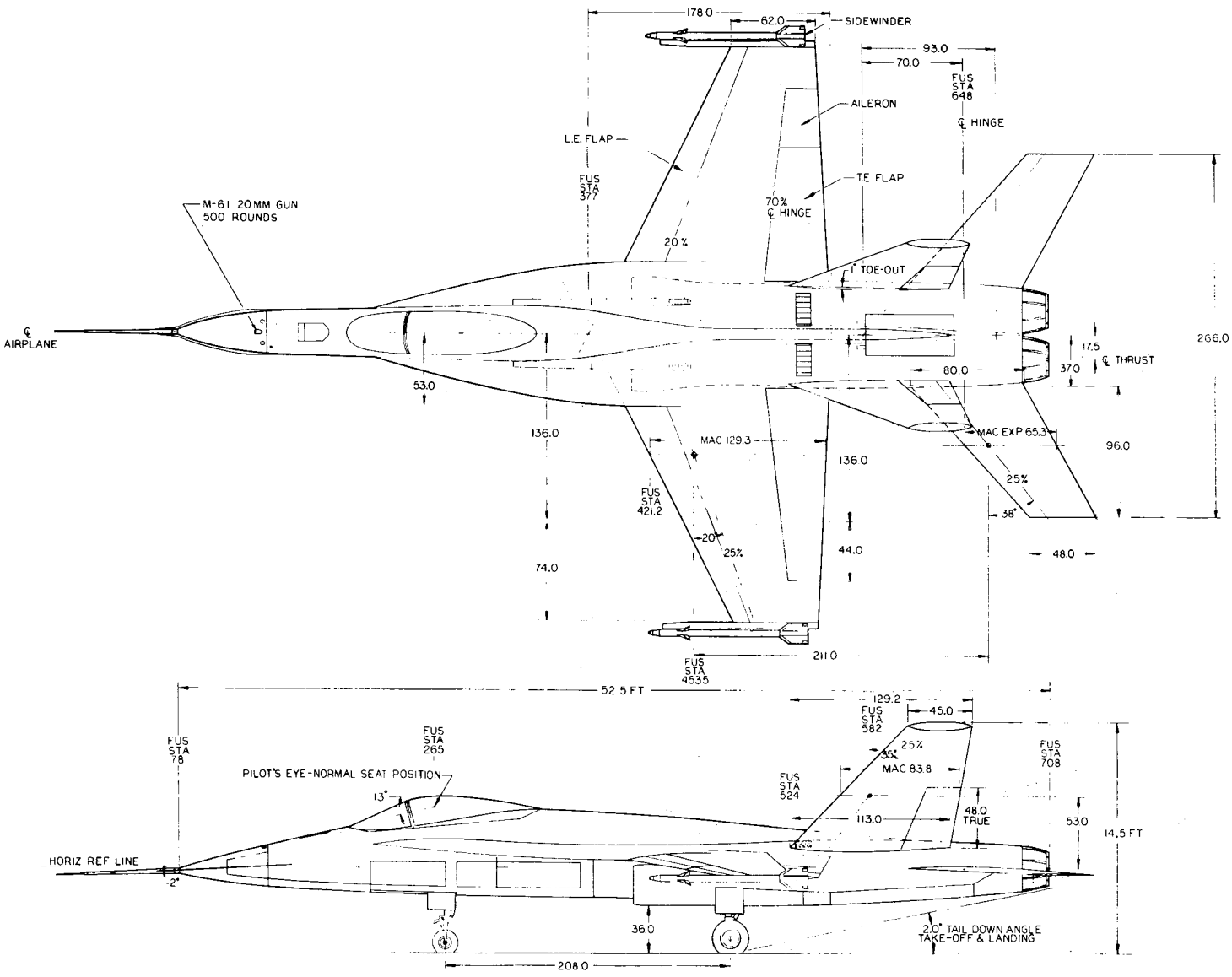

Figure 1. - YF-17 Baseline Aircraft

YF-17 METALLIC DESIGN

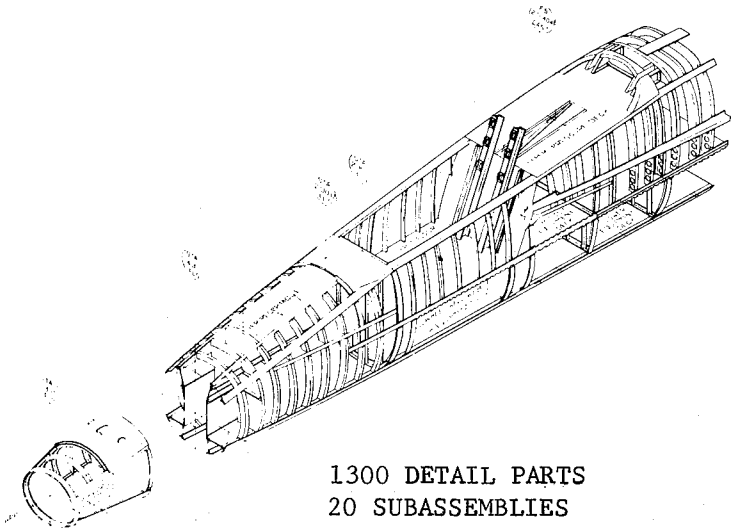

1300 DETAIL PARTS
20 SUBASSEMBLIES

COMPOSITE DESIGN

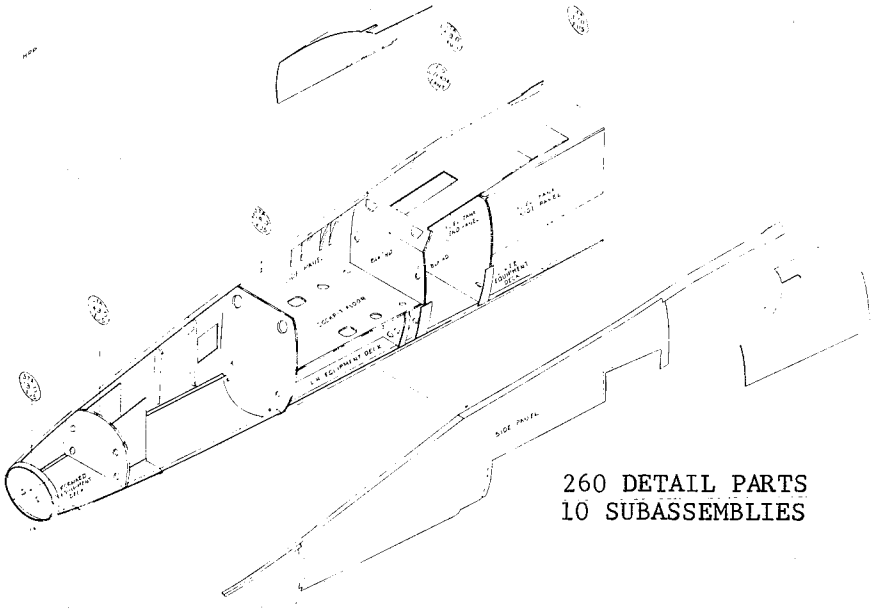

260 DETAIL PARTS
10 SUBASSEMBLIES

Figure 2. Effects of Simplified Design

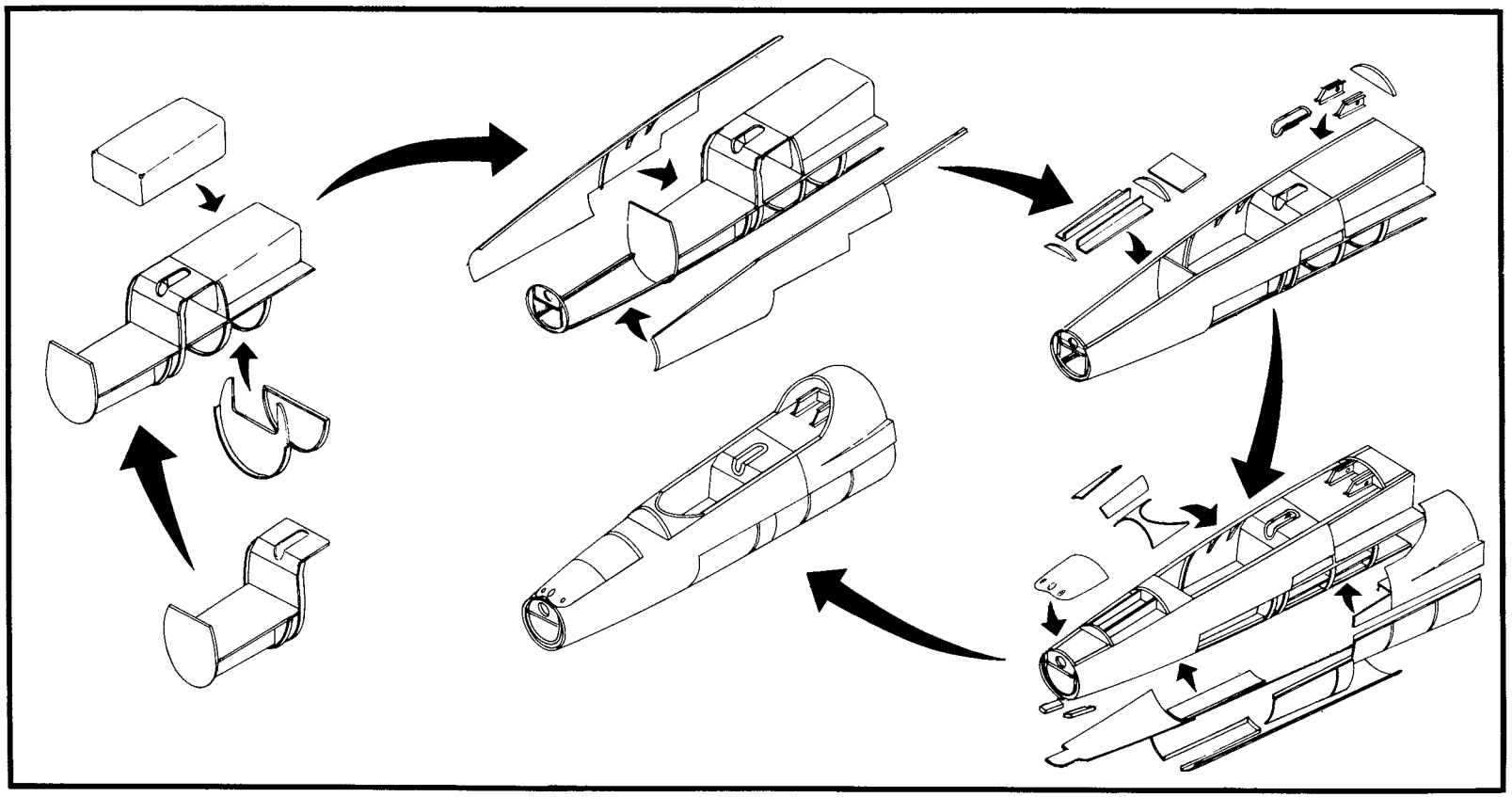

Figure 3. - Final Assembly Sequence

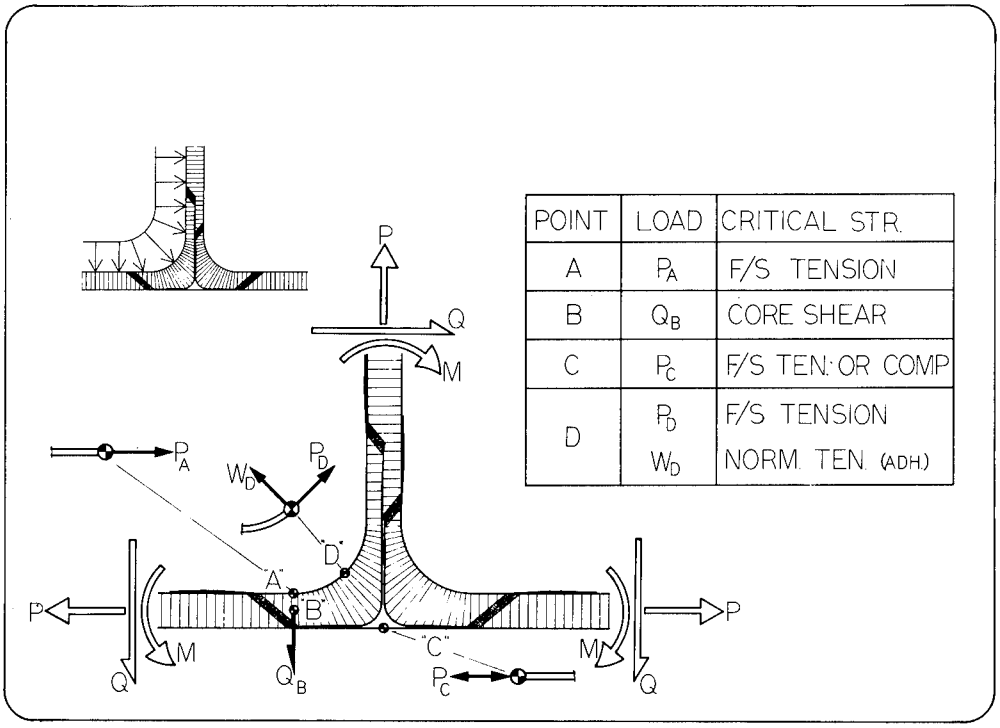

POINT	LOAD	CRITICAL STR.
A	P_A	F/S TENSION
B	Q_B	CORE SHEAR
C	P_C	F/S TEN. OR COMP
D	P_D	F/S TENSION
	W_D	NORM. TEN. (ADH.)

Figure 4. - Cockpit Joint Loading Diagram

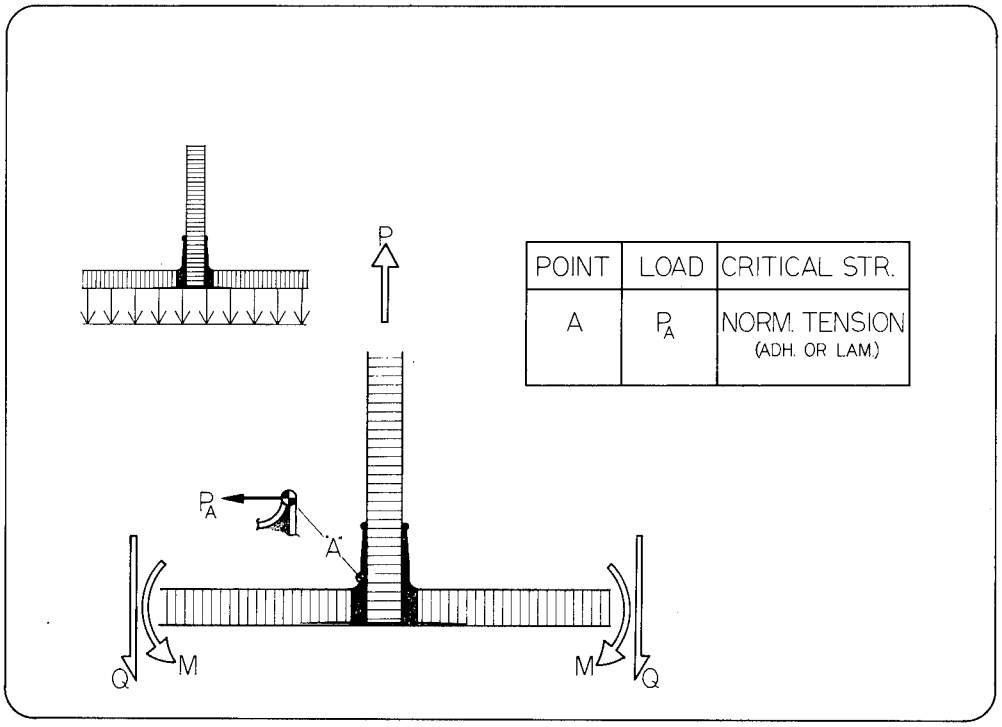

POINT	LOAD	CRITICAL STR.
A	P_A	NORM. TENSION (ADH. OR LAM.)

Figure 5. - Socket Joint Loading Diagram

LOADING CONDITION	SPECIMEN CONDITION	TEST TEMP.	FAILURE UNIT LOAD
COMPRESSION 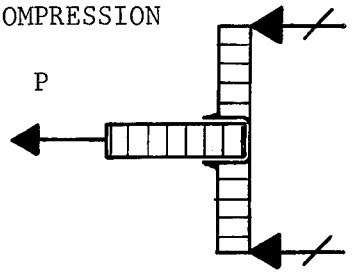	DRY	102°C (215°F)	15.2×10^3 N/m (87 lb/in)
	DRY	-55°C (-67°F)	45.9×10^3 N/m (262 lb/in)
	DRY	R.T.	53.7×10^3 N/m (307 lb/in)
	WET	R.T.	42.0×10^3 N/m (240 lb/in)
	DRY	R.T.	52.0×10^3 N/m (4) (298 lb/in)
TENSION 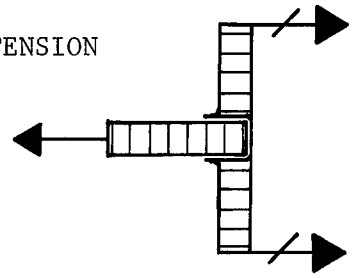	DRY	102°C (215°F)	6.48×10^3 N/m (37 lb/in)
	DRY	R.T.	27.8×10^3 N/m (159 lb/in)
TRANSVERSE TENSION 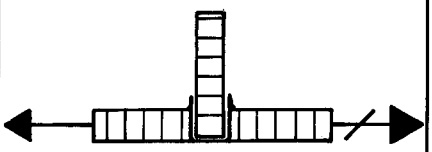	DRY	102°C (215°F)	96.5×10^3 N/m (551 lb/in)
	DRY	R.T.	156×10^3 N/m (893 lb/in)
	WET	R.T.	140×10^3 N/m (800 lb/in)
BENDING 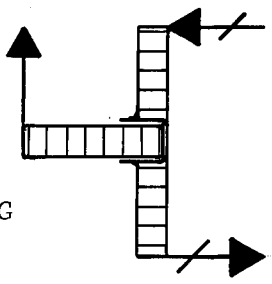	DRY	R.T.	21.0×10^3 N/m (120 lb/in)

1. ALL SPECIMENS VACUUM BAG CURED
2. MEASUREMENTS WERE MADE IN ENGLISH UNITS
3. WET DENOTES 45 DAYS IMMERSION IN 82°C (180°F) WATER
4. RESIDUAL STRENGTH AFTER 32,000 CYCLES WITH MIN. LOAD/MAX. LOAD = 0.2

Figure 6. - Socket Joint Test Results

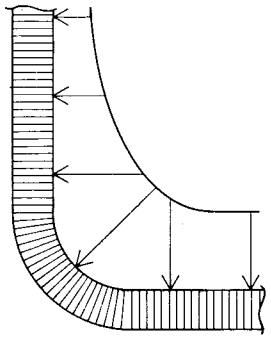

POINT	LOAD	CRITICAL STR.
A	Q_A	CORE SHEAR
B	P_B	F/S TENSION
	W_B	NORM. TEN. (ADH.)
C	P_C	F/S COMP.
	W_C	NORM. TEN. (ADH.)

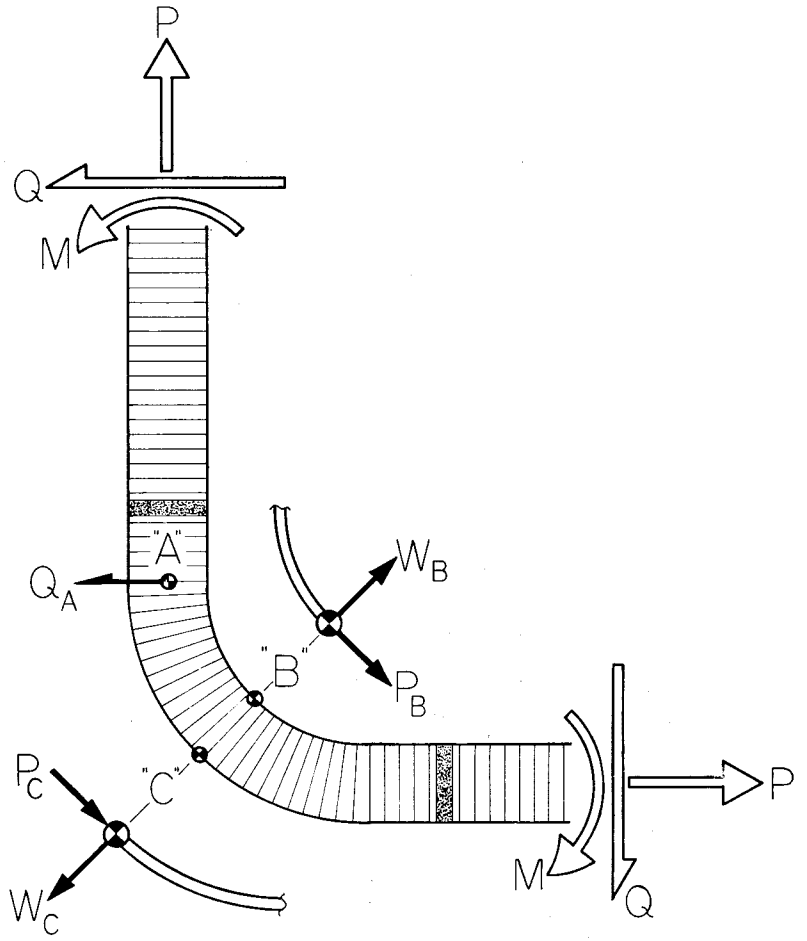

Figure 7. - Tank Corner Loading Diagram

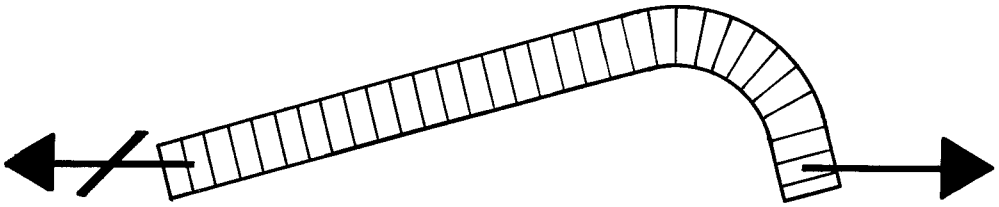

SPECIMEN CONDITION	LOADING	TEST TEMP.	FAILURE UNIT LOAD	% DES. ULT.
AC DRY	STATIC	R.T.	120×10^3 N/m (684 lb/in)	150
AC DRY	STATIC	-55°C (-67°F)	129×10^3 N/m (738 lb/in)	162
AC DRY	STATIC	57°C (135°F)	109×10^3 N/m (625 lb/in)	138
AC DRY	R.S.	R.T.	129×10^3 N/m (738 lb/in)	162
VB DRY	STATIC	R.T.	137×10^3 N/m (780 lb/in)	171
VB DRY	STATIC	57°C (135°F)	124×10^3 N/m (712 lb/in)	157
VB DRY	R.S.	R.T.	135×10^3 N/m (767 lb/in)	168
VB WET	STATIC	R.T.	131×10^3 N/m (750 lb/in)	165
VB WET	STATIC	-55°C (-67°F)	131×10^3 N/m (750 lb/in)	165
VB WET	STATIC	57°C (135°F)	131×10^3 N/m (750 lb/in)	165
VB WET	R.S.	R.T.	130×10^3 N/m (745 lb/in)	164

1. AC DENOTES AUTOCLAVE CURE 345×10^3 N/m^2 (50 PSI)
2. VB DENOTES VACUUM BAG CURE 103×10^3 N/m^2 (15 PSI)
3. R.S. DENOTES RESIDUAL STRENGTH AFTER 32,000 CYCLES WITH MIN. LOAD/MAX. LOAD = 0.2
4. WET DENOTES 45 DAYS IMMERSION IN 57°C (135°F) JP 4 FUEL
5. MEASUREMENTS WERE MADE IN ENGLISH UNITS

Figure 8. - Tank Corner Test Results

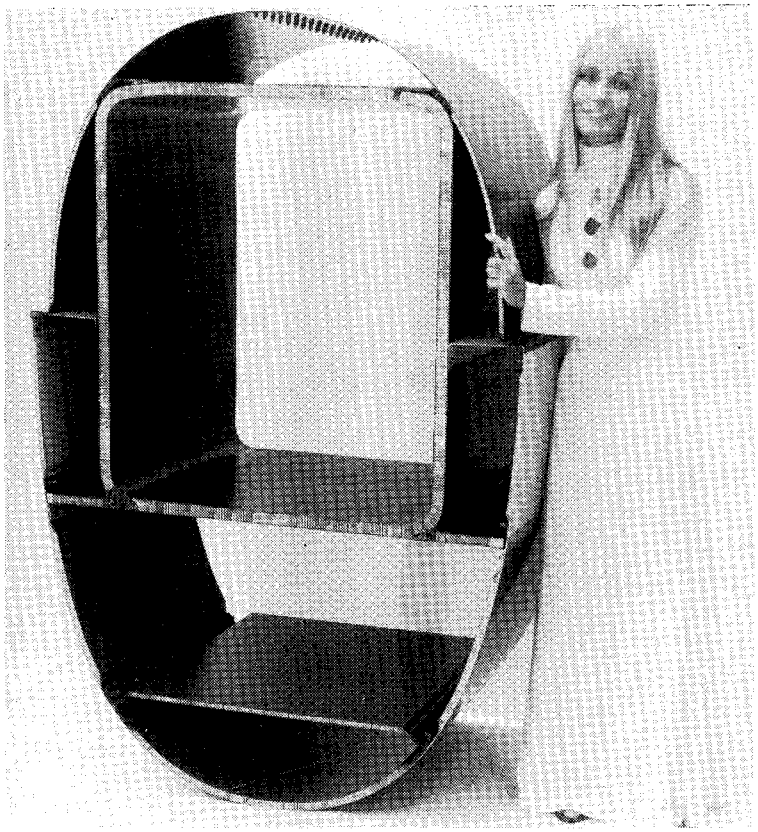

Figure 9. - Two Foot Fuselage Component

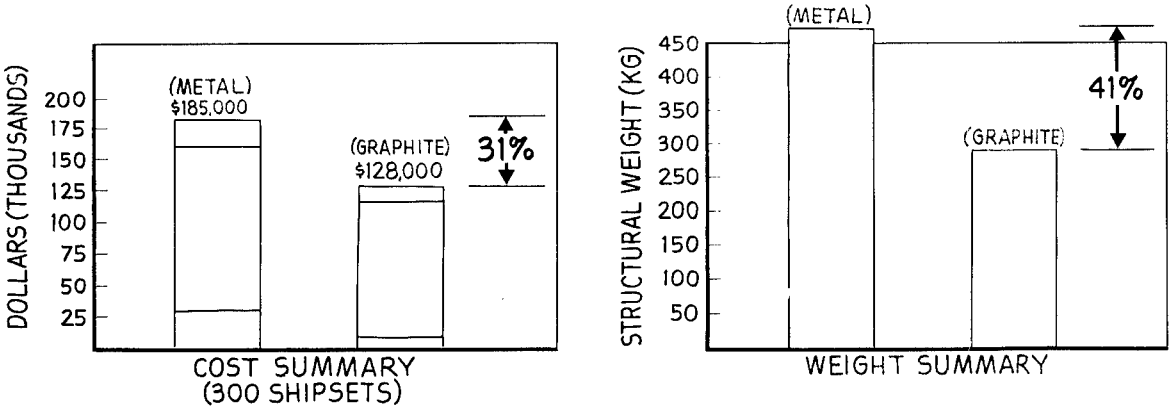

Figure 10. - Metallic Composite Cost & Weight Comparison

SHUTTLE ORBITER - GRAPHITE/EPOXY PAYLOAD BAY DOORS

By D. Garcia, Rockwell International Space Division
and C. E. Halstead, Rockwell International Tulsa Division

SUMMARY

Rockwell International is fabricating the Orbiter Payload Bay Door (PBD) from graphite/epoxy. Presented in this paper is a summary review of the test results, design approaches, production activity, and lessons learned to date.

INTRODUCTION

In November 1974, Rockwell International was authorized by NASA to design and fabricate the Space Shuttle PBD structure, utilizing graphite/epoxy composite material. The decision to produce the PBD with graphite/epoxy was based on a preliminary design study and the fabrication of 4-foot by 15-foot (1.22-m by 4.57-m) demonstration panel completed in May 1974. The study, which included a review of available graphite/epoxy data throughout the industry, concluded that the structure weight would be reduced by 23 percent, while maintaining the delivery schedule for the first flight orbiter and resulting in minimum program cost impact over the then aluminum baseline design. In addition, the study indicated that the on-orbit distortions of the PBD, resulting from the extreme temperature environment would be appreciably reduced. The purpose of this paper is to present the progress accomplished to date and highlight the major challenges and their resolutions.

PBD STRUCTURE SYSTEM DESCRIPTION AND DESIGN REQUIREMENTS

The Orbiter PBD (Figure 1) is a 60-foot (18.29-m) structure, consisting of a left- and right-hand forward and aft door, hinged at the mid-fuselage, and attached at the forward and aft fuselages and the top centerline by mechanical latches. The doors, when closed, are fixed at the aft fuselage bulkhead and allowed to move longitudinal at the forward fuselage. In addition to the translating capability at the forward bulkhead latch, there are four expansion joints located at Stations 1284 (32.61 m), 1122 (28.50 m), 939 (23.85 m), and 757 (19.23 m). These translating joints are provided to accommodate the longitudinal movement caused by thermal expansion and mechanical deflections resulting from body bending. The PBD is designed to accommodate vehicle torsional loads, aerodynamic pressure loads, and cargo bay vent lag pressures.

In addition to the foregoing, the doors are designed for 100 flights and 10 years service life. The PBD will be exposed to a maximum acoustic level of 163 db during boost, on-orbit temperatures of -170 F (160.9 K) to +220 F (377.6 K), and a maximum reentry temperature of +350 F (449.8 K).

The structure is made up of typical 15-foot (4.57-m) subassemblies (Figure 2) consisting of a graphite/epoxy honeycomb sandwich panel, solid graphite/epoxy laminate frames, expansion joint frames, torque box, seal depressor, centerline beam, intercostals, gussets, end fittings, and clips.

In addition, there are aluminum shear pins, titanium fittings and attachment clips, and Inconel 718 floating and shear hinges. With the exception of the skin panel, the total assembly is joined together by mechanical fasteners.

The skin panel (Figure 3) is made up of precured inner and outer skins constructed of a single 7-mil (0.00018-m) fabric sandwiched between two 4-mil (0.00010-m) tapes, a Nomex 1/8-inch (0.0032-m) honeycomb core, and bonded together with 0.06 lb/ft^2 (0.29 Kg/m^2) unsupported adhesive. The outer skin incorporates doublers consisting of 13-mil (0.00033-m) fabric and 4-mil (0.00010-m) tape located at the torque box and frame attachment areas. These doublers are incorporated during the initial curing of the outer skin. The skin panels are closed out with 7-mil (0.00018-m) and 13-mil (0.00033-m) fabric during final sandwich bonding.

A typical frame is depicted in Figure 4. The initial design included an insert located at the point of highest stress (knee); however, based upon development test, it has been determined that the insert is not required. The frames consist of multiple $\pm$45-degree 13-mil and 7-mil (0.00033-m and 0.00018-m) fabric and 90-degree and 0-degree 4-mil (0.00010-m) tape plies, layed up and tailored to provide the necessary design stiffness and strength. A typical expansion joint and seal assembly is shown in Figure 5. The graphite/epoxy seal retainer incorporates a silicone rubber pressure seal and quartz fibrous pile thermal barrier. Five tubular shear pins per side are provided at each expansion joint to accommodate longitudinal translation of each door panel. The shear pins are integrated with the panel assemblies through titanium bosses in the expansion joint frames. The titanium bosses incorporate self-aligning bearings and are mechanically fastened to the graphite/epoxy frames.

PROGRAM CHALLENGES

The completion of the Graphite/Epoxy Trade Study and the fabrication of a 4-foot by 15-foot (1.22-m by 4.57-m) demonstrator panel, in May 1974, provided assurance that the conversion from aluminum to graphite/epoxy could be accomplished. The major challenges associated with the decision to proceed with the change were evident.

There was no question concerning the technical and manufacturing ability to accomplish the Graphite/Epoxy Payload Bay Door Program; the major challenge was to accomplish the preliminary design analysis, the development testing, the

production design release, the tooling, the completion of the development testing, and the delivery of the first flight hardware within a period of 15-1/2 months. In addition to the foregoing, qualification of graphite/epoxy prepreg suppliers and the establishment of design allowables had to be accomplished.

A detailed integrated program plan was established to accomplish the major milestones, as shown in Figure 6. A Preliminary Design Review (PDR) was held on 26-28 February 1975, and the first production drawing was released on 28 March 1975. The final production drawing was completed and released on 24 October 1975.

A Critical Design Review (CDR) is scheduled for 2-4 December 1975, and the first PBD for Orbiter 101 will be delivered to Palmdale, California on 3 March 1976.

Design Allowables

The graphite/epoxy materials selected to fabricate the PBD were 13-mil (0.00033-m) and 7-mil (0.00018-m) fabric and 4-mil (0.00010-m) tape. Preliminary testing indicated that either the 934/T300 or 5208/T300 systems would meet the thermal and mechanical properties required. However, there was insufficient testing throughout the industry to provide design allowables over the range of environments required for the Shuttle PBD. It, therefore, was decided that a conservative set of preliminary design allowables, based on industry experience, would be used for the design and analysis of the PBD. A design allowables and supplier qualification test program was performed concurrently with the production design and drawing release in order to validate the acceptability of the preliminary design allowables. The testing has validated the selected preliminary design allowables as shown on Charts I, II, and III.

Payload Bay Door Mass Properties

The aluminum PBD specification weight at the time of conversion to graphite/epoxy was 4150 pounds (1882.4 Kg). The present graphite/epoxy PBD specification weight is 3108 pounds (1409.8 Kg). Rockwell International committed to a minimum weight savings of 900 pounds (408.2 Kg) or 23 percent. The present book weight, based upon calculation from released production drawings (95 percent released), is 3082 pounds (1398.0 Kg), as shown on Chart IV.

Development Test

A development test program was initiated at the offset to provide empirical data in order to design and analyze various elements of the doors that were considered critical. The program included acoustic, thermal, static structural, cyclic, mechanical joint, and environmental tests.

The development testing is basically complete and the results have shown that the critical elements, i.e., frames, panel/frame joints, hinge joints, etc., are capable of withstanding the design limit loads and life cycle requirements including a scatter factor of four. The intermediate frame, as an example, has been cycled up to 19,000 times at design load without failure, has also been exposed to design limit load in both compression and tension at room temperature for the Orbiter life cycle requirements, and then subjected to ultimate in both directions without failure.

The frames, when loaded to failure, withstood 230 to 260 percent of design limit load before failing. In addition, elevated temperature tests have been completed providing the same results. The testing has been instrumental in finalizing the detail design. Very few major changes have been required, as a result of the development test program.

Production Tooling and Fabrication

In order to provide the maximum amount of experience and learning within the Production Operations organization, it was decided to have all development test articles tooled and produced by the Operations personnel that would be responsible for the fabrication of the flight articles. They would also be required to utilize the same facilities and equipment as that planned for production. In order to assure that all procedural systems and documentation were "debugged" prior to release of Orbiter 101 PBD, the PBD development test program was performed with the production type procedures, engineering drawings, planning, inspection, processing, and controls required for flight hardware. Because of this approach, the production of the Orbiter 101 doors has progressed with an exceptional understanding by the Manufacturing personnel for what is necessary to produce high quality graphite/epoxy production parts.

The basic tooling concept selected for fabricating the PBD can be summarized as follows:

a. All frame tools are fabricated from high temperature epoxy resin systems and have a built-in adjustment for controlling contour.

b. The constant contour 15-foot (4.57-m) bond tools are fabricated from steel and have a contour adjustment capability.

c. The 15-foot (4.57-m) compound contour bond tools are fabricated from high temperature epoxy resins and also feature a contour adjustment capability.

d. All small and/or flat parts, where thermal differential between the tool and part is not critical, are made with aluminum tools.

The tooling approach taken has proved to be successful in the fabrication of high quality graphite parts. It has, however, required extensive effort to fabricate the tools themselves. Maintaining tooling contour and dimensional tolerances has presented only minor problems. The areas of major challenge

fell in the actual fabrication of the high temperature epoxy resin layup dies (LUD). In order to overcome blistering and surface cracking of the LUD during curing, it was necessary to control the environment and resin mixing and application during tool layup. A special mixing and gun system were utilized to assure homogenious and timely application during tool fabrication.

Another problem encountered was tool leakage of the initial tools during the 350 F, 85 psi (449.8 K, 5.86 x 10^5 N/m^2) and vacuum check. This problem has also been controlled by the foregoing actions to resolve blistering and surface cracking.

Final assembly of the Orbiter 101 PBD is being accomplished at the present time. The bringing together of the frame, skin panels, gussets, intercostals, closeouts, and metal parts is almost complete. However, prior to these being assembled into a completed assembly, it was necessary to develop the techniques for planning, scheduling, layup, trim, and drilling the various detail parts. These techniques were perfected, as stated before, during the development test program.

A tracking system was established to provide continuous visibility on the status of each detail part. Planning was formated in such a manner to provide kitting, layup, processing, and quality verification of critical engineering requirements. Special debulk tools were necessary to assure proper layup of tape at compound contoured areas.

Layup techniques were perfected on development hardware with the Engineering and Processing personnel providing continuous direction and guidance.

Rockwell International's Tulsa Division Manufacturing Engineering developed drilling techniques and equipment, in conjunction with the Rockwell International Industrial Division, that will consistently drill close tolerance holes within $\pm$0.0005 inch (0.0000127 m) in graphite/epoxy laminates. Trimming has been performed with diamond cutters and has proved to be easily accomplished.

Nondestructive Testing (NDT)

Rockwell International has had extensive experience with ultrasonic and X-ray inspecting of composite structures over the last 12 years. The application of these inspection techniques required establishing standards for the specific PBD design and determining acceptance criteria. The approach being taken with the PBD is a conservative one; in that, each discrepancy indicated by NDT is evaluated and is not allowed in flight hardware, unless previous exposure by testing deems it acceptable or reparable.

CONCLUDING REMARKS

On 14 November 1975, one year will have elapsed since NASA authorized Rockwell International to proceed with a graphite/epoxy PBD. That decision was a major step forward in the use of lightweight advance composite material as a primary aerospace structure. The decision was a sound one then, and based upon the progress to date, remains justified.

ACKNOWLEDGEMENT

This paper was made possible by the confidence and direction provided by the Johnson Space Flight Center and the Rockwell International Space Division Program Management. Special acknowledgement must also be given to the Rockwell International Tulsa Division Payload Bay Door (PBD) Program team, without them this work would never have been accomplished.

Bill Waldorf	PBD Project Engineer
Doug Welch	PBD Analysis Supervisor
Jim Anderson	PBD Design Supervisor
Fred Smith	PBD Design Supervisor
Willie Pound	PBD Production Operations Manager
Bill DuFresne	PBD Manufacturing Engineering Supervisor
Dick Schmigle	PBD Test Engineer and M&P Administrator
Ed Morris	PBD Facilities Administrator
Ted Miller	PBD Material Procurement Administrator

In addition, all the members of the Rockwell International Tulsa Division have contributed to its success.

Chart I

GRAPHITE/EPOXY PHYSICAL/MECHANICAL PROPERTIES

7-mil Fabric (0.00018 Metre)

PROPERTY	AC-50 "PRELIM" DESIGN ALLOWABLES		SPECIFICATION REQUIREMENT*		QUAL TEST DATA (AVERAGE)**	
	RT	350 F (449.8 K)	RT	350 F (449.8 K)	RT	350 F (449.8 K)
WARP TENSILE STRENGTH, N/m^2	$58.5 = 4.03 \times 10^8$	$45.6 = 3.14 \times 10^8$	$55.0 = 3.79 \times 10^8$	$55.0 = 3.79 \times 10^8$	$63.6 = 4.39 \times 10^8$	$68.7 = 4.74 \times 10^8$
WARP TENSILE MODULUS, N/m^2	$9.58 = 6.61 \times 10^{10}$	$10.1 = 6.96 \times 10^{10}$	$8.5 = 5.86 \times 10^{10}$	$8.3 = 5.72 \times 10^{10}$	$9.6 = 6.62 \times 10^{10}$	$9.4 = 6.48 \times 10^{10}$
FILL TENSILE STRENGTH, N/m^2	$58.5 = 4.03 \times 10^8$	$45.6 = 3.14 \times 10^8$	$55.0 = 3.79 \times 10^8$	$55.0 = 3.79 \times 10^8$	$65.1 = 4.49 \times 10^8$	$72.0 = 4.96 \times 10^8$
FILL TENSILE MODULUS, N/m^2	$9.58 = 6.61 \times 10^{10}$	$10.1 = 6.96 \times 10^{10}$	$8.5 = 5.86 \times 10^{10}$	$8.3 = 5.72 \times 10^{10}$	$9.1 = 6.27 \times 10^{10}$	$9.3 = 6.41 \times 10^{10}$
WARP COMPRESSION STRENGTH, N/m^2	$43.9 = 3.03 \times 10^8$	$36.0 = 2.48 \times 10^8$	$45.0 = 3.10 \times 10^8$	$35.0 = 2.41 \times 10^8$	$52.6 = 3.63 \times 10^8$	$37.0 = 2.55 \times 10^8$
WARP COMPRESSION MODULUS, N/m^2	$9.58 = 6.61 \times 10^{10}$	$10.1 = 6.96 \times 10^{10}$	$8.3 = 5.72 \times 10^{10}$	$7.8 = 5.38 \times 10^{10}$	$9.9 = 6.83 \times 10^{10}$	$9.1 = 6.27 \times 10^{10}$
FILL COMPRESSION STRENGTH, N/m^2	$43.9 = 3.03 \times 10^8$	$36.0 = 2.48 \times 10^8$	$45.0 = 3.10 \times 10^8$	$35.0 = 2.41 \times 10^8$	$60.0 = 4.14 \times 10^8$	$41.5 = 2.86 \times 10^8$
FILL COMPRESSION MODULUS, N/m^2	$9.58 = 6.61 \times 10^{10}$	$10.1 = 6.96 \times 10^{10}$	$8.3 = 5.72 \times 10^{10}$	$7.8 = 5.38 \times 10^{10}$	$9.5 = 6.55 \times 10^{10}$	$8.8 = 6.07 \times 10^{10}$
IN-PLANE SHEAR STRENGTH, N/m^2	$8.1 = 5.58 \times 10^7$	$2.6 = 1.79 \times 10^7$	—	—	—	—
IN-PLANE SHEAR MODULUS, N/m^2	$1.0 = 6.89 \times 10^9$	$0.45 = 3.10 \times 10^9$	—	—	—	—
LONGITUDINAL FLEXURAL STRENGTH, N/m^2	—	—	$85.0 = 5.86 \times 10^8$	$65.0 = 4.48 \times 10^8$	$91.8 = 6.33 \times 10^8$	$81.1 = 5.59 \times 10^8$
LONGITUDINAL FLEXURAL MODULUS, N/m^2	—	—	$8.0 = 5.52 \times 10^{10}$	$7.5 = 5.17 \times 10^{10}$	$9.1 = 6.27 \times 10^{10}$	$9.0 = 6.21 \times 10^{10}$
INTERLAMINAR SHEAR STRENGTH, N/m^2	—	—	$7.0 = 4.83 \times 10^7$	$5.5 = 3.79 \times 10^7$	$8.4 = 5.79 \times 10^7$	$6.6 = 4.55 \times 10^7$
WARP TENSILE STRAIN, μ-IN./IN.	6100	4510	—	—	—	—
FILL TENSILE STRAIN, μ-IN./IN.	5980	4850	—	—	—	—
WARP COMPRESSION STRAIN, μ-IN./IN.	4570	3560	—	—	—	—
FILL COMPRESSION STRAIN, μ-IN./IN.	4480	3820	—	—	—	—
IN-PLANE SHEAR STRAIN, μ-IN./IN.	8100	5780	—	—	—	—
FIBER VOLUME, %	—		60 ± 4		59.3	
SPECIFIC GRAVITY	—		1.56 (REF)		1.58	
CURED PLY THICKNESS, METRES	—		0.000185 ± 0.0000126		0.000183	

*TB0130-001, REVISION D.
**AVERAGE OF THREE MATERIAL BATCHES.

Chart II

GRAPHITE/EPOXY
PHYSICAL/MECHANICAL PROPERTIES
13-mil Fabric (0.00033 Metre)

PROPERTY	AC-50 "PRELIM" DESIGN ALLOWABLES		SPECIFICATION REQUIREMENT*		QUAL TEST DATA (AVERAGE)**	
	RT	350 F (449.8 K)	RT	350 F (449.8 K)	RT	350 F (449.8 K)
WARP TENSILE STRENGTH, N/m^2	$58.5 = 4.03 \times 10^8$	$45.6 = 3.14 \times 10^8$	$75.0 = 5.17 \times 10^8$	$70.0 = 4.83 \times 10^8$	4.39×10^8	$68.7 = 4.74 \times 10^8$
WARP TENSILE MODULUS, N/m^2	$9.58 = 6.61 \times 10^{10}$	$10.1 = 6.96 \times 10^{10}$	$9.3 = 6.41 \times 10^{10}$	$8.5 = 5.86 \times 10^{10}$	6.62×10^{10}	$9.4 = 6.48 \times 10^{10}$
FILL TENSILE STRENGTH, N/m^2	$58.5 = 4.03 \times 10^8$	$45.6 = 3.14 \times 10^8$	$65.0 = 4.48 \times 10^8$	$65.0 = 4.48 \times 10^8$	4.49×10^8	$72.0 = 4.96 \times 10^8$
FILL TENSILE MODULUS, N/m^2	$9.58 = 6.61 \times 10^{10}$	$10.1 = 6.96 \times 10^{10}$	$9.3 = 6.41 \times 10^{10}$	$8.5 = 5.86 \times 10^{10}$	6.27×10^{10}	$9.3 = 6.41 \times 10^{10}$
WARP COMPRESSION STRENGTH, N/m^2	$43.9 = 3.03 \times 10^8$	$36.0 = 2.48 \times 10^8$	$65.0 = 4.48 \times 10^8$	$50.0 = 3.45 \times 10^8$	3.63×10^8	$37.0 = 2.55 \times 10^8$
WARP COMPRESSION MODULUS, N/m^2	$9.58 = 6.61 \times 10^{10}$	$10.1 = 6.96 \times 10^{10}$	$8.5 = 5.86 \times 10^{10}$	$8.0 = 5.52 \times 10^{10}$	6.83×10^{10}	$9.1 = 6.27 \times 10^{10}$
FILL COMPRESSION STRENGTH, N/m^2	$43.9 = 3.03 \times 10^8$	$36.0 = 2.48 \times 10^8$	$65.0 = 4.48 \times 10^8$	$50.0 = 3.45 \times 10^8$	4.14×10^8	$41.5 = 2.86 \times 10^8$
FILL COMPRESSION MODULUS, N/m^2	$9.58 = 6.61 \times 10^{10}$	$10.1 = 6.96 \times 10^{10}$	$8.5 = 5.86 \times 10^{10}$	$8.0 = 5.52 \times 10^{10}$	6.55×10^{10}	$8.8 = 6.07 \times 10^{10}$
IN-PLANE SHEAR STRENGTH, N/m^2	$8.1 = 5.58 \times 10^7$	$2.6 = 1.79 \times 10^7$	—	—	—	—
IN-PLANE SHEAR MODULUS, N/m^2	$1.0 = 6.89 \times 10^9$	$0.45 = 3.10 \times 10^9$	—	—	—	—
LONGITUDINAL FLEXURAL STRENGTH, N/m^2	—	—	$100.0 = 6.89 \times 10^8$	$73.0 = 5.03 \times 10^8$	6.33×10^8	$81.1 = 5.59 \times 10^8$
LONGITUDINAL FLEXURAL MODULUS, N/m^2	—	—	$8.6 = 5.93 \times 10^{10}$	$8.0 = 5.52 \times 10^{10}$	6.27×10^{10}	$9.0 = 6.21 \times 10^{10}$
INTERLAMINAR SHEAR STRENGTH, N/m^2	—	—	$7.0 = 4.83 \times 10^7$	$5.5 = 3.79 \times 10^7$	5.79×10^7	$6.6 = 4.55 \times 10^7$
WARP TENSILE STRAIN, μ-IN./IN.	6100	4510	—	—	—	—
FILL TENSILE STRAIN, μ-IN./IN.	5980	4850	—	—	—	—
WARP COMPRESSION STRAIN, μ-IN./IN.	4570	3560	—	—	—	—
FILL COMPRESSION STRAIN, μ-IN./IN.	4480	3820	—	—	—	—
IN-PLANE SHEAR STRAIN, μ-IN./IN.	8100	5780	—	—	—	—
FIBER VOLUME, %	—		62 ± 4		63.6	
SPECIFIC GRAVITY	—		1.60 (REF)		1.59	
CURED PLY THICKNESS, METRES	—		0.00033 ± 0.000019		0.000326	

*TB0130-001, REVISION D.
**AVERAGE OF TWO MATERIAL BATCHES.

Chart III

GRAPHITE/EPOXY PHYSICAL/MECHANICAL PROPERTIES

(4-mil Tape (0.00010 Metre)

PROPERTY	AC-50 "PRELIM" DESIGN ALLOWABLES		SPECIFICATION REQUIREMENT		QUAL TEST DATA (AVERAGE)	
	RT	350 F (449.8 K)	RT	350 F (449.8 K)	RT	350 F (449.8 K)
LONGITUDINAL TENSILE STRENGTH, N/m^2	$165.0 = 1.14 \times 10^9$	$120.0 = 8.27 \times 10^8$	$180.0 = 1.24 \times 10^9$	$165.0 = 1.14 \times 10^9$	$212.7 = 1.47 \times 10^9$	$205.2 = 1.41 \times 10^9$
LONGITUDINAL TENSILE MODULUS, N/m^2	$20.9 = 1.44 \times 10^{11}$	$22.0 = 1.52 \times 10^{11}$	$18.0 = 1.24 \times 10^{11}$	$18.0 = 1.24 \times 10^{11}$	$20.1 = 1.39 \times 10^{11}$	$21.6 = 1.49 \times 10^{11}$
TRANSVERSE TENSILE STRENGTH, N/m^2	$6.47 = 4.46 \times 10^7$	$4.02 = 2.77 \times 10^7$	—	—	—	—
TRANSVERSE TENSILE MODULUS, N/m^2	$1.67 = 1.15 \times 10^{10}$	$1.3 = 8.96 \times 10^9$	—	—	—	—
LONGITUDINAL COMPRESSION STRENGTH, N/m^2	$135.0 = 9.31 \times 10^8$	$80.4 = 5.54 \times 10^8$	$180.0 = 1.24 \times 10^9$	$135.0 = 9.31 \times 10^8$	$234.3 = 1.62 \times 10^9$	$143.5 = 9.89 \times 10^8$
LONGITUDINAL COMPRESSION MODULUS, N/m^2	$20.9 = 1.44 \times 10^{11}$	$22.0 = 1.52 \times 10^{11}$	$18.0 = 1.24 \times 10^{11}$	$18.0 = 1.24 \times 10^{11}$	$20.8 = 1.43 \times 10^{11}$	$20.5 = 1.41 \times 10^{11}$
TRANSVERSE COMPRESSION STRENGTH, N/m^2	$15.52 = 1.07 \times 10^8$	$8.4 = 5.79 \times 10^7$	—	—	—	—
TRANSVERSE COMPRESSION MODULUS, N/m^2	$1.67 = 1.15 \times 10^{10}$	$1.3 = 8.96 \times 10^9$	—	—	—	—
IN-PLANE SHEAR STRENGTH, N/m^2	$6.75 = 4.65 \times 10^7$	$2.4 = 1.65 \times 10^7$	—	—	—	—
IN-PLANE SHEAR MODULUS, N/m^2	$0.65 = 4.48 \times 10^9$	$0.4 = 2.76 \times 10^9$	—	—	—	—
LONGITUDINAL FLEXURAL STRENGTH, N/m^2	—	—	$225.0 = 1.55 \times 10^9$	$150.0 = 1.03 \times 10^9$	$264.7 = 1.83 \times 10^9$	$166.0 = 1.14 \times 10^9$
LONGITUDINAL FLEXURAL MODULUS, N/m^2	—	—	$18.0 = 1.24 \times 10^{11}$	$17.0 = 1.17 \times 10^{11}$	$18.2 = 1.25 \times 10^{11}$	$17.3 = 1.19 \times 10^{11}$
INTERLAMINAR SHEAR STRENGTH, N/m^2	—	—	$12.0 = 8.27 \times 10^7$	$6.0 = 4.14 \times 10^7$	$16.3 = 1.12 \times 10^8$	$8.6 = 5.93 \times 10^7$
LONGITUDINAL TENSILE STRAIN, μ-IN./IN.	7890	5450	—	—	—	—
TRANSVERSE TENSILE STRAIN, μ-IN./IN.	3870	3100	4000	4000	5072	5687
LONGITUDINAL COMPRESSION STRAIN, μ-IN./IN.	9290	6460	—	—	—	—
TRANSVERSE COMPRESSION STRAIN, μ-IN./IN.	6450	3650	—	—	—	—
IN-PLANE SHEAR STRAIN, μ-IN./IN.	10380	6000	—	—	—	—
FIBER VOLUME, %	—		63 ± 4		65.0	
SPECIFIC GRAVITY	—		1.57 (REF)		1.60	
CURED PLY THICKNESS, METRES	—		0.000112 ± 0.0000101		0.000116	

Chart IV

PAYLOAD BAY DOOR WEIGHT STATUS

ITEM	BOOK	Kg	SPEC	Kg
HONEYCOMB PANEL	(1027)	(465.8)		
PANEL SKINS	707	320.7		
PANEL CORE (NOMEX, 3 PCF) (48 Kg/m^3)	172	78.0		
PANEL BOND (R398, 0.06 PSF) (0.29 Kg/m^2)	148	67.1		
LIQUID SHIM — EPON 934	10	4.5		
FRAME — INTERMEDIATE	556	252.2		
FRAME — CLOSEOUT	409	185.5		
HINGES	198	89.8		
SECONDARY	(148)	(67.2)		
DRIVE MOTOR SUPPORT	7	3.2		
RADIATOR SUPPORT	16	7.3		
CENTERLINE	81	36.7		
FWD BULKHEAD INTERFACE	26	11.8		
AFT BULKHEAD INTERFACE	18	8.2		
HARDWARE	146	66.2		
RADIATOR ATTACH	7	3.2		
TORQUE BOX	135	61.2		
SEAL SUPPORT	(113)	(51.3)		
CENTERLINE — LEFT HAND	15	6.8		
CENTERLINE — RIGHT HAND	10	4.5		
FWD BULKHEAD	16	7.3		
AFT BULKHEAD	14	6.4		
EXPANSION JOINT	58	26.3		
EXPANSION JOINT	226	102.5		
LIGHTNING PROTECTION	107	48.5		
TOTAL WEIGHT (POUNDS) (Kg)	3082	1397.9	3108	1409.8

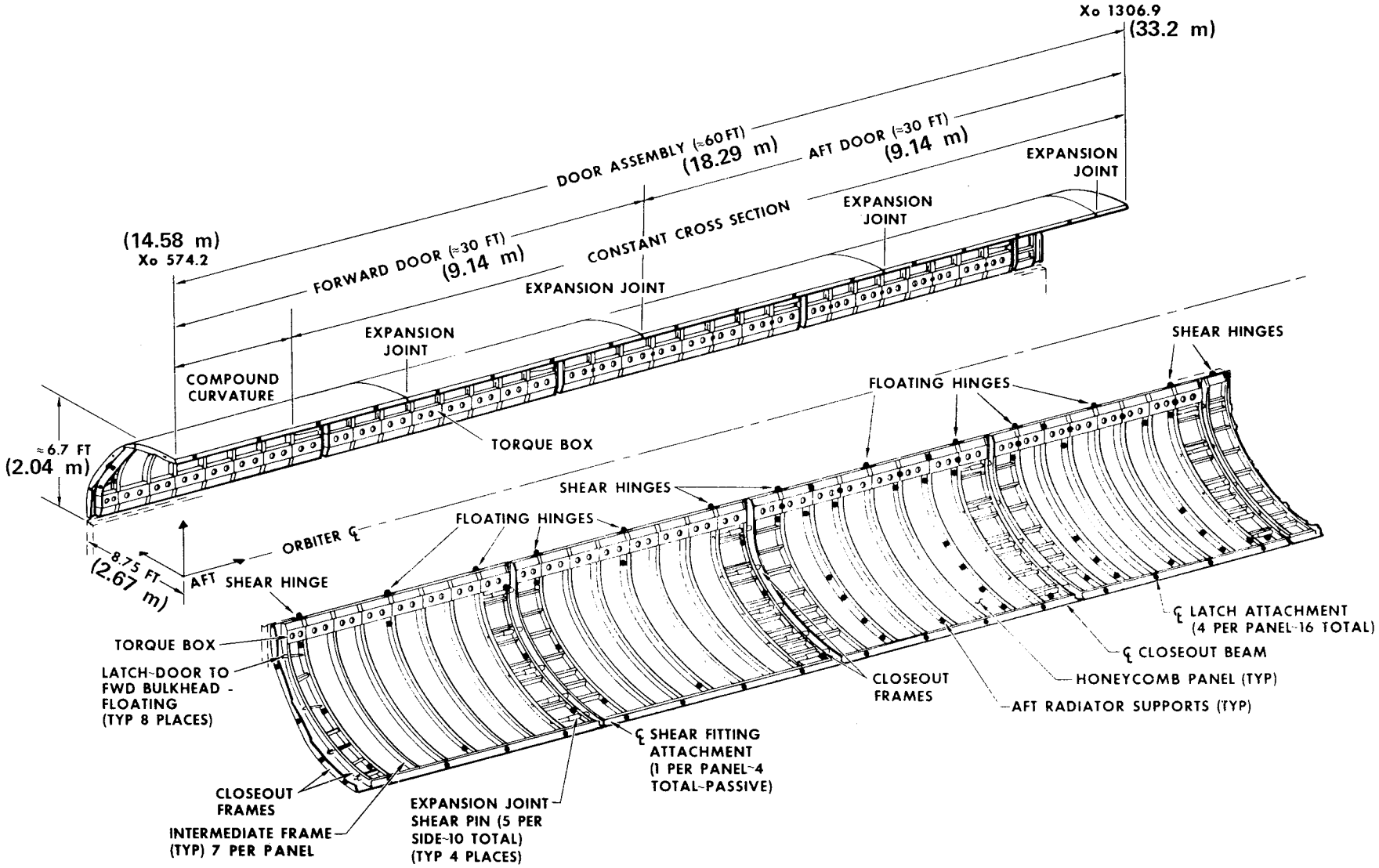

Figure 1.- Payload bay door - baseline configuration.

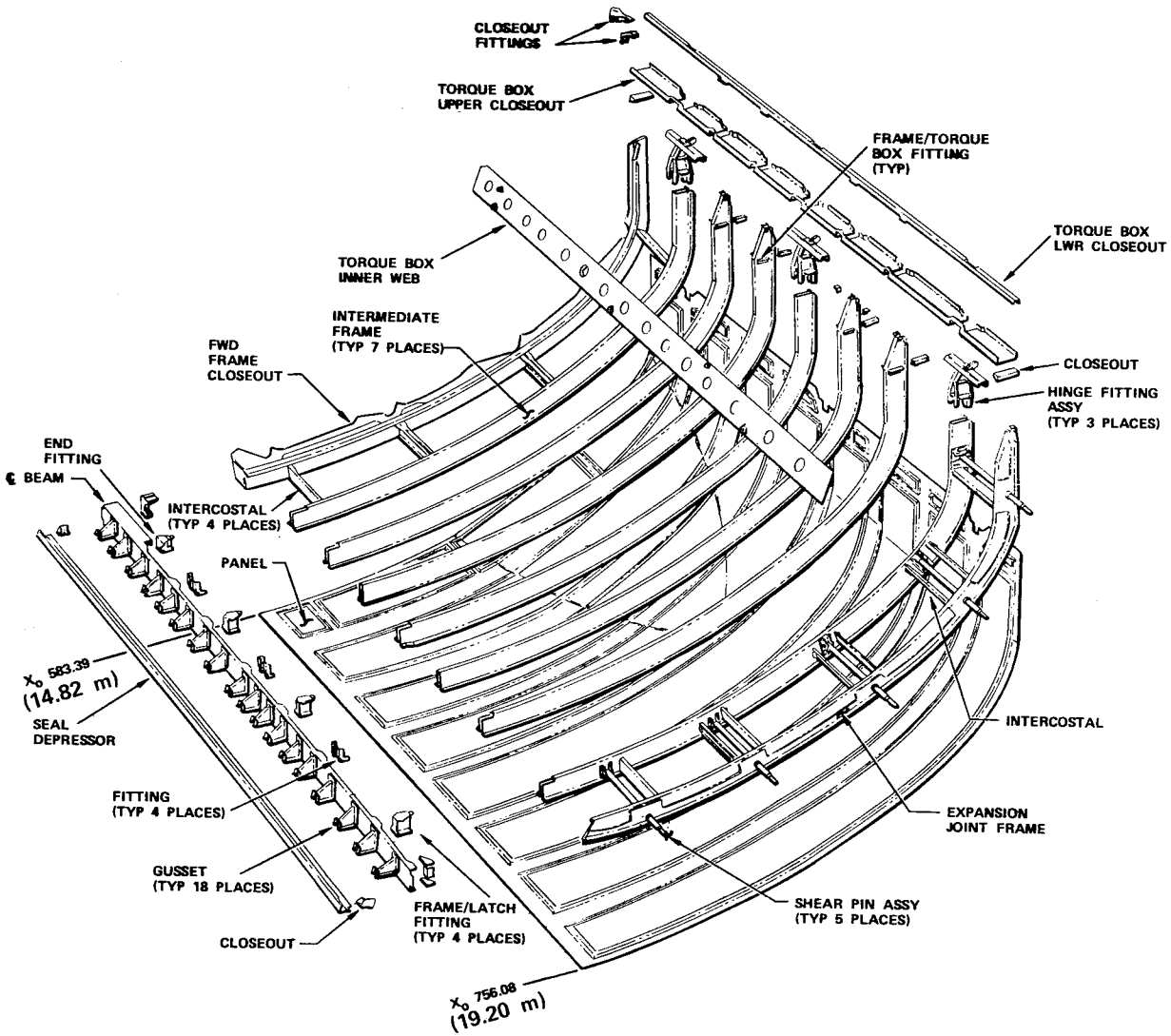

Figure 2.- Payload bay door - panel segment (typical).

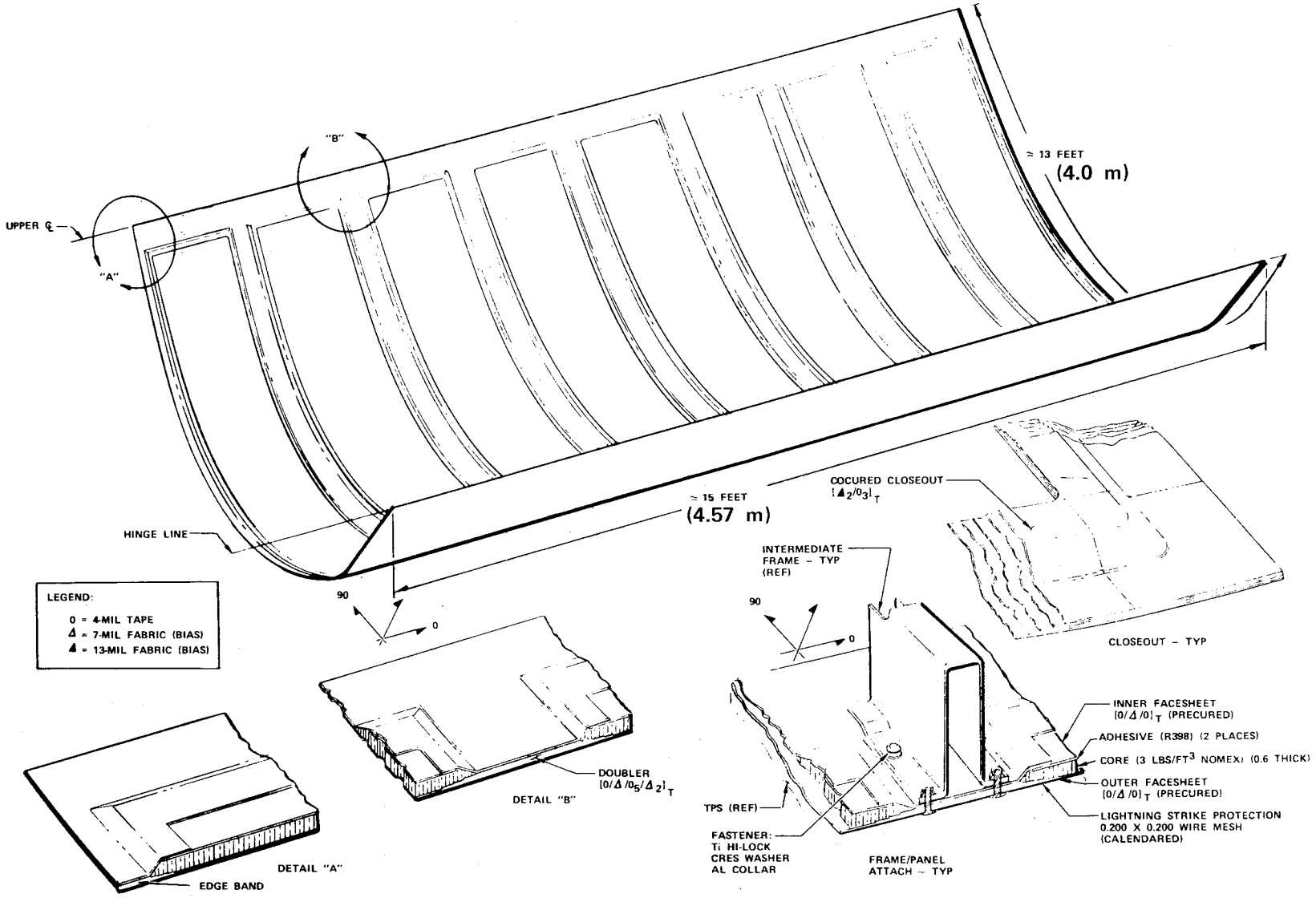

Figure 3.- Payload bay door - skin panel (typical).

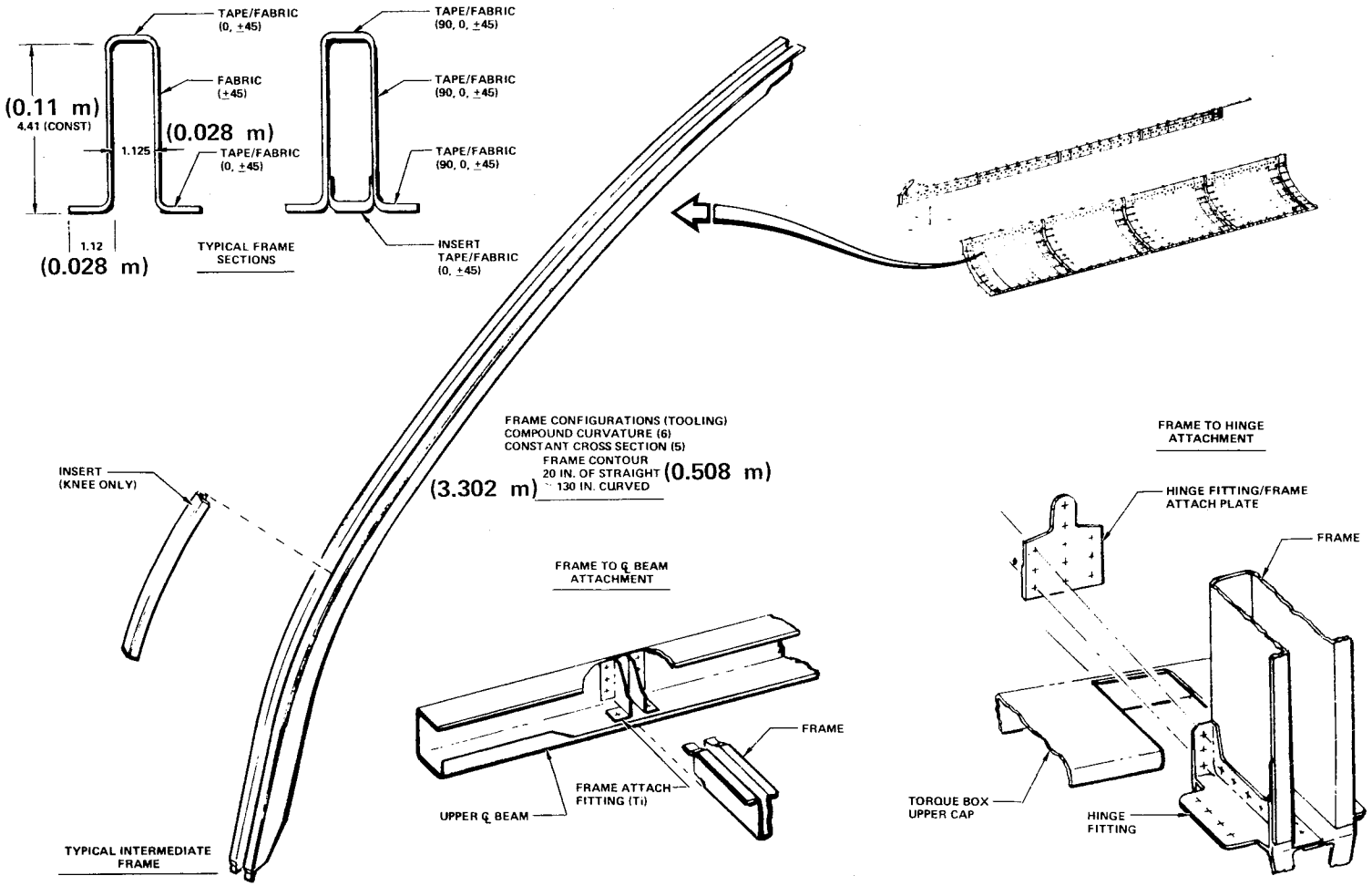

Figure 4.- Payload bay door - intermediate frame (typical).

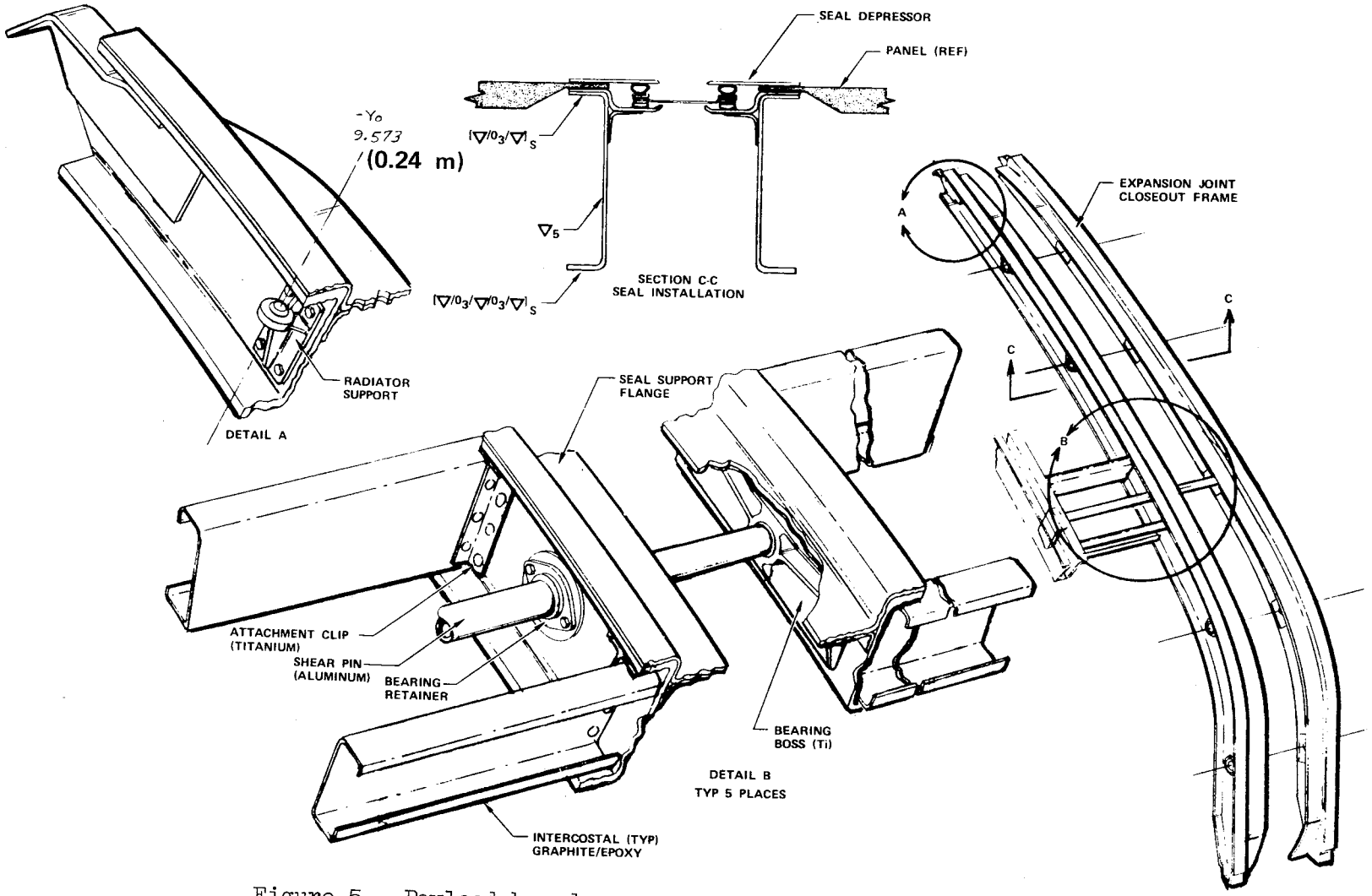

Figure 5.- Payload bay door - expansion joint and shear pin.

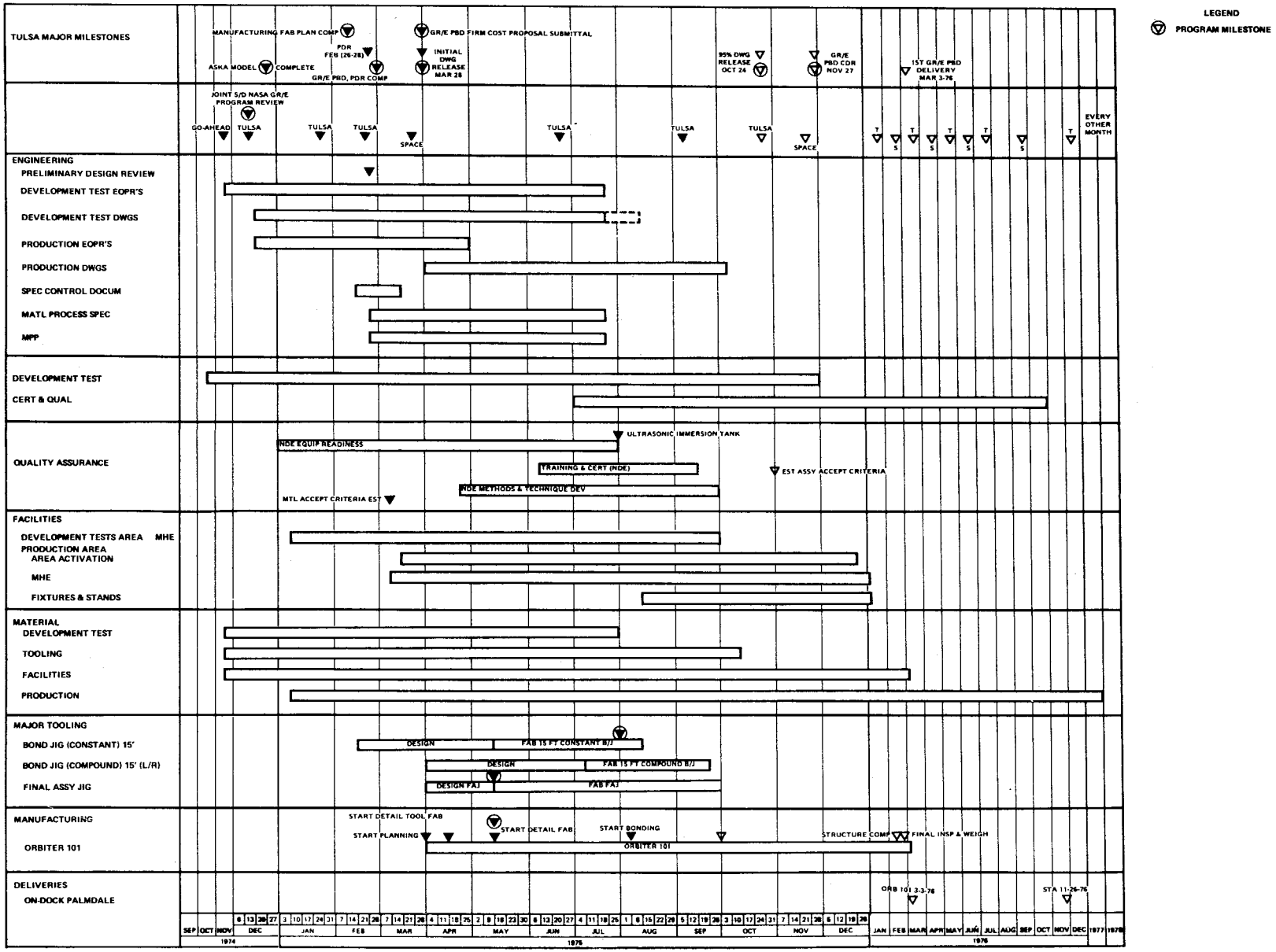

Figure 6.- Graphite/epoxy program master schedule - space shuttle payload bay doors.

B-1 COMPOSITES WEAPONS BAY DOOR

By Dr. Leslie M. Lackman and Dean S. Klivans

Rockwell International Corporation
Los Angeles Aircraft Division

INTRODUCTION

In the past few years, the successful completion of advance composite contracts to industry, along with industry independent research and development (IR&D) programs, has clearly demonstrated the integrity of composites for structural use. Weight savings payoffs of up to 30 percent have been attained, and there have been firm production commitments of advanced composite materials on the F-14, F-15, and B-1 aircraft. A significant decrease in raw material costs for boron and graphite prepregs has occurred in the last few years and will continue for more years to come. As a consequence, it is now being shown that the ability exists to develop composite designs that not only save weight, but will be cost-competitive with existing comparable metal parts, and will maintain reliability and reproducibility.

These objectives are now being obtained through the use of simplified design concepts, strong engineering/manufacturing interface, low-cost manufacturing concepts, optimum use of hybrid materials, and trading back weight savings for cost reductions.

B-1 WEAPONS BAY DOOR

An important, recently completed Los Angeles Aircraft Division (Rockwell International) IR&D program has been the design, fabrication, and test of an advanced composite version of the B-1 weapons bay door. This is a large component of secondary structure, measuring 4 by 15 feet, with a maximum thickness of 4 inches. Figure 1 shows the location of the six weapons bay doors on the B-1 aircraft.

The program objectives were to (1) establish confidence in composites, (2) demonstrate weight savings, (3) validate manufacturing costs, (4) demonstrate structural integrity, and (5) provide flight service qualified hardware.

METAL CONFIGURATION

The metal version of the door (see figure 2 for a cross section) consists of a 0.016-inch aluminum inner skin, 0.030-inch aluminum outer skin, a full-depth aluminum honeycomb core at 3.1 pounds per cubic foot density, a primary structural aluminum J-beam longitudinally down the center, and aluminum Z-sections utilized as closeouts along the four sides. There are four cutouts in the core along one side of the door, with inserted machined aluminum rib fittings for attachment of the door to the operating and support mechanism. The rib fittings are adhesively bonded to the core and skins and are mechanically fastened to the web of the center beam.

COMPOSITE CONFIGURATION

The composite door was designed to perform the same function as the metal door and to operate within the same constraints. The basic constraints which had to be satisfied include matching the outer mold line, allowing for the linkage system and store drop-angle clearance on the inner mold line, providing access to the actuator attach fitting from the exterior surface, insuring adjustment capability at the actuator attach points, meeting edge sealing requirements, and withstanding the service life and environment of the B-1 aircraft.

These constraints, in conjunction with efficient composite design practices, dictated a general structural configuration of the composite door quite similar to the metal configuration. In the first-generation design of the advanced composite weapons bay door, emphasis was placed on obtaining maximum weight savings. This design resulted in the use of the aluminum honeycomb core (as in the metal component), graphite/epoxy skins, and a rectangular tube center beam of graphite/epoxy replacing the aluminum J-beam of the metal component. Although the resultant weight savings of 30 percent was significant, the cost analysis showed that the center beam was a high-cost item and that further consideration of its redesign should be undertaken in order to obtain a more favorable cost savings.

In the second-generation design, the change in the basepoint design was the use of more dense aluminum honeycomb core with unidirectional graphite/epoxy caps, instead of the rectangular graphite/epoxy center beam tube. Although this redesign has reduced the weight savings below the 30-percent savings of the original design, the significant reduction in cost warrants its use. The design (shown in figure 2) therefore consists of a full-depth aluminum honeycomb sandwich. The inner and outer skins are three plies of graphite/epoxy [90/$\pm$45], and the center beam consists of upper and lower six-ply unidirectional

graphite/epoxy caps bonded to 8 and 12-pound per foot cubed aluminum honeycomb core. The 12-pound core is at each rib fitting. The main parts of the honeycomb core, on both sides of the center beam, are of 3.1 pounds per foot cubed density. The edge members along the four sides of the door consist of laidup epoxy fiberglass in the shape of a "Y". These serve as a closeout for the honeycomb core and as a land for the door seals. The machined aluminum rib fittings are generally similar to those used in the metal door.

STRUCTURAL ANALYSIS

Thermal Mismatch

The problem of thermal mismatch between the [90/±45] graphite/epoxy skins and aluminum ribs was examined. The purpose of this analytical study was to determine which material could be used to relieve the thermally induced shear stresses in the bond line between the graphite/epoxy skins and the aluminum rib incurred during cocuring. The approach taken was to sandwich another material between the bond of skins to rib, to attempt to soften the thermally induced stresses.

It was determined from these studies that the lowest shear stresses were present when one ply of unidirectional high-tensile strength (HTS) graphite/epoxy was sandwiched into the bond between the [90/±45] graphite/epoxy skins and the aluminum rib. These data were incorporated into the final weapons bay door design.

Finite Element Analysis

In order to assess the structural behavior of the composite weapons bay doors, several studies were conducted using the automated system of kinematic analysis (ASKA) finite element model of the structure. These studies yielded several types of data, including (1) stress distributions throughout the structure, (2) deflections, and (3) reaction forces at the roller track attach and swing-link attach points. In the case of the reaction forces, these loads were used to size the detail stress check of the aluminum rib fitting parts. The first of these studies was conducted for a configuration using 12 plies of unidirectional graphite/epoxy for the center beam caps. Four conditions were examined and proved to be more than structurally adequate. It was decided to change the design configuration to six plies instead of 12, and two critical conditions were analyzed. An AC-3 computer program (point stress analysis) was run to obtain margins of safety for these conditions, and the minimum margin obtained was +0.17. These margins were based on predicted skin allowables obtained by use of unidirectional high-strength graphite/epoxy allowables at 270°F and the use of conventional lamination theory.

Two additional ASKA finite element studies were conducted for the present configuration in order to assess the effect of a nuclear blast environment. These two studies consisted of (1) assessing the structural (dynamic) behavior due to a nuclear burst overpressure, and (2) assessing the effects of the thermal flash associated with the nuclear blast. The results of both of these studies showed low skin stresses; therefore, no strength problem was indicated.

Detail Stress Analysis

Based on the previously discussed ASKA finite element studies, loads, stresses, and reactions, conventional hand-calculation stress analysis methods were employed to stress-check the various detail parts of the door. These included core shear checks, stress analysis of the aluminum rib fittings and attached hardware, bond line checks, and margin-of-safety calculations. All parts of the design were of adequate strength.

Design Allowables

Existing design allowables data for HTS graphite/epoxy from the third edition of the "Advanced Composites Design Guide" were utilized throughout the composites weapons bay door design development effort. At the inception of this program, unidirectional properties for the T300/5208 graphite/epoxy were generated via beam tests, and the data indicated that T300/5208 graphite/epoxy material had higher unidirectional properties than the HTS material. Based on the results of the unidirectional material properties test, it was decided to utilize the HTS properties, without any knockdown factors, for preliminary design. Humidity tests at room temperature and 270°F were conducted for the laminate orientations and configurations utilized in the door at a later date in the program, and very little degradation (less than 10 percent in compression) in properties was observed. Furthermore, no composite initiated failures were indicated in either the subcomponent or full-scale door tests, hence tending to validate the design as developed with the HTS properties being utilized. The design allowables data are as follows:

Orientation	Property	Room Temp Value	270°F Value
$[0]_{6T}$	E_x (Msi)	21.00	20.00
	E_y (Msi)	1.70	1.20
	G_{xy} (Msi)	0.65	0.45

Orientation	Property	Room Temp Value	270°F Value
$[0]_{6T}$	ν_{xy}	0.21	0.23
	ν_{yx}	0.017	0.014
	F_x^{tu} (ksi)	180.00	178.00
	F_y^{tu} (ksi)	8.00	5.80
	F_x^{cu} (ksi)	180.00	130.00
	F_y^{cu} (ksi)	30.00	21.00
	F_{xy}^{su} (ksi)	12.00	10.70
$[0/\pm45]_T$	E_x (Msi)	9.00	8.50
	E_y (Msi)	3.50	3.20
	G_{xy} (Msi)	3.70	3.40
	ν_{xy}	0.31	0.32
	ν_{yx}	0.72	0.74
	F_x^{tu} (ksi)	78.00	70.00
	F_y^{tu} (ksi)	32.00	19.00
	F_x^{cu} (ksi)	78.00	57.00
	F_y^{cu} (ksi)	40.00	27.00
	F_{xy}^{su} (ksi)	46.00	42.00

Fatigue Analysis

A limited fatigue analysis effort is currently in work on the program. This effort consists of fabrication of IITRI-type coupons simulating various areas of the door structure (e.g., basic skin, skin plus center beam cap, skin and edge closeout), fatigue testing (cyclically loaded) to obtain basic S-N data, and a Miner's rule cumulative damage type of analysis based on the developed test data and the applicable weapons bay door analytical fatigue spectrum.

SUBCOMPONENT STATIC TEST

An advanced composites weapons bay door subcomponent was successfully static tested to validate the proposed design prior to release of the design drawings for fabrication of the full-scale door. The subcomponent consisted of a one-fourth section of the full-scale door (see figure 3), and included one aluminum rib fitting with drag brace attach point, a swing-link attach fitting, and door support roller tracks.

The first load condition tested represented the door closed at M=0.95 and a 1-G cruise, which is a deflection-critical case. The panel was loaded to 100 percent design limit load, with no failure. The test showed a maximum deflection of 0.160 inch at the edge of the panel furthest away from the actuator attach point. This compared to a predicted deflection of 0.222 inch from the ASKA finite element analysis of the composite door, and a 0.197-inch predicted deflection for the metal door.

The second and final load condition represented a door open 63 degrees at M=1.8 yaw condition, which is a strength-critical case. Both ultimate air pressure loads and drag loads were applied simultaneously to the test panel. The loading was applied up to 120 percent of design ultimate before any sign of failure was observed. While holding at 120 percent, a loud cracking noise was heard, and the load was removed. No visible sign of failure was apparent except for an approximate 2-inch wide bulge on the inner skin, indicating a disbond between the skin and honeycomb core. Ultrasonic inspection of the panel verified this disbond.

FULL-SCALE DOOR STATIC TEST

Fabrication

Based on the test results on the subcomponent panel, the program continued into the fabrication phase of the full-scale static test door. The fabrication sequence consisted of first making a major subassembly comprised of (1) all of the aluminum honeycomb core segments bonded together using a foaming adhesive, (2) the four aluminum rib fittings bonded to the core subassembly using a foaming adhesive, and (3) the laidup fiberglass edge members. The inner and outer skins, each of 3-ply [90/±45] T300/5208 graphite/epoxy, were laid up as separate uncured subassemblies. The final assembly then consisted of the application of the skins to the core subassembly and the autoclave cocuring of the complete assembly. Figure 4 shows the completed assembly ready for delivery to the structural lab for static test.

Static Test

The door was installed in a test fixture with the capability of applying the test loading as shown in figure 5. The instrumentation consisted of a total of 23 deflection gages and 45 strain gages. The loading was applied in increments of 10 percent of design ultimate load. After each 10 percent addition, the load was held and the strain gage and deflection gage readings were taken. The panel failed at a reading of 99 percent of design ultimate load. Figure 6 shows the fracture line of the failure and the failure mode. The failure analysis concluded that the initial failure occurred in the bond between the 12-pound honeycomb core and the base web of the aluminum fitting. (See section AA of figure 6.) Section AA shows how the core and skins sheared away from the aluminum fitting. An examination of the surface of the fitting web indicated that the MB-6607 foaming adhesive in that area did not make the proper load-carrying bond with the fitting.

The following summarizes maximum deflections of both the metal and composite doors as predicted by ASKA finite element analysis, as well as actual deflections observed from the static tests. These deflections are relative to the attach linkage points, and rotation or translation of the door due to the linkage movement under load are not included.

Door-Closed Condition - Limit Loads

δ metal = 0.197 in. (ASKA predicted)
δ composite = 0.222 in. (ASKA predicted)
δ composite = 0.160 in. (subcomponent test)

Door-Open Condition - Ultimate Loads

δ metal = 0.482 in. (ASKA predicted)
δ composite = 0.511 in. (ASKA predicted)
δ composite = 0.400 in. (subcomponent test)
δ composite = 0.324 in. (full-scale test)

Test Conclusions

Basic structural integrity of the composite weapons bay door was demonstrated by both the subcomponent test, which incurred a bond failure at 120 percent of design ultimate, and by the full-scale door test, which failed at 99 percent of design ultimate due to an inadequate foaming adhesive bond. In the case of the subcomponent, no composite failure occurred, and it should be added that the test was more severe than actual aircraft conditions, from the standpoint of the larger residual bond stresses present at the test temperature (room temperature) due to cocure bonding at 350°F, versus the actual operating airload temperature of 190° to 260°F. Additionally, the full-scale door failed, as verified by analysis of strain gage data, due to an approximate 50 percent inadequate foaming adhesive bond in one fitting

area. The combined skin stresses in the area of that fitting of the full-scale door indicated margins-of-safety of +0.80 at 90 percent of design ultimate load. Hence, it was indicated that the door skins failed due to overload after the inadequate foaming adhesive bond failed at 99 percent of design ultimate load.

FLIGHT ARTICLE

Based on having verified the structural integrity of the composite design by analysis and structural test, one more weapons bay door was fabricated. The manufacturing procedures and the quality and reliability procedure used were those that would be established for a production effort. This door has been fully qualified as a flight article, and is planned to be installed on one of the B-1 flight test aircrafts.

COMPARATIVE WEIGHT AND COST SUMMARY

At the beginning of this program in 1973, the predicted weights were 147.6 pounds for the metal door and 119.0 pounds for the composite door, resulting in a 19.4 percent weight savings. The current calculated weight for the production metal door is now 149.9 pounds and, for the composite door, is 125.0 pounds, for a weight savings of 16.6 percent.

During this program effort, a cost-tracking system was established which could be used for accumulating the costs on near-future production of composite doors so that these costs could be compared to the metal door costs, thus verifying what the actual cost savings would be versus the predicted cost savings. Based on cost information developed using this cost-tracking system during the fabrication of these first two doors, the current prediction for the production of 240 ship sets of doors (1440) indicates a total cost savings of 10.3 percent. The following uses the metal costs at 100 percent as a baseline for each of the cost factors considered, and relates the composite costs in terms of percent of the metal costs:

Nonrecurring	Metal (%)	Composite (%)
Tooling hours	100	104.3
Tooling material $	100	74.5
Recurring		
Fabrication hours	100	77.5
Material $	100	111.2
General & Administrative	100	89.7
TOTAL	100	89.7

ACKNOWLEDGEMENT

Acknowledgement is hereby given to the following personnel who have been responsible in the key areas noted for the successful completion of this important program: F. F. MacDonald, Program Manager; D. Van Putten, Structural Design; J. Rohlen, Structural Analysis; T. McGann, Materials and Producibility; J. Jacques, Structural Test; H. Thomason, Manufacturing; and W. Heimerdinger, Quality Reliability and Assurance.

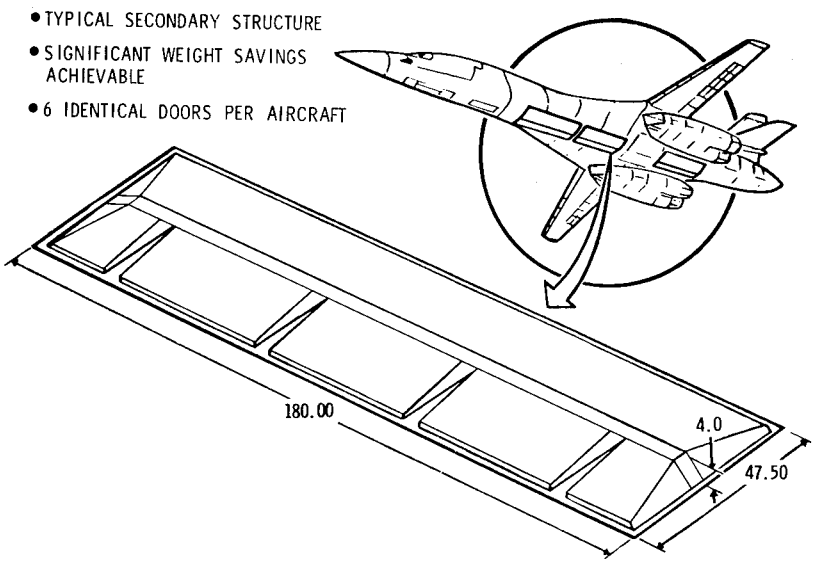

Figure 1. B-1 Weapons Bay Door

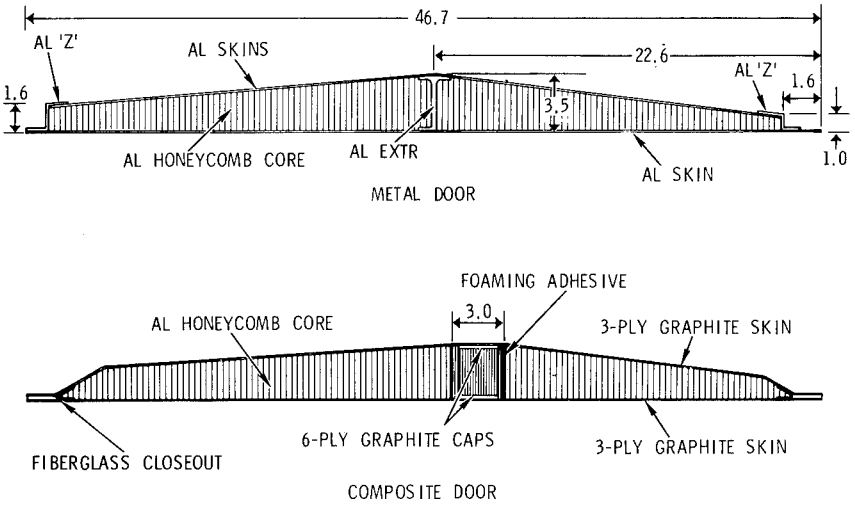

Figure 2. Configuration Cross Sections

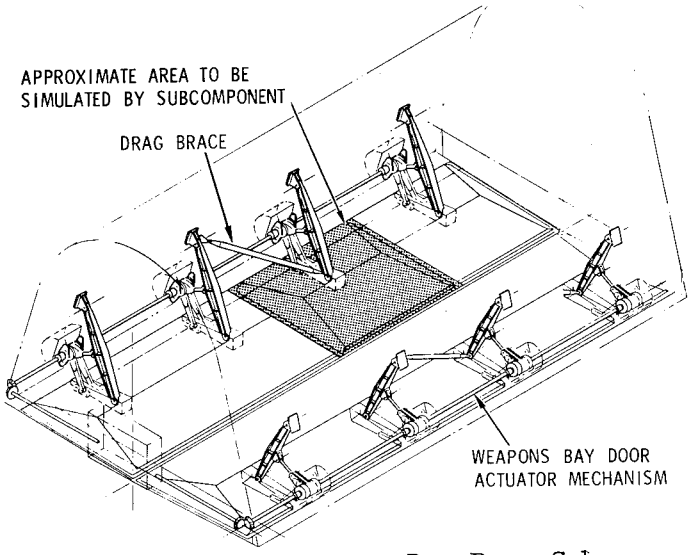

Figure 3. Weapons Bay Door Subcomponent

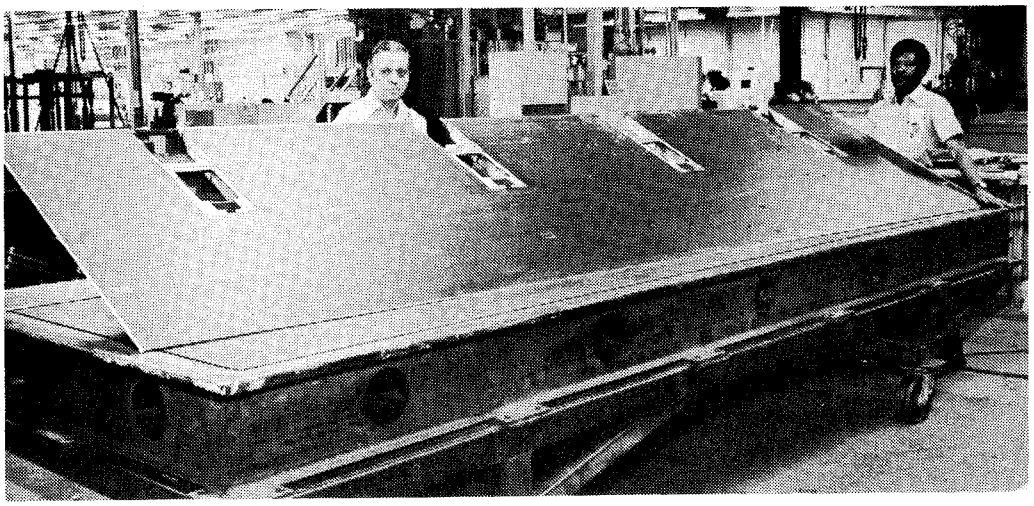

Figure 4. Composite Weapons Bay Door

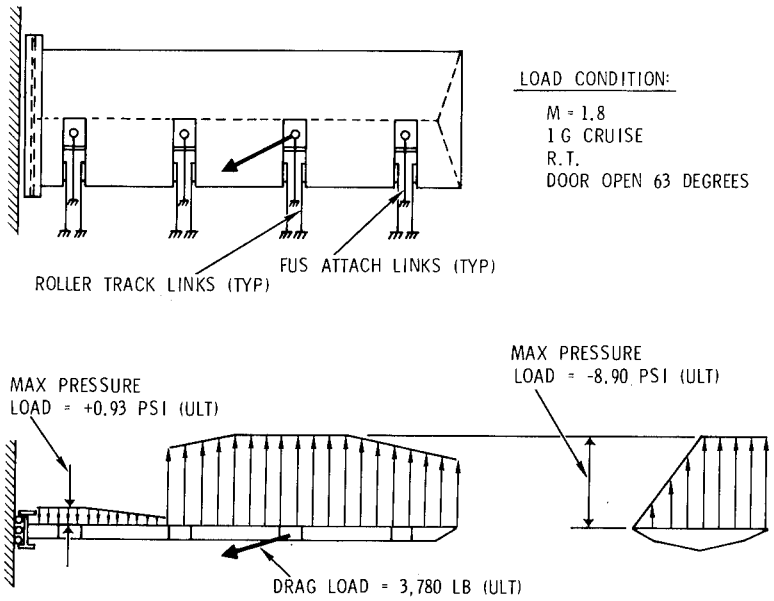

Figure 5. Static Test Loading Configuration

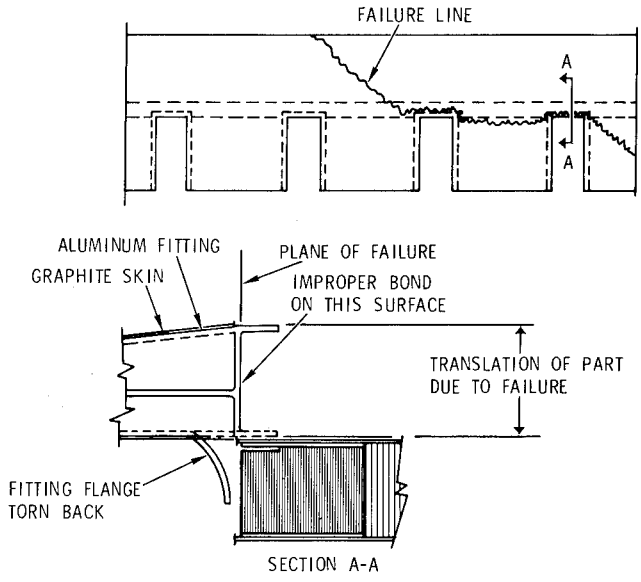

Figure 6. Static Test Failure

DEVELOPMENT OF AN A-7D ADVANCED COMPOSITE OUTER WING FOR PRODUCTION AND IN-SERVICE EXPERIENCE

By

C. R. Foreman - Vought Systems Division
LTV Aerospace Corporation

C. Tanis - Air Force Materials Laboratory

ABSTRACT

An advanced composite outer wing for the USAF A-7D aircraft has been designed, fabricated, and tested by Vought Systems Division. This work was conducted under the "Advanced Composites Production/Service Experience program sponsored by the Air Force Materials Laboratory. The program includes the fabrication of a series of production outer wings for use on A-7D aircraft in service. Static testing of wing # 1 was conducted in September and October, 1974. The composite wing failed prematurely at 120% of design limit load. A thorough failure analysis was conducted, and the causes of the premature failure were determined. The wing design was modified to correct the deficiencies found. Redesign verification specimens were built and tested to prove the design modifications. Vibration and inertia tests were conducted on wing # 2 for direct comparison to data from metal wing tests. New static and flight/fatigue test articles (wings # 3 and # 4) have been fabricated, and static testing has been started. Wing # 4 will be used for structural durability demonstration tests. These tests include proof test, flight tests, fatigue testing, P_{xx} proof tests at maximum service temperature, and a residual strength test. The wing will be moisture conditioned prior to fatigue testing. A considerable amount of experience in the design and fabrication of flightworthy advanced composite aircraft hardware has been obtained from this program. A summary of lessons learned from this program, particularly from the premature wing failure, are presented.

INTRODUCTION

In 1973, the Air Force Materials Laboratory Non-Metals and Composites Branch initiated a program to fabricate and put into service a quantity of advanced composite primary wing structures. Specific objectives of this program were to:

- Establish manufacturing technology and production experience
- Establish factual production cost data
- Obtain in-service operational experience
- Establish confidence in highly loaded composite primary structure

Vought Systems Division of LTV Aerospace Corporation was awarded a contract in 1973 to conduct a program aimed at meeting these objectives. Twenty-four left side advanced composite outer wing structures for the Air Force A-7D aircraft were to be fabricated under normal production conditions. Two of the composite outer wings were scheduled for ground and flight testing, and twenty-two were scheduled for installation on in-service A-7D aircraft. The program title is "Advanced Composite Production/Service Experience", and the contract number is F33615-73-C-5066. The engineering design of the A-7D composite outer wing was a VSD IR&D program, conducted in support of the Air Force program.

DISCUSSION

Description of the A-7D Composite Outer Wing

The A-7D outer wing was selected for use in the Production/Service Program because it is a primary wing structure that can be easily installed on or removed from the aircraft. This is possible because of the wingfold feature of the A-7D. A view of the A-7D aircraft is shown in Figure 1. The wingfold lines are shown, and the left side advanced composite outer wing structure is shown as the shaded area. The outer wing has a span of 2.4 meters and a chord at the wingfold joint of 2.9 meters. Total outer wing area is 5.2 square meters. Wing airfoil thickness (t/c) is seven percent.

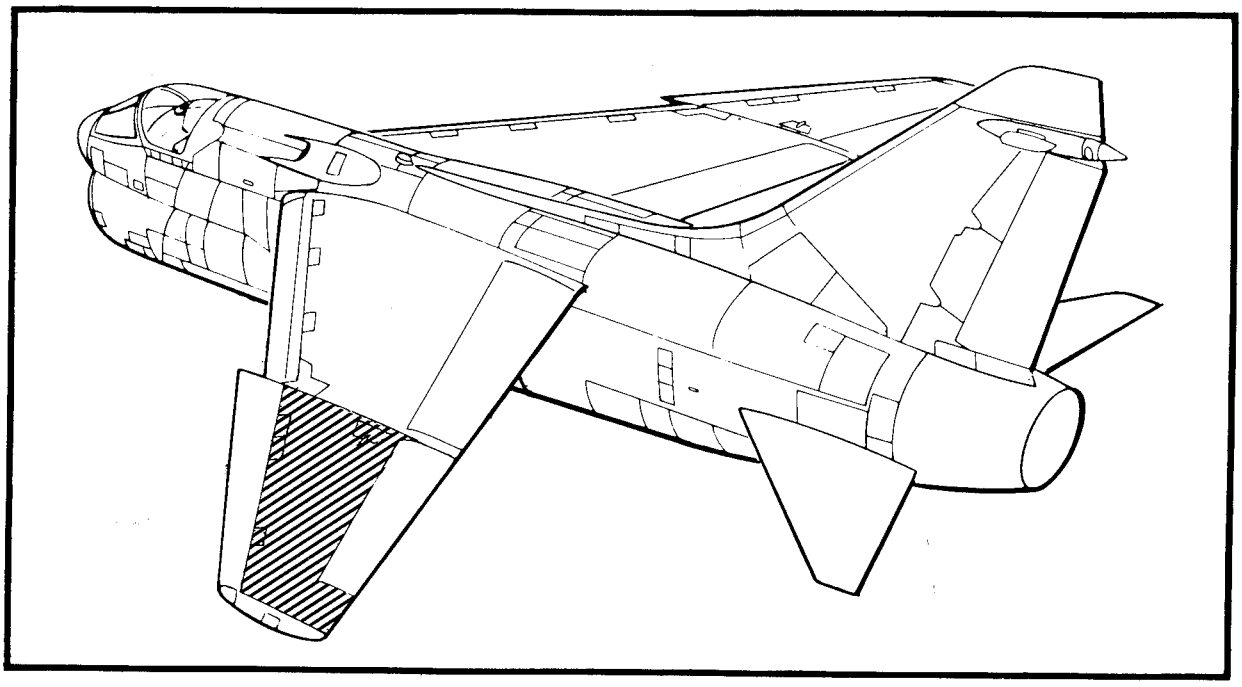

FIGURE 1 COMPOSITE OUTER WING INSTALLED ON AIR FORCE A-7D AIRCRAFT

The main structural box of the outer wing is constructed of advanced composite materials, as shown in Figure 2. The existing A-7D metal leading edge spar, fixed trailing edge, and wingfold rib were retained. The standard metal leading edge flap and aileron are also used. The composite main box area is 2.2 square meters. Maximum wing skin running load at the inboard end (wing fold splice joint) is 2.8 MN/m (16,000 lb/in.).

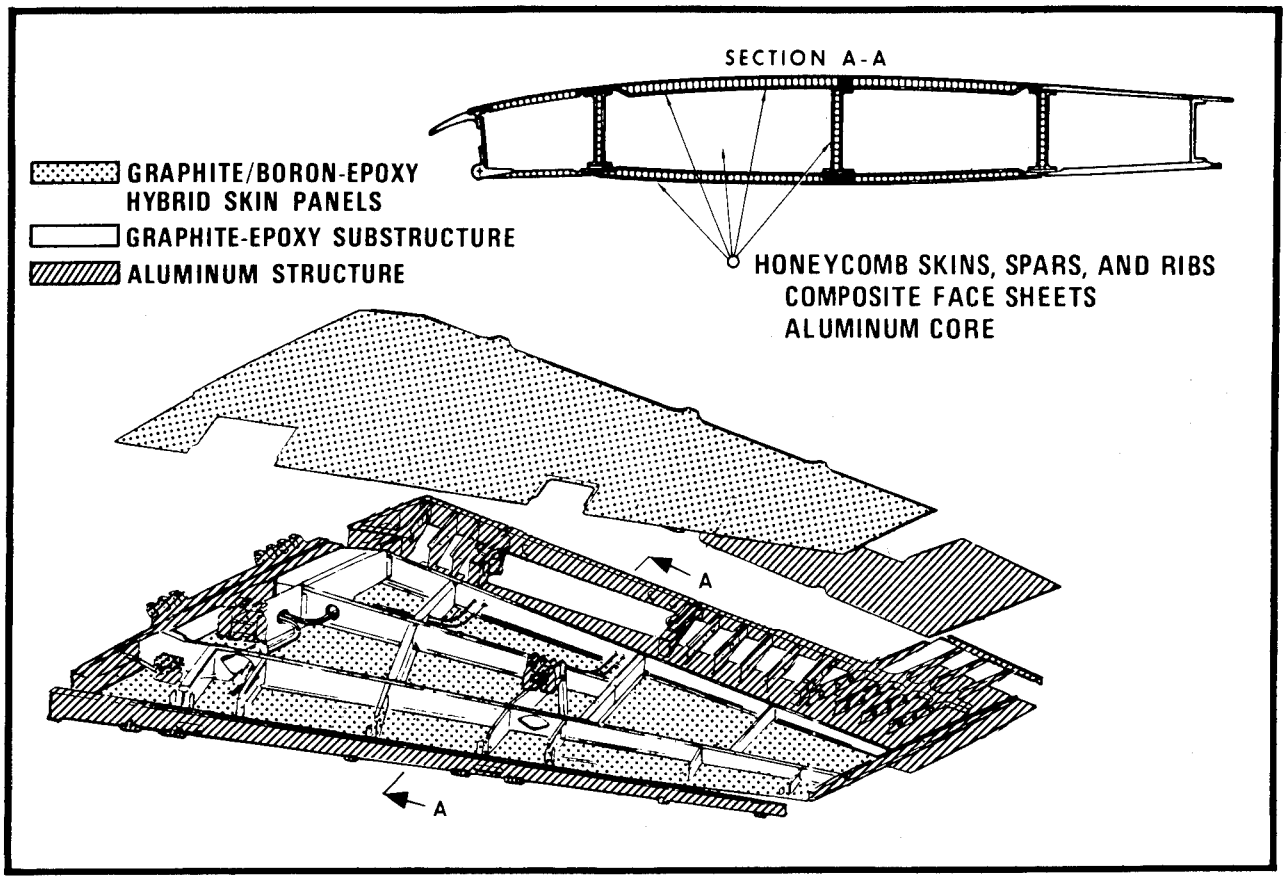

FIGURE 2 STRUCTURAL DESCRIPTION

Details of the composite wing box construction are presented in Figure 2. Upper and lower skins are honeycomb sandwich panels with graphite/boron-epoxy hybrid faces and aluminum core. The hybrid skin face materials used are NARMCO 5208/T-300 graphite prepreg and AVCO 5505 boron prepreg. Cure temperature for the skins is 177 °C (350°F). These skin panels contain numerous internal inserts and doublers at points of concentrated loads. The front, mid, and rear spars are graphite/epoxy. The webs are sandwich construction with aluminum core. Flanges are solid graphite/epoxy laminate approximately 0.5 cm thick. All of the seventeen rib sections are graphite/epoxy. Part of the ribs are solid laminate construction, and part are honeycomb sandwich construction. Narmco 5209/T-300 graphite prepreg material, cured at 127 °C (260°F) is used for all of the substructure.

The most highly loaded part of the composite outer wing structure is the wingfold splice joint, described in Figure 3. The purpose of this joint is to splice wing skin loads into the aluminum wingfold rib. Internal splice plates (4 total) are used to form double shear joints. The skins and the graphite/epoxy splice plates each contain six .41 mm thick titanium shims. The wing skins transition from boron/graphite hybrid construction to all graphite construction in the area of the splice joint. The skins and splice plates are both mechanically fastened and bonded to the aluminum wingfold rib. The fasteners by themselves (no bond) are designed to take ultimate load with no failure.

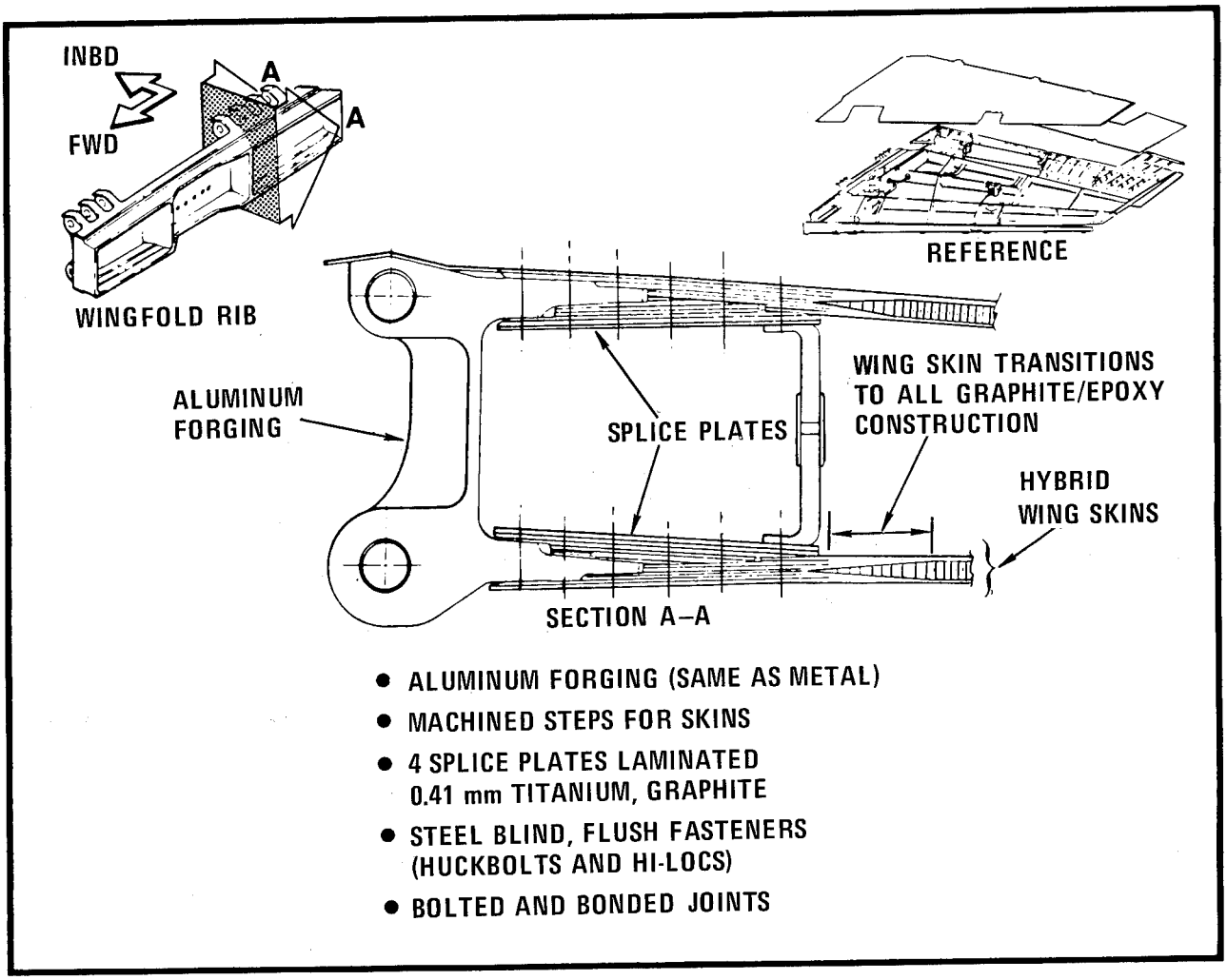

FIGURE 3 WINGFOLD SPLICE JOINT DESIGN

Assembly of the composite wing components is accomplished both with mechanical fasteners and bonding. Fasteners are used in all wingfold splice area rib-to-skin joints and in all spar-to-skin joints. In the original design, all other joints (rib-to-skin, rib-to-spar) were bonded only. A paste adhesive, 3 M's EC-3445, is used for all assembly bonding. Final assembly curing is done in an oven at 121 °C (250°F).

Program Status

Static testing of the # 1 composite outer wing was conducted during the August through October time period last year (1974). Static testing was to have been followed immediately by proof testing, flight testing, and fatigue testing of wing #2. However, the static wing failed prematurely at 120% D.L.L. in the maximum bending condition. All program work was temporarily stopped, and a detailed failure analysis was conducted during November and December 1974.

The causes for the premature failure were determined, and the necessary design revisions were started in February 1975. The current program status, starting at that time and projected to the end of the program, is shown in Figure 4. The wing redesign was completed and the new static test article, wing #3, has been fabricated. The completed wing #3 is shown in Figure 5, prior to installation in the static test fixture. In this photograph, the aileron with tension pads is installed, but the leading edge flap is not installed.

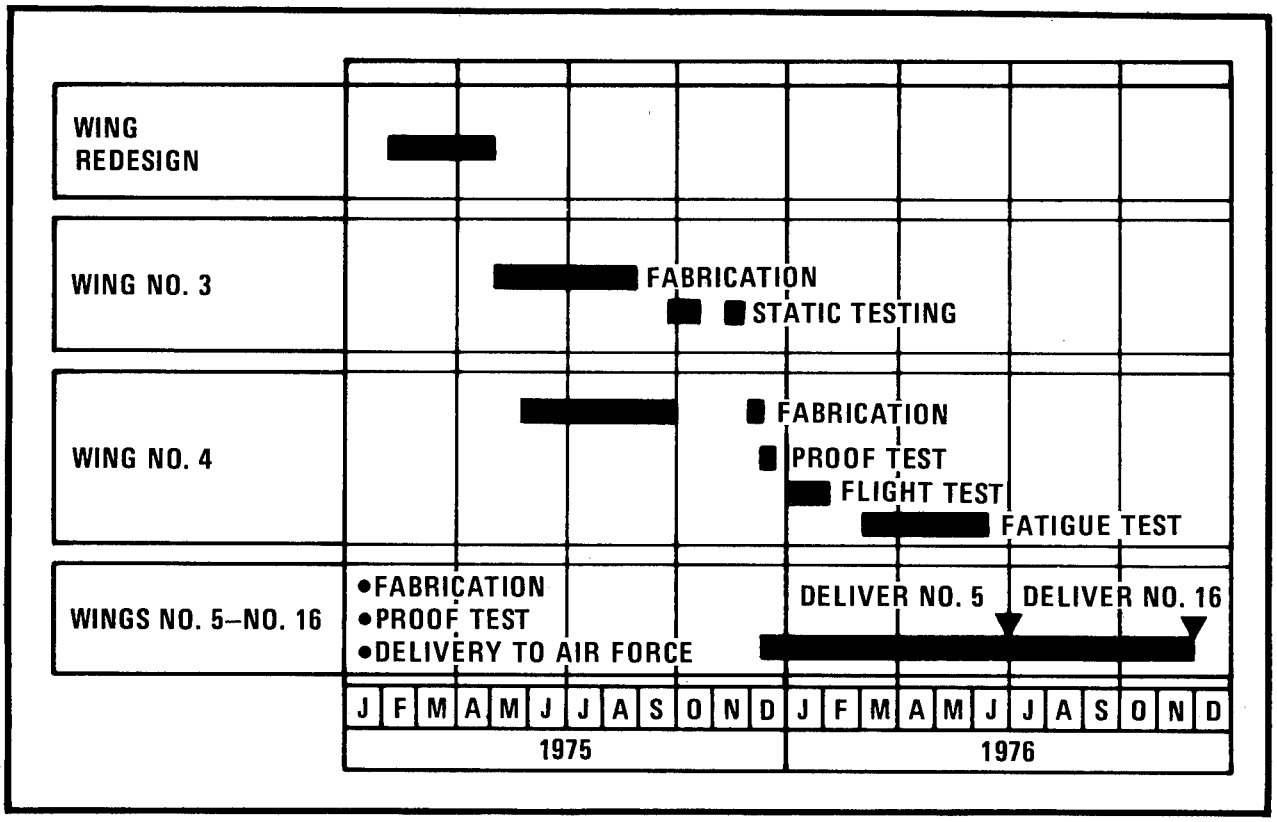

FIGURE 4 PROGRAM STATUS

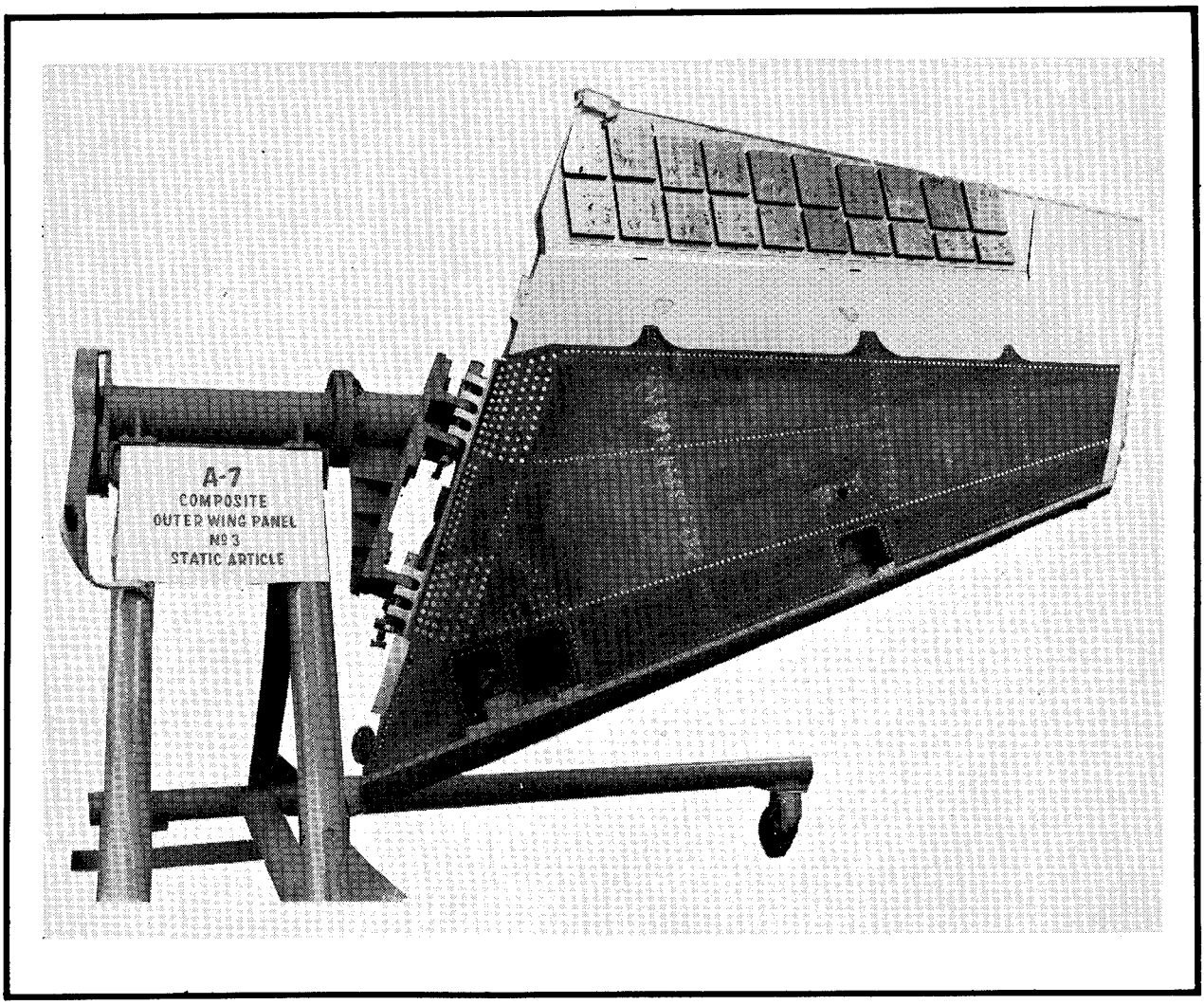

FIGURE 5 OUTER WING # 3 STATIC TEST ARTICLE

Wing # 4, the flight/fatigue test article, is complete except for final assembly bonding. Static testing of wing # 3 was started in late September. However, testing has been delayed until mid-November so that the lower skin can be locally reinforced in two areas.

After successful completion of the static tests, the # 4 wing will be completed and then proof tested, flight tested, and fatigue tested. Fabrication of outer wings # 5 through # 16 will be initiated immediately after completion of static testing. Wing # 5 will be delivered to The Air National Guard in approximately July, 1976, and wing # 16 will be delivered in about December, 1976. Reduction in the number of production composite outer wings from the original twenty-two to twelve is a result of additional expenses due to wing redesign, fabrication of two more test articles, and additional static testing.

Inertia and Vibration Tests

The primary design criteria at the start of the program was that the A-7D composite outer wing must be dynamically equivalent to the metal outer wing. This is necessary to assure that flutter margins for the wing are not changed. Specifically, it was required that the first three modal frequencies be within $\pm$ 5% of the metal wing, and that the mass and mass distribution be the same.

The composite wing skins were sized by varying ply orientations (% 0° plys vs. % $\pm$ 45° plys) and thicknesses to match the metal wing EI and GJ distributions. The original plan was to match mass and distribution by attaching ballast weights to the spars. However, because of the small amount of weight saved in the final design, the addition of ballast weights was not required. Tests were conducted on both composite and metal outer wings to determine c.g. locations and rolling and pitching moments of inertia. It was concluded from these tests that good inertial similarity exists between the metal and composite outer wings.

Comparison of modal frequencies between two metal and composite outer wings was made by conducting vibration tests. The wings were mounted vertically in a fixture which picks up the wing fold lugs and attaches rigidly to the test lab floor. Therefore, the wings were cantilevered from a fully-fixed base. (In actual practice, the base only approaches being fully fixed.) A summary of the tests conducted is presented in Figure 6. Tests were conducted without the aileron installed, but with

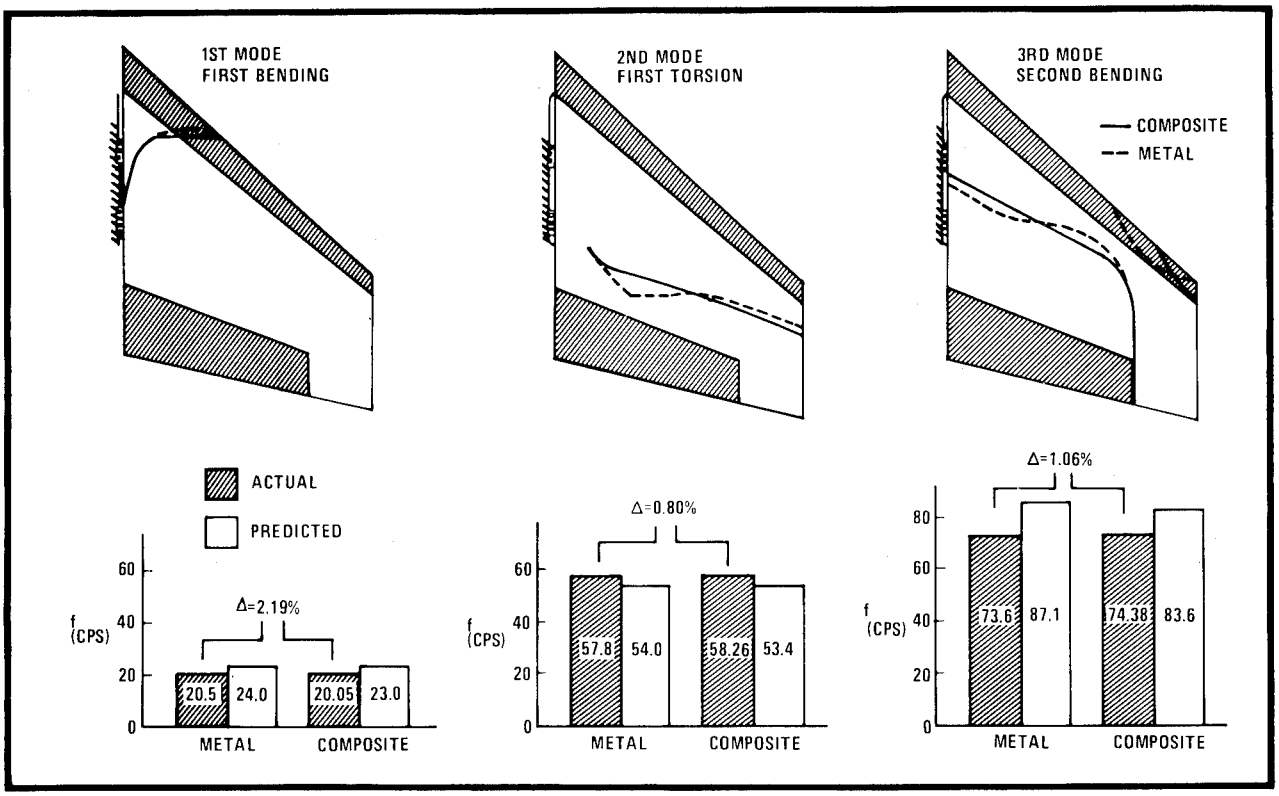

FIGURE 6 COMPARISON OF METAL AND COMPOSITE WING VIBRATION TEST RESULTS

the L.E. flap. This data shows that an excellent match of frequencies between metal and composite outer wings was obtained for the first three modes. Analytical frequency predictions were also reasonably accurate compared to test values. Most of the difference that does exist is due to the fact that the mounting fixture is not completely rigid as assumed in the analysis.

Static Tests - Wing # 1

For static testing, the A-7D composite outer wing is attached to a standard metal A-7 center wing. The center wing is mounted in a support tower. An actual A-7 center wing structure is used instead of steel test structure because the load distribution in the wing fold lugs and wing fold joint is quite sensitive to the stiffness characteristics of the attach structure. Counter balancing hydraulic actuators are used on the center wing to prevent overloading.

Loads are applied to the main box structure by compression pads located over the front and rear spars. Seven load frames and a whiffle-tree arrangement are used to correctly distribute the loads to the compression pads. The aileron is loaded by tension pads, and the L.E. flap by compression pads.

The # 1 static test wing was instrumented with 183 strain gages and 10 deflection transducers. This instrumentation required 419 data channels. 70 axial and 113 rosette strain gages were used. All instrumentation was recorded at each load increment up to 120% D.L.L. Approximately twenty gages were monitored and plotted during the test.

Static testing of the A-7D outer wing involves four critical design conditions:

- o LFR-2 Level Flight Roll, 0g pushover, maximum download on L.E. flap
- o RPO-2A Rolling Pullout, unsymmetric 5.6g, maximum wing torsion
- o HA(D-1) Symmetric Pullout, 7.0g, maximum wingfold joint loads
- o LA(D-1) Symmetric Pullout, 7.0g, maximum wing bending, i.e., maximum skin load

The maximum negative load condition, IMA (D-1), is not included in the test conditions. It is a -3.0g condition, or only 43% of the maximum positive bending load, and is not critical for any portion of the structure. During the static testing last year, the following maximum loads were obtained for each test condition:

- o LFR-2 150% (ultimate)
- o RPO-2A 100% (limit) 120%, Wing # 2
- o HA(D-1) 100% (limit)
- o LA(D-1) 120% (wing failure)

During the initial LFR-2 tests, some debonding occurred between four L.E. ribs and the front spar, and between the upper skin and the L.E. spar. These joints were repaired and reinforced, and the LFR-2 condition was retested. Ultimate load was successfully achieved.

After testing the remaining three conditions to limit load, ultimate load tests were started. The wing failed catastrophically at 120% D.L.L. level, while instrumentation data was being taken. The composite main box structure completely separated at approximately one-fourth span. Fracture lines and locations are described in Figure 7. The lower (tension) skin fracture surfaces were very clean and straight, except at the rear spar aileron tab area. The upper (compression) skin fracture surfaces were very jagged, with a considerable amount of splintering and delamination.

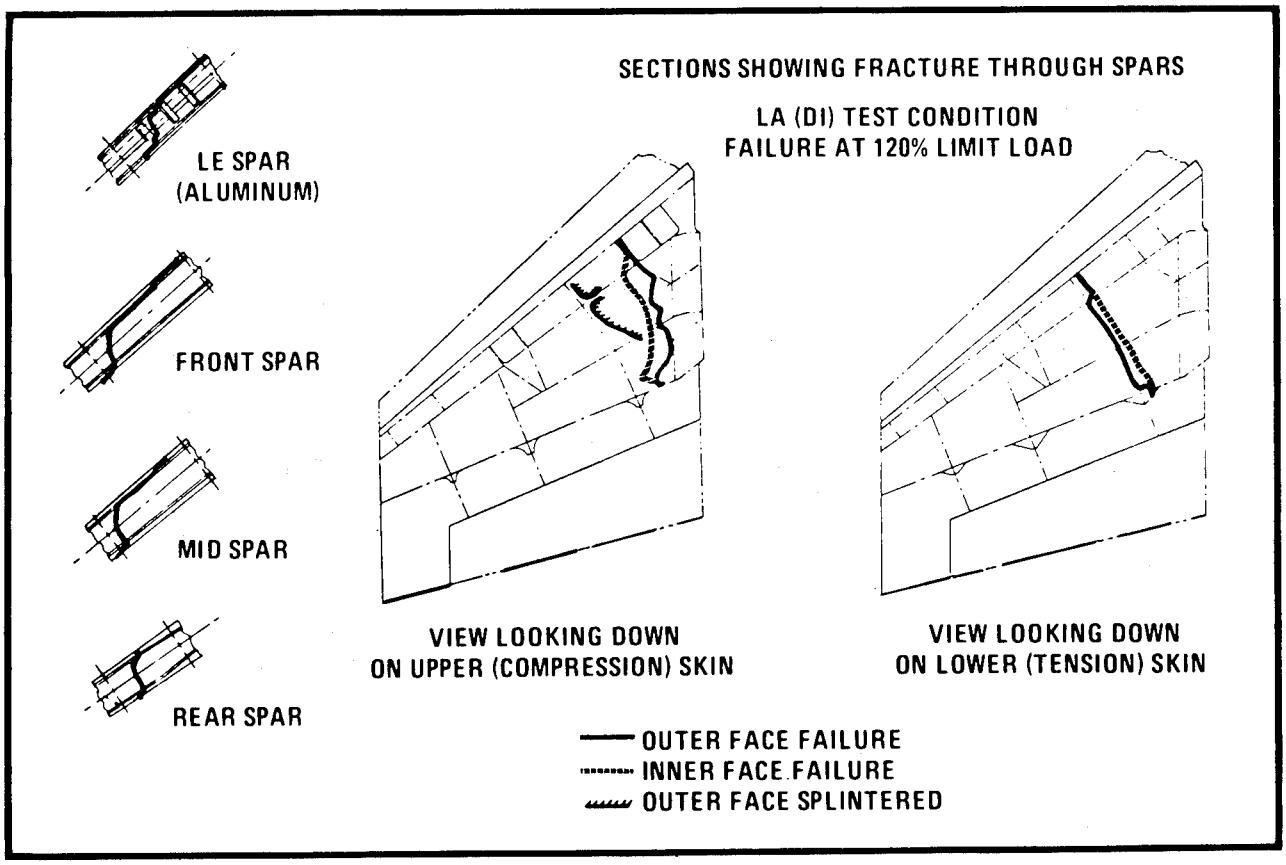

FIGURE 7 FAILURE LOCATION, WING # 1 STATIC TEST

Failure Investigation

Immediately after the wing failure a comprehensive failure investigation was initiated. The following is a summary of the work conducted:

(1) Verification of Applied Loads - Test fixture load linkage geometry was rechecked. Hydraulic cylinder load cells were recalibrated. Conclusion: test loads were correctly applied.

(2) Material and Process Evaluation - Debond of lower skin aileron tab titanium insert was investigated. Photomicrographs of skin laminates were prepared and analyzed. Material fiber volumes and per-ply thicknesses were determined. Conclusions: Titanium insert was debonded before test, but was not primary cause of failure. Skin laminates had low void content and correct ply thicknesses.

(3) Material Property Data - Quality Control specimen data was reviewed. Tension, compression, and flatwise tensile specimens were cut from the wing skins and tested (A total of 80 specimens were prepared and tested). Conclusion: The mechanical strength properties of the # 1 wing material were acceptable, and did not contribute to the premature failure.

(4) Analysis of Strain Gage Data - Plots of individual gages were made at many locations. Spanwise and chordwise strain plots were made of gages in the vicinity of the wing skin fracture lines. Conclusion: The point of maximum strain in the tension skin is in the inboard, aft corner of the skin, adjacent to the inboard aileron tab. The fracture line goes through this point of maximum strain.

(5) Rib Flange Doubler Specimen Tests - The wing skins contain internal graphite/epoxy doublers over the inboard, mid, and outboard rib flanges. These doublers fit into a rabbited section of the h/c core, as shown in figure 8 (a). In the original design, these doublers are constructed of 100% longitudinal plies (90° from the 0° skin orientation). The purpose of these rib flange doublers is to provide additional rib flange area in the skin, and to shear the concentrated load from the aileron tab into the skins. The failure lines in the tension skin followed the edge of the rib flange doubler very closely. This raised the suspicion that the flange doubler could have contributed to the premature wing failure. Verification specimens simulating the skin face/rib flange doubler interface were fabricated and tested. These specimens and test results are shown in Figure 8 (a). These tests showed that the rib flange doublers result in a stress concentration in the skin faces of K_T=1.19. Conclusion: The rib flange doubler/skin interface does cause a stress concentration in the skin. However, the K_T was not of sufficient magnitude to cause the premature wing failure.

(6) Wing # 2 Tests - Wing # 2 was completed shortly after failure of wing # 1. Wing # 2 was heavily strain-gage instrumented in the area of the lower skin around the inboard aileron tab and fracture line. The wing was tested to 70% D.L.L. in the LA(D-1) condition. Strain-gage data was plotted and analyzed. Strain values were extrapolated to the 120% failing load level. This indicated a maximum strain of 3,770 μ in/in. Analysis of the rosette gage data showed the maximum principal strain to occur

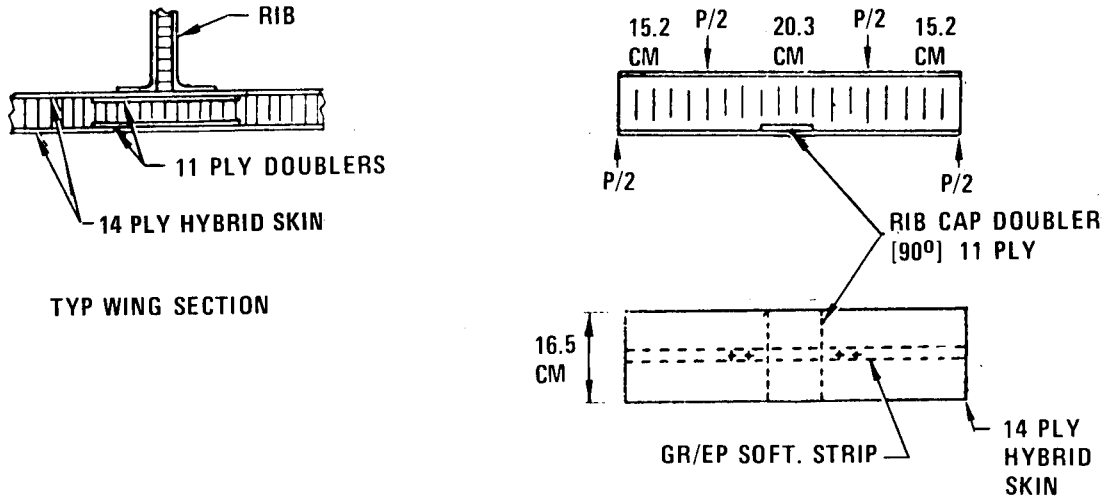

4 SPECIMENS TESTED
AVG FAILING LOAD
95.5 KN WITHOUT DOUBLER
80.3 KN WITH DOUBLER
K_T = 1.19

(A) RIB FLANGE DOUBLER SPECIMENS

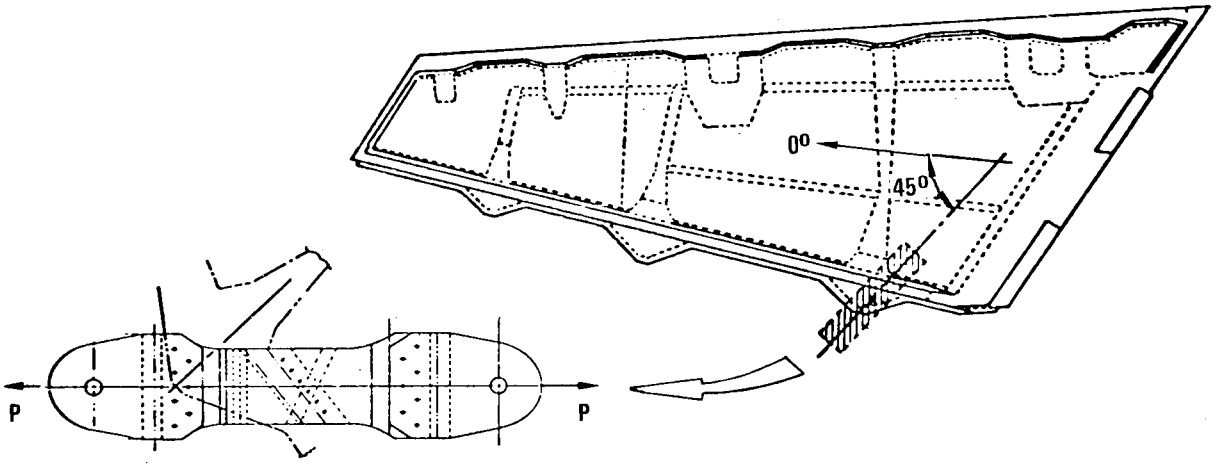

3 SPECIMENS TESTED
MINIMUM STRAIN AT FAILURE IN CRITICAL AREA = 3,500 μ IN./IN.

(B) OFF – AXIS AILERON TAB SPECIMEN

FIGURE 8 FAILURE INVESTIGATION SPECIMENS

15° from the 0° skin ply orientation. This "off-axis" maximum strain vector is evidence of the biaxiality resulting from the aileron tab tension load (the aileron tab load is applied approximately 90° to the wing 0°, or spanwise bending, direction). Conclusion: The maximum tension skin strain was 60% higher than predicted by the NASTRAN math model, and this strain occurred 15° off of the 0° skin ply orientation.

(7) Strain Allowable Specimens - Two types of specimens were fabricated and tested to determine the failing strain level in the ± 45° graphite/epoxy softening strip in the trailing edge of the skin, over the rear spar. Both types of specimens were designed to represent loads applied 45° to the skin 0° direction. This, of course, results in a 0°, 90° ply orientation in the specimens. The 0°, 90° ply orientation represents the worst case, or lowest failing strain, that could occur in the skin. This would occur if the principal strain in the outer panel were at an angle of 45° to the spanwise direction, thus aligning itself with the ± 45° plies. There is some conservatism in this specimen design approach, since the maximum principal strain lies 15° from the spanwise direction. The first type of specimens tested were a series of ten tension coupons consisting of 12 plies in a balanced 0°, 90° layup. The average failure strain of the specimens with fastener holes was 4,450 μ in/in. The allowable strain was set at a value of 90% of 4,450, or 4,005 μ in/in. The second type of specimens fabricated and tested were "off-axis" tensile specimens. These relatively complex specimens, described in Figure 8 (b), represented a 10.2 cm wide section of the lower wing skin at the inboard aileron tab area. The minimum failure strain value obtained from the three specimens was 3,500 μ in/in, at a gage that is best representative of the free-field condition in the most critical region. Conclusion: A conservative allowable strain value for the lower skin trailing edge softening strip is 3,500 μ in/in. This correlates quite well with the 3,770 μ in/in strain value predicted at 120% D.L.L. from tests of wing # 2.

All of the analysis and testing work described in items (1) through (7) above resulted in a clear definition of the cause of the failure of wing # 1 at 120% D.L.L. The possibility of a compression skin failure was ruled out fairly early in the investigation. The physical evidence of the fracture surfaces indicated a tension skin failure. Also, compression test coupons cut from the upper skin failed at fairly high load levels. The area of failure initiation was narrowed down to the inboard aileron tab of the lower skin.

The conclusions from the failure analysis are summarized in Figure 9. The failure initiation point (point "A") is located at a rear spar fastener hole in the area of maximum skin strain. The stress concentration caused by interruption of spanwise graphite plies to make room

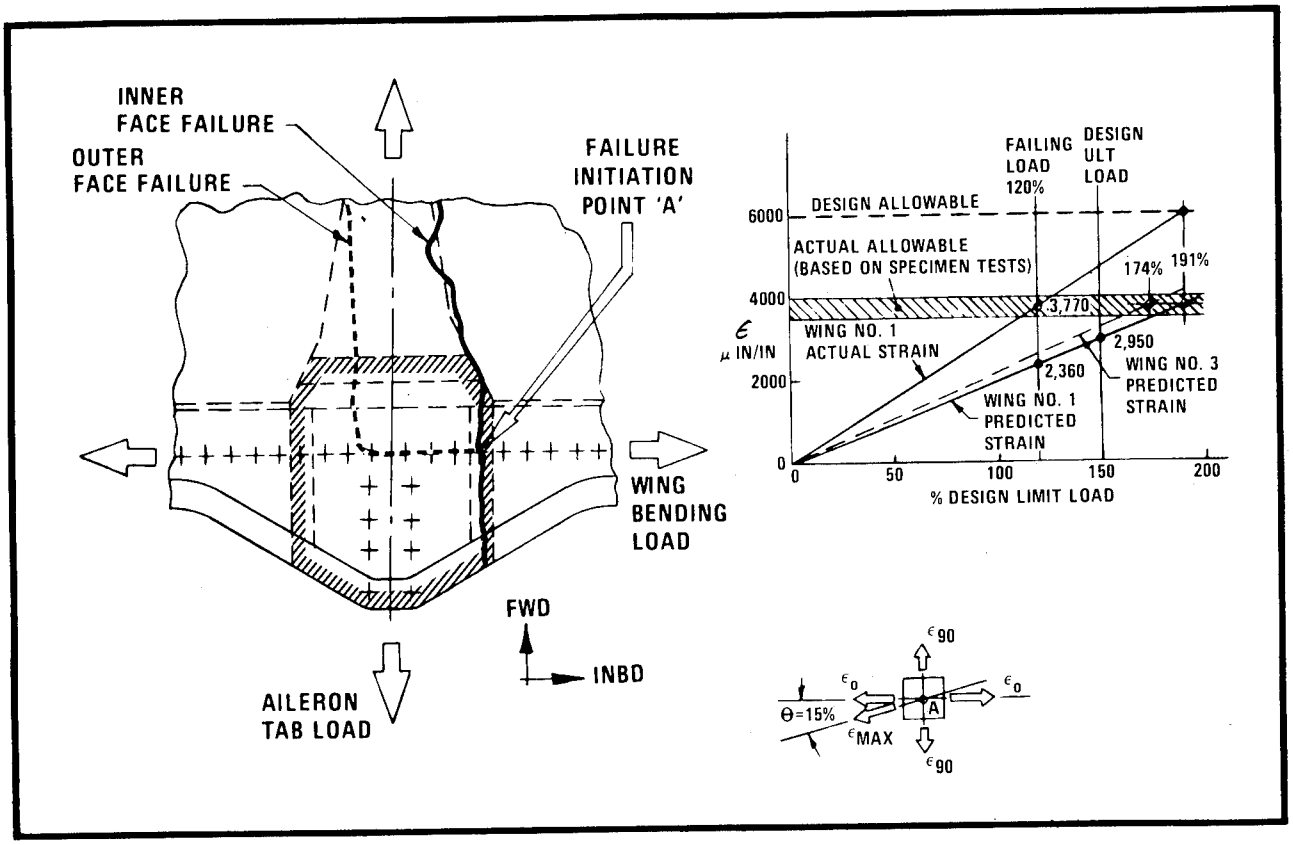

FIGURE 9 CONCLUSIONS FROM FAILURE ANALYSIS

for the titanium insert may have contributed to the early failure. Also, the partial debond of the titanium insert to outer skin face joint could have reduced the failing strain level. Once the failure started, it progressed down the edges of the rib flange doublers, because of the stress concentration caused by the doublers. The primary causes of the premature failure are presented in the graph in Figure 9. As mentioned above in item (6), the maximum skin strain was approximately 3,770 μ in/in, instead of 2,360 as predicted by the original NASTRAN math model. Also, the design allowable strain in the $\pm$ 45° softening strip is in the range of 3,500 to 4,000 μ in/in, instead of the 6000 μ in/in allowable used in the original design. Thus, the high margin of safety predicted during the wing design was really -20%, or failure at 120% D.L.L. If the actual strain had been as predicted by the NASTRAN model (2950 μ in/in at ult.) failure would have occurred at 191% D.L.L., using the actual strain allowable of 3,770 μ in/in.

Failure Redesign

Redesign of the A-7D composite outer wing was conducted in early 1975 to correct the deficiencies uncovered during static testing of wing # 1. The design changes incorporated are summarized in Figure 10.

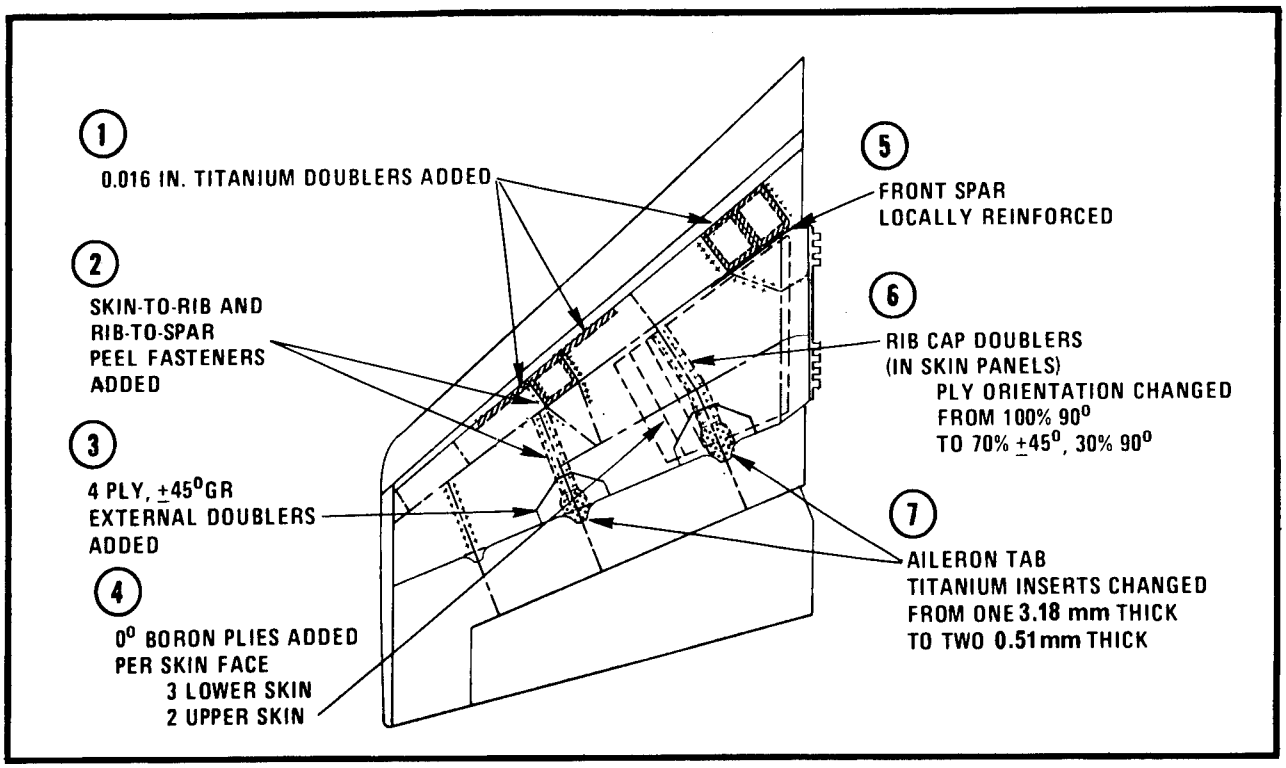

FIGURE 10 DESIGN CHANGES

The first design changes made were the result of L.E. rib-to-skin and rib-to-spar debonds, and fastener hole bearing failure in the upper skin L.E. access doors. Change # 1 shown in Figure 10 is the addition of .41 mm thick titanium doublers around the edges of the access doors and in the leading edge of the skin. Also, L.E. rib-to-front spar clips were added.

One of the most significant changes made to the wing was the addition of "peel" fasteners in skin-to-rib and rib-to-spar joints (design change # 2 in Figure 10). A major feature of the original design was that these joints were bonded - only (no fasteners). Thus, there were fastener holes in the skins only in the softening strips, over the spars. No drilling through boron was required. Peel fasteners were added during redesign for two main reasons. First, the average rib flange bond failing stress was somewhat less than the allowable used for design (13.8 MN/m^2 at ultimate). Secondly, it was decided that it was almost impossible to provide the level of manufacturing quality control and post cure inspection necessary for primary aircraft structure such as the A-7D outer wing.

Fasteners were added at 7d to 10d spacing in the skin-to-rib joints, and approximately 5d spacing in the rib-to-spar joints. A series of fifteen specimens were fabricated and tested to determine the feasibility of putting fastener holes in the boron/graphite hybrid areas of the wing skins. These specimens are shown in Figure 11 (a). The

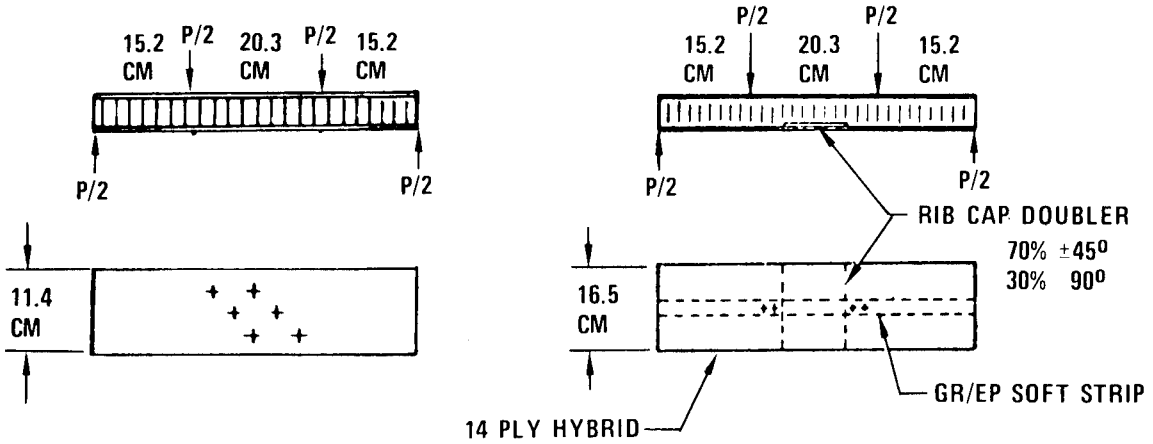

15 SPECIMENS, 4 PATTERNS TESTED
7D SPACING SELECTED
K_T = 1.64 (BASED ON STRAIN)

(A) BORON K_T SPECIMENS

3 SPECIMENS TESTED
AVG FAILING LOAD
95.5 KN WITHOUT DOUBLER
87.4 KN WITH DOUBLER
K_T = 1.09

(B) RIB FLANGE DOUBLER SPECIMEN
(NEW DESIGN)

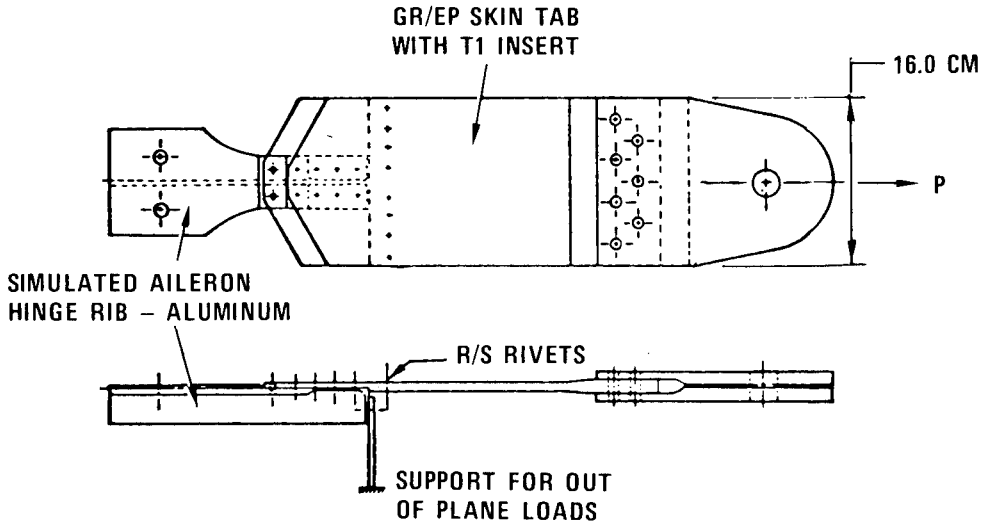

3 SPECIMENS TESTED
P_{AVG} = 14,380 K_g FAILING LOAD
(321% D.L.L.)

(C) AILERON TAB JOINT SPECIMEN

FIGURE 11 REDESIGN VERIFICATION SPECIMENS

7D minimum fastener spacing configuration selected for the skins results in a strain concentration of K_T= 1.64. The maximum skin strains in the areas of the added fasteners are low enough so that adequate margins of safety are maintained.

Design change #3 in Figure 10 is the addition of 4 ply, $\pm$ 45° graphite/epoxy external doublers over the inboard and mid aileron tab areas of the upper and lower skins. These doublers locally provide a reduction in strain in the skin around the aileron tab areas.

Design change # 4, however, provides the major reduction in skin strains. Three additional 0° boron plies have been added to each face of the lower skin, and two to each face of the upper skin. These 0° boron plies were added to the inboard portion of the wing, as shown in Figure 10. The predicted reduction in wing #3 skin strain is 34%, and is shown as the dashed line in the graph in Figure 9. Thus, the predicted failing load level for this particular area of the skin is 174% of D.L.L.

Strain gage data from the limit load RPO-2A test condition last year indicated that strains in the front spar around the inboard cutout, and inboard of that cutout, were higher than predicted. These strains would produce a marginal strength situation at ultimate load, based on failing strain levels obtained from previous front spar cutout specimen tests. Therefore, the inboard section of the front spar has been reinforced in wing # 3. This is shown as design change # 5 in Figure 10. Five plies of graphite were added to each face of the honeycomb web, from the inboard cutout to the inboard end of the spar. Also, the graphite reinforcing angle over the cutout was enlarged.

The wing skin rib flange doublers, discussed previously in the failure investigation section, were redesigned. This is shown as design change # 6 in Figure 10. Ply orientation of the inboard and mid rib flange doublers was changed from 100% 90° (chordwise) plies to 70% $\pm$ 45°, 30% 90° plies. This was done so that the modulus and thermal coefficient of expansion would more closely match that of the wing skin faces, reducing the K_T in the skins due to the doublers. New specimens, shown in Figure 11(b), containing the revised doubler ply orientation, were fabricated and tested. These specimens were identical except for doubler orientation to those described in Figure 8(a). The results of these specimen tests showed that the stress concentration due to the doublers was reduced from K_T 1.19 to K_T+1.09.

Design change # 7 shown in Figure 10 is a modification of the titanium inserts in the aileron tabs. Titanium inserts are required to provide the necessary bearing strength for the aileron hinge rib fastener loads. In the original design, one machined insert 3.18 mm thick was used. This thick insert abruptly interrupted many of the skin softening strip graphite plies. It's stiffness also caused some "bridging" problems in the tab areas during layup and curing of the skins. This thick insert was replaced by two .51 mm thick titanium inserts of the same general size and shape. Aileron tab joint specimens were fabricated and tested to verify this design change. These specimens are

described in Figure 11 (c). The average failing strength of the three specimens was 321% of D.L.L.; considerably above the required load. This design change produced a much more efficient aileron tab design; i.e., stronger and somewhat lighter.

All of the design changes described in the proceeding paragraphs have been incorporated into wing # 3 static test article and wing # 4 flight/fatigue test article. They will, of course, also be incorporated into production wings # 5 through # 16.

Static Tests - Wing # 3

Static testing of wing # 3 was started in late September, as shown in the program status in Figure 4. Wing # 3 must be tested to ultimate load in three conditions: RPO-2A, HA(D-1), and LA(D-1). During testing of the RPO-2A condition (maximum wing torsion), a localized delamination and fracture occurred in the thin (4 ply per face) inboard front bay area of the lower wing skin, at 138% of D.L.L. This fracture resulted from a locally high shear strain adjacent to an inboard L.E. rib and the front spar.
This skin fracture has been repaired by bonding on an external doubler over the damaged area. The bond adhesive was cured by placing the wing in an oven. This repair resulted in a one month delay in the static test program. The repair has been completed and testing will be resumed during the second week in November.

Structural Durability Demonstration - Wing # 4

The A-7D composite outer wing is primary, critical to flight safety structure, and will be flown on in-service aircraft with no imposed flight restrictions. It must, therefore, be flight qualified under the latest Air Force structural durability demonstrations requirements for composite structures.

These requirements are by no means firm at this time, and are constantly being improved and better defined. Composites structural durability requirements have not yet been formalized into Military Specifications.

During the past year and a half, VSD and the Air Force have worked closely together to add environmental considerations to the original wing # 4 structural durability demonstration plan. The original plan included proof testing, flight testing, fatigue testing (under ambient conditions), and residual strength testing to failure. The latest plan is illustrated in Figure 12. The thirty-day accelerated presoak and "P_{xx}" proof test have been added to the plan.

The latest Air Force requirements for fatigue testing of flight safety critical composite structure specify that testing must be done under representative service temperature and humidity environmental conditions. Since the A-7D is a subsonic aircraft, most all flight time will occur with wing temperature of 24°C (75°F) or less.

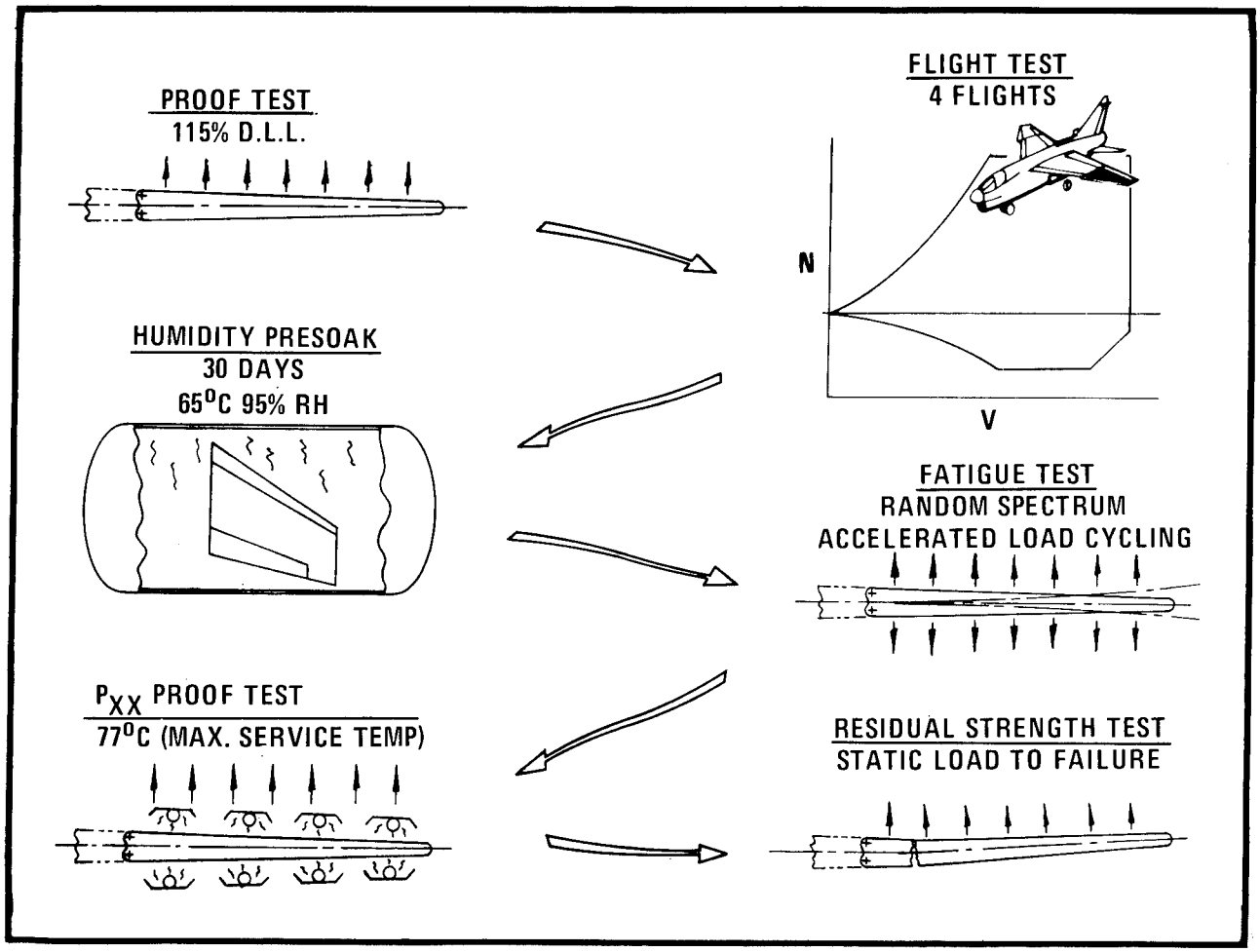

FIGURE 12 STRUCTURAL DURABILITY DEMONSTRATION, WING # 4

It is desired, however, that the fatigue test article absorb and contain a moisture level approximating the level that would be achieved after long term exposure in a high humidity environment. For the A-7D composite outer wing, this seems to be about .8 to 1.2% moisture (by weight).

The problem, then, is to obtain this moisture level in wing # 4 within a reasonable length of time, prior to fatigue testing. Absorption calculations show that thirty days at 95% relative humidity and 65°C (150°F) would result in approximately the desired moisture content in the composite materials. The present plan to obtain these conditions for presoak is to place the wing into an autoclave. Steam will be injected into the autoclave to obtain saturated air at 65°C. A "trial run" will be made before presoaking wing # 4 to uncover any problems and determine how closely the temperature and humidity can be controlled.

Desorption calculations show that drying-out of the wing during fatigue cycling occurs quite slowly at ambient test laboratory conditions. Therefore, maintenance of a humidity environment during fatigue testing will not be required.

After completion of fatigue testing to the prescribed number of equivalent flight hours, a demonstration of the ability of the structure to carry "P_{xx}" loads at maximum service temperature is required by the Air Force. P_{xx} is the maximum average internal member load that will occur in the outer wing once in "M" times the inspection interval. In the case of the A-7D outer wing, P_{xx} load is equal to design limit load. Maximum service temperature for the A-7D outer wing occurs after the aircraft sets on the runway for several hours on a clear, 43°C (110°F) day. This maximum wing temperature is 77°C (170°F). The method to be used for obtaining the 77°C wing structure temperature has not been finalized at this time. The temperature will most probably be obtained with heat lamps surrounding the wing during testing.

After successfully passing the P_{xx} test, the # 4 outer wing will be statically tested to failure to determine its residual strength. This will be done using LA(D-1) test loads, so that test results will be directly comparable to that of the static test wing # 3 failing load test. Results of wing # 3 static test and wing # 4 residual strength test will be used to determine the proof test load level required for production wings # 5 through # 16. Each production outer wing will be proof tested prior to delivery to the Air Force and installation on A-7D aircraft.

CONCLUSIONS

A considerable amount of knowledge and experience in the design and fabrication of flightworthy advanced composite aircraft hardware has been obtained from this program. The premature wing failure was disappointing and disruptive from the standpoint of achieving the main program objectives. However, the additional probing, testing, and analysis required because of the failure has been a technically rewarding experience, and has significantly increased the experience and data base available for designing future advanced composites structures. A summary and discussion of accomplishments and lessons learned are presented in the following paragraphs.

Accomplishments

The most tangible accomplishments of the program to date are the four composite outer wing structures which have been fabricated. Significant improvements and innovations in materials processing, fabrication, and quality assurance techniques were required for the fabrication of these wing structures. Several specific program accomplishments should also be mentioned:

(1) The composite wing matched stiffnesses and frequencies of the metal wing within ± 2%. This was done at the start of the

wing design program using relatively simple "hand" calculations. This further demonstrates the feasibility of using composite materials to precisely tailor structural stiffness distributions.

(2) One of the four required static test conditions, LFR-2, has been successfully tested to ultimate load. This condition is critical for the L. E. flap support structure and most of the L. E. ribs.

(3) The specific causes of the premature failure were identified and verified with specimen tests.

(4) The wing design was revised to eliminate the structural deficiencies found from static testing, and a new static test wing (# 3) was fabricated.

(5) A structural durability test plan has been developed. This plan is the first application of the new Air Force composite structures durability requirements to a major structural component.

The most important accomplishment is yet to be attained: successful completion of the static test program. This should be done by the end of November.

Lessons Learned

It is felt that many of the experiences and lessons learned from the program, particularly those from the failure investigation, might be of benefit to other people in government and industry who are involved with similar composites technology and programs. Undoubtedly, some of the "lessons learned" presented will be long-accepted practice for some organizations. Seven of the more important lessons learned are presented and discussed below.

(1) Design and analysis of "real world" wing structures are considerably more complex than box beam technology. A single cell box beam, similar in construction and materials to the complete outer wing, was fabricated and successfully tested. Much optimism about the future success of the composite outer wing was generated from the success of this box beam. However, none of the problem areas encountered in the composites wing structure were represented in the simplified box beam design. For instance, the box beam rib-to-skin and rib-to-spar bond joints were not highly loaded, because no torsion load was applied to the box beam. Aileron tab biaxial loading and L. E. flap hinge and actuator loads were not applied to the box beam. The lesson learned is that, while simplified box beams are quite valuable in providing early verification of a new wing design, their limitations in representing the real structure should be understood and kept in mind.

(2) Current NDI techniques are not adequate for inspection of bonds in primary structure. Ultrasonic (through - transmission or pulse-echo) NDI is the best technique currently available for inspection of com-

posite laminates and bond joints. Ultrasonic NDI will show, with good reliability, whether a joint is bonded, but cannot distinguish between 10 percent and 100 percent bond strength. Detail inspection of the # 1 static wing after failure revealed some joints with poor bonds and low bond strengths which had not been detected during the extensive quality inspection during fabrication. This, of course, is the reason that the Air Force requires proof test inspection of every production article of flight safety critical components containing structural bonds. The use of structural bonds without fasteners in primary structure should be carefully evaluated during the preliminary design stages.

(3) Use fasteners in joints where high loads are transferred. The original composite outer wing design included bonded - only rib-to-skin and rib-to spar joints. It was thought that if the allowable average stress in the bond joint were kept well below the adhesive lap shear test strength (less than 33%), the peel forces would not be a problem. Bond failures occured in the # 1 static test article at approximately 15% of the adhesive lap shear strength. It was concluded that the all-bonded joint design was feasible but not very efficient at the lower stress level. Also, all bonded joints subjected to large peel forces are very vulnerable to bond void defects. Such bond defects are difficult to detect with NDI, and can cause bond failures at very low stresses. The lesson learned, then is that fasteners should be used in joints where high loads are transferred.

(4) Access for inspection and repair is essential. Since the A-7D composite outer wing is a bonded structure, access to the interior bays for repair is possible only by cutting access holes in the upper or lower skins. This, of course, would be worse damage than that being repaired. The interior of the structure is accessible for inspection by use of a fiber optics boroscope. Accessibility for inspection and repair was considered during the preliminary design. It was decided at that time that the requirement to repair any of the composite wings in service in the inaccessible areas was very unlikely. If major, unrepairable damage did occur, the composite wing would be taken off the aircraft and the metal wing reinstalled. This approach overlooked the fact that internal repair might be required due to problems during static or fatigue testing. Repair of bond joints in the L.E. area of the wing were accomplished, but not without difficulty and added expense. The lesson from this is that access for inspection and repair should be designed into the structure, because it is impossible to anticipate damage and problems which can arise during fabrication, testing, and in-service use.

(5) Off-axis strain components significantly reduce allowable strains. As was discussed previously, the failure analysis and testing conducted showed a significant reduction in strain allowable in the aft edge of the skin, adjacent to the aileron tab. The tab load, acting at 90° to the spanwise bending load, caused the maximum principal strain to shift 15° "off-axis". This reduced the failing strain level in the + 45° softening strip (in the fastener area) from approximately 6,000 μ in/in to about 3,700 μ in/in. The lesson here is: watch for off-axis principal strains due to biaxial loading and concentrated loads inputs, and use reduced strain allowables where necessary.

(6) Secondary bonding should be minimized. Use co-cure bonding where possible. The composite outer wing contains a considerable amount of both secondary and co-cure adhesive bond joints. Because of the limitations of existing NDI techniques (as discussed in item (2) above), it is essential that the production bond process be as reliable and repeatable as possible. Experience from the program has clearly shown that co-cure bonds are more reliable in production than secondary bonds. The possibility of "bridging" between two bond surfaces is minimized. The possibility of bond surface contamination is significantly reduced.

(7) Consideration must be given to quality inspection in basic design concept. Most, but not all, of the A-7D composite outer wing structure is inspectable after final assembly. Quality inspection procedures were considered during preliminary design, but a specific, detailed inspection plan was not developed until after the design was completed. Experience on the outer wing has highlighted the fact that such a plan should be developed concurrent with the basic design.

DEVELOPMENT AND TEST OF A GRAPHITE/EPOXY WINGBOX

G. C. Krumweide and E. E. Spier

General Dynamics Convair Division

ABSTRACT

Integrally stiffened graphite/epoxy skin panels were designed and fabricated for a wingbox test that was representative of a Convair Navy VSTOL Model 200 fighter aircraft wing. Considerable development effort was expended to accomplish the cocuring of I-shaped stiffeners and pseudo-isotropic skins. A thermal pressure forming process using elastomeric tooling was developed, enabling large flat, stiffened panels to be net formed. Current analysis techniques were employed to size the structure for representative Navy aircraft wing loads: bending, torsion, and internal pressure from fuel head in maneuvers. The wingbox was extensively strain-gaged on the compression side and tested under various loading conditions. The output of the strain gages indicated that the compression loading was reasonably uniform over the cross sections, even though the loads were introduced by discrete loads through an aluminum substructure. The test results exceeded all expectations, which demonstrated the feasibility of using all graphite/epoxy stiffened skins in aircraft wing structures.

INTRODUCTION

A program was performed to demonstrate the applicability of integrally stiffened graphite/epoxy panels for compressive aircraft structures such as a pressurized wing compression cover. Analysis readily demonstrates sizable weight savings over metal counterpart structures. However, unique tooling and fabrication techniques needed to be developed to produce those structures recommended by analysis. Accordingly, a wingbox test program was initiated to develop the necessary manufacturing methods and prove the analytical predictions for strength and stability.

After considerable manufacturing development efforts, the integrally stiffened graphite/epoxy wingbox panels were fabricated with I-section stiffeners cocured with pseudo-isotropic skins. The A-S/3501 graphite/epoxy system was used. The designs for both the upper and lower skin panels were strongly influenced by the manufacturing approach (i.e., skin "steps" were incorporated in the design rather than tapers). Stiffener buildups were abrupt steps rather than gradual thickness variations.

An aluminum substructure was employed at one end of the wingbox to properly introduce specified bending and shear loads, while the aluminum substructure at the other end provided the required reactions to the applied loads. Thus, the graphite/epoxy wingbox was located at the center of a cantilever beam. Provision was made to apply internal pressure to the wingbox.

The design and analysis of the compression cover was performed using typical flight loads from a Convair Navy VSTOL Model 200 fighter aircraft wing. The compression cover was extensively strain-gaged, and tests for various loads and combinations of loads were performed. All tests were conducted with no evidence of impending failure, and the strain gage readings showed that nearly uniform internal compression strains were developed as planned. Also, high internal pressure loads were applied without developing large strains in any of the strain gages.

DESIGN

The primary objective of this program was to develop an advanced wingbox test specimen using graphite/epoxy panels and an aluminum substructure. The technical approach with respect to the design and analysis of the upper and lower panels and the aluminum substructure was:

1. The upper panel was designed for Convair Navy VSTOL Model 200 wing loads, primarily compression..
2. The lower panel was designed to pattern the upper panel but was made thicker and incorporates provisions for access into the inside of the wingbox.
3. The aluminum substructure was designed to distribute desired loads uniformly to the upper panel and to facilitate fuel pressure cycling.

The design of the upper panel is shown in Figure 1. Basically, the 3- by 4-foot panel consists of a 0.06-inch (12-ply) skin stepwise thickened to 0.24-inch (48-ply) and is stiffened with nine I-cross-section stiffeners. Both the skin and the cocured inplace stiffeners are made from A-S/3501 graphite/epoxy.

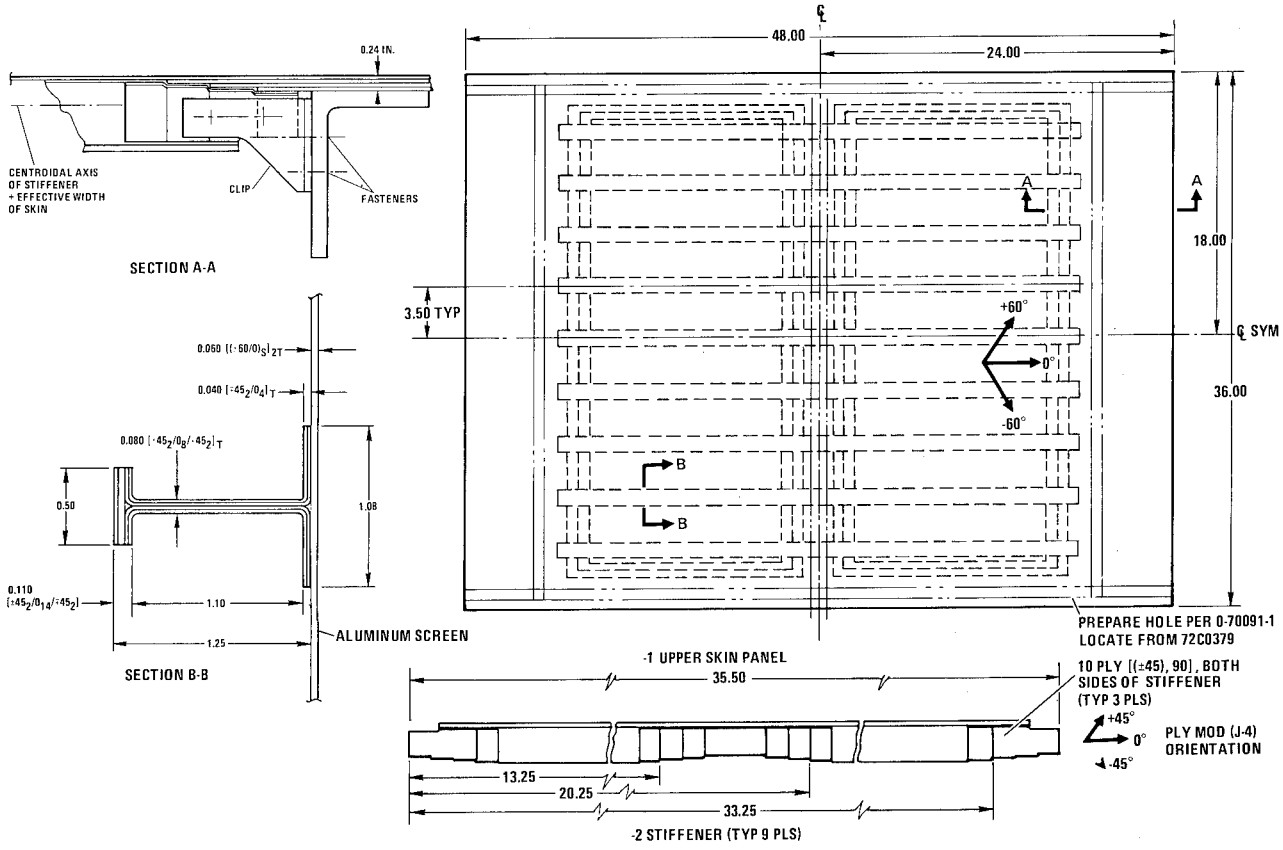

Figure 1. Upper panel design configuration.

The I-cross-section stiffeners were sized, spaced (3.5-inch pitch), and supported at their ends in a manner that would prevent the skin from buckling below limit load (5.5g roll). Fabrication problems which occurred during buildup of smaller compression test panels led to removal of a unidirectional

(0-deg) ply module in the web of these I-cross-section stiffeners. As shown in Figure 2, these unidirectional plies wrap the corners to form a portion of the stiffener cap and base.

The 12-ply modules that form the basic skin of the panel have been made identical and are symmetrical within themselves. This allows a single material orientation to be laid up and the various skin plymodule configurations to be "dinked" out, regardless of which side of the material is facing up. This skin design approach is intended to simplify the manufacturing aspects in producing multiple thickness skins. The aluminum screen material called for on the outer surface of the upper panel (shown in Section B-B of Figure 1) is to provide for lightning strike and EMC protection for the actual aircraft.

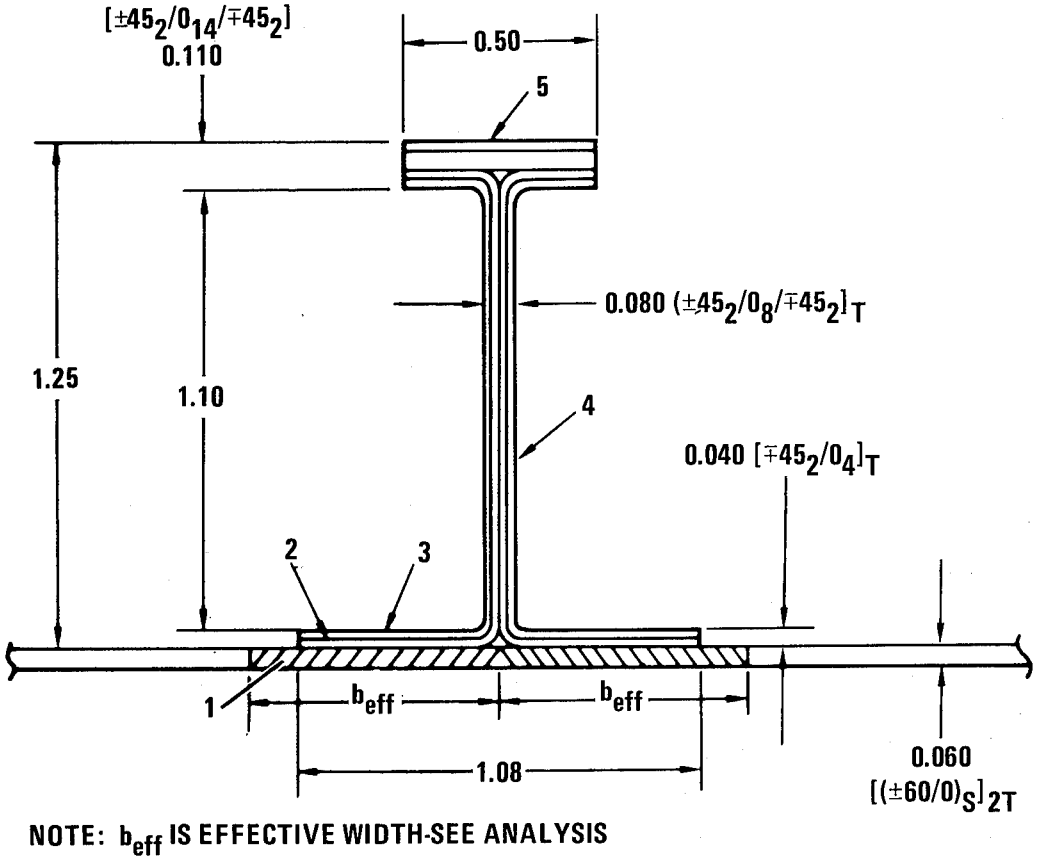

Figure 2. Cross section of I-section integral stiffeners.

The aluminum end clips attached to both ends of the stiffeners shown in Figure 1 provide positive reactions for the pressure load. The stiffeners are locally built up under these end clips to provide for fastener bearing and to eliminate peaking stresses at the end of the stiffeners. One task in the test program was to determine if the end clips could be omitted without premature failure due to the high internal pressure.

The wing testbox is shown in Figure 3, where the upper 48-inch test panel is somewhat representative of a pressurized stiffened compression panel for the Model 200 VSTOL aircraft. The compression test panel is designed to withstand representative load conditions, which were developed by loads and reactions as shown.

The upper compression panel shown in Figure 3, covers the two middle bays of the test box. It is supported by three transverse ribs and the closing longitudinal spar members. The lower skin panel is basically the same design as the upper skin panel except for the addition of a 12-ply plymodule to the entire panel and a general beef-up around access ports. No lightning strike protection was incorporated into its outer surface.

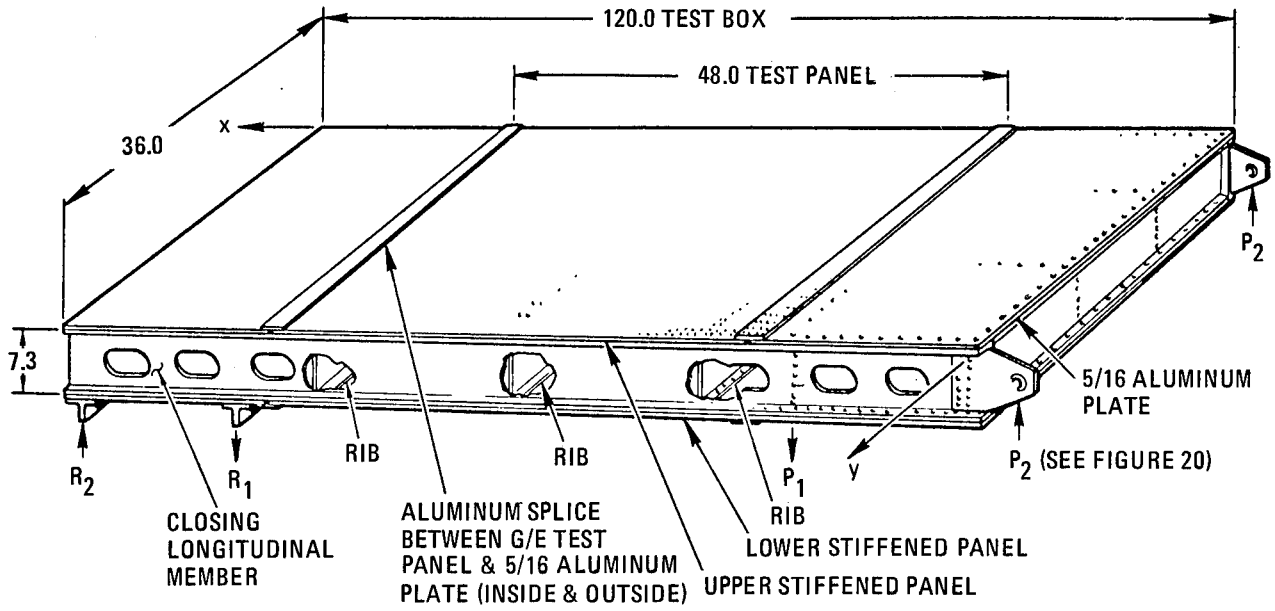

Figure 3. Wingbox test assembly.

The extra plymodule allows a fairly simple design to be used for the "flush-mounted" access doors. Here, the outer two 12-ply plymodules that form the basic skin (0.12-inch thick) are identical and only have to have coinciding circular (10-inch diameter) cutouts in them to provide the necessary recess for the access doors.

The two access doors are identical as shown in Figure 4. Plymodules cut from the upper panel, coupled with two additional 6-plymodules of the same basic orientation, were used to fabricate these doors. Removal of an annular 0.2-inch width of material from one of the 6-ply plymodules, in the area of the "to be molded" seal groove, allows for better definition of this formed groove.

Incorporation of this molded-in seal groove, as well as the molded-in countersunk holes depicted in Detail 'B' of Figure 4 was done to:

1. Prove feasibility of such a design.
2. Improve the hole strength and wear characteristics.
3. Reduce fabrication costs.

The configuration for the basic test wingbox is shown in Figure 3. The total length and width of the assembled box is 10 by 3 feet, respectively. The depth of the box assembly was determined by the 7-inch channel section that is used to build the aluminum substructure.

The center two bays of the test box were made fuel-tight by using a polysulfide sealant in the interface of all attaching components before riveting them together. Rivets were also coated with sealant before they were driven. Between the two fuel-tight ribs is a center rib that has been "scalloped" to allow stiffeners on both the upper and lower graphite/epoxy panels to pass through.

The upper panel was left unfinished to evaluate the following effects:

1. Graphite/epoxy and fuel compatibility.
2. Fuel containment capability (under pressure).
3. Corrosion-related effects on mounting structure and around fasteners.

It was expected that an uncoated surface will allow better failure analysis investigation should failure occur.

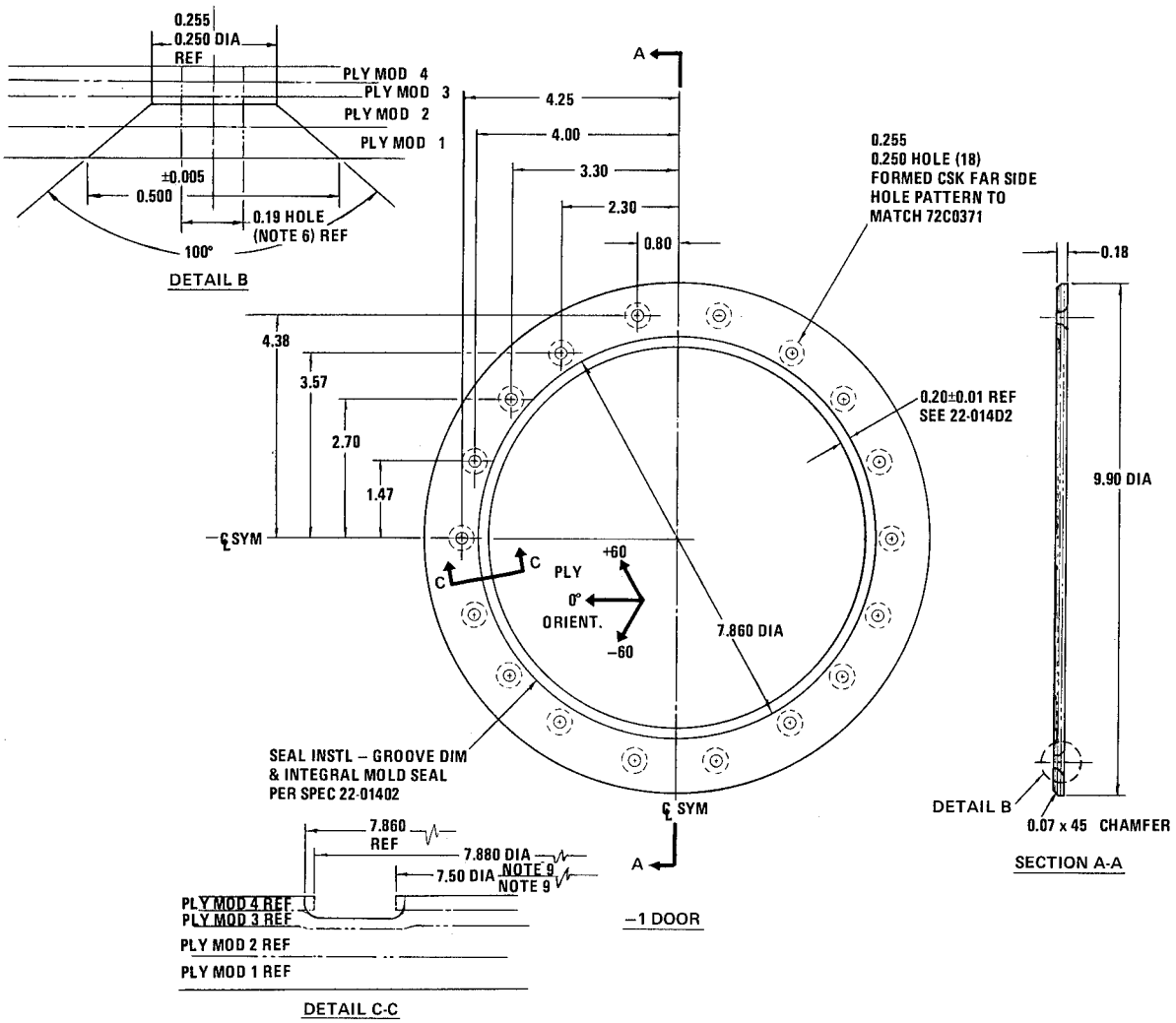

Figure 4. Access door.

The lower panel was finished with the latest state-of-the-art surface protection. Both the inside and outside surfaces of the panel were protected. The intent of such protection was to:

1. Serve as a control panel for the unfinished upper panel.
2. Evaluate coating system compatibility with the graphite/epoxy in a wet wing environment.
3. Evaluate the amount of corrosion-inhibiting protection offered.

THERMAL-PRESSURE-FORMING (TPF) PROCESS

The idea of using an elastomeric compound for tooling purposes is not particularly new – furniture manufacturers have been using these materials for years. But, using the thermal expansion of these elastomeric tooling materials as a means of applying proper pressure at the right temperature during heat-curing of the part is a relatively new development. Various formulations of these elastomeric compounds, each having certain chemical, thermal, and material handling characteristics, were examined and experimented with in recognition of their potential in lowering tooling costs and improving manufacturing techniques for reinforced plastics and composites. The TPF process developed and reported here is an outgrowth of this type of experimentation. The following summarizes the development status of the TPF process:

1. Properties of the selected elastomeric compound (Dapco 38-3) have been determined so that tooling can be designed properly.
2. The design requirements have been determined with respect to meeting panel design objectives, production assembly method, and curing press procedures.
3. Heating profile/cure cycle for the panels have been delineated to optimize panel quality and tool turnaround time.
4. Finished part quality, net formed, is such that minimum cleanup is required.
5. Finished parts are coatable, if required, when removed from the mold. No machining, deburring, strain relieving, degreasing, chemical filming, or protective priming is required for these parts.

TOOL DESIGN AND FABRICATION

The fundamental tooling approach is to build an exact dimensional model of the finished panel, cast silicone rubber (38-3) over the model to form a female mold (with respect to stiffeners), cure the mold, remove the model, install the graphite/epoxy, and cure the part. Essentially, this is the process, except certain requirements are placed on the tool so that it is reusable with rapid turnaround.

Model

Model features that must be incorporated into the design are that it provide proper tool expansion allowances, that it be dimensionally compatible with the actual part, and that its geometry permits it to be freely separated from the mold or production mold (PDMO). Figure 5 shows the model used for the upper panel.

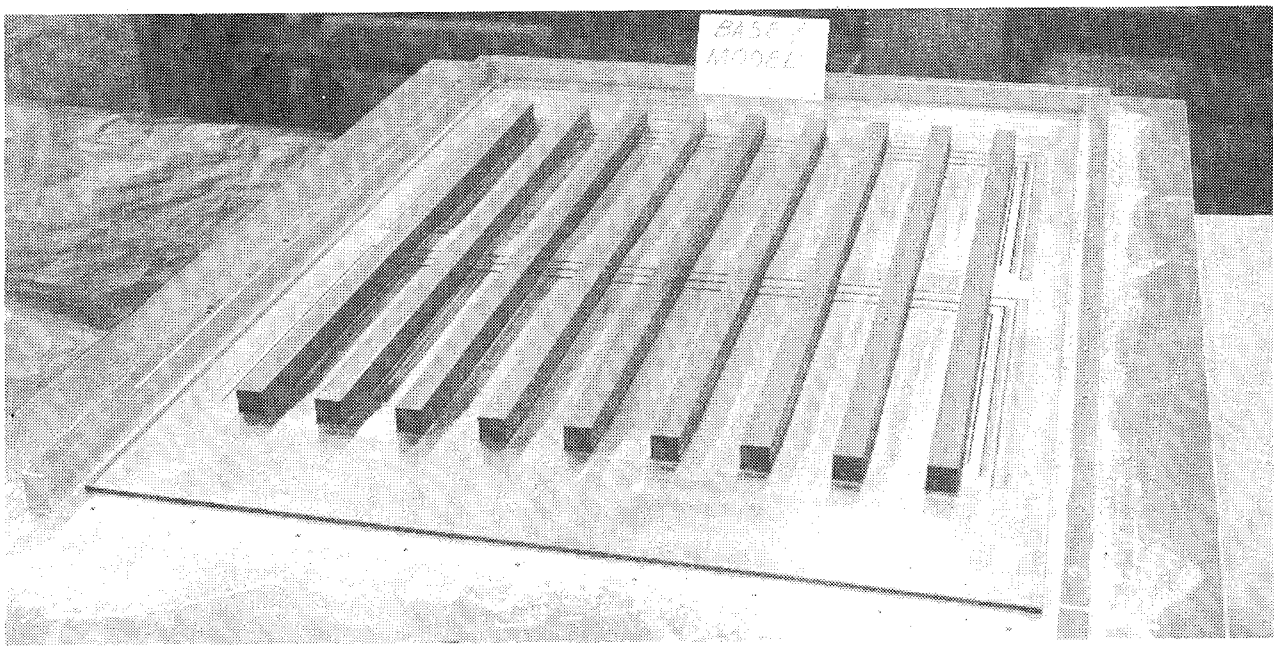

Figure 5. Model used for the upper panel.

Cap

For the TPS process described, the cap is designated that portion of the PDMO used to form the lower stiffener surface of the panel during cure, the cap is on top when the PDMO is placed in the curing press. The hard tooling portion of the cap (Figure 6) is a flat plate of 0.5-inch thick aluminum. Tackwelded to the plate are rectangular bars of aluminum that correspond to the midpoints of the model stiffeners and for the full length of these stiffeners.

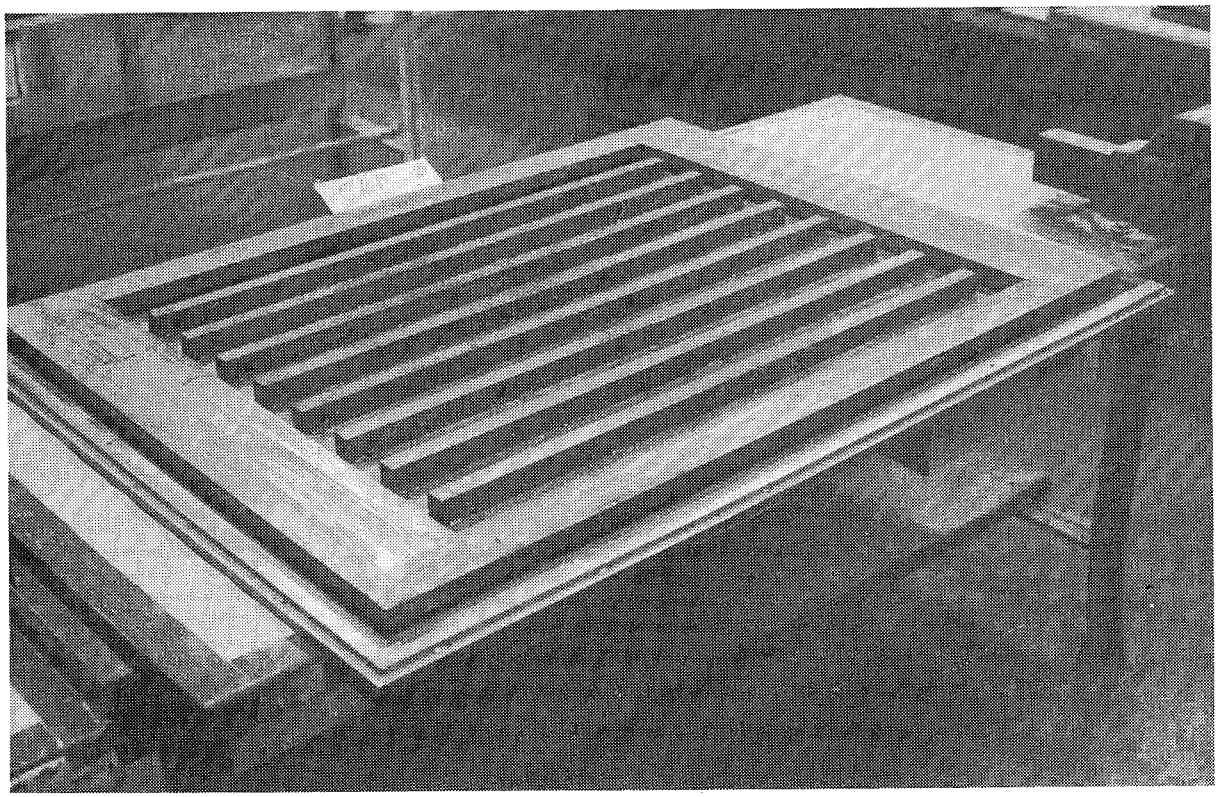

Figure 6. Cap portion of PDMO before casting of silicone rubber.

Base

The base portion of the PDMO was also made from 0.5-inch aluminum plate, as illustrated in Figure 5. A picture frame of aluminum bar (bar in foreground not in place) is bolted to the base and is used to confine the silicone rubber during initial pour and to restrain it from lateral expansion during heating.

Cast

Silicone rubber was cast into the hard tooling portions of the PDMO by "gravity" pouring the rubber into the cavity created between the cap and the model. The model was temporarily attached to the base. In preparation for this room-temperature cast of the silicone rubber, the base (previously Frekoted and baked) and the model were coated with a liquid detergent. This soap provided excellent release characteristics after cure of the silicone rubber.

PANEL ASSEMBLY

Aluminum mandrels used to form the stiffeners are wrapped with plymodules of prebled (190±10F for 15 minutes) A-S/3501 material, as shown in Figure 7. The trimmed panel skin shown being installed in Figure 8 was an assembly of prebled plymodules preplied together. The coordinated tooling used to build the model and cut and stack these plymodules was Mylar templates.

Steam Press Cure

The panel was cured in the steampress. The temperature was increased, under a 90 psi pressure, from room temperature to 350F in one hour.

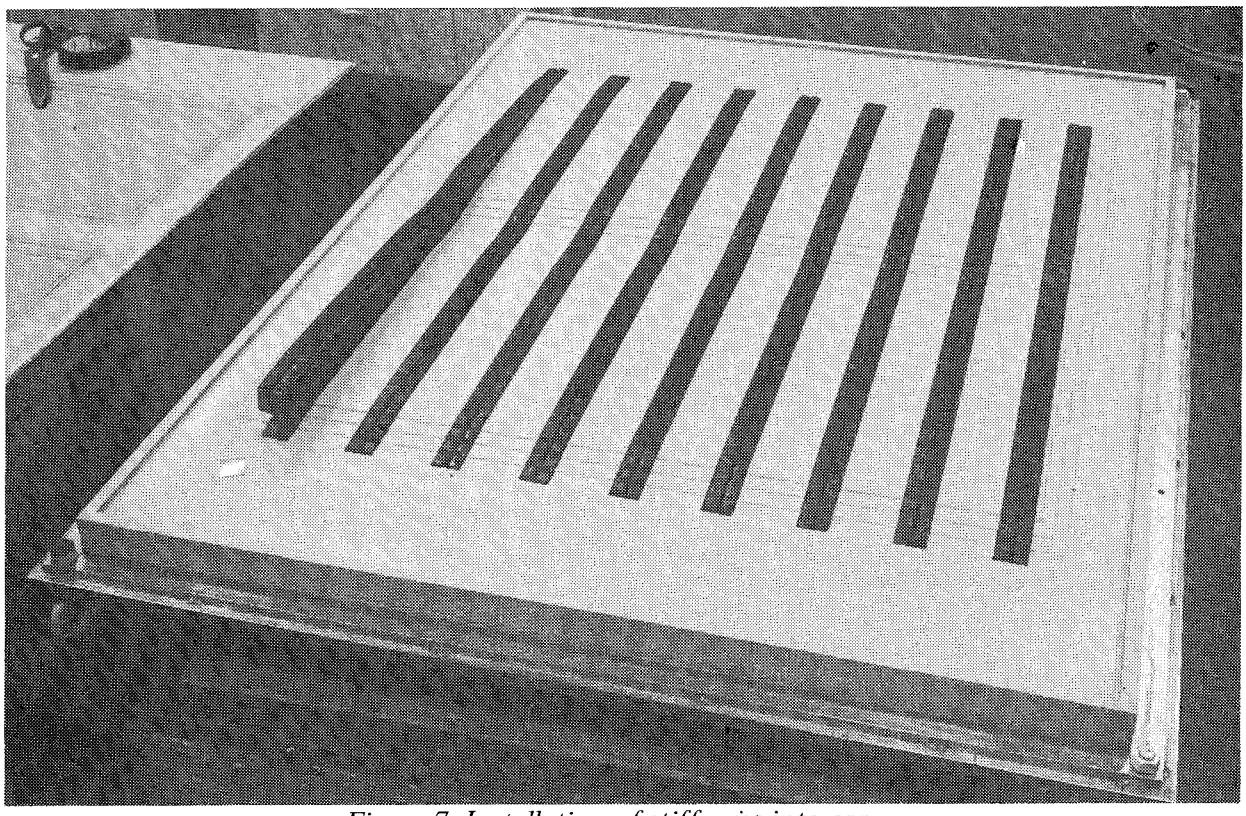

Figure 7. Installation of stiffeners into cap.

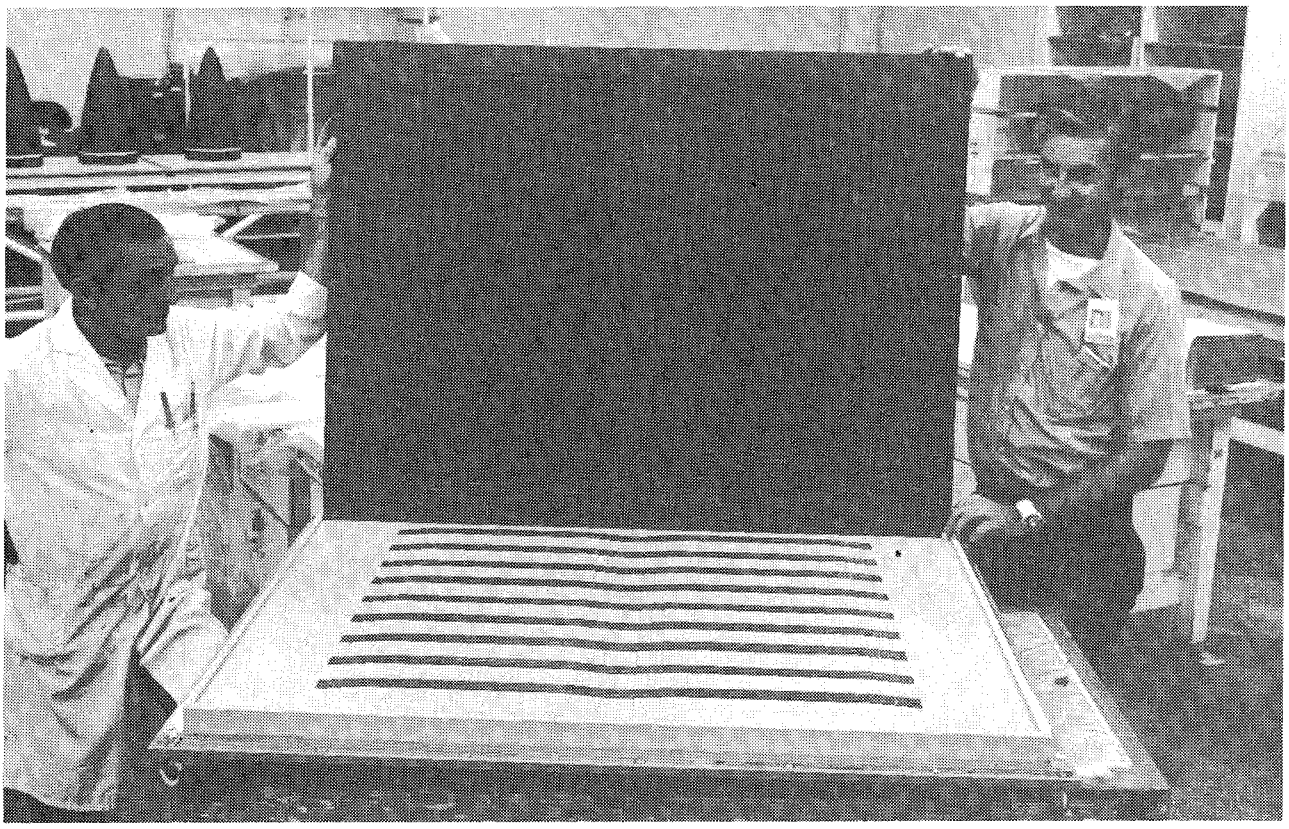

Figure 8. Installation of skin into cap.

FINISHED PANEL CHARACTERISTICS

Aluminum Screen Surface

The outer screen surface of the panel had some minor blemishes. A few resin-starved areas in the screen existed for no apparent reason. On the surface directly over the stiffener, it appeared that there was good penetration of the resin into the screen. They appeared to be higher pressure application areas.

Stiffener-Mounted Surface

The significance of this TPF process lies in the fact that the panel surface in Figure 9 was net formed. Very little sanding to remove flash was required. The stiffeners and the panel thickness steps were well defined. Transitions from stiffeners to panel and panel steps in thickness were gradual and free of voids.

General Appearance

Not readily apparent in the photograph is a slight bow in the panel due to the thermal expansion differences of the aluminum screen, ply orientation differences between skin and stiffeners and forming pressure variations across the panel. Net edges were achieved except in one small area, where the prebled material for the panel skin was not trimmed within the ±0.03-inch requirement. This area (gap) filled with resin and is generally characterized by a porous surface.

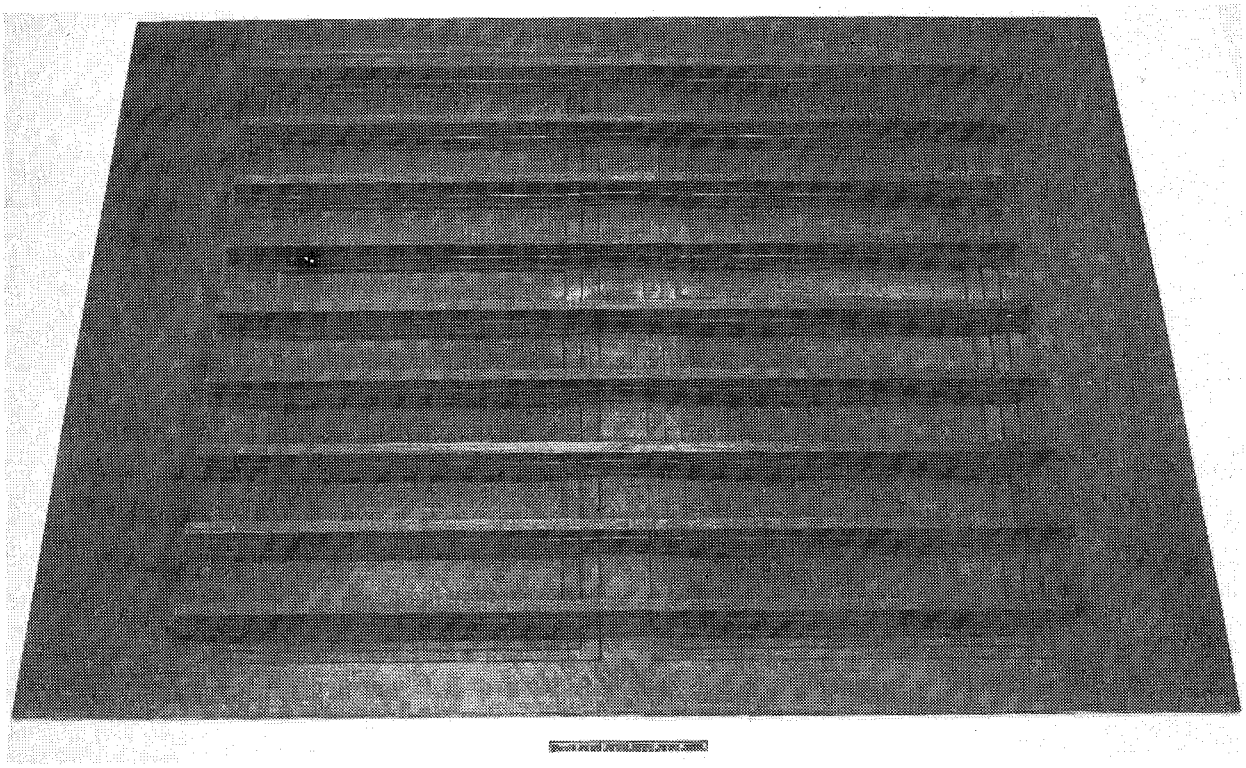

Figure 9. Lower, stiffened surface of the cured panel.

ACCESS DOORS

An acceptable technique for producing low-cost, high-quality doors was developed during this program, in which five doors were fabricated. The basic design configuration did not change, although the fabrication technique for hole preparation and seal groove preparation was altered for each subsequent door.

ANALYSIS

The stability analysis of the compression panel is confined to compression loads only since this can be accomplished by simple means. The general instability of the panel due to combined compression and in-plane shear would require a more sophisticated method of analysis, possibly involving an extensive computer program. Accordingly, only the allowable compression loads for the panel are determined in the analysis that follows: (see Ref. 1 for test data and nomenclature).

Buckling of Panel Between Stiffeners

$b = 3.5$ in.

$P_x^{cr} = 1{,}435$ lb

$\sigma_x^{cr} = 6{,}919$ psi } Ref. 1

Crippling Strength of Stiffener

A crippling test of a representative panel for the compression panel was performed in Ref. 1. A photograph of the failed specimen is shown in Figure 10; the cross section is shown in Figure 2. The crippling load for the panel was 40,600 lb. Thus, the allowable crippling load per stiffener is found by the expression

$$P_{ST}^{cc} = (40{,}600 - 2\,P_x^{cr})/3 = 12{,}565 \text{ lb}$$

It was found in Ref. 1 that

$A_{ST} = 0.180$ in.^{2}

$E_{ST}^{c} = 9.56 \times 10^6$ psi

where the compressive elastic modulus of elasticity is a "weighted average" value for all the elements of the stiffener cross section. The weighted average crippling strength of the stiffener is

$$\sigma_{ST}^{cc} = P_{ST}^{cc}/A_{ST} = 12{,}565/0.180 = 69{,}806 \text{ psi}$$

Section Properties

For stability analysis of the stiffened panel, it is convenient to convert all elements of the stiffener to "equivalent" elements for the same elastic compressive modulus as that of the skin ($\bar{E}_x^c = E_{SK}^c$). Accordingly, by use of section property data from Ref. 1, "equivalent" section properties for the stiffener and varying effective widths of skin combined were determined and plotted as shown in Figure 11.

Column Analysis (No Eccentricity)

The iterative column analysis recommended in Ref. 1 was followed, which required that at the last iteration an assumed load was sufficiently close to the calculated allowable. The last iteration used in the present analysis for the column strength for zero eccentricity of the applied load is presented as follows where the same nomenclature as that found in Ref. 1 is used:

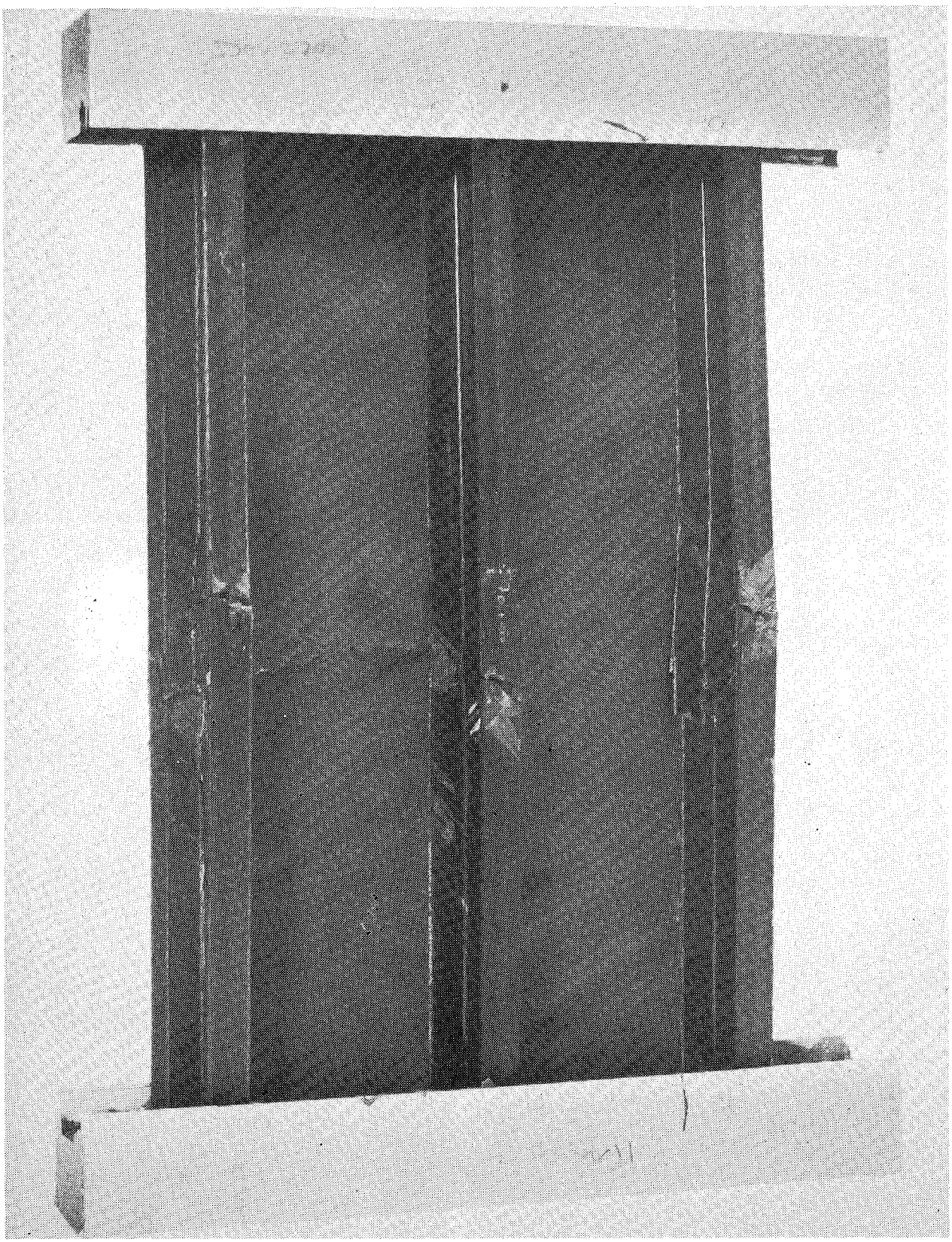

Figure 10. Failed compression panel specimen.

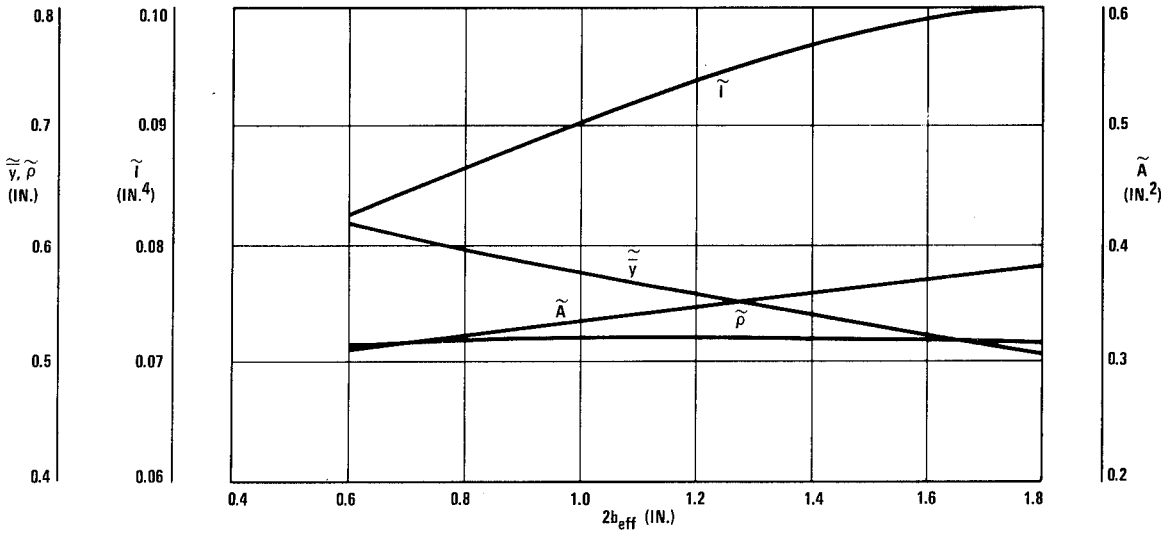

Figure 11. Section properties of stiffener plus effective width of skin after conversion of entire section to E^c_{SK} .

Assume that the load in the stiffener plus effective-width skin is

$$\tilde{P}^c_x = 12{,}200 \text{ lb.}$$

Thus, the load in the stiffener is

$$P^c_{ST} = \tilde{P}^c_x - P^{cr}_x = 12{,}200 - 1{,}453 = 10{,}474 \text{ lb}$$

and the stiffener stress is

$$\sigma^c_{ST} = P^c_{ST} / A_{ST} = 59{,}706 \text{ psi}$$

The corresponding strain in the stiffener is

$$\epsilon^c_{ST} = \sigma^c_{ST} / E^c_{ST} = 59{,}706 / 9.56 \times 10^6 = 0.00624$$

As stated in Ref. 1, the strain in the effective-width of skin is assumed identical to that of the stiffener. Thus,

$$\epsilon^c_{SK} = 0.00624$$

Now, the average stress in the effective-width of skin is

$$\sigma^c_{max} = E^c_{SK} \; \epsilon^c_{SK} = 6.275 \times 10^6 \times 0.00624 = 39{,}190 \text{ psi}$$

and the effective-width of skin is

$$2b_{eff} = 2\,(b/2)\sqrt{\sigma^{cr}_x / \sigma^c_{max}} = 3.5\sqrt{6{,}919/39{,}190} = 1.47 \text{ in.}$$

With all the elements of the stiffener converted to the compressive elastic modulus of the skin, the section properties of the stiffener plus a total of 1.47 inches of effective skin as found in Figure 11 are

$\tilde{A} = 0.362$ in.^{2} $\qquad \tilde{\bar{y}} = 0.534$ in.

$\tilde{I}_x = 0.0978$ in.^{4} $\qquad \tilde{\rho}_x = 0.52$ in.

The effective area of skin is

$$\tilde{A}_{eff} = 1.47 \times 0.06 = 0.088 \text{ in.}^2.$$

The crippling load in the stiffener including the effective width of skin is

$$\tilde{P}_x^{cc} = \tilde{P}_{ST}^{cc} + \sigma_{max}^{c} \tilde{A}_{eff} = 12{,}565 + 39{,}190 \times 0.088 = 16{,}020 \text{ lb}$$

The corresponding "weighted average" crippling stress becomes

$$\tilde{F}_x^{cc} = \tilde{P}_x^{cc}/\tilde{A} = 16{,}020/0.362 = 44{,}263 \text{ psi}$$

The column length is 19 inches and the end fixity coefficient is assumed to be 1.0. Therefore, $L'/\rho = L/(\sqrt{C}\,\tilde{\rho}_x) = 19/0.52 = 36.54$.

The allowable column stress as found by the Johnson parabolic equation is

$$\tilde{F}_x^{co} = \tilde{F}_x^{cc} - \frac{(F_x^{cc})^2 \, (L'/\tilde{\rho}_x)^2}{4\pi^2 \, \bar{E}_x^c} = 44{,}263 - \frac{44{,}263^2 \times 36.54^2}{4\pi^2 \times 6.275 \times 10^6} = 33{,}703 \text{ psi}$$

and the allowable column load is

$$\tilde{P}_x^{co} = \tilde{F}_x^{co} \, \tilde{A} = 33{,}703 \times 0.362 = 12{,}200 \text{ lb}$$

which agrees exactly with the assumed load. The allowable running compressive load (stress resultant) is

$$\tilde{N}_x^{co} = \tilde{P}_x^{co}/b = 12{,}200/3.5 = 3486 \text{ lb/in.}$$

Eccentric Column Analysis

The eccentricity of the column load in the panel is illustrated in Figure 12, which

$$e = \tilde{\bar{y}} - 0.24/2 = 0.53 - 0.12 = 0.41 \text{ in.}$$

It should be noted that the section where the stiffener has been converted to the modulus of the skin is still being used in this analysis. Accordingly, the theoretical Euler load for the column is

$$P_{Euler} = \pi^2 \bar{E}_x^c \, \tilde{I}_x/L^2 = \pi^2 \times 6.275 \times 10^6 \times 0.0978/19^2 = 16{,}778 \text{ lb}$$

By using Figure 26.8 in Ref. 2 for analysis, we need the plasticity ratio

$$\eta = \tilde{P}_x^{co}/P_{Euler} = 12{,}200/16{,}778 = 0.73$$

Also, we need the allowable bending moment for the section

$$M_{allow} = \frac{F_x^{cu} \, \tilde{I}_x}{\tilde{\bar{y}}}$$

Recent testing of the ±60/0 laminate showed the ultimate compressive strength to be

$$F_x^{cu} \approx 123{,}000 \text{ psi}$$

Thus,

$$M_{allow} = 123{,}000 \times 0.0978/0.534 = 22{,}527 \text{ psi}$$

The base eccentricity is

$$e_o = M_{allow}/\tilde{P}_x^c = 22{,}527/12{,}200 = 1.85$$

The eccentricity ratio becomes

$$R_e = e/e_o = 0.41/1.85 = 0.22$$

Now, by using the values for R_e and η the value on the ordinate of the Figure in Ref. 2 becomes

$$\tilde{P}_{ecc}^{co}/\tilde{P}_x^{co} = 0.67$$

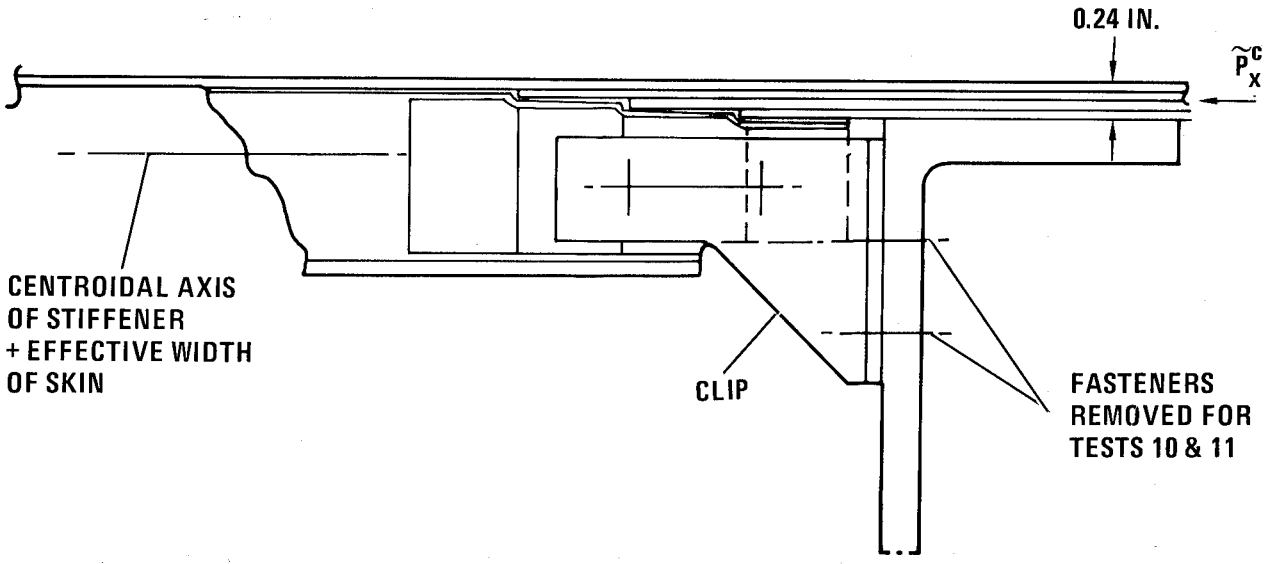

Figure 12. Stiffener to end rib attachment.

Now, the allowable load for the eccentric column is

$$\tilde{P}_{ecc}^{co} = 0.67 \times 12{,}200 = 8{,}174 \text{ lb}$$

The running allowable load (stress resultant) for the eccentric column is

$$\tilde{N}_{ecc}^{co} = \tilde{P}_{ecc}^{co}/b = 8{,}174/3.5 = 2{,}355 \text{ lb/in.}$$

WINGBOX TESTING

A sketch of the total basic wingbox test structure, including the aluminum substructure, is shown in Figure 13. At one end of the wingbox cantilever loads are applied. The intermediate spars were provided to ensure a relatively uniform strain distribution over the cross section of the compression panel located in the fuel-tight area. A sketch of the applied loads and reactions is shown in Figure 14. The structural test setup is shown in Figures 15 and 16.

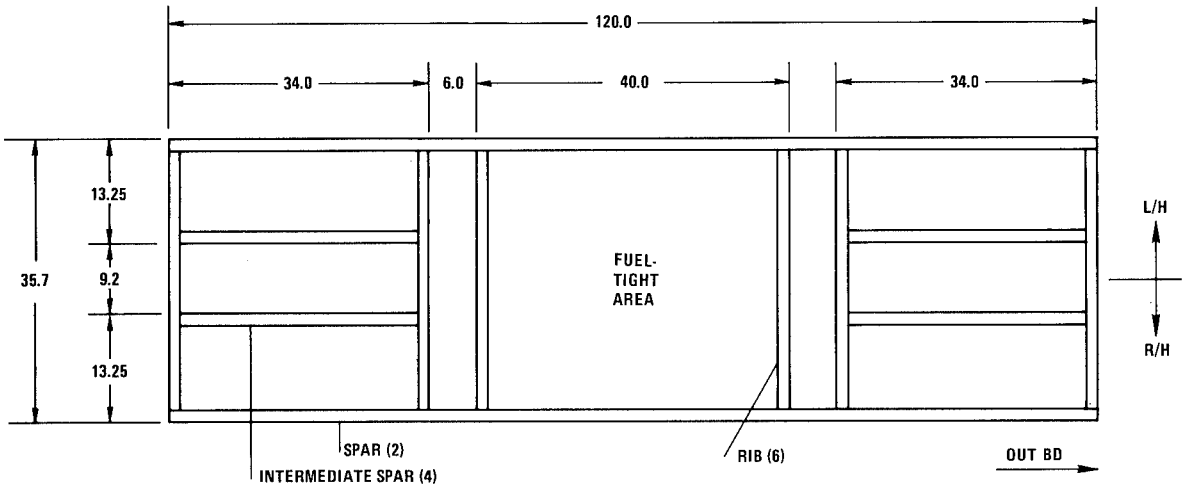

Figure 13. Test box basic structure and orientation (looking at upper surface).

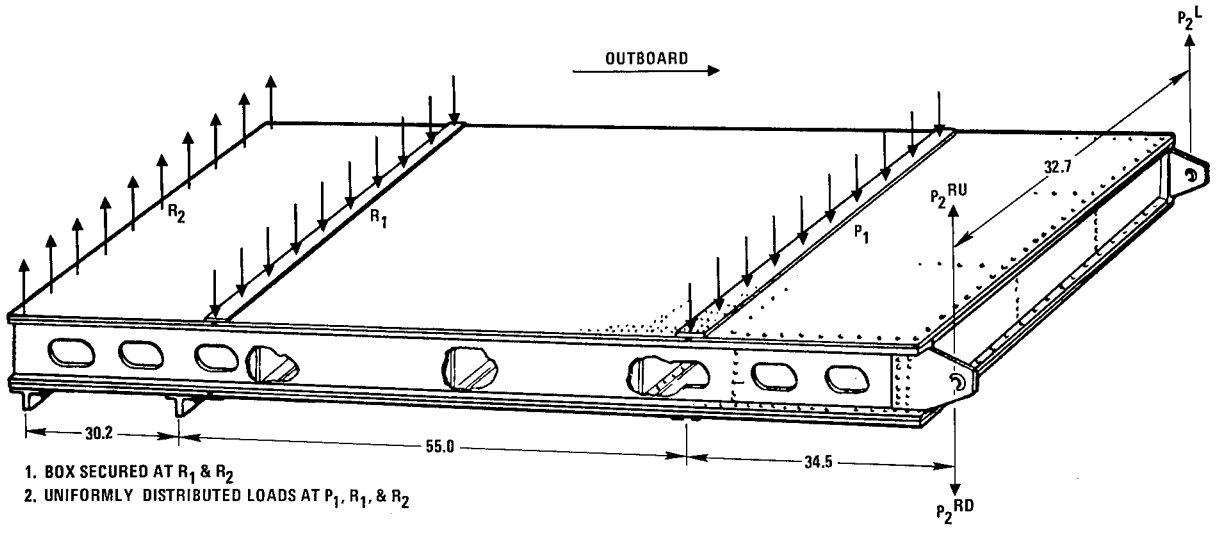

Figure 14. Test box loads and load locations.

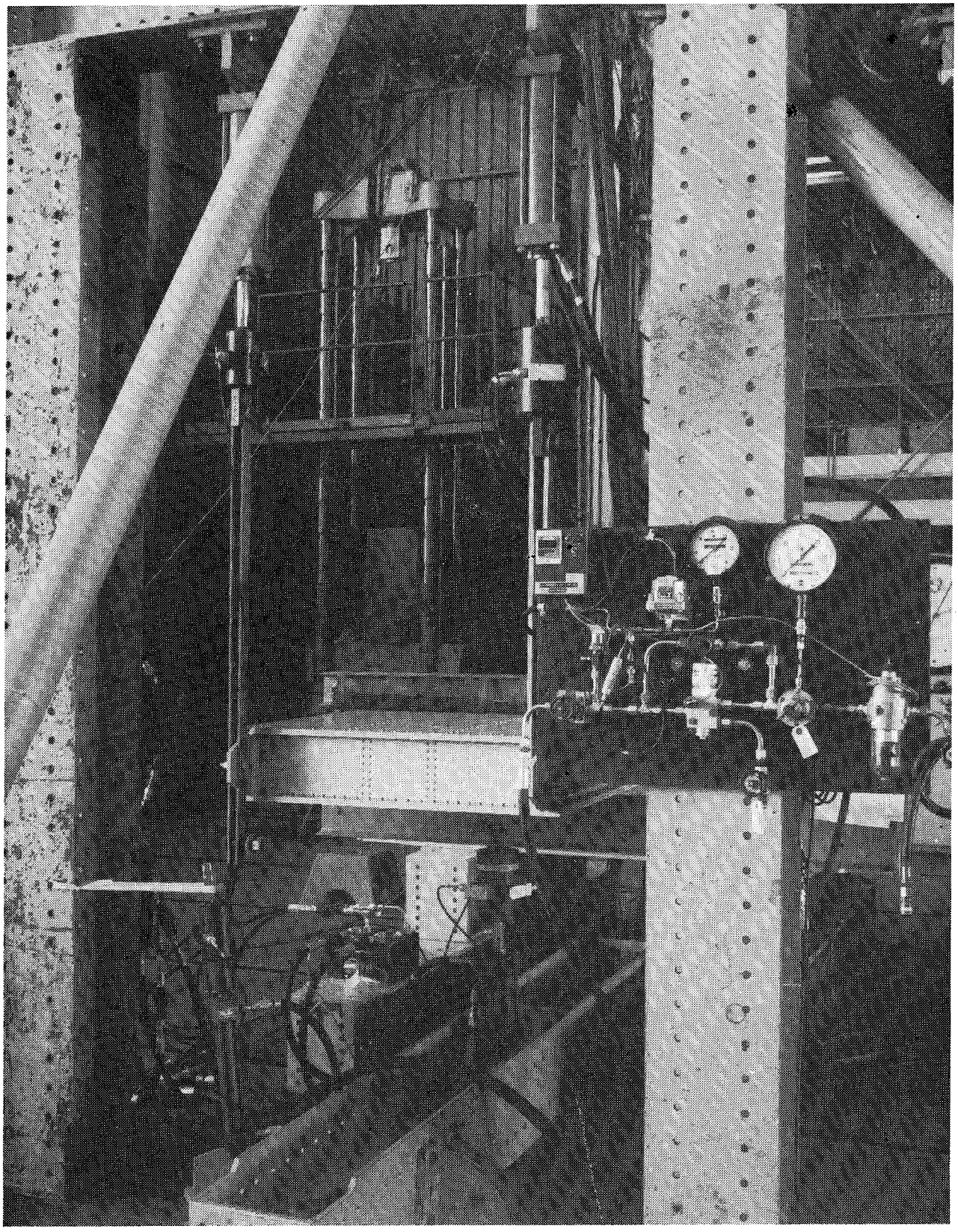

Figure 15. Structural test setup.

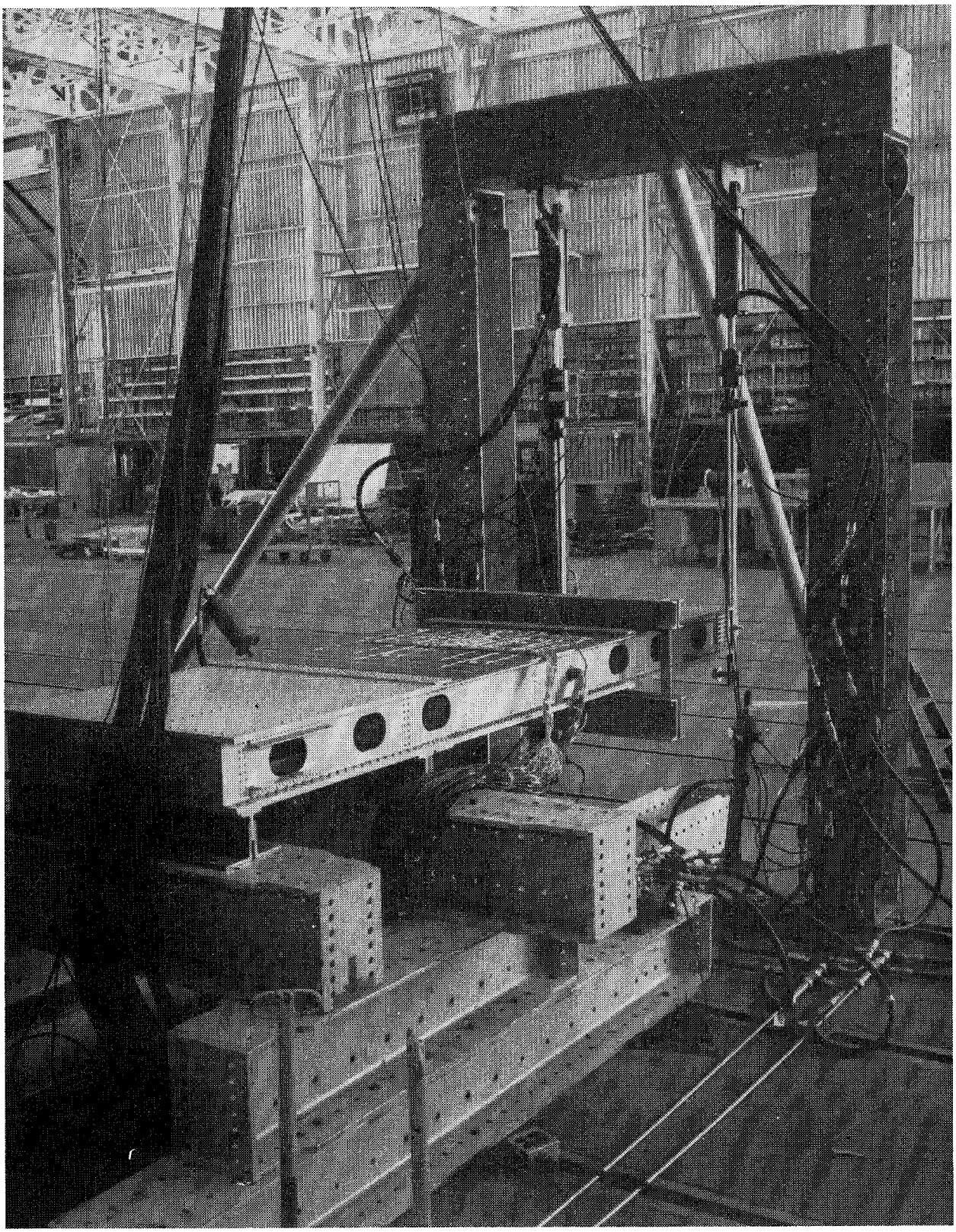

Figure 16. Structural test setup.

Several static, fatigue, and environmental tests were performed on the wingbox. Provisions were provided for pressurizing and automatically pressure cycling the box. Corrosion protection provisions were added inside and outside for future evaluation. The following instrumentation was provided on the compression panel:

23 internal axial gages
48 external axial gages
6 external (3-leg) rosettes

The strain gages are shown in Figures 17 and 18. Figure 19 is a photograph of the gages in place. Each of the four loading cylinders had load cells attached to the cylinder piston rod. Each load cell had three strain gage bridges which were used for load programming control, load monitoring, and data recording. A pressure transducer was installed in the pressurizing system, and its output was recorded and monitored. Four deflection dial gages were located along the right-hand spar as shown in Figure 20. A fifth gage was located at the outboard end of the left-hand spar. These deflection dial gages were removed after Test 3.

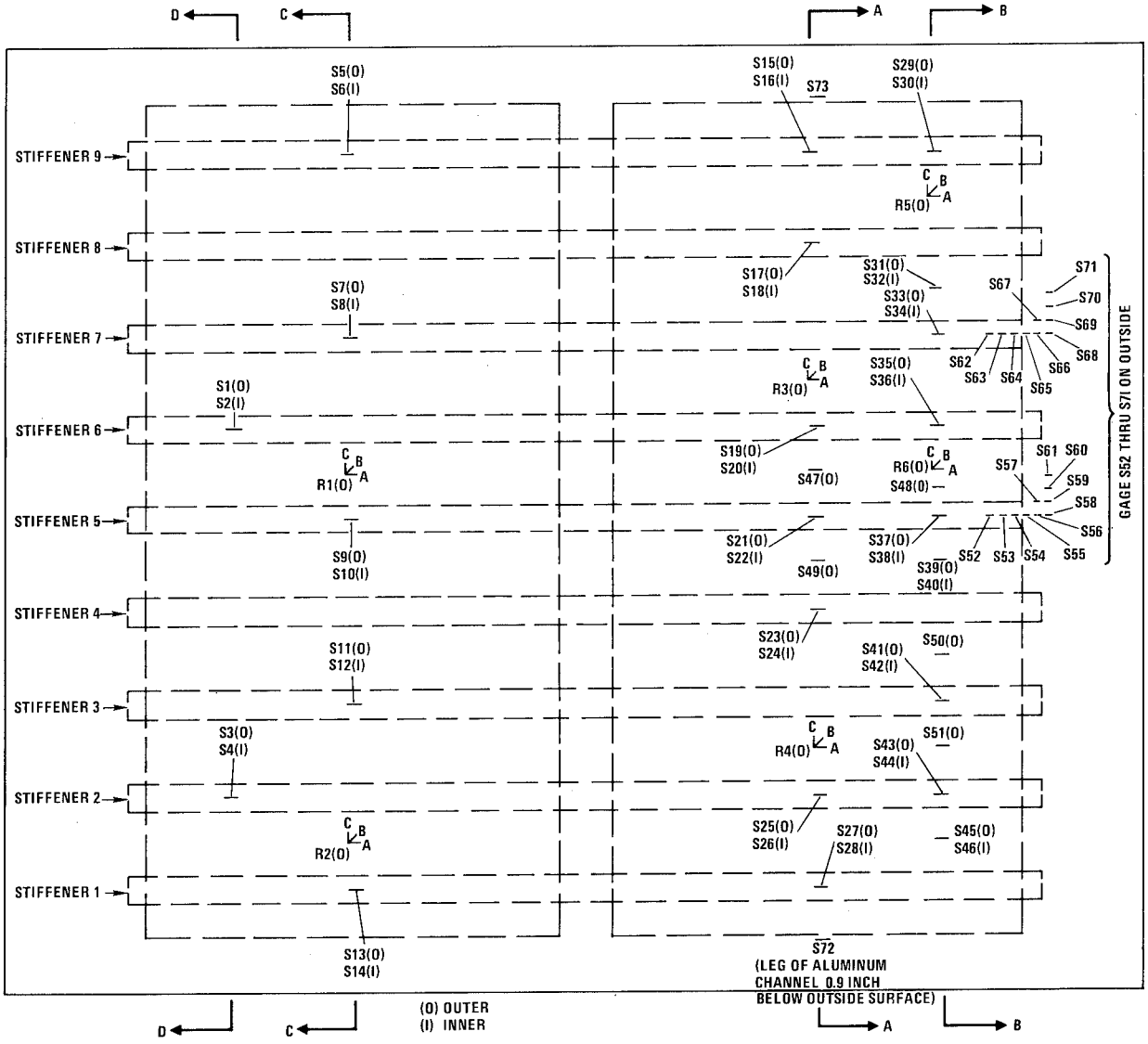

Figure 17. Strain gages on compression panel.

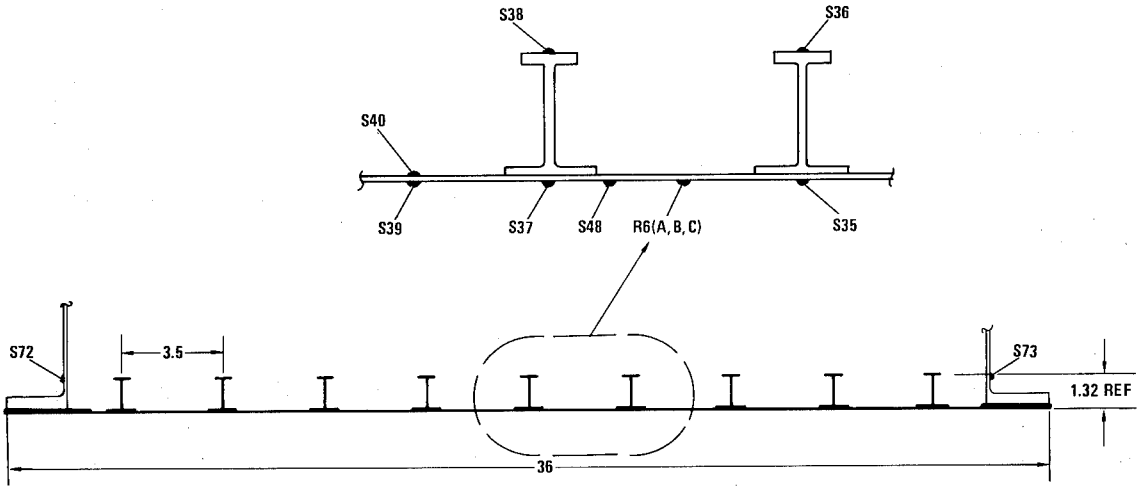

Figure 18. Section B-B — stiffened panel cross section with strain gage locations.

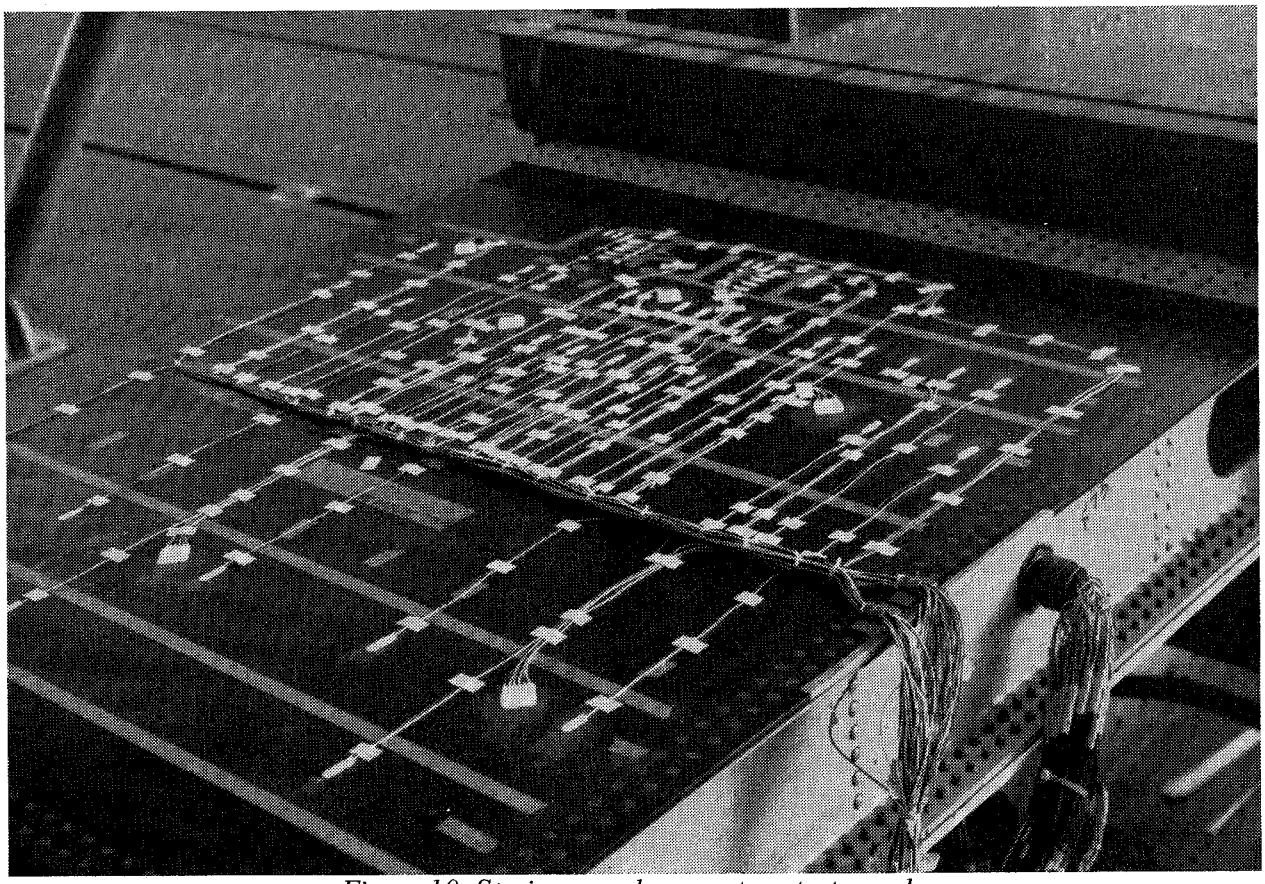

Figure 19. Strain gage placement on test panel.

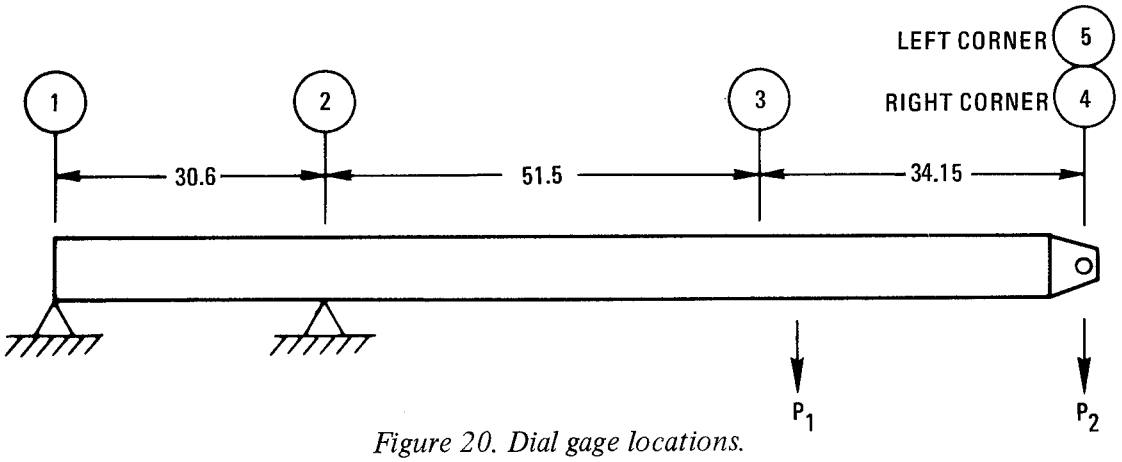

Figure 20. Dial gage locations.

Seven loading tests and four fuel tank pressure tests were performed, where one of the loading tests included pressurization. The fuel tank portion of the test box was loaded in bending, torsion and combined torsion and bending. Transverse shear was suppressed by the manner of loading. The fuel tank pressure was cycled to 12 psi for 1,790 cycles and to 20 psi for 4,000 cycles. A 72-hour leak check was conducted at 2 psi. Freon or jet fuel was used to pressurize the tank. The last two tests were performed with 72 fasteners removed which attach stiffener clips to the ribs. These clips provide support to the ends of the stiffeners. The elimination of clips would be very desirable for the cost savings available in the fabrication of actual wing structures.

A summary of the tests performed is presented in Table 1. However, only those tests shown in Table 2 are reported in this paper. Actual measured loads and pressure are recorded in Table 2, as well as calculated internal loads in the test section. The maximum average compression was 1,900 pounds per inch, and the maximum shear flow was 600 pounds per inch. A schematic sketch showing the deflection pattern and loads for the compression side due to pure bending is shown in Figure 21. Figure 22 shows the deflections and loads at the outboard end of the structure due to bending (Test 9). A plot of deflections from the dial gages for Test 1 is shown in Figure 23, along with predicted deflections for Test 9. As shown in Figures 21 and 22, there are discrete reaction points (Q and S) that may react local bending moments that may develop in either the compression or tension sides of the beam. The simplified analysis for internal loads shown in Table 2 obviously does not account for the possiblity of these loads being present. Thus, since bending moments could be present in the compression structure, close correlation between predicted and actual strains is not expected. Therefore, the valuable information to be derived from the strain gages is how uniform the strains are across a given cross section.

Table 1. Summary of testing performed on wingbox test specimen.

Test No.	Type of Test	Tank Fluid	Pressure (psi)	Recording Increments
1	Bending (90% max.)	Freon	0	10%
2	Bending & Torsion (90% max.)	Freon	0	10%
3	Bending & Torsion	Freon	16.2	10%
4	Maximum Bending & Torsion	Freon	0	10%
5	Pressure Cycling (1790 cycles)	Freon	12	
6	Leak Check (72 hours)	Jet Fuel	2	
7	Pressure Cycling (4,000 cycles)	Jet Fuel	20	
8	Maximum Torsion	Air	0	10%
9	Maximum Bending	Air	0	10%
10	Maximum Bending & Torsion (fasteners removed)	Air	0	10%
11	Pressure (fasteners removed)	Freon	25	20%

Table 2. Summary of reported static tests

Test No.	Type of Test	Press. (psi)	P_2^L (lb)	P_2^{RU} (lb)	P_2^{RD} (lb)	P_1 (lb)	Apparent Average Calculated Internal Load			
							M (in.-lb)	N_x (lb/in.)	T (in.-lb)	N_{xy} (lb/in.)
3	2/3 Maximum Bending & Torsion + Pressure	16.0	10,527	12	893	9,661	332,790	1,266	186,520	403
4	Maximum Bending & Torsion		15,917	-42	1,395	14,579	499,560	1,901	282,360	610
9	Maximum Bending		7,330	7,343		14,622	499,319	1,900		
10	Fasteners Removed Maximum Bending & Torsion		15,890	-30	1,388	14,600	499,319	1,900	282,020	609
11	Fasteners Removed Maximum Pressure	25.0								

$M = (P_2^L + P_2^{RU} - P_2^{RD}) \times 34.5$ $\qquad N_x = M/(7.3 \times 36) = M/262.8$

$T = (P_2^{RD} + P_2^L - P_2^{RU}) \times (32.5/2)$ $\qquad N_{xy} = T/2A = T/[2(7.3 \times 31.7)] = T/462.8$

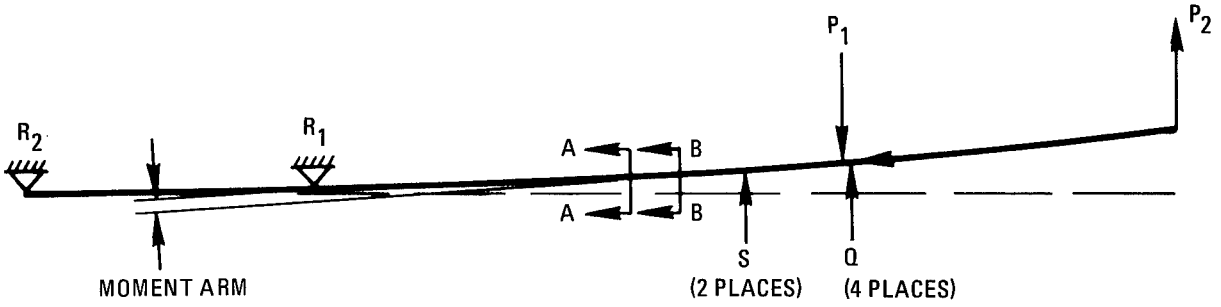

Figure 21. Schematic of deflected beam due to bending load only (Test 9).

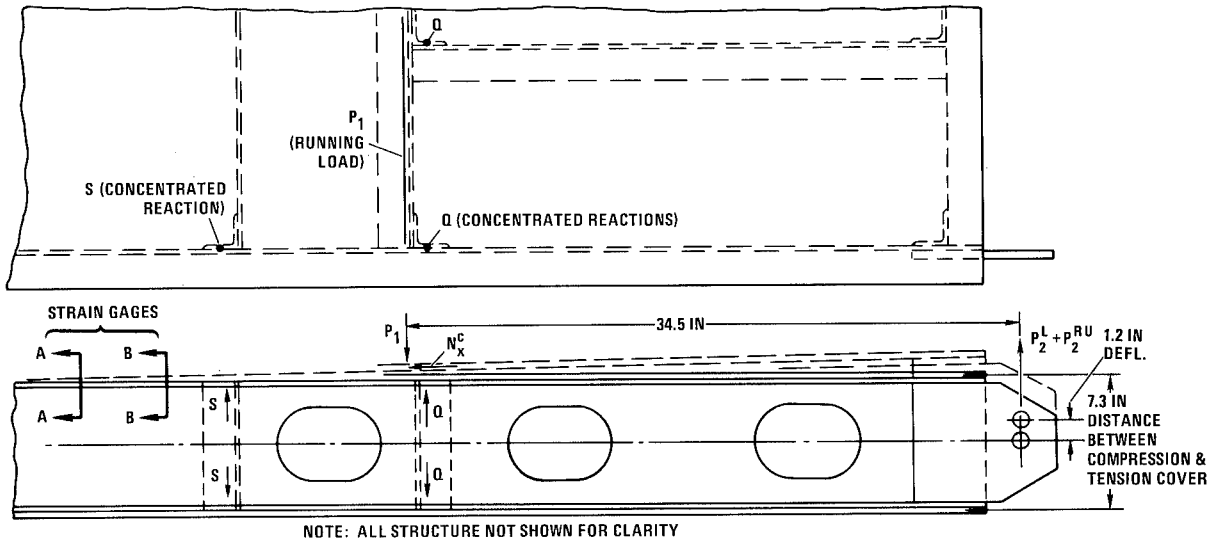

Figure 22. Outboard end of test under pure bending (Test 9).

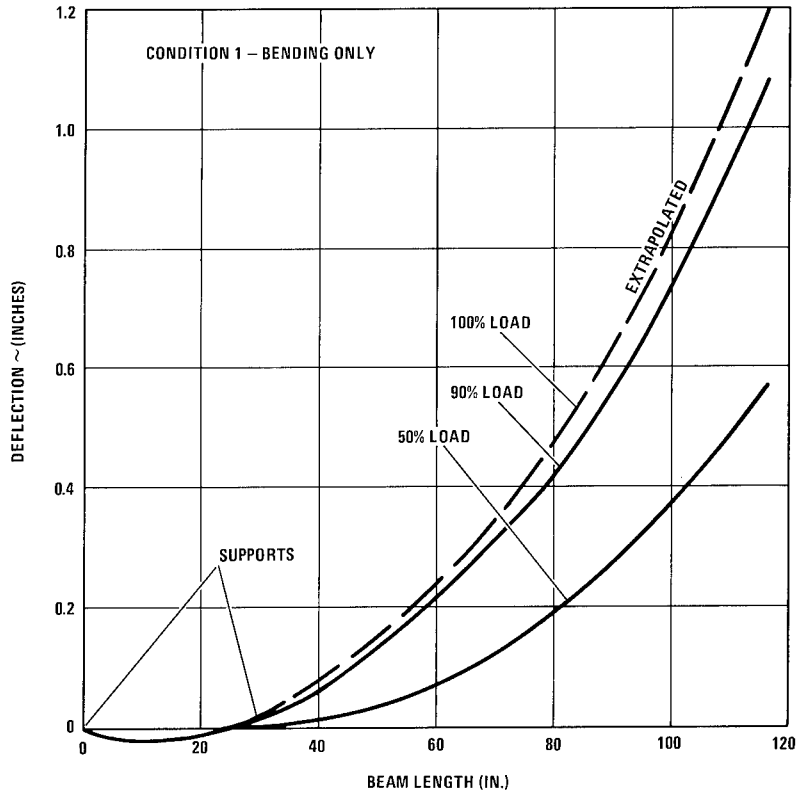

Figure 23. Plot of measured test box deflection (Test 1).

Strain gage readings for Test 9 (bending load only) for Section A-A of Figure 17 are shown in Figure 24, where all the strain gages are in compression. The strains on the outer surface of the skin are reasonably uniform with some drop off at the sides, including the projected strain on the aluminum spars. Notice that certain gages located at the corresponding Section D-D (at mid-length of columns) show good agreement with the plot of strains at Section A-A. Also, strains for the maximum bending and torsion conditions are shown in Figure 25. For Test 4 (zero pressure) and Test 10 (zero pressure and the end clip fasteners removed), the compressive strains are nearly the same. A plot of strains for Tests 10 and 11 superposed result in strains for 16 psi pressure and the fasteners removed, which show much higher strains than the corresponding 16-psi pressure case (Test 3) where the fasteners are intact. However, Test 3 provides only two-thirds of the maximum bending and torsion loads. Even so, there is still a sizable comparable difference. Plots of the strains on the inner surface of the outstanding flanges of the stiffeners are shown in Figure 26 for maximum bending and torsion.

Results of Test 11 at Section A-A are shown in Figure 27, where the strains are fairly uniform except for the drop-offs of strain at stiffeners 1 and 9 nearest the side spars.

Plots of strain readings are also shown for Section B-B in Figures 28 through 30. The significant difference in these plots are the back-to-back gages on the skin, some from Section D-D noted in brackets. It is apparent in the plots that bending strains are present in the skin. The strain gages on the skin near the terminus of the stiffener were thought to divulge devastating strains due to pressure when the fasteners supporting the end clips were removed. However, this was not the case, as can be observed in the plots of Figure 31. Thus, it has been shown that the metal clips were unnecessary. It should be re-emphasized that the strain gage readings cannot be predicted by the simplified method of analysis present in this paper.

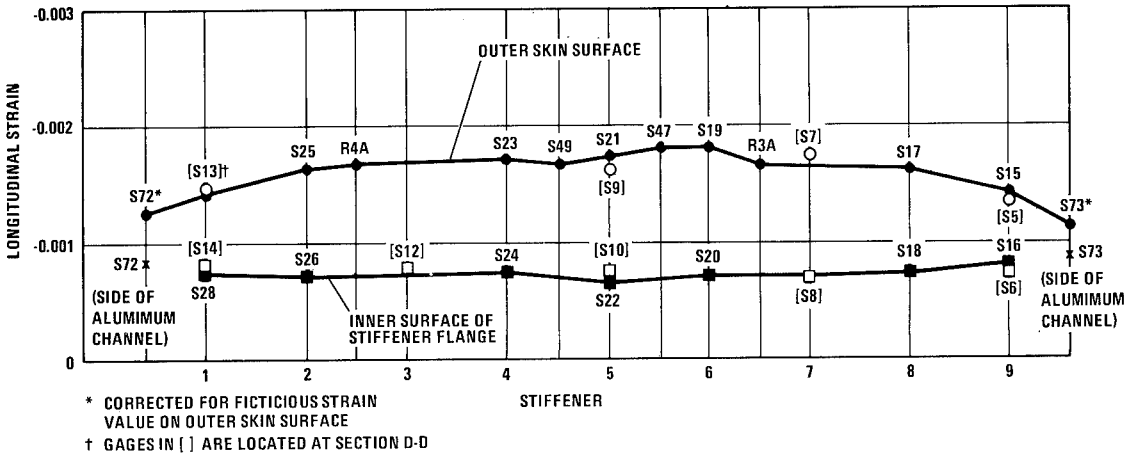

Figure 24. Strains at Section A-A for maximum bending load only (Test 9).

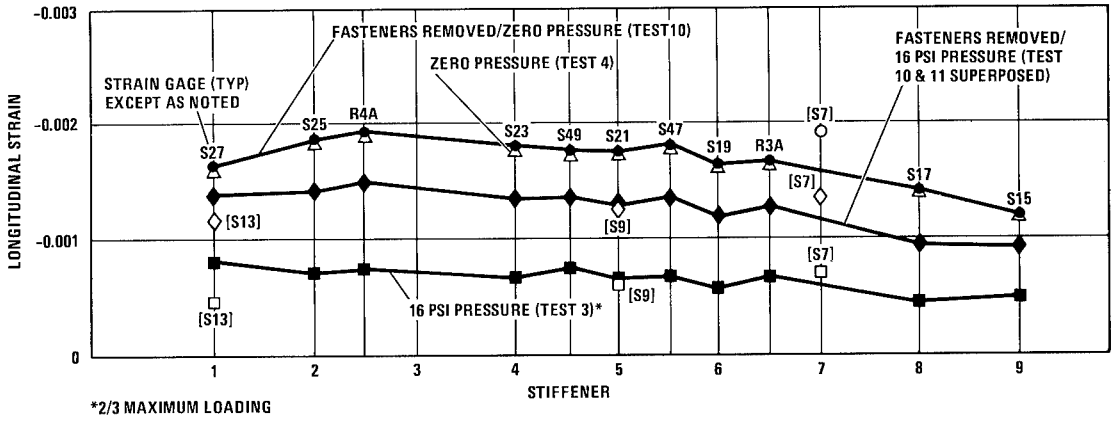

Figure 25. Strains at Section A-A on outer skin surface for maximum bending and torsion (except as noted).

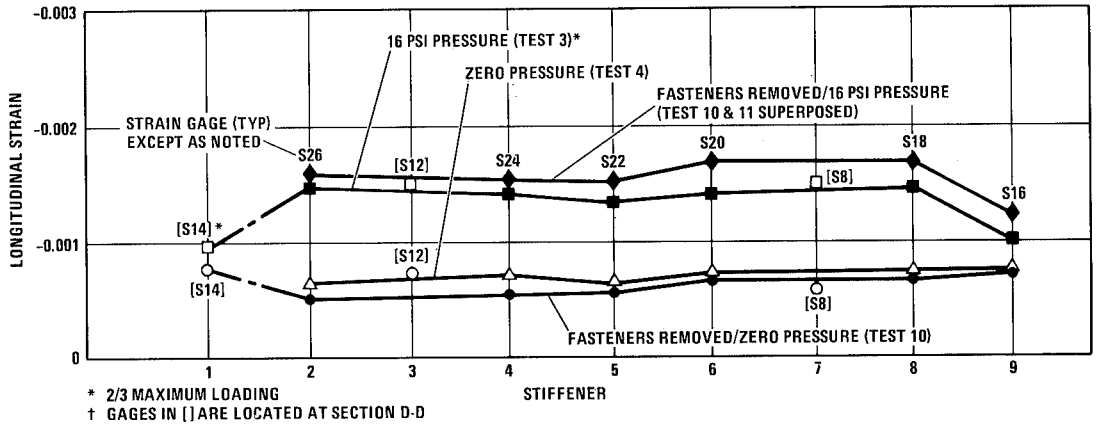

Figure 26. Strains at Section A-A on inner surface of stiffener flange for maximum bending and torsion (except as noted).

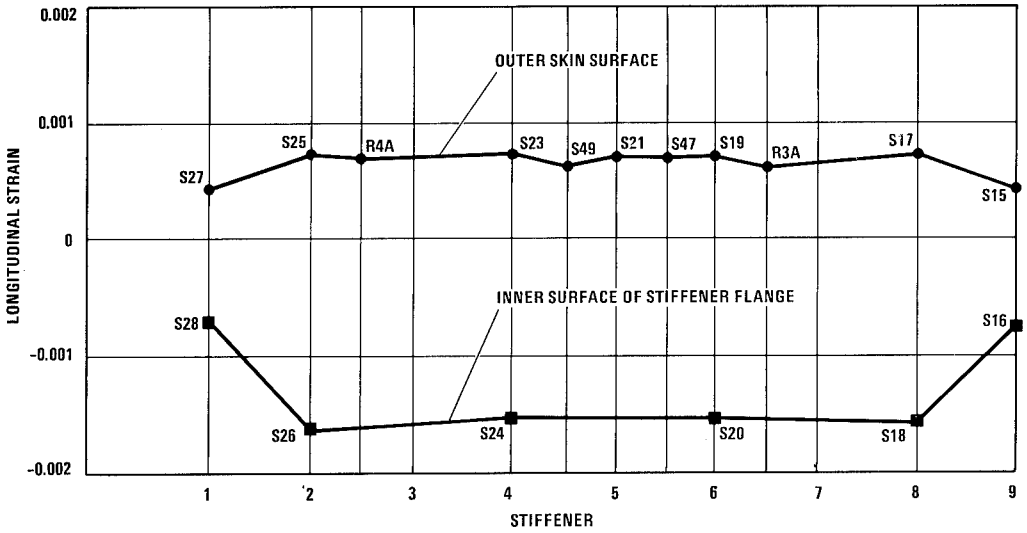

Figure 27. Strains at Section A-A for 25 psi pressure load (Test 11).

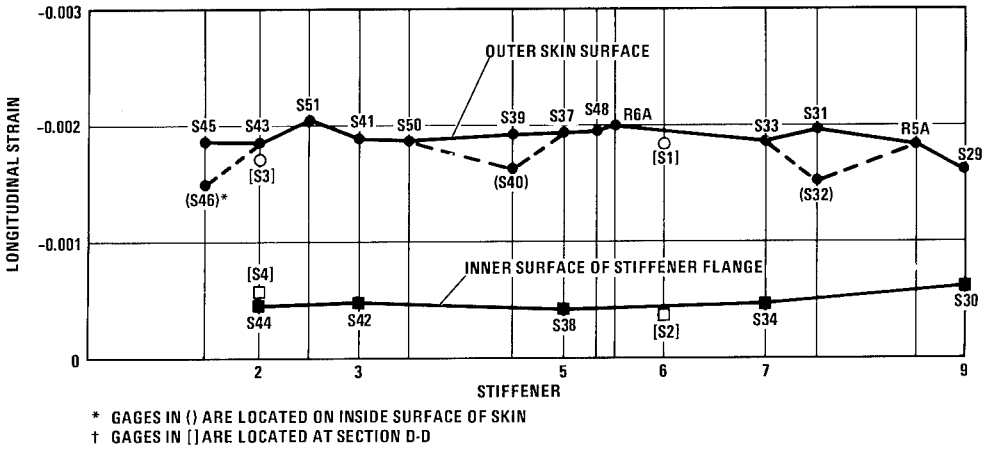

Figure 28. Strains at Section B-B for maximum bending load only (Test 9).

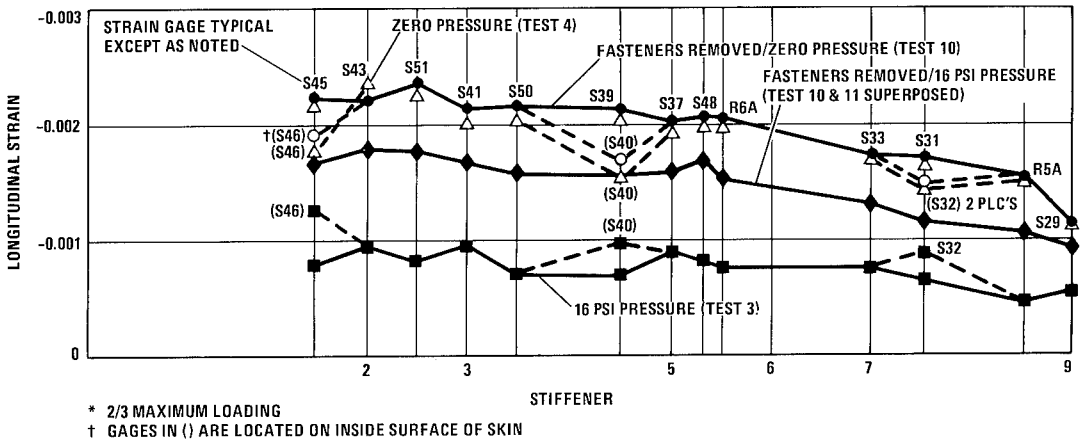

Figure 29. Strains at Section B-B on outer skin surface for maximum bending and torsion (except as noted).

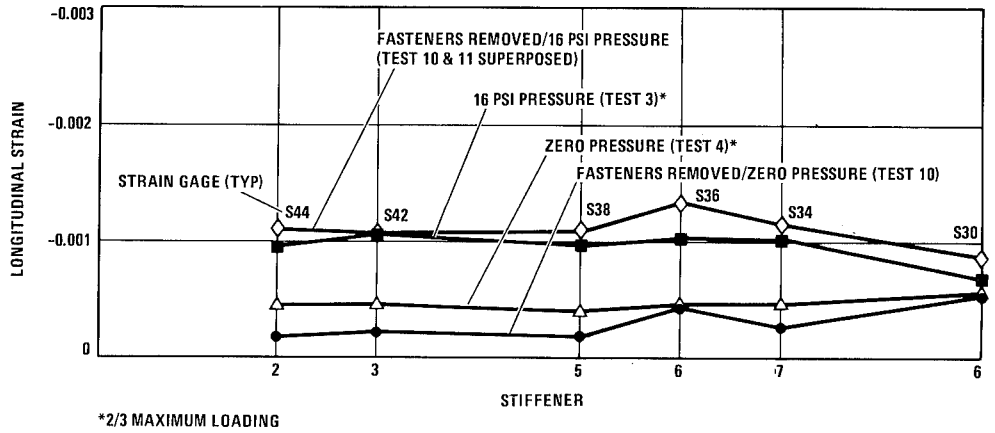

Figure 30. Strains at Section B-B on inner surface of stiffener flange for maximum bending and torsion (except as noted).

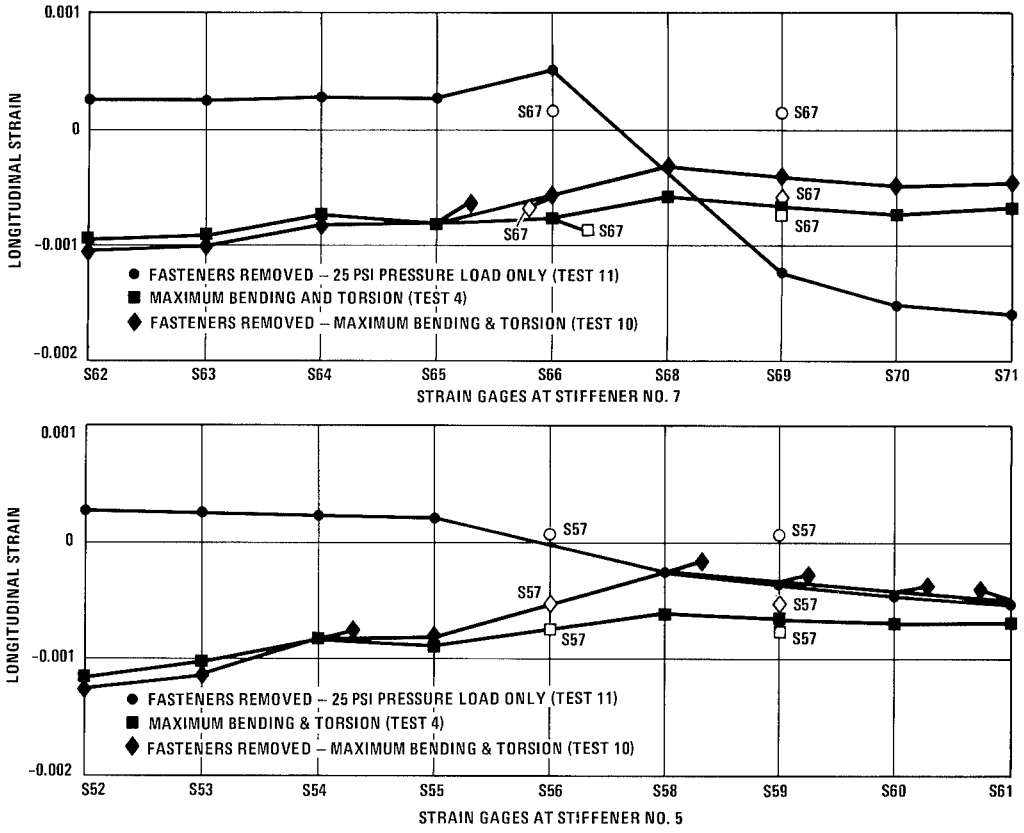

Figure 31. Strains on outer skin surface at end of stiffeners.

CONCLUSIONS

For application in wet wing areas, graphite/epoxy panels, used in conjunction with standard attachment and sealing systems, have been proven extremely satisfactory. The thermal-pressure-forming process used to fabricate these graphite/epoxy skin panels appears to have large-volume cost benefits and will provide panels that are of excellent quality.

The test method and fixture design utilized for providing a uniform load distribution to the test skins panels was quite satisfactory. Since no failures occurred in the test program, it can be assumed that the methods of analysis employed were conservative. Most surprising was the capability of withstanding high internal pressure when the ends of the stiffeners were not clipped to the aluminum ribs. Analysis of this loading condition was not attempted.

Evident from the successful completion of this program is that other graphite/epoxy structures such as large curved panels, 360-degree cylinders or cones can be produced, using the TPF process, at low cost, particularly when large volume production runs are necessary.

ACKNOWLEDGMENT

The authors wish to acknowledge the valuable assistance and major contributions made to this program by: Mr. R.C. "Chris" Christopher (Manufacturing Development of graphite/epoxy net formed doors and stiffened panels) and Mr. N.L. "Norm" Frederick (Manufacuring Development of graphite/epoxy machining and assembly techniques). The general program leadership furnished by Mr. Dave Forest and Dr. Jim Ashton; the valuable technical discussion with Messrs. Jim Spurgeon, Gerald O'Barr, Mike Varlas, Joe Comber, and Jules Hertz along with Drs. Ray Adsit and Paul Merz are also gratefully acknowledged. The test support of the completed wing box by Messrs. Don Bowers and Bob Niebrugge is most appreciated as is the contribution by Convair technicians and shop personnel.

REFERENCES

1. Spier, E.E., "Crippling/Column Buckling Analysis and Test of Graphite/Epoxy Stiffened Panels," AIAA Paper 75-753, 16th AIAA/ASME/SAE Structures, Structural Dynamics, and Materials Conference, Denver, Colorado May 27-29, 1975.
2. Shanley, F.R., Strength of Materials, Fig. 26-8, pg. 644, McGraw-Hill (1957).

MILITARY AIRCRAFT FLIGHT COMPONENT DEVELOPMENT

W. R. Royston

Research & Engineering Division
BOEING AEROSPACE COMPANY
Seattle, Washington

ABSTRACT

An ongoing program to develop an advanced composite military aircraft component for a Boeing Company product is reviewed. The candidate components, selected from the AWACS, Compass Cope, ALCM and YC-14 programs are described. Procedures by which the component, the YC-14 outboard elevator is selected are outlined. Structural design trades with resulting weight and cost evaluations are presented. Material selection, design configuration, joining methods and fabrication approaches are discussed. Proposed subcomponent and full scale tests, both static and dynamic, are described.

INTRODUCTION

It has become increasingly apparent over the past few years that the aircraft industry is committed to a growing application of advanced composites for both primary and secondary air vehicle structure. Hardware programs, funded by industry, the Air Force and NASA have confirmed the early projections of increased performance and reduced costs over metal structure. The Boeing Company recognizes these facts and has instituted a long term IR&D program structured to develop and build the data bank necessary for full participation in future advanced composite projects. The first phase of this program will be of two years duration and involves the selection and development of an airplane structural component: State-of-the-art techniques and data will be incorporated in the design, and on completion, the component will be ground tested with the capability of flight test. In the second phase of this program which will run a further four years, a more complex structure will be studied and developed. This paper deals with the phase one activity to date.

COMPONENT SELECTION

The component for development was selected from several candidates in accordance with criteria formulated to include program objectives and constraints. The many objectives were divided into four main groups and each group was allotted a weighting factor corresponding to its relative importance to the program goals. In addition, each objective was rated within its group. This formed a two-tier selection process and the four groups with their respective weighting factors are defined in Table 1.

TABLE 1

o TECHNOLOGY	(50)*	o CAPITALIZE	(30)*
Primary structure		Performance	
Man rated		Cost	
Typical structure		Production potential	
Adaptable to design change			
Weight			
Cost			
o DEMONSTRATE	(10)*	o REPRESENTATIVE	(10)*
Complexity		Manned aircraft	
Size		R.P.V.'s	
Payoff		Missiles	
Composite utilization		Space	
Flight test		Ships	
Production potential			

* Weighting Factor

Program restraints stated that all candidate components must:

- Be within the current manufacturing and design capability of The Boeing Company.
- Show potential technical advancement over previous advanced composite programs at Boeing.
- Stay within budget.
- Stay inside schedule.
- Constitute a real design requirement.

Seven candidate components were selected (see Figure 1). Advanced composite design drawings were made for each candidate and compared with the current design in accordance with the selection criteria. These candidates were the:

INBOARD WING, Compass Cope (RPV), a straight constant section structural wing box with integral fuel tanks.
Current design: All aluminum, three spar box with honeycomb supported covers.
Advanced composite design: All Gr/Ep, three spar box with nomex honeycomb supported covers.

HORIZONTAL STABILIZER, Compass Cope, a straight constant section structural box.
Current design: Two aluminum spars, honeycomb supported fiberglas covers.
Advanced composite design: All Gr/Ep, two spars and honeycomb supported covers.

WING, ALCM (Air Launched Cruise Missile), a straight, tapered wing section, five feet semi-span, pivoted at root.
Current design: Upper and lower machined aluminum wing half sections, bonded on chord plane. Steel pivot fittings.
Advanced composite design: Full depth nomex flexcore, Gr/Ep covers. Titanium pivot fittings.

FUSELAGE, ALCM, a highly pressurized non-cylindrical fuel tank.
Current design: All welded aluminum.
Advanced composite design: All Gr/Ep laminate shell subassemblies, longerons and body frames. Mechanically fastened assembly.

RUDDER, AWACS, (707 airplane).
Current design: Conventional aluminum.
Advanced composite design: All Gr/Ep, two spars, corrugated support structure and laminate skins. Full depth honeycomb aft of rear spar.

HORIZONTAL STABILIZER, YC-14, (Medium STOL Transport), a carry-through structural box with tapered cross section.
Current design: Aluminum, four spars and ribs, square edged honeycomb supported covers.
Advanced composite design: All Gr/Ep, multi-spar, honeycomb supported covers, rib webs and spar webs.

INBOARD AND OUTBOARD ELEVATORS AND TABS, YC-14.
Current design: Aluminum, conventional stiffened skin elevator and full depth honeycomb tab.
Advanced composite design: All Gr/Ep, two spar elevator with honeycomb sandwich covers and full depth honeycomb tab.

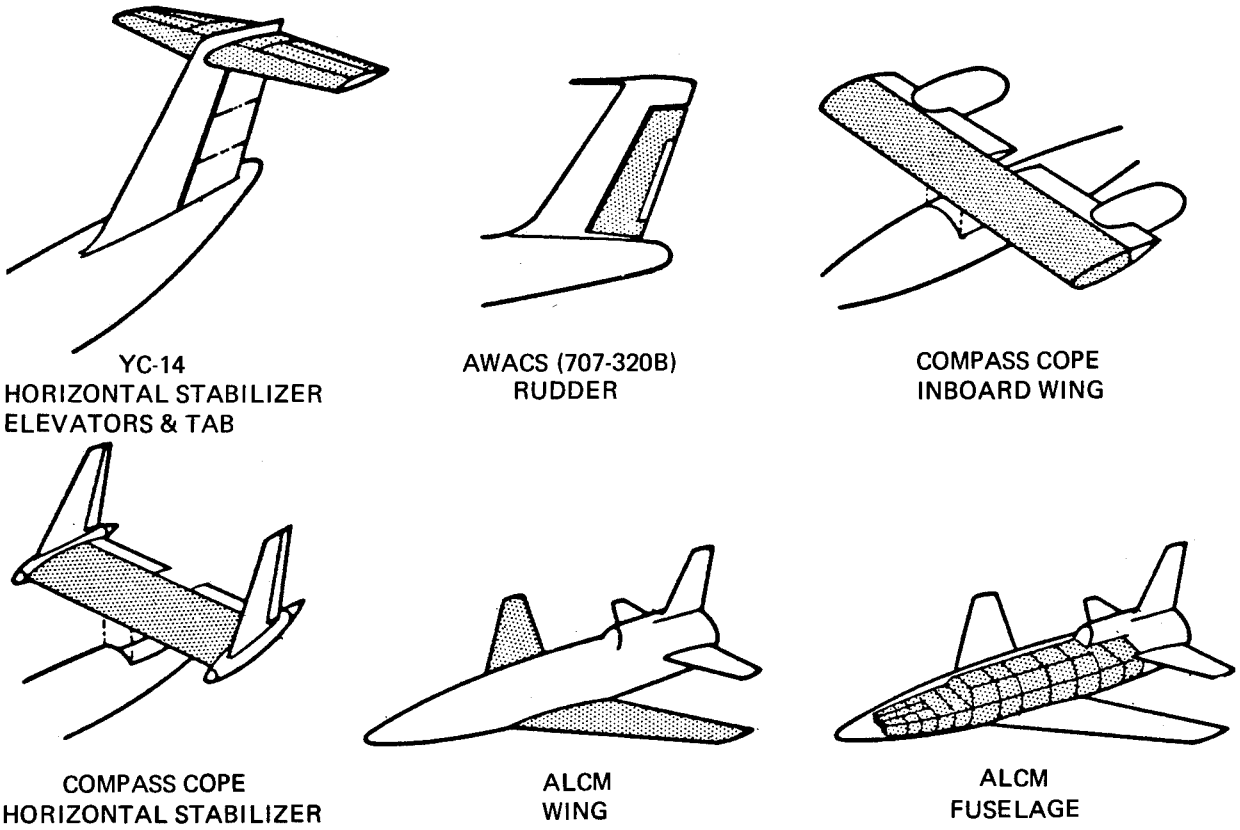

Figure 1. Candidate Components

Manufacturing costs and weights were determined for both the current design and the advanced composite design for each candidate component. These are shown in Tables 2, 3, and 4.

Table 2. Cost Comparison Composite/Metal

Component	Advanced composite cost / Metal baseline cost	
	1st component	100th component
Inboard wing—Compass Cope	1.43	1.16
Horizontal tail—Compass Cope	.83	.69
Wing—ALCM	2.06	1.74
Fuselage—ALCM	.80	.52
Rudder—AWACS	1.17	.95
Stabilizer structural box—YC-14	1.57	1.26
Elevator and tab—YC-14	.73	.60

Table 3. Weight Comparison

Component	Weight baseline design kg (lb)	Weight adv comp design kg (lb)	Δ weight kg (lb)	Graphite/ epoxy usage kg (lb)	Weight saving (%)
Inboard wing–Compass Cope	280 (619)	193 (426)	87 (193)	124 (274)	31
Horizontal tail–Compass Cope	33 (73)	16.3 (36)	16.7 (37)	13.6 (30)	50
Wing–ALCM	15.4 (34)	9.06 (20)	6.34 (14)	3.2 (7)	41
Fuselage–ALCM	144 (317)	116 (256)	28 (61)	79.4 (175)	19
Rudder–AWACS	394 (868)	302 (667)	92 (201)	46.6 (103)	23
Horizontal tail structural box–YC-14	920 (2029)	674 (1487)	246 (542)	401 (886)	27
Outboard elevator and tab (H/C)–YC-14	270 (596)	177 (391)	93 (205)	47.5 (105)	34

Table 4. Weight Comparison YC-14 Horizontal Stabilizer

Component	Weight baseline design kg (lb)	Weight adv comp design kg (lb)	Δ weight kg (lb)	Graphite/ epoxy usage kg (lb)	Weight saving (%)
Structural box (left hand and right hand)	920 (2029)	675 (1487)	245 (542)	401 (886)	27
Outboard elevator (2)	468 (1034)	296 (654)	172 (380)	71 (157)	37
Outboard tab (2)	71.6 (158)	58 (128)	13.6 (30)	25.4 (56)	19
Inboard elevator (2)	84 (186)	63.2 (140)	20.8 (46)	33.5 (74)	25
Inboard tab (2)	25.8 (57)	21.8 (48)	4.0 (9)	13.6 (30)	16
Total	1570 (3470)	1115 (2460)	457 (1010)	545 (1200)	29

Merit points were then awarded to each component based on the program objectives listed in Table 1. These were then summed in order to arrive at a rating for each component in the four groups, "Technology," "Demonstrate," "Capitalize," and "Representative." See Tables 5, 6, 7, and 8.

Table 5. Technology

Components \ Selection criteria	Weighting factor	Primary structure	Man rated	Typical structure	Adaptable to design change	Weight	Cost	Weight factor x rating/100
		10	5	20	5	30	30	
Inboard wing–Compass Cope		10	0	9	9	7	-3	4.45
Horizontal tail–Compass Cope		10	0	6	7	10	4	6.75
Wing–ALCM		10	0	2	4	9.5	-5	2.95
Fuselage–ALCM		10	0	6	5	3	0	3.35
Rudder–AWACS		0	10	6	6	4	-1	2.90
Horizontal tail–YC-14								
Outboard elevator and tab		0	10	6	8	8	5	6.00
Outboard box elevator and tab		10	10	10	9	7	0	6.05
Structural box (left hand)		10	10	9	9	6	-2	4.95
Inboard box outboard elevator		10	10	10	9	8	3	7.25

Table 6. Demonstrate

Components \ Selection criteria	Complexity	Size	Payoff	Composite utilization	Flight test	Production potential	Others	Average rating
Inboard wing–Compass Cope	9	7	4	6	5	5	5	5.86
Horizontal tail–Compass Cope	7	3	10	2	5	5	5	5.29
Wing–ALCM	5	1	4	1	4	5	5	3.57
Fuselage–ALCM	9	2	3	5	4	5	5	4.71
Rudder–AWACS	6	8	3	4	10	9	9	7.00
Horizontal tail–YC-14								
Outboard elevator and tab	6	6	9	4	8	8	9	7.14
Outboard box elevator and tab	10	9	6	7	8	8	9	8.14
Structural box (left hand)	8	8	4	8	8	8	9	7.57
Inboard box outboard elevator	9	7	9	6	8	8	9	8.0

Table 7. Capitalize

Components \ Selection criteria	Performance	Cost	Others	Production potential	Average rating
Inboard wing—Compass Cope	6	-3	6	6	3.75
Horizontal tail—Compass Cope	8	4	6	6	6.0
Wing—ALCM	6	5	6	7	3.5
Fuselage—ALCM	3	0	6	7	4.0
Rudder—AWACS	3	-1	3	7	3.0
Horizontal tail—YC-14					
Outboard elevator and tab	10	5	8	8	7.75
Outboard box elevator and tab	9	0	8	8	6.25
Structural box (left hand)	8	-2	8	8	5.5
Inboard box outboard elevator	9	3	8	8	7.0

Table 8. Representative

Components \ Selection criteria	Manned aircraft	RPV's	Missiles	Space	Ships	Average rating
Inboard wing—Compass Cope	8	9	5	5	7	6.8
Horizontal tail—Compass Cope	7	8	5	4	7	6.2
Wing—ALCM	2	5	9	4	6	5.2
Fuselage—ALCM	4	6	9	4	2	5.0
Rudder—AWACS	6	4	5	4	5	4.8
Horizontal tail—YC-14						
Outboard elevator and tab	7	7	6	4	6	6.0
Outboard box elevator and tab	9	8	6	5	8	7.2
Structural box (left hand)	8	8	4	6	7	6.6
Inboard box outboard elevator	9	9	5	5	8	7.2

In Table 9, the respective weighting factors are applied to these ratings and the final component ranking is achieved.

Table 9. Component Rating

Components \ Selection criteria	Technology (50)	Demonstrate (10)	Capitalize (30)	Representative (10)	Total	Rank
Inboard wing–Compass Cope	4.45	5.9	3.7	6.8	463	6
Horizontal tail–Compass Cope	6.75	5.3	6.0	6.2	633	4
Wing–ALCM	2.95	3.6	3.5	5.2	341	9
Fuselage–ALCM	3.35	4.7	4.0	5.0	385	7
Rudders–AWACS	2.90	7.0	3.0	4.8	353	8
Horizontal tail–YC-14						
Outboard elevator and tab	6.0	7.1	7.8	6.0	665	2
Outboard box elevator and tab	6.05	8.1	6.3	7.2	645	3
Structural box (left hand)	4.95	7.6	5.5	6.6	555	5
Inboard box outboard elevator	7.25	8.0	7.0	7.2	725	1

The Compass Cope horizontal tail is a stiffness designed, flutter critical structure built currently with fiberglas cover panels. Substituting Gr/Ep for fiberglas, a low E material, has the decided advantage of reducing weight (50%) and manufacturing costs (31%), this being largely due to labor savings with reduced ply lay-up. This component was rated fourth in the program. The Compass Cope inboard wing ranked sixth. This component showed a good weight savings (31%) but a cost increase of 16% over the aluminum design.

The ALCM fuselage ranked seventh in spite of estimated weight savings of 19% and a cost reduction of 48%. Its low ranking was due mainly to its non-representative structure in the terms of the selection criteria and its low contribution to improved flight performance.

The AWACS rudder with a weight savings of 23% and a cost reduction of 5%, ranked low since it is secondary structure. It was awarded low ratings for technical complexity and improved flight performance.

The ALCM wing showed a high weight savings of 41%, but a manufacturing cost increase of 74% contributed to its ranking being the lowest of all the candidates.

In making the manufacturing cost comparisons in Table 2, it was ascertained that the development and fabrication costs of the YC-14 horizontal stabilizer structural box overran the budget constraint on this program. The stabilizer box, however, being primary structure, offered potential technical advancement in many areas and in order to retain the stabilizer box in the program, it was decided to pair sections of the box with elevators and tabs.

The YC-14 stabilizer components all showed good weight savings and potential cost reductions. As a result, the horizontal stabilizer components ranked high on the list of candidates. The combination of outboard elevator and inboard section of the structural box ranked highest making these components the final selection in the development program.

SELECTED COMPONENT DESCRIPTION

The YC-14 prototype (see Figure 2) is an advanced medium STOL transport airplane of around 90,000 kg (200,000 lb.) gross weight currently under development by The Boeing Company on an Air Force contract. It is a twin engined airplane using upper surface blowing to derive its STOL capability. Its large "T" tail has a span of 16.8 meters (55 feet) and a maximum chord of 4.5 meters (14.7 feet). The horizontal stabilizer structural box is a full span torsion box with a maximum chord of 1.7 meters (5.5 feet).

The inboard section of this stabilizer selected for advanced composite development has a span of 3.7 meters (12 feet), and includes the load introduction points at the vertical fin attachment. A full span elevator is hinged to the stabilizer rear spar. This elevator comprises four sections, two inner and two outer, the left hand outboard section, 5.8 meters (19 feet) in length being selected for redevelopment. Figure 3 shows the location of the two selected components on the YC-14. Design details of both the structural box and the outboard elevator are shown in Figures 4 and 5, respectively. These designs were made during the original component selection process and do not necessarily illustrate the final thinking on these components.

At this point in the program, the design effort was directed to the elevator and there has been no further study to date on the stabilizer structural box.

The current aluminum elevator is a two spar box structure with twelve ribs and stiffened cover panels. Six hinge fittings on the front spar attach to the stabilizer and five hinge fittings on the rear spar attach to the elevator tab. In addition, two actuator and four reaction link fittings are provided on the front spar. Chordwise loading at these fittings is reacted by inspar ribs placed at each fitting location. All hinge, actuator and reaction link fittings were retained for use on the advanced composite elevator which was designed to be fully interchangeable with the current elevator.

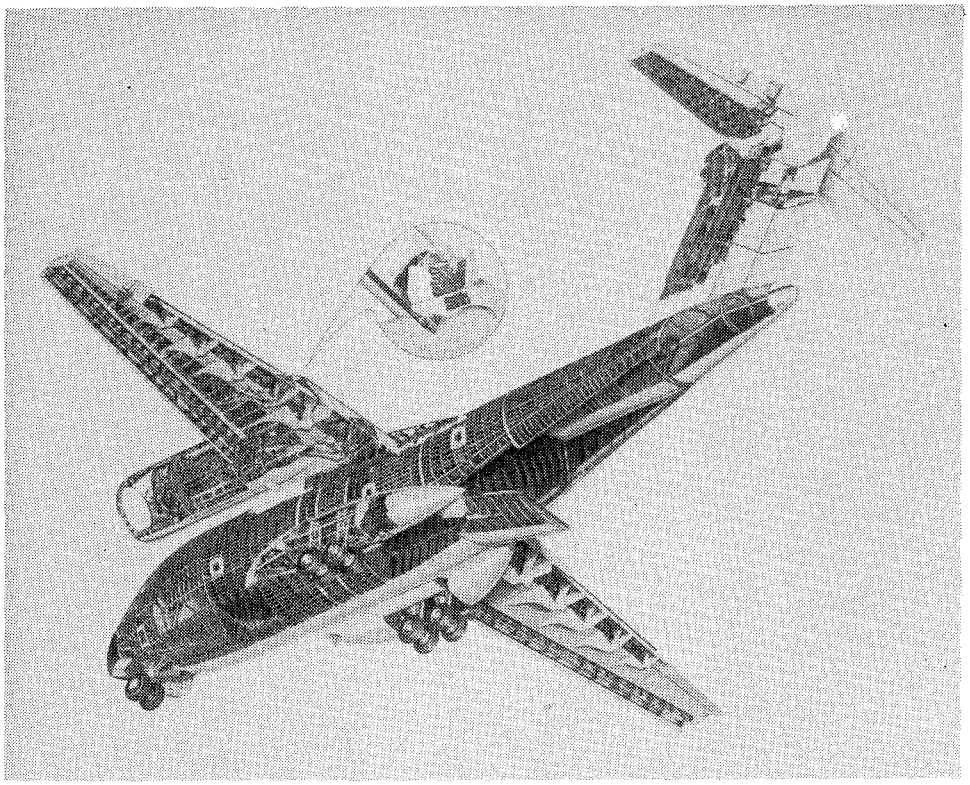

Figure 2. YC-14 Prototype Airplane

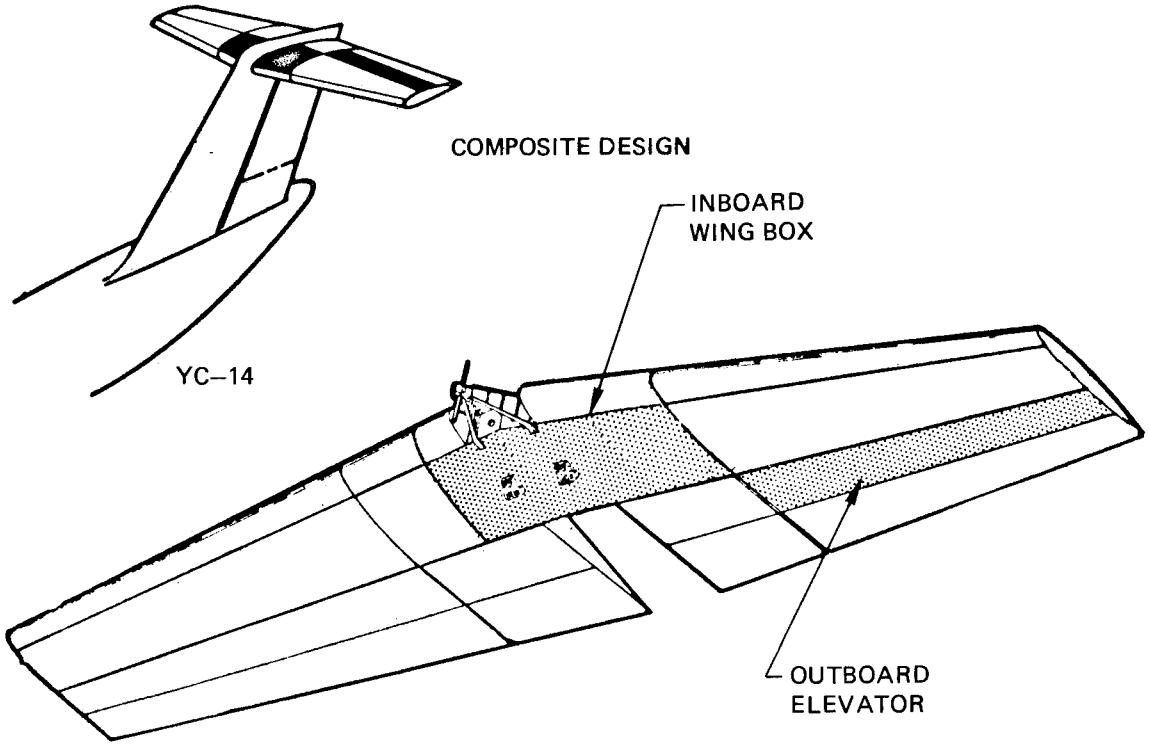

Figure 3. YC-14 O/B Elevator and I/B Structural Box

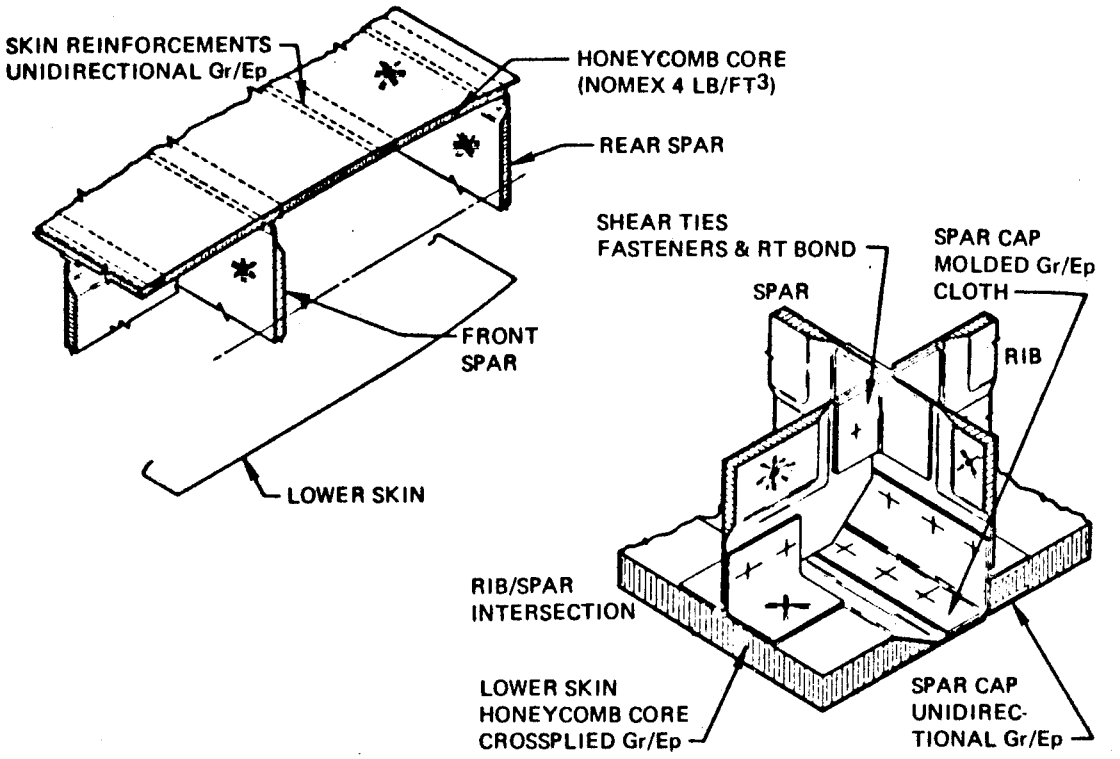

Figure 4. YC-14 Horizontal Stabilizer-Structural Box Details

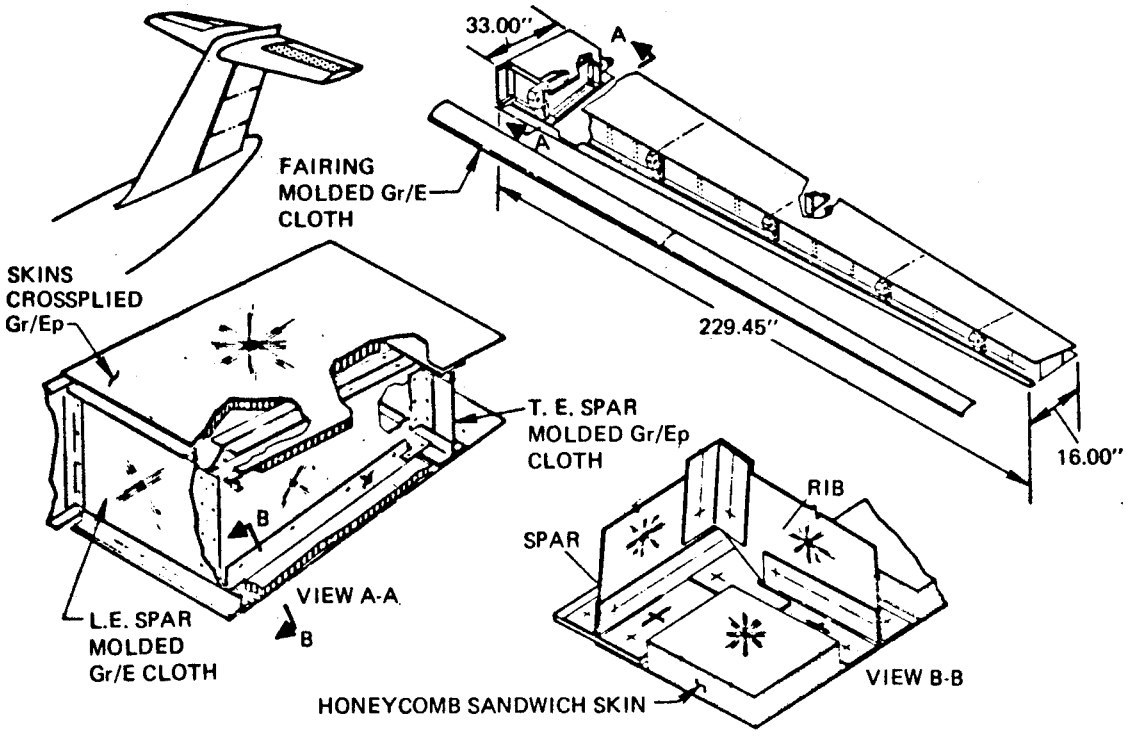

Figure 5. YC-14 Elevator-Honeycomb Sandwich Composite Design

COMPONENT DESIGN STUDIES

Drawings were prepared for nine different advanced composite elevator design concepts. These were:

Honeycomb Design (Figure 6) uses nomex core to stablize Gr/Ep cover panels, spar and rib webs. This concept was considered to be an efficient, low cost method of supporting the thin gage, lightly loaded structure.

Honeycomb Design - Gr/Ep Hinge Fittings (Figure 7), a similar design to the previous one with redesigned Gr/Ep hinge fittings at the four double rib locations. 19% of the current elevator weight is in the hinge, actuator, and reaction link fittings attached to the front and rear spars. This design was an attempt to reduce that weight. It was eventually considered a high risk design. Consequently, all other Gr/Ep concepts utilize the current aluminum fittings.

Skin/Continuous Stringer Design (Figure 8) uses Gr/Ep covers supported by full span longitudinal hat section stiffeners and stiffened Gr/Ep laminate spar and rib webs. This is a conventional stiffening approach which minimizes the number of cover panel stiffeners but introduces cut-outs and shear ties at all ribs.

Skin/Discontinuous Stringer Design (Figure 9) a similar design to the previous one but the stringers are discontinuous at each rib. This design eliminates the rib cut-outs and shear ties but increases the stiffener part count. Both of these longitudinally stiffened designs have the disadvantage of increasing the elevator EI above the required limits, thus inducing higher bending loads than necessary due to stabilizer deflections. A number of chordwise stiffened concepts, designed to reduce these bending loads, were also evaluated.

Chordwise Corrugated Stiffened Skin Design (Figure 10) uses Gr/Ep cover panels supported by a Gr/Ep chordwise corrugated member. Spar and rib webs are stiffened Gr/Ep laminates.

Chordwise Honeycomb Stiffened Skin Design (Figure 11), this concept uses Gr/Ep cover panels stiffened with narrow honeycomb strips having a Gr/Ep facing ply. Spar and rib webs are stiffened Gr/Ep laminates. This was an attempt to reduce weight by substituting the full span corrugation in the previous design with intermittent stiffening elements.

Waffle Design 0^{o}-90^{o} Laminates (Figure 12) uses Gr/Ep cover panels supported by a Gr/Ep laminated waffle grid bonded in position. Spar and rib webs are stiffened Gr/Ep laminates. Difficulties arose in this design in developing a satisfactory edge bond between the waffle and the cover panel. The following design was an attempt to overcome this problem.

Waffle Design 0^{o}-90^{o} Honeycomb Stiffeners (Figure 13), this concept uses Gr/Ep cover panels supported by narrow honeycomb strips having a Gr/Ep facing ply. This honeycomb waffle grid is bonded to the cover panels in the 0^{o}-90^{o} direction. Spar and rib webs are stiffened by similar honeycomb stiffeners bonded vertically to the webs.

Waffle Design $\pm 45^{o}$ Honeycomb Stiffeners (Figure 14), a similar design to the previous one with the waffle grid positioned at $\pm 45^{o}$. This is a variation on the previous concept and was proposed since torsional stiffness requirements design the cover panels. Here the $\pm 45^{o}$ waffle adds to this stiffness with a resultant slight weight savings. The manufacturing complexity is increased by this concept and is reflected in relatively increased costs.

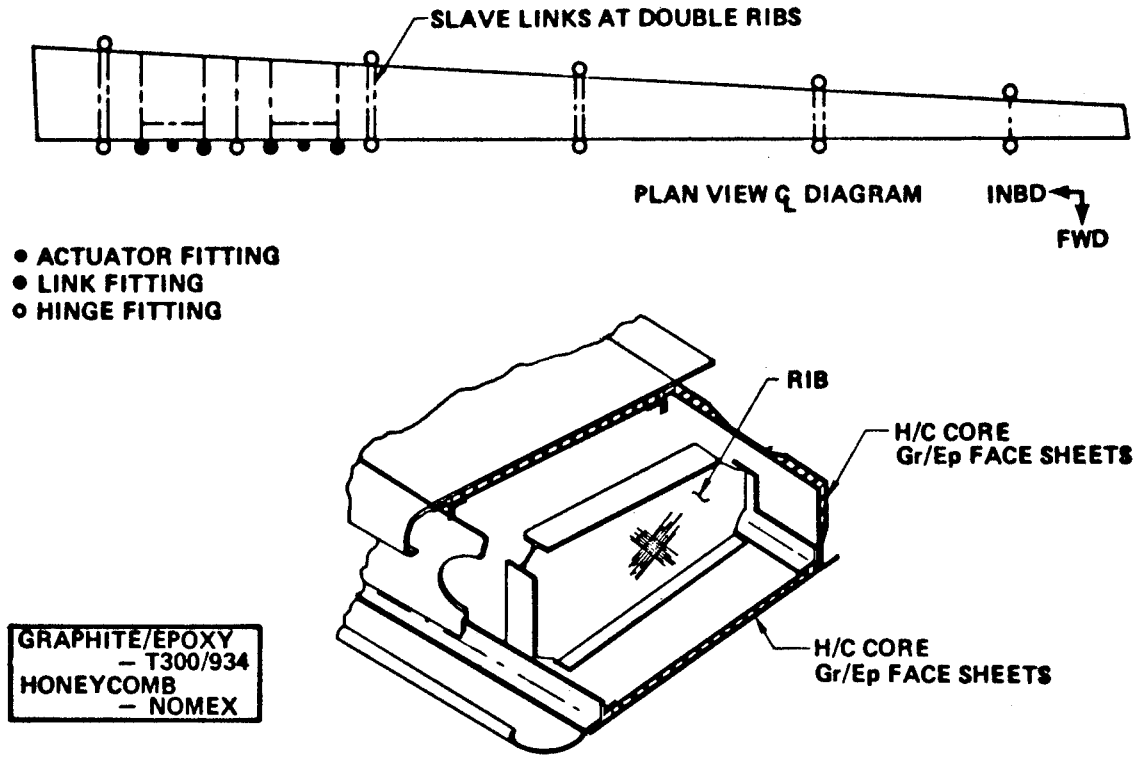

Figure 6. YC-14 Elevator Gr/Ep Honeycomb Design

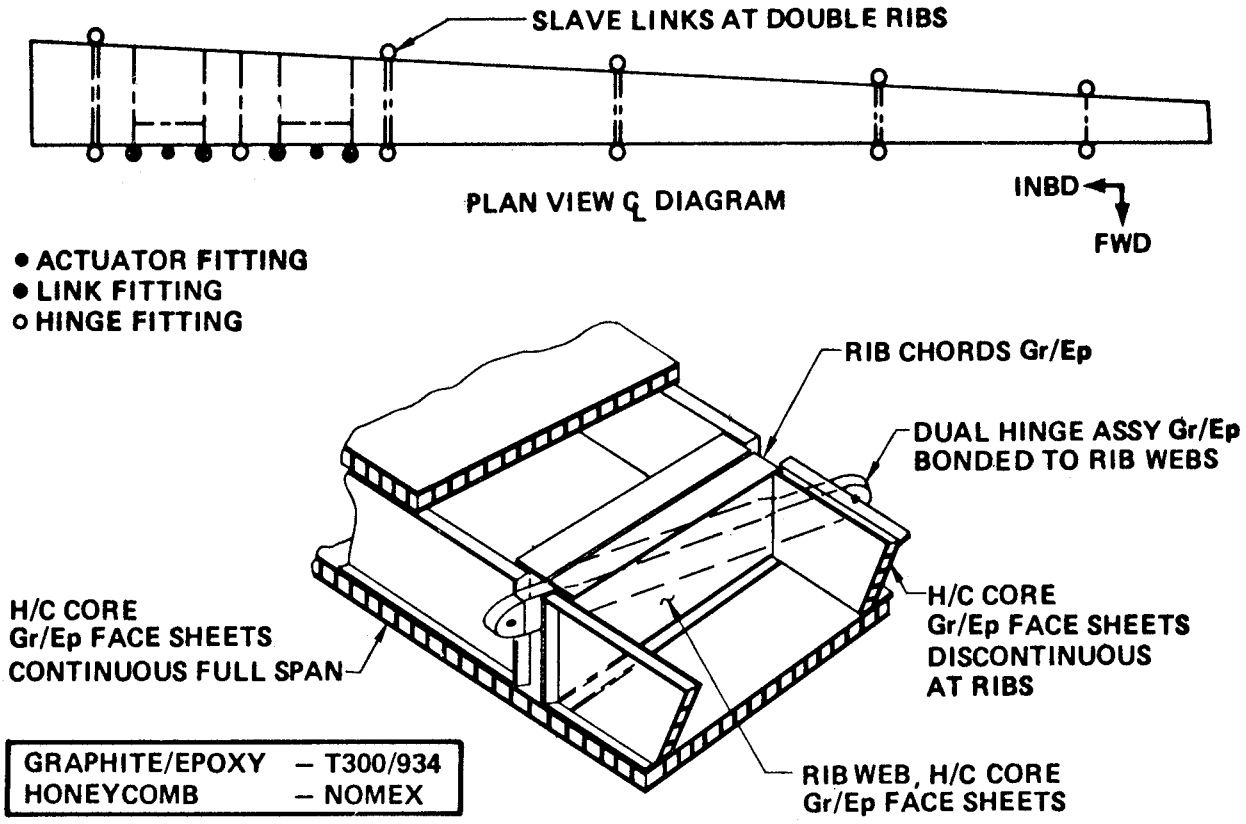

Figure 7. YC-14 Elevator Gr/Ep Honeycomb Design – Gr/Ep Hinge Fittings

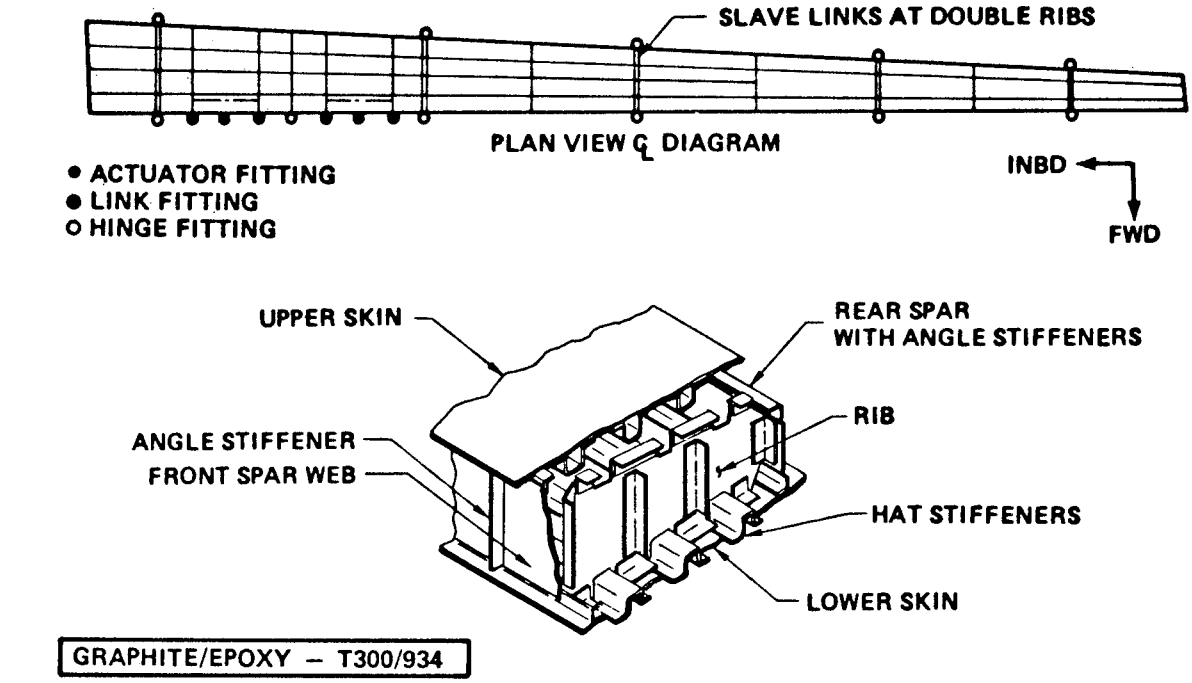

Figure 8. YC-14 Elevator Gr/Ep Skin/Continuous Stringer Design

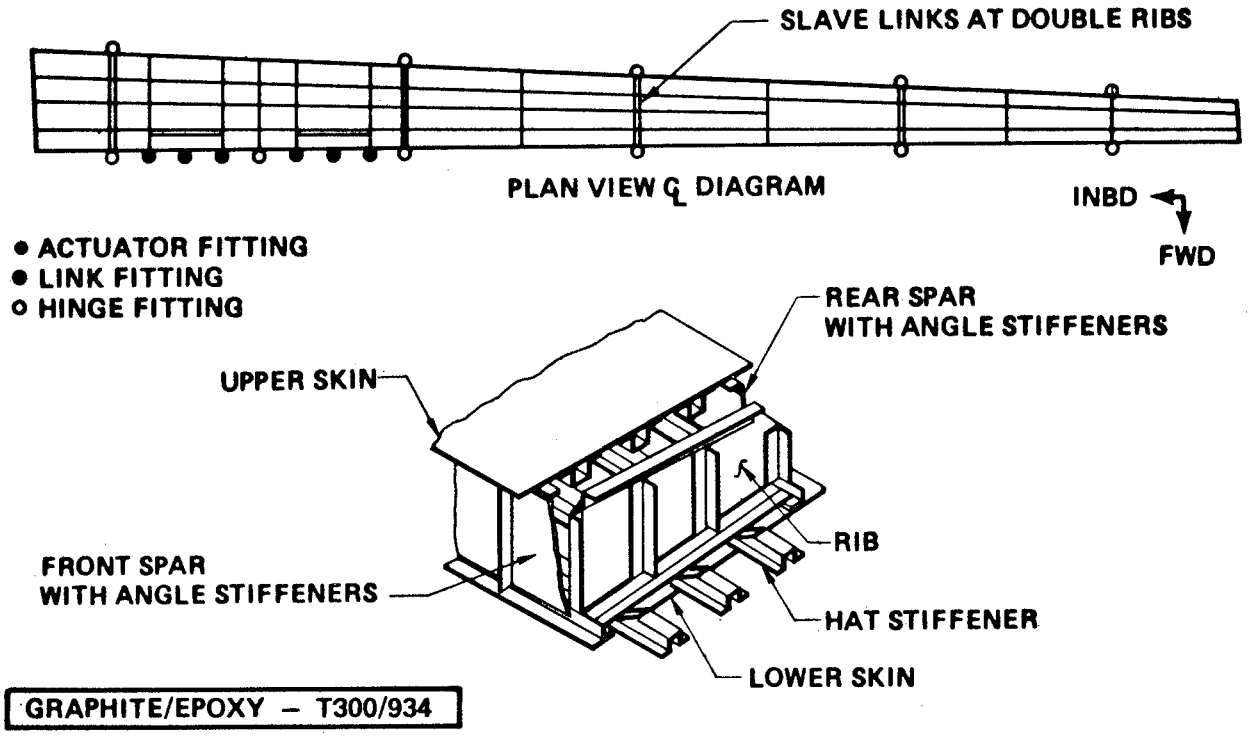

Figure 9. YC-14 Elevator Gr/Ep Skin/Discontinuous Stringer Design

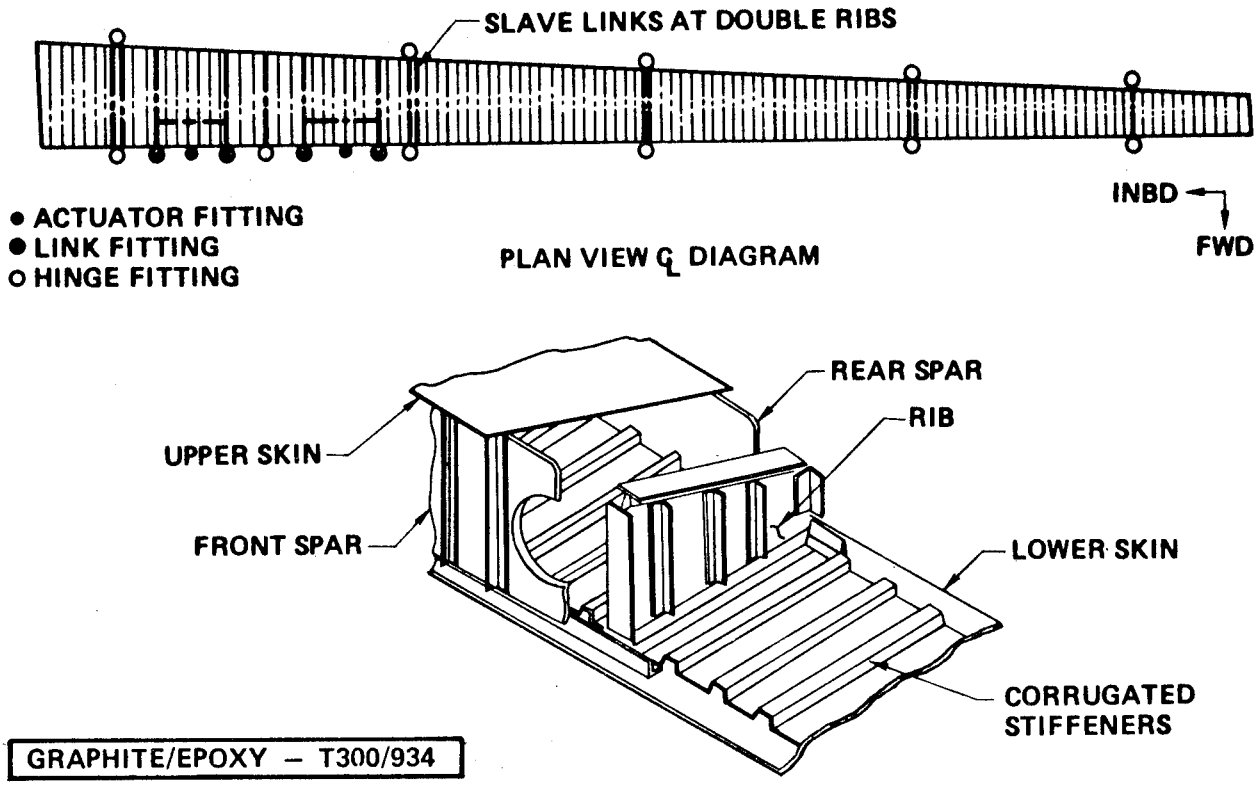

Figure 10. YC-14 Elevator Gr/Ep Chordwise Corrugated Stiffened Skin Design

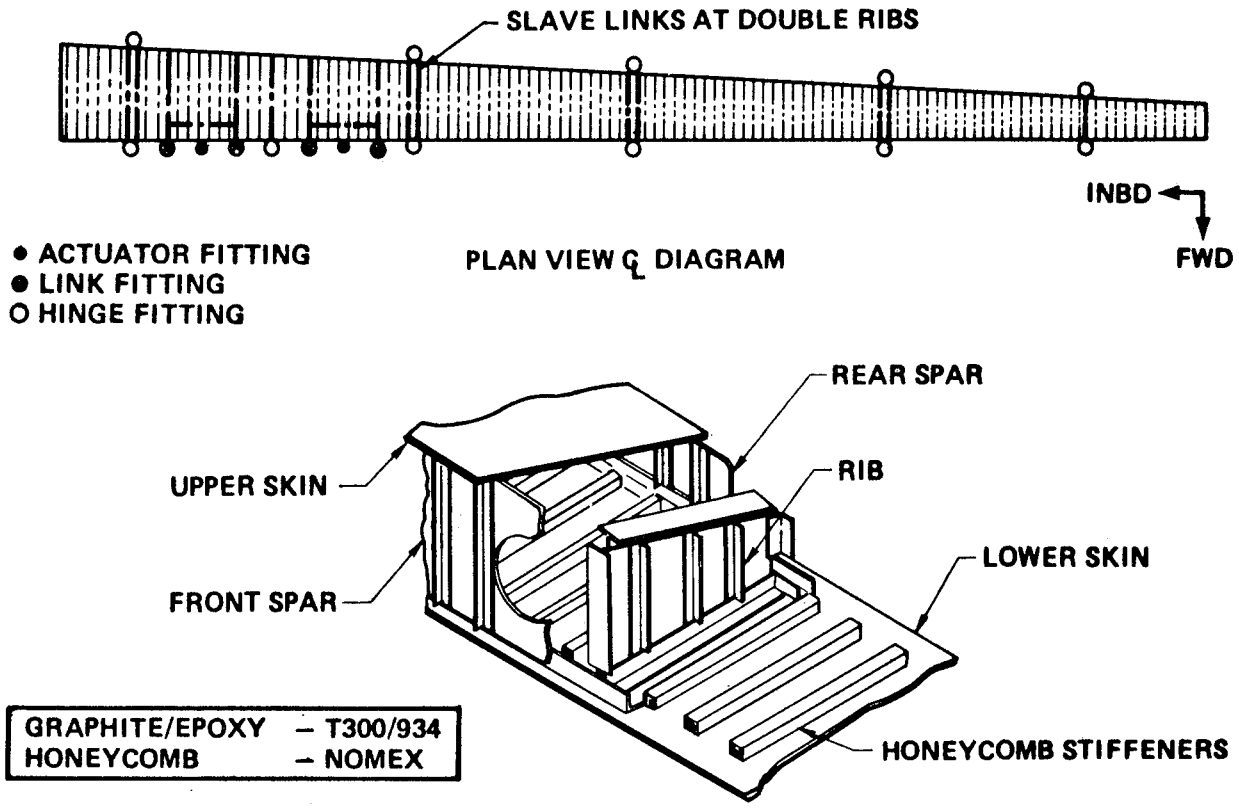

Figure 11. YC-14 Elevator Gr/Ep Chordwise Strap H/C Stiffened Skin Design

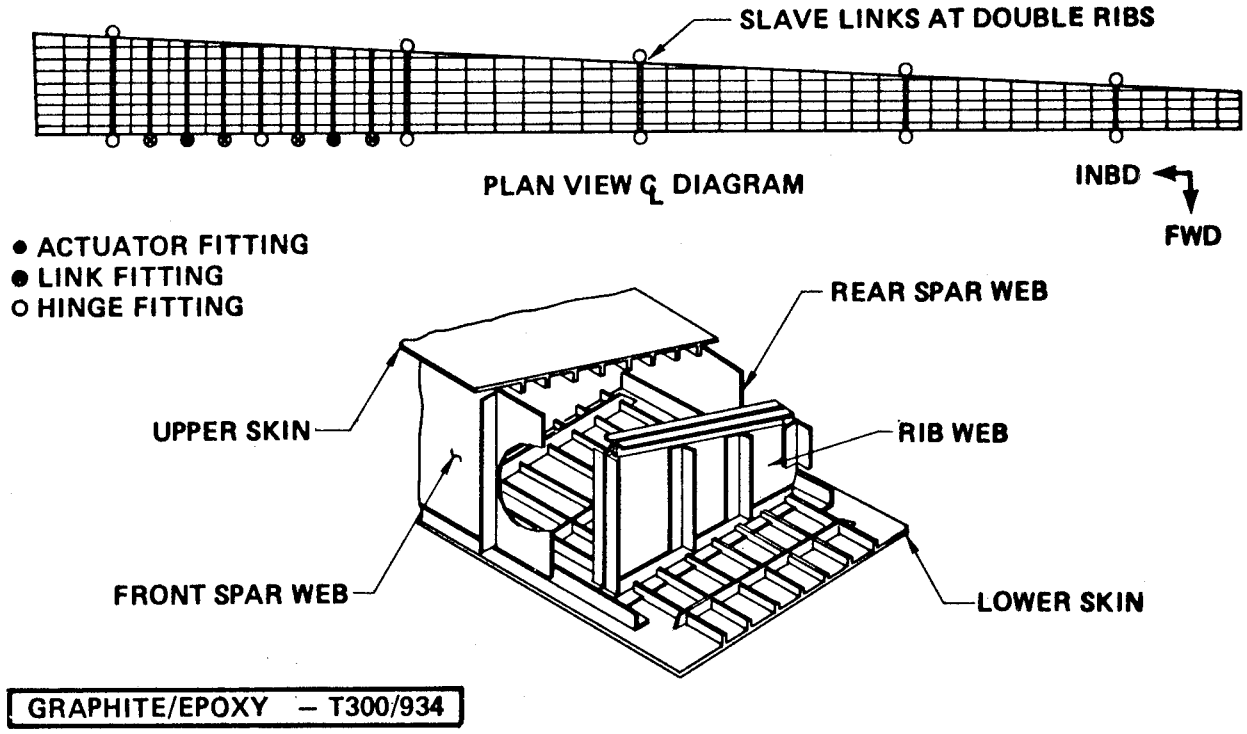

Figure 12. YC-14 Elevator Gr/Ep Waffle Skin Design 0^{o}–90^{o} Laminate Stiffeners

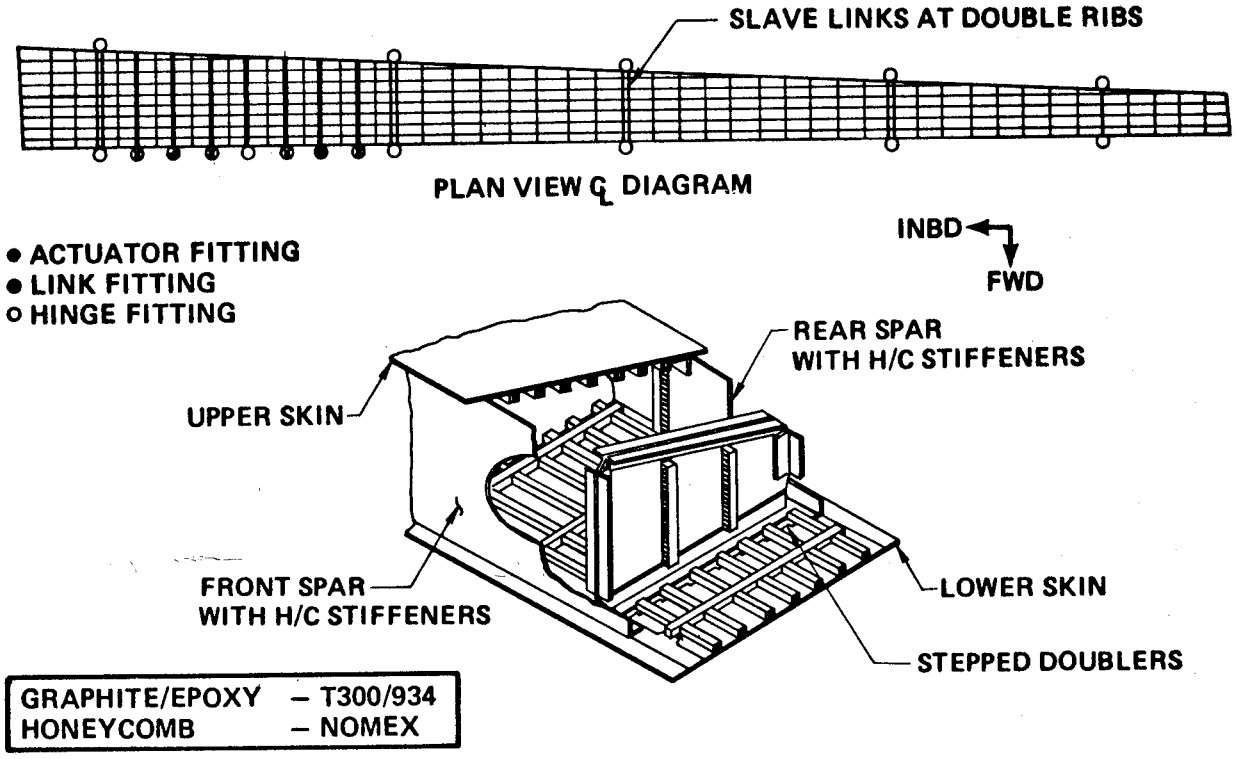

Figure 13. YC-14 Elevator Gr/Ep Waffle Skin Design 0^o–90^o Strap H/C Stiffeners

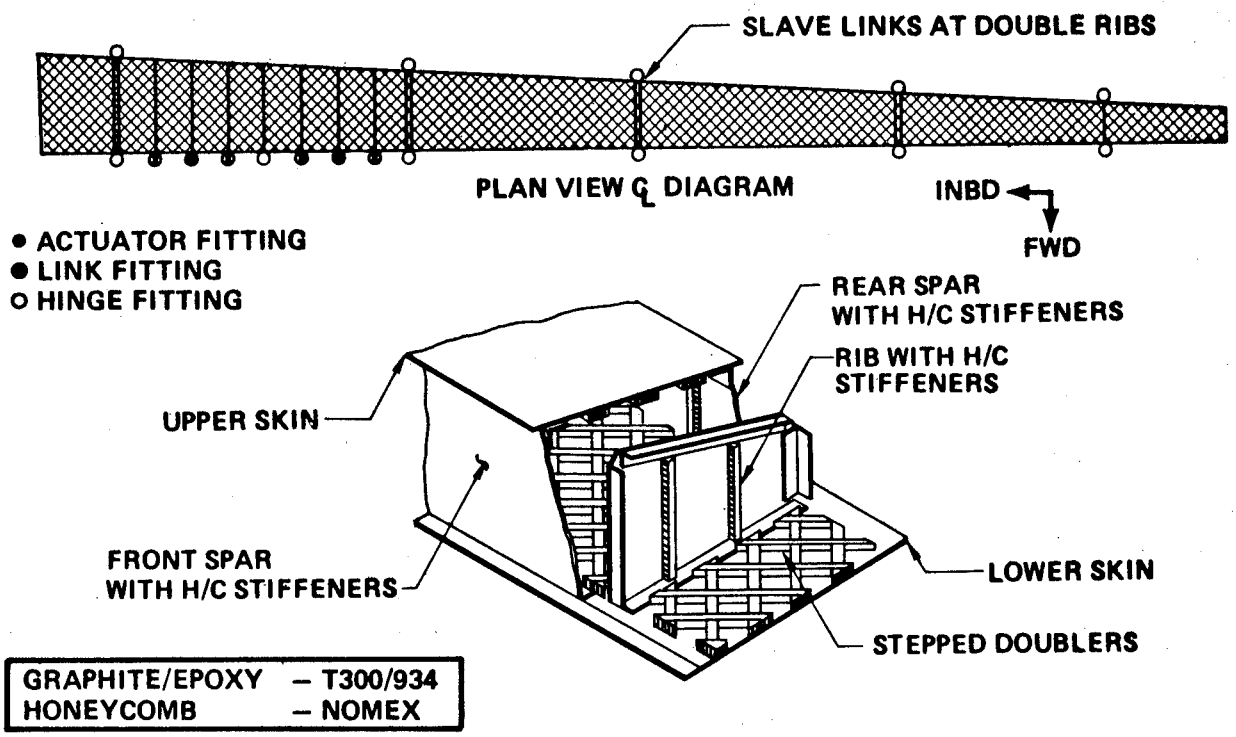

Figure 14. YC-14 Elevator Gr/Ep Waffle Skin Design $\pm 45^o$ Strap H/C Stiffeners

These nine concepts were then rated using a weighting system applied as follows:

Cost	35
Weight	35
Materials & Processes	5
Quality Control	5
Fatigue and Fracture	5
Damage Tolerance	5
Maintainability	10

These evaluations are shown in Tables 10, 11, and 12, with the final rating summary in Table 13. This shows the honeycomb design ranked first with the alternate honeycomb design a close second. The honeycomb design was therefore selected as the final concept with the proviso that further evaluation of rib and spar shear web design was required. As a result, a rib web and spar web study was initiated.

Table 10. Concept Rating

Dwg no.	Concept	M&P	Fatigue fracture	Damage tolerance	Q/C	Maintainability	
						Ease of repair	Damage susceptibility
100	H/C design	10	7	7	2	8	6
105	H/C design -Gr/Ep hinge ftgs	8	6	7	0	6	6
101	Skin/stringers - continuous	2	6	8	7	7	10
104	Skin/stringers - discontinuous	5	5	8	7	7	10
107	Corrugated stiff skin - chordwise	6	7	8	9	5	10
108	H/C stiff skin - chordwise	1	6	7	6	6	8
103	Waffle des $0^{o}/90^{o}$ - lam stiff	4	4	7	9	6	10
106	Waffle des $0^{o}/90^{o}$ - H/C stiff	1	5	7	5	5	8
109	Waffle des $\pm 45^{o}$ - H/C stiff	1	4	7	0	5	8

Table 11. Weight Comparison

Dwg no.	Concept	Total weight kg	Total weight (lb)	Gr/Ep usage kg	Gr/Ep usage (lb)	Weight saving kg	Weight saving (lb)	Weight saving (%)	Rating	Rank
100	H/C design	59.4	(131.52)	30.0	(66.33)	43.0	(94.98)	41.9	8.8	2
105	H/C design-Gr/Ep hinge fittings	53.0	(117.91)	33.0	(72.74)	49.2	(108.59)	47.9	10.0	1
101	Skin/stringers—continuous	72.5	(160.43)	49.2	(108.65)	29.9	(66.07)	29.2	6.1	8
104	Skin stringers—discontinuous	73.0	(161.47)	49.5	(109.78)	29.4	(65.03)	28.7	6.0	9
107	Corrugated stiffened skin—chordwise	71.5	(158.17)	47.6	(105.06)	30.9	(68.33)	30.2	6.3	7
108	H/C stiffened skin—chordwise	68.5	(152.85)	44.2	(97.60)	33.4	(73.65)	32.4	6.8	6
103	Waffle design $0^{o}/90^{o}$—laminate stiffeners	67.0	(147.57)	43.5	(95.84)	35.8	(78.93)	34.8	7.3	5
106	Waffle design $0^{o}/90^{o}$—H/C stiffeners	66.2	(146.09)	41.5	(91.86)	36.4	(80.41)	35.5	7.4	4
109	Waffle design $\pm 45^{o}$—H/C stiffeners	59.4	(132.03)	34.4	(76.03)	42.7	(94.47)	41.7	8.7	3

Table 12. Cost Comparison—100th Article

Dwg no.	Concept	Fab cost ($) (1) (3)	Material cost ($) (2)	Total ($)	Compared to alum design (46,894) (4)	Rating
100	H/C design	32,045	2,466	34,511	.73	10.0
105	H/C design—Gr/Ep hinge fittings	34,170	2,596	36,766	.78	8.6
101	Skin/stringers—continuous	37,315	3,231	40,546	.86	6.3
104	Skin/stringers—discontinuous	37,102	3,232	40,334	.86	6.3
107	Corrugated stiffened skin—chordwise	35,530	3,112	38,642	.82	7.3
108	H/C stiffened skin—chordwise	35,870	2,707	38,577	.82	7.4
103	Waffle design $0^{o}/90^{o}$—lam stiffeners	39,015	2,762	41,777	.89	5.4
106	Waffle design $0^{o}/90^{o}$—H/C stiffeners	40,715	2,651	43,366	.92	4.5
109	Waffle design $\pm 45^{o}$—H/C stiffeners	48,365	2,242	50,067	1.08	0

(1) 85% learning curve—same for Gr/Ep and aluminum structure
(2) Gr/Ep cost 100th article assumed to be $25/lb
(3) Excludes tooling
(4) Aluminum material cost increased by a factor of 1.36 (Ref. material cost management)

Table 13. Rating Summary ①

Dwg no.	Concept	Cost	Weight	Others	Total	Rank
100	H/C design	350 (1)	308 (2)	200 (3)	858	1
105	H/C design—Gr/Ep hinge fittings	301 (2)	350 (1)	165 (7)	816	2
101	Skin/stringers—continuous	220 (5)	214 (8)	200 (3)	634	7
104	Skin/stringers—discontinuous	220 (6)	210 (9)	210 (2)	640	6
107	Corrugated stiffened skin—chordwise	256 (4)	221 (7)	225 (1)	702	3
108	H/C stiffened skin—chordwise	259 (3)	238 (6)	170 (6)	667	4
103	Waffle design $0^{o}/90^{o}$—lam stiffeners	189 (7)	256 (5)	200 (3)	645	5
106	Waffle design $0^{o}/90^{o}$—H/C stiffeners	158 (8)	259 (4)	155 (8)	572	8
109	Waffle design $\pm 45^{o}$—H/C stiffeners	0 (9)	305 (3)	125 (9)	430	9

① Rating x weighting factor

SHEAR WEB STUDY

This study encompassed four shear resistant shear web concepts, honeycomb stiffened, corrugation stiffened, "Tee" stiffened and bead stiffened. Figures 15 to 22 show these concepts applied to both spar and rib webs. Weight and cost comparisons are presented in Tables 14 and 15.

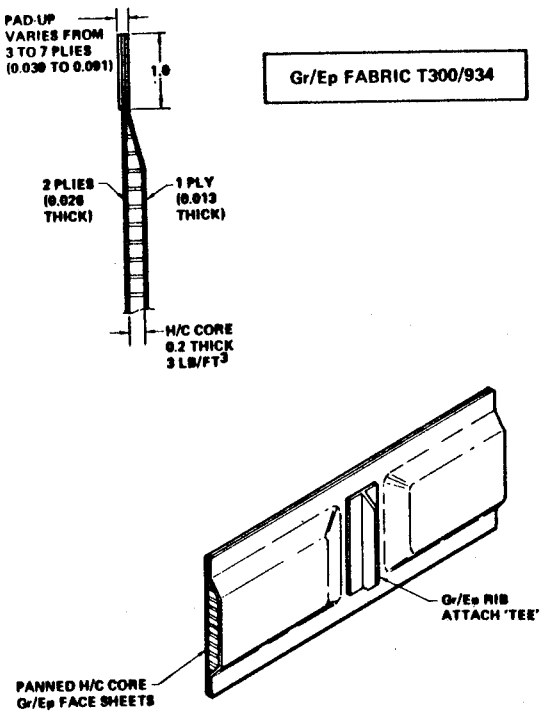

Figure 15. YC-14 Elevator Gr/Ep Spar Web Study — Honeycomb Stiffened

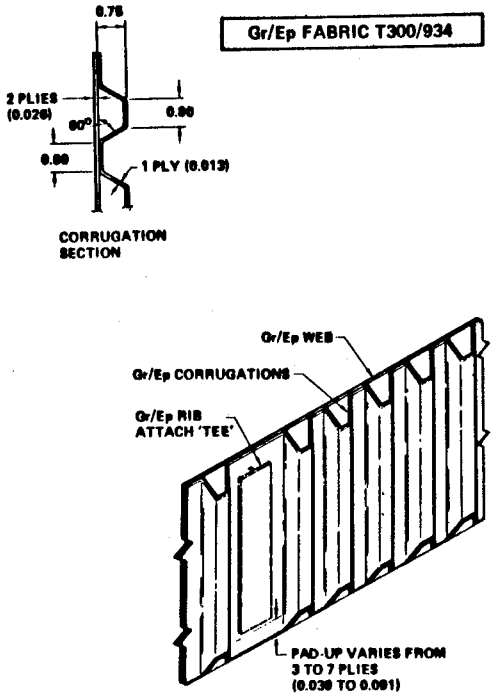

Figure 16. YC-14 Elevator Gr/Ep Spar Web Study — Corrugation Stiffened

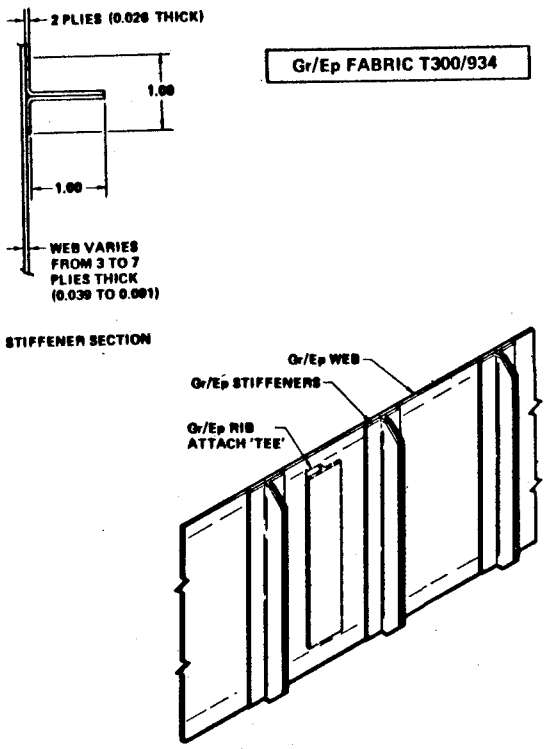

Figure 17. YC-14 Elevator Gr/Ep Spar Web Study — 'Tee' Stiffened

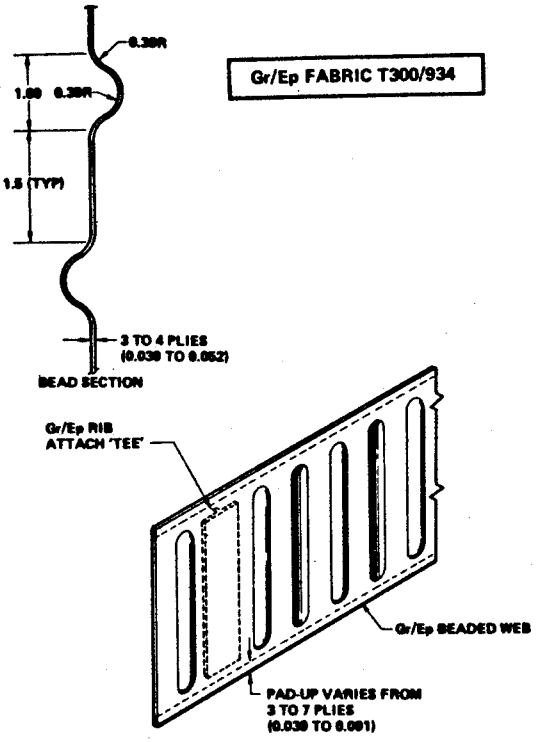

Figure 18. YC-14 Elevator Gr/Ep Spar Web Study — Beaded Stiffeners

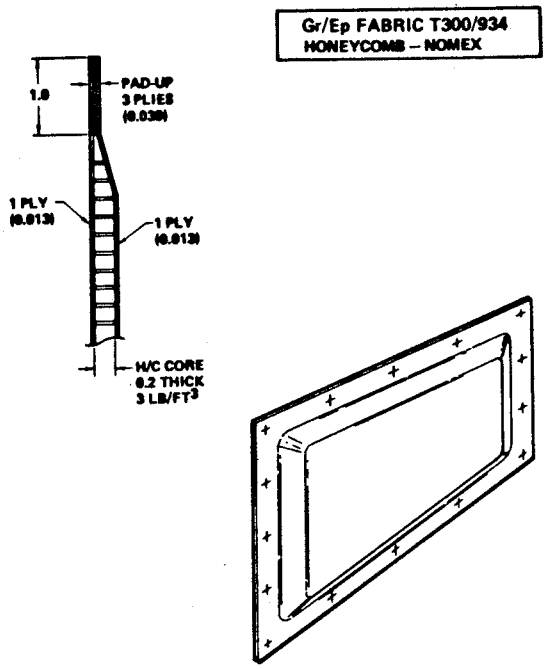

Figure 19. YC-14 Elevator Gr/Ep Rib Web Study – Honeycomb Stiffened

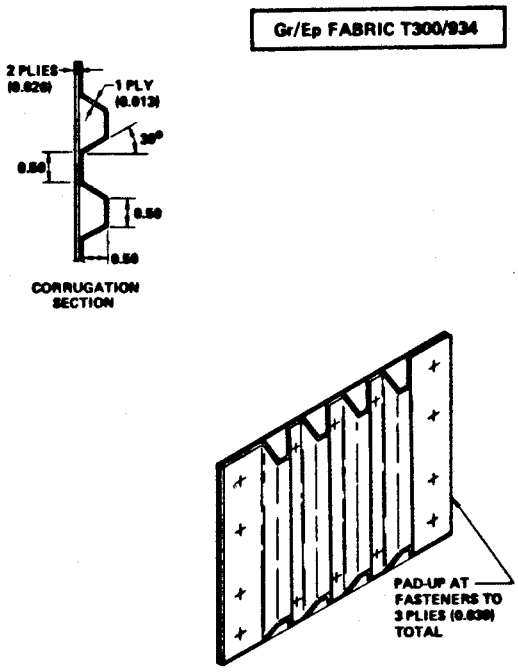

Figure 20. YC-14 Elevator Gr/Ep Rib Web Study – Corrugation Stiffened

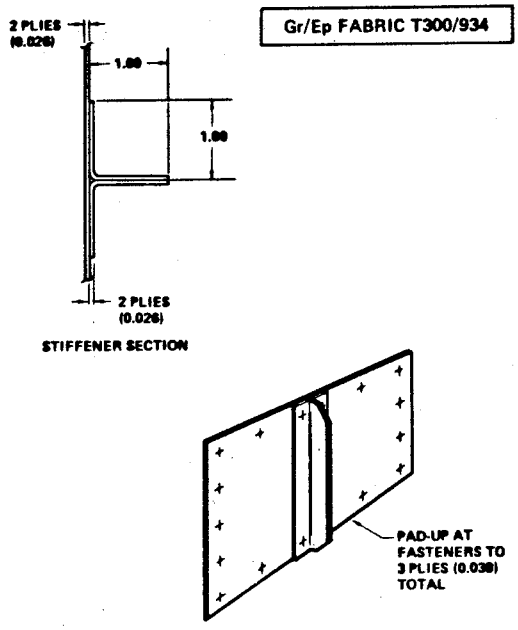

Figure 21. YC-14 Elevator Gr/Ep Rib Web Study – Tee Stiffened

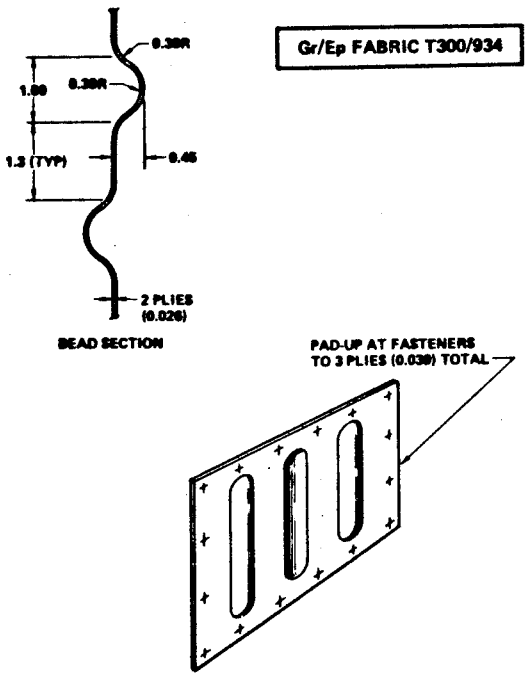

Figure 22. YC-14 Elevator Gr/Ep Rib Web Study – Beaded Stiffeners

Table 14. YC-14 Elevator, Spar and Rib Study—Weight Comparison

Component	Concept	Total weight kg	(lb)	Total saving kg	(lb)	Weight saving	Rank
Front spar (Gr/Ep)	Honeycomb	3.58	(7.89)	2.36	(5.21)	39.8	1
	Corrugated	3.64	(8.04)	2.29	(5.06)	38.6	2
	'Tee' stiffened	3.76	(8.30)	2.17	(4.80)	36.6	4
	Beaded	3.72	(8.20)	2.22	(4.90)	37.4	3
Rear spar (Gr/Ep)	Honeycomb	2.16	(4.76)	0.24	(0.52)	9.8	1
	Corrugated	2.17	(4.79)	0.22	(0.49)	9.3	2
	'Tee' stiffened	2.30	(5.09)	0.08	(0.19)	3.6	4
	Beaded	2.20	(4.87)	0.19	(0.41)	7.8	3
Ribs (Gr/Ep)	Honeycomb	2.73	(6.03)	0.5	(1.10)	15.4	4
	Corrugated	2.29	(5.06)	0.94	(2.07)	29.0	3
	'Tee' stiffened	1.83	(4.01)	1.43	(3.12)	43.7	2
	Beaded	1.62	(3.67)	1.54	(3.46)	48.5	1

Table 15. YC-14 Elevator Spar and Rib Study—Manufacturing and Tooling Cost (100th Article)

Component	Concept	▷1 Fab $	▷2 Fab mat'l $	▷3 Tooling $	Total $	Rank
Front spar (Gr/Ep)	Honeycomb	2,346	368	39	2,753	2
	Corrugated	2,414	428	118	2,960	4
	'Tee' stiffened	2,125	420	59	2,604	1
	Beaded	2,295	412	196	2,903	3
Rear spar (Gr/Ep)	Honeycomb	1,649	253	32	1,934	2
	Corrugated	1,700	300	96	2,095	4
	'Tee' stiffened	1,505	296	47	1,848	1
	Beaded	1,615	289	158	2,062	3
Ribs (Gr/Ep)	Honeycomb	2,261	272	21	2,554	1
	Corrugated	3,408	216	63	3,687	4
	'Tee' stiffened	2,576	327	31	2,934	3
	Beaded	2,465	285	105	2,855	2

▷1 85% learning curve

▷2 25 $/lb graphite/epoxy material cost

▷3 Tooling fab and tool material cost

DESIGN, ANALYSIS AND TEST

Previous study results indicated a design concept with honeycomb supported cover panels and "Tee" stiffened shear webs on both ribs and spars to be the most optimum design solution. More detailed design and analysis, however, showed that the rib stiffeners and web pad-ups at fastener locations could be eliminated by adding one extra $\pm 45^{o}$ Gr/Ep fabric ply to the rib web. This proved to be a slightly heavier but less costly solution and was adopted. In addition, a decision was made to use a post-buckling shear web design on both front and rear spars after a STAGS analysis showed that with this approach strains were well within allowable limits. This showed a further weight and cost reduction. A STAGS-B code model for the front spar nonlinear post-buckling analysis is shown in Figure 23.

Finally, a design concept with honeycomb supported cover panels, laminate shear resistant rib webs and laminate post-buckling spar webs was selected as shown in Figure 24. This design was broken down into several bonded subassemblies and mechanically fastened on final assembly.

An integrally bonded cover panel and spar chord assembly was adopted (see Figure 25). Cover panels were of sandwich construction with two Gr/Ep plies at $\pm 45^{o}$ per face sheet and .25 thick nomex honeycomb core. 90^{o} Gr/Ep reinforcing plies were added to the face sheets selectively at hinge locations to react chordwise hinge loads. These cover panels were cocured and then bonded to precured spar chords which were Gr/Ep angles with 0, $\pm 45^{o}$, 90 ply orientation. Rib chords, made from $\pm 45^{o}$ Gr/Ep angles were bonded to the cover inner face sheet (see Figure 26).

Spar webs were Gr/Ep laminates with plies at $\pm 45^{o}$ stiffened with Gr/Ep angles bonded in position. These webs were padded at fastener locations.

Rib webs were $\pm 45^{o}$ laminates with no stiffeners or pad-ups. Figure 27 shows a typical rib assembly.

A beam at each actuator location, (see Figure 28) carries actuator loads across to the reaction link ribs. These "I" beams were made of two back-to-back Gr/Ep channels and mechanically fastened in position.

The outboard elevator is subjected to induced bending due to its multi-hinge attachment to the horizontal stabilizer. These bending loads can be minimized by reducing the elevator EI to a minimum. In addition, a high torsional stiffness is a requirement since the elevator is actuated at the inboard end only. Both of these objectives were achieved by using $\pm 45^{o}$ Gr/Ep plies only in the cover panels and spar webs.

In order to verify analytic strength and stiffness predictions for the elevator, a section of the elevator box has been designed and is now being fabricated for test. This test component (see Figure 29), is a two-meter (seven foot) long box section incorporating five ribs, six hinge fittings, an actuator fitting and two reaction link fittings. This represents the most complicated structural section of the elevator and in addition to providing test data, its fabrication also gives manufacturing feasibility.

Two static tests are currently proposed for the component, one in torsional shear and one in bending. Each test will be to limit load only and strains and deflections will be recorded. The component will not be tested to failure at this time and will eventually be used in tests to compile various damage, moisture content, dynamic and lightning strike data.

Detailed SAMECS finite element computer models have been built for internal loads analysis of both the elevator and the component test box. Both models simulate the advanced composite design and are defined in Table 16. The finite element test component model is shown in Figure 30. A total of 16 flight maneuver and ground gust load cases were evaluated and the test component analysis results were used to define the test loading conditions required to simulate load responses of the full size elevator.

Analysis results on the elevator indicate the advanced composite design has cover panel and spar web ultimate loads that are within 4% of the aluminum elevator loads; torsionally, the composite design is considerably stiffer, showing 30% less wind up than the aluminum design.

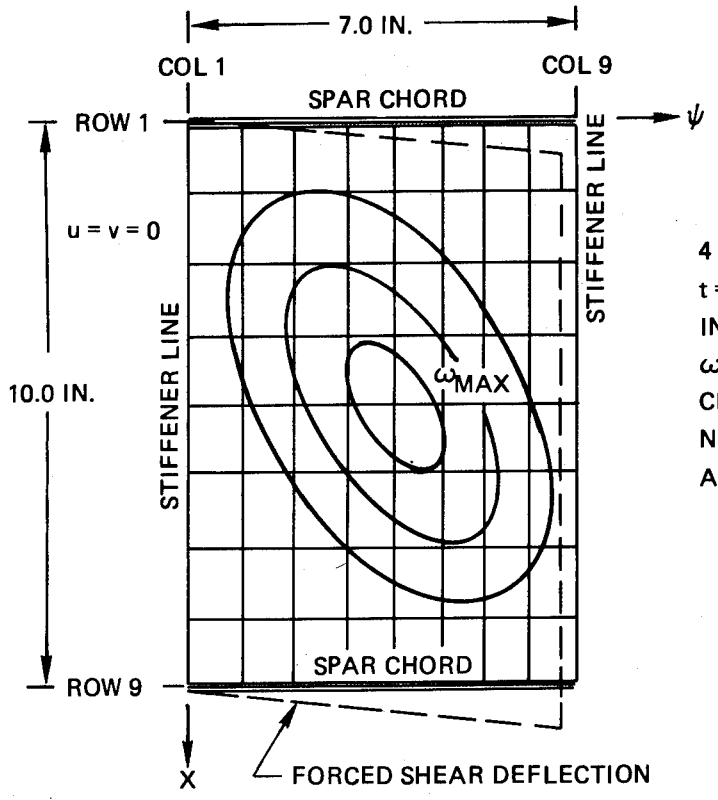

Figure 23. STAGS-B Code Model of Forward Spar Panel for Non-Linear (post) Buckling Analysis

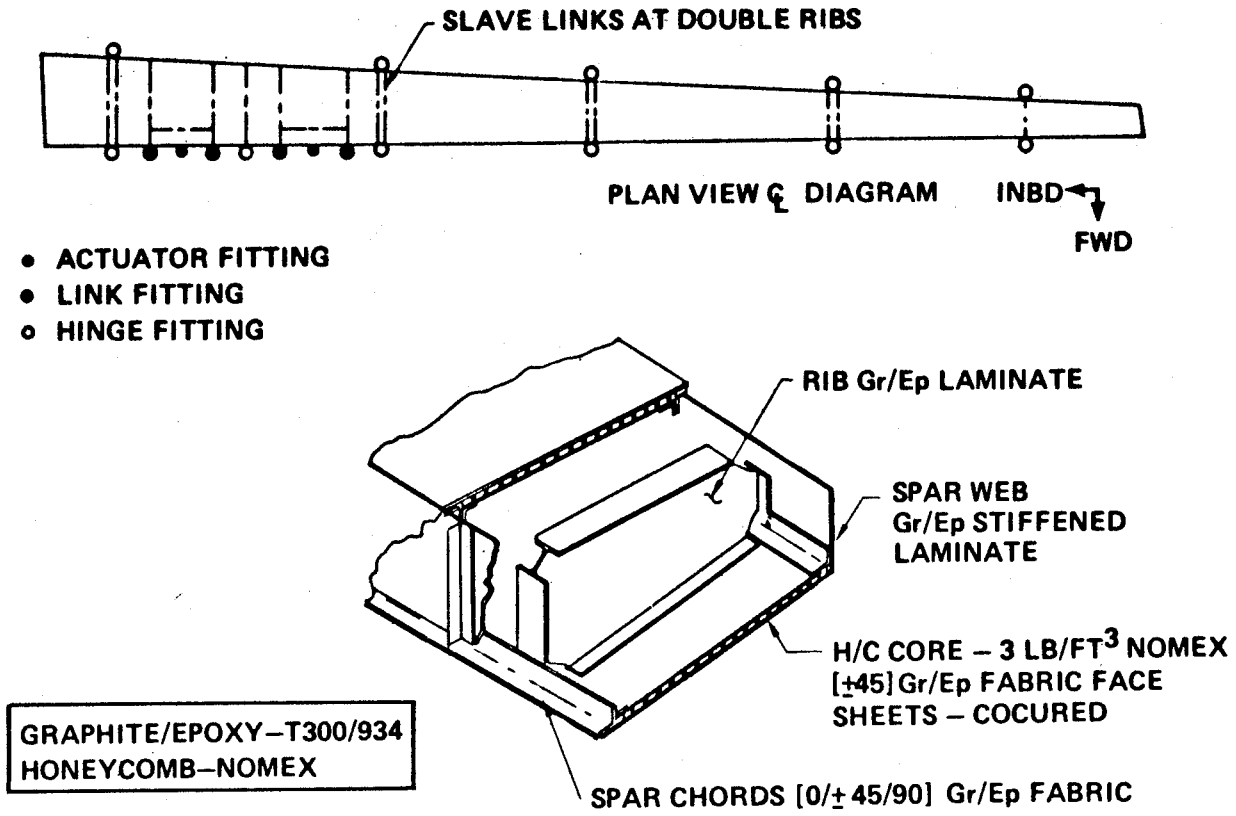

Figure 24. YC-14 Elevator Gr/Ep Selected Design Concept

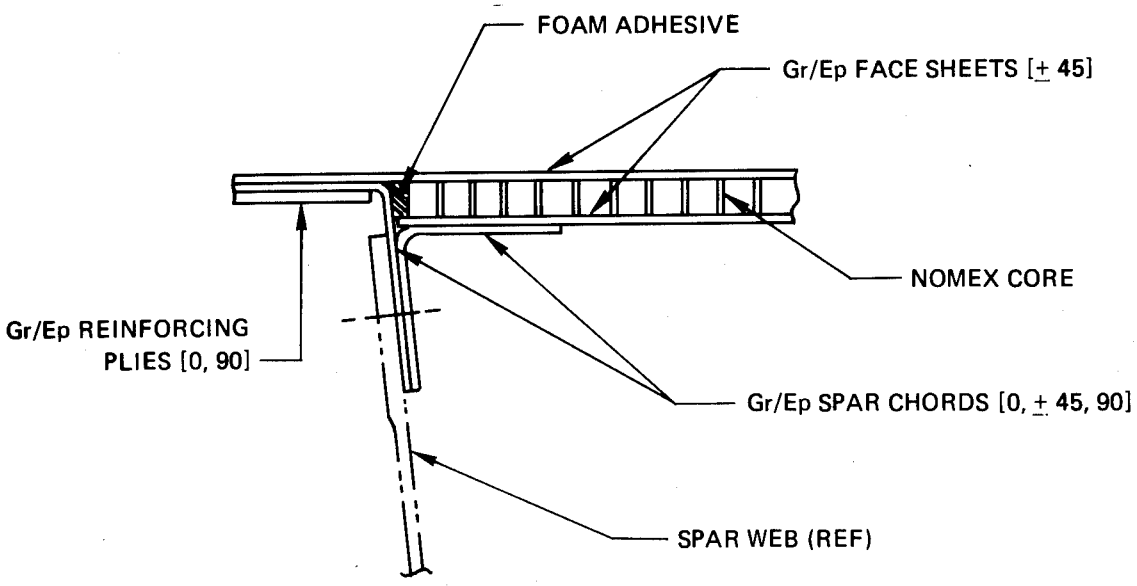

Figure 25. Integrally Bonded Spar Chord/Cover Assembly

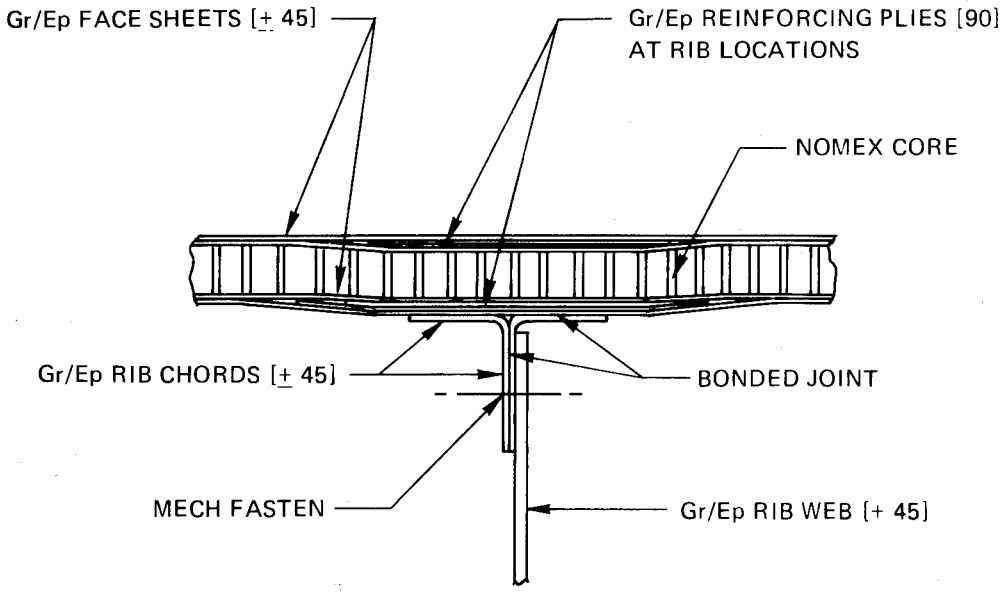

Figure 26. Rib/Cover Attachment

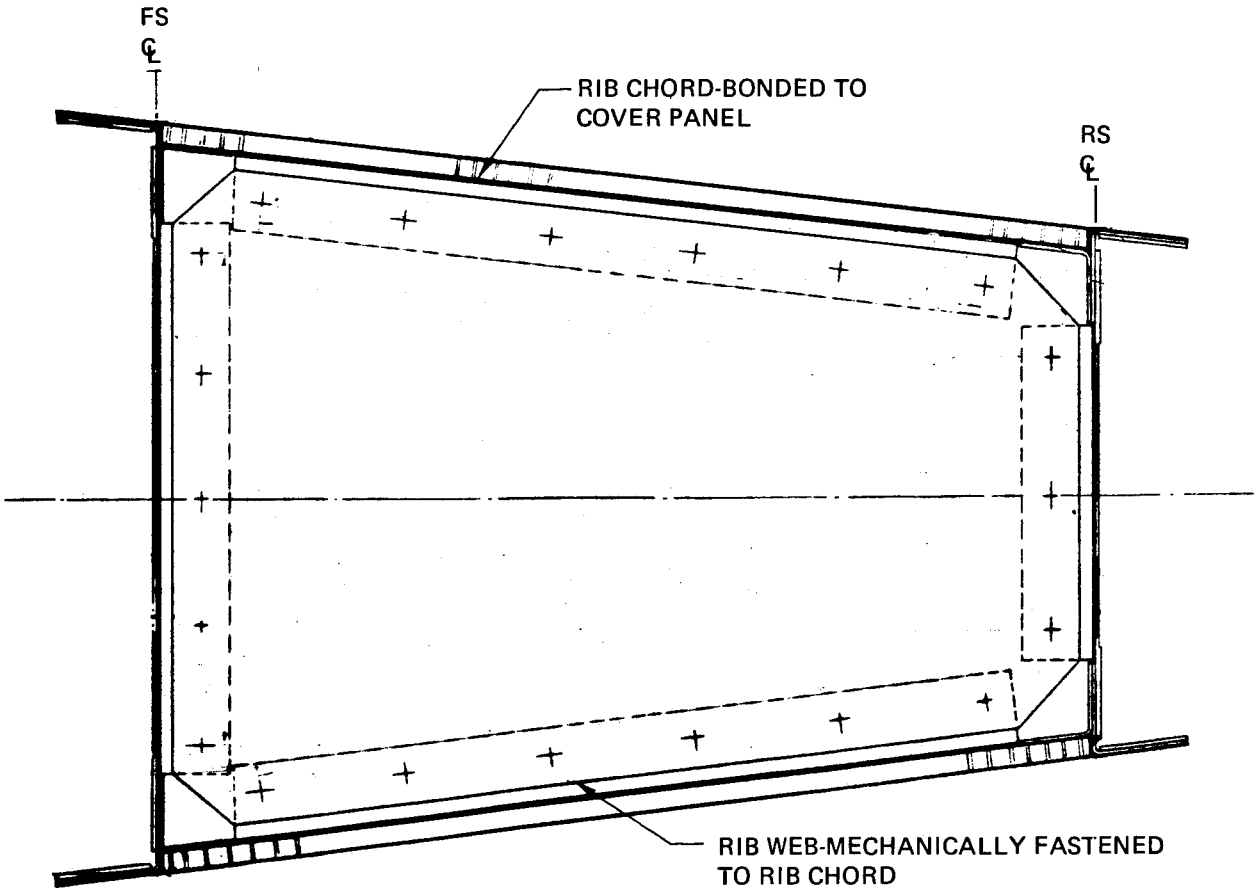

Figure 27. Typical Rib Assembly

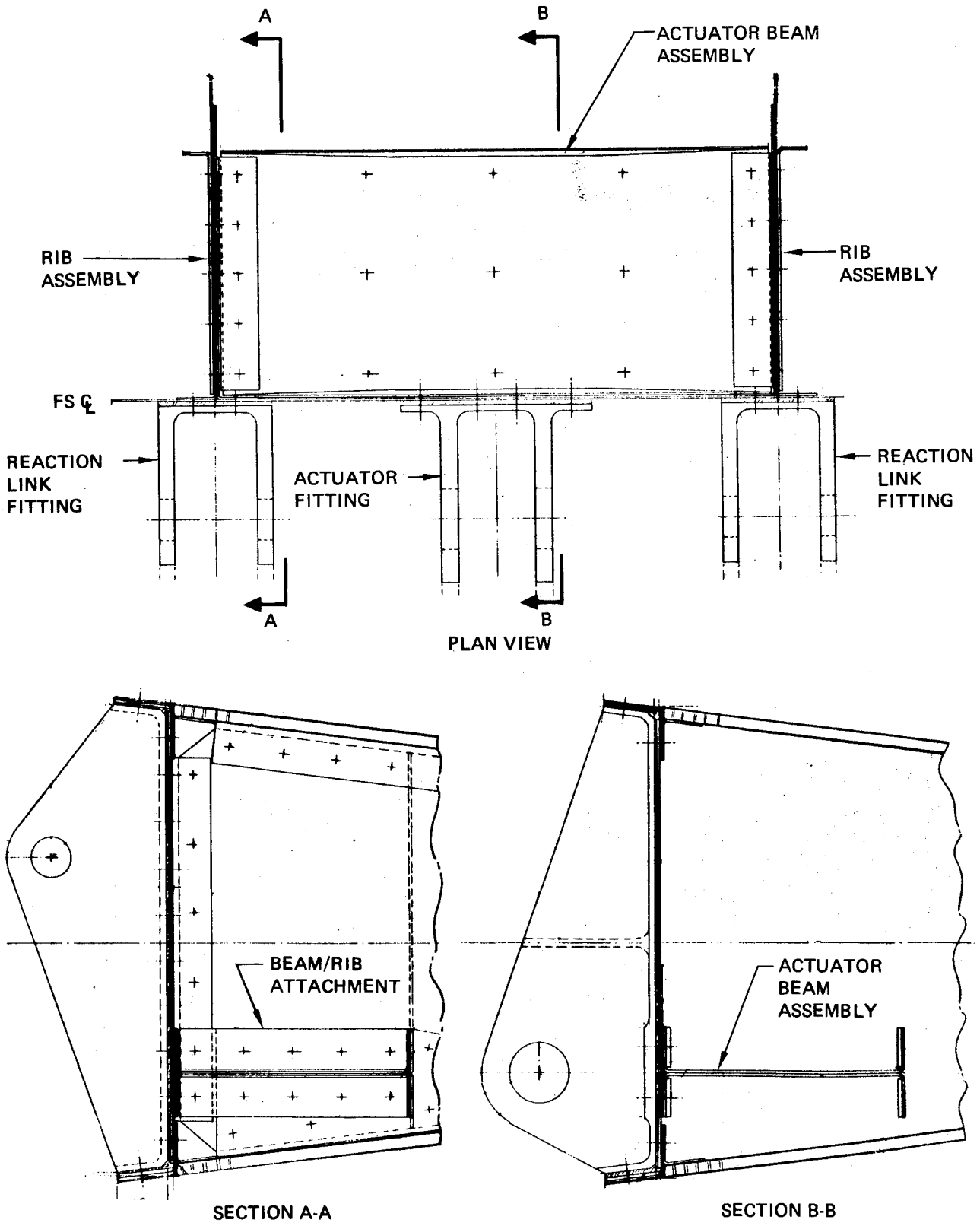

Figure 28. Actuator Beam Assembly

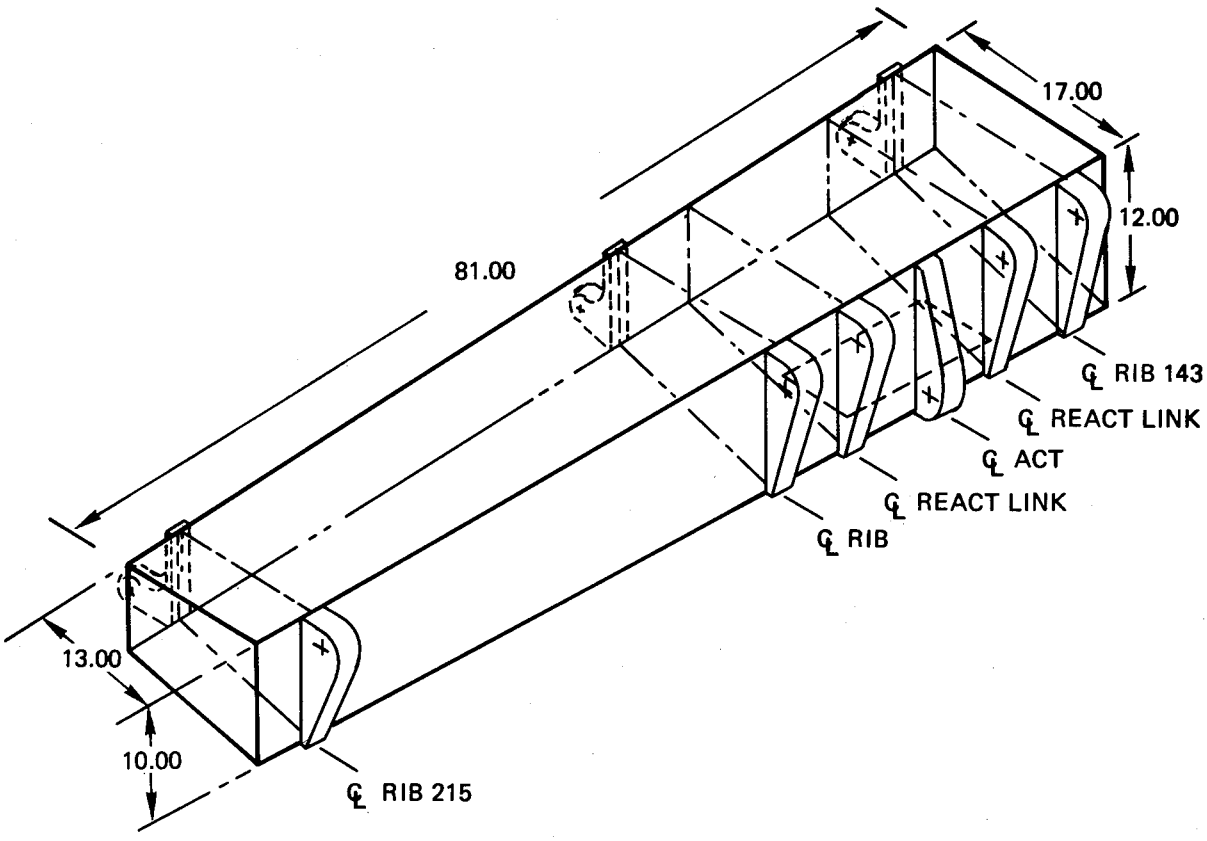

Figure 29. Test Component YC-14 Elevator

Table 16. SAMECS Finite Element Models for Internal Loads Analyses

	Number nodes	Number elements*		Number unit load cases
		plates*	beam	
Test component	59	61	98	8
Full size elevator	152	163	378	32**

*Orthotropic general plates used for covers,shear plates used for spars, ribs, and actuator beam

**Includes 8 induced elevator hinge deflection cases

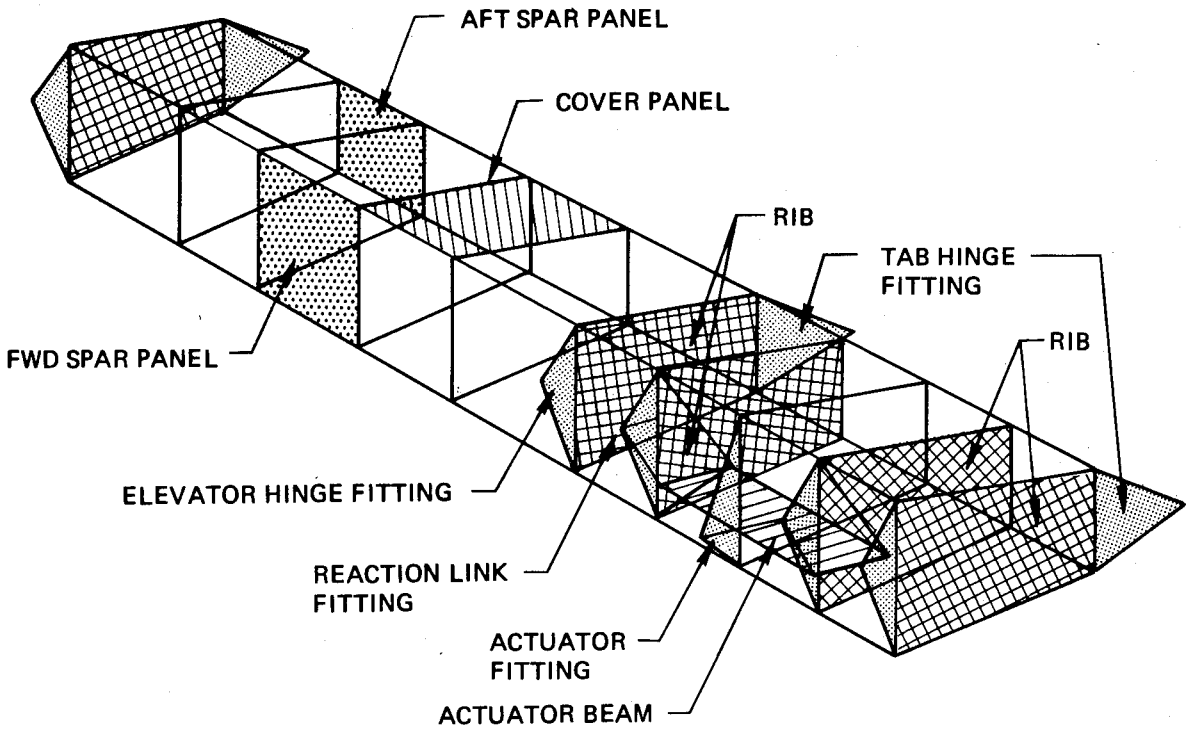

Figure 30. SAMECS Finite Element Test Component Model

MATERIAL SELECTION

Two of the guidelines applied to material selection for this program were that "state-of-the-art" materials should be used, and that material selected should be suitable for other programs. These guidelines prompted the use of T300 fibers. Good quality pre-impregnated tape of this material was available from several suppliers. The material was priced lower than most fibers and could be used for many applications.

Both 250°F and 350°F resin systems were considered. The lower temperature cure system was preferred from the manufacturing standpoint and strength degradation at elevated operating temperatures was not a problem on this program. However, a 350°F curing cycle was selected because of its wider potential application to other programs.

All available data indicated the Fiberite 934 system to be a good choice. It was widely used in industry and more design data was available to us on this material than any other. Cost trade studies showed that it was more economical to use woven prepreg than tape in this structure. Furthermore, it was projected that woven graphite had many other structural applications. Based on this, the decision was made to use woven graphite prepreg T300/934.

Previous results gained with 3M's AF 143 film adhesive in fiberglas sandwich panels indicated its potential application to Gr/Ep sandwich construction. A cocured test panel was fabricated using T300/934 prepreg, AF 143 adhesive film and nomex honeycomb core. This construction showed good strength resolution and this system was chosen for the sandwich cover panels. Woven graphite fabric was selected for use on all other applications on the elevator, with the exception of some local reinforcing plies of tape in the cover panels.

MATERIAL ALLOWABLES

A test program is well under way to provide structural design data for T300/934 laminates and is summarized in Table 17. The eleven items provide the data necessary for the final design of the elevator. The $-120^{o}F$ test temperature was selected to provide material property data relevant to high altitude RPV's and interpolation will provide the $-65^{o}F$ data for the YC-14 elevator. The test program will provide data representative of materials procured from Fiberite and processed according to Boeing specifications. Some tests will include the environmental effects of temperature and humidity and typical manufacturing and service damage will be evaluated. To gain statistical confidence, these data will be combined with other data bases for the same material system.

Mechanical fastening is used for the elevator final assembly. To combat the galvanic corrosion problem associated with graphite and certain metals in contact, it was decided to restrict graphite fastener combinations to those with less than .3 volts electrode potential difference. As a result, all fasteners are either titanium or A286 corrosion resistant steel. No squeeze or driven rivets were used as our experience showed these processes damaged the Gr/Ep laminates. Titanium fasteners with a rotating locking collar were used in areas with access to both sides of the fastener. Where blind fasteners were dictated, a corrosion resistant steel blind bolt with no hole filling properties was selected. Titanium hexagon head bolts with nut plates were also used at some of the hinge fitting attachments. Mechanical testing of all selected fastener applications is in progress.

Table 17. T-300/934 Structural Design Data Program

Item number	Test description	Number of specimens tested		
		-120°F	RT	+180°F
1	Boeing certification tests of prepreg properties		18	
2	Basic laminate properties	11	41	11
3	Cocured sandwich properties	2	2	2
4	Fracture strength of open holed laminates	1	4	1
5	Tension strength at loaded fastener holes		4	
6	Static strength of adhesive and fastened joints	10	57	10
7	Fracture and fatigue strength of defective joints	3	24	3
8	Static strength of stiffened shear webs		2	
9	Lot certification data and humidity effects	4	35	20
10	Joint and element coupon tests		8	
11	Static and fatigue strength of fabric lap splices		24	
		31	219	47
		Total tests =	297	

CONCLUSIONS

This IR&D program is progressing into the full scale component fabrication stage. The elevator design is finalized, and material property and structural element tests have verified both the material selection and design concept. The test component is completely designed and fabrication is well under way.

This program will produce a flight worthy outboard elevator for the YC-14 with an estimated weight reduction of 35% and a cost reduction of 20%.

LOW COST COMPOSITE AIRFRAME STRUCTURES*

By Melvin J. Rich
Sikorsky Aircraft Division
United Technologies Corporation

and Raymond L. Foye
Langley Directorate, U.S. Army Air Mobility R&D Laboratory

SUMMARY

This paper presents the results of design and development of a cocured integrally molded skin/stringer/frame (CSSF) concept for low cost airframe structures. The concept consists of integrally stiffened laminates of Kevlar® 49 broadgoods and graphite tape. The integral stiffening provides stability during lay-up, cure and for subsequent structural loading.

In this paper the selection of a compatible material system is described along with the fabrication methods, and the structural element tests to date. The results of these tests have verified the strength and stability of stringers, frames, joints and the ability of composite skins to withstand post-buckled static and fatigue loadings.

INTRODUCTION

The application of advanced composites to airframe structures has generally indicated typical weight savings between 20 and 30 percent for fixed wing aircraft. Greater weight savings appear to be possible as a result of re-sizing of the aircraft in the initial design phase. A detail preliminary type of design study (Reference 1) of a helicopter fuselage has indicated a somewhat similar trend (18.4 percent).

* The major portion of this paper reports the results of joint NASA/Army funded contracts NAS1-11688 and -13479.

A more significant problem appears to be in reducing costs through the use of advanced composites. This paper will present the progress obtained through two NASA/Army funded programs (References 1 and 2) that show the promise of both significant weight and overall cost reductions for helicopter airframe structures. Inherent in these programs are: (1) the introduction of hybrid composites to reduce material costs; (2) the use of large molded single cocured structural sections to reduce labor costs for assembly and installation; (3) the concept of integral stiffening to provide stability during fabrication and subsequent loadings; (4) the light weight solution of using composite skins for postbuckled strength (diagonal tension).

The objective of the first study program was to assess the application of advanced composite materials to helicopter airframe structures and to project quantitative improvements in vehicle costs and performance. To attain this objective, the study utilized the Sikorsky model CH-53D, a current production (Figure 1) transport helicopter, for comparison of composite with current conventional construction. Composite materials potentially offer substantial weight saving, reduction in number of parts and possible reduction in manufacturing costs for the higher stressed skin/stringer panels and forged frames and beams. This is particularly true of the size, weight, and performance class of the CH-53D helicopter, which involves a greater proportion of structure than do smaller rotary wing aircraft.

Figure 1. CH-53D High Speed Military Transport Helicopter.

As shown in Figure 2, the CH-53D is of conventional construction involving the large usual number of parts and multitude of detail fastening and assembly. The conventional airframe structure was detailedly investigated and the results are illustrated in Figure 3. As expected most of the airframe is constructed of aluminum (88%) with some use of low cost composites (fiberglass 7%) for fairing type structures. Most of the airframe structure is designed by strength and rigidity (81%). A large proportion of the structural weight is in the skin/stringers and frames (66%). The major cost was found to be in labor, with assembly and installation being the major item (63%).

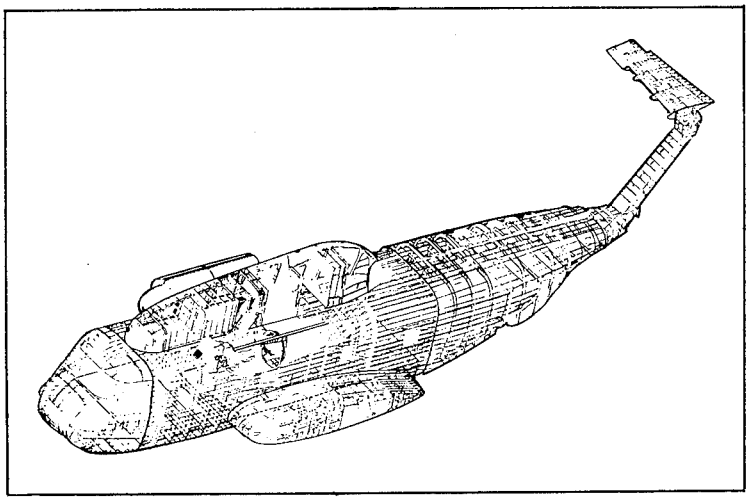

Figure 2. Current CH-53D Airframe Conventional Construction.

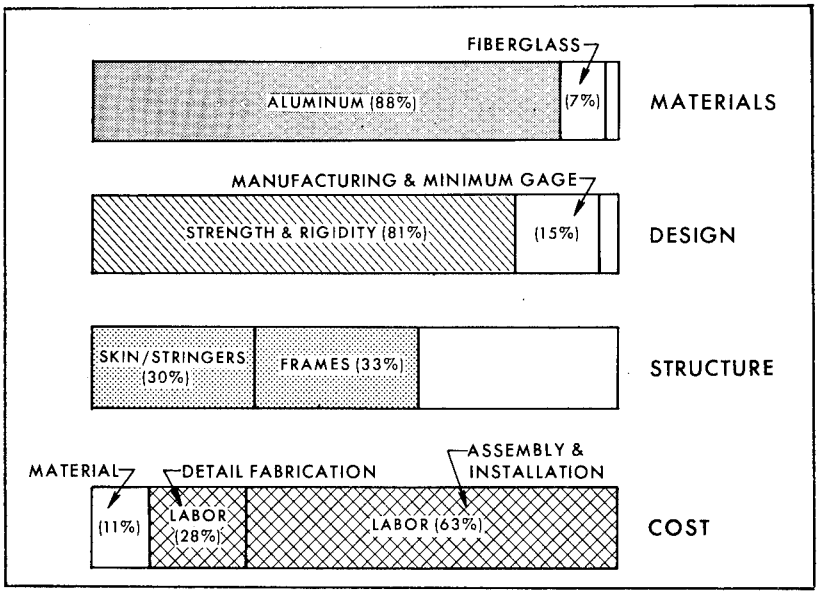

Figure 3. Conventional Airframe is Primarily Aluminum Alloy, Major Weight in Shell, and Major Cost is Due to Labor.

The results of the evaluation of the conventionally constructed CH-53D indicated that: (1) even for this size helicopter the load intensity was low and to compete with aluminum construction very light gage composite skins utilizing postbuckled strength (diagonal tension) would be required; (2) the large proportion of frame weight required some integral molded design to achieve low weight and cost and (3) the type of structure needed some stabilization to achieve an integral design capable of being molded in a one stage cure.

The first study program (Reference 1) indicated an 18.4 percent weight reduction as illustrated in the weight breakdown chart of Figure 4. The overall results were an increased productivity of seven percent and life cycle cost reduction of five percent. It was also concluded that further design and experimental testing, and manufacturing investigations were needed to simplify joint designs, verify structural concepts and develop a single cocure structural system.

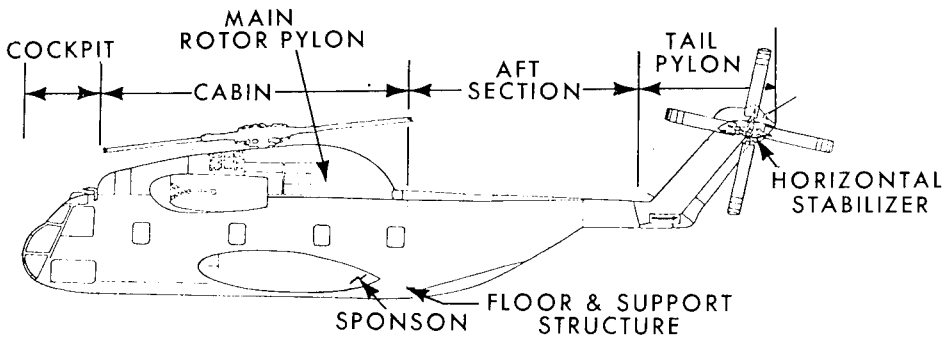

SECTION	WEIGHTS LB CURRENT DESIGN	COMPOSITE DESIGN	% WEIGHT REDUCTION
COCKPIT	564	471	16.5
CABIN	2424	1897	21.7
SPONSON	767	657	14.3
AFT	1159	947	18.3
FLOOR & SUPPORTS	449	402	10.5
MAIN ROTOR PYLON	297	257	13.4
TAIL PYLON	315	256	18.7
HORIZONTAL TAIL	102	72	29.4
	6077	4959	18.4

Figure 4. Composites Reduce Airframe Weight by 18.4%.

SYMBOLS

N_z	Aircraft load factor
q	Shear flow, lb/in.
CSSF	Cocured skin stringer frame
P	Load
W	Panel width, inches
D	Panel depth inches
E	Modulus of elasticity, psi
S	Stress, ksi

DESIGN CONCEPTS

Historically the lightest weight metal airframe design solution has been the skin/stringer/frame concept utilizing the skin for its postbuckled strength (diagonal tension). In composite structures it has been presumed that post-buckled strength could not be used for laminates with epoxy matrices, and thus design solutions always defaulted to sandwich construction with its inherent greater resistance to buckling. As described in Reference (1) the evaluation favored the skin/stringer/frame concept from the limited evidence of composite skins being capable of high fatigue resistance for cyclic loads in the post-buckled mode.

In addition, a composite design with greater section modulus for stringers and frames (than usual metal construction) provides a portal beam effect with inherent rigidity even without skins. Thus, it is practical to design the composite construction with the skins acting in almost a pure diagonal tension field. This concept lends itself to using lower cost advanced composites such as Kevlar 49 and to lay up the large sheet sections from broadgoods oriented to the ± 45 degree direction. The result is a highly efficient structure, even for the low load intensity for helicopter airframes.

The low loading intensities for helicopter airframe impose another problem, that is the light gage thickness for stringers and frames introduce local crippling limitations for the high strength graphite/epoxy materials. To enable efficient use of thin laminate graphite/epoxy, stabilization is required. One solution, that also lends itself to low cost fabrication, is to stabilize with a polyurethane foam core. This integral stiffening provides the stability during lay-up, cure, and for subsequent structural loadings.

Another consideration is that cocuring is the only composite fabrication concept that promises to lower costs compared to present aluminum construction. On the basis of structural efficiency the CSSF is superior to sandwich construction for lightly loaded or minimum gage applications.

The design concept for the airframe shell, shown in Figure 5, provides structural continuity, stabilization of the higher loaded thin graphite/epoxy gage stringers and frames to avoid crippling, use of a lower cost Kevlar 49 ± 45 broadgoods skin loaded only in tension, and the potential of a single cure cycle fabrication. Molded in large segments the assembly costs will be reduced since a minimum number of mechanical fasteners are used. A fabricated segment shown in Figure 6, was constructed of all graphite/epoxy, using Kevlar 49 only as a protective shell covering for the outer skin. Further studies (Reference 2) revealed that the use of all Kevlar 49 for the composite skin was a lower cost and weight solution and practical due to the greater rigidity referred to by the foam stabilized hat sections of the stringers and frames. Kevlar 49 was selected over fiberglass because of its better thermal compatibility with graphite and lower weight.

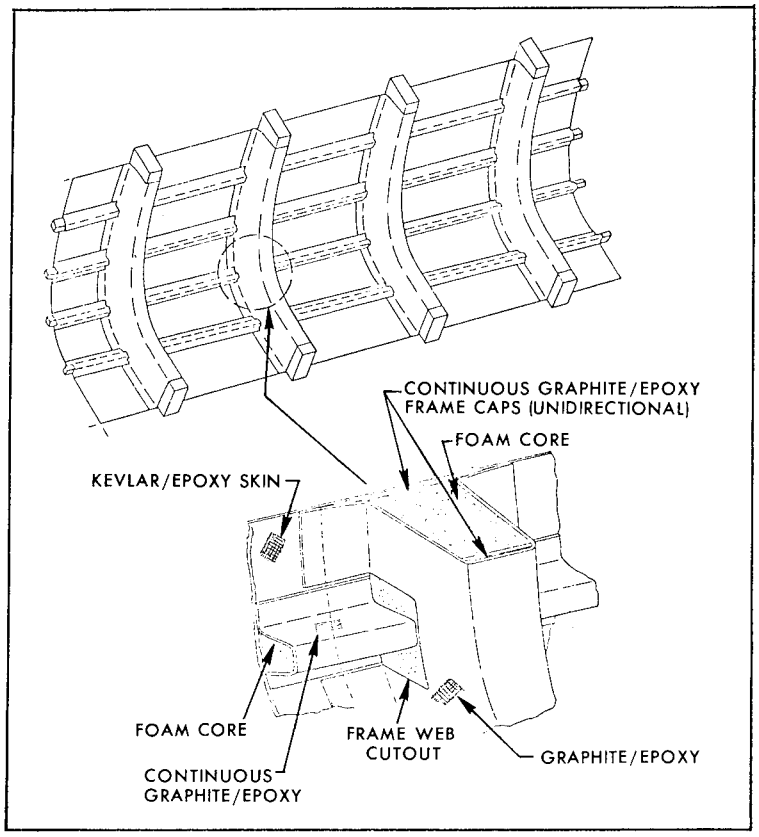

Figure 5. Integral Shell Construction Provides Structural Continuity with Potential for Single Cure Cycle Fabrication.

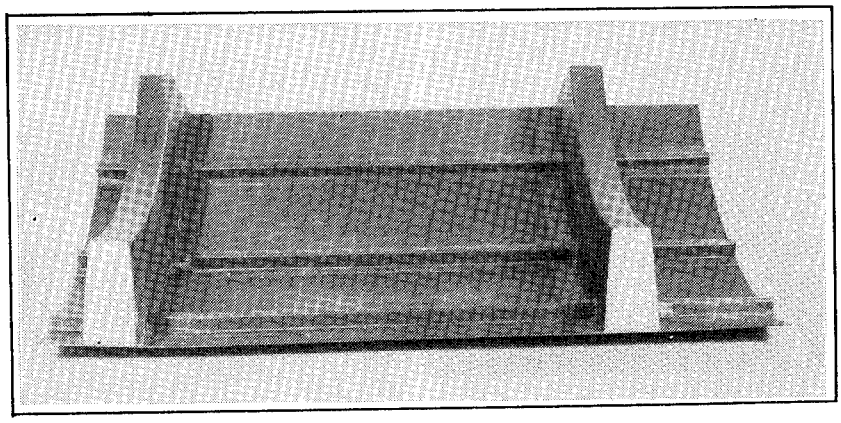

Figure 6. Single Cure Composite Fuselage Section.

The initial design concept for joining major sections was to integrate titanium fittings with the graphite hat sections. Further studies (Reference 2) showed a simpler lower cost solution was to use simple composite channel sections, which are illustrated in Figure 7. Thus, problems of thermal compatibility and providing a single cocure system are resolved with the CSSF System as described, and verification of this concept is provided from the results of the structural testing described later in this paper.

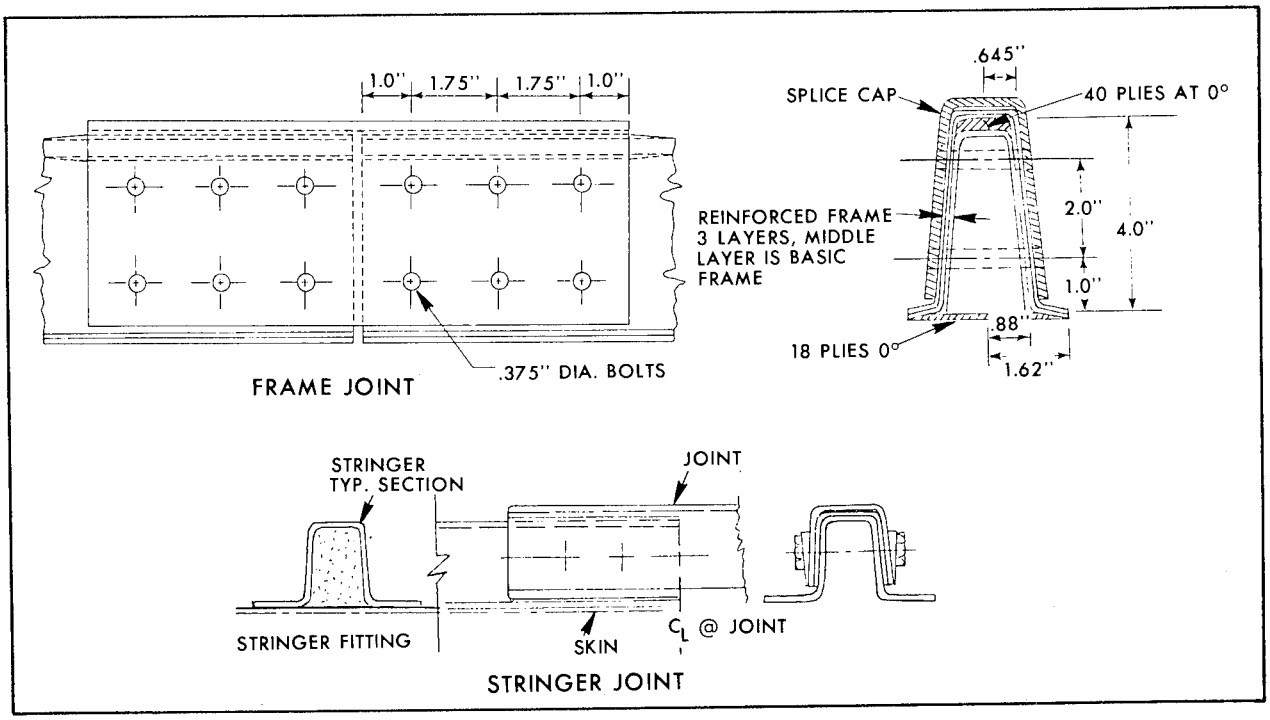

Figure 7. Bolted Composite Channel Sections Provide Simple Mechanical Joints.

MATERIALS

The objective of the Materials Selection Phase of Reference (2) was to select a combination of graphite and Kevlar 49 with a compatible resin system, and a foam filler that permitted a single stage cocure.

Laminate Material Selection

The criteria for selection of the resin system was that it be: (1) suitable for impregnation of both T-300 graphite and Kevlar 49; (2) lowest available cure temperature with minimum heat distortion of 165°F upper helicopter operating temperature; (3) maximum cure temperature of 250°F for compatibility with foam system and (4) lowest pressure cure to provide low void laminate with a fiber volume fraction of at least 50 percent.

A summary of the test results for three candidate resin systems, shown in Table I, indicates that the criteria is met for cure pressures of 25 psi and above. This fact is important since one problem area is obtaining sufficient pressure at the intersection of the stringer and frame (as shown in Figure 5). NARMCO 5209/T-300 graphite and NARMCO 5209 Style 281 - Kevlar 49 were selected on the basis of the test results and current available costs.

Table I Material System Evaluation Results

Material System	Process Variable	Laminate Thickness	Flexure		Shear (ksi)	Comment
			S (ksi)	E x 10^6 (psi)		
NARMCO 5209/T-300 Graphite NARMCO 5209 Style 281-Kevlar® 49	50 psi	0.080	255	18.8	12.7	Low void content graphite and Kevlar
	25 psi	0.082	248	17.9	12.8	Low void content graphite and Kevlar
	Vacuum	0.085	222	17.3	11.0	Medium void content graphite and Kevlar, Kevlar resin rich
3M-SP-288/T-300 Graphite NARMCO 3203 Style 281-Kevlar 49	50 psi	0.072	242	17.9	12.9	Low void content graphite, High void content Kevlar
	25 psi	0.076	224	17.0	13.0	Low void content graphite, High void content Kevlar
	Vacuum	0.080	215	16.2	11.7	Low void content graphite, High void content Kevlar
FERRO-E293 Style 248 T-300 Graphite FERRO-E293 Style 281-Kevlar 49	50 psi	0.092	234	18.7	12.1	Low void content graphite and Kevlar
	25 psi	0.102	211	17.2	11.9	Low void content graphite and Kevlar
	Vacuum	0.100	185	16.4	10.6	High void content graphite and Kevlar

Foam Material Selection

The integral shell construction concept requires that the foam core be able to support and produce the shape of the frame and stringer hat section. From past experience with CH-53 fiberglass canopies it was found a rigid polyurethane foam was stable during cure cycles. A literature search indicated only one material, Stathane 8747 (8 lbs/cubic foot), met the process requirements specified for the candidate laminating systems. Stathane has a room temperature strength of 210 psi and a 250°F temperature strength of 190 psi, which is suited for autoclave processing.

Representative frame core sections were cast and put through autoclave cycles of 250°F and pressures of 50 psi and showed no measurable distortion.

Foam permeability and absorption of laminating resin were considered a potential problem area. Test results showed that the combination of release agents, preheat of foam and foaming tools, produce a "self skin" on the foam component. This "self skin", which is a layer of collapsed cells, produces a surface which proved to be impermeable to the laminating resin systems for the specified criteria of pressure and temperature.

FABRICATION

Various tooling concepts were investigated. A female tool concept was the final selection to produce an airframe component with a finished outer or aerodynamic surface. The evaluation indicated that the female tool would be less complex than a male one and have less mass to permit faster heat up rates and reduced cycle time.

As illustrated in Figure 8, a locating skeleton framework will have to be developed to act as a positioning jig during lay-up and a holding fixture during cure. This tooling concept of the female OML (Outside Mold Line) was fabricated from two candidate materials, i.e., (1) steel plate, and (2) glass/epoxy sandwich construction.

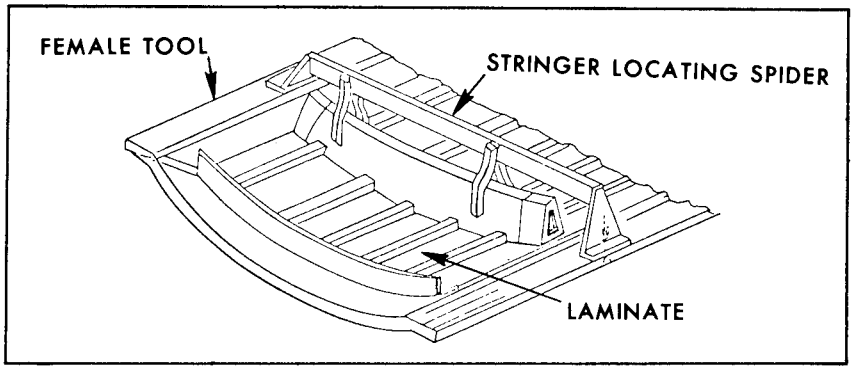

Figure 8. Female Tool Allows Easier Fabrication.

The steel plate was selected over the glass/epoxy sandwich because of a better thermal match with graphite/Kevlar and dimensional stability. Sample parts were fabricated and checked for dimensional and quality control. Finally all static test specimens (a total of eight) were fabricated using the designated materials from the materials evaluation and the tooling concept and materials described. Thus the test results will include the effects of the fabrication concepts developed.

Final evaluation will be made in the Phase II part of the program when fabricating the larger skin/stringer/frame panel shown in Figure 6. Further structural evaluation will be obtained from the fatigue testing of frames cut out from the large panel.

TEST EVALUATION

Stringers, Frames, and Joints

Phase I of the low cost composite structures investigation (Reference 2) required design and static testing of stringers, frames, and stringer and frame joints. In subsequent work of Phase II it is planned to fatigue test three frame sections.

The static test specimens were fabricated on the same tooling which was developed for manufacturing technology. The stringer and frame specimens such as illustrated in Figure 9 were tested at what was considered the most critical sections, i.e., at the intersection area.

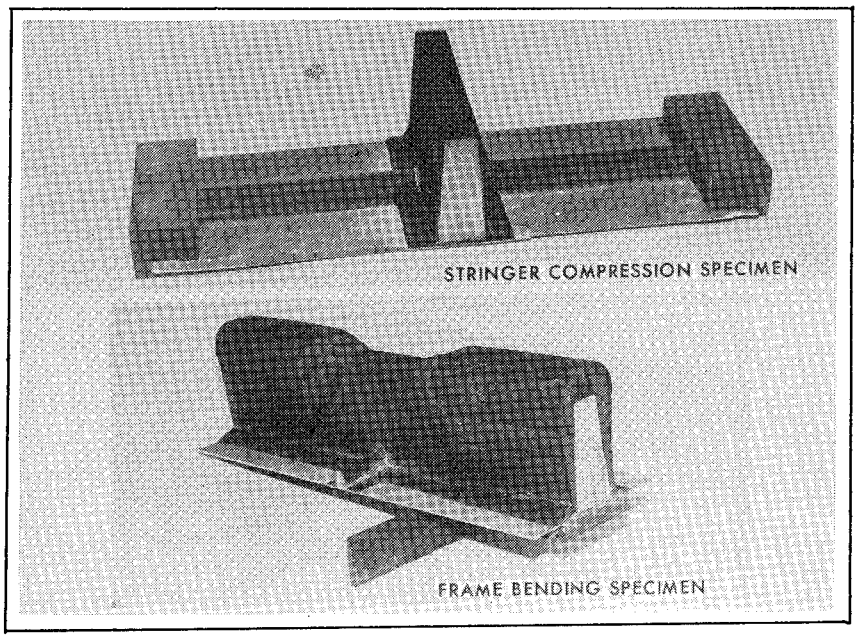

Figure 9. Specimens Tested at Critical Intersection.

The test results are tabulated in Table II and comparison is made with predicted failure load (and mode) with zero margins of safety. In general, the test results correlate well with predictions except for the frame joint, which proved to be very conservative.

Table II Comparison of Analysis and Test Results

Structure and Type Loading	Design Ultimate Load	Predicted Failure Load Zero Margin of Safety	Test Failure Load (Average)*	Ratio of Test to Predicted Failure Load	Ratio of Test to Design Load	Comments
Stringer Compression	4,500 Lb (Column)	7,070 Lb (Crippling)	6,650 Lb	.94	No equiv. test	Demonstrates crippling is not a problem and adequate margins of safety should exist for column mode
Stringer Splice Compression	3,000 Lb	3,300 Lb	3,400 Lb	1.03	1.13	
Frame Axial and Bending	16,600 Lb 100,00 In. Lb	19,260 Lb 116,000 In. Lb	15,200 Lb 98,000 In. Lb	.84	.98	While test verifies design the analytical prediction is significantly higher than test results
Frame Splice Axial and Bending	3,300 Lb 20,000 In. Lb	5,380 Lb 32,600 In. Lb (For Total Fracture)	8,040 Lb 49,470 In. Lb	1.49	No data for fiber failure mode	Comparison shows that a more precise analytical procedure is needed for complex splices where axial and bending loads are introduced. In addition some conservatism is probably due to hole size effect

*2 Specimens of each type

As a result of these tests it is expected that stringer and frame sections and stringer joints will stay the same as initially designed. However some reduction in the size of the frame joint is warranted due to the evidenced over-strength.

Skin Shear Panels

Understanding the postbuckling of composite panels is essential to the application of composite materials to the CSSF construction. Adequate methods of analyzing the postbuckled stiffness and strength of composite shear panels are not yet available. The result has been that designers have legislated a shear resistant criteria to avoid postbuckling and therefore sandwich construction has been favored.

However, a substantial proportion of the helicopter fuselage is lightly loaded and legislating shear resistant skins imposes both a weight and cost penalty on the design. Thus the use of thin laminates in diagonal tension becomes an attractive alternate providing the skin structures are capable of withstanding the operational static and fatigue loadings. Therefore a test evaluation was made of various composite shear panels to evaluate their ultimate postbuckled strength, fatigue resistance for design loadings of the CH-53D, and the static residual strength with and without damage.

Four types of composite shear test panels were fabricated. These were:

Type	Description
I	Graphite/epoxy, fiber Type A in unidirectional tape. Laminates at $(\pm 45)_S$, .04 inches thick.
II	Same as Type I with Kevlar 49/ epoxy laminates on inner and outer face orientated at 0/90 to panel edges. Total thickness .068 inches.
III	All Kevlar 49/epoxy laminate. Unidirectional tapes at $(\pm 45)_S$, .046 inches thick.
IV	Same as Type III except using woven 181, .043 inches thick.

All of the panels had some amount of initial curvature, usually on the order of 2 or 3 times the panel thickness. This was attributed to residual compressive stresses developed in the panel as a result of bonding the titanium edge strips at 250°F. This curvature prevented obtaining experimental determination of initial buckling loads.

The test fixture schematically shown in Figure 10 was designed to minimize corner stresses which are usually a problem for picture frame type fixtures. The test panel is bolted into the center section and the axial load P is resolved into pure shear. The test panels are 6 inch by 10 inch (rectangular) framed on the sides by fiberglass and a titanium strip, all bonded to the edges. The edges of the test panel are attached to the test fixture by .375 inch bolts on 1.375 inch centers. Each of the panels had their corners slotted at 45° to the panel edges. These slots extended through the titanium edge strips but not into the test section. The purpose of these slots was to prevent the titanium edge strips carrying any shear load by portal bending at the corners. Figure 11 is a photograph of the test setup.

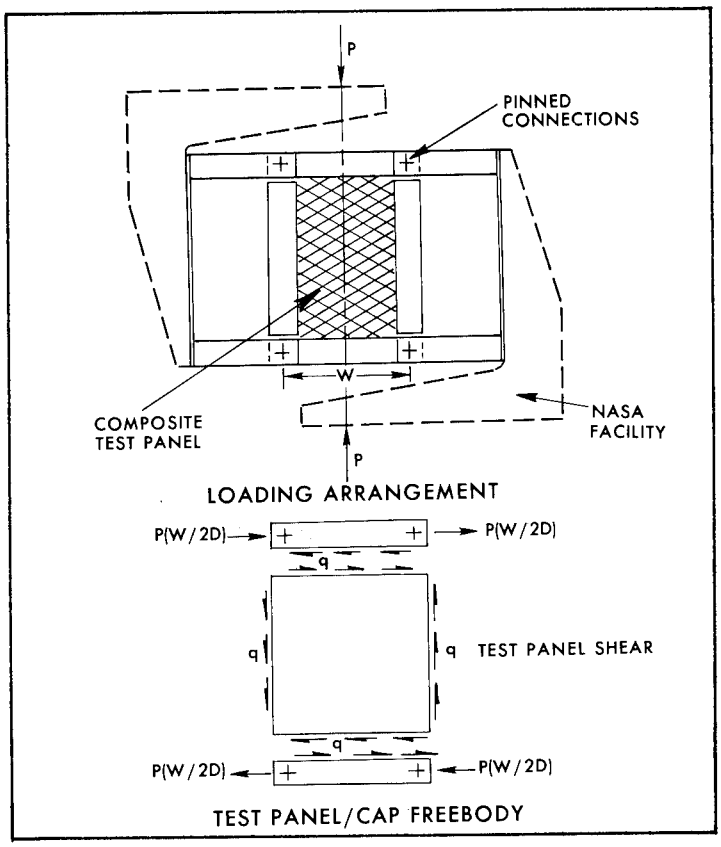

Figure 10. Test Panel Loading Arrangement.

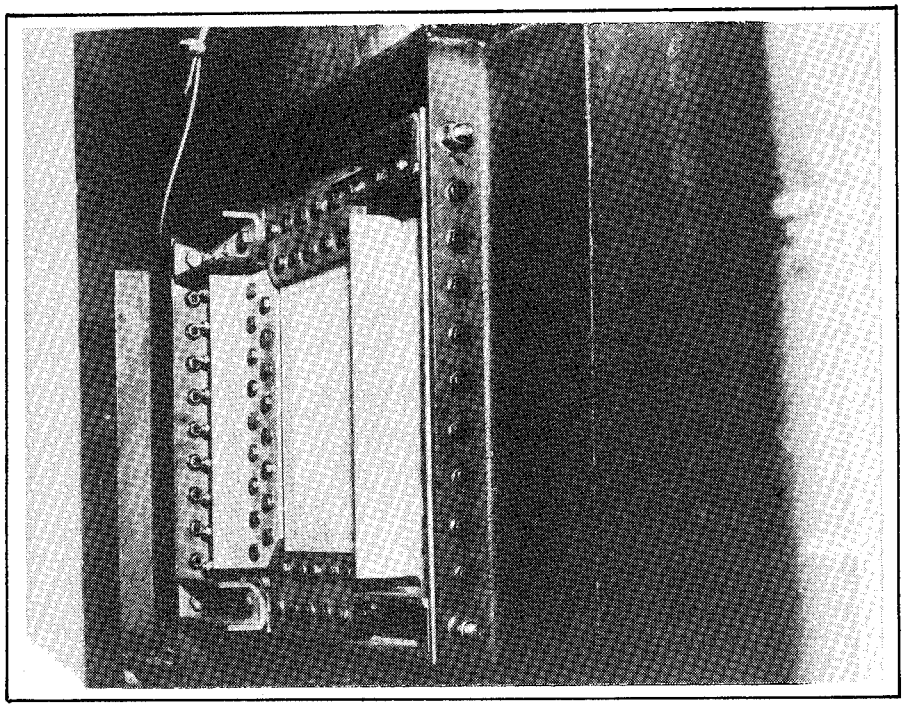

Figure 11. Test Panel Arrangement.

The testing was accomplished at the NASA/Langley facilities. The cyclic or static load to the test jig was applied through a double acting hydraulic unit operating only in the compression mode. A sinusoidal hydraulic pressure profile was used in all the cyclic tests at a 5Hz rate. The test schedule, presented in Table III, was randomized for spectrum testing. One lifetime represents a 4000 hour usage of the CH-53D helicopter, which includes the limit shear load condition.

Table III CH-53D Airframe Load Spectrum

Peak Load Factor, $N_{z_{max.}}$	No. of Cycles* (4000 Hrs.)	Panel Shear (Lbs./In.)	Test Panel Shear Load
3	1	285	3,600
2.8	4	266	3,360
2.6	8	247	3,120
2.4	24	228	2,880
2.2	74	209	2,640
2.0	194	190	2,400
1.8	743	171	2,160
1.6	1,521	152	1,910
1.4	103,613**	133	1,670
1.2	12,552**	114	1,440
1.0	(REF)	95	1,200

* Cycled from load factor of 1.0 to peak load factor

** Includes lumped gust and landing spectrum

Note: Design ultimate static strength is 428 lb/in.

Five specimens of each panel type were tested as follow:

(a) One specimen test to static failure.

(b) Three specimens tested for one lifetime and then tested for static residual strength.

(c) One specimen tested to one lifetime, then damaged by a hole

in center of panel in shape of a fully tumbled 7.62mm armor piercing projectile (elongated) axis normal to direction of maximum tensile stress, then cycled for one more lifetime, and finally loaded to fracture for residual strength.

The test results of the twenty specimens are presented in Table IV. All specimens successfully passed the cyclic tests, even with the reported overloads. The test ultimate shear stress well exceeded the design ultimate requirement even with simulated ballistic damage. For example, the ultimate design shear flow for the panel is 428 lb/in, and for the Type IV Kevlar panel would be a shear stress of 10 ksi. Thus the composite skins have residual strengths well beyond ultimate design requirements. The design and test shear results are compared in Figure 12.

Table IV Summary of Composite Panel Test Results

Panel Type	Specimen No.	Ultimate Shear Strength (ksi)	Residual Shear Strength (ksi)	Comments
I (Graphite/epoxy)	1	42.1 (1600)*	-	
	2	-	39.8 (1510)	
	3	-	32.4 (1390)	
	4	-	38.0 (1480)	
	5	-	36.4 (1370)	Ballistic damage + 2 life times
II (Graphite/epoxy and Kevlar^{R} 49)	16	23.4 (1610)	-	
	17	-	27.0 (1800)	
	18	-	23.4 (1520)	
	19	-	21.6 (1560)	
	20	-	17.4 (1180)	Ballistic damage + 2 life times
III (Kevlar 49 Tapes)	6	19.8 (921)	-	
	7	-	18.2 (864)	
	8	-	16.7 (793)	Overload 1X 9.2 ksi
	9	-	17.0 (782)	Overload 3225X to 7.8 ksi
	10	-	14.9 (678)	Ballistic damage + 2 life times
IV (Kevlar 49 Woven)	11	21.4 (909)	-	
	12	-	30.4 (1307)	
	13	-	25.5 (1100)	
	14	-	42.4 (1780)	
	15	-	14.1 (606)	Ballistic damage + 2 life times

*Shear lb/in based on actual thickness of each panel.

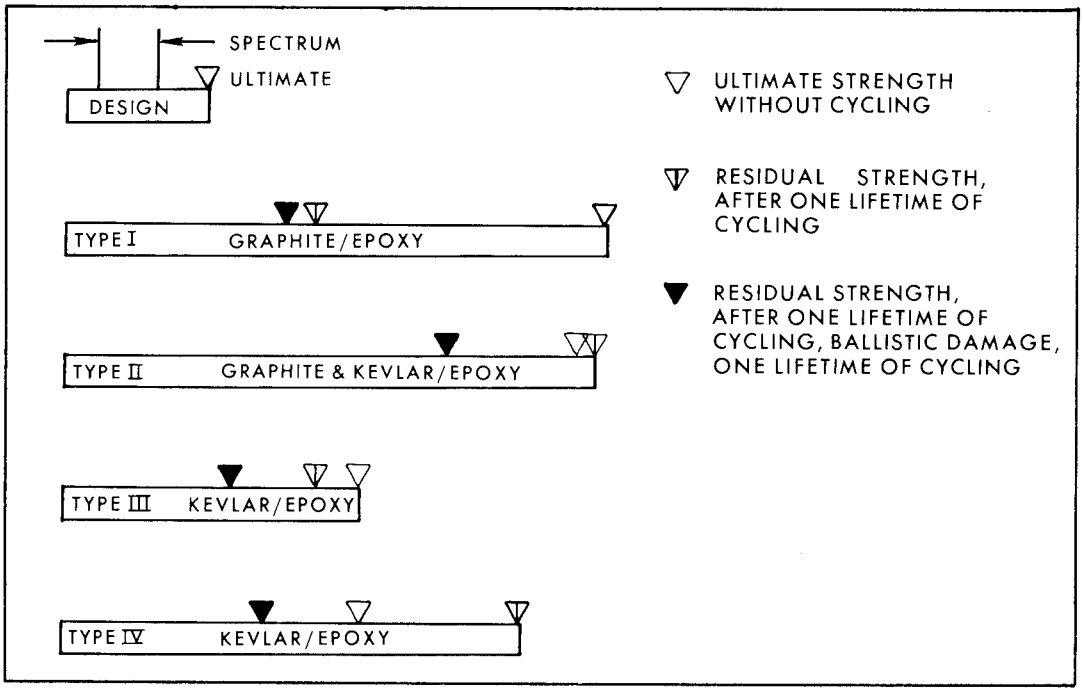

Figure 12. Composite Shear Panels Exceed Design Requirements.

The test results confirm the use of composite skins in diagonal tension. The Kevlar 49 woven (broadgoods) panels appear to be more than adequate for the CH-53D loadings and offer a low cost solution for the CSSF design concept.

It should be noted that the effects of shear reversal, interaction effects with compression or tensile loadings, or the effects of curvature have not been tested. These combinations should be tested for needed information of a design data phase.

CONCLUDING REMARKS

The development of a low cost composite airframe is progressing very well. The results to date for the CSSF design concept are most promising:

- A compatible material system is available for a single stage cocured structure.
- Static test results have verified the CSSF design concept for stringers, frames, and joints.
- Fatigue test results of composite skins verify the ability to use postbuckled strength for cyclic loadings.

The results to date indicate the CSSF design concept will be more efficient than originally projected in the first program (Reference 1). Since the static test results confirm the crippling strength is not a limitation then, with minor geometry changes, the stringer column lengths can be extended (frame to frame). Thus far fewer intermediate frames will be required and both cost and weight can be reduced. The static tests also indicate that the major frame joints were conservatively designed and again correspondingly both weight and cost will be reduced. The spectrum tests of shear panels have shown that more than adequate strength exists for the helicopter design loads. The ability to withstand the design spectrum loads even with imposed damage confirm that the Kevlar 49 broadgoods will be a low cost solution. Furthermore it is indicated that it may be practical to reduce the skin gage from 4 ply (.040 inches) to 3 ply (.030 inches), again providing reduced weight and cost.

The second phase of the program (Reference 2) will involve fabrication of large sections of the airframe and include fatigue testing of the primary frame structures. The final review will include a re-evaluation of weight and cost and promises to show significant improvements over that originally projected for the CSSF concept.

However the full development of a low cost composite airframe will require considerable further effort. As shown in Figure 13 the detail design, acquiring full design data, fabrication of a total (or significant portion) of an airframe, testing, and obtaining service experience are the steps to acquiring the confidence to commit to production. The effort has been started and the results obtained to date point towards a successful program.

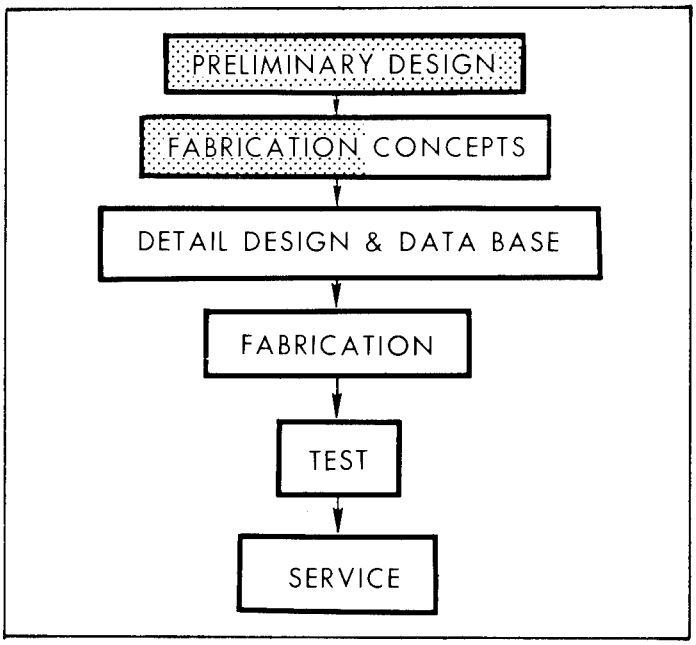

Figure 13. The Path to Developing Low Cost Composite Airframe Structures.

REFERENCES

1. Rich, M. J., Ridgley, G. F., and Lowry, D. W., "Application of Composites to Helicopter Airframe and Landing Gear Structures", NASA CR-112333, June, 1973.

2. Adams, K. M., Lucas, J. J., "Study to Investigate Fabrication and Test of Low Cost Concepts for Large Hybrid Composite Fuselage - Phase I", NASA CR-132731, September, 1975.

COST REDUCTION WITH COMPOSITES IN B-1 SLATS

By W. Andrew Pitman

Lockheed-Georgia Company

SUMMARY

The advanced composite wing leading-edge slat designed for the Air Force B-1 aircraft offers excellent cost saving, as well as weight saving in excess of 15%, in comparison with the all-metal baseline slat. Innovative design/fabrication concepts were elected to reduce fabrication costs. Experience in fabricating three slats has confirmed the feasibility of the design and fabrication concepts and has indicated that the projected cost savings are real.

The design of the slat is explained and related to the tooling and fabrication concepts. Key portions of the slat rely upon the Thermal Expansion Molding Process, which is an important factor in cost saving. This process and its effect on the design and on the resulting molded parts are described. The design validation tests and their results are reported.

INTRODUCTION

The wing leading-edge slats were among the secondary structures selected by Rockwell International and the Air Force to evaluate the potential of composites for saving cost and weight on the B-1. From among the total of 14 slat segments on the aircraft, the Number 3, left-hand segment, Figure 1, was selected as that most suitable for the evaluation.

Two minimum cost saving and weight saving objectives were established during the program:

Cost saving	28%
Weight saving	12.5%

The cost target was based on cumulative average production costs at the 241st unit estimated for both the all-metal baseline slat and the composite design.

SLAT DESIGN

Design Criteria

The program objectives had to be attained with no favors allowed the composite design. The B-1 requirements for form, fit, and function applied, including, of course, elevated temperature exposure, lightning exposure, as well as the strength, stiffness, and configuration envelopes. Principal sizing of the major composite members proved to be stiffness-controlled. Bending and torsional stiffness requirements proved quite demanding. Aerodynamic considerations also dictated challenging limits on permissible trailing-edge deflections under load.

Detail Design

The design of the metallic baseline slat is shown in Figure 2. The construction is generally typical of sheet-metal slat structures, but close examination would show heavier than normal spar caps. Lockheed's composite counterpart is illustrated in Figure 3 and Figure 4. Note the quite heavy spar capstrips which are required to provide the necessary bending stiffness. The spar capstrips are predominantly unidirectional graphite/epoxy. As the design was firmed up, it turned out that the bending stiffness (EI) was most effectively (and almost exclusively) provided by the spar, while the torsional stiffness was provided by the two-cell box formed by the leading edge and the full-depth sandwich "eyebrow" panel aft of the spar. The skins of these cells, including the spar web, were thus planned for $\pm 45^{\circ}$ graphite laminates. Finally, optimization analyses showed that a combination of 0° and 90° plies added to the eyebrow skins was necessary, in conjunction with the system of three ribs, to constrain peak deflections of the trailing edge to the maximum allowed by the criteria at any point along the length of the slat.

The remainder of elements of the complete slat structure are shown in Figure 4. The principal materials used are shown in Table I.

Tracking of Projected Cost

In the design of the slat, estimates of the cost saving possible with the design described above followed the history shown in Figure 5. For the early design, when the proposal was formulated, criteria were incomplete. As these were rounded out and refined, projected cost savings varied considerably. The basis of cost comparison is the projected cumulative average cost over 241 units, as shown in Figure 6. The initial optimism reflects an inadequate accounting for the effects of flutter-prevention stiffness criteria (EI and GJ). Subsequent savings in the cost-saving projections reflect the process of homing in on the final balance between cost-saving and weight-saving objectives, established by Rockwell at 28% and 12.5%, respectively. It will be noted that the projected cost savings achieved are about 36%. This excellent cost saving is complemented by a weight saving of 15%. Results

from fabrication of three test articles confirm the feasibility of attaining at least a 15% weight saving.

COST REDUCTION MEASURES

Part Count Reduction

The means of saving cost with composites in the B-1 slat will be discussed in terms of the principal design and fabrication approaches most heavily contributing to total result. It is interesting, however, to observe the applicability of the time-honored index: relative part counts of baseline and composite designs. The index shows the appropriate trend, since the composite slat gives a part count of 21 versus the metallic baseline count of about 100.

Fabrication Approaches

Two principal fabrication approaches are credited with the cost savings projected:

- Thermal Expansion Molding of the spar and leading edge
- Cocuring of the eyebrow assembly

These fabrication approaches are possible, of course, only because the design was based on their use. The manner in which these approaches fit into the complete fabrication plan is depicted in Figure 7. The Elastomeric Molding approach used on the leading edge, shown in Figure 8, enables production of a unit assembly directly from wet prepreg material, complete with integrally cocured aluminum-screen lightning protection on the exterior surface and fiberglass T-section stiffeners on the interior surface. The elastomeric tool segments not only position the fiberglass stiffeners, but they also generate lateral pressure to form the outstanding stiffener legs and transmit the autoclave pressure to the stiffener bases and to the shell laminate. A leading-edge unit with elastomeric tool segments still in place is shown in Figure 9, while a molded leading edge with elastomeric segments removed is shown in Figure 10.

Thermal Expansion Molding

The thermal expansion molding concept for the spar is diagrammed in Figure 11. Though the payoff on success is quite handsome, this complex part presented a challenge. It is evident from the cross section in Figure 11 and the view of the front side in Figure 12 that many details were molded into a single-unit assembly. The combination of part design, tool design, and processing required a great deal of ingenuity and perseverance. Work has continued independently of the funded program to consolidate the generally successful efforts in making these assemblies for the slats. The approach is definitely successful, and comparison

with the alternative of a more conventional spar fabrication approach demonstrates the payoff. The fabrication sequence for a conventionally made spar is illustrated in Figure 13. Basically, it involves a step-by-step buildup of elements with final assembly bonding in a bond fixture processed by autoclaving.

A cost comparison was made between the elastomeric-molded spar and a conventionally made spar built up in the sequence shown in Figure 14. The estimated cost difference is a rather dramatic 25%.

Cocuring

The previously described spar becomes cocured, along with the other elements identified in Figure 15, into the "eyebrow" panel assembly. The aluminum honeycomb core is precut in segments to contour and planform. The aluminum ribs and actuator retainer block are incorporated into the layup in final form, as is the precured fiberglass trailing-edge closeout. The facing sheets, however, are laid into the eyebrow bond fixture as wet prepreg The cocuring operation accomplishes in the one processing, illustrated in Figure 16, the bonding together of core, ribs, spar, and trailing-edge closeout simultaneously with the curing and bonding of the hybrid face sheets.

The cost saving inherent in the eyebrow cocuring is apparent. The most important saving is in recurring cost, but the saving in tooling cost is considerable.

Any cocuring operation involves an exchange of risks; that is, some risks are reduced in exchange for other increased risks. In the case of the slat, reduced cost and the improved reliability inherent in cocured bonds compared with secondary bonds are exchanged for two principal areas of increased risk: (1) the risk of losing several valuable parts in the event of process failure, and (2) the risk of out-of-tolerance contour in the event of movement of or between uncured parts. The contour control problem is particularly pertinent to the slat, because both upper and lower surfaces of the eyebrow from aerodynamic surfaces and close tolerances are required. Our experience confirmed expectations that the necessary tolerances could be held while cocuring. We further feel that the superior integrity potential of a cocured assembly outweighs any real increment of risk of losing high-value parts. Therefore, the cost savings from simplified tooling and fabrication are free and clear savings.

Material Cost Effects

The very attractive savings in fabrication cost are, of course, partially offset by a somewhat higher material cost for the composite slat. It is of interest to examine one instance in which a higher cost was accepted in order to use boron in the eyebrow facings in lieu of a nominally all-graphite layup. This choice was elected to achieve a necessary increment of weight saving. The trend effect of the tradeoff is shown in Figure 17. It will be noted that all-boron facings gave maximum weight saving but at a rather steep relative cost. All-graphite facings gave the lowest cost. The so-called "all-graphite" facings,

however, were felt by Lockheed to require use of "insulating" plies of fiberglass between graphite and aluminum materials. The combination which used two plies of boron, one each at the inner and outer surfaces of each facing, proved to make an excellent hybrid with the graphite, since it provided nearly minimum cost and weight levels. Incidentally, this combination provided two other bonuses: (1) avoidance of face strength loss due to graphite dimpling into the core, and (2) a substantially tougher eyebrow than that which would have resulted if all-graphite facings had been retained.

CONCLUDING REMARKS

The aggregate effect of cost influences of composites use, as exemplified in Lockheed's work on the B-1 slat design and development, points to the importance of design, tooling, and fabrication approaches which take advantage of the unique attributes of composites. Their unique attributes are considered to include greater amenability to combining many fabrication and assembly operations into a few operations. Thereby the pronounced cost savings summarized in Figure 18 are attainable, and they overwhelm the now small material cost handicap of composites.

It is gratifying to report that the composite slat sustained static test loading in the most critical condition up to 134% of design ultimate load. The fatigue test is well advanced, but not completed at the time of this writing. Some failures of fasteners have been experienced, but they are unrelated to the use of composites in the design. Since they are readily correctable, they are hardly more important than nuisances.

The initial flight of a B-1 with a composite slat is expected later this year.

TABLE I - APPLICATION OF MATERIALS

PART	MATERIAL
Leading Edge	Graphite: 8 plies, $\pm 45^{\circ}$ Fiberglass: 2 plies, 120 fabric prepreg Aluminum screen: 120 mesh
Spar - Capstrips	Graphite: 66 plies (lower) and 42 plies (upper), 0° Fiberglass: Transverse tie and pad-up plies as required
- Webs	Graphite: 12 plies, $\pm 45^{\circ}$
Core	Corrosion resisting aluminum (5056)
Internal ribs and actuator fitting	Aluminum, 7075-T73
Trailing edge closeout	Fiberglass
Eyebrow panel face sheets - Upper	Aluminum screen: 120 mesh Boron: 1 ply each at 0° and 90° Graphite: 6 plies at $\pm 45^{\circ}$ plus 2 plies at 90° in outboard bay
- Lower	Same as upper face, less aluminum screen
Trailing edge wedge	Aluminum, 7075-T73
External (removable) fittings	Aluminum, 7075-T73

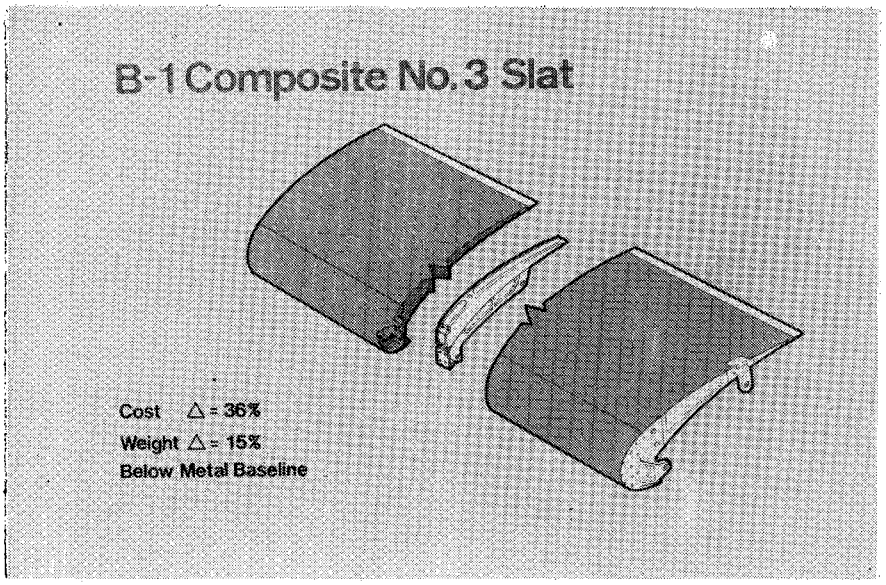

Figure 1. Slat Development Article

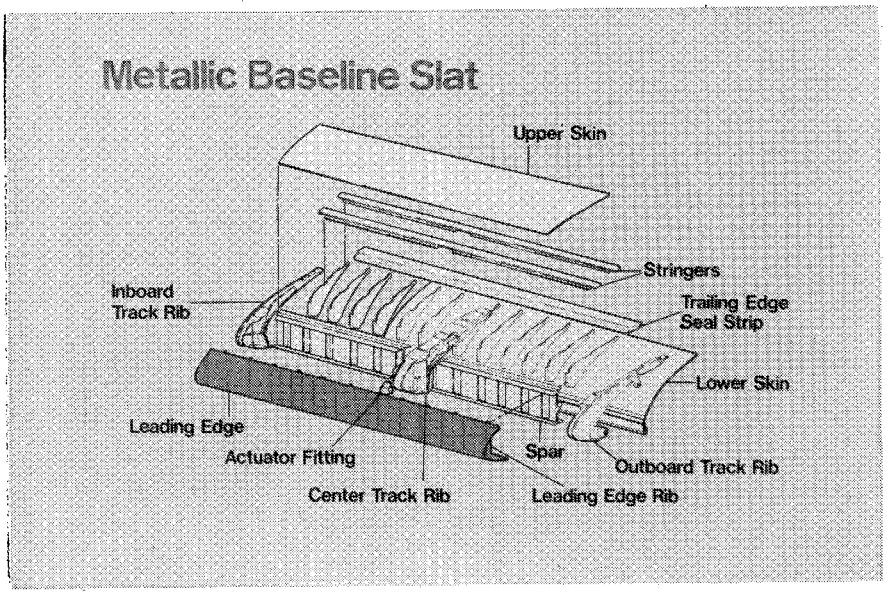

Figure 2. Metal Slat Design

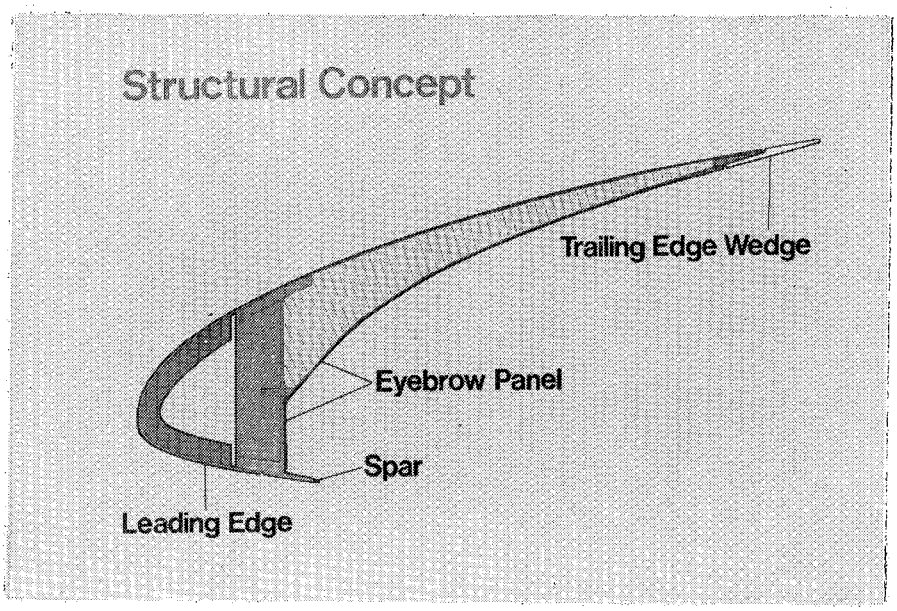

Figure 3. Composite Slat Cross Section

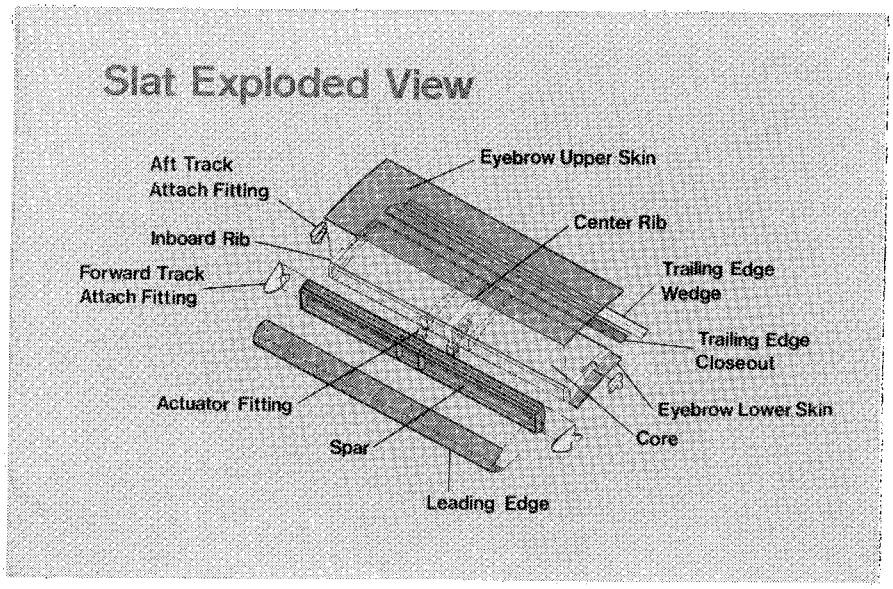

Figure 4. Details of Complete Slat

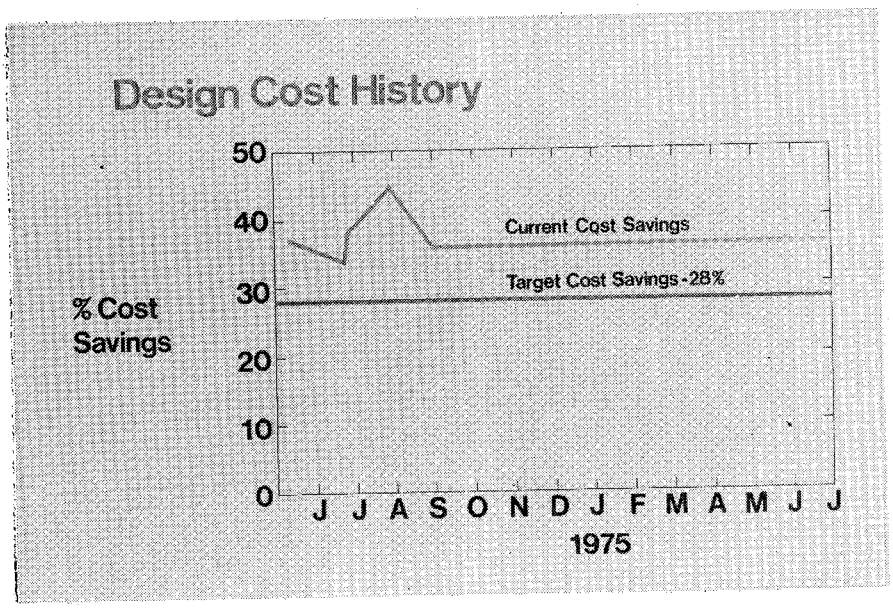

Figure 5. Cost Tracking Chart

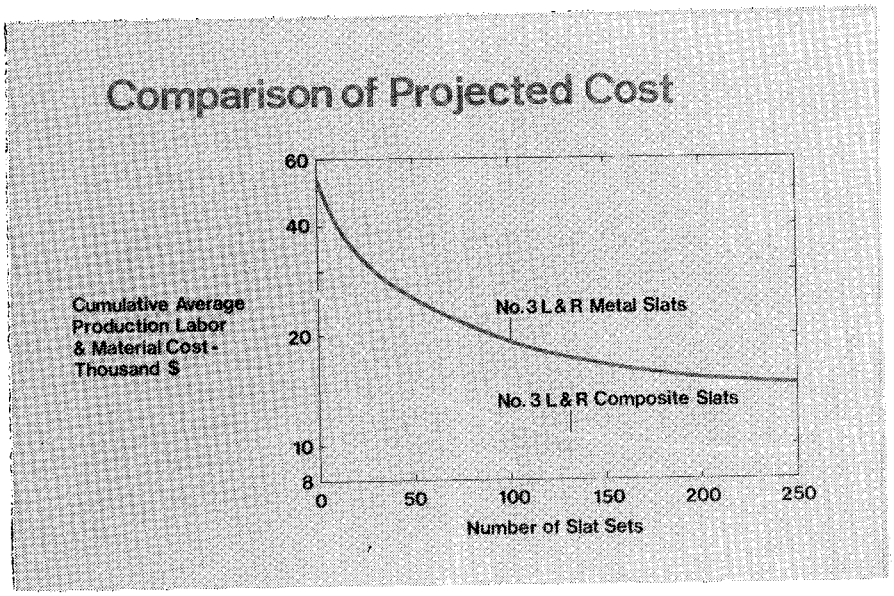

Figure 6. Comparative Cost Projection

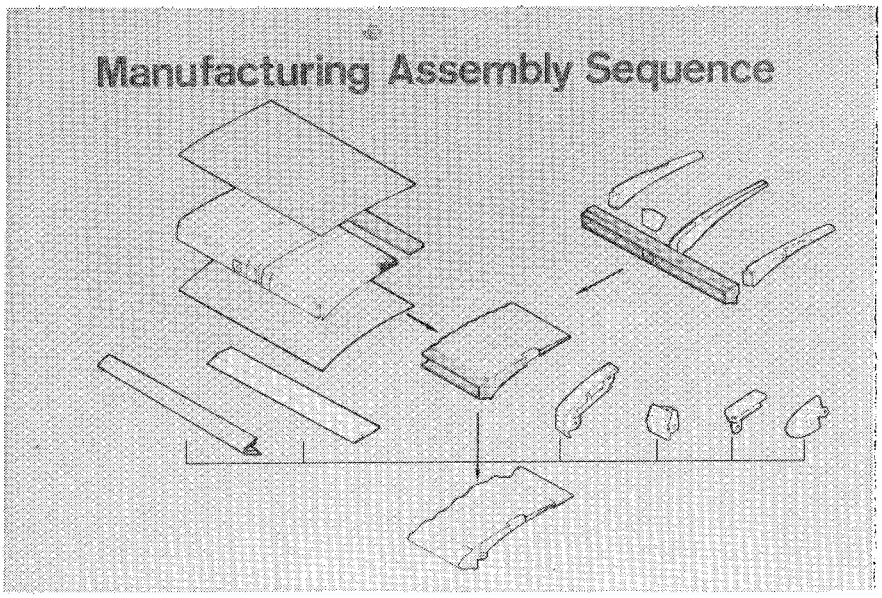

Figure 7. Flow of Assembly Operations

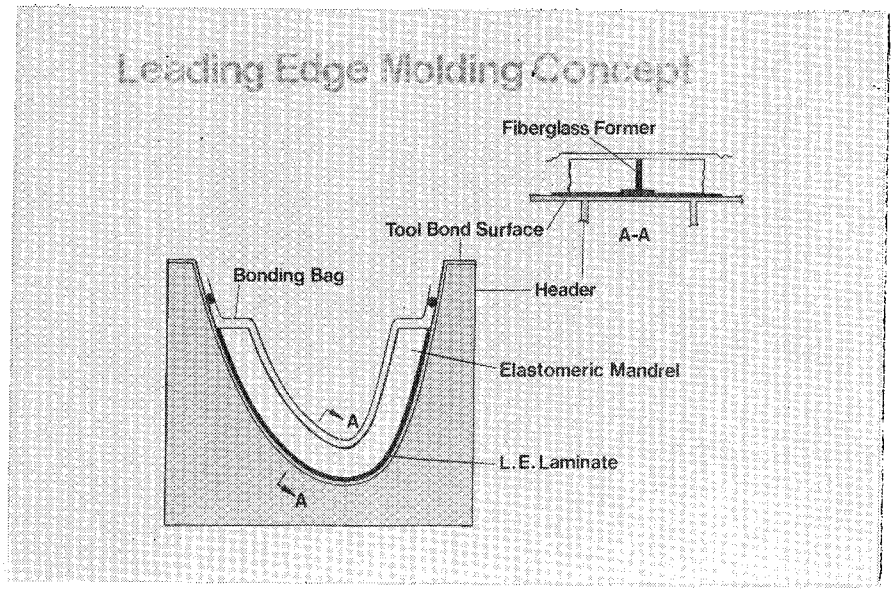

Figure 8. Open-Faced Elastomeric Molding of Leading Edge

Figure 9. Removal of Leading Edge Elastomeric Tooling

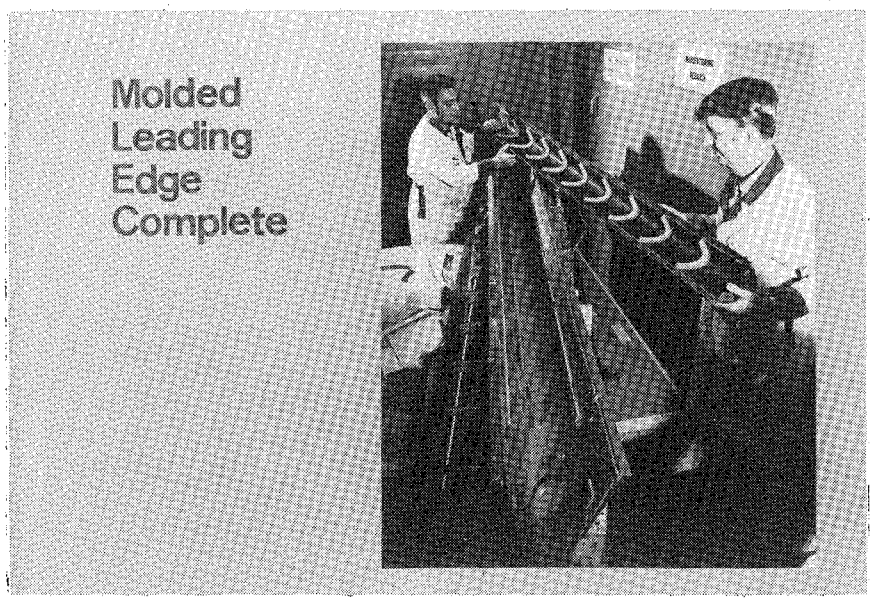

Figure 10. Removal of Cured Leading Edge

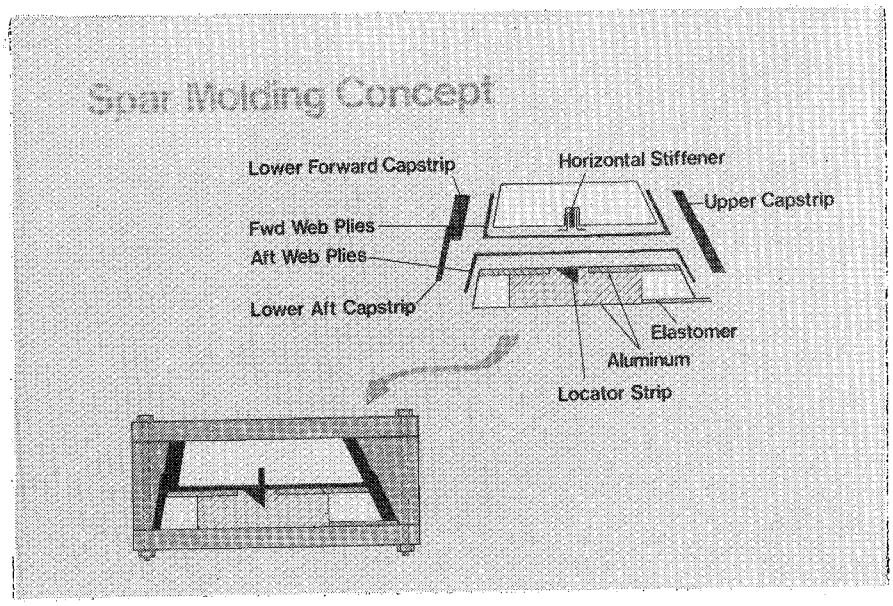

Figure 11. Closed-Tool Elastomeric Molding of Spar

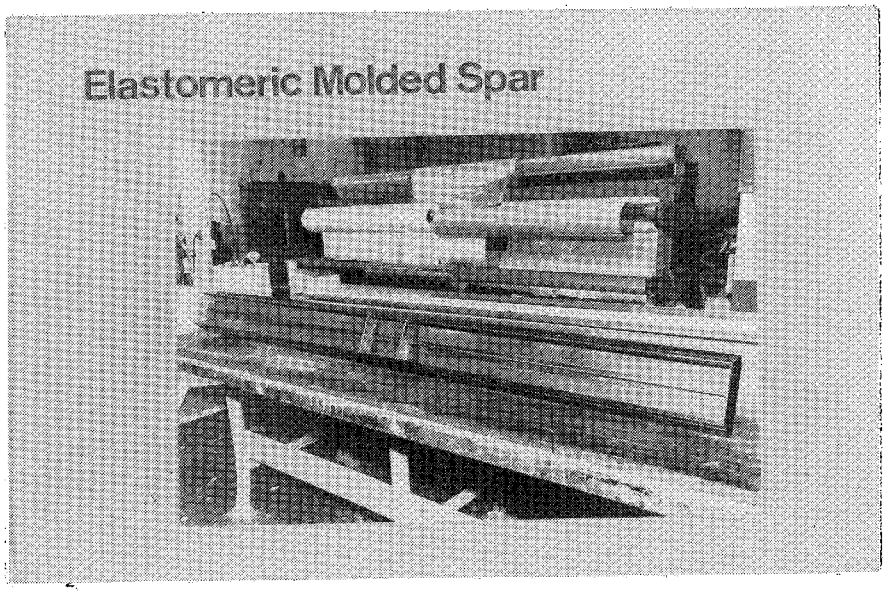

Figure 12. Front Side of Spar

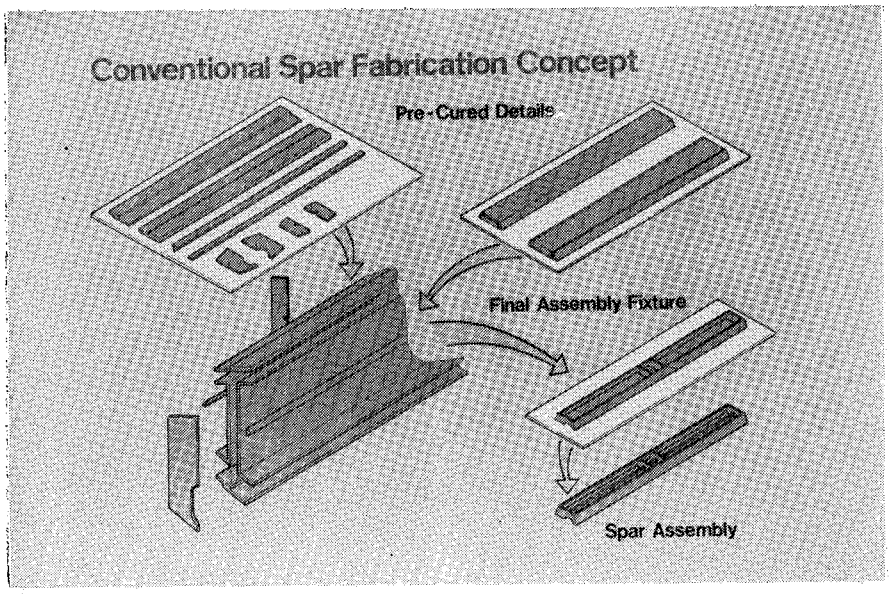

Figure 13. Fabrication and Assembly Sequence for Spar Made by Conventional Method

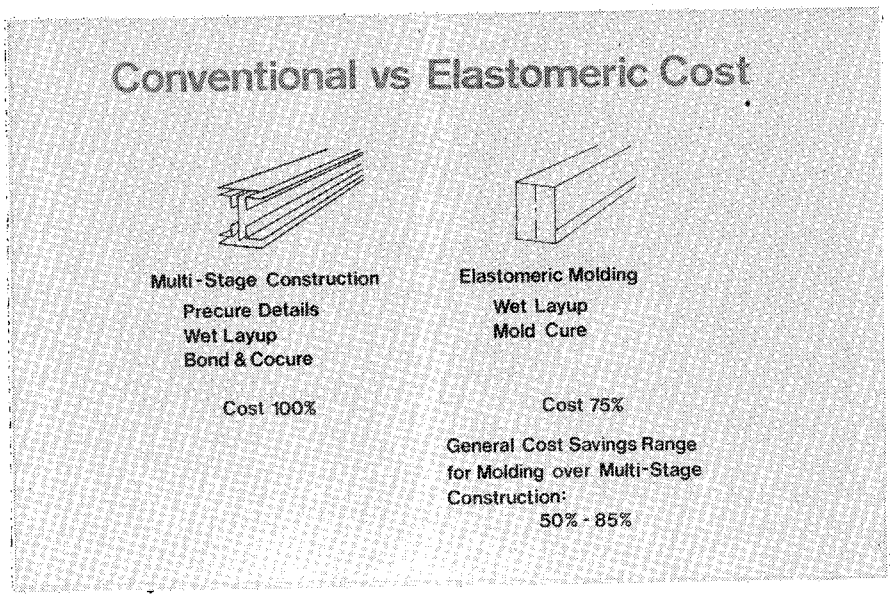

Figure 14. Cost Comparison between Built-Up and Elastomeric Molded Spars

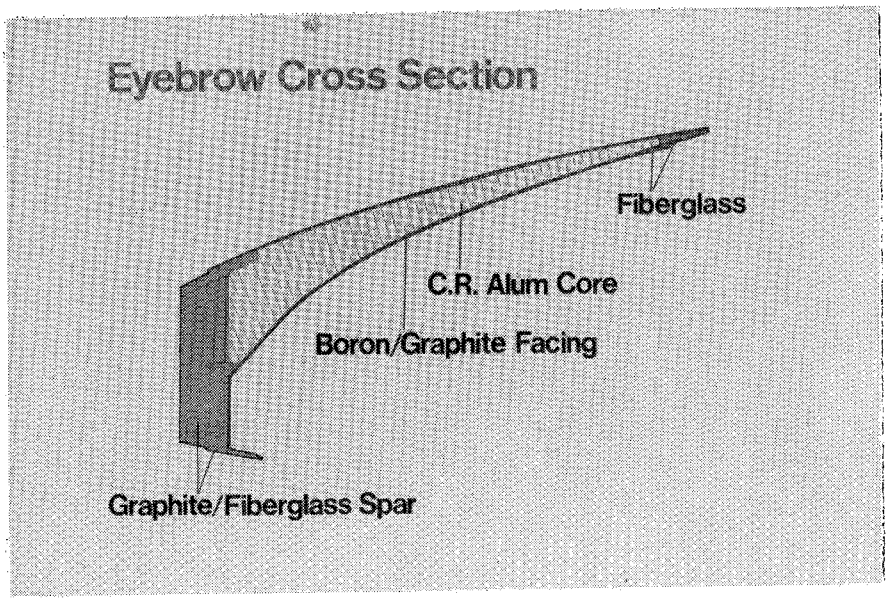

Figure 15. Eyebrow Assembly Details

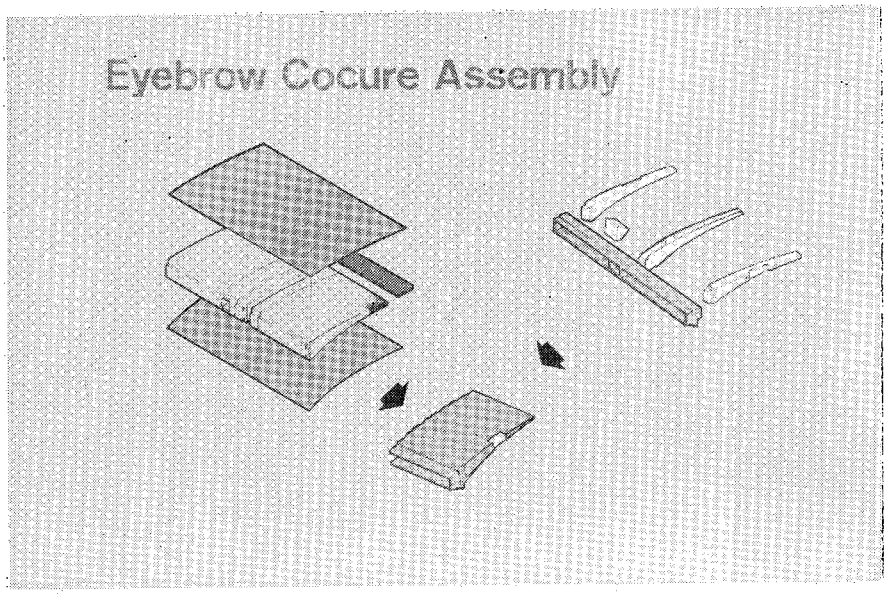

Figure 16. Elements Cocured to Make Eyebrow Panel

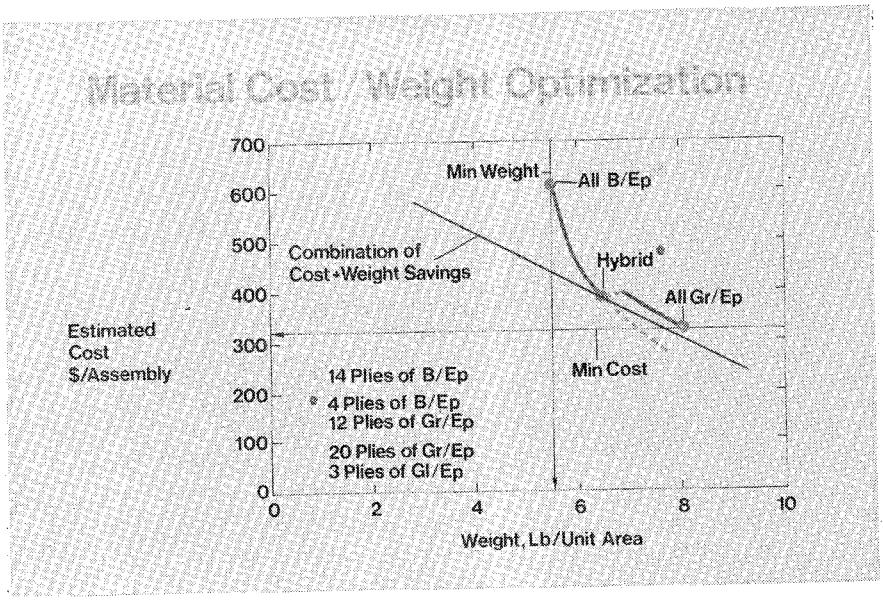

Figure 17. Trade-Off between Boron and Graphite in Eyebrow Facings

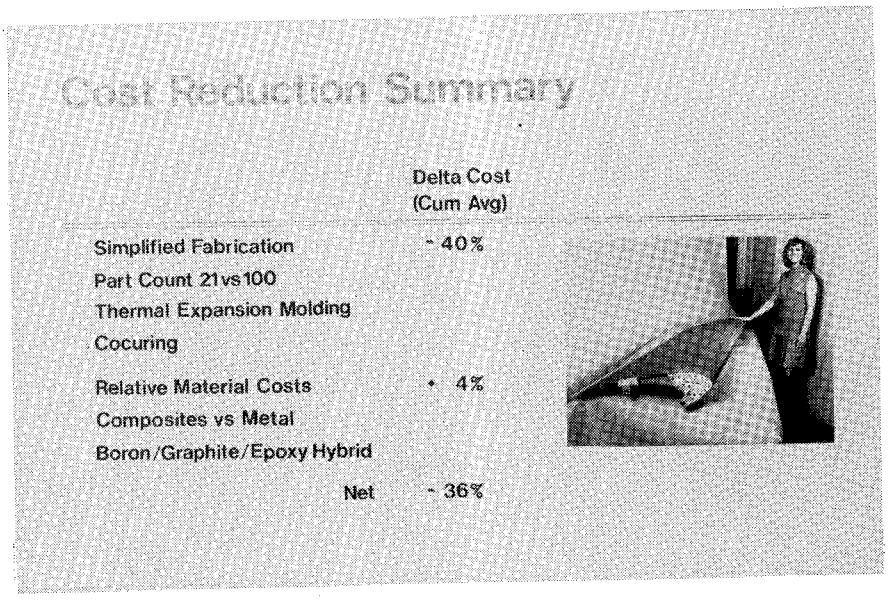

Figure 18. Principal Factors Affecting Cost Savings on Composite Slat

DESIGN, FABRICATION AND TEST FOR AN F-14A GRAPHITE/EPOXY MAIN LANDING GEAR STRUT DOOR

By R. Carlson, G. Lubin and A. Cowles
Grumman Aircraft Corporation

INTRODUCTION:

In 1972 Grumman Aerospace Corporation initiated a study of potential applications for the use of high modules graphite composites in aircraft structure. The main objective of this program was to demonstrate design feasibility and optimum cost, weight and performance benefits. After a preliminary survey of different types of current production aircraft assemblies, the F-14 main landing gear strut door was chosen as a demonstration article since it represented an excellent example of a complex metal honeycomb assembly with compound curvature, several highly loaded areas and a large number of detail parts.

BACKGROUND:

The present F-14A production main landing gear strut door consists of a single piece formed and chem milled aluminum outer skin, a three piece formed and chem milled inner skin, aluminum honeycomb core and numerous zee and channel type closure members. A machined titanium fitting is used to actuate the opening and closing of the door and two aluminum hinges provide attachment points. The hinges, actuator and several stiffeners are riveted to the bonded panel to complete the assembly. In total, there are 73 detail parts.

Under an internal research and development (IRAD) program, Grumman fabricated an all graphite/epoxy skin - aluminum honeycomb core door to display design feasibility. The objective of this program was to fabricate a main landing gear (MLG) strut door which would be less costly to produce than the present metal door at no sacrifice in weight or performance. This door was tested by the Naval Air Development Center in 1974 and passed all static and fatigue tests required, and further withstood loads as high as 250% of design limit load at 335°F without sustaining damage. This particular door was approximately 10% lighter than the current metal door.

Under a Navy funded follow on contract, the original composite design for the main landing gear strut door was revised to make the door fully flightworthy, incorporate several additional design and manufacturing concepts and to the cost savings design concepts, it is expected that up to $1,000 per door savings may be obtained.

Design Concepts

The F-14 graphite/epoxy main landing gear strut door, which is located between Fuselage Station 501.187 and Fuselage Station 573.75 in the outboard sponson area, is of honeycomb sandwich construction using graphite-fiberglass/epoxy composite inner and outer skins with aluminum honeycomb core. It is hinged off the sponson wall at Station 521.827 and Station 555.80, and is actuated

by a titanium fitting at Station 534.62. The composite door is designed with a slight warpage at both the forward and aft inboard corners. When closed, this design feature provides a preload to the door to minimize edge gapping when the door is subjected to critical aerodynamic pressures. The warpage of the composite door differs from that of both designs of its F-14 production metal counterpart. The metal door used on the first 184 F-14 production aircraft had a slight twist at the inboard forward corner and an 0.43-in warpage at the in-board aft corner. On Aircraft No. 185 and subsequent, the metallic door will be built with zero warpage at the inboard aft corner. The composite doors differ from both of these designs by having 0.100-in warpage at the inboard aft corner.

In an effort to produce a part at minimum cost, several design changes were made to the IRAD design. These changes were as follows:

- Eliminated the fore and aft (zee) edge members by use of the fiberglass plies on the inner skin to effect the honeycomb core edge closures.
- Increased central honeycomb core densities to eliminate the need for core edge blocks, thereby reducing the number of core details required to be pre-fitted and spliced.
- Eliminated the inboard (zee) edge member aft of the forward core cut-out.
- Selected scrim-backed graphite/epoxy tape for air passage skin to obtain the improved handling characteristics of woven broadgoods, while retaining strength levels approximating those of conventional graphite/epoxy materials.
- Eliminated use of edge filler along core to reduce weight and cost.
- Reduced density of the honeycomb core from 9.5 to 8.0 lb per square foot adjacent to and forward of the actuator fitting, thereby reducing weight and improving formability of core in this area.
- Eliminated rounded inside/outside corner trims on most graphite/epoxy plies in order to reduce fabrication time.
- Used production cast aluminum hinge fittings and titanium actuator fittings.

The air passage skin is a graphite-fiberglass/epoxy hybrid using a layer of fiberglass fabric type 7781 on both external surfaces of the skin at $\pm$ 45° to the longtudinal axis. These layers of fiberglass in additional to preventing potential galvanic corrosion, were used to replace full layers of graphite or a 1:1 basis. This substitution does however increase the weight of the skin as a result of the per ply thickness of fiberglass being substantially greater than that of graphite. The remainder of the skin is graphite/epoxy construction with orientations at 0°, 90° and $\pm$ 45° as required to withstand the applied loads. The total number of plies varies from four (2 layers fiberglass, 2 layers graphite) to twenty eight (2 layers fiberglass, 26 layers graphite). Two small titanium doublers are laminated into the air

passage skin, as well as the inner skin, in the areas of the hinges. These doublers are interposed between the graphite layers to provide additional bearing strength. To reduce fabrication costs by eliminating the graphite/epoxy edge members along 50% of the perimeter of the assembly, the graphite build up for the lower leg of the zee type edge member was manufacturered as part of the air passage skin. Similarly, the upper portion of the zee member was laminated into the inner skin. Where necessary, honeycomb core ribbon direction or density was changed to carry the shear loads originally carried in the graphite zee member vertical wall. Two layers of fiberglass are all that is used as a close out in place of the graphite zee member.

To minimize lay up time for the compound contoured air passage skin, carrier type (style 104 fiberglass scrim support) graphite prepreg was chosen. This material over gentle or moderate curves has excellent handling characteristics, well suited for mylar transfer type lay up. Although the carrier type graphite prepreg has allowables that are 92 - 95% of those for unsupported graphite, the addition of the carrier increases skin gauge and component weight. Due to complexity of the inner skin, the carrier type graphite could not be used, and the conventional unsupported graphite was substituted. To further reduce graphite prepreg lay up time, the internal trimmed edges of the graphite plies were made with 45° corners instead of rounded corners used on the IRAD door to permit more rapid trimming.

The core subassembly for both the metallic production MLG strut door and the IRAD composite door contained thirty one honeycomb core details. At the sacrifice of some weight, the number of core details was reduced to twenty two in the final composite door. With full production tooling, the number of core details could still be further reduced. Since the inner skin was co-cured with the honeycomb core to the air passage skin, core machining was held to a minimum. Where necessary additional adhesive was used to minimize costly core refinement by hand sanding.

To control overall program costs, the machined titanium actuator from the production door was used. Normally riveted into place on the metallic production door, this fitting was packed with honeycomb core, spliced to the core sub-assembly and bonded into the graphite/epoxy composite door assembly. This enhances the design by permitting a much more uniform distribution of loads from the actuator into the door. In order to carry the high shear loads from centrally located actuator fitting to the forward and aft hinges, the honeycomb core was cut along the outboard edge to accept a 15 ply co-cured fiberglass channels. At the hinge locations, small titanium doublers were added along the vertical wall of the channels to act as a reinforcement when installing the blind fasteners used in attaching the hinges.

In addition to the fiberglass channels, graphite/epoxy zee members are laid up in these outboard areas. These zee members are a maximum twenty four plies in thickness and are co-cured with the inner skin. A third zee member at the inboard forward area of the door, up to 38 plies of graphite, is used to maintain assembly stiffness in this area. The problems on this area are caused by the close fit of the landing gear assembly requiring

the removal of a part of the honeycomb section.

With the exception of the precured air passage skin and the prespliced core subassembly, the remainder of the fiberglass, graphite and adhesive is co-cured to eliminate fit up problems and after bond discrepancies, such as voids. The assembly is then completed by the mechanical attachment of two seals, the hinges and a metal fairing to permit landing gear clearance. In all there are 38 separate details to make up the composite MLG Strut Door compared to 73 details for the metallic production door.

Weight Factors

The composite MLG Strut Door demonstrated only a .6 pound weight savings of the present metallic production door, the composite door weighing 34.3 lbs.

The IRAD graphite door had achieved an approximate four pound weight savings, but in an effort to optimize cost effectivenss and the addition of the fiberglass barrier layers to prevent potential galvanic corrosion, this weight savings was lost.

The use of carrier type graphite prepreg to reduce lay up time resulted in 0.6 pound weight increase. The use of four layers of style 7781 fiberglass prepreg in lieu of four layers of graphite/epoxy added an additional 2.2 pounds. The simplification of honeycomb core details further increased the weight by one pound.

Although the graphite edge members at the forward and aft ends of the door were not longer evident as separate details, they were built into the air passage and inner skins. Consequently, although the assembly was less expensive to manufacture, there was no weight savings on this particular item.

Materials

As a result of examining the manufacturing problems when fabricating the IRAD composite MLG shut door, it was decided that the scrim support graphite prepreg would be greatly beneficial during lay up of the air passage skin. Consequently, a sample of Hercules 3501/AS-SCRIM material was tested. As a result of these tests, the minimum allowables for this material was established at approximately 92 - 95 per cent of the conventional unsupported graphite prepreg. These allowables may be found in Table 1.

The remainder of the materials used in the construction of the door are in common use at Grumman and include;

- Hercules 3501/AS graphite/epoxy - (Hercules Corp); prepreg for inner skin and zee members.
- Trevarno F-161/7781 fiberglass prepreg (Hercules Corp)
- Narmco 2054/7743 fiberglass prepreg - (Whitaker Corp)

- Metlbond 329 epoxy film adhesive - (Whitaker Corp)
- AF 3002 core splice adhesive - (3M Co)
- Aluminum Honeycomb Core - 2024 - T81; 5.0 lbs/cu ft to 8.0 lbs/cu ft density

Design Data Generation

The work on coupons, subscale specimens and the IRAD door is detailed in Ref. 1. The processing parameters were also discussed in that article. The information generated was used to fabricate this new MLG strut door.

Analytical Considerations

The F-14A main landing gear strut door is subjected to aerodynamic pressures at a peak temperature of 160°C. The two critical design conditions are simulated landing and take-off with the door open at room temperature, and maximum bursting pressure with the door closed during a flight maneuver at 160°C. The aerodynamic pressure is carried mainly as a torsional shear flow and secondly as a flexural stress to the skins. A rib redistributes the out-of-plane loads associated with the depressed area adjacent to the pivot fitting and also serves to redistribute the torsional shear flows resulting from the reduced cross-section in this area. The door design was based on the peak design ultimate loads provided from wing tunnel test data. Load is transferred from the laminates into the hinges and actuator fitting by a combination of adhesive bond shear and bolt shear.

Testing

The test program for the graphite epoxy MLG strut door is being performed at the Naval Air Development Center, Warminster, Pa. The door will be tested in three different static conditions. The sequence for the different load cases are as follows:

- Elevated Temperature/Crushing Load - This load case simulates the aircraft flying a Mach 2.4 with the door being exposed to 315°F. The door will be subjected to a positive limit pressure of 3 psi in the closed and locked position. The door will be tested to both limit load and design ultimate.
- Room Temperature/Door Open - This load case simulates the aircraft flying below 260 knots with the door open and exposed to a lateral gust during landings or take off. The limit pressure varies from .65 psi to 1.5 psi at the forward edge. This load case will be run to limit load and design ultimate.
- Room Temperature/Door Closed - The MLG Strut Door will be failed in this condition which represents the aircraft flying at subsonic speeds with the door closed and locked. The door will be subjected to negative bursting loads where the limit pressures range from -2 psi to -2.7 psi along the aft edge. After exposing the door to limit load, the door will be loaded to design ultimate and then to failure.

Since the IRAD door was exposed to these same tests as well as a full fatigue spectrum and was loaded to 250% of design limit load without failure, it is anticipated that the newly designed door will perform in a similar manner. Based on being stiffness critical, the composite door was well above the required strengths.

Fabrication

Based on the experience gained when fabricating the IRAD MLG strut door, fabrication criteria and material handling procedures were developed for the fabrication of the new series of graphite/fiberglass epoxy doors.

Since only a limited number of door assemblies were to be fabricated, prototype tooling was manufactured. For the molding of the air passage skin and the curing of the bonded assembly, a high temperature epoxy plastic tool was built. Reinforced by fiberglass cloth, this tool included an aluminum pocket to accept the hooked titanium actuator fitting which extends beyond the trim of the door. (Figure 1) The addition of side rail blocks, fabricated from high temperature rubber, enables this same fixture to be used as a bonding fixture. To assure smooth vertical walls on the zee members of the door, .040" thick aluminum shims were attached to the rubber blocks at the assembly to side rail block interface.

Due to the increased thickness of the edge of the composite door when compared to the metal door, the hinges were shifted inboard by approximately one-eighth of an inch to eliminate interference between the door edge and the mating land area on the aircraft structure. To accomplish this, an assembly fixture with the new hinge locations was manufactured using an existing F-14 production hydraulic model. (Figure 2)

To expedite the graphite tape layup procedure and ensure proper tape alignment, contoured layup tools were fabricated using fiberglass fabric laid up to the internal contours of both outer and inner skins. The location, direction and boundaries of each layer of graphite and fiberglass plies were drawn on the outside of each of these tools enabling the technicians to rapidly lay up each ply. (Figure 3) After each ply was laid up, the tool was inverted, placed in the bonding fixture and the graphite heat tacked down to the preceeding ply. The lay up tools were indexed ensuring the exact location of each layer. These tools were also used to locate the titanium doublers which were laminated into both inner and outer skins.

The air passage skin was laid up (Figure 4) and precured to permit its fabrication under the normal laminating pressure (85 psi) to assure the maximum mechanical properties, and to permit detailed ultrasonic inspection. The carrier type graphite was used in the manufacture of the air passage skin. After every six to eight plies were stacked together, the lay up was compacted using a PVA vacuum bag. This was done to prevent bridging in the compound contoured areas. Metlbond 329 IA epoxy film adhesive was used to bond the internal titanium doublers. Narmco's 2054/7743 fiberglass prepreg was used as a structural filler at the internal edges of these same titanium doublers. During the curing operation, fiberglass or paper bleeder was used in varying amounts to insure adequate resin flow and air removal.

After dimensional and ultrasonic inspection, the cured skin was placed back into the mold and the core assembly prefitted. The core consisted of 22 individual details, some of which were pre-bonded into the lateral recesses of the pivot fitting to insure core continuity. Most of the abrupt curvature changes were eliminated by core scarfing. After prefit, the core blocks were spliced together and cured using the existing bonding tool. (Figure 5) The core assembly was machined in two locations to accept the fiberglass channels adjacent to the titanium actuator. At the same time as the honeycomb core was spliced, an adhesive isolation fit check was performed between the core and the air passage skin.

Prior to the start of the final layup, the titanium actuator was liquid shimmed to the air passage skin using a two part room temperature curing epoxy. This was necessary since the production titanium actuator fitting did not precisely match the contour of the graphite/epoxy skin.

The first step in the lay up for the bonded door assembly was to remove the nylon peel ply from the inner surface of the air passage skin. Using the results of the adhesive isolation fit check, the Metlbond 329 adhesive was applied to the skin; extra adhesive being added in specific areas to insure the structural integrity of the bondline. The F161/7781 fiberglass prepreg channels the next item laid up. This was done on cast epoxy lay up tools to permit compaction of the uncured FRP lay up. With the appropiate adhesive in place the uncured fiberglass channels were then located on the honeycomb core and the core placed against the air passage skin. A layer of Metlbond 329 IA adhesive was laid up to the inner surface of the core. It was found that while the scrim type graphite tape worked well on the air passage skin, this was not the case with inner skin because of the many areas of involved curvature. At these areas the unsupported graphite was more effective since it was sufficiently flexible to be used without extensive tailoring. Since the unsupported tape is slightly less costly and marginally stronger, and since there was no advantage of using both types of graphite prepreg on the inner skin, a decision was made to use unsupported tape on the entire inner skin.

The first fiberglass layer from the inner skin was wrapped over the edges of the core, down the core's vertical wall and onto the air passage skin. (Figures 6 & 7) As with the air passage skin, the inner skin had two titanium doublers inserted into the laminate at the hinge attachment locations. Again the graphite lay up was compacted down with a vacuum bag after every six or so layers. Prior to the lay up the final layer of fiberglass for the inner skin, the two outboard and the one inboard zee members, made entirely from graphite, were laid up. (Figures 8 & 9)

After completion of the lay up, the fiberglass bleeder system was applied. Paper bleeder was not chosen for the same reasons that carrier type graphite prepreg could not be used; it resulted in too many wrinkles. The side rail blocks for the bonding fixture were set in place. These blocks provided the only source of pressure to the vertical walls of the zee members during the bonding operation. The assembly was then vacuum bagged and autoclave cured at a reduced pressure, 45 psi. During the bonding cycle, an aluminum

caul plate was used on the upper flange of the inboard compression critical zee member. This was done to prevent any fiber wrinkling which would reduce the compression strength.

After cure and postcure, the part was trimmed, ultrasonically inspected and X-rayed. Both through transmission and pulse echo ultrasonic techniques were used. X-ray revealed that the compaction of the vertical walls of the graphite zee members and the fiberglass channels was excellent. The two hinges, a metal fairing to permit landing gear clearance and two small seals were mechanically fastened in place. The fasteners were installed wet with sealant. Two teflon bumpers were bonded in place as a final touch. (Figures 10 & 11)

Installation on F-14A Aircraft

Since the thickness of the edges of the composite door was greater than that of the metallic production door at the inboard and outboard edges, some minor modification to the aircraft was required to accept the graphite door. On the inboard edge, the door stop had to be trimmed away for approximately eight inches to permit the door to rest along the remainder of the five foot length. On the outboard edge, most of the interference with the land on the aircraft structure was relieved by the shifting of the hinges inboard 1/8 inch. There was however, one area where the outboard land of the aircraft had to be cut away to alleviate interference. Once this rework was accomplished, no further rework to the aircraft was necessary to allow for the re-installation of the metallic production door. While the fit up of the door on the aircraft was less than what was desired, the composite door fit no worse than the production door. The lack of positive control on the opening in the aircraft structure to accept either doors greatly contributed to the observed mismatches. In any event, the observed mismatches would not affect aircraft performance. (Figure 12)

Program Pay Offs

Since the final test results on the newly designed door are not yet available the ability of the door to meet critical loads must be based on the experience with the IRAD door. Since however, the door design is stiffness critical it can be assumed that the second door will perform in a similar manner to the IRAD door and will successfully meet all strength requirements. This ability to meet critical loads will prove that graphite/fiberglass epoxy door can be used in a direct substitution for aluminum in this particular design. On the basis of strength and stiffness, it can be considered a suitable construction material for aircraft structures. From the weight standpoint, the latest door does not offer a marked improvement but the weight saving was not planned to be a critical factor in this design.

Beyond the test article, nine ship sets of right and left hand doors will be fabricated to accurately determine cost advantages. The experience with previous composite parts shows that for the first and the second unit, the start up costs are extremely high due to the necessary process and tool development peculiar to the configuration of this part. The production history

of high performance composites is limited at present and only after a production start-up can all the variables be optimized. After the 5th unit all primary problems will be practically eliminated and the true cost can be determined.

Conclusions

As a result of preliminary evaluation and limited production experience, it appears that the graphite/fiberglass epoxy main landing gear door will result in substantial cost savings and limited weight savings. In addition, experience will be compiled for a hybrid design with very drastic curvatures and the use of ply on ply lay up technique. The proposed flight evaluation program will further prove out the feasibility of this design. The controlled production cost analysis techniques and the development of the learning curve data will assist in accurately calculating the potential economic factors. The flight experience will bring out any unexpected service problems and the fiberglass interlayers between aluminum and graphite should eliminate or reduce to a minimum any possible galvanic corrosion problems. Since a landing gear door is subjected to considerable impact damage from runway debris during take off and landings, the improvement in impact strength of graphite composite brought out by the fiberglass layers will be evaluated.

References: (1) Carbon Fibrics Can Be Cost Competitive, by G. Lubin and S. Dastin
International Conference on Carbon Fibrics, Their Place In Modern Technology, London, 1974.

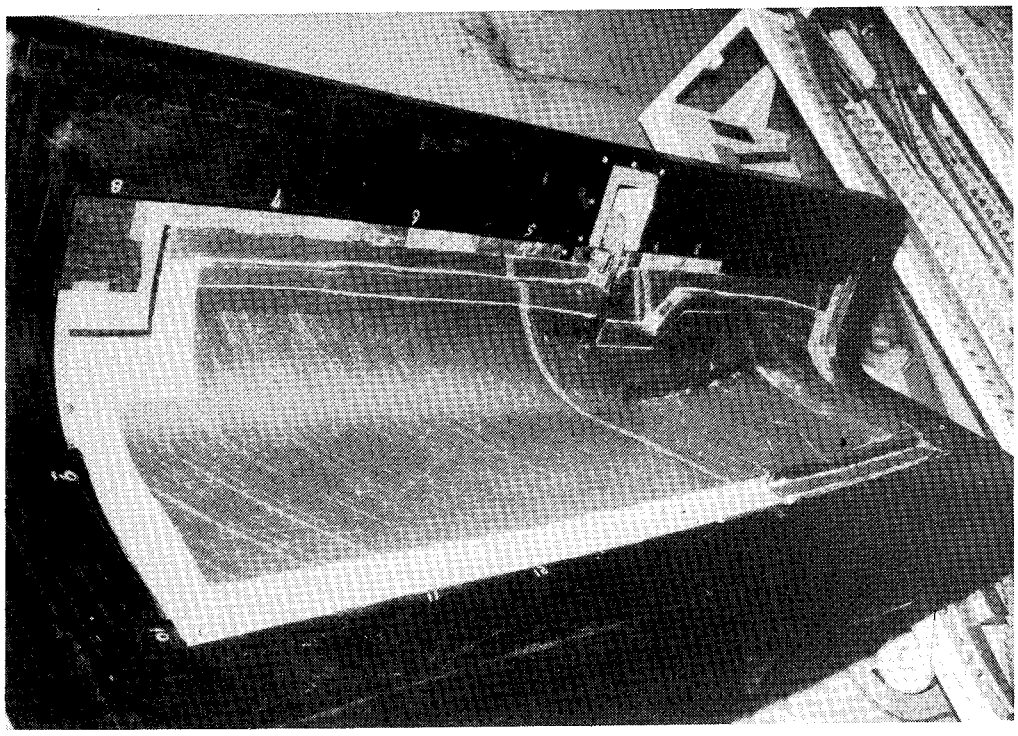

Figure 1.- Graphite door - inner skin layup.

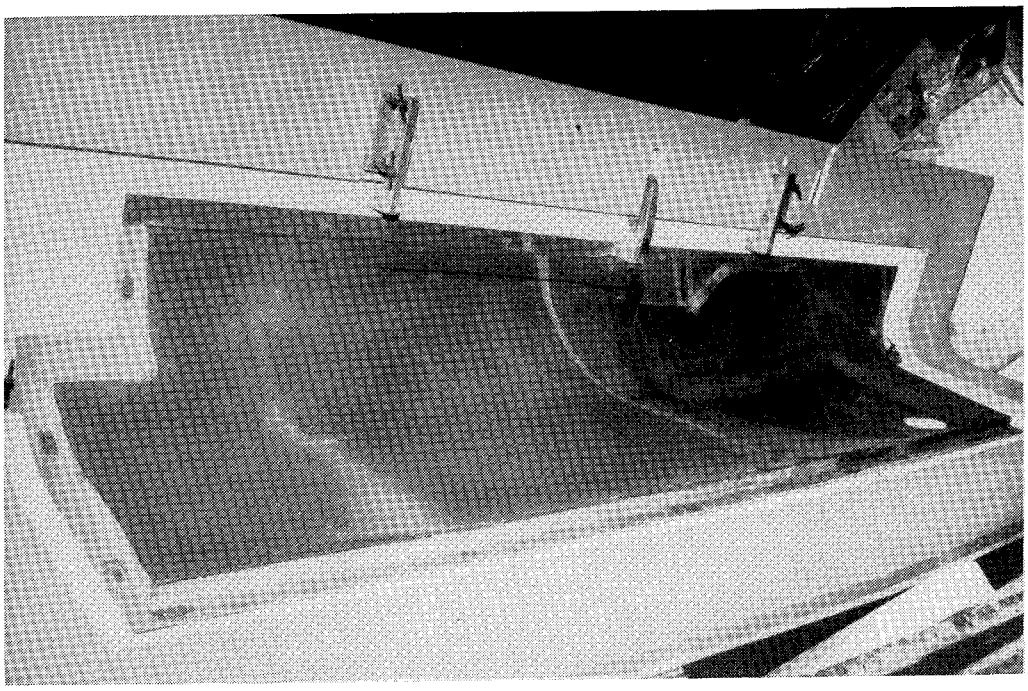

Figure 2.- Graphite door in assembly fixture.

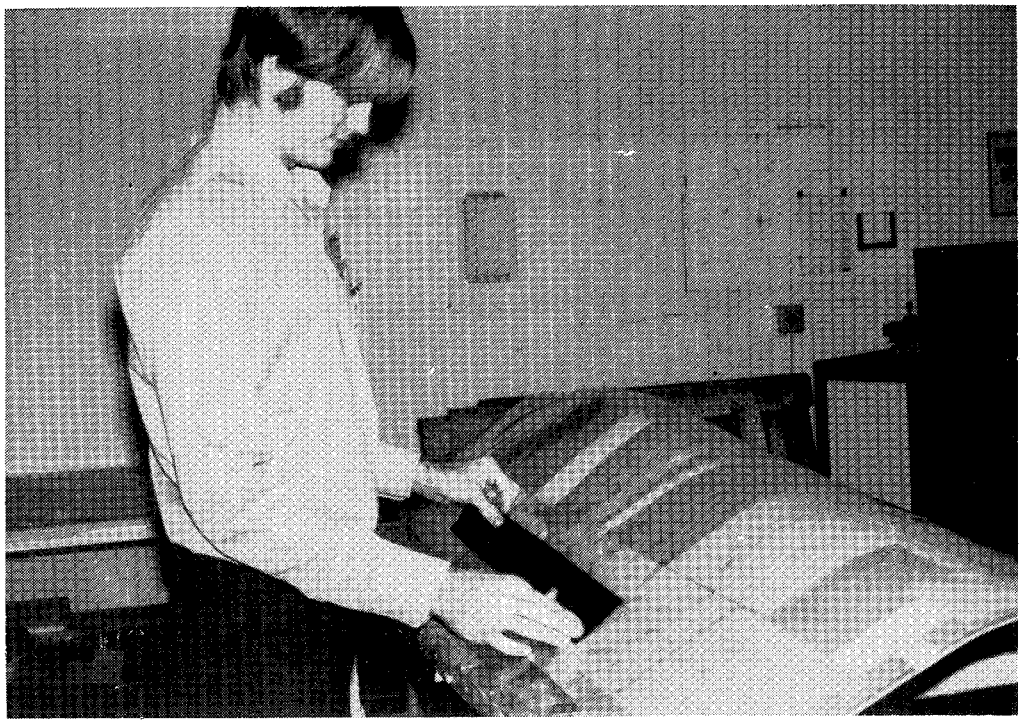

Figure 3.- Graphite door - layup on transfer tool.

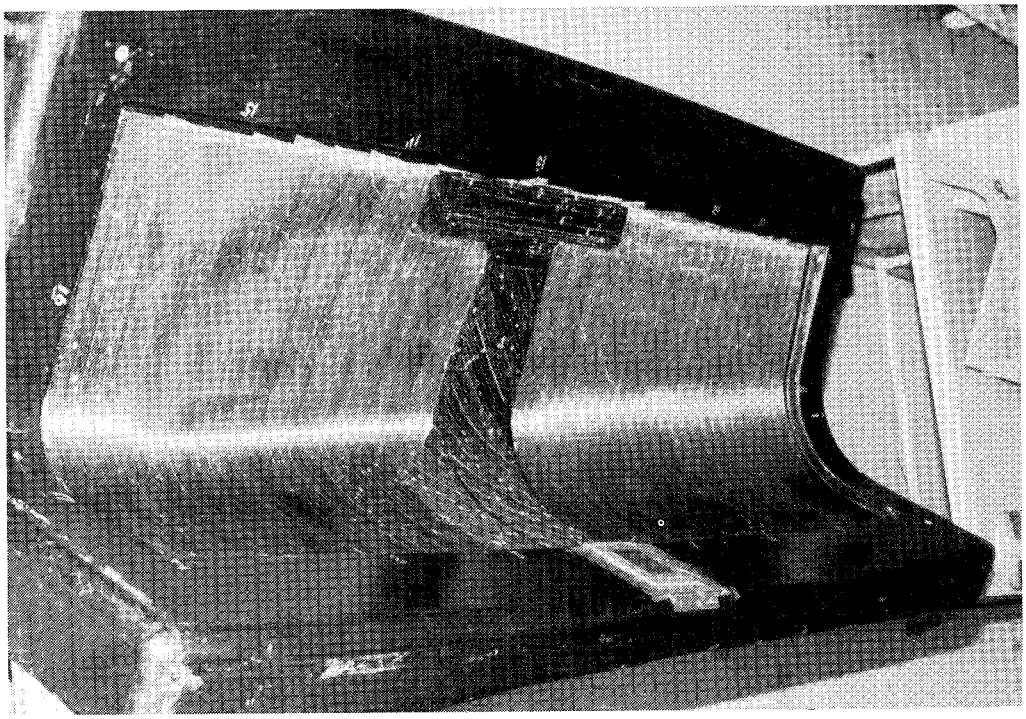

Figure 4.- Graphite door - outer skin layup.

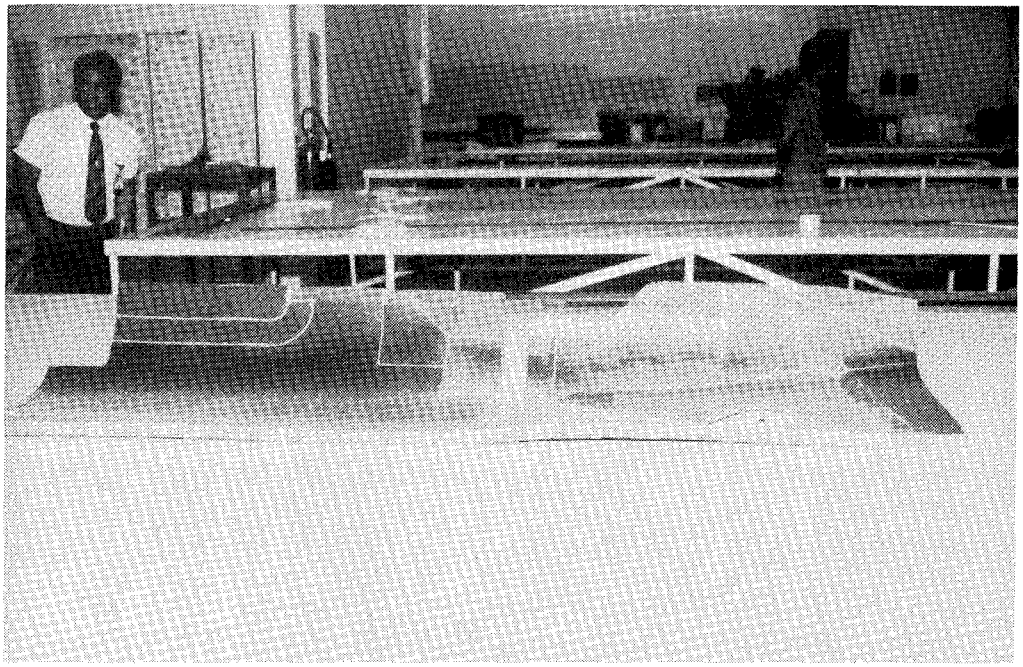

Figure 5.- Graphite door - core assembly.

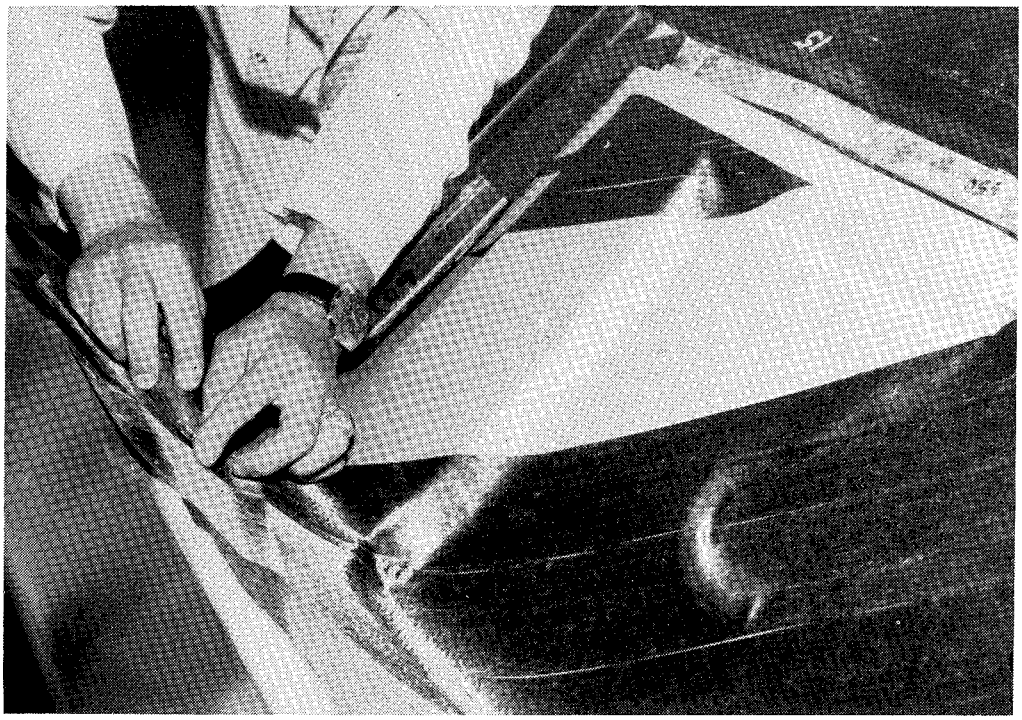

Figure 6.- Graphite door layup detail of inner skin - 45 degree ply.

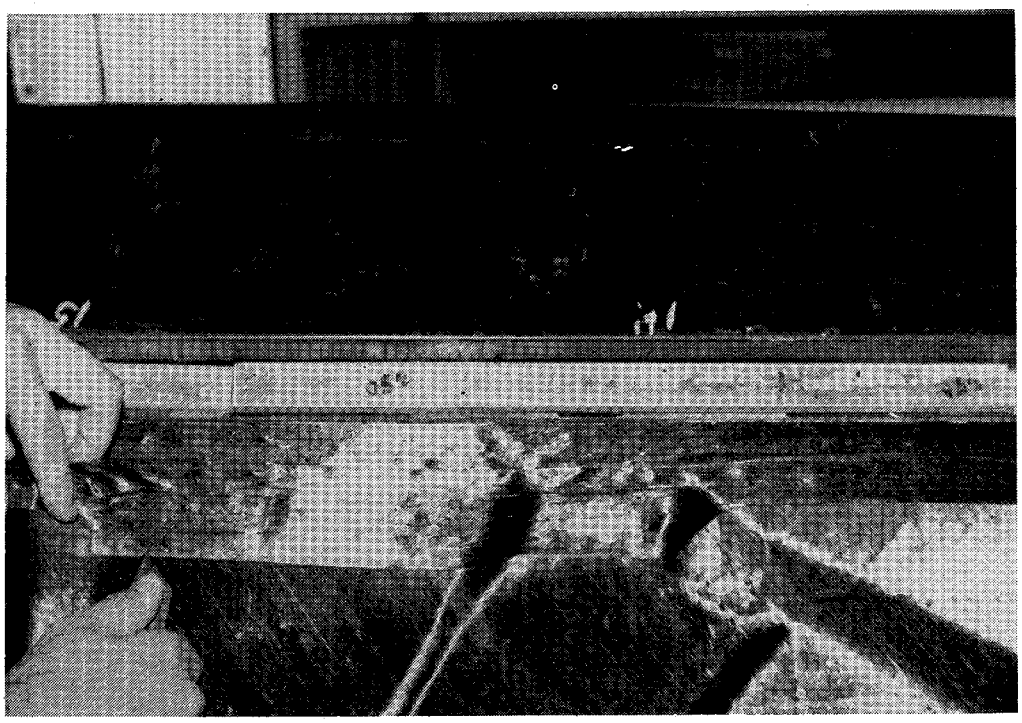

Figure 7.- Graphite door layup detail of inner skin - 0 degree ply.

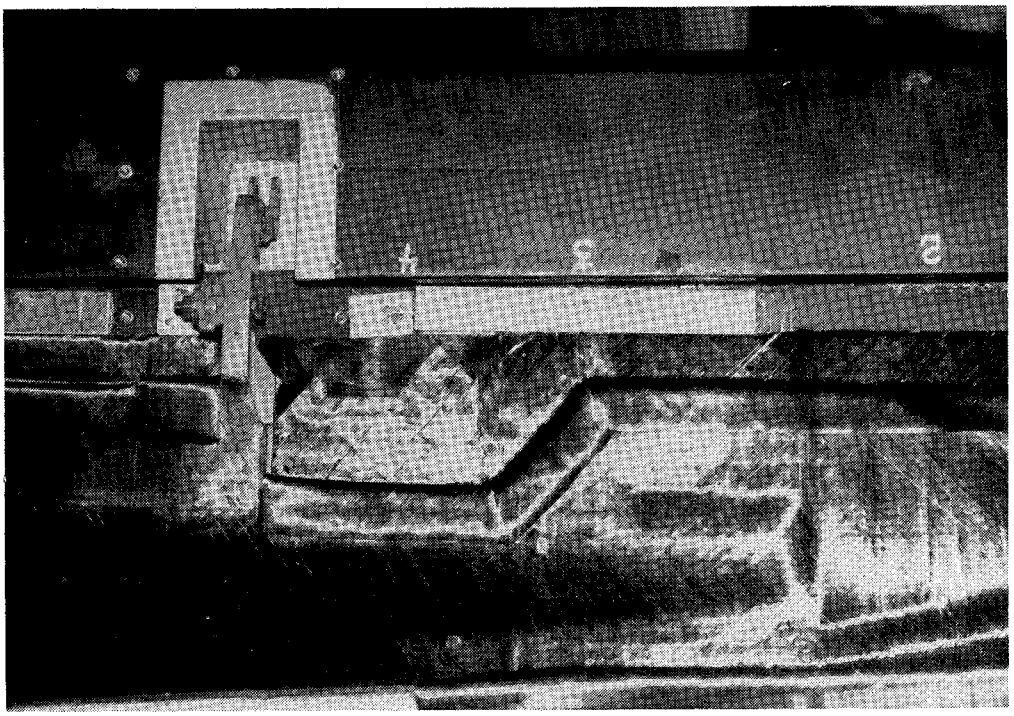

Figure 8.- Graphite door - pivot fitting and edge buildup.

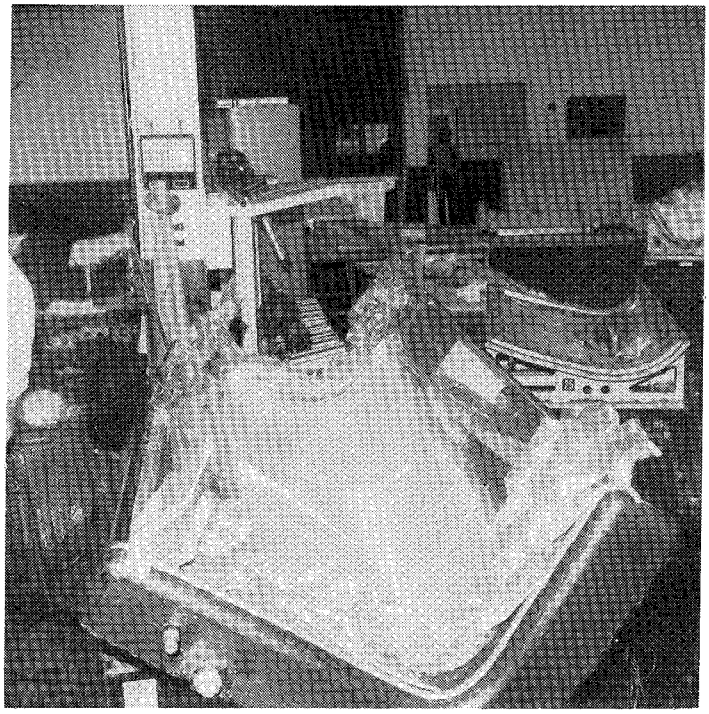

Figure 9.- Graphite door - outside skin with bag.

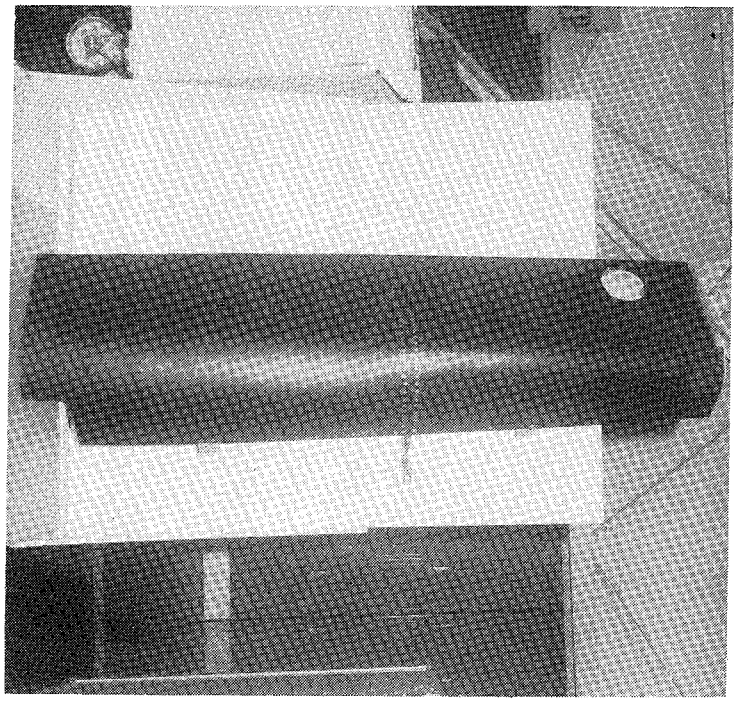

Figure 10.- Graphite door - outside view.

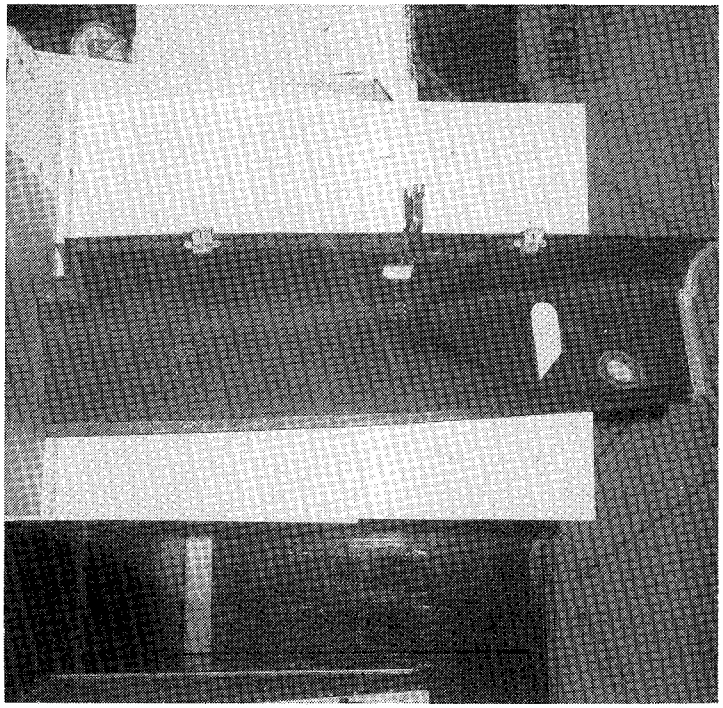

Figure 11.- Graphite door - inside view.

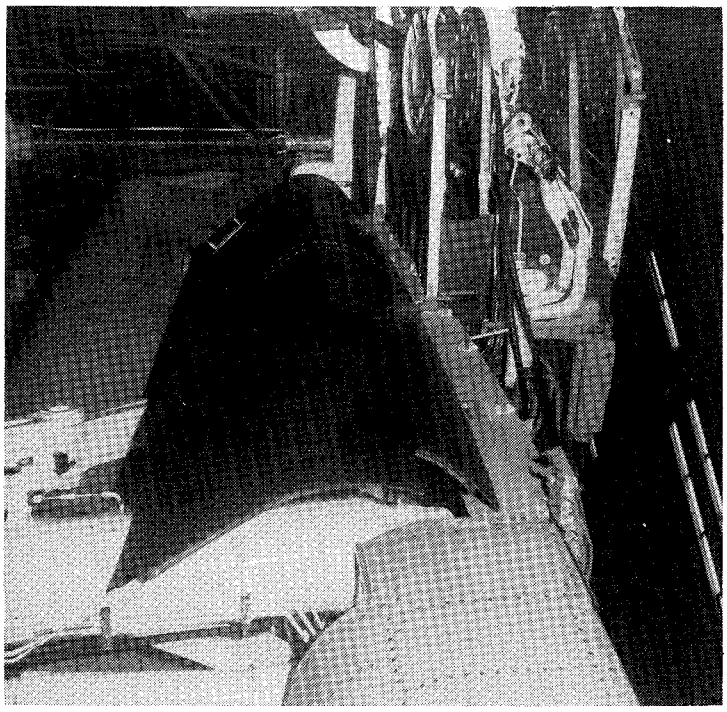

Figure 12.- Graphite door in place on ship - landing gear down.

A THERMALLY INERT CYLINDRICAL TRUSS CONCEPT

By Paul T. Nelson, TRW Systems and
Michael H. Krim, Perkin-Elmer Corp.

SUMMARY

A design approach incorporating a series of features tending to first minimize thermally induced distortions and then compensating for residual strains in the members is presented. Along with a rigorous application of athermalization, the design of a structurally efficient and producible truss is developed. The stability and structural requirements are based on optical requirements of the Large Space Telescope.

INTRODUCTION

The cylindrical truss concept described in this paper is designed to provide a stable support for the secondary mirror in a Ritchey-Cretien optical system. Stability requirements, on the order of microns, over the length of the structure are critical to optical performance.

The truss is a three-bay configuration having 16 struts per bay and three rings bounding the bays. The aft bay struts are directly connected to the primary mirror support ring as illustrated in Figure 1.

To meet stability requirements over the wide range of anticipated operational temperatures, graphite/epoxy has been selected as the basic material.

The design requirements applied to the truss are consistent with the Large Space Telescope (LST) requirements. While gross misalignments can be periodically corrected, temporal stability must be adequate so orbital temperature ripple and temperature changes caused by various viewing attitudes do not cause unacceptable system misalignment.

This paper primarily addresses the thermal stability problem. While stiffness and weight are important considerations, these structural aspects are straightforward.

SYMBOLS

R	mirror radius
S	length of a single bay
T	temperature or temperature change
α	coefficient of thermal expansion, CTE
Δ	decenter of truss
δ	lateral displacement of a single bay
Δf	defocus
ε	error
ℓ	length of a strut
ℓ_1	distance from primary to secondary mirror vertexes
ℓ_2	distance from primary mirror vertex to focal plane
μ	micrometer or micron

DESIGN REQUIREMENTS

Optical tolerances determine the stability requirements for the metering truss. In terms of truss performance, these may be expressed as despace, decenter, and tilt errors. The relationship between these error sources and defocus is given by:

$$\Delta f = \left\{ \begin{array}{l} \left[(2\ell_1 - R_1 + R_2) \dfrac{R_2}{2} + \left(\dfrac{R_1 R_2}{2} - R_2 \ell_1 \right) \right] \partial R_1 \\ + \left[(2\ell_1 - R_1 + R_2) \left(\dfrac{R_1}{2} - \ell_1 \right) - \left(\dfrac{R_1 R_2}{2} - R_2 \ell_1 \right) \right] \partial R_2 \\ + \left[(2\ell_1 - R_1 + R_2)(-R_2) - 2 \left(\dfrac{R_1 R_2}{2} - R_2 \ell_1 \right) \right] \partial \ell_1 \end{array} \right\} \div (2\ell_1 - R_1 + R_2)^2$$

The symbols are defined in Figure 1.

The radius of curvature changes, ∂R, are caused by both uniform ($\Delta \overline{T}$) and gradient ($\Delta T'$) temperature distribution changes in the mirrors

$$\partial R = R \alpha \Delta \overline{T} + \frac{R^2 \Delta \alpha \Delta \overline{T}}{h} + \frac{R^2 \alpha \Delta T'}{h}$$

The first term applies to the uniform growth of a uniform material, the second is due to bending in a uniform temperature field due to axial material inhomogeneities ($\Delta\alpha$), and the last term represents the bending of the mirror due to an axial (back-to-front) temperature difference.

After accounting for the ∂R terms and the change in the mechanical focal plane position, $\partial \ell_2$, only 186μ remains available for despace effects, which via the above equation limits $\partial \ell_1$ to 1.6μ (64 millionths of an inch). This error allocation is beyond the scope of this paper. This 1.6μ is further divided between two sources: local effects in the primary mirror mount area and growth of the truss. On an RSS basis, evenly dividing $\partial \ell_1$, the total axial change in length of the truss must not exceed 1.1μ.

Tilt and decenter tolerances, not developed in this paper, are 1 arc-second and 5μ respectively.

It should be noted that the Δf equation is an excellent preliminary design tool for structural engineers involved with telescope design.

The metering structure in the LST will experience many different temperature conditions. We have selected the hot and cold cases shown in Figure 2 as a design model. When the telescope is reoriented from one position to the other, the temperature change (ΔT) in the structure is equivalent to the difference in temperature distributions, as shown in the lower left corner. These changes could occur during an interrupted, or between successive, scientific observations. Dimensional stability must be maintained within the allowable limits in the presence of these changes to achieve satisfactory viewing periods.

To initially calibrate the design task, the following simplistic relationships were employed to identify preliminary expansivity requirements:

Axial displacement (despace) $\quad \Delta_A = \frac{1}{2}\,\alpha \ell \Delta T_1$

Lateral displacement (decenter) $\quad \Delta_L = \frac{\ell^2\,\alpha\,\Delta T_2}{2h}$

Angular displacement (tilt) $\quad \theta = \frac{\ell\,\alpha\,\Delta T_2}{h}$

From these equations the initial expansivities (α) are:

Despace	0.016×10^{-6}	$in/in/^{o}F$
Decenter	0.054×10^{-6}	$in/in/^{o}F$
Tilt	0.138×10^{-6}	$in/in/^{o}F$

The 0.016 despace value is the governing design requirement.

The remaining important design requirements are stiffness, strength, and weight. To preclude deleterious interaction with the pointing and control system, a minimum fixed-base first bending mode frequency of 25 Hz was established. The secondary mirror and ancillary optical and electronic equipment on the secondary support structure weigh 70 pounds. Load and safety factors are in accordance with Reference 1.

DESIGN APPROACH

For a number of reasons which we will not discuss here, the use of active thermal control techniques to reduce temperature fluctuations as a means of controlling distortion was not a satisfactory solution. This leaves the designer with four general areas in which he can operate to achieve dimensional control: 1) select low or near-zero CTE constructional materials, 2) apply athermalization techniques to kinematically compensate for undesirable dilations, 3) optimize the geometry to minimize the contribution of the more expansive elements such as joints and transverse CTE in secondary support arms, and 4) tailor individual component members to near-zero or other finite effective CTE values.

This paper discusses a truss structure for the LST. The tradeoffs between a shell and truss are outside the scope of this paper. Suffice to say that the primary reason a truss was selected over a shell configuration is because it is amenable to greater control over the ensemble expansivity. Because it does have many elements, one has the following options:

a) Assemble the parts and expect the probability that individual members cancel via randomness.

b) Measure and locate the members in optimal positions.

c) Measure, select, and reject.

d) Measure, adjust/tune members to near-zero CTE and assemble in optimal positions.

We believe, and will show, that the latter approach is the proper one to take when dealing with a structure of this size and of ±1 micron stability.

Material Selection

Since we know of no suitable constructional material with "zero" expansivitiy, we must settle for materials with near-zero CTE values. Because a high natural frequency of the truss is also a requirement, graphite/epoxy was selected as the most suitable basic material. Boron and glass cloth are also used in small amounts for property tailoring and to offset the negative CTE of the selected graphite/epoxy system. Table 1 shows a comparison of several low expansion materials. The graphite and boron composite properties are of typical unidirectional laminates. Tailoring can be accomplished to alter the properties by use of hybrid techniques or by adding cross plies.

Table 1. Low CTE Materials Comparison

	CTE (μ-in/in/^{o}F)	E/ρ (in x 10^{-6})
Invar 36	0.6	70
Unispan LR-35	0.3	70
Aluminum alloys	12.5	104
Titanium alloys	4.9	100
ULE	±0.016	124
Cer-Vit	±0.016	144
Graphite/epoxy (HM-S/934, unidirectional)	-0.38	530
Graphite/epoxy molding (hy MAT 7534)	0.23	150
Boron/epoxy	2.5	530
Glass cloth/epoxy	6.7	52

In theory, given the properties of the constituent graphite fibers and resin matrix, zero CTE laminates can be configured. However, material property variations, tolerances on resin content, and processing variables

of as much as ±0.05μ-in/in/^{o}F negate this as a possibility even under the tightest controls. Since the material properties cannot be specified without tolerances, the additional finesse of athermalization, geometry optimization, and component tuning is applied.

Design and analysis to date have been based on available materials test data. Because of the accuracy that we are interested in for the LST metering truss, the particular incoming materials batches would be partially characterized after receipt. These data would then be used to fine-tune the nominal truss design; e.g., cross-ply angles or adjust number of plies. Boron, Style 112 glass, Celanese chopped GY-70 fibers, and Hercules HM-S fibers are used. Fiberite 934 resin was selected because, based on available data, it appeared most suitable from a resin flow, outgassing, and microcracking point of view.

As indicated earlier, two characteristics that must be recognized by the designer in the application of graphite/epoxy to precision optical structures are:

a) Material and process variables can cause the α of the finished part to deviate as much as 0.05 x 10^{-6} in./in./^{o}F from the nominal value predicted by laminate analysis.

b) The variability of α with temperature ($d\alpha/dT$) could be a significant factor in a structure subjected to a 170^{o}F temperature gradient.

Solutions for both these problems have been developed and form the basis for the remainder of this paper. The solutions include the Dual-α Tuned Strut which is described later.

Athermalization

Athermalization is the technique of controlling the expansivity of an ensemble structure by the use of compensating expansions of individual elements. Figure 3 shows graphically how it works in a truss where it is desired to maintain a constant length although individual structural elements dilate under temperature change. To accomplish this it is necessary to understand the deformation mechanics.

Despace

The derivation for axial deformation may be found in Reference 2. With reference to Figure 4, the deformation of a single bay where the temperature gradient is linear from top to bottom rings is exactly:

$$\Delta S = \frac{1}{S}\left[\frac{1}{2}\ell^2\alpha_S + R^2\,\partial_R\,(\cos\theta - 1)\right](\Delta T_T + \Delta T_B)$$

ΔT_T = temperature change of top ring

ΔT_B = temperature change of bottom ring

This was obtained by differentiating S with respect to R_T, R_B and ℓ and setting ∂R equal to $R\alpha_R\,\Delta T_R$. Also for a circular truss, $R_T = R_B$. This implies that the strut temperature is equal to the average of the two bounding rings. This is not always true and the effect of $T_S \neq (T_T + T_B)/2$ on deformation will be discussed later in the discussion of athermalization errors.

For a three-bay truss, the axial deformation is as follows, where temperature subscripts apply to the first (main), second, third, and fourth rings:

$$\Sigma\Delta S = \frac{1}{S}\left[\frac{1}{2}\ell^2\alpha_S + R^2\alpha_R\,(\cos\theta - 1)\right](\Delta T_1 + 2\Delta T_2 + 2\Delta T_3 + \Delta T_4)$$

Decenter and Tilt

Using the exact expression for the displacement of a single bay, approximate equations describing decenter and tilt caused by a lateral (circumferential) gradient may be derived. With reference to Figures 1 and 5, it is apparent from elementary mechanics that $\rho = R/\varepsilon$ and $\varepsilon = \Delta S/S$ where ΔS is the displacement derived from Figure 4. By substitution:

$$\varepsilon = \frac{1}{S^2}\left(T_{R_1} + T_{R_2}\right)\left[\frac{1}{2}\ell^2\alpha_s + R^2\alpha_R\,(\cos\theta - 1)\right]$$

for a lateral gradient ΔT_n, i.e., $\pm T_1$, $\pm T_2$, etc.

$$T_{R_1} = \frac{\Delta T_1}{2}, \quad T_{R_2} = \frac{\Delta T_2}{2}$$

$$\therefore \varepsilon = \frac{1}{2S^2} \left(\Delta T_1 + \Delta T_2\right) \left[\frac{1}{2} \ell^2 \alpha_s + R^2 \alpha_R \left(\cos \theta - 1\right)\right]$$

Therefore the radius of curvature, ρ, is

$$\rho = \frac{2RS^2}{\left(\Delta T_1 + \Delta T_2\right) \left[\frac{1}{2} \ell^2 \alpha_s + R^2 \alpha_R \left(\cos \theta - 1\right)\right]}$$

$$\theta = \frac{S}{\rho} \text{ for small angles}$$

$$\theta = \frac{\left[\frac{1}{2} \ell^2 \alpha_s + R^2 \alpha_R \left(\cos \theta - 1\right)\right] \left(\Delta T_1 + \Delta T_2\right)}{2RS}$$

Further, since $\delta = S^2/2\rho$

$$\delta = \frac{\left[\frac{1}{2} \ell^2 \alpha_s + R^2 \alpha_R \left(\cos \theta - 1\right)\right] \left(\Delta T_1 + \Delta T_2\right)}{4R}$$

Extending the above single bay analysis to a three-bay truss and referring to Figure 6, it is apparent for small angles that the tilt and decenter are cumulative. Hence,

$$\theta_4 = \frac{\Delta T_1 + 2\Delta T_2 + 2\Delta T_3 + \Delta T_4}{2RS} \left[\frac{1}{2} \ell^2 \alpha_s + R^2 \alpha_R \left(\cos \theta - 1\right)\right]$$

Also, since

$$\Delta = \delta_2 + \theta_2 \left(2S\right) + \delta_3 + \theta_3 S + \delta_4$$

$$\Delta = \frac{\Delta T_1 + 2\Delta T_2 + 2\Delta T_3 + \Delta T_4}{4R} \left[\frac{1}{2} \ell^2 \alpha_s + R^2 \alpha_R \left(\cos \theta - 1\right)\right]$$

$$+ S \left\{ \frac{\Delta T_1 + \Delta T_2}{2RS} 2 \left[\frac{1}{2} \ell^2 \alpha_s + R^2 \alpha_R \left(\cos \theta - 1\right)\right]\right.$$

$$+ \frac{\Delta T_2 + \Delta T_3}{2RS}\left[\frac{1}{2}\ell^2\alpha_s + R^2\alpha_R\ (\cos\theta - 1)\right]\Bigg\}$$

Rearranged,

$$\Delta = \frac{\left[\frac{1}{2}\ell^2\alpha_s + R^2\alpha_R\ (\cos\theta - 1)\right]}{4R}(5\Delta T_1 + 8\Delta T_2 + 4\Delta T_3 + \Delta T_4)$$

CTE Requirements and Potential Errors

An examination of the despace, decenter, and tilt equations show that the distortion in all three cases will be zero when the following holds true:

$$\frac{1}{2}\ell^2\alpha_s + R^2\ (\cos\theta - 1)\,\alpha_R = 0$$

From this it appears that a thermally inert structure for any material systems will exist if

$$\frac{\alpha_R}{\alpha_S} = -\frac{\ell^2}{2R^2\ (\cos\theta - 1)}$$

Using the dimensions of our design model,

$$\frac{\alpha_R}{\alpha_S} = -\frac{(71)^2}{2(56)^2\ (\cos 22.5 - 1)} = 10.58$$

The above holds true, however, only if

$$\Delta T_s = \frac{1}{2}\left(\Delta T_{R_T} + \Delta T_{R_B}\right)$$

(linear strut gradient) which is not necessarily true in a transient environment. In fact, the higher the nominal α values selected, the more sensitive the system becomes.

Variations in member expansivities from a design nominal or measurement uncertainties associated with tuning elements must be anticipated.

Substituting the ℓ, R, and θ parameters into the $\Sigma\Delta S$ equation shown earlier,

$$\Delta S = 37.36\ (\alpha_S + \varepsilon_S) - 3.52\ (\alpha_R \pm \varepsilon_R) \times (\Delta T_1 + 2\Delta T_2 + 2\Delta T_3 + \Delta T_4)$$

And since, from the temperature model, Figure 2,

$$(\Delta T_1 + 2\Delta T_2 + 2\Delta T_3 + \Delta T_4) = 84$$

the above can be expressed as:

$$\Delta S = 3136\ (\alpha_S \pm \varepsilon_S) - 295.6\ (\alpha_R \pm \varepsilon_R)$$

If α_S and α_R, the nominal values are balanced, the despace error caused by α errors (ε) is

$$\Delta\Delta S = 3136\ (\pm \varepsilon_S) - 295.6\ (\pm \varepsilon_R)$$

Assuming a random spread of errors among all the members

$$\Delta\Delta S = \left[\left(3136\ \frac{\varepsilon S}{\sqrt{2}}\right)^2 + \left(295.6\ \frac{\varepsilon R}{\sqrt{2}}\right)^2\right]^{1/2}$$

For a ring variability of $\pm 0.05 \times 10^{-6}$ in./in./^{o}F, assuming it will not be tuned like the struts and setting $\Delta\Delta S$ to two-thirds of the total despace budget (this is the major contributor in a balanced truss design):

$$27 \times 10^{-6} = \left[(2217\ \varepsilon_S)^2 + 1.1 \times 10^{-10}\right]^{1/2}$$

$$\varepsilon_S = 0.012 \times 10^{-6}\ \text{in./in./}^{o}\text{F}$$

Thus, the strut and ring specifications become:

$$\alpha_S = 0.012_{max} \pm 0.012\ \mu\text{-in./in./}^{o}\text{F}$$

$$\alpha_R = 0.125_{max} \pm 0.05\ \mu\text{-in./in./}^{o}\text{F}$$

Lower values of α_S and α_R nominals are preferable. In any case, the part-to-part tolerances of ±0.012 and ±0.05 still apply. Note that if the struts are built such that $\alpha_S = 0 \pm 0.012$ then the rings can be 0 ± 0.125. Thus the tuned struts, described in the next section, relax the more complex ring design and manufacturing requirements.

Another potential error source as previously mentioned is due to a nonlinear temperature gradient in the strut. For a balanced system where

$$\frac{1}{2} \ell^2 \alpha_S = - R^2 \alpha_R (\cos \theta - 1)$$

a temperature difference between the actual strut temperature and $(\Delta T_T + \Delta T_B)/2$, denoted as $\Delta T_{\ell/R}$, will produce a despace error,

$$\varepsilon\Delta_S = \frac{1}{S}\left(\alpha_S \frac{\ell^2}{2}\right) \Delta T_{\ell/R}$$

or

$$\varepsilon\Delta_S = \frac{1}{S}\left[R^2 \alpha_R (\cos \theta - 1)\right] \Delta T_{\ell/R}$$

For all three bays, where S = 67.7 in., R = 56 in. and $\theta = 22.5^o$ (our design model) the error is:

$$\Sigma\varepsilon\Delta_S = 10.58\, \alpha_R\, \Delta T_{\ell/R}$$

The solution to this equation for a range of α_R and Δ_T is shown in Table 2.

It was assumed $\Delta T_{\ell/R}$ would not exceed 5^oF. Figure 2 illustrates the temperature excursion of the rings after changing orientation. Note that there is as much as 21^oF end-to-end differential which may not be at all times linear.

The horizontal bound was placed below 13μ-inches which is one-third of the total despace allowable. Hence the <u>maximum</u> design value for the ring expansivity is 0.125×10^{-6} in./in./^oF. This results in a strut α of

$$\alpha_S = \frac{0.125}{10.58} \times 10^{-6}$$

$$\alpha_S = 0.012 \times 10^{-6} \text{ in./in./}^{o}\text{F}$$

Obviously, lower values of α_R and α_S will decrease sensitivity to this effect. The best system would have α_R and α_S equal to zero. However, this is not as easy to accomplish with a ring, or ring segments, as it is with straight strut elements because of the curvature in the rings.

Table 2. Errors Due to Nonlinear Strut Gradient, $\Delta T_{\ell/R}$ as a Function of α_R, $\Sigma\varepsilon\Delta_S \times 10^6$ in.

αR \ $\Delta T_{\ell/R}$	1	2	3	4	5	6
0.5	5.29	10.5	15.9	21	26.5	31.7
0.25	2.64	5.25	7.95	10.5	13.25	15.85
0.125	1.32	2.62	3.97	5.25	6.62	7.92
0.062	0.66	1.31	1.98	2.62	3.31	3.96
0.032	0.33	0.65	0.99	1.31	1.65	1.98
0.016	0.16	0.33	0.49	0.66	0.83	0.99

CTE Tuning

The rings are fabricated in one-eighth sections and after appropriate thermal cycling, are tested to determine their effective CTE along the chord from one end to the other. For the given geometry, the effective CTE required for mating the four struts and joint fittings is approximately one-tenth (α_R/α_L = 10.58). Since the effective lengths of the end fittings are small by comparison with the struts, and moreover because their CTE is controlled with reasonably good accuracy, their "nominal" value is used in computing the required CTE for the struts to obtain the required effective CTE for the combination. This additional finesse enhances, but is not absolutely critical to, truss thermal stability. As described earlier, a strut expansivity of $\pm 0.012 \times 10^{-6}$ in./in./^{o}F allows relaxation of the ring requirements at the expense of approximately 0.6 μ despace. The local tuning described here reduces this to almost zero.

Three strut tuning principles were considered. The Dual-Alpha concept is described in detail, and a variable-alpha method is briefly presented and a tunable end-fitting principle is described in Reference 3.

Dual-Alpha Strut

The Dual-α Strut is a relatively simple concept which enables the attainment of a specific expansivity from parts whose as-cured α variability exceeds the design allowables.

The concept is illustrated in Figure 7 which shows a single strut constructed (laminated) so the expansivities on either side of a transition zone bound the desired end-item expansivity. All tuning (i.e., α-adjustment) operations are performed in the post-cured condition, thus accounting for all material and process variables. Tuning is accomplished using the as-cured material only. Additional parts or tuning "spacers" which usually are of a different material and different thermal diffusivity are not required. This enhances stability in a <u>transient</u> thermal environment.

The laminate design and laminate process controls are such that the properties shown in the figure are achieved when a zero-expansivity member is desired, for example. Tuning is based on the following equation:

$$\alpha_0 = \frac{\alpha_1 \ell_1 + \alpha_2 \ell_2}{\ell_0}$$

and when $\alpha_0 = 0$

$$\ell_1 = -\frac{\alpha_2}{\alpha_1} \ell_2$$

Since ℓ_2 equals $\ell_0 - \ell_1$

$$\ell_1 = -\frac{\alpha_2}{(\alpha_1 - \alpha_2)} \ell_0$$

The tuning operations are performed in the order described below:

Step 1 Measure the expansivity (α) of either side of the initially oversize strut (using a Fizeau interferometer).

Step 2 Solve for ℓ_1 from the above equation and measure it from the transition zone.

Step 3 Trim side ℓ_1 to length.

Step 4 From the end of ℓ_1 measure back ℓ_0 and trim off side ℓ_2.

That is all that is required to tune the strut to zero expansivity in this example.

It should be noted that a step 5 will be performed until confidence in the tuning procedure is developed.

Step 5 Measure the overall expansivity (α_0) using a long path dilatometer.

Scatter, or variability, in the achieved α_0 depends on the precision with which α_1 and α_2 are measured. Using high-finesse Fizeau interferometry and a frequency stabilized laser, coefficient of expansion measurements have been made at Perkin-Elmer to an accuracy of 1×10^{-8} (Reference 1). The effect of this error on the overall strut behavior was investigated.

It was assumed that α' in the equation

$$\ell_1 = - \frac{\alpha_2'}{\alpha_1' - \alpha_2'} \ell_0$$

could either represent zero measurement error or an error of (+) or (-) 1×10^{-8}. Thus the length ℓ_1 could be trimmed to an erroneous value. The net effect of these errors was calculated using

$$\alpha_0 = \frac{\alpha_1 \ell_1 + \alpha_2 \ell_2}{\ell_0}$$

In this equation, $\alpha_{1,2}$ did <u>not</u> include the measurement error. This error was applied only in the trimming equation. Table 3 shows the results obtained from these calculations.

Note that for the combinations shown in Table 3, the $\pm 0.012 \times 10^{-6}$ tolerance is satisfied. This will be true for all combinations. Further, it may be inferred that it is not necessary to have knowledge of the exact center of the transition zone.

Table 3. α_0 Error Due to α_1 and α_2 Measurement Errors

α_1 0.05×10^{-6}
α_2 -0.05×10^{-6} (ACTUAL VALUES)

α'_1	0.05	0.04	0.06
α'_2	-0.05	-0.04	-0.06

(MEASURED VALUES) $\times 10^{-6}$

Combinations	ℓ_1	ℓ_2	α_0
0.05/-0.05	35 In.	35 In.	0×10^{-6}
0.05/-0.04	31.1	38.9	-0.00557
0.05/-0.06	38.1	31.8	0.0045
0.04/-0.05	38.9	31.1	0.00557
0.04/-0.04	35	35	0
0.04/-0.06	42	28	0.01
0.06/-0.05	31.8	38.1	-0.0045
0.06/-0.04	28	42	-0.01
0.06/-0.06	35	35	0

α_1 $.05 \times 10^{-6}$
α_2 -0.01×10^{-6} (ACTUAL VALUES)

α'_1	0.05	0.04	0.06
α'_2	-0.01	0	-0.02

(MEASURED VALUES) $\times 10^{-6}$

Combinations	ℓ_1	ℓ_2	α_0
0.05/-0.01	11.66 In.	58.33 In.	0×10^{-6}
0.05/ 0	0	70	-0.01
0.05/-0.02	20	50	0.0071
0.04/-0.01	14	56	0.002
0.04/ 0	0	70	-0.01
0.04/-0.02	23.33	46.66	0.01
0.06/-0.01	10	60	-0.0014
0.06/ 0	0	70	0
0.06/-0.02	17.5	52.5	0.005

α_1 0.01×10^{-6}
α_2 -0.01×10^{-6} (ACTUAL VALUES)

α'_1	0.01	0	0.02
α'_2	-0.01	0	-0.02

(MEASURED VALUES) $\times 10^{-6}$

Combinations	ℓ_1	ℓ_2	α_0
0.01/-0.01	35 In.	35 In.	0×10^{-6}
0.01/ 0	0	70	-0.01
0.01/-0.02	46.66	23.33	0.0033
0/-0.01	70	0	0.01
0/ 0	-	-	0.01 or -0.01
0/-0.02	70	0	0.01
0.02/-0.01	23.33	46.66	-0.0033
0.02/ 0	0	70	-0.01
0.02/-0.02	35	35	0

α_1 0.01×10^{-6}
α_2 -0.01×10^{-6} (ACTUAL VALUES)

α'_1	0.01	0	0.02
α'_2	-0.1	-0.09	-0.11

(MEASURED VALUES) $\times 10^{-6}$

Combinations	ℓ_1	ℓ_2	α_0
0.01/-0.1	63.64 In.	6.36 In.	0×10^{-6}
0.01/-0.09	63	7	-0.001
0.01/-0.11	64.17	5.833	0.0008
0/-0.1	70	0	0.01
0/-0.09	70	0	0.01
0/-0.11	70	0	0.01
0.02/-0.1	58.33	11.66	-0.0083
0.02/-0.09	57.27	12.72	-0.0099
0.02/-0.11	59.23	10.76	-0.0069

Effects of Axial Gradients on Dual-α Struts

In the preceding section, it was shown how the struts could be tuned for zero-expansivity when the temperature change is uniform along the strut length. The effect of an axial gradient on a strut tuned in this manner results in an apparent expansivity. The value of this "error" was computed for a variety of α_1 and α_2 combinations. For most combinations, the error is acceptably small.

Consider a strut subjected to the temperature change shown in Figure 8. The total expansion is:

$$\Delta \ell_0 = (\alpha_1 \ell_1 + \alpha_2 \ell_2) \ \Delta \overline{T} + \alpha_1 \ell_1 \ \frac{T_3}{2} + \alpha_2 \ell_2 \left(T_3 + \frac{T_2 - T_3}{2} \right)$$

where T_2 and T_3 are measured from T_1.

$$\Delta \ell_0 = (\alpha_1 \ell_1 + \alpha_2 \ell_2) \ \Delta \overline{T} + \alpha_1 \ell_1 \ \frac{T_3}{2} + \alpha_2 \ell_2 \left(\frac{T_2 + T_3}{2} \right)$$

Since $T_2 \equiv \Delta T'$ and $T_3 = \ell_1 / \ell_0 \ \Delta T'$,

$$\Delta \ell_0 = (\alpha_1 \ell_1 + \alpha_2 \ell_2) \ \Delta \overline{T} + \frac{1}{2} \left[\alpha_1 \ \frac{\ell_1^{\,2}}{\ell_0} + \alpha_2 \ell_2 \ \left(1 + \frac{\ell_1}{\ell_0} \right) \right] \Delta T'$$

For a $\Delta \overline{T}$ balance,

$$\Delta \ell_0 = \frac{1}{2} \left[\alpha_1 \ \frac{\ell_1^{\,2}}{\ell_0} + \alpha_2 \ell_2 \ \left(1 + \frac{\ell_1}{\ell_0} \right) \right] \Delta T'$$

and, since $\ell_1 = - \alpha_2 / \alpha_1 \ \ell_2$ and $\ell_0 = \ell_1 + \ell_2$, the equation finally becomes

$$\Delta \ell_0 = \frac{1}{2} \alpha_2 \ell_2 \ \Delta T'$$

Dividing by ℓ_0 and setting

$$\frac{\ell_2}{\ell_0} = - \frac{\alpha_1}{\alpha_1 - \alpha_2}$$

the expression for $\alpha_{0_{\text{effective}}}$ is

$$\alpha_{0_{\text{eff}}} = \left| \frac{\alpha_1 \alpha_2}{2(\alpha_1 - \alpha_2)} \right|$$

The solution to this equation, for a range of α values is shown in Table 4. There are combinations in this table which are out of tolerance. However, in practice the struts will be arranged with alternating high and low α ends as shown in Figure 9. It was shown (Reference 2) that this further reduces $\alpha_{0_{eff}}$ for a strut pair by about a factor of 10. This is because the effective α of an opposing pair is

$$\alpha_{0_{eff\text{-}pair}} = \frac{1}{2}\left[\frac{\alpha_1\alpha_2}{\alpha_1 - \alpha_2} - \frac{\alpha_3\alpha_4}{\alpha_3 - \alpha_4}\right]$$

where

$\alpha_1 = +$

$\alpha_2 = -$

$\alpha_3 = +$

$\alpha_4 = -$

as shown in Figure 8.

Table 4. α_0 Errors Due to α_1 and α_2 Errors When an Axial Gradient Exists

$$\alpha_{0_{eff}} = \left|\frac{\alpha_1\alpha_2}{2(\alpha_1 + \alpha_2)}\right|$$

	α_2										
α_1	0.1	0.09	0.08	0.07	0.06	0.05	0.04	0.03	0.02	0.01	0
0.1	0.025	0.024	0.022	0.021	0.019	0.017	0.014	0.011	0.008	0.004	0
0.09	0.024	0.023	0.021	0.019	0.018	0.016	0.014	0.011	0.008	0.004	0
0.08	0.022	0.021	0.02	0.019	0.017	0.015	0.013	0.011	0.008	0.004	0
0.07	0.021	0.019	0.019	0.018	0.016	0.015	0.013	0.011	0.008	0.004	0
0.06	0.019	0.018	0.017	0.015	0.015	0.014	0.012	0.010	0.008	0.004	0
0.05	0.017	0.016	0.015	0.015	0.014	0.013	0.011	0.009	0.007	0.004	0
0.04	0.014	0.014	0.013	0.013	0.012	0.011	0.01	0.009	0.007	0.004	0
0.03	0.011	0.011	0.011	0.011	0.010	0.009	0.009	0.008	0.006	0.004	0
0.02	0.008	0.008	0.008	0.008	0.008	0.007	0.007	0.006	0.005	0.004	0
0.01	0.004	0.004	0.004	0.004	0.004	0.004	0.004	0.004	0.003	0.003	0
0	0	0	0	0	0	0	0	0	0	0	0

Alternatively, the struts could be tuned for a $\Delta T'$, rather than a $\Delta\overline{T}$, balance by setting

$$\ell_1 = \frac{-\frac{\alpha_2}{\alpha_1}\ell_2 \pm \sqrt{\left(\frac{\alpha_2}{\alpha_1}\ell_2\right)^2 - 4\frac{\alpha_2}{\alpha_1}\ell_2\ell_0}}{2}$$

if the gradient (slope) is reasonably constant over a range of nominal temperatures. Of course there will now be an error in the uniform soak, or $\Delta\overline{T}$ balance. It is believed that the former approach, coupled with alternating strut ends is preferable as it accounts for both components of temperature change.

Variable-Alpha Structure

The variable-alpha principle is based on the laminate property variation as a function of the cross-ply angle. This is demonstrated in Figure 10 for three types of structure where the laminate configuration is $[0_3/\theta/90_2/-\theta/0_3]$ and θ varies uniformly from 40 degrees at one end to 56 degrees at the other. The corresponding CTE varies from -0.06 in./in./in./^{o}F at one end to +0.06 in./in./in./^{o}F at the other as shown in Figure 10b The CTE at the midsection is zero. Figure 10c shows a method for tuning a structural element to a desired plus or minus CTE and specified length, ℓ_o.

The variable-alpha principle lends itself to a highly producible strut, laying successive tapes of variable-angle laminate so that the rectangular tapes overlap slightly. The tubes can be rolled, tape wound, or laid by hand. It is an alternate to the foregoing dual-α principle and much of the dual-α discussion applies to variable-α structure. The dual-α was selected because of higher stiffness to weight ratio and lower thermal stresses.

LAMINATE CONFIGURATIONS AND SELECTION CRITERIA

Fiber types, resins, and laminate configurations were selected uniquely for each candidate structural member. Criteria used in selection of constituent materials and laminate configuration included: 1) availability of supporting test data; 2) adequate safety margins due to external, induced,

and thermal loads; 3) sensitivity due to material and process variations; 4) outgassing characteristics; 5) physical and mechanical properties; 6) stability of property characteristics after reasonable and appropriate thermal cycling, and 7) their adaptability to the part for which selected.

The specific fiber types selected for particular applications on the basis of the above criteria include Hercules HM-S, Celanese GY-70, AVCO Boron, and Style 112 glass. Fiberite 934 resin is used throughout in the laminates while Epon 934 adhesive is used for some secondary bonding applications.

In addition to the aforementioned selection criteria, the hybrid laminates of HM-S, boron, and glass was chosen on the basis of high specific stiffness (E/ρ) and suitable CTE. The pure HM-S/934 laminate configuration selection was also influenced by the combination of high stiffness (E) and near-zero CTE. Use of hy-MAT 7534 is based on low CTE and producibility.

The materials and laminate configurations selected for concepts presented here have the properties shown in Table 5.

Table 5. Nominal Laminate and Molding Properties of Materials Selected for Specific Designs (Detail Concepts)

	CTE Microstrain/^{o}F	E_x MSI	F_x KSI
HMS B HMS $[112/0_6/0/0_6/112]$	-0.07	30.2	115
HMS B HMS HMS HMS HMS HMS $[112/0_6/0/0_2/112/0/112/0/112/0/112/0/112]$	+0.06	30.5	113
HMS/934 $[0_3/\pm 64/\mp 64/0_3]$	0	18.5	52
hy MAT 7534	0.23	9.2	20
HMS/934 $[0_3/+48/90_2/-48/0_3]_s$	0	20.0	50

Note: 112 - Style 112 glass
HMS - Hercules HM-S fiber
B - Boron fiber

DETAIL CONCEPTS

The detail concepts described are the component parts of a right cylinder truss that meet the requirements stated earlier. Studies leading to these particular concepts were oriented to developing a truss structure that minimized thermal strain in constituent members. However, recognizing that materials and processes are imperfect, even under the best of controls, cost effective means of fine tuning compensating members is incorporated.

Ring

The base of the truss is attached to an isothermal metallic main ring. Each bay is separated by a truss-core composite ring and there is a similar truss-core ring at the end. The truss-core concept is shown in Figure 11. It is made of HM-S/934 and has $[0_3/\pm 64/\mp 64/0_3]_3$ caps and $[0_3/\pm 64/\mp 64/0_3]$ diagonal core members. The CTE is theoretically zero. Cap sections and core sections are made in one-eighth sections of a circle and are secondarily bonded together. Since all members of the truss core ring are made of similar materials and laminate configurations, distortions in the ring due to differential thermal forces are virtually nonexistent.

Strut

The struts are designed for tuning to compensate for unavoidable CTE tolerances in the rings. The dual-alpha strut is made with the two laminate configurations as previously described. Its initial length is sufficient to tune the strut CTE positively or negatively sufficient to compensate for maximum allowable variations in the interfacing rings. The inner 10 plies of both sections are identical. From there outward, layers of Style 112 glass cloth are interleaved to raise the CTE of the larger cross-section. Since all HM-S fibers and the boron lamina are unidirectional, a high specific stiffness ($E/\rho > 500 \times 10^6$) is obtained. The higher CTE of the single boron layer makes it a powerful compensator for the negative expansivity of the graphite and also enhances the axial stiffness.

Ring-Strut Joint Fitting

The fitting is short in the longitudinal direction and has a low CTE ($\alpha < 0.23$ strain/^{o}F); therefore, its expansivity and contribution to distortion is minimized. It is molded hy-MAT 7534 and made in sections as shown in Figure 12. The wedge allows the truss assembly to operate without elastically deforming any members, and when located, the wedge is bonded with the strut members. Although not considered necessary, the wedge, and hence the entire joint, can be readily locked in place with mechanical fasteners such as a graphite/epoxy dowel.

The short axial length of the fitting reduces the effect of its axial contribution to expansion but its effect is further reduced by its consideration in tuning the dual-α struts. Thus, the effective CTE of the struts from ring to ring is optimized by accounting for the fittings. Anomalies that sometimes occur in bonded joints is kept to a minimum because of their short lengths.

Secondary Mirror Support

The secondary mirror support, as shown in Figure 13, is a very critical element of the truss. All of the finesse applied to the main truss structure could be lost in a poor secondary mirror support system. In the main truss, the main concern was to reduce to zero all axial expansion. Now at the end of the truss it is necessary to not only match the circumferential expansion of the ring but also maintain X-axis stability using anisotropic materials.

To accomplish this we have indeed matched the circumferential expansion of the ring by using the same laminate configuration. Axial stability of the secondary mirror mounting plane is achieved by setting it in the plane of the outer ring and making the entire support structure symmetrical about that plane. Thus, the higher transverse expansion in the radial arms and hub caused by the higher transverse CTE ($\alpha_y > \alpha_x$) is balanced about the ring plane. Accordingly, the nominal movement of the secondary mirror mounting plane is zero. Notwithstanding the above, consideration was also given to minimizing α_y, even though the geometry arrangement tends to negate its effect.

Another critical area of the secondary support structure is the ring-arm attachment. As previously discussed, a low-expansion molded fitting is used to join the struts to the ring. The effective axial length of the fittings was minimized to reduce their contribution to error and over and above that, their expansion was compensated for in tuning the struts to obtain the desired overall effective CTE of the strut-fitting systems for athermalization.

The same concern exists in the fitting-secondary support radial arm attachments. The sensitivity of the attachment does not warrant athermalization because of the impact of small changes in ring radius. It is, nonetheless, prudent to practically minimize this distortion. This is done by narrowing the inside ring flanges at the junctures of the radial arms so that the arms can attach directly to the fittings and, thus, the high transverse expansion of the flange is not in the load path. The arms have cutouts allowing them to attach to the fitting inside the flange, close to the struts, as shown in Figure 14.

ASSEMBLY METHOD

The method of assembly is depicted in Figure 15. It illustrates the assembly breakdown and its relation to a plan for assembling the truss in an unstressed condition. No part requires elastic deformation in order to fit into the final assembly. All parts are prefit and pin aligned prior to curing. Following is a brief outline of the fabrication method for the major details:

a) Strut tubes are substantially made on a semi-automated rolling table. The outer laminae, including boron and glass cloth, are laid up manually.

b) All flat laminates are of the same general pattern. They are laid up full thickness as uncured prepreg laminates and are then trimmed and applied to the respective mold; e.g., radial arm, center hub, truss core flange, etc.

c) The ring-strut fitting components are substantially compression molded to net size. Allowance is made for fitting critical parts at the ring assembly.

Locating platforms, adjustable radially and vertically are required to facilitate prefitting and ambient cure bonding.

TRUSS PERFORMANCE CALCULATIONS

The truss described in this paper was modeled for solution by NASTRAN. The objective of this work was to obtain confirmation of the despace, decenter, and tilt equations presented in this paper. Confirmation is necessary in order to employ them for preliminary design purposes. Exact confirmation (within 1 percent) was obtained for the despace equations. This was true regardless of whether the strut ends were modeled as pinned on fixed joints. Decenter and tilt confirmation was within 25 percent. Variance on this order was expected inasmuch as the closed-form solutions are only approximate as stated earlier.

CONCLUSIONS

A cylindrical truss, constructed using existing composite material and process controls, can be designed to satisfy micron-level stability requirements when subjected to the severe LST environmental conditions. It requires a sophisticated concern for detail and application of not only the best suited materials, but the judicious development of athermalization techniques and geometry optimization.

REFERENCES

1. "Space Shuttle System Payload Accommodations," JSC 07700.

2. Krim, Michael H., "Design of Highly Stable Optical Support Structure," AAS 75-206.

3. Nelson, Paul T., "A Strut with Infinitely Adjustable Thermal Expansivity and Length," NASA TMX-3274.

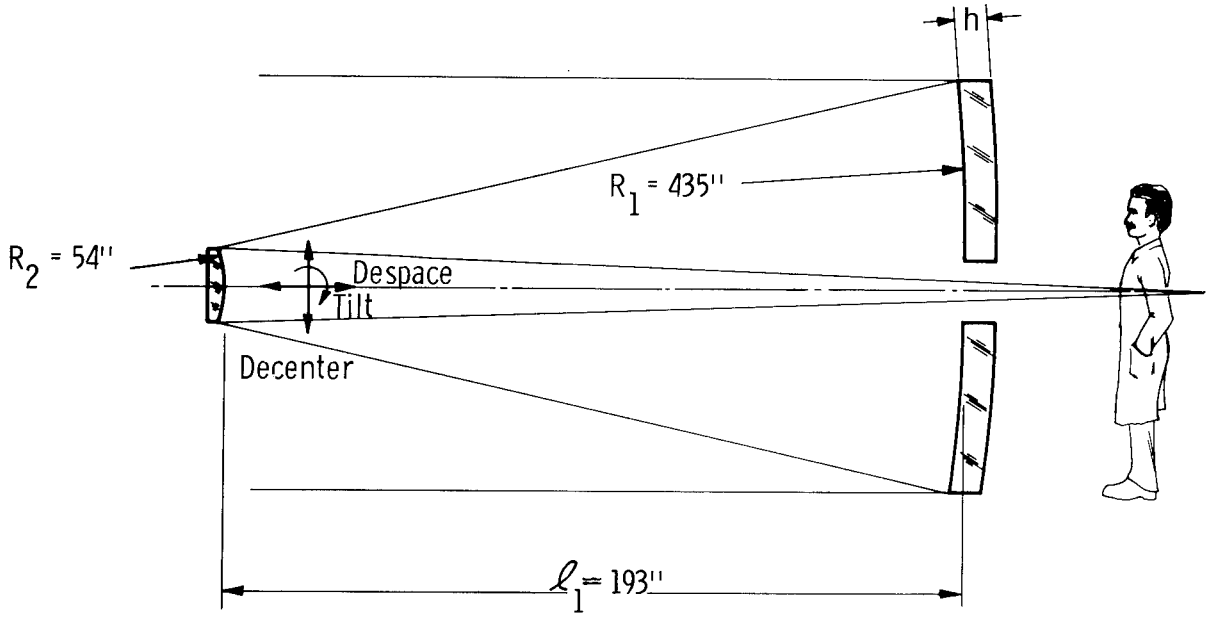

Figure 1. Optical System Parameters

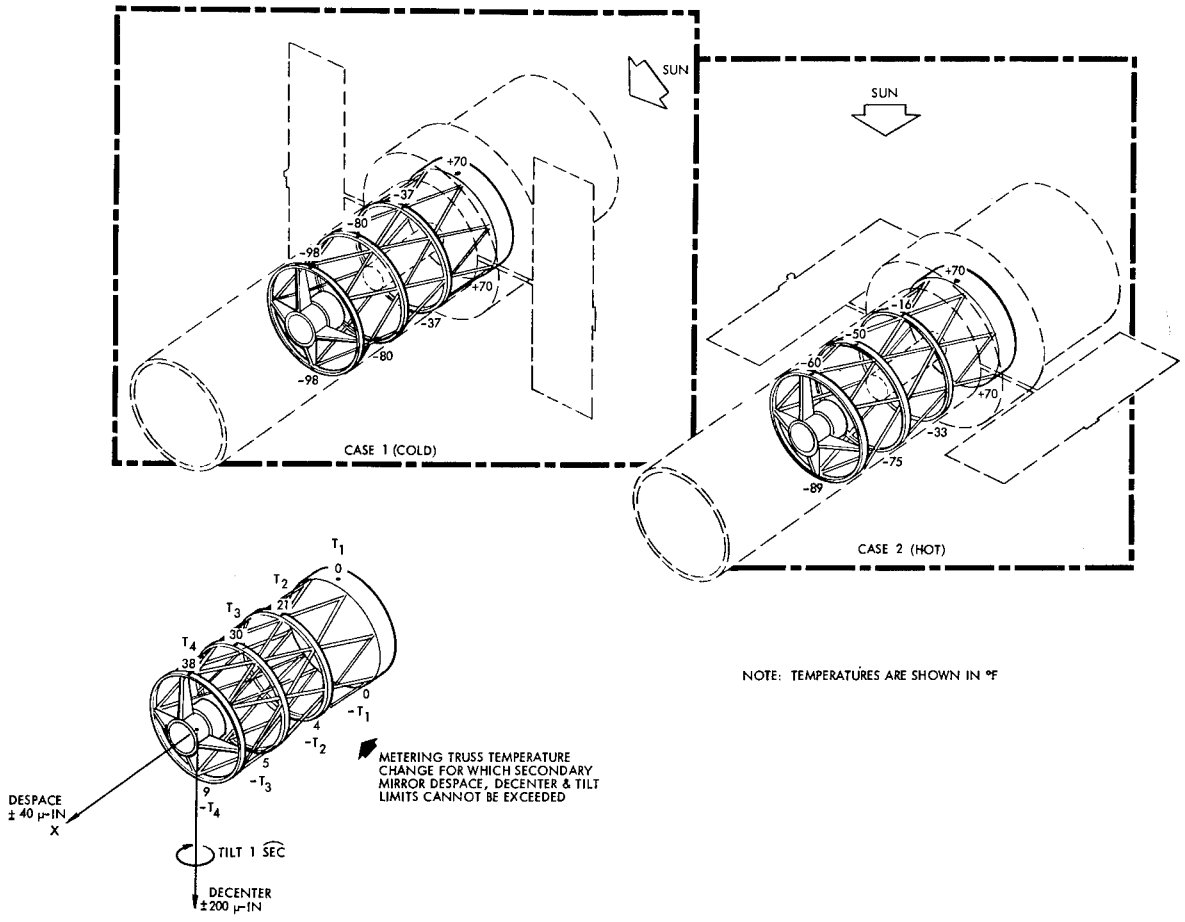

Figure 2. Temperature Model for Which Stability Must be Maintained Within Given Limits

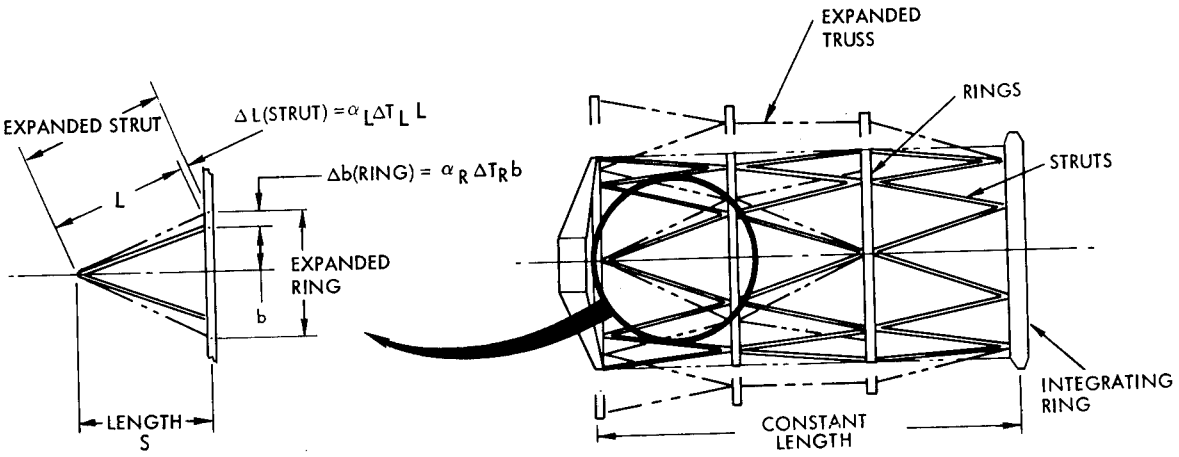

Figure 3. Athermalized Right Cylindrical Truss

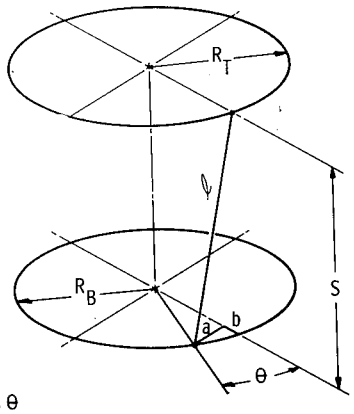

$$a = R_B \sin\theta$$

$$b = R_T - R_B \cos\theta$$

$$S^2 = \ell^2 - a^2 - b^2$$

$$S = \left[\ell^2 - R_B^2 \sin^2\theta - R_T^2 + 2 R_B R_T \cos\theta - R_B^2 \cos^2\theta\right]^{\frac{1}{2}}$$

$$\text{AND } \Delta S = \frac{1}{S}\left[\frac{\ell^2 \alpha S}{2} + R^2 \alpha_R (\cos\theta - 1)\right]\left(\Delta T_T + \Delta T_B\right)$$

Figure 4. Truss Bay Geometry

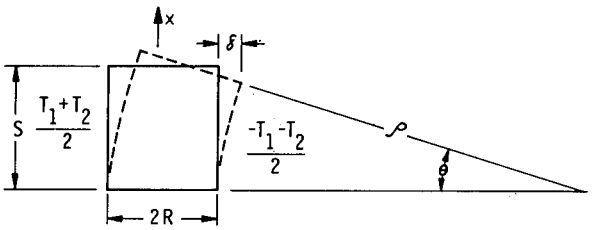

Figure 5. Lateral Displacement of a Single Bay Due to Lateral Temperature Gradients as Shown in Figure 1

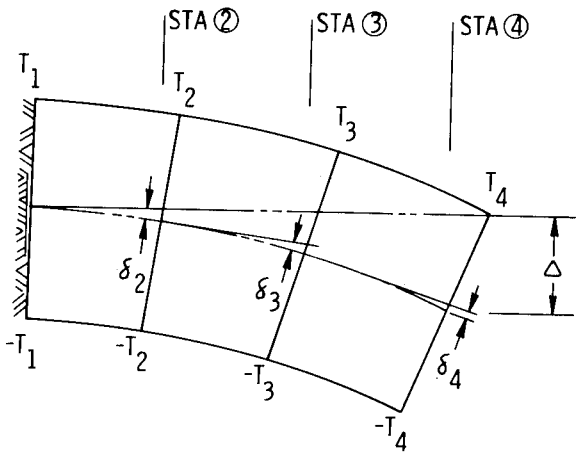

Figure 6. Decenter of Truss

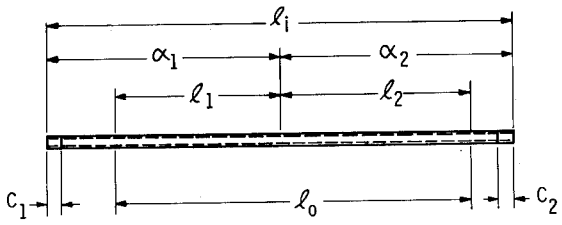

ℓ_i INITIAL AS-MANUFACTURED LENGTH

ℓ_o DESIRED FINAL LENGTH

C_1, C_2 MEASUREMENT COUPONS REMOVED FROM ℓ_i FOR INTERFEROMETRIC TESTING

ℓ_1 TOTAL LENGTH OF α_1 IN FINAL (ℓ_o) STRUT

ℓ_2 TOTAL LENGTH OF α_2 IN FINAL (ℓ_o) STRUT

α_1 $0^{+0}_{-\varepsilon}$

α_2 $0^{+\varepsilon}_{-0}$

} WHERE ε IS THE AS-CURED VARIABILITY

Figure 7. Dual-α Strut

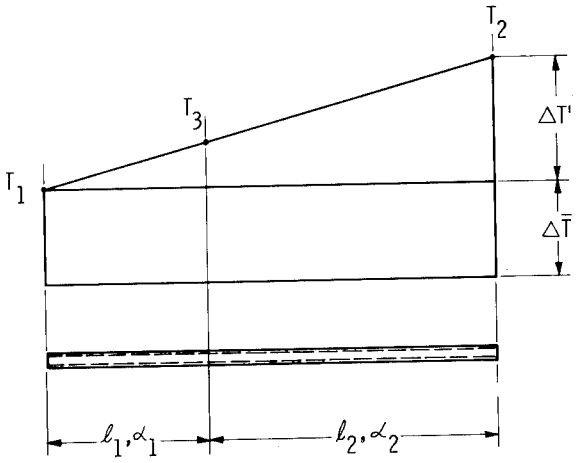

$$\alpha_{eff} = \left| \frac{\alpha_1 \alpha_2}{2(\alpha_1 - \alpha_2)} \right| \text{ for } \Delta T'$$

Figure 8. General Strut Temperature Profile

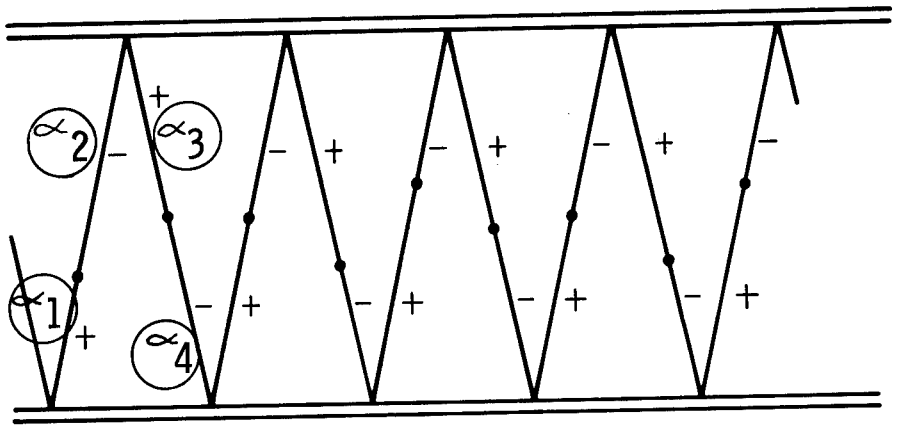

Figure 9. Alternating Strut Arrangement

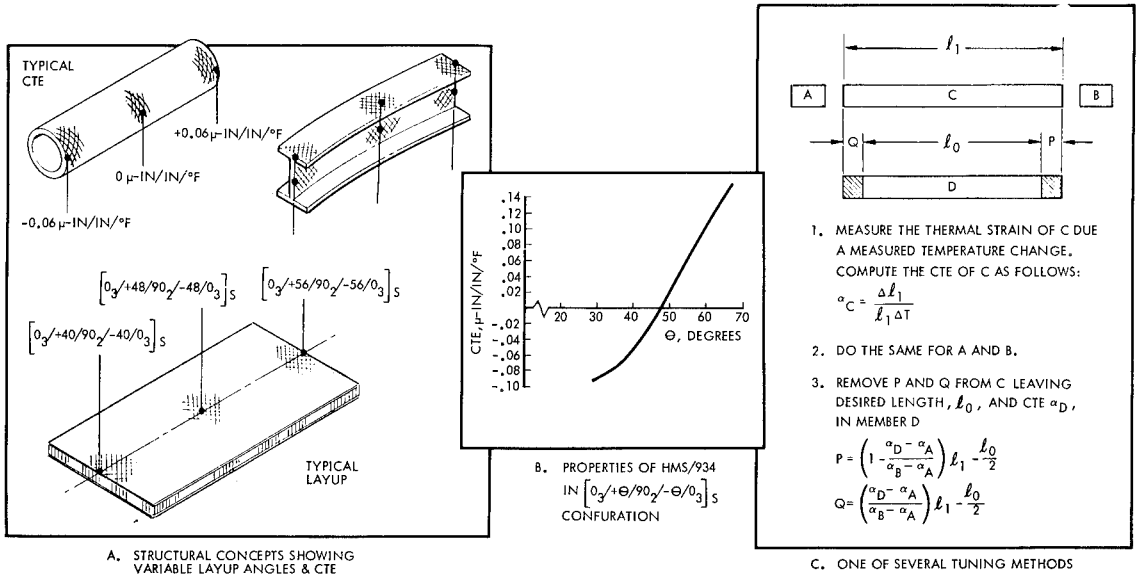

Figure 10. CTE Tuning Principle for Various Types of Structural Elements

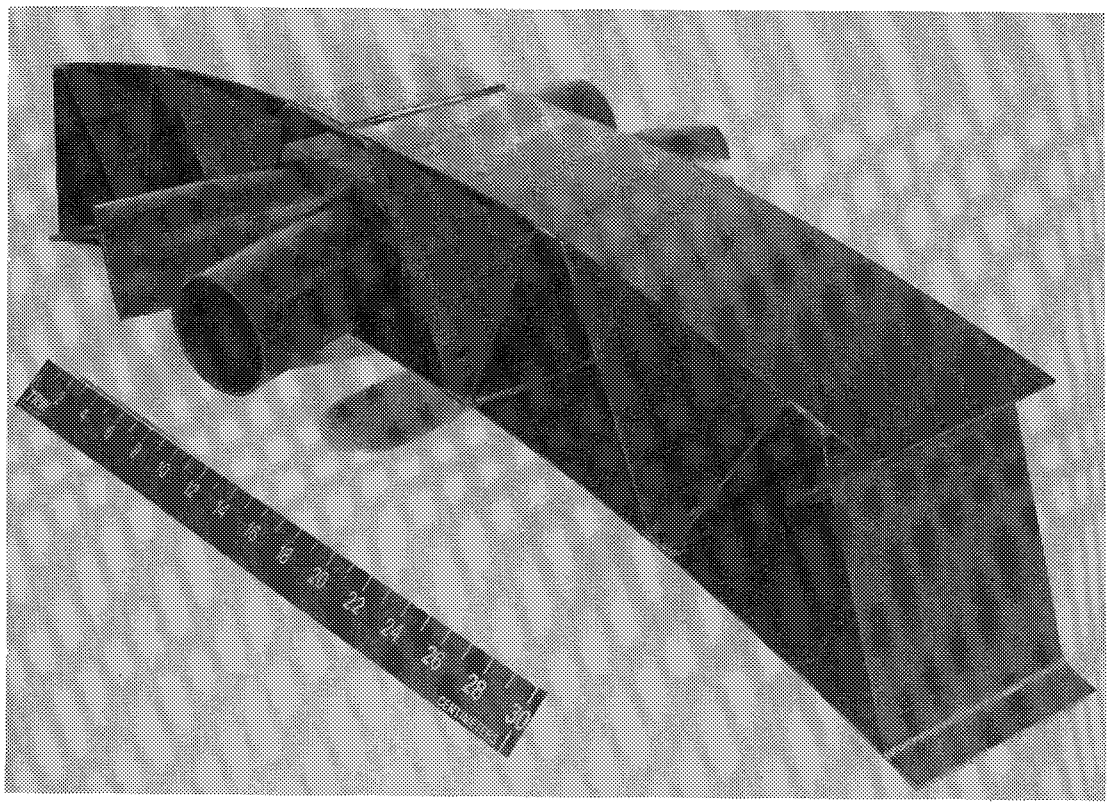

Figure 11. Truss-Core Ring Section

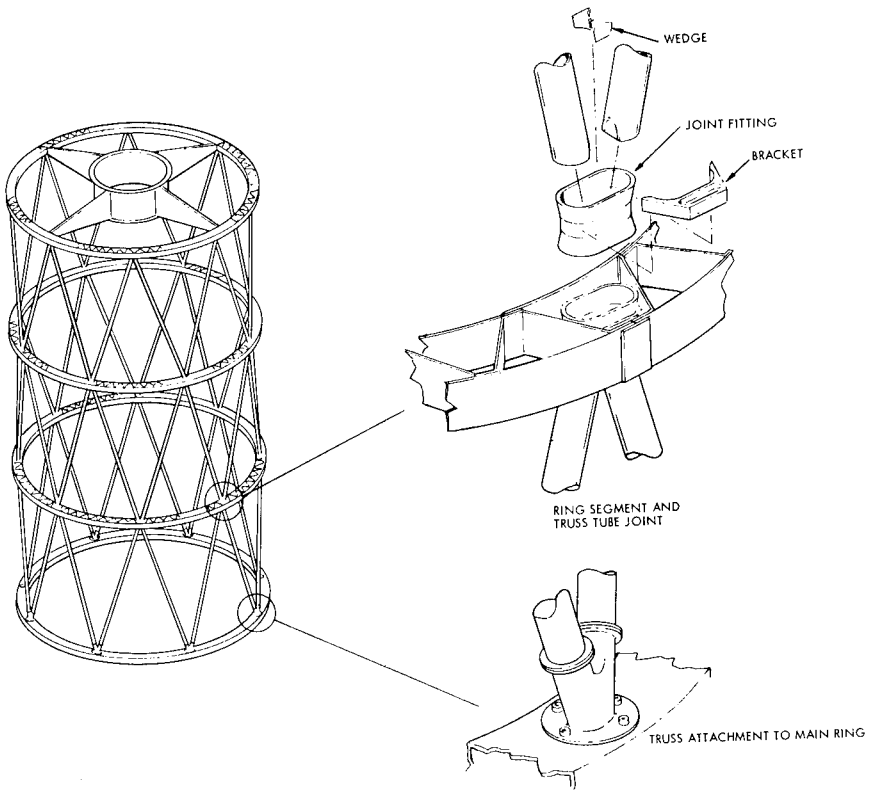

Figure 12. OTA Metering Truss

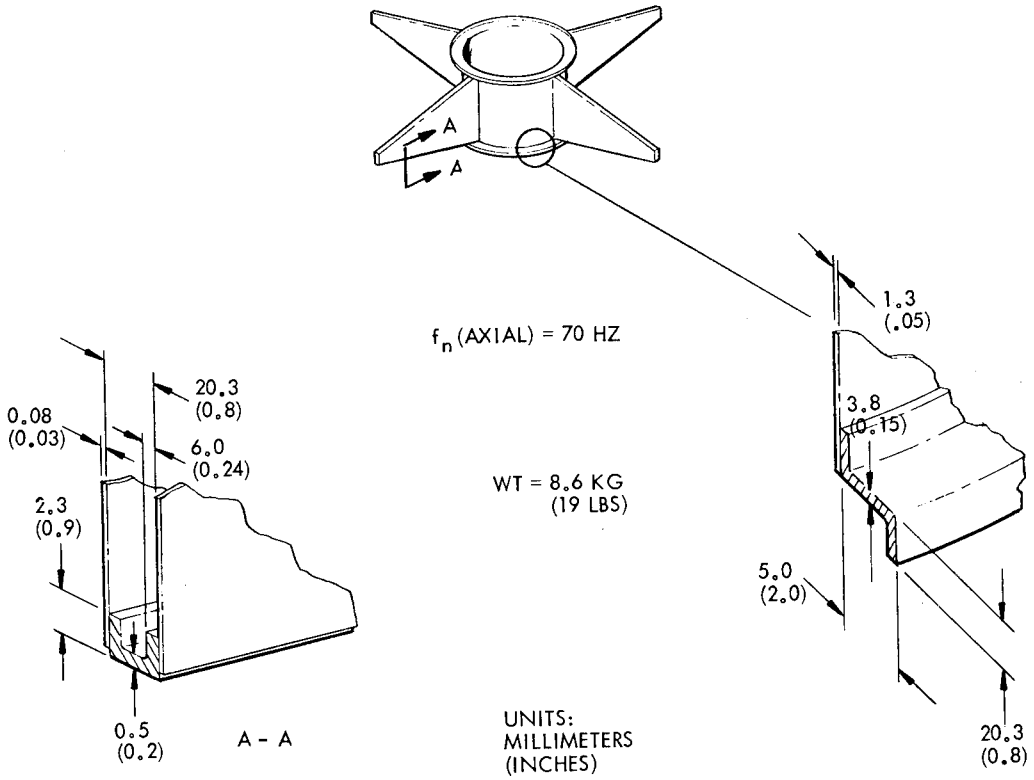

Figure 13. Graphite/Epoxy Secondary Mirror Support

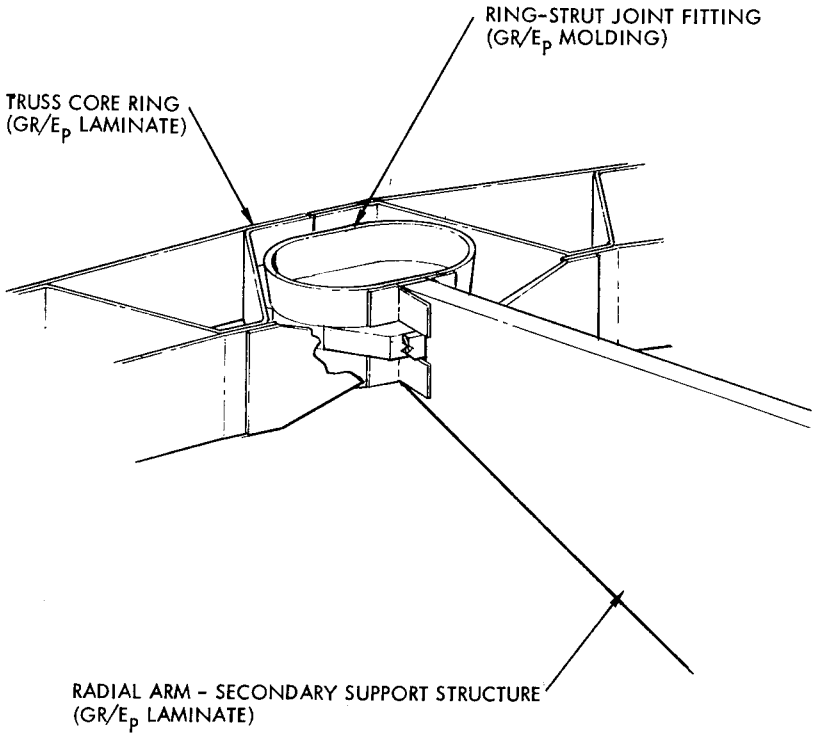

Figure 14. Attachment of Radial Arm to Outer Ring Joint Fitting

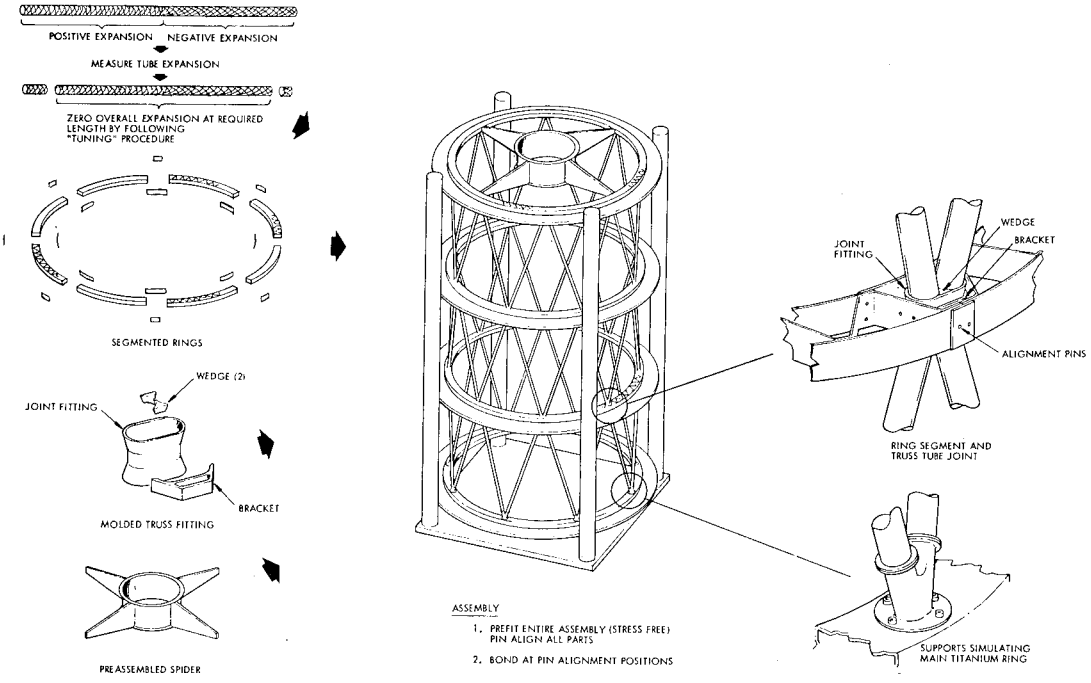

Figure 15. OTA Metering Truss Assembly Method

GENERAL COLLAPSE AND JOINT ANALYSIS OF A LAUNCH VEHICLE GRAPHITE/EPOXY CONICAL ADAPTER

E. E. Spier and G.D. Heller
General Dynamics Convair Division

ABSTRACT

A graphite/epoxy (HM-S/X904B) conical adapter for a launch vehicle flight mission is analyzed for stability and local strength at the end of integral flange joints. The stability analysis is performed by a linear/nonlinear finite-difference computer code (STAGS, structural analysis of general shells) where both bifurcation and nonlinear collapse solutions are obtained. The strength of the flanged joints was obtained by a finite-element computer code (SOLID SAP), where failure was initiated primarily by interlaminar tension. Tests of flange joint specimens in conjunction with the analysis permitted determination of lower-bound allowables for interlaminar tension.

The conical adapter is stiffened only by one ring near mid-length, and the cutouts are stiffened locally by one-sided doublers. The mathematical model for the finite-difference stability analysis included the forward aluminum adapter and 10.5 inches of simulated Atlas vehicle structure. The bifurcation analysis combined with conventional knock-down factors resulted in virtually the same allowable loading as that obtained by the nonlinear collapse analysis, where assumed initial imperfections were included. These imperfections were assumed to have the same wave form as that of the bifurcation solution and maximum amplitudes of approximately one-third the thickness. A bifurcation analysis for the shell without cutouts resulted in only a modest increase in allowable loading, thus indicating the adequacy of the reinforcing doublers.

NOMENCLATURE

A_{ij}	=	Extensional elastic constant of anisotropic shell wall
D_{ij}	=	Flexural elastic constant of anisotropic shell wall
E^c	=	Compressive modulus of elasticity
E^c_{11}, E^c_{22}	=	Longitudinal and transverse compressive modulus of elasticity of unidirectional composite material, respectively
E^t_{22}	=	Transverse tensile modulus of elasticity of unidirectional composite material
F^{cu}_{11}, F^{cu}_{22}	=	Longitudinal and transverse ultimate compressive strength of unidirectional composite material, respectively
F^{cu}	=	Ultimate compressive strength
G_{12}	=	Shear modulus of rigidity of unidirectional composite material
L	=	Length of shell
M	=	Total external applied bending moment
M_X', M_Y'	=	Local stress couples in shell wall
$M_X'Y', M_Y'X'$	=	Local twisting stress couples in shell wall
m	=	Number of longitudinal half waves

N_X', N_Y'	=	Local stress resultants in shell wall
$N_{X'Y'}, N_{Y'X'}$	=	Local shearing stress resultants in shell wall
n	=	Number of circumferential full waves
P_x	=	Total external applied compression load in x-direction
P_z	=	Total external applied shear load in z-direction
$P_{X'}, P_{Y'}, P_{Z'}$	=	Local applied axial loads
$\bar{P}$	=	Entire limit loading on overall structure in STAGS analysis
p	=	Pressure loading
R	=	Radius of circular cylinder
R, R_1	=	Minimum and maximum radii of truncated conical shell, respectively
t	=	Thickness
u, v, w	=	Local meridional, hoop, and radial displacement components
w_{max}	=	Amplitude of maximum initial imperfection in w-direction
X, Y, Z	=	Coordinate system for reference surface of STAGS mathematical model
ΔY	=	Delta Y, the circumferential difference in angle (degrees) between adjacent grid lines (columns)
X , Y , Z	=	Local coordinates: meridian, hoop, and normal, respectively
x, y, z	=	Global coordinates
$\beta_{X'}, \beta_{Y'}$	=	Local rotations
Γ	=	Knock-down factor
Γ_a^c, Γ_b^c	=	Axial and bending knock-down factors for compression, respectively
Γ_s	=	Knock-down factor for shear loads that cause compression
Γ_p	=	Knock-down factor for external pressure
Γ_{wa}^c	=	"Weighted average" knock-down factor for axial and bending loads resulting in combined compression
λ	=	Eigenvalue in bifurcation buckling analysis; characteristic of the attenuation length
ν	=	Poisson's ratio in isotropic material
ν_{12}, ν_{21}	=	Major and minor Poisson's ratio in unidirectional composite material
θ	=	Angle corresponding to local coordinate Y

INTRODUCTION

A graphite/epoxy conical adapter supports a satellite on top of the Atlas launch vehicle. There is an aluminum cylindrical adapter forward, which supports the satellite and aerodynamic fairing. Loads are assumed capable of acting in any direction for the design of the conical adapter, permitting it to withstand maximum loads in the region of major cutouts.

Graphite/epoxy used for the conical adapter is high-modulus graphite (HM-S)/epoxy (X904B), which is most efficient for a stiffness (stability) critical structure. Stresses are, in general, quite low. The liquid oxygen boiloff valve results in a 10-inch diameter cutout that must be reinforced. All other cutouts in both adapters are similarly reinforced except for the small vent holes in the conical adapter, which need no reinforcement. The conical adapter is bolted to metal rings at both ends. There is one mid-ring to support the shell against external pressure.

The mission is subjected to several loading conditions, most critical of which is the maximum $q\alpha$ case, a room-temperature condition for the conical adapter. This loading condition causes meridional and hoop stresses in the conical adapter, which tend to cause local buckling or general collapse of the shell. The stability analysis of the structure is performed with a computer code called STAGS, which solves either bifurcation buckling or nonlinear collapse analyses. The bifurcation analysis requires use of knock-down factors. On the other hand, nonlinear collapse analysis accounts for nonlinear incremental displacements and the corresponding redistribution of stresses up to the point of collapse without knock-down factors. Both types of analysis are performed for the present problem.

Graphite/epoxy integral ring joints of the conical adapter are modeled in a finite-element analysis. Also, some simulated tests of the joints were performed. By comparison between analysis and test, preliminary allowable interlaminar tensile strength is obtained.

DESIGN

The graphite/epoxy conical adapter must support the applied loads without local or general instability for a factor of safety of 2.0 (Air Force requirement). The larger cutouts, which accommodate the boiloff valve and access doors, must be reinforced by the addition of local doublers. In metal structures, it is generally considered good design to provide the cross-sectional area of the doubler to be 1.72 times the cross-sectional area of the cutout. For the graphite/epoxy adapter it was arbitrarily established that twice the cross-sectional area of the cutout would be provided in the reinforcing doublers. This was decided because the brittle graphite/epoxy will not yield locally in areas of high stress as metals do.

Drawings of the conical adapter are shown in Figures 1 through 4, where the dimensions shown are in inches. The shell wall is a pseudo-isotropic layup of 24 plies and a minimum total thickness of 0.132 inch, which corresponds to a ply thickness of 0.0055 inch. The layup is $[(90/\pm45/0)_S]_{3T}$, where the 90-degree plies on the outside provide maximum resistance to external pressure and a resulting maximum margin of safety for combined stresses in the shell. The attachment rings at the ends are integral with the conical shell, where the only metal employed is that of aluminum radius blocks for tension loads. The forward flange is designed to interface with the flange of the aluminum alloy cylindrical adapter and the aft flange is designed to interface with the existing steel ring on the booster. The mating flanges are joined by bolting. However, the flanges are considerably thicker than the conical shell to minimize the magnitudes of the interlaminar shear and tensile stresses, the allowables of which are quite low.

Some preliminary finite-element analysis and testing of simulated joints were performed to substantiate the geometry of the joints shown. The geometry of the Z-section mid-ring was established by engineering judgment following hand analysis by use of Reference 1 and a comparison to a similar all-aluminum conical adapter. The predominantly 90-degree fibers in the flanges are for the maximum bending stiffness of the ring, while the zero-degree fibers in the web provide torsional stability support for the outstanding flange.

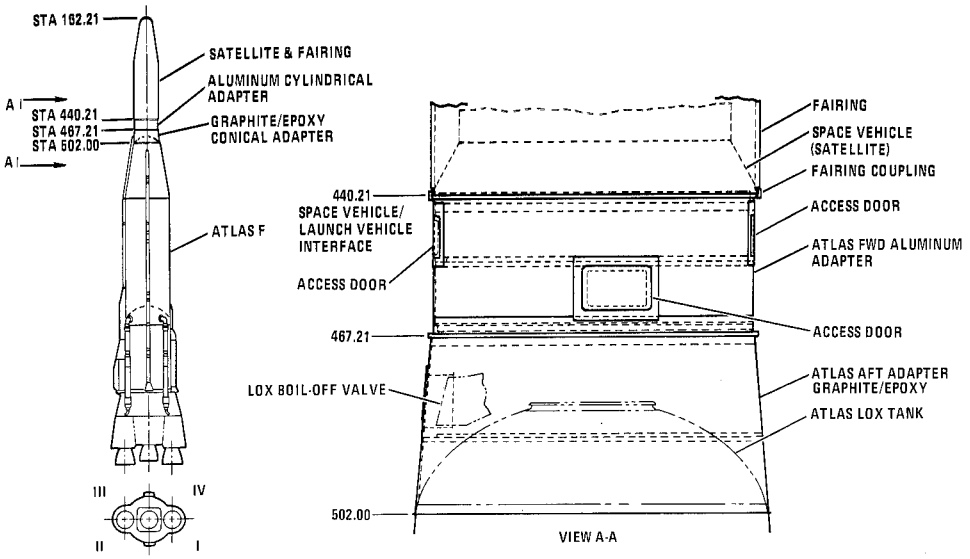

Figure 1. Launch configuration and adapters.

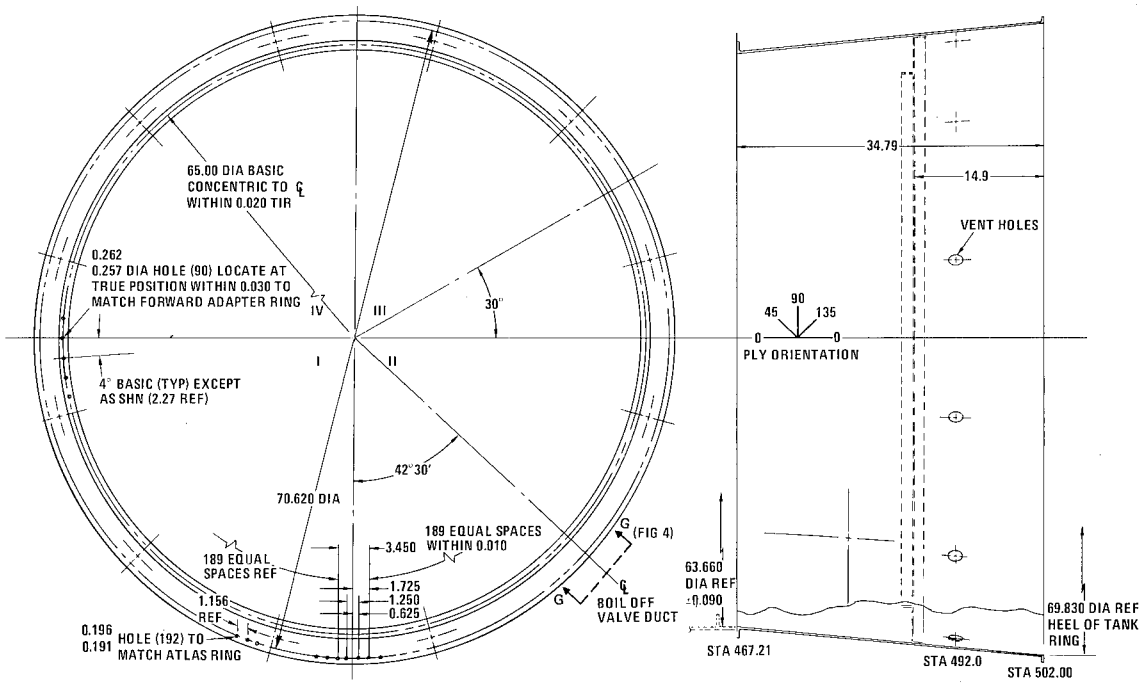

Figure 2. Graphite/epoxy conical adapter.

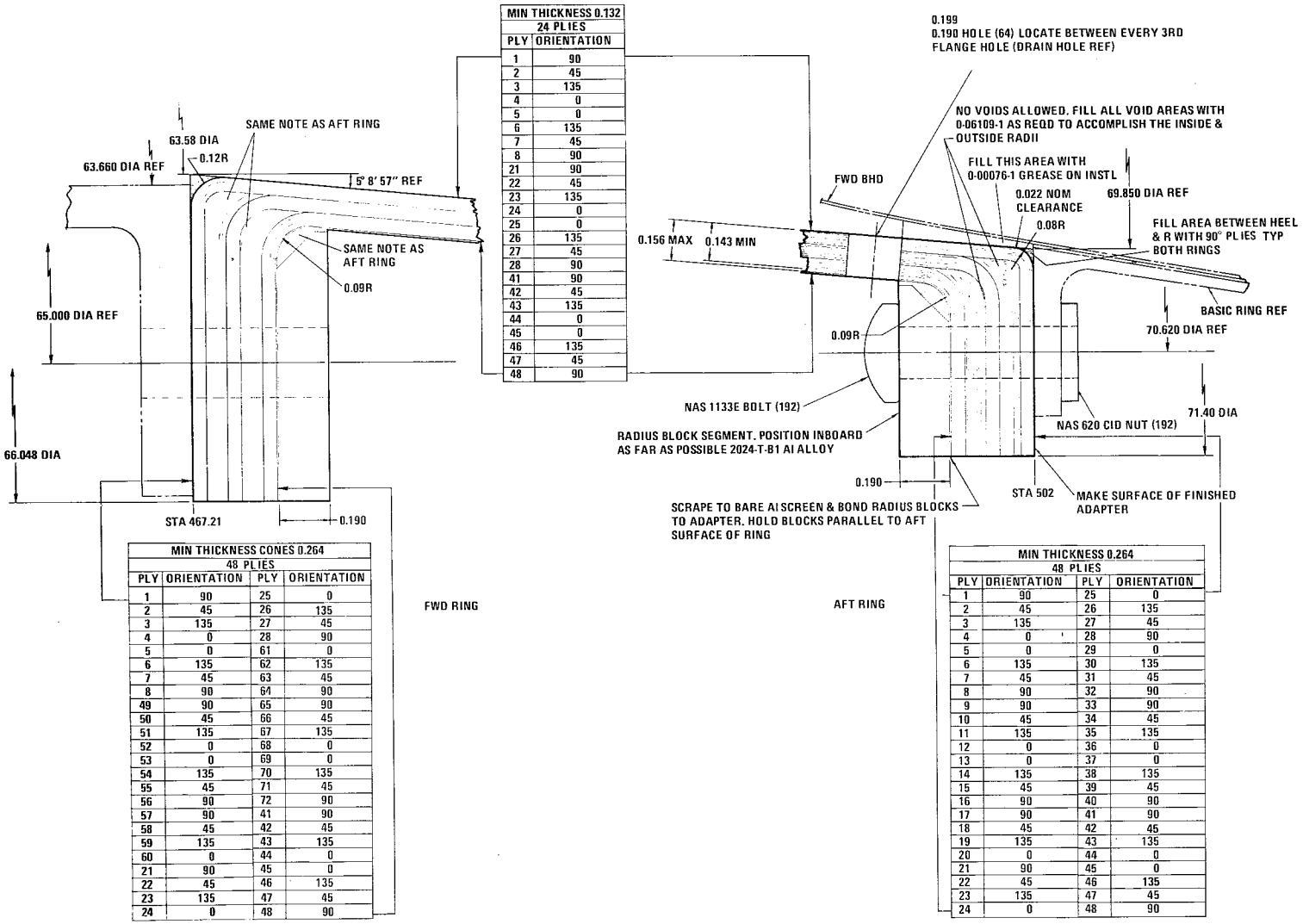

MIN THICKNESS 0.132	
24 PLIES	
PLY	ORIENTATION
1	90
2	45
3	135
4	0
5	0
6	135
7	45
8	90
21	90
22	45
23	135
24	0
25	0
26	135
27	45
28	90
41	90
42	45
43	135
44	0
45	0
46	135
47	45
48	90

MIN THICKNESS CONES 0.264			
48 PLIES			
PLY	ORIENTATION	PLY	ORIENTATION
1	90	25	0
2	45	26	135
3	135	27	45
4	0	28	90
5	0	61	0
6	135	62	135
7	45	63	45
8	90	64	90
49	90	65	90
50	45	66	45
51	135	67	135
52	0	68	0
53	0	69	0
54	135	70	135
55	45	71	45
56	90	72	90
57	90	41	90
58	45	42	45
59	135	43	135
60	0	44	0
21	90	45	0
22	45	46	135
23	135	47	45
24	0	48	90

MIN THICKNESS 0.264			
48 PLIES			
PLY	ORIENTATION	PLY	ORIENTATION
1	90	25	0
2	45	26	135
3	135	27	45
4	0	28	90
5	0	29	0
6	135	30	135
7	45	31	45
8	90	32	90
9	90	33	90
10	45	34	45
11	135	35	135
12	0	36	0
13	0	37	0
14	135	38	135
15	45	39	45
16	90	40	90
17	90	41	90
18	45	42	45
19	135	43	135
20	0	44	0
21	90	45	0
22	45	46	135
23	135	47	45
24	0	48	90

Figure 3. Integral end rings of conical adapter.

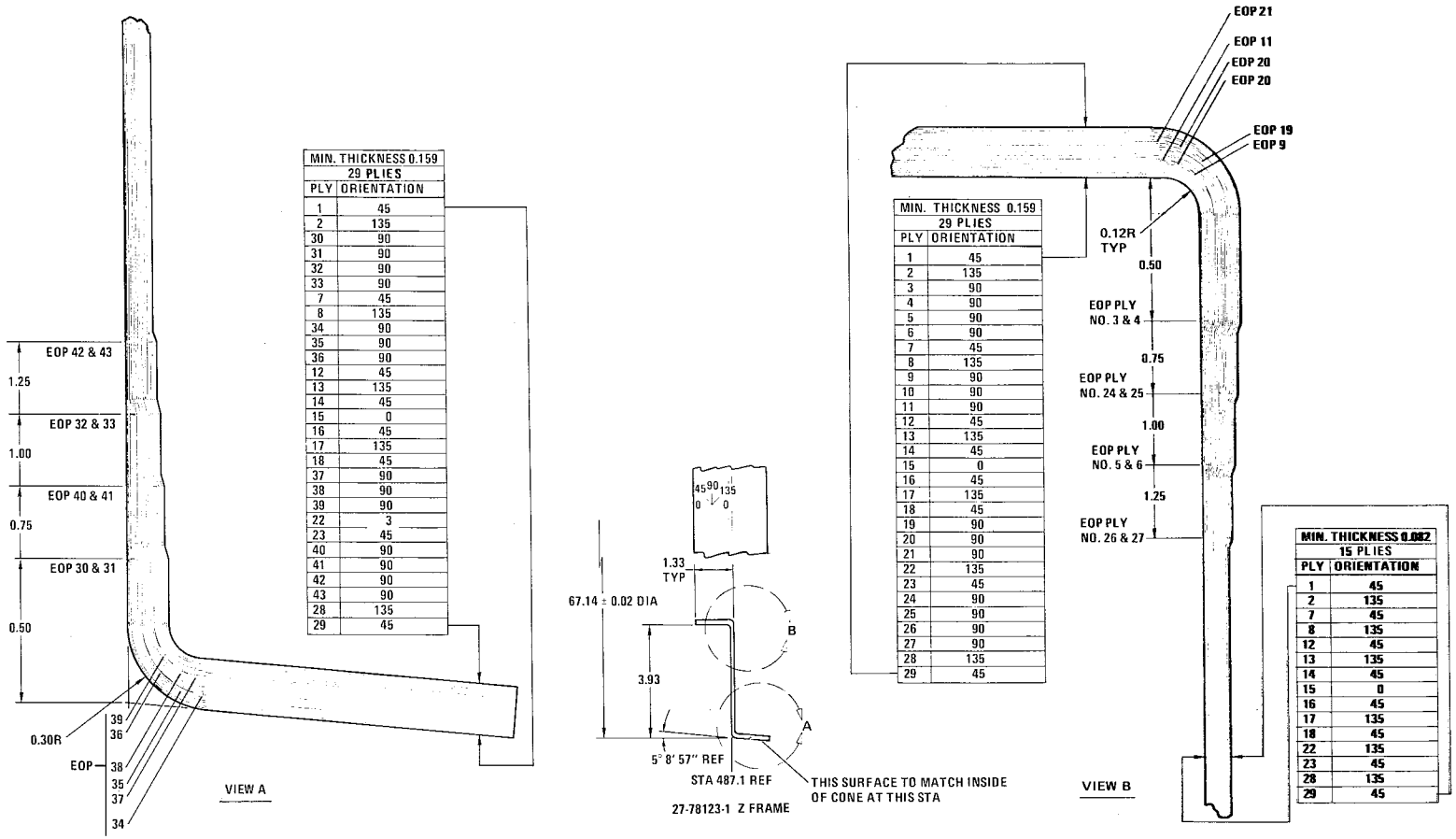

Figure 4. Mid-ring of graphite/epoxy conical adapter.

MATERIAL PROPERTIES

The material selected for the conical adapter is HM-S/X904B graphite/epoxy, which is a high-modulus, moderate-strength system. Considerable testing for both lamina and laminate mechanical properties was performed. For the present problem, room-temperature compressive properties are of primary interest. The Air Force requirements are that minimum test data be used for material allowables. Both lamina and laminate test data was analyzed to establish the minimum allowable mechanical properties. Test data of interest are:

Lamina

12 Test Specimens	2 Test specimens	9 Test Specimens
$F^{cu}_{11_{avg}}$ = 119,000 psi	$F^{cu}_{22_{avg}}$ = 17,900 psi	$F^{tu}_{22_{avg}}$ = 3,600 psi
$F^{cu}_{11_{max}}$ = 130,100 psi	$F^{cu}_{22_{max}}$ = 18,800 psi	$F^{tu}_{22_{max}}$ = 4,310 psi
$F^{cu}_{11_{min}}$ = 113,000 psi	$F^{cu}_{22_{min}}$ = 17,000 psi	$F^{tu}_{22_{min}}$ = 2,736 psi
$E^{c}_{11_{avg}}$ = 24.5×10^6 psi	$E^{c}_{22_{avg}}$ = 1.04×10^6 psi	$E^{t}_{22_{avg}}$ = 0.97×10^6 psi
$E^{c}_{11_{max}}$ = 26.3×10^6 psi	$E^{c}_{22_{max}}$ = 1.05×10^6 psi	$E^{t}_{22_{max}}$ = 1.06×10^6 psi
$E^{c}_{11_{min}}$ = 23.3×10^6 psi	$E^{c}_{22_{min}}$ = 1.03×10^6 psi	$E^{t}_{22_{min}}$ = 0.83×10^6 psi

Longitudinal tensile properties are higher than the compressive properties, and are of no interest in this discussion. However, the tensile transverse properties are of interest for use in determining laminate properties by use of lamination theory. See Figure 2 for ply orientation.

Laminate $[(90/\pm45/0)_S]_{3T}$

27 Test Specimens (21 tested in 0-degree direction, 6 in 90-degree direction)	26 Test Specimens (20 tested in 0-degree direction, 6 in 90-degree direction)
F^{cu}_{avg} = 48,900 psi	E^{c}_{avg} = 9.45×10^6 psi
F^{cu}_{max} = 58,000 psi	E^{c}_{max} = 10.1×10^6 psi
F^{cu}_{min} = 41,250 psi	E^{c}_{min} = 8.8×10^6 psi

By the use of lamination theory, the laminate test data was used to establish minimum allowable lamina mechanical properties for use in the STAGS computer analysis. By assuming that

$E^{c}_{0° \text{ or } 90°_{min}}$ = 8.8×10^6 psi

$\nu_{12} = \nu_{21}$ = 0.34 (estimated)

$E^{c}_{22_{min}} = E^{t}_{22_{min}}$ = 0.9×10^6 psi

G_{12} = 0.6×10^6 psi (estimated)

the resulting value for the unidirectional compressive modulus became

$$E^{c}_{11} = 24.0 \times 10^6 \text{ psi}$$

which is somewhat higher than the minimum value (23.3×10^6 psi) from the lamina tests

By the use of lamination theory, the complete minimum-stiffness matrix for the shell wall was found by letting

$E_{11} = 24 \times 10^6$ psi $\quad G_{12} = 0.6 \times 10^6$ psi

$E_{22} = 0.9 \times 10^6$ psi $\quad \nu_{12} = 0.34$

The resulting values for the stiffness matrix are:

$$\begin{bmatrix} A_{11} & A_{12} & A_{13} & & & \\ A_{21} & A_{22} & A_{23} & & & \\ A_{31} & A_{33} & A_{34} & & & \\ & & & D_{11} & D_{12} & D_{13} \\ & & & D_{21} & D_{22} & D_{23} \\ & & & D_{31} & D_{32} & D_{33} \end{bmatrix} =$$

$$\begin{bmatrix} 1.288 \times 10^6 & 4.035 \times 10^6 & -1.340 \times 10^{-2} \\ 4.035 \times 10^5 & 1.288 \times 10^6 & -5.020 \times 10^{-1} \\ -1.340 \times 10^{-2} & -5.020 \times 10^{-1} & 4.421 \times 10^6 \end{bmatrix} \text{ lb/in.}$$

$$\begin{bmatrix} 1742 & 575 & 23 \\ 575 & 2020 & 23 \\ 23 & 23 & 631 \end{bmatrix} \text{ lb-in.}$$

Stiffnesses for other elements of the conical adapter, such as the mid-ring and cutout reinforcements, were also determined.

STAGS COMPUTER CODE

The computer code STAGS (Structural Analysis of General Shells – Ref. 2) was developed to analyze the behavior of general stiffened or unstiffened shells under arbitrary static thermal and mechanical loading. An important feature of the code is its capacity to include the effects of nonlinearities due to finite displacements and rotations. Multiple shells joined at common junctures may be included in the analysis, where each shell is considered as a separate branch. The shell surface of each branch is subdivided by means of a finite-difference grid made up of rows and columns. This results in a set of subareas in each branch. At junctures, the grid lines of adjoining branches must connect to common nodes (intersection of rows and columns). The strain energy density for each subarea is expressed in terms of displacement components and their derivatives at the nodes. The resulting equations are put in finite-difference form; then, the internal strain energy, together with the potential energy of applied loads, is summed over the surface of each shell branch. By employing the principle of stationary total potential energy, a system of nonlinear algebraic equations results. These equations are then solved by use of a modified Newton-Raphson numerical technique. Cutouts can be properly accounted for by specifying zero thickness at the affected nodes. The code is capable of performing any of the following types of analysis:

Linear

This analysis is limited to the linear terms of the nonlinear algebraic expressions. The resulting output may include linear displacement components and rotations, stress resultants, stress couples, and internal stresses in the shell wall. In addition, internal loads and stresses in stiffeners may be printed out.

Nonlinear

This analysis begins with some small initial load step, which results in a linear solution for this load step only. By successive incremental load steps, the nonlinear terms in the algebraic expressions are

included in the solutions. Thus, nonlinear displacement components and rotations are accounted for. The modified Newton-Raphson solution must converge within a prescribed set of constraints described in the strategy section of Ref. 2. The grid point with the most rapidly changing displacement component or rotation is where convergence is tested. After convergence has been reached, all pertinent information concerning the point is printed out.

A load-displacement (or rotation) plot, as shown in Figure 5, will show the degree of nonlinear behavior taking place. When this plot approaches a horizontal direction, general collapse of the shell structure is about to take place. Confirmation of collapse is obtained when the determinant of the stiffness matrix also "collapses." This determinant is printed out after each Newton step, which is a refactoring of the stiffness matrix of the mathematical model. The procedure usually followed in the nonlinear analysis is to increment the load steps up to some prescribed maximum load, say 0.5 of limit load. Then, after being satisfied of the results and the strategy being employed, the run can be restarted at one of the last three load steps, which are saved on magnetic tape. A restart run always begins with a Newton step and the determinant of the stiffness matrix is recalculated. With proper planning, sufficient Newton steps can be performed to allow a reasonable plot of the determinant of the stiffness matrix.

It should be noted that the cost of Newton steps comprises the major cost of the total nonlinear run. As the load-deflection curve approaches the horizontal, smaller and smaller load steps with more corresponding Newton steps are necessary, which results in sizable increases in computer time. Thus, it is wise not to carry the solution too near the collapse point to avoid astronomical computer costs. The nonlinear behavior can be confined to only certain branches if so desired. Initial waviness of the shell if known or assumed can be mathematically included in the computer solution by use of a user-written subroutine (WIMP) usually involving sine and cosine terms.

Bifurcation

A classical bifurcation buckling analysis is implemented in the STAGS program. A linear analysis is initially performed as it provides the linear prebuckling displacements for the lowest eigenvalue solution, which defines the bifurcation point. A discussion of the strategy for bifurcation analysis is beyond the scope of this paper (Ref. 2). The bifurcation point is defined to be equal to the eigenvalue (λ) times the applied loading ($\bar{P}$), as shown in Figure 6. The effect of applicable knock-down factors is also shown. Knock-down factors (Γ) are obtained from Ref. 1, to account for the discrepancy between test and theory due to the effect of initial imperfections and boundary conditions.

The global axes coordinate systems (x, y, z) for a circular cylindrical shell and a conical shell are shown in Figure 7. The basic surface coordinates (X, Y) along with the length (L) and appropriate radii (R for cylinder, R, R_1 for cone) define the shell reference surface. The mid-surface of the shell wall is measured a distance Z from the reference surface, where Z is measured positive in the positive local Z direction. The local coordinate system (X , Y , Z) and the sign convention for stress resultants and stress couples are shown in Figure 8. Also, the sign convention for the displacement components (u, v, w) and rotations (β_X', β_Y') are shown in Figure 9.

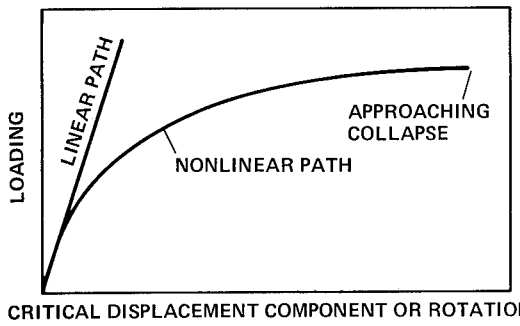

Figure 5. Nonlinear load-deflection plot.

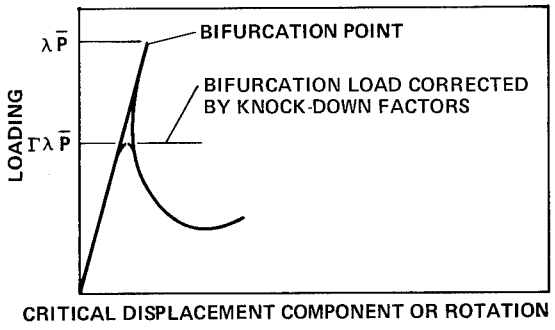

Figure 6. Bifurcation buckling path.

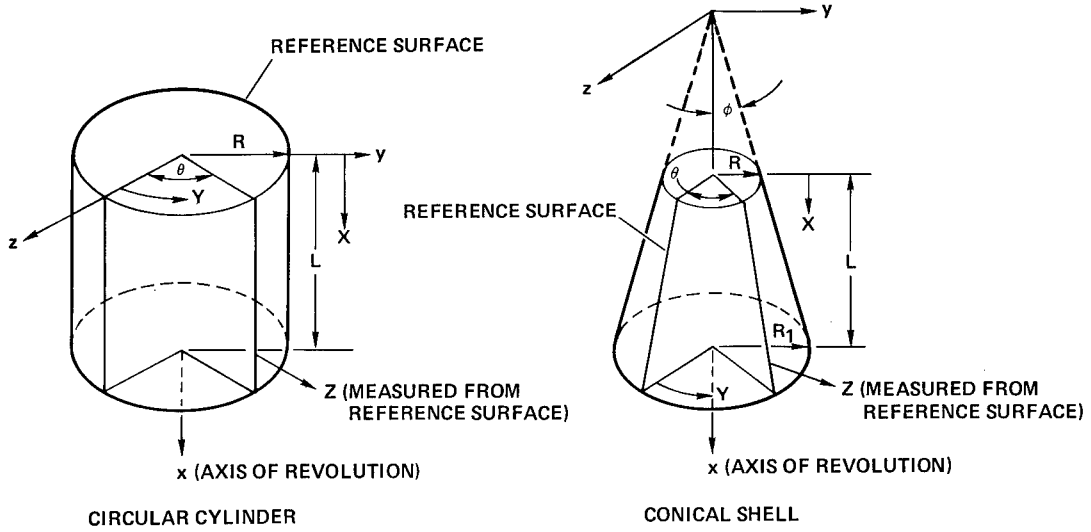

Figure 7. Shell coordinate systems.

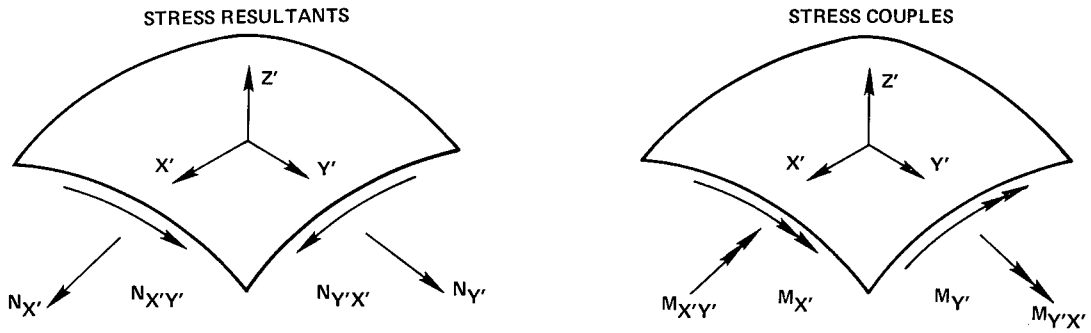

Figure 8. Local coordinate system (X,Y,Z) and sign convention for stress resultants and stress couples.

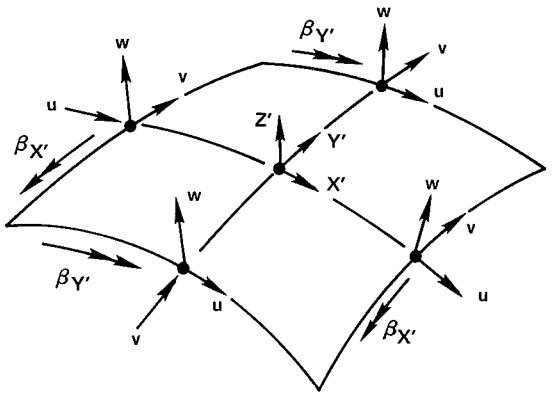

Figure 9. Sign convention for displacement components and rotations.

MATHEMATICAL MODEL

The mathematical model for the STAGS computer analyses shown in Figure 10 includes the forward aluminum adapter, the graphite/epoxy conical adapter, and 10.5 inches of Atlas "cylindrical" shell (actually conical). The Atlas bulkhead is omitted, but the effect of the internal pressure on the bulkhead was treated as a tensile preload in the Atlas segment. The STAGS code designates each shell as a branch when they are joined at junctures. Consequently, the forward aluminum adapter is designated as Branch 1, the graphite/epoxy conical adapter as Branch 2, and the Atlas structure as Branch 3. The reference surface of the mathematical model coincides with the mid-surface of Branch 2, as shown in Figure 10. Since this paper is concerned only with the stability of Branch 2, both Branches 1 and 3 are limited to linear displacements in either the bifurcation or the nonlinear collapse analyses.

It is sufficient to model one-half of the structure (180 degrees), and impose symmetric boundary conditions at Y equal to zero and 180 degrees. This is justified in that the critical loading condition (maximum α q) causes compressive stresses predominantly by the applied bending moment, which results in symmetric displacements. However, for bifurcation buckling analysis, both the symmetric and antisymmetric mode must be considered to obtain the minimum bifurcation load. Each branch of the model is partitioned into rows (X-direction) and columns (Y-direction), where the columns in each branch must coincide.

The boundary condition at Row 1 of Branch 1 is unrestrained, and the boundary condition of Row 8, Branch 3 is clamped. Note that much of the column spacing beyond Y equal to 90 degrees is about twice as large as corresponding spacing less than Y equal to 90 degrees. Actually, the initial model had wide spacing in both regions, but spurious circumferential deflection modes developed due to compression in the region of Y less than 90 degrees. The model as shown provided reasonable deflection modes. It is of interest to note that the maximum width to thickness ratio (4/0.132) for the spurious mode was equal to 30, and reducing this ratio to 15 eliminated the problem. The spurious deflection mode resulted in a very conservative value for the eigenvalue.

The cutouts are shown in a flat pattern layout of the mathematical model in Figure 11. In Branch 2 the boiloff valve cutout and the access door cutout were modeled 180 degrees apart for expediency in analysis at each cutout, although their locations are actually quite different. The bending moment that imposes compression in the boiloff valve area need only be reversed in the analysis to impose maximum compression in the access door. The cutout for the boiloff valve is reinforced by rectangular stiffening for maximum efficiency, even though the cutout is circular. Circular cutouts are more detrimental than rectangular cutouts in the stability of monocoque cylinders (Ref. 3). Corresponding cutouts in the forward adapter (Branch 1) are included with their respective reinforcements. The nodes identified by the solid circles designate zero thickness in the shell wall. The boundary of the cutout is located halfway between the node and the adjacent row or column of the shell with finite thickness.

LOADS

The critical loading condition for the graphite/epoxy conical adapter is maximum αq, where the applied bending moment results in peak compression in line with the centerline of the boiloff valve cutout. The loading is due to a combination of the aerodynamic fairing load and inertia relief of the payload at Sta. 440 of the forward adapter. In addition, external pressures are applied to both the forward and conical adapters. However, the pressure on the forward adapter is neglected since the ensuing analysis concerns only the stability of the conical adapter.

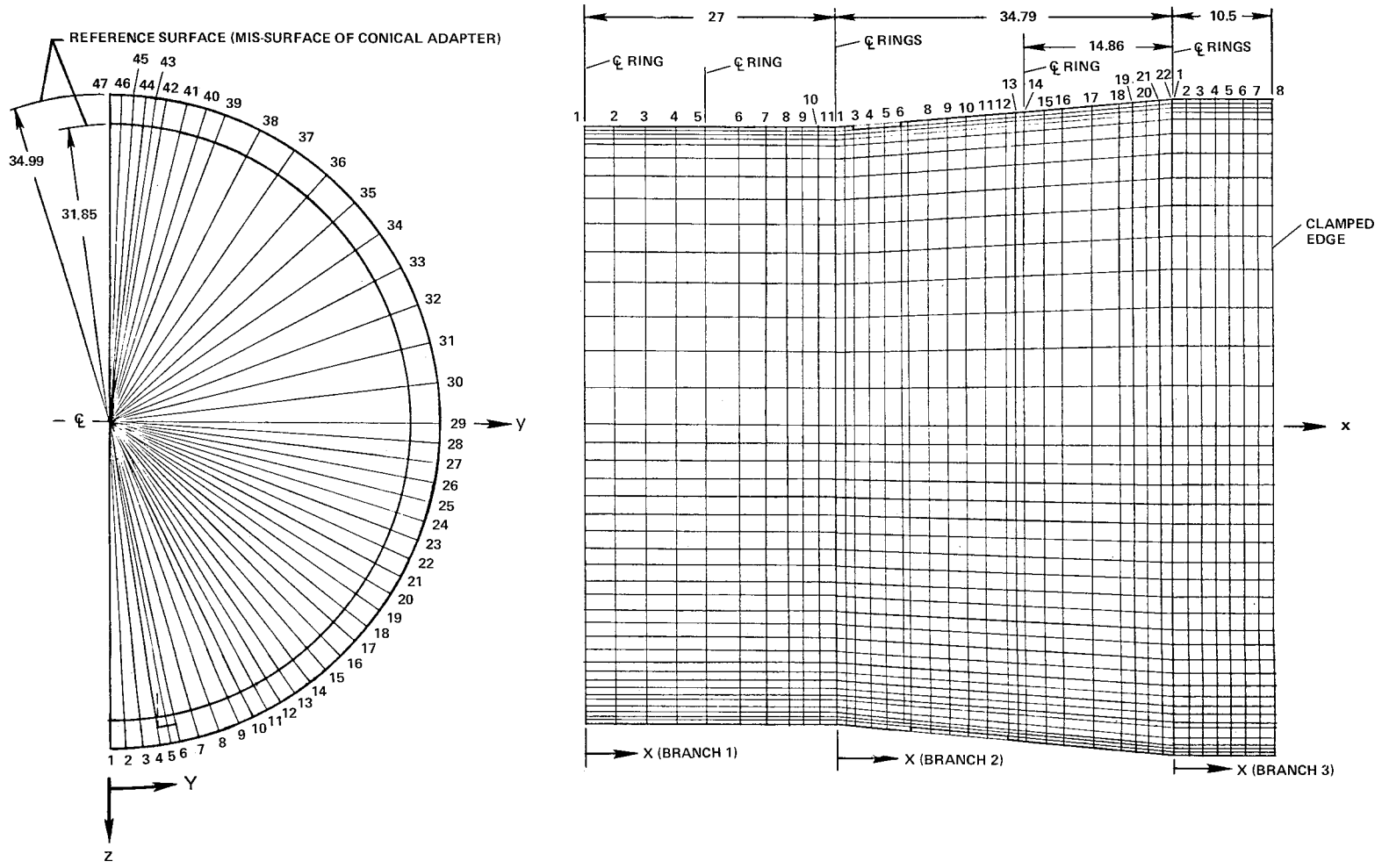

Figure 10. Mathematical model for STAGS computer analysis.

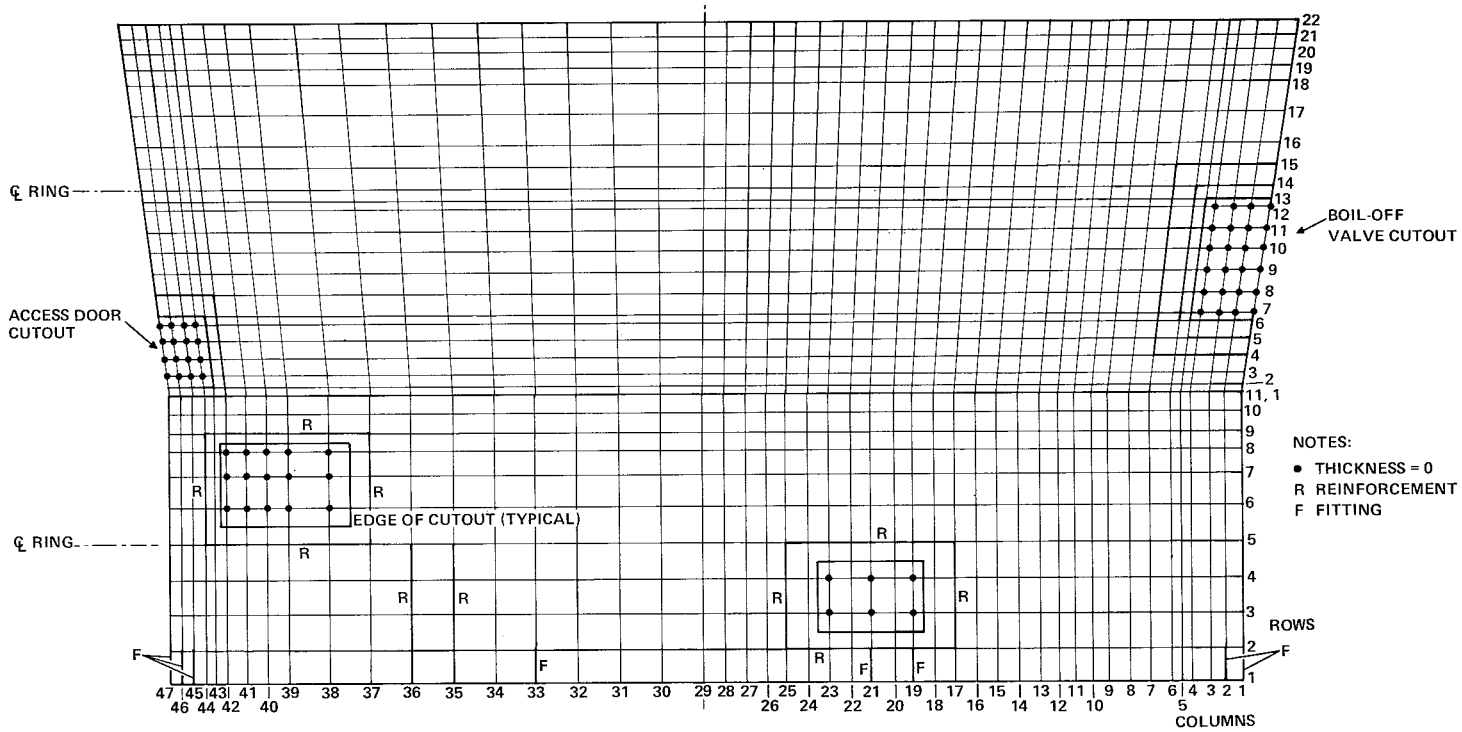

Figure 11. Flat pattern of mathematical model of Branches 1 and 2.

The net applied limit loads are shown in Figure 12, which are the result of the following limit loads:

Fairing

$M = 1.21 \times 10^6$ in.-lb

$P_x = 9{,}980$ lb

$P_z = 6{,}620$ lb

Payload (satellite)

$M = -0.28 \times 10^6$ in.-lb

$P_x = 8{,}130$ lb

$P_z = -2{,}440$ lb

External pressure on conical adapter

At Station 467: p = 1.12 psi

At Station 502: p = 1.84 psi

The fairing loads are distributed uniformly, but the payload is connected at discrete points through fittings which result in local bending moments applied at the reference surface. The loads include a net compressive hoop load at Sta. 440 due to the presence of a Marmon clamp that is preloaded to attach the spacecraft to the cylindrical adapter. The internal pressure load on the Atlas bulkhead was included as a pretension in Branch 3 of the mathematical model of Figure 10.

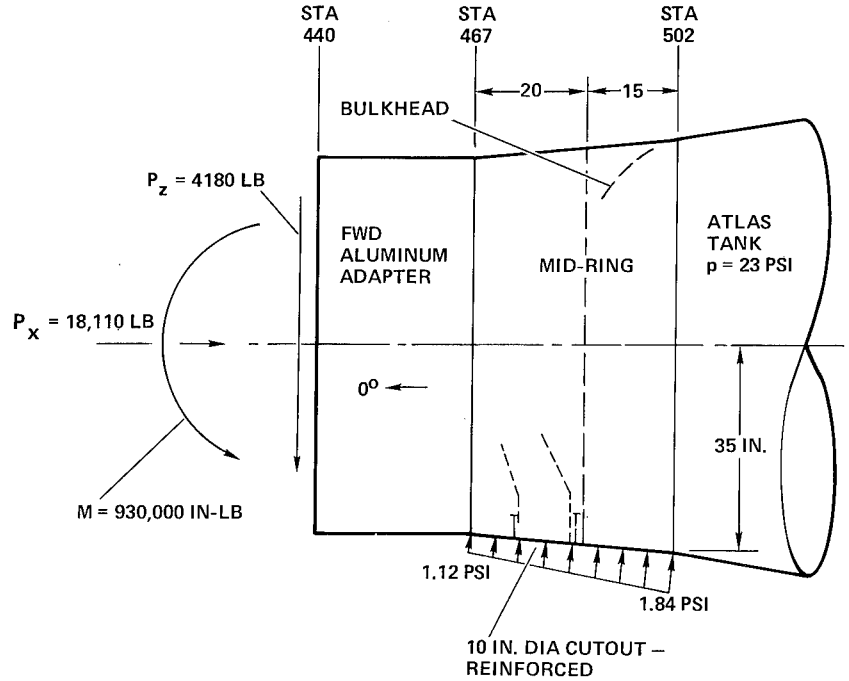

Figure 12. Graphite/epoxy conical adapter and adjacent structures with maximum a q loading.

STABILITY ANALYSIS

Stability of the conical adapter is determined by the use of the STAGS computer code. Both bifurcation and nonlinear collapse analyses were performed. The effect of expected initial waviness in manufacturing (initial imperfections) is accounted for in the bifurcation analysis by the use of knock-down factors (Ref. 1) and in the nonlinear analysis by imposing an initial deflection pattern by use of a user-written subroutine called WIMP. The mathematical model shown in Figures 10 and 11 is used, but Branches 1 and 3 are not permitted to buckle in either the bifurcation or the nonlinear collapse analysis. The cutouts and corresponding reinforcements, plus all rings in the three branches, are included in the STAGS computer solutions. Also, eccentricities of the ring and stiffener cross-sections are included in the analysis.

The effects of knock-down factors (Γ) are included at the outset by amplifying the applied loads by the reciprocal of the appropriate knock-down factors; i.e., knock-up the loads. The radius of the conical shell was assumed to be 35 inches and the original minimum thickness was assumed to be 0.143 inch (actually now 0.132 inch). For a radius thickness ratio of 35/0.143 equal to 245, the axial and bending knock-down factors, as found from Ref. 1 are:

$$\Gamma_a^c = 0.44 \quad \cdot \quad \Gamma_b^c = 0.56$$

Approximately 79% of the maximum compression is due to the bending moment, leaving 21% due to axial load. Thus, a "weighted average" knock-down factor for the compression loads is found by the expression

$$\Gamma_{wa}^c = 0.79 \times 0.56 + 0.21 \times 0.44 = 0.53$$

Thus, all compression loads applied at the forward end of the aluminum adapter are amplified by the reciprocal relation

$$1/\Gamma_{wa}^c = 1/0.53 = 1.886$$

Since the shear results in bending stresses, the shear loads were amplified by

$$1/\Gamma_s = 1/\Gamma_b^c = 1/0.56 = 1.786$$

Also, Ref. 1 recommends a knock-down factor for external pressure (Γ_p) to be 0.75. Therefore, the external pressure on the conical adapter is amplified by the reciprocal relation

$$1/\Gamma_p = 1/0.75 = 1.33$$

Now, by using these amplified (knock-up) loads for bifurcation analysis, no further corrections concerning knock-down factors are required. The actual loads are retained for the nonlinear analysis.

Bifurcation analysis was performed with the STAGS code for the mathematical model with and without cutouts. The results are shown in Figure 13, where the load factors indicated refer to the eigenvalues (λ) from the computer solutions. Load factor is defined as being "times limit load." The critical point in both cases was on Row 17 (X = 26.75 inch) and the model without cutouts had the critical point at Column 1 (Y = θ = 15.6 degrees). It is interesting to note that the critical row was unaffected by the boiloff valve cutout; only the critical column was affected. The eigenvalue for the model with cutouts is 3.233, while that for the model without cutouts is 3.387. There is not much difference in the eigenvalues, but the reinforcements around the large cutout did not completely restore the shell to its original buckling strength. A bifurcation analysis was performed where the cutouts had no reinforcements, and the resulting eigenvalue was only 1.41. A bifurcation analysis for the shell without cutouts by the use of Ref. 1 and 4 resulted in an eigenvalue of 1.86 (Figure 13). This is due to the extreme conservatism in the recommended linear interaction relationship for combined compression and external pressure. Also, it must be assumed in the use of Ref. 1 and 4 that all rings are sufficiently rigid to provide simple support to the individual shell segments. Then, the analysis checks only bifurcation buckling of the shell wall between rings.

A nonlinear analysis of the model with cutouts was performed up to a load factor of 2 times limit load, as shown in Figure 13. Note that the critical nodal point is the same as that for the corresponding bifurcation analysis. This analysis assumes that the shell is perfect except for the cutouts. Actually, it is impossible to build a perfect shell, be it made from metal or fibrous composites. Accordingly, a user-written subroutine called WIMP was employed to input an initial waviness in the shell. This was accomplished by using an equation of the form

$$w = w_{max} \sin (m \pi X/L) \cos (nY)$$

where the number of axial half and circumferential full waves, m and n, respectively, are selected to coincide with the bifurcation buckling pattern. Those values became

$m = 3 \qquad n = 14$

and the maximum displacement component was conservatively assumed to be

$w_{max} = 0.04$ inch

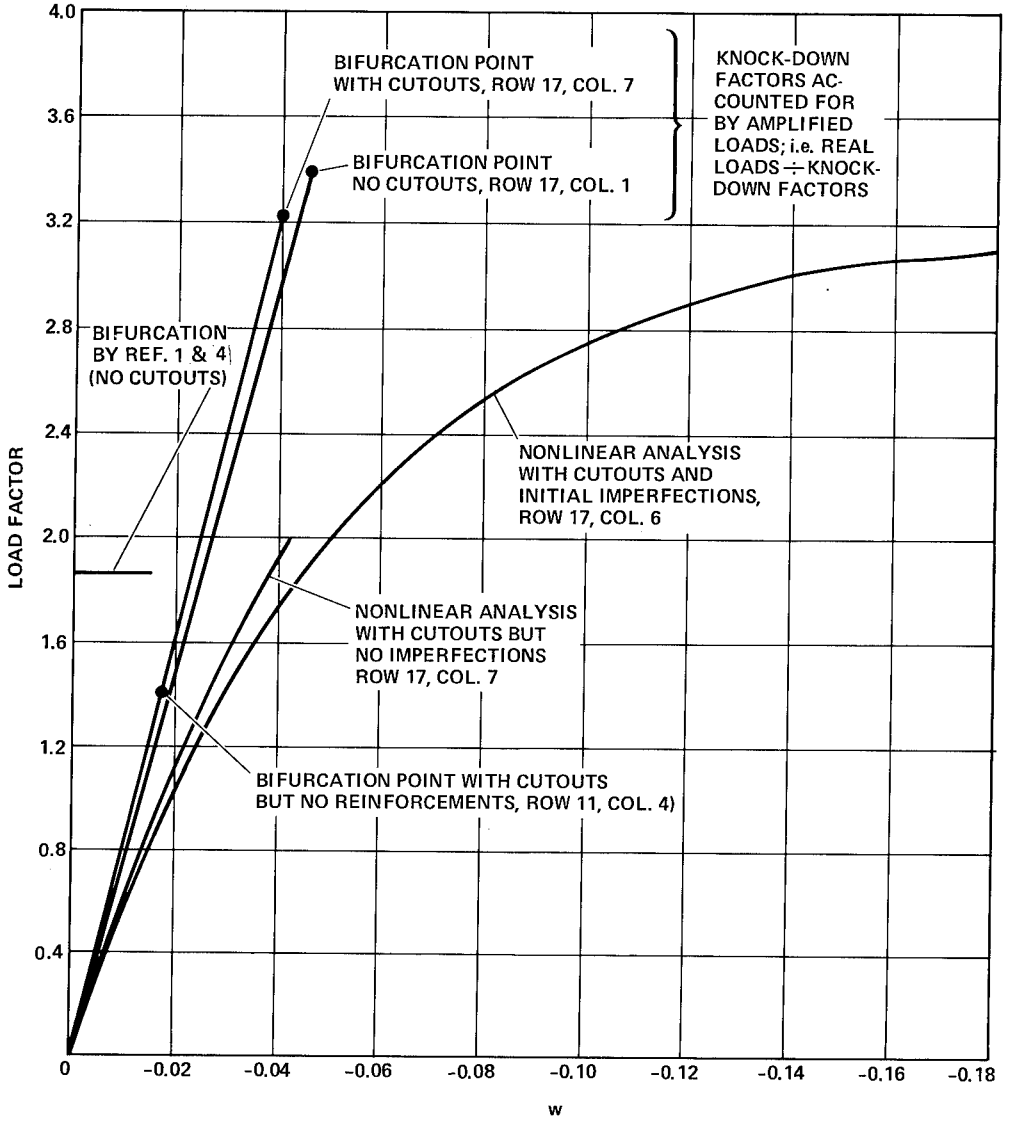

Figure 13. Bifurcation and nonlinear collapse analysis results.

Results of the nonlinear analysis for the model with cutouts and the assumed initial imperfections are shown in Figures 13 and 14, where the curve in Figure 14 indicates that the solution was carried nearly to collapse (load factor = 3.175). Confirmation is demonstration by a plot of the determinant of the stiffness matrix, as shown in Figure 15, where at maximum load the determinant is equal to approximately 1/100 as much as the initial determinant. The critical point for the nonlinear collapse analysis is at the same Row (17),but at Column 6 (Y = θ = 12.1 degrees) rather than Column 7 as before. The bifurcation and nonlinear collapse solutions are remarkably close so that for the present

problem the more expensive nonlinear computer run was unnecessary. However, no generalizations can be made from this for any other shell structures. In fact, if the actual waviness was much less than assumed, the load factor at collapse could be considerably higher than the bifurcation eigenvalue.

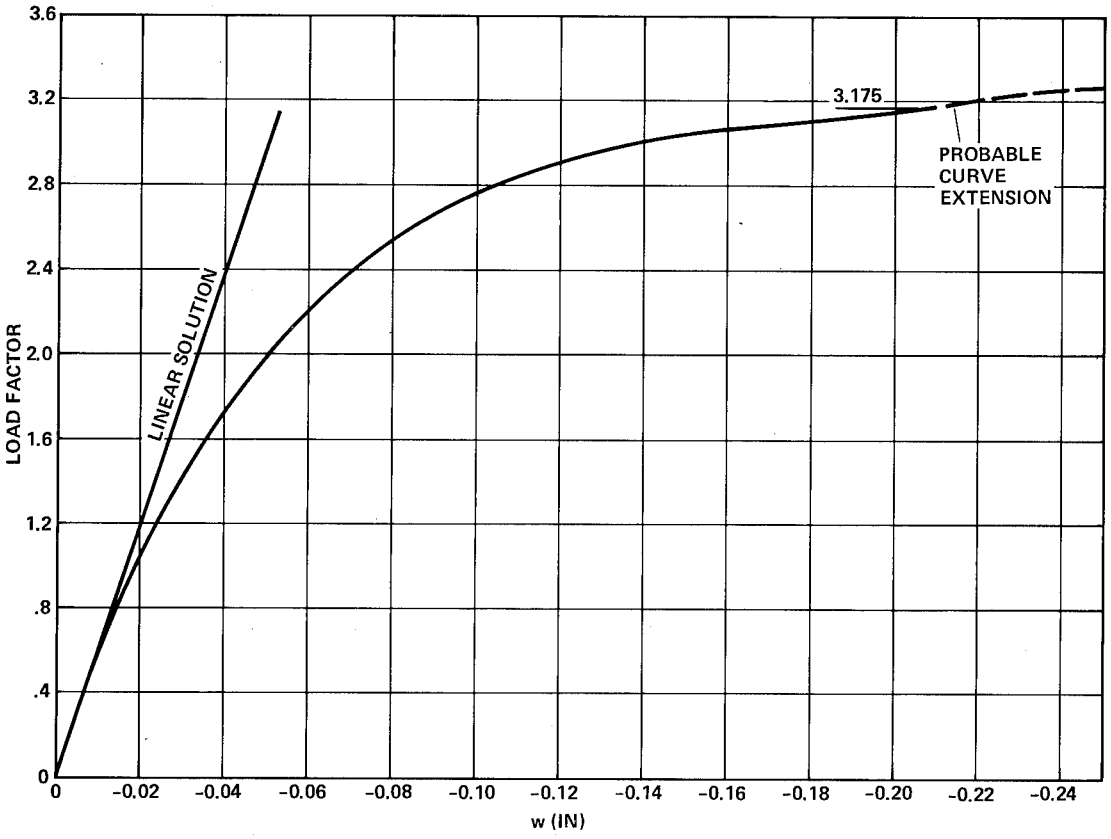

Figure 14. Nonlinear collapse of adapter with cutouts and initial imperfections at Row 17, Column 6.

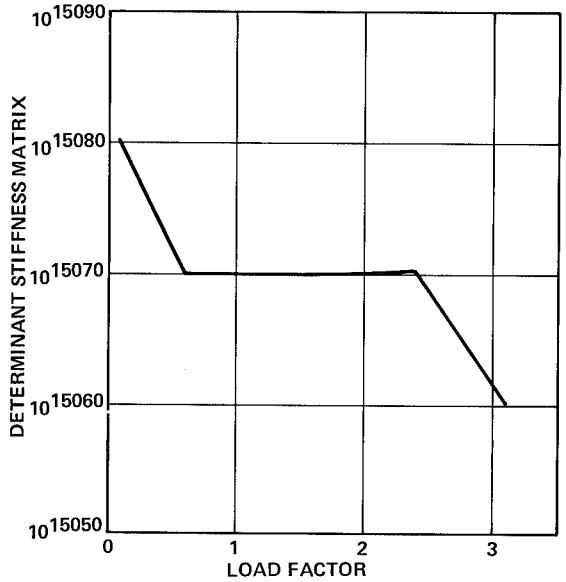

Figure 15. Determinant of stiffness matrix versus load factor.

All data presented from here on refers to the mathematical model with cutouts, and the nonlinear analysis includes initial imperfections. Plots of the normalized displacement component w are shown in Figure 16 for the first 90 degrees around the circumference along Row 17 for the bifurcation, nonlinear, and linear solutions.

Note that for the first 20 degrees the three solutions nearly coincide, and that the overall general shapes of the curves are quite similar. The bifurcation curve shown was used to establish the number of circumferential full waves to be used in the user-written subroutine WIMP for the input of initial imperfections in the nonlinear analysis. Actual nonlinear displacement components (u, v, w) are shown in Figure 17, where the linear displacement component w is also shown. Note the great difference in magnitudes of this displacement between the linear and nonlinear solutions. The displacement components u, v are quite small, as expected. The magnitude of w for the mid-ring is shown in Figure 17 for reference, and the relatively small displacement components w seem to indicate that its cross-section was more than adequate.

The linear and nonlinear rotations (β_X', β_Y') along Row 17 are shown in Figure 18. The significantly higher nonlinear circumferential rotations (β_Y') follow a similar path as the nonlinear displacement components (w) in Figure 17. This is as expected since the rotations (β_Y') are proportional to the derivatives of w with respect to the circumference.

The linear and nonlinear stress resultants are shown along Row 17 in Figure 19. The difference between the maximum value of N_X' from the linear and nonlinear solutions is not too great. However, note the large difference in the maximum value for N_Y' from the linear and nonlinear solutions. The nonlinear stress couples along Row 17 are shown in Figure 20.

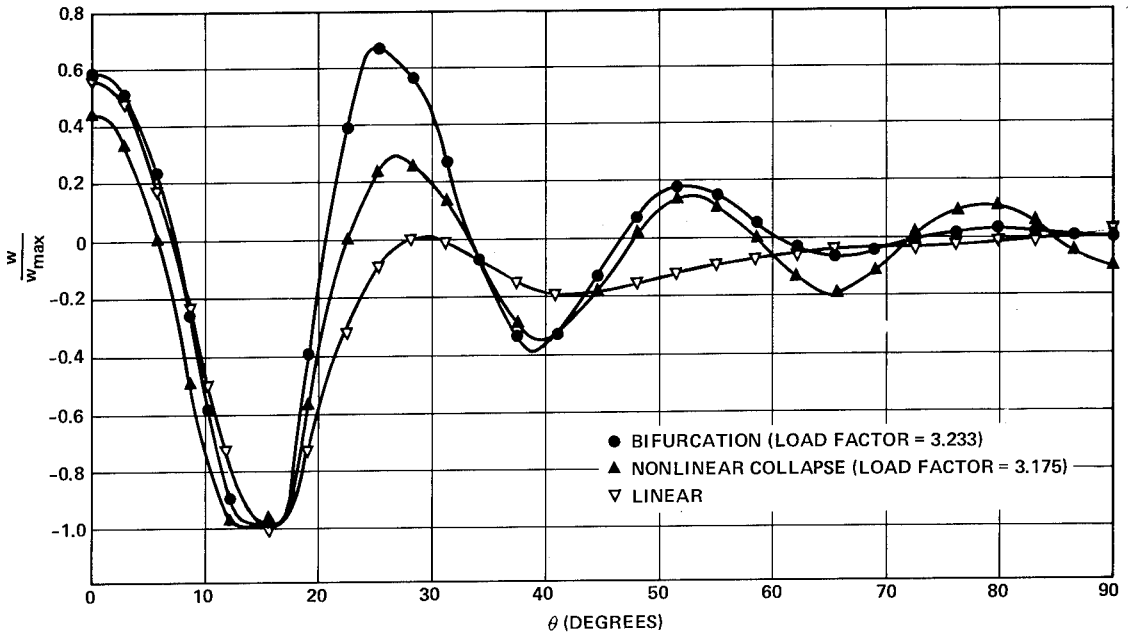

Figure 16. Normalized displacement components (w) along Row 17.

To complete the stability picture, it is appropriate to plot certain data along Column 6. Accordingly, the displacement components (u, w) are shown in Figure 21, which clearly shows that the aft portion of the adapter was much more critical; i.e., the nonlinear displacement components w_{NL} forward of the mid-ring are relatively small when compared to w_{NL} aft of the mid-ring. Similar results are found for the rotations as shown in Figure 22. At first it might appear that an additional ring at Row 17 would result in a thinner wall for the same collapse load; but the primary critical loading is axial compression, not hoop compression, and the allowable axial load is virtually unaffected

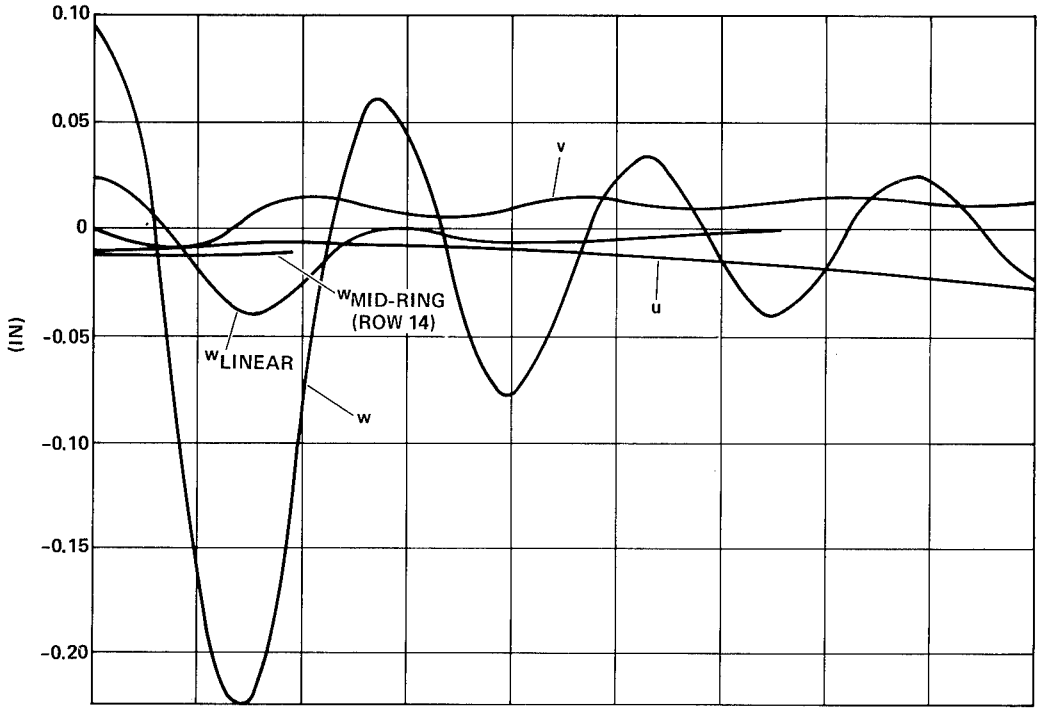

Figure 17. Nonlinear displacement components along Row 17 for load factor = 3.175.

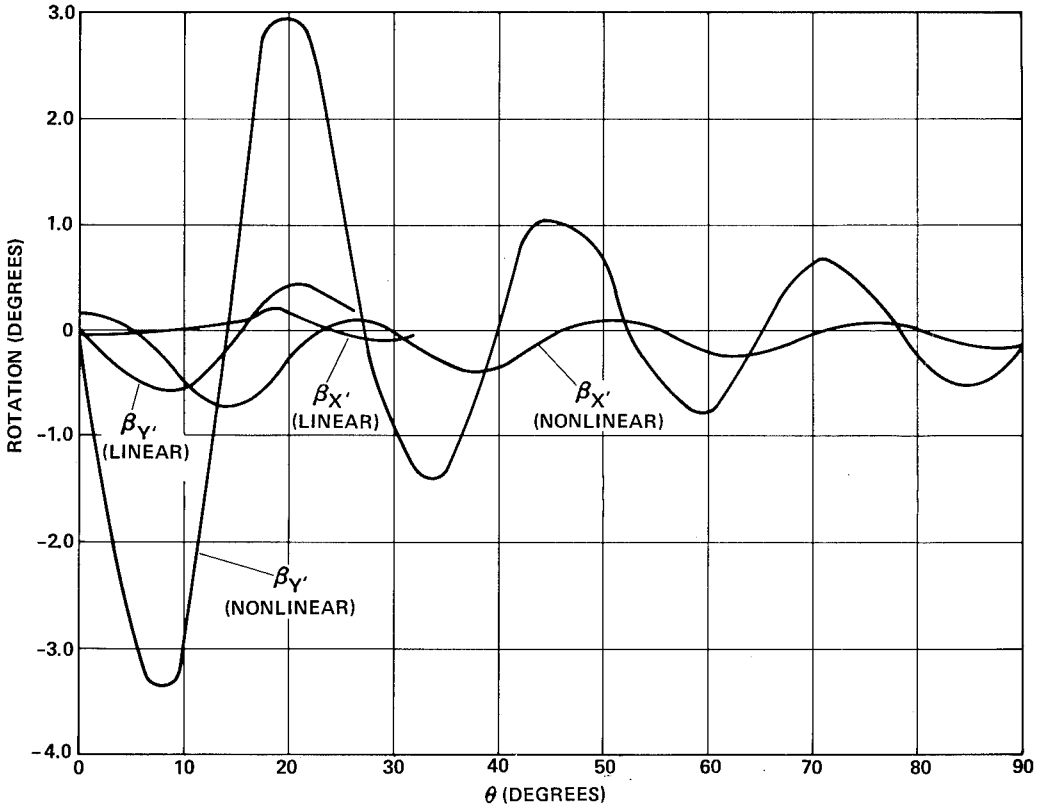

Figure 18. Linear and nonlinear rotations along Row 17 for load factor = 3.175.

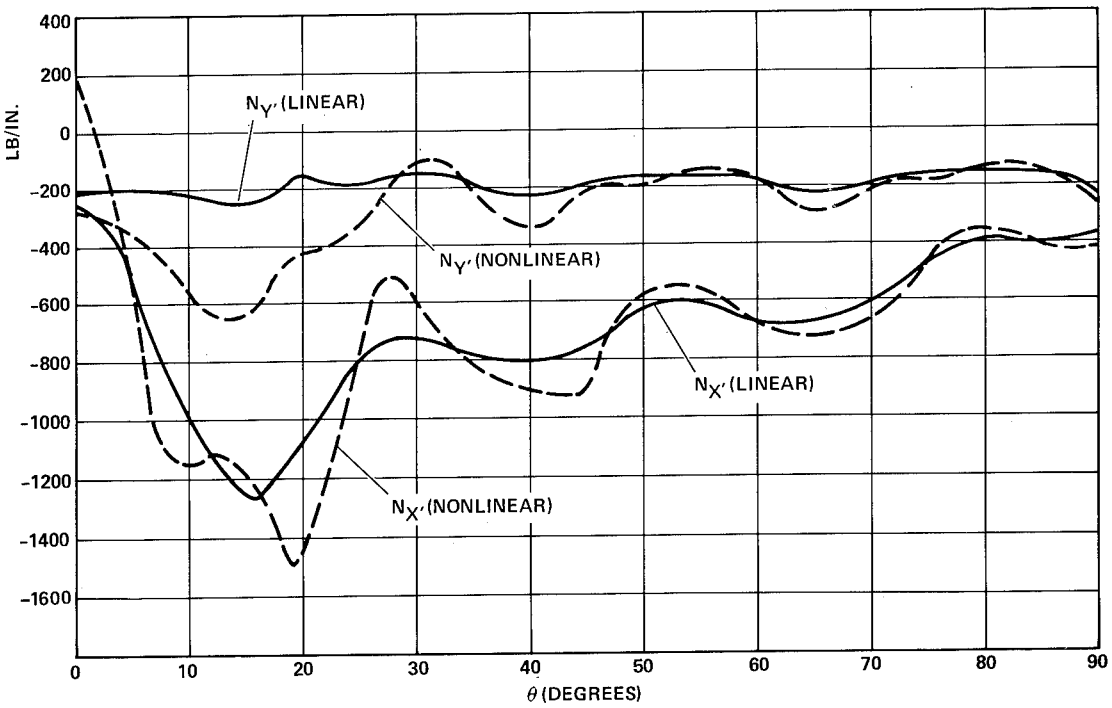

Figure 19. Linear and nonlinear stress resultants along Row 17 for load factor = 3.175.

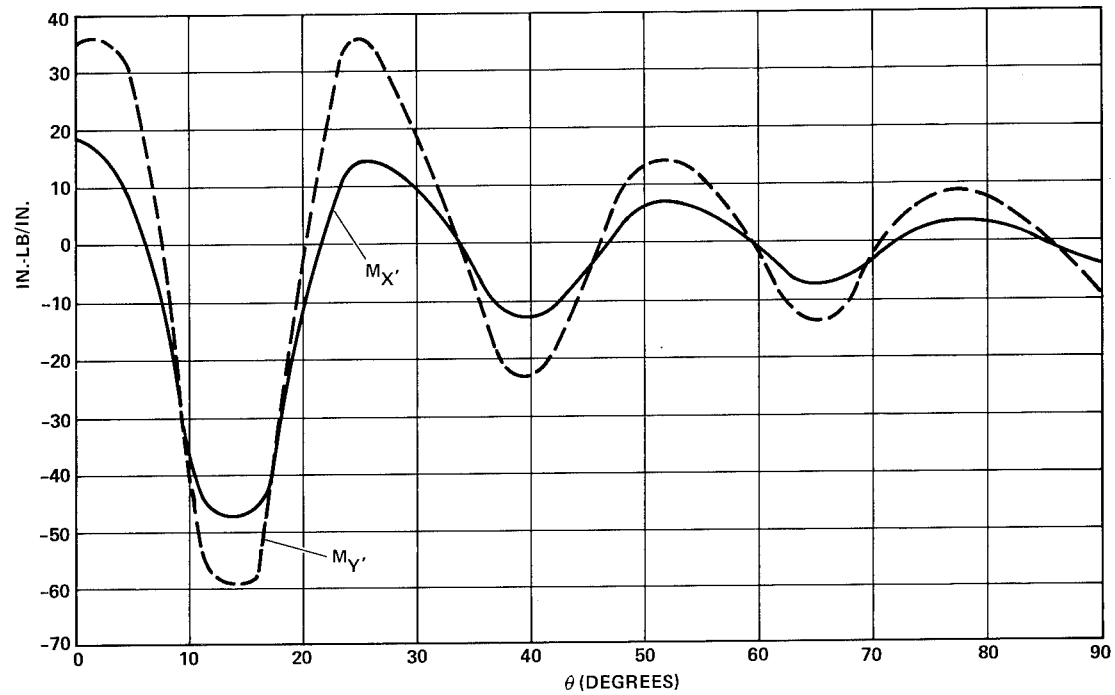

Figure 20. Nonlinear stress couples along Row 17 for load factor = 3.175.

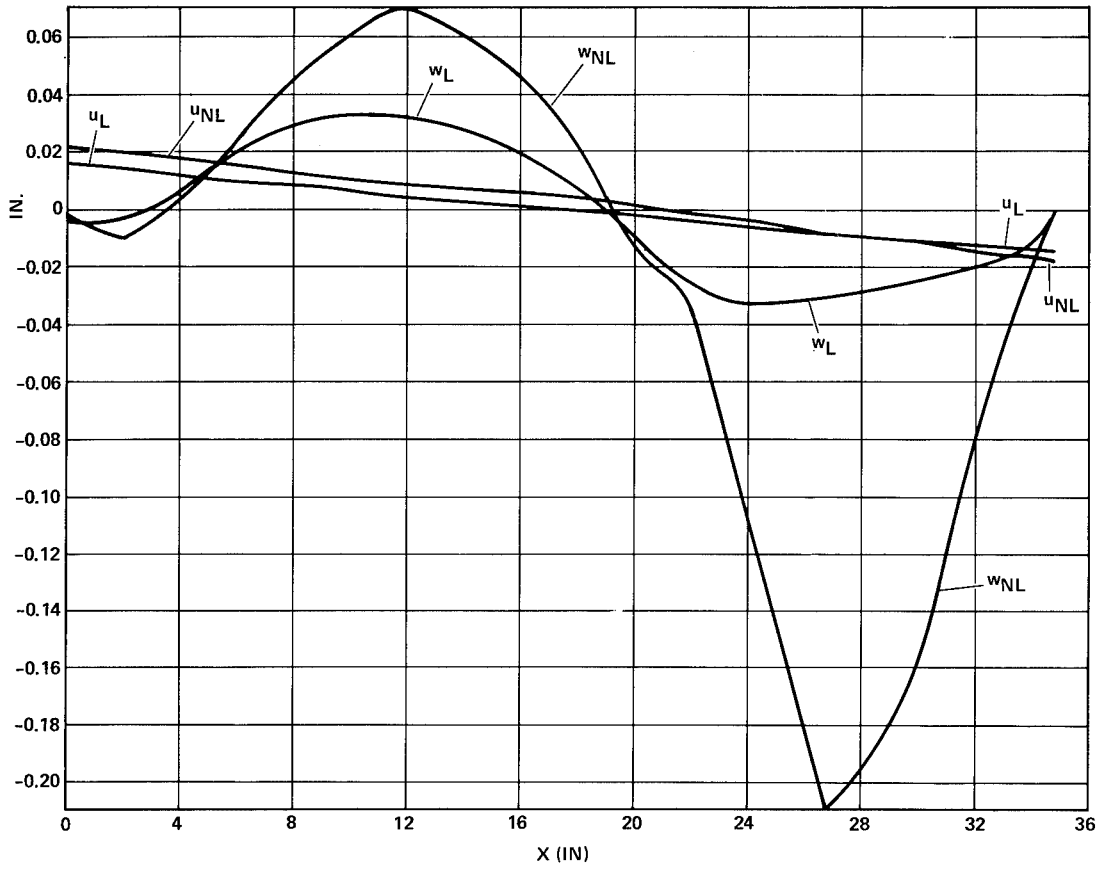

Figure 21. Linear and nonlinear displacement components along Column 6 for load factor = 3.175.

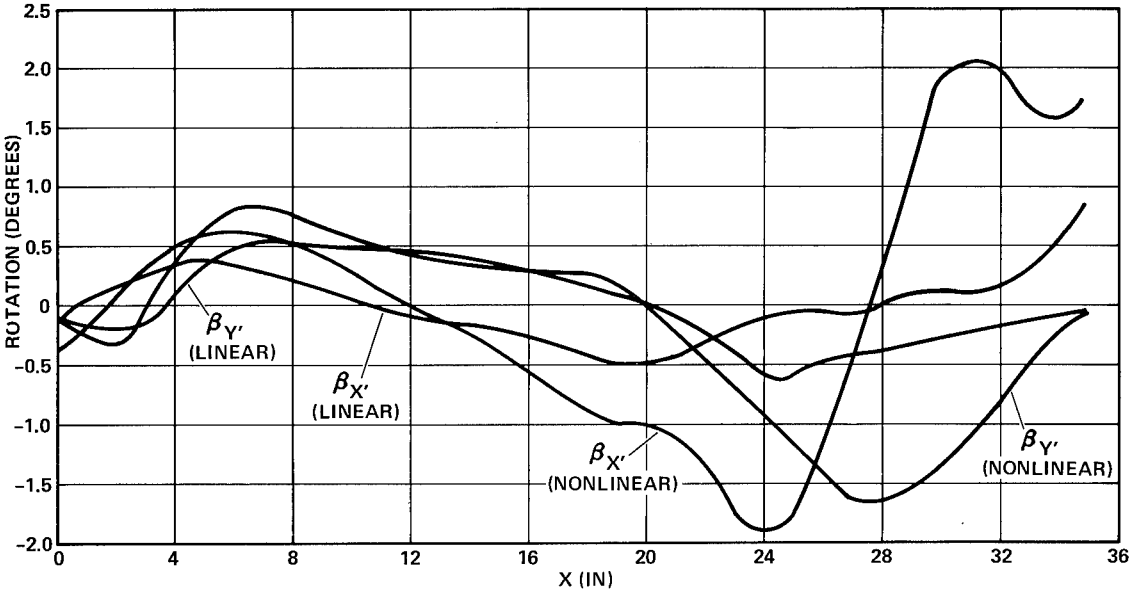

Figure 22. Linear and nonlinear rotations along Column 6 for load factor = 3.175.

by the presence of intermediate rings in this case. As a matter of interest, the stress resultants are shown along Column 6 in Figure 23.

A comparison of the three rings in the conical adapter is shown in Figure 24, where plots of the displacement components (w) are shown. The forward ring has the greatest displacements, while the mid and aft rings have approximately similar magnitudes of maximum displacement. This serves to show that the mid-ring was adequately designed, and some weight reduction may be warranted.

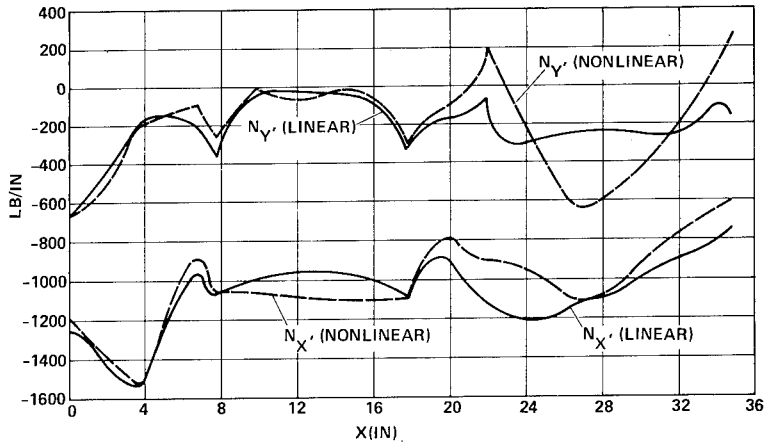

Figure 23. Linear and nonlinear stress resultants along Column 6 for load factor = 3.175.

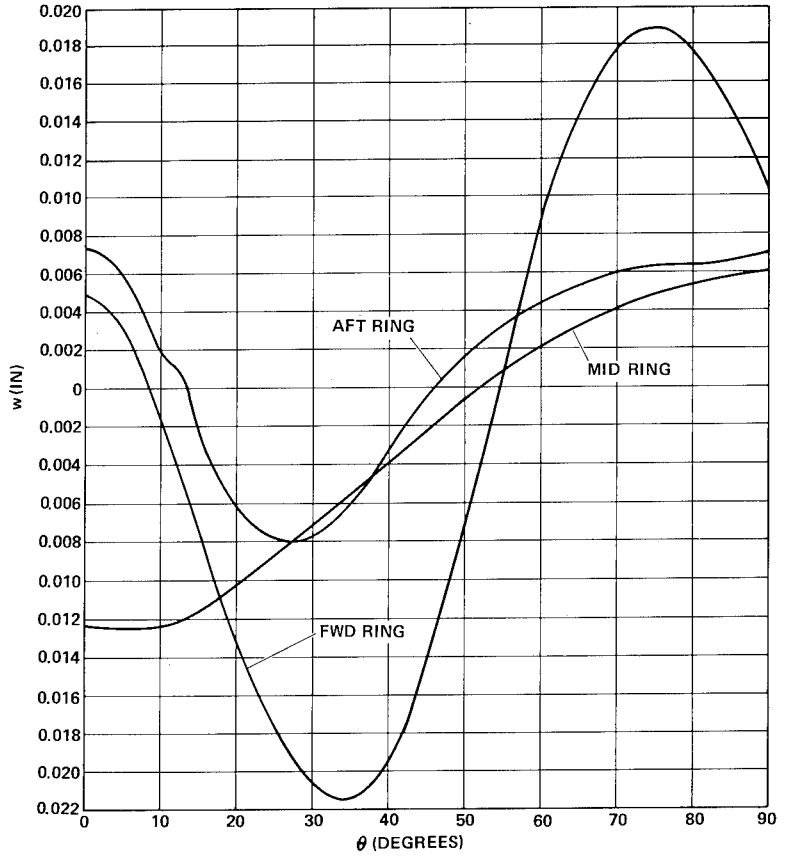

Figure 24. Nonlinear displacement component (w) of rings for load factor = 3.175.

INTEGRAL RING FLANGE JOINTS

The graphite/epoxy forward and aft rings on the conical adapter were designed to be integral with the shell. Figures 2 and 3 show the geometry and layups of the integral laminated rings. Previous experience with integral ring joints in composite shell structures has indicated that problems can result from compression loads in the shell, which result in significant interlaminar tension stresses in the corners of the joints. Premature failure of the shell can result due to these interlaminar tension stresses. The interlaminar tensile strength is quite low since there are no fibers in this direction. Accordingly, an analytical investigation of this phenomenon was undertaken in conjunction with a small test program to ensure the structural adequacy of the joints.

A finite-element analysis was performed for both the forward and aft joint configurations. The mathematical models included the metal mating rings and four inches of the conical shell. The length of shell used in the analytical model was established to be the appropriate attenuation length ($x = 4$ inches) by the use of Ref. 5, where $\lambda x = \pi$ and $\lambda = 4\sqrt{3(1-\nu^2)/(R^2t^2)}$. Figure 25 illustrates the aft ring joint configuration loaded in compression. Shown in the joint are the Atlas (Sta. 502) mating ring, the epoxy filler under the heel of the flange, and an aluminum radius block for reacting tensile loads.

The complete finite-element model, excluding the radius block and fillet, is shown in Figure 26. Details of the joint area in the finite-element model, which includes both the radius block and the fillet, appear in Figure 27. An analysis of the joint shown in Figure 28 without the potted fillet was performed to ascertain its effect upon the interlaminar tension values.

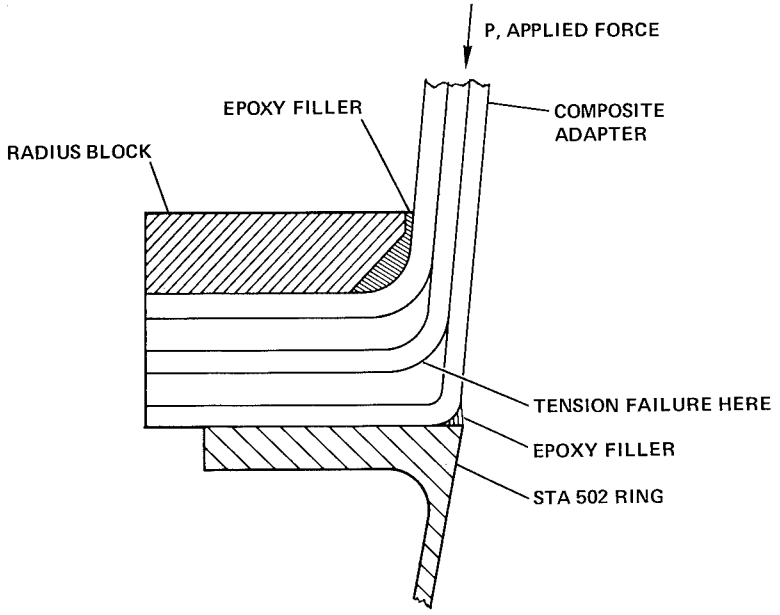

Figure 25. Aft ring joint.

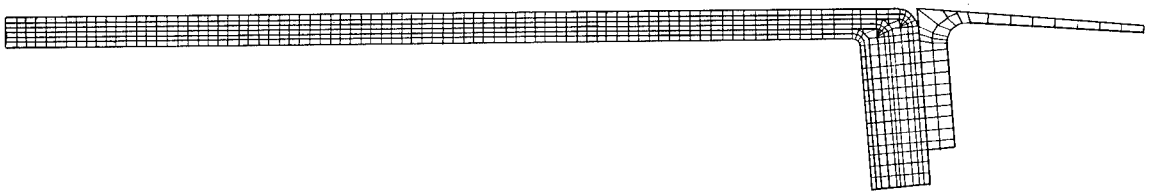

Figure 26. Finite-element model of aft ring joint.

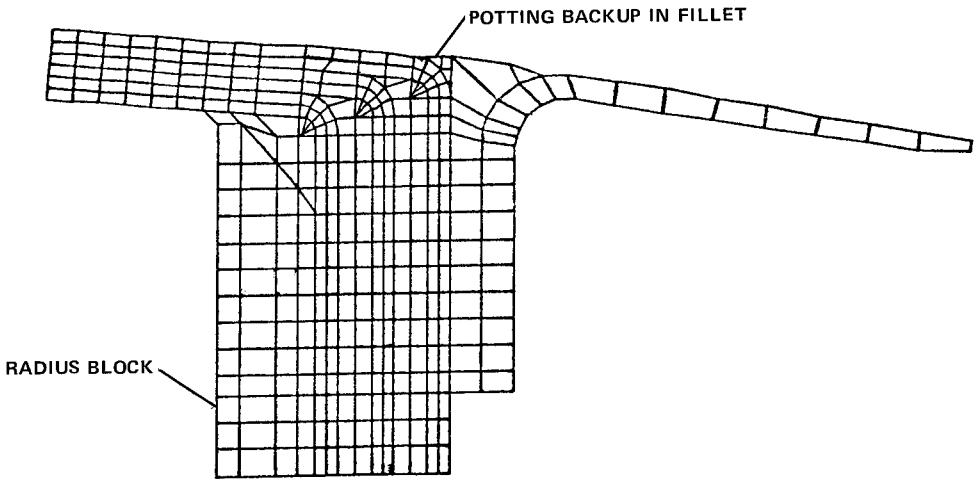

Figure 27. Finite-element model of aft ring with radius block and potting backup.

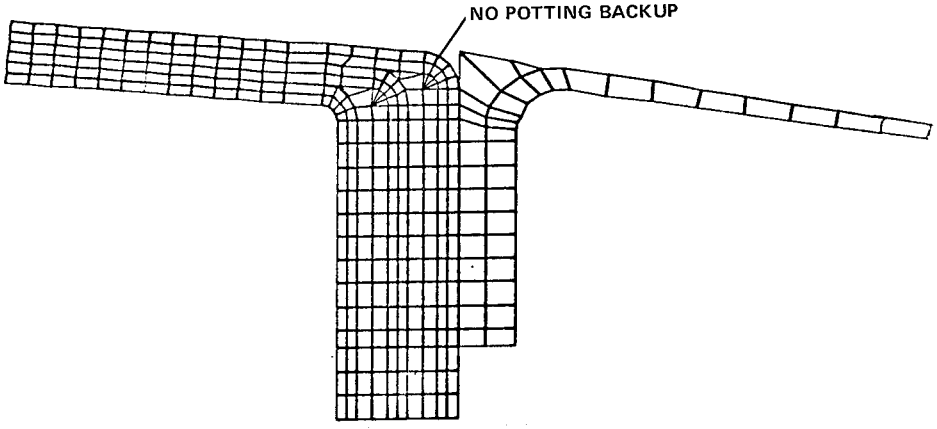

Figure 28. Finite-element model of aft ring without radius block or potting backup.

In the finite-element model, there are six elements through the thickness of the shell and ten elements through the flange, excluding the metal ring. Each element consists of four plies of pseudo-isotropic graphite/epoxy. The notation for laminate coordinates in the finite-element model are shown in Figure 29. Average material properties for unidirectional and the pseudo-isotropic laminate are presented in Table 1. Average values for material properties were used in the finite-element model since a prediction of average interlaminar tensile stresses was desired for correlation purposes with the planned tests. Minimum properties were used earlier for design purposes.

The computer code used in the analysis is a finite-element program, SOLID SAP (Ref. 6), which was developed at the University of California at Berkeley and modified for use at Convair. It performs static linear analysis of three-dimensional structural systems. An axisymmetric analysis was made. The finite-element model was verified using a graphic interface with the computer (Ref. 7). Figures 26, 27, and 28 are hard copies of the pictures on the cathode ray tube. After execution of the computer code, deflected plots may also be displayed on the cathode ray tube. Figure 30 shows such a plot where the deflections are greatly exaggerated.

Four joint test specimens were fabricated and tested, two in tension and two in compresssion. The specimens are shown in Figure 31 after testing. The first tensile specimen did not have a radius block for support, and failed at a tensile load of 1,024 pounds. The second tensile specimen with the radius block did not fail, but the bolt yielded excessively at a tensile load of 1,782 pounds. Figure 32 is a closeup view of the two tensile specimens. Without the radius block, the composite joint failed in

interlaminar tension as shown. The composite material appears intact where the radius block was used, and bending of the bolt is observed. The finite-element analysis for the joint with the radius block verified analytically the structural adequacy of the composite due to tensile loading.

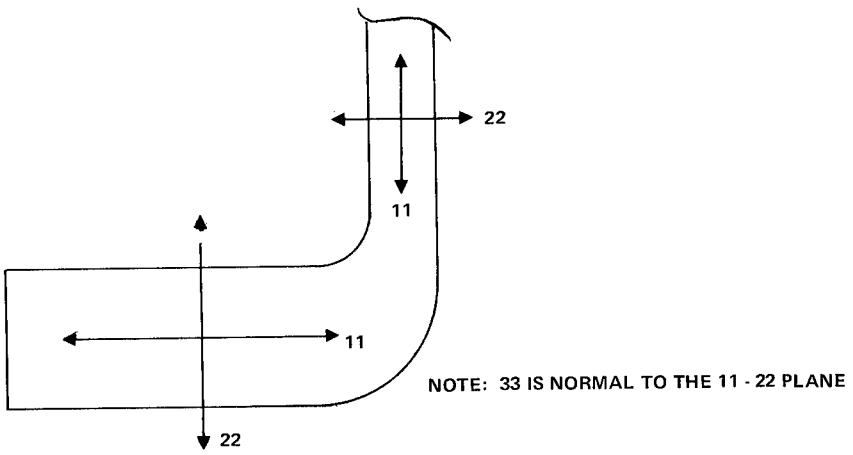

Figure 29. Notation for coordinate axes in finite-element model of joints.

Table 1. Average material properties.

Unidirectional		0/±45/90*	
E_{11} (psi)	26.1×10^6	E_{11} (psi)	9.52×10^6
E_{22} (psi)	0.9×10^6	E_{22} (psi)	0.90×10^6
G_{12} (psi)	6.3×10^6	E_{33} (psi)	9.52×10^6
ν_{12}	0.32	G_{12} (psi)	0.63×10^6
		ν_{12}, ν_{23}	0.03024
		ν_{13}	0.312

*The directions 11, 22, 12, 13, & 23 refer to elements in the finite-element analysis, as shown in Figure 29, which has no relation to the notation for unidirectional composites

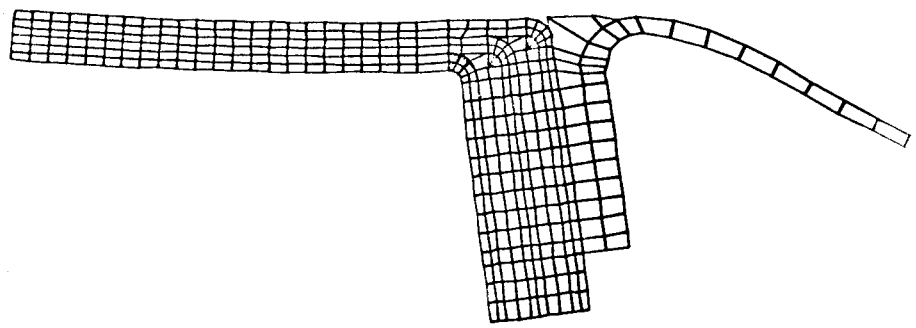

Figure 30. Deformed model of aft ring joint due to compression load.

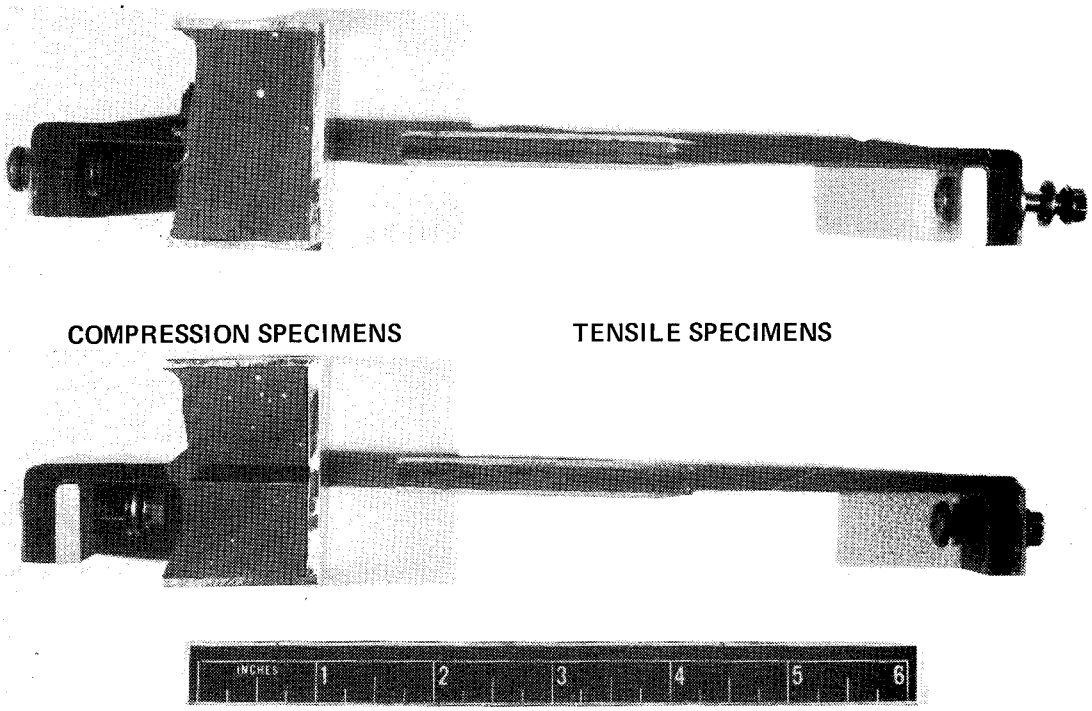

Figure 31. Tensile and compressive joint specimens (two each) after testing.

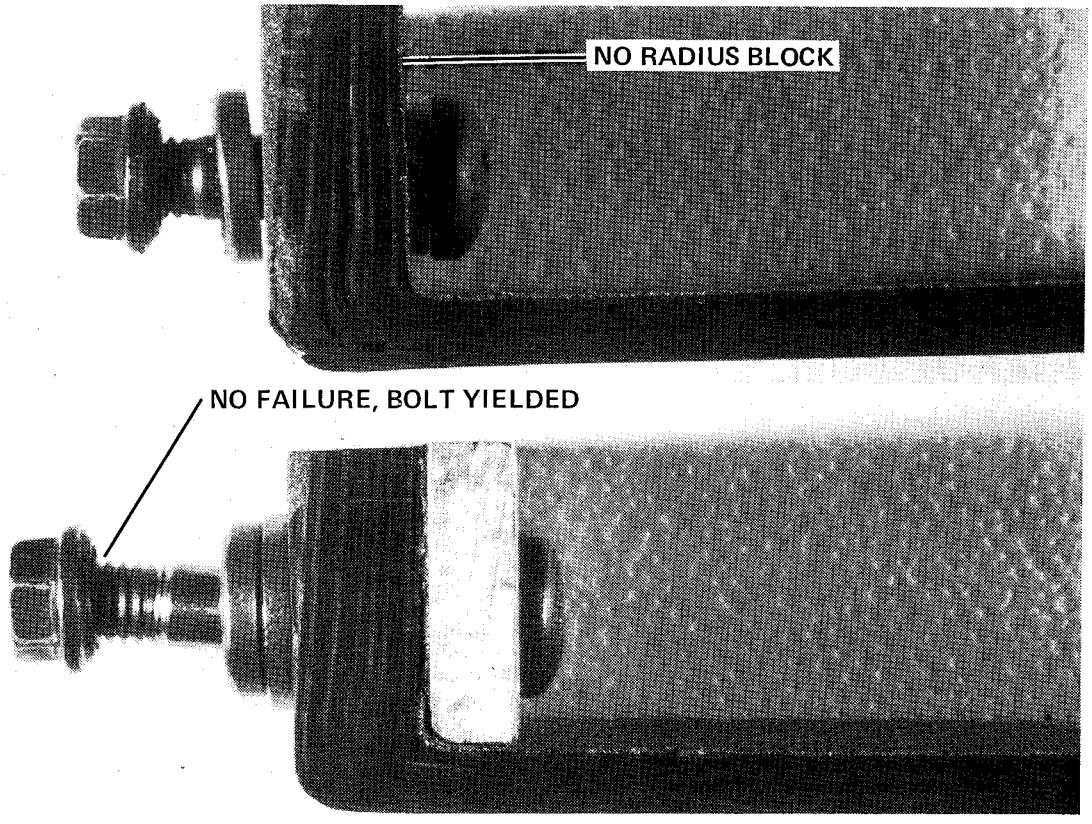

Figure 32. Tensile specimen after testing.

The two compression specimens failed in interlaminar tension at the same location, as shown in Figure 33, where the failure in one specimen is quite pronounced. The failure loads for the specimens were 1,466 and 1,596 pounds. The corresponding finite-element analysis indicated that the highest interlaminar tensile stress did, indeed, occur where the failures took place. Also, the addition of potting in the fillet of the heel of the specimens would reduce the resulting interlaminar tension to approximately 77% of the value without potting.

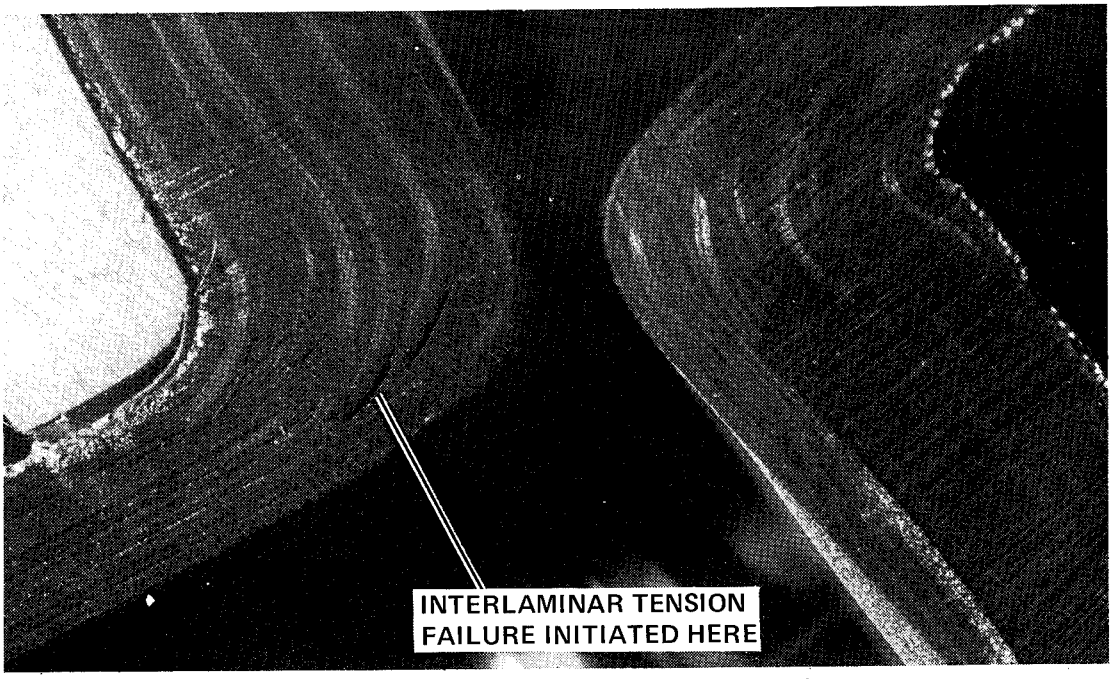

Figure 33. Enlarged views of compression test specimens.

There is no reliable test data concerning allowable interlaminar tensile stresses; consequently, a comparison of the joint tests reported here and a corresponding plane-strain finite-element analysis was performed to establish estimated interlaminar tension allowables. Here, the model was changed to duplicate the actual test specimens: 1.1 inches wide and 1 inch long resting on a fixed surface instead of the flexible match angle. This was then compared to the axisymmetric analysis to determine the applicability of the test results to the real structure, which compared favorably. The average compressive stress in the shell portion of the test specimens was $\sigma^c = 10{,}600$ psi. From the axisymmetric and plane-strain finite-element solutions, corresponding interlaminar stresses were found to be

$$\sigma_{22}^{c} \text{ (axisymmetric)} = 0.178\ \sigma^c$$

$$\sigma_{22}^{c} \text{ (plane-strain)} = 0.191\ \sigma^c$$

Thus, the average allowable interlaminar tension stress so established is

$$F_{22}^{cu} \approx 1{,}950 \text{ psi}$$

which is consistent with the wide scatter of previously unpublished test data at Convair.

CONCLUSIONS

Because of its versatility, the STAGS computer code is an excellent tool for analysis of shell structures that are subjected to possible local buckling or general collapse. In the case of the problem presented in this paper, the monocoque shell structure behaves in such a manner that local buckling and general collapse are synonymous. Had axial stringers been present, local buckling might have occurred in the skin panels before general collapse.

The existing version of STAGS does not accommodate discrete point supports such as those provided by beams or rods; however, this capability will be made available during 1975 by an additional finite-element routine to be used in conjunction with the finite-difference method. Thus, a wide class of complex asymmetric structures may then be analyzed for stability by the STAGS code.

The mathematical model must be generated with utmost care since any solution (linear, bifurcation, nonlinear) is vulnerable to an ill-conditioned model. What started out as a very ill-conditioned model in this program turned out to be excellent with only a few changes that involved the circumferential grid-spacing. Some of the important facts that came to light in this program regarding the mathematical model and subsequent analysis are:

1. Do not make drastic changes in grid spacing abruptly; make all changes gradually.
2. Make all grid patterns reasonably small in all areas of compression, particularly the circumferential grid spacing where a large number of half waves usually appear at buckling. For the present problem it was found that a maximum circumferential spacing no larger than 15 times the thickness was more than adequate.
3. Gradually open up the grid-spacing in tension areas because the fewer number of grid lines the less computer time will be required.
4. Reinforcing large cutouts by one-sided doublers whose cross-sectional area is twice that of the cutout will not completely restore this shell to its original buckling strength, but nearly so.
5. A bifurcation buckling analysis for combined compression and external pressure by the use of Ref. 1 or 5 will result in an overweight structure because of the much too conservative linear interaction expression

   $$R = R_c + R_p$$

   that is recommended in Ref. 1. The interaction of the total loading is accurately accounted for in the STAGS computer code by the total potential energy theory that is employed.

6. In the present problem, the nonlinear collapse analysis with initial imperfections that had amplitudes of about a third of the shell thickness resulted in an allowable load factor that was virtually the same as that from a bifurcation analysis where lower-bound knock-down factors were employed.
7. Potted-in radius blocks are required for the integral rings to adequately react the tension loads. Potting under the heel substantially reduces the interlaminar tension when subjected to compression loads. Finally, interlaminar tension is not significant for the tension condition with the potted radius blocks under the bolts. In conclusion, it appears to be a very feasible design approach to use integral ring joints for the type of structure reported in this paper.

ACKNOWLEGEMENT

The authors are deeply indebted to the following persons for their helpful advice during the course of this work:

Lockheed Palo Alto Research Laboratory (STAGS Analyses); B.O. Almroth. F.A. Brogan, and E. Meller.

California Institute of Technology (STAGS Analyses): Prof. C.D. Babcock, Jr. and J. Arbocz.

General Dynamics Convair Division (STAGS Analyses): G.W. Smith and G. Wang.

Significant contributions to the program were provided by the following Convair personnel: W.J. Wallace (design), R.O. Morin (design), N.R. Adsit (testing), G. Harrison (stress), and F. Harris (loads).

Also, appreciation is extended to R.S. Shorey, G.W. Norris, and J.L. Minos for their encouragement in the preparation of this paper.

REFERENCES

1. NASA Space Vehicle Design Criteria (Structures), "Buckling of Thin-Walled Circular Cylinders," Report NASA SP-8007, August 1968.
2. Almroth, B.O., et al, "User's Manual for STAGS," Vol. 3 – User's Instructions, Report LMSC-D358197, Structural Mechanics Laboratory, Lockheed Palo Alto Research Laboratory, Palo Alto, California, January 1974.
3. Brogan, F, and Almroth, B.O., "Buckling of Cylinders with Cutouts," AIAA Paper No. 69-92, AIAA 7th Aerospace Sciences Meeting, New York City, New York, January 1969.
4. NASA Space Vehicle Design Criteria (Structures) "Buckling of Thin-Walled Truncated Cones," Report NASA SP-8019, September 1968.
5. Hetenyi, M., *Beams on Elastic Foundation,* University of Michigan Press, Ann Arbor, Michigan.
6. CASD-CIH-74-008, "SOLID SAP: User's Manual," September 1974.
7. CASD-CIH-74-002, "A General-Purpose Finite-Element Graphics Program: User's Manual," February 1974.

COMPOSITE NACELLE STRUCTURES - DC-9 NOSE COWL

By Robert A. Elkin

Rohr Industries, Inc.

INTRODUCTION

The program described in this paper was undertaken to obtain an in-depth evaluation of the problems and payoffs associated with applying advanced composites to jet engine nacelles. The program had two objectives.

(1) Expand Rohr's experience and expertise in the design and manufacture of composites to flight-worthy composite nacelle hardware.

(2) Obtain a flight service evaluation of composite nacelle hardware.

The program was divided into four tasks: design, manufacture, test and in-service evaluation. The first three have been completed and have met the first program objective. The second objective will be met by the flight service task which is expected to begin shortly.

DESIGN TRADEOFF STUDIES

The design task began with a weight/cost tradeoff study. Following some preliminary evaluations of a typical nacelle, a nose cowl assembly was selected for more detail study. Two basic designs of a typical nose cowl were compared; a composite configuration, and an advanced conventional aluminum version. Manufacturing cost drawings were prepared for various composite concepts. These were used to estimate weights and production costs for each of the major details and subassemblies. Tooling costs for the more promising concepts were also evaluated.

The initial portions of the tradeoff analyses used the current material and labor costs. A sensitivity analysis was then conducted to evaluate the effects of projected composite material cost reductions, various rates of inflation on labor and other material costs, and their effect upon the overall cost of each design.

The conclusion derived from the tradeoff study was that the application of composites to nacelle structures, specifically a nose cowl assembly, will result in a significant cost competitive weight savings by about 1979 (see Table I). If a dollar value is placed upon weight saved, composite application is cost effective now for many areas of nacelles.

Following completion of the tradeoff studies a decision was made to proceed with the detail design of a DC-9 nose cowl with a graphite composite outer barrel assembly. The production outer barrel assembly, currently manufactured by Rohr Industries as part of the DC-9 nose cowl, is shown in Figure 1. A comparison of some of the pertinent features of the production aluminum, and the composite designs, is shown in Table II.

DESIGN CONSIDERATIONS

In addition to the basic structural aspects, strength and stiffness, the detail design considered all applicable environmental factors. These included elevated temperatures resulting from use of the anti-icing system, lightning protection, riveted joint strength, galvanic corrosion of fasteners, impact resistance and repair techniques, and the response of the composite structure in a high sound pressure field (sonic fatigue resistance).

Thermal Analysis

A thermal analysis was conducted to establish the maximum temperatures to which the outer barrel structure would be exposed due to operation of the nose cowl anti-icing system. During icing conditions these temperatures are well within the capability of the epoxy matrix. However, it was found that there are unusual circumstances which could cause excessive temperatures in certain areas. These maximum temperatures occur with takeoff power, on a 49°C (120°F) ambient day, and the anti-icing turned on. This would only occur with a failure in the anti-icing system. Under these conditions the analysis indicated two areas of concern. The composite skin temperature, in the vicinity of the opening in the outer barrel through which the expended anti-icing air is exhausted overboard, would reach 229°C (444°F). The other area was the junction of the outer barrel and the nose lip, where the analysis indicated a temperature of 204°C (400°F) in the composite.

For the first area, further analysis indicated that the local application of insulation would limit the skin temperature to under 176°C (350°F). However, there was no convenient way to insulate the composite in the second area, at the nose lip junction. Since the likelihood of the conditions resulting in the high temperatures is small, and if it occurred at all would be of short duration (several minutes), it was decided to establish reduced properties for this area by conducting tests at 204°C (400°F). The area in question is where the composite skin is riveted to the nose lip. Therefore fatigue tests of riveted joint specimens were conducted at 204°C (400°F). The results of these tests showed that the strength of the joint was considerably greater than required.

Lightning Protection

The nacelle on a DC-9 is in a Zone 2 lightning area. This means that it is not subject to a direct lightning strike, but may be subject to a restrike or sweep stroke attachment. The associated current of these is significantly lower than that of a direct strike. This allowed the use of a passive lightning protection system based upon the dielectric shielding approach recently patented by M. Amason and J. Kung of Douglas Aircraft Company (Reference 1). This approach is significantly lighter, for this application 38 percent lighter, than a conductive aluminum mesh lightning protection system.

Riveted Joints

It was planned to assemble the composite outer barrel into an entire nose cowl assembly using production details for the remainder of the assembly. This meant that, despite the problems with rivets in composites that have been reported in the literature, the outer barrel would be assembled by riveting. Design substantiation tests revealed relatively few problems associated with installing rivets in graphite epoxy. Several precautions, however, are required. When drilling the rivet hole the back side of the composite skin should be supported to prevent any splintering of the back side plies. Standard high speed drills are acceptable for drilling, but they must be sharpened or replaced frequently. For countersinking, a diamond tool should be used. Installation of the rivets may be accomplished by normal squeezing or bucking procedures. However, if the upset head of the rivet is against the composite, a washer, with a close tolerance hole, should be used.

Galvanic Corrosion

The corrosion of fasteners, specifically rivets, due to the difference in electrical potential between the graphite skin and the fastener, was also investigated during the design task by a series of tests. Riveted joint test specimens were subjected to salt spray for 30 and 60 day periods. Aluminum, monel, and titanium rivets were evaluated. Salt spray impingement was on the flush head side of a portion of the specimens, and the upset head on the remainder. Both protected and unprotected rivets were exposed. As was expected, the unprotected aluminum rivets were badly corroded after 30 days, and several fell apart after 60 days exposure. Neither the monel nor the titanium rivets showed any signs of corrosion or loss of strength, even when unprotected. The coated aluminum rivets also held up well. However, since the durability of the coating during several years in service could not be guaranteed, a conservative approach was decided upon, and monel rivets were selected for use.

Sonic Fatigue Resistance

The nacelle of any jet engine is subjected to high sound pressure levels, or sonic fatigue. Through many years of experience in designing and building nacelles for nearly all of the free world's jet aircraft, Rohr has found that sonic fatigue cannot be ignored. An extensive study was therefore undertaken to establish the sonic fatigue response and resistance of graphite composites compared to metallic structures. Six panels were fabricated, one all aluminum and the others graphite. The aluminum panel had a skin the same gauge, and stiffeners of the same configuration and spacing, as the production DC-9 outer barrel. All of the graphite panels were an eight ply, quasi-isotropic layup. Two panels were unstiffened, two had a single stiffener (different stiffener configurations), and the fifth had stiffeners spaced as the aluminum panel. Four of the graphite panels and the aluminum panel are shown in Figure 2. All panels were instrumented and tested at the Institute of Sound and Vibration in Southhampton, England.

The results of those tests showed composites to be more than adequate for the application. The panels showed no sign of damage after several hours at sound pressure levels 23 db higher than the DC-9 sound pressure levels at the response frequency of the panel. After initial tests one of the unstiffened panels was subjected to impact damage by dropping a steel ball from a sufficient height to allow complete penetration. One jagged, splintered hole was made near the center of the panel, and another near an edge. The panel was subsequently subjected to four hours at sound pressure levels 5 db above the DC-9 levels at the response frequency of the panel. Examination of the panel before and after the test showed no propagation of the impact damage.

The results of the sonic fatigue tests of the panels were used to predict the response of the outer barrel. As discussed in a later section, these predictions were basically confirmed in a test of the completed nose cowl on an engine.

FINAL DESIGN

Some of the details of the final design of the nose cowl assembly, and the composite outer barrel, are shown in Figure 3 and 4. The basic outer barrel is composed of two skin halves joined by riveting at an upper and lower axial splice. To avoid the requirement for a separate splice, and a second row of rivets at each joint, one of the skin halves joggles to go under the other skin. This same approach is used at the forward joint, where the outer barrel joggles to go inside the nose lip assembly and is riveted in place. At the aft end, there is a joggle and then a flange. Nut plates are riveted to the flange, and the aft bulkhead of the nose cowl is subsequently attached by bolting. A rub strip is fastened in the aft joggle area with nylon rivets. The cowl door of the nacelle closes against the rub strip.

The basic skin of the outer barrel is eight plies of graphite epoxy oriented in a quasi-isotropic pattern. In all rivet joint areas the skin is

built up with an additional eight plies, also in a quasi-isotropic pattern. Included in the outer barrel assembly is an aluminum air exit scoop. This directs the expended anti-icing air overboard, through an opening in the barrel structure. The brackets that support the duct, which carries the anti-icing air to the nose lip, are also riveted to the composite skin.

The structural analysis of the outer barrel was performed with the use of the NASTRAN finite element analysis program. Rohr's composite analysis program, COMPOSITE, was used to establish the stiffnesses and buckling coefficients of the oriented layup. A fail-safe analysis of the outer barrel was conducted by removing a large section from the NASTRAN model, and rerunning the program to establish the increase in the stresses in the vicinity of the cutout.

MANUFACTURE

The skins were laid up and cured in a fiberglass tool. A female plaster splash was taken from the master model of the DC-9 nose cowl. This was used to make a male plaster plug on which the fiberglass tool was laid up and cured. The tool was maintained as a full 360^{o} section in order to better maintain contour. However, the two skin halves were laid up and cured sequentially. A removable insert was used in the tool to form the joggle for the axial splice joint of each skin half.

The graphite epoxy prepreg was purchased as 12-inch wide tape. This was used to layup the large sheets of multiple ply oriented broadgoods. Flat pattern templates were then used to cut the large pieces of broadgoods which were laid in the tool. The slight compound contour of the skin posed no problems in the layup of the large multiple ply sheets. The layup in the aft flange, however, did require some development before a wrinkle and void free corner could be formed.

Simple sheet metal templates were used during the layup to assure proper location of doubler plies. One such template is shown in Figure 5. In this photo the basic skin layup has been completed, and the required doubler plies around the anti-icing air exit scoop opening are being applied.

After completion of the layup the part was bagged and cured. Standard edge dam, bleeder, and bagging methods for graphite epoxy were used. A heavy rubber caul sheet was used to assure uniform pressure distribution during cure. Since the tool was fiberglass, and therefore somewhat porous, an envelope style vacuum bag was utilized. The cure was conducted in an autoclave at $176^{o}C$ ($350^{o}F$) and 0.69 MN/m^{2} (100 psi).

A thorough transmission ultrasonic inspection, as depicted in Figure 6, was used to check for delaminations or void areas. In addition, destructive tests were conducted on specimens cut from in-process control panels. These panels were laid up and cured at the same time as the skin laminate, using the same batch of material.

The composite outer barrel was mated to production sheet metal assemblies of the inner barrel, nose lip, and aft bulkhead, to form a complete DC-9 nose cowl. Location of outer barrel trim lines and rivet holes was accomplished with the production jigs and templates used for the conventional sheet metal outer barrel. Holes in the composite were drilled with standard high speed

drills and, where required, countersunk with a diamond tool. Figure 7 shows the assembly almost complete. Riveting of the nose lip to the outer barrel is depicted in Figure 8.

GROUND TEST

A ground test, on a JT8D engine, was conducted to verify the response of the outer barrel in the high sonic environment surrounding a jet engine. Instrumentation for the test, consisting of seven biaxial and eight uniaxial strain gages, was installed prior to assembly of the outer barrel with the remainder of the nose cowl. In addition, four small diaphram microphones, to measure the sound pressure levels on the inside and outside surface of the composite skin, were installed at the time of test.

The test was conducted in a test cell at Pacific Southwest Airlines (PSA's) engine overhaul facility located in San Diego. Figures 9 and 10 show the nose cowl mounted on the engine being prepared for, and ready for test. The cables hanging from lower portion of the nose cowl led to an instrumentation van where the sound pressure levels, strain gage readings, engine vibration, and engine RPM were recorded on magnetic tape for subsequent evaluation.

During the test the strain gages, microphones, and engine RPM were also monitored in real time as the engine power was slowly increased from idle to takeoff power. The engine was then run at the several speeds which produced the greatest response in the outer barrel, as indicated by the highest strain readings.

The test results were basically as predicted. The location of the maximum stresses was not precisely as expected; it was adjacent to the axial splice rather than adjacent to the outer barrel/nose lip joint. However, the stress levels due to the sonic exitation were quite low, as predicted. The maximum stresses were in the order of 2.41 MN/m^2 (350 psi).

IN-SERVICE EVALUATION

The final phase of the program is the in-service evaluation. This flight service evaluation will be conducted on a regularly scheduled commercial carrier for a period of approximately two years. In addition to the routine maintenance and inspections normally conducted by the airline personnel, Rohr plans to conduct a more thorough periodic inspection. This will include both a visual and ultrasonic inspection. The latter inspection will utilize an ultrasonic thickness gage. This instrument utilizes a reflected wave transducer and its use does not require access to the inside of the outer barrel. The thickness gage will be used to detect and map any delamination in the outer barrel skin. Of course no delaminations are expected to occur, and the inspections will only be a precautionary measure.

The in-service evaluation will commence upon completion of the few remaining Federal Aviation Administration requirements for a Supplemental Type Certificate, and completion of negotiations with the selected airline. Both of these tasks are expected to be completed shortly.

REFERENCE

1. Amason, M. P. and Kung, J. T.: Aircraft Lightning Protection System. U. S. Patent No. 3,906,308, September 16, 1975.

TABLE I.

DESIGN TRADEOFF STUDIES

WEIGHT SAVINGS
12.2 kg (26.9 lb.)
24 PERCENT
COST REDUCTION (1979)*
2 PERCENT

*BASED UPON GRAPHITE EXOXY
PREPREG COST = $55/kg($25/lb.)

TABLE II.

OUTER BARREL DESIGN COMPARISON

	ALUMINUM	COMPOSITE	PERCENT REDUCTION
FRAMES	3	0	100
DETAIL PARTS	25	10	60
RIVETS	1200	250	79
WEIGHT: kg (lb)	10.9 (24.1)	5.8 (12.7)	47

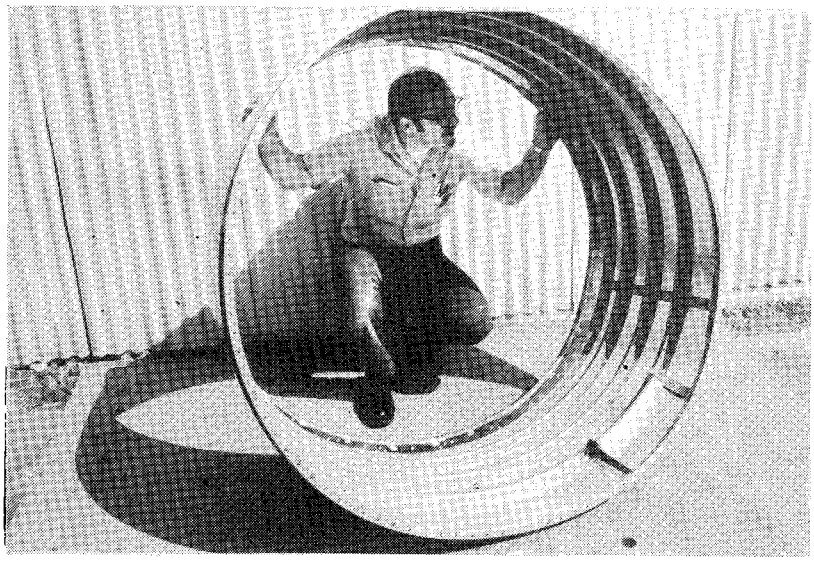

FIGURE 1

Production DC-9 Nose Cowl Outer Barrel Assembly

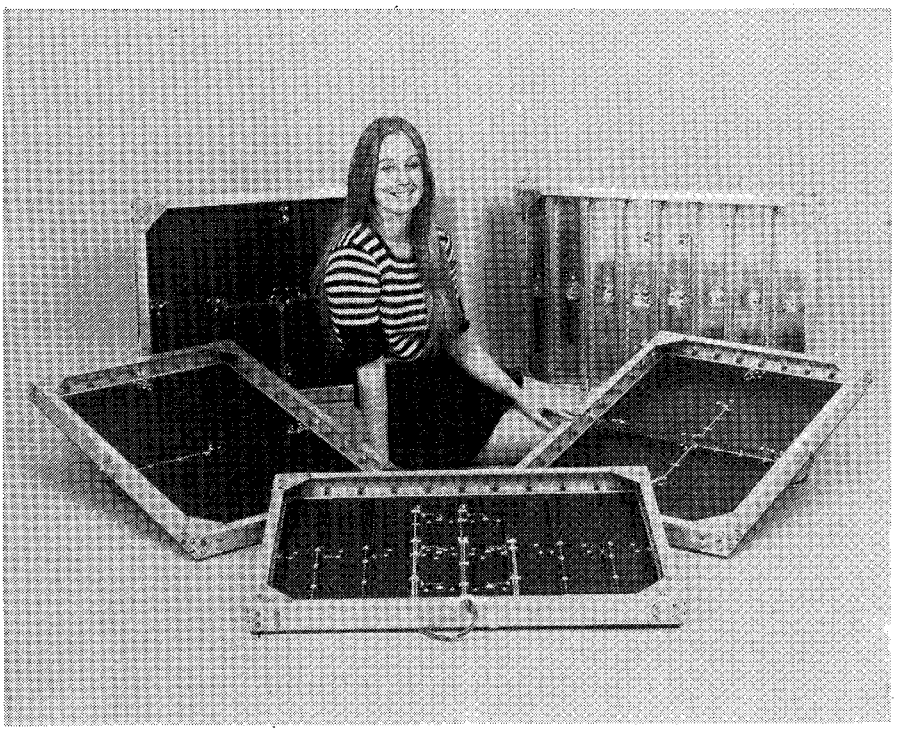

FIGURE 2

Sonic Fatigue Test Panels

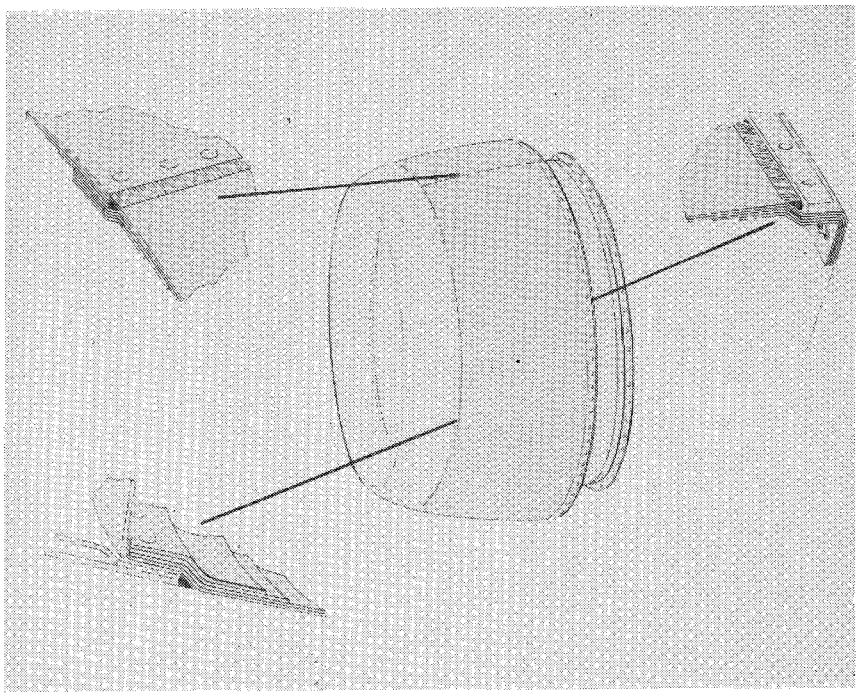

FIGURE 3

Composite DC-9 Nose Cowl Outer Barrel

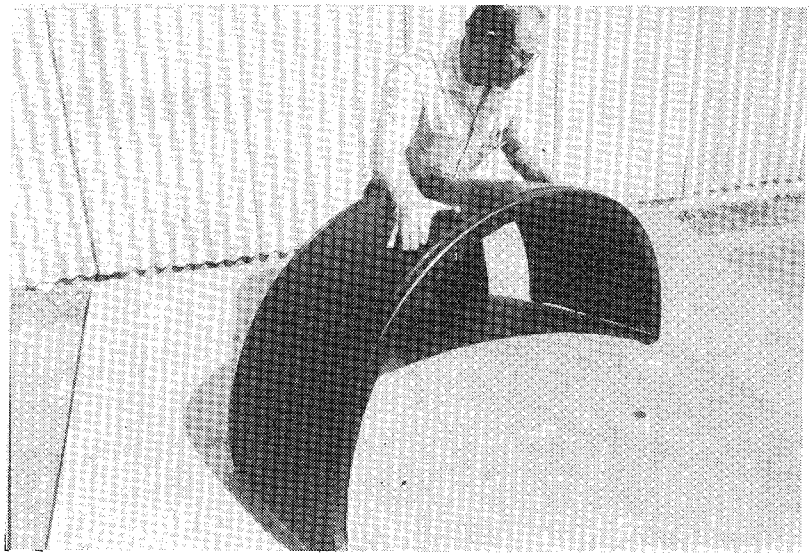

FIGURE 4

Composite Outer Barrel Half

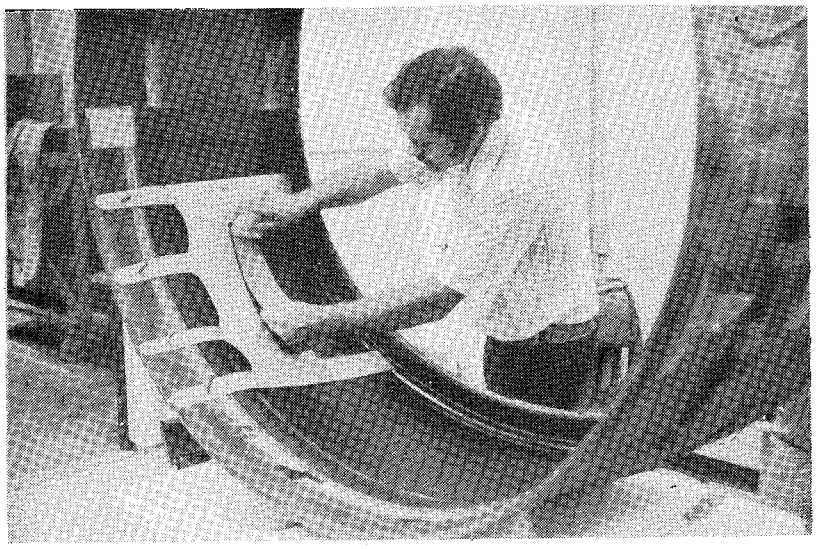

FIGURE 5

Outer Barrel Layup

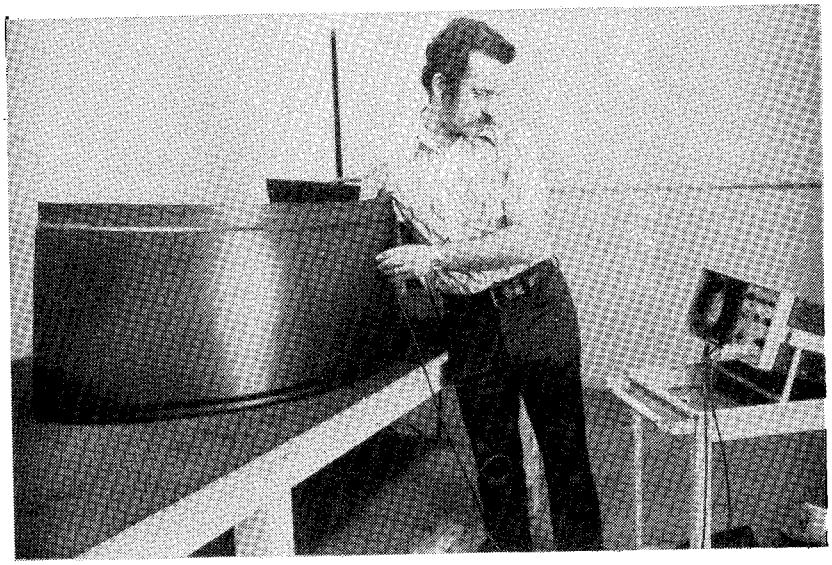

FIGURE 6

Ultrasonic Inspection

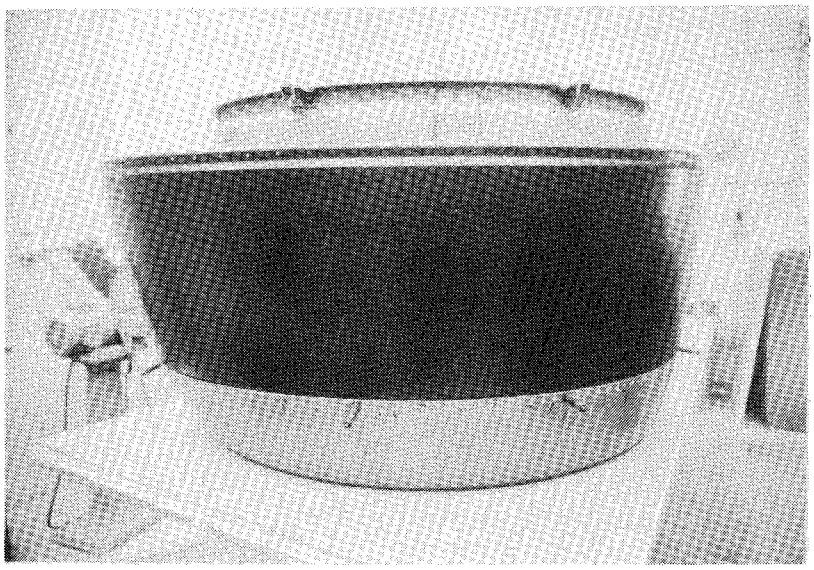

FIGURE 7

Nose Cowl Assembly

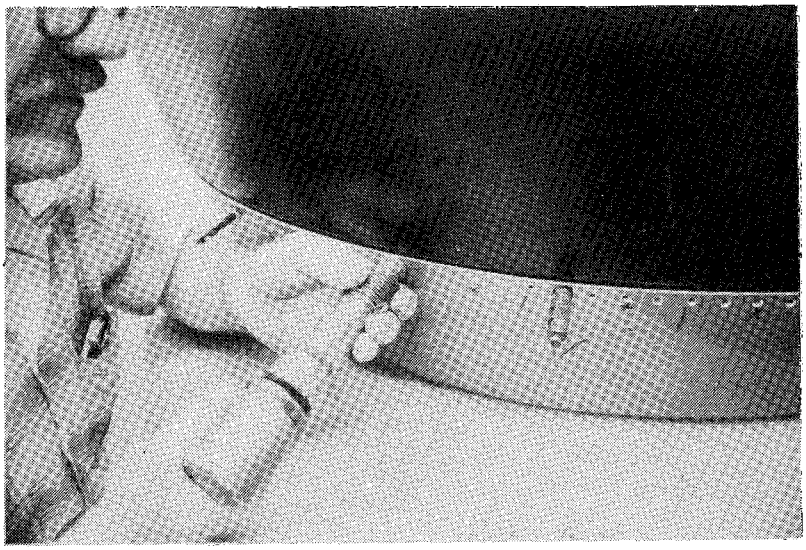

FIGURE 8

Nose Lip/Outer Barrel Riveted Joint

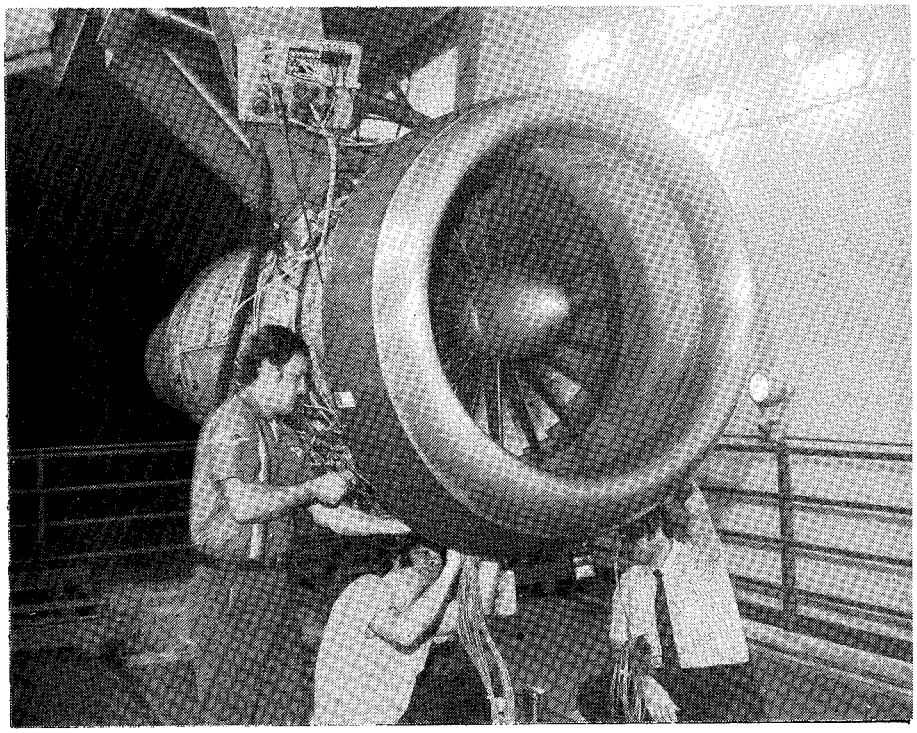

FIGURE 9

Engine Ground Test - Installation

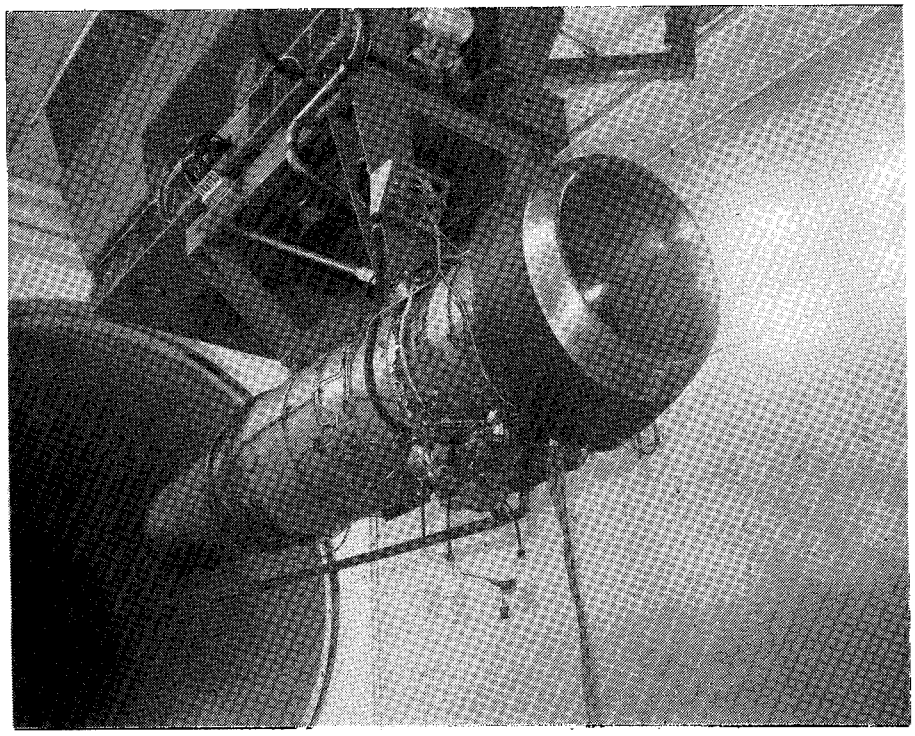

FIGURE 10

Engine Ground Test Setup

COMPOSITE NACELLE STRUCTURES -

B-1 ENGINE NACELLE RAMP

By

Norman O. Brink

Rohr Industries, Inc.

INTRODUCTION

The application of advanced composite materials to airframe structures is becoming cost and weight effective. The trend for weight and cost reduction of advanced composite structures is achieved through efficient utilization of materials, a minimum number of detail parts and improved fabrication techniques. The engine nacelle structure is one area of the aircraft in which appreciable weight/cost savings may be achieved utilizing advanced composite materials.

The nacelle on a supersonic aricraft, such as the B-1, is a complex structure because the cross-sectional area must be changed for effective air flow to the engine throughout the aircraft's speed regime. The structural complexity is due to the stiffness required to minimize deflections. The stiffness requirement and the complex contours within the nacelle indicate the potential application of advanced composite materials to this area of the airframe. Rohr Industries has completed a preliminary design of an advanced composite supersonic nacelle ramp under a subcontract to Rockwell International, Los Angeles Aircraft Division (USAF Contract No. F33-615-72-C-5111). The selected component was the second of a series of three movable ramps located in the engine nacelle of the B-1 air vehicle. The location of the Engine Nacelle Ramp No. 2 and its relation to the nacelle is shown in figure 1. The program required the development of advanced composite ramp configurations which meet the design criteria with a lower weight and achieved lower cost during production. This paper will discuss the advance composite design trade off study, the laminate structural property determination, and the production cost evaluation.

TECHNICAL DISCUSSION

Design Criteria and Baseline Configuration

The design criteria for the composite movable ramp were the same used for the prototype metallic Ramp No. 2. The composite ramp design had to meet the same form, fit, and function requirements as the prototype to provide interchangeability. The major functional requirements are listed in table I and the overall size envelope of the ramp is shown in figure 2. The target weight for the composite ramp design was 25.0 Kg (55 lb.) although the prototype had a weight of 30.0 Kg (66 lb.).

The envelope thickness for Ramp No. 2 was established by adjacent structure and actuator clearance requirements. The maximum thickness for the aft portion of the ramp was 3.8 cm (1.5 inches). To provide clearance for the torque tube at a point 12.7 cm (5 inches) aft of the forward hinge fitting the thickness was reduced to 2.54 cm (1.0 inch). In addition, two local areas were limited to a maximum thickness of 0.3 cm (0.12 inch) to provide clearance for the rotary actuators.

The complexity of the ramp is increased by the requirement for boundary layer control (BLC) through skin perforation on the aft 3/4 of the ramp area. The open area of 11 percent of the solid area was achieved on the prototype design by drilling the holes through the metal skin in the shaded sections shown in figure 2. One of the major efforts during the composite ramp design was the development of the procedure for fabricating large area perforated laminates with adequate strength. The results of this effort will be discussed later.

The critical design load on the ramp structure was caused by the transient "hammer shock" over-pressure condition. The pressure ranged from 76 to 145 KN/m^2 (11 to 21 psi) over the surface of the ramp. In addition, concentrated axial loads of 115.6 KN (26,000 lb.) were applied to the hinges during the pressure loading. The majority of this axial load was due to the kinematic arrangement of the three ramps making up the inlet nacelle control system.

Composite Ramp Design Evolution

At the beginning of the preliminary design task, three basic structural arrangements were formulated for the composite Ramp No. 2:

Arrangement A -- Full depth sandwich construction in which the maximum envelope of the ramp was used for sandwich thickness. The longerons were buried and integral within the sandwich.

Arrangement B -- Thin, constant-depth sandwich panel with integrated "strongback" longerons for stiffness and axial strength.

Arrangement C -- Single, perforated skin with a stiffening grid consisting of longerons and closures.

Several variations of each of the arrangements were configured in sufficient detail to establish the stiffness, part count, and weight of each. The goal was to lower cost and weight while still meeting the criteria.

At the end of the design evaluation, two configurations were selected for additional design definition and manufacturing analysis. One configuration consisted of sandwich construction. The second configuration was a single skin with beam stiffeners. The final two configurations are discussed in the following sections.

Stiffened Sandwich Composite Ramp No. 2

The stiffened sandwich composite Ramp No. 2 configuration is shown in figure 3. The constant-depth sandwich was located at the aft portion of the ramp. The moldline skin of the sandwich extended forward to the hinge line. The backside skin of the sandwich portion of the ramp required twice the perforated area of the moldline skin to prevent chocking of the BLC system. The skins consisted of (0/90/+45) 2S 3501/AS graphite epoxy.

The stiffeners consist of $(0_5/90)$ laminae layers laid up to the required thickness of 0.22 and 0.11 cm (.088 and .044 inch) for the backside and moldline side respectively. The composite sandwich configuration allows the stiffeners to be cocured with the skins. The stiffeners were also canted to provide a direct load path between the forward and aft fittings. Use of the canted stiffeners allowed a compact aft single lug to be designed.

The forward fitting was designed as a steel investment casting (17-4-PH) and provided the load path around the 0.32 cm (0.125 inch) maximum thickness region. Since the fitting extends aft to the constant-depth sandwich, the complex stress distribution in the transition thickness region is carried by the metallic element. This design approach resulted in a relatively heavy forward fitting but allowed for efficient material utilization elsewhere in the design.

Provisions for the side elastomeric seals were incorporated into the moldline laminate. Additional reinforcement was incorporated along the laminate edge to provide the necessary thickness for the fasteners.

Stiffened Single Skin Composite Ramp No. 2

The stiffened single skin ramp configuration meeting the load and deflection requirements is shown in figure 4. The materials used in the composite design included 3501/AS graphite epoxy, CE9000/7581 fiberglass epoxy, HRP core and 17-4 PH steel.

The design assumed a rectangular stiffening grid in order to provide panel sizes of approximately the same size. The narrow dimension determined the waviness allowed (approximately 0.1 cm [0.04 in.] for the given spacing, under the limit load). In order to meet the waviness criterion the perforated skin was 0.34 cm (0.132 in.). The perforated area of the skin used 0.36 cm (0.14 in.) diameter holes in order to obtain the required open area for the BLC system of the ramp.

The single skin design required narrow sandwich beam stiffeners to limit deflection. For the beam caps, the $(0_4/\pm45)$ laminate system was used to provide high axial stiffness and also some torsional stiffness. The use of the $(0_4/\pm45)$ orientation at the intersection of the longeron caps and the aft transverse beam also provided a nearly quasi-isotropic laminate ($0_2/90_2/\pm45$ effectively) at the point where the fitting fasteners penetrate the laminate. For the single skin design, the moldline and backside caps were .58 and .76 cm (0.23 and 0.30 inches) thick respectively. To provide for additional stiffness the backside

cap was widened to 7.6 cm (3.0 inches) over the portion of the panel with the high bending moments. The caps were separated to the envelope thickness by HRP fiberglass core with a density of 12 lb/ft^3.

In the thickness transition region of the ramp, molded fiberglass epoxy wedges were specified. The beam wedges eliminated the requirement to machine a tapered section of HRP core to match the contour.

The steel forward fitting was designed to attach to the longerons prior to bonding the perforated skin laminate. The fitting was relatively compact with an efficient use of the material. The aft fitting, on the other hand, was larger because of the single lug and the necessity to beam the loads to the longerons.

A preliminary manufacturing plan and weight analysis was prepared to determine the cost/weight tradeoff of this configuration with a composite sandwich configuration and the metallic design of the Ramp No. 2.

Weight Analysis and Comparison

The detail weight breakdown for the sandwich and stiffened single skin configurations is shown in table 2. For the stiffened single skin design the graphite epoxy material was approximately 38.1 percent of the total ramp weight. The steel fittings made up 34.4 percent of the total ramp weight. The remainder of the stiffened single skin ramp weight consists of adhesives, honeycomb core, fasteners, and fiberglass epoxy. The seals and fairings were assumed to be 2.7 Kg (5.95 lbs.) which was the same value calculated for the prototype metallic ramp.

The sandwich configuration weight breakdown is presented in table 2. For this configuration the graphite epoxy weight was 24.8 percent of the total ramp weight. The steel fittings made up 44.3 percent of the total weight. The remainder of the sandwich weight consisted of core, adhesives, fiberglass and seals.

Cost Analysis and Comparison

The starting point for the cost analysis of the ramp designs was the manufacturing plan written from the engineering drawings. The three major cost elements of fabrication labor, material and tooling were obtained from the manufacturing plan. The ground rules for the cost analysis included:

- 964 units or 241 shipsets
- 16 units (4 shipsets) per month production rate
- Customer directed material costs and labor rate including:
  --Graphite epoxy broadgoods @ $20/lb.
  --Fiberglass epoxy broadgoods @ $3/lb.
  --Metal @ 1974 dollars plus 8 percent/year escalation factor through 1983
  --Labor wraparound rate of $15/hour

One thousandth unit standard labor hours were assigned to each manufacturing operation listed on the manufacturing plan. The factors representing realization, learning curve and rework were included in the labor hours. For this cost analysis, a realization factor of 0.68 to 0.77 was assumed and represents the efficiency of shop personnel conforming to the manufacturing plan. The learning curve (L.C.) factors averaged 0.88. The learning curve resulted from historical data for each of the major functions, such as layup, bond, and machine shops. The rework and scrap factor amounted to a 5 percent increase on the labor hours. The cumulative average hours were obtained by summing the hours under the learning curve and dividing by the number of units.

Functional services were factored into the cumulative average hours. These services included quality assurance, tool maintenance, shop tools, tool cleanup, etc. The functional services resulted in an additional 57 percent in the cumulative average manhours for the composite designs.

The cost of each item for the stiffened single skin and sandwich configurations has been tabulated and is presented in tables 3 and 4, respectively. The tables provide the cumulative average manhour, fabrication labor cost, and material cost for the major items making up the composite ramp configurations. The cumulative average cost was $2569 and $2483 for the stiffened single skin and sandwich configurations respectively.

In order to provide a baseline for the cost comparison, a metallic ramp meeting the 25 Kg (55 lb.) target weight was configured. The configuration consisted of a single perforated skin with formed metal stiffeners. The total part count was 49 with 25 different items. Based on the material and detail parts, a manufacturing plan was written and the costs were developed. The resulting cost of the metallic ramp included $1015 for labor and $2485 for materials resulting in a cumulative average cost of $3500. The relatively high material cost was due largely to the assigned material escalation cost factors.

A comparison of the composite costs with the metal baseline is shown in table 5. The projected cost savings were 27 and 29 percent for the stiffened single skin and sandwich respectively.

Perforated Laminate Development

As already noted, the Engine Nacelle Ramp No. 2 requires skin porosity for boundary layer control. One of the major objectives of this program was to establish a fabrication procedure for perforating advanced composite laminates. The procedure had to be adaptable to large area laminates with a minimum of sixteen plies in a quasi-isotropic layup. In addition, the selected procedure had to be cost effective for a possible production run.

Several different techniques were evaluated and rejected because of low reliability in producing good quality holes, excessive complexity, or limited adaptability. From this evaluation, and in light of the ramp design criteria, it was determined that the laminate thickness required holes to be formed in the prepreg by pins and the hole shape maintained during cure. The method

selected produced good quality laminates and was adaptable to large areas. The tooling required a three part mold as shown in figure 5 and consisted of:

1) A pin plate in which the tapered pins are pressed and staked,
2) A stripper plate to aid in separating the laminate from the pins, and
3) A base plate to serve as the moldline surface and provide pressure to the laminate during a press cure.

The fabrication sequence using this tooling method consisted of the following steps:

1) A debulked laminate, shown on figure 5, was placed on the base plate.
2) The stripper plate was placed on top of the laminate layup and indexed to the base plate.
3) The pin plate was placed on top of the stripper plate and indexed. The mold was placed in a press and closed to force the pins through the layup.
4) The laminate was subjected to its cure cycle.
5) After cooling, the laminate was removed from the disassembled mold (see figure 6).

The pin spacing selected for this perforated laminate evaluation was a 0.89 cm (0.352 inch) hexagonal pattern with a nominal hole diameter of 0.33 cm (0.1285 inch), resulting in an open area of 12 percent.

The basic evaluation panel was a 30.5 cm (12 in.) square with a central perforated area of 20.3 cm (8 in.) square. This panel size was selected to enable all the specimens to be taken at any point on the panel. The square panel also allowed test specimens to be cut from the perforated laminate X and Y directed as shown in figure 7.

Examination of figure 7 indicates the reason for the two test directions even though the laminate is quasi-isotropic (0/90/$\pm$45) 2S. The hexagonal hole pattern provides a series of wide bands of material between hole rows in the X direction. On the other hand, in the Y direction a greater number of narrow bands of laminated material exists. At the onset of the test program, this difference in material distribution was thought to make a large change in the structural properties.

Perforated Laminate Test Specimens

Three types of structural tests were performed on the perforated laminate--tension, compression and in-plane (rail) shear. The majority of the testing was performed at 310^{o}F, the critical design temperature of the ramps. The specimens were conventional in shape and followed the suggestions outlined in the Advanced Composite Design Guide. The tensile specimens were the straight-sided, tabbed-end configuration 30.5 cm (12 in.) long. However, the width was increased to approximately 3.8 cm (1-1/2 in.) to minimize the hole effects. The tensile specimens, as with the other two test specimen configurations, were machined between hole rows so the edges were smooth.

The compression specimens were of the edgewise sandwich compression configuration with a width of 6.4 cm (2-1/2 in.) and a length of 10.2 cm (4 in.). The core, 8 lb/ft^3 density, used to bond the laminates together was selected to assure that the faces would not disbond during test. To minimize the core supporting the load during test, all specimens were made with the core ribbon running transverse to the loading direction. The ends of the specimens were machined square and perpendicular to the loaded direction.

The third type of test, in-plane shear, was performed using the rail shear method.

Perforated Laminate Test Results

The average test results are summarized in table 6 for the perforated laminate evaluation. The definition of the terms longitudinal (X) direction and transverse (Y) direction define the testing orientation with respect to the hexagonal perforation pattern as shown in figure 7. Generally these data exhibited structural properties acceptable for the ramp design. These data provide a good indication of the perforated laminate structural properties since the coefficient of variation was low, even the small test sample (7 to 10 percent). The test evaluation served its purpose of providing the structural properties for perforated laminates using a process technique applicable to fabrication of the ramp skins.

CONCLUSIONS

This program indicated that advance composite components in a supersonic nacelle will have lower weight than their metal counterparts. In addition, production cost savings of 27 percent to 29 percent were achieved with composite structure designs because of a low detail-part count resulting in labor cost savings. The projected material cost trends were also favorable for the composite designs. The activity of this program on the B-1 Engine Nacelle Ramp No. 2 showed that the composite designs would have weight savings of 14 percent to 20 percent over the metal baseline. The technology developed on this program is now being extended to another area of the B-1 Nacelle. Rohr Industries is under contract to Rockwell International, Tulsa Division (AFFDL Contract No. F33 615-75-C3153) to develop an advanced composite Engine Nacelle Ramp No. 3.

Table 1.- B-1 Engine Nacelle
Ramp No. 2 Design Criteria.

- NORMAL PRESSURE CRITICAL
- CONCENTRATED HINGE LOADS
- STIFFNESS FOR DEFLECTION LIMITATION
- DESIGN TEMPERATURE = 307° F
- PERFORATED SKIN FOR BLC
  - AFT 3/4 AREA
- TARGET WEIGHT 25.0 Kg (55 LB)

TABLE 2

WEIGHT COMPARISON FOR

ENGINE NACELLE RAMP NO. 2

ITEM	COMPOSITE DESIGNS Kg (lb.) SINGLE SKIN		SANDWICH	
FWD FITTING (2)	3.49	(7.68)	6.61	(14.57)
AFT FITTING (2)	3.89	(8.56)	2.21	(4.86)
SKIN MOLDLINE	3.04	(6.69)	2.33	(5.14)
SKIN-BACKSIDE		--	1.39	(3.07)
CAP	5.04	(11.1)	1.22	(2.68)
CORE	1.25	(2.75)	1.72	(3.78)
OTHER COMPONENTS	1.50	(3.52)	0.83	(1.83)
ADHESIVES	0.45	(1.0)	0.91	(2.0)
SEALS	2.70	(5.95)	2.70	5.95
TOTAL (EXCLUDES FINISH & LIGHTNING PROTECTION)	21.45	(47.25)	19.92	(43.88)

TARGET WEIGHT = 25.0 Kg (55 LB.)

PROTOTYPE WEIGHT = 30.0 Kg (66 LB.)

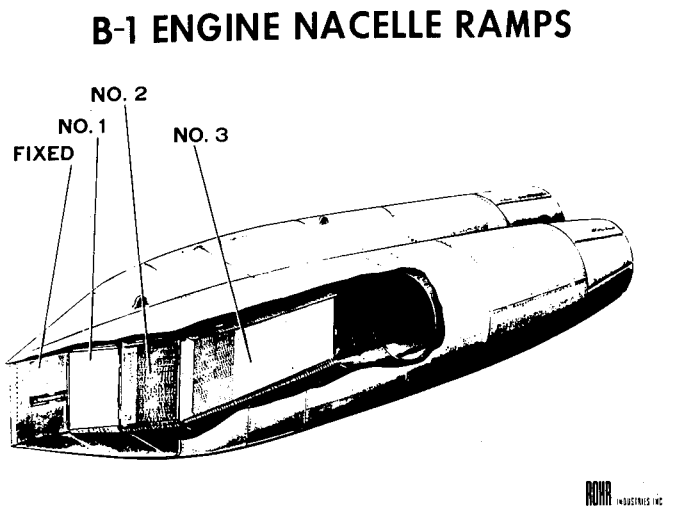

Figure 1.- B-1 Engine Nacelle Ramps.

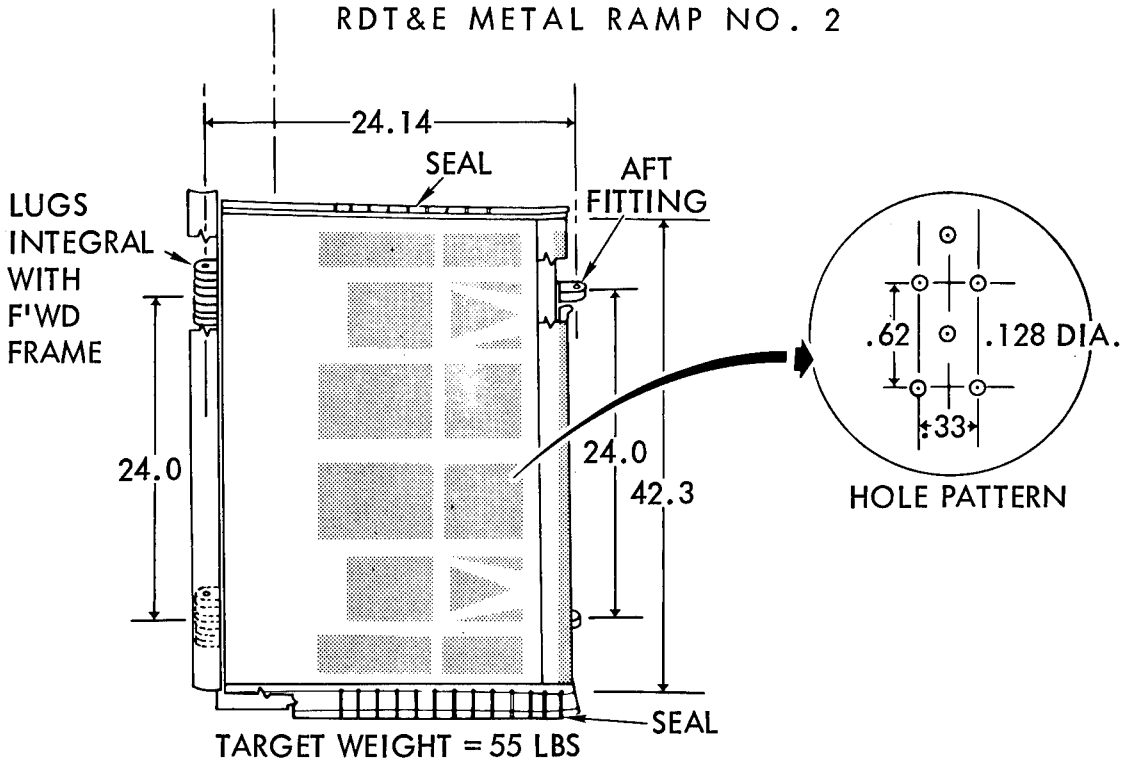

Figure 2.- Ramp design envelope.

SANDWICH DESIGN

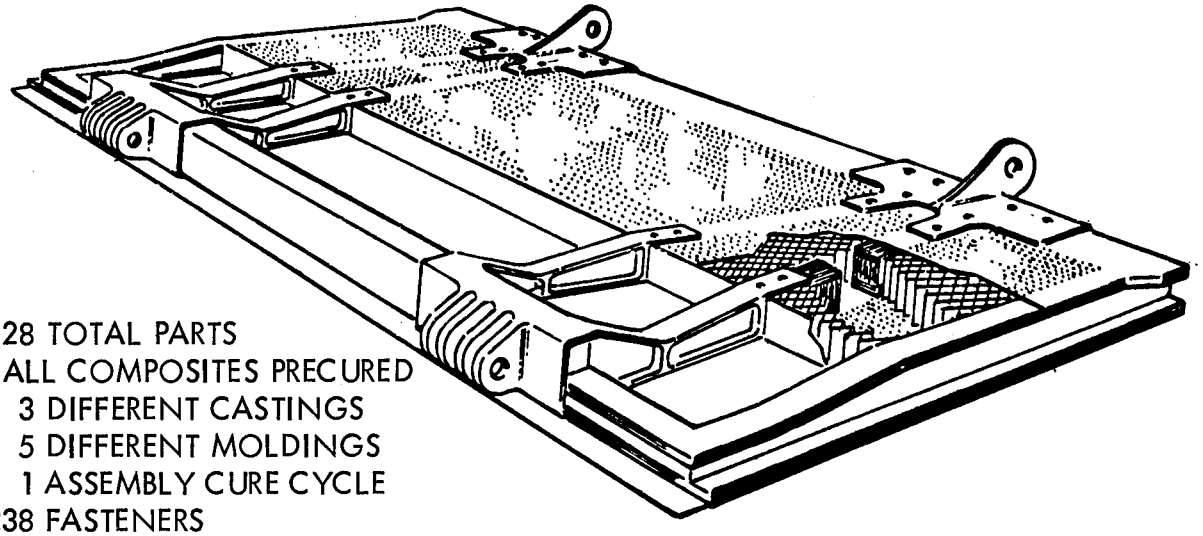

28 TOTAL PARTS
ALL COMPOSITES PRECURED
3 DIFFERENT CASTINGS
5 DIFFERENT MOLDINGS
1 ASSEMBLY CURE CYCLE
238 FASTENERS

Figure 3.- Sandwich design.

STIFFENED SINGLE SKIN

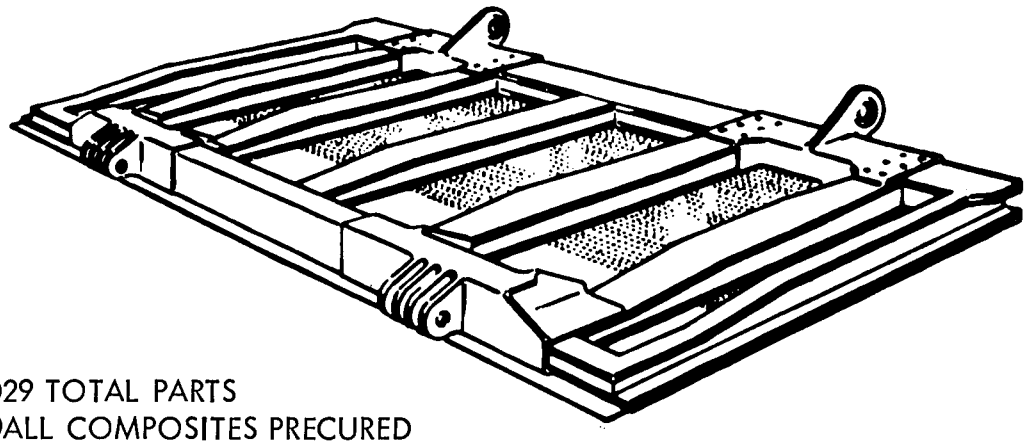

- 29 TOTAL PARTS
- ALL COMPOSITES PRECURED
- 4 DIFFERENT CASTINGS
- 6 DIFFERENT MOLDINGS
- 1 ASSEMBLY CURE CYCLE
- 181 FASTENERS

Figure 4.- Stiffened single skin.

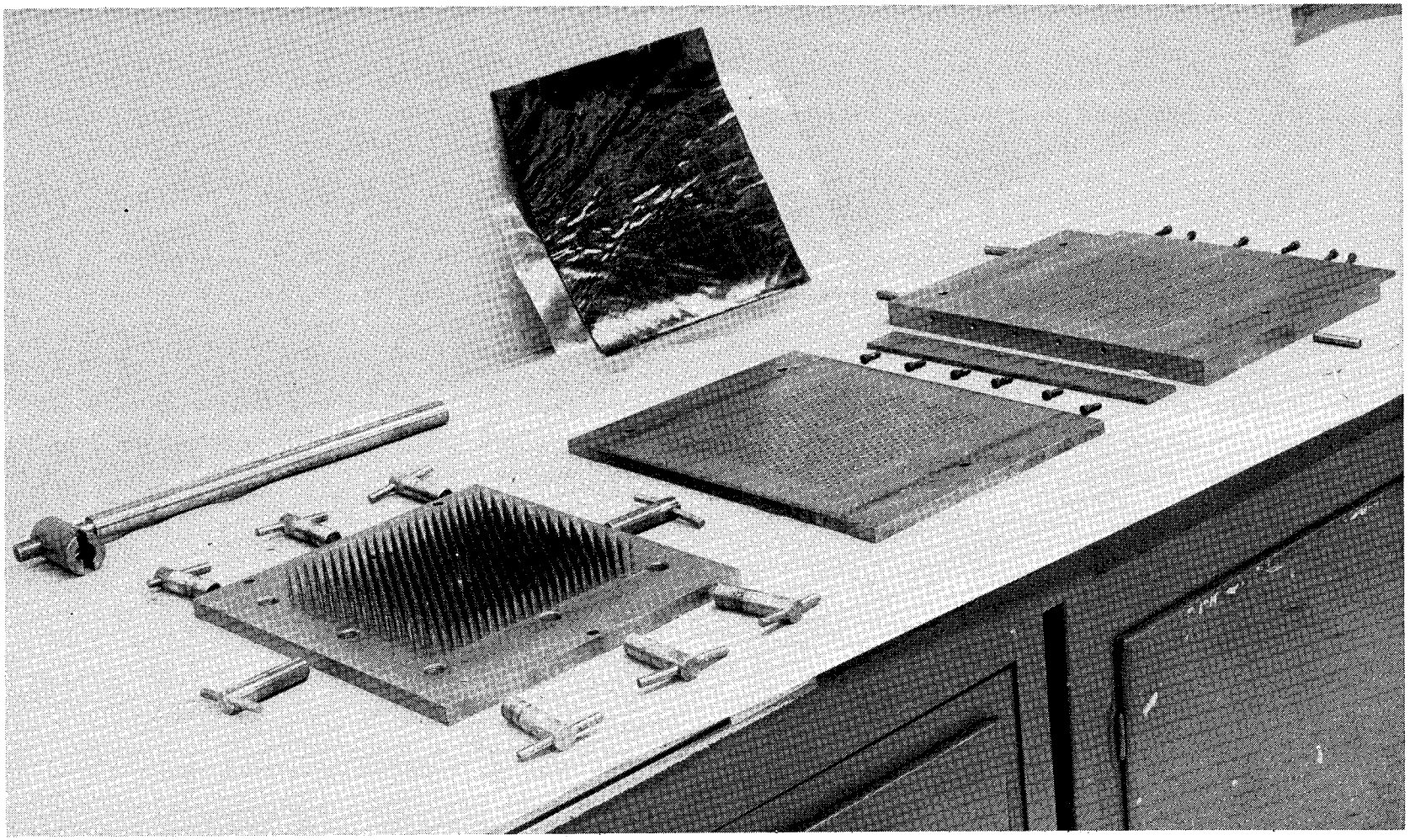

Figure 5.- Tool for fabricating perforated laminates.

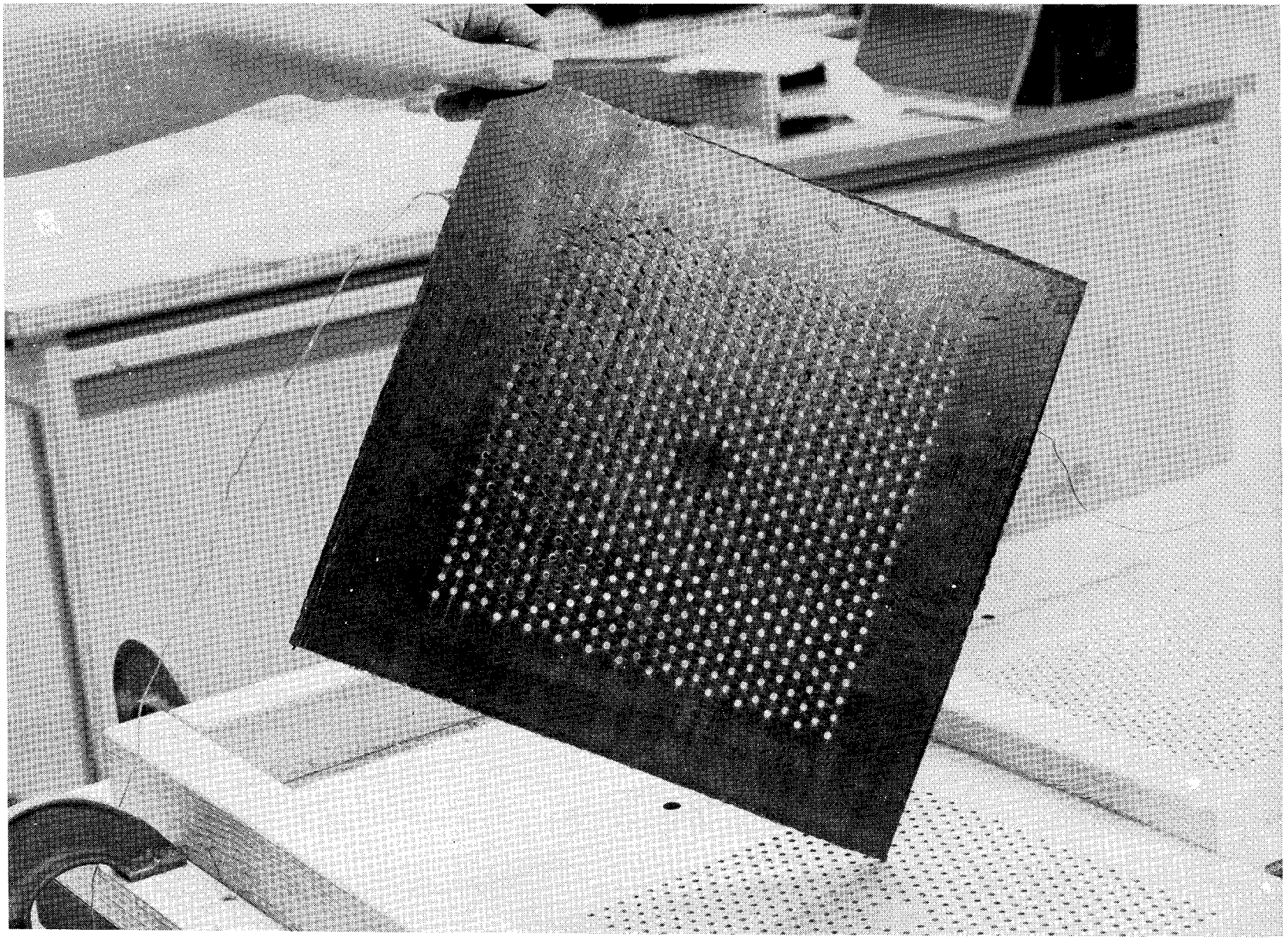

Figure 6.- Perforated laminate test panel.

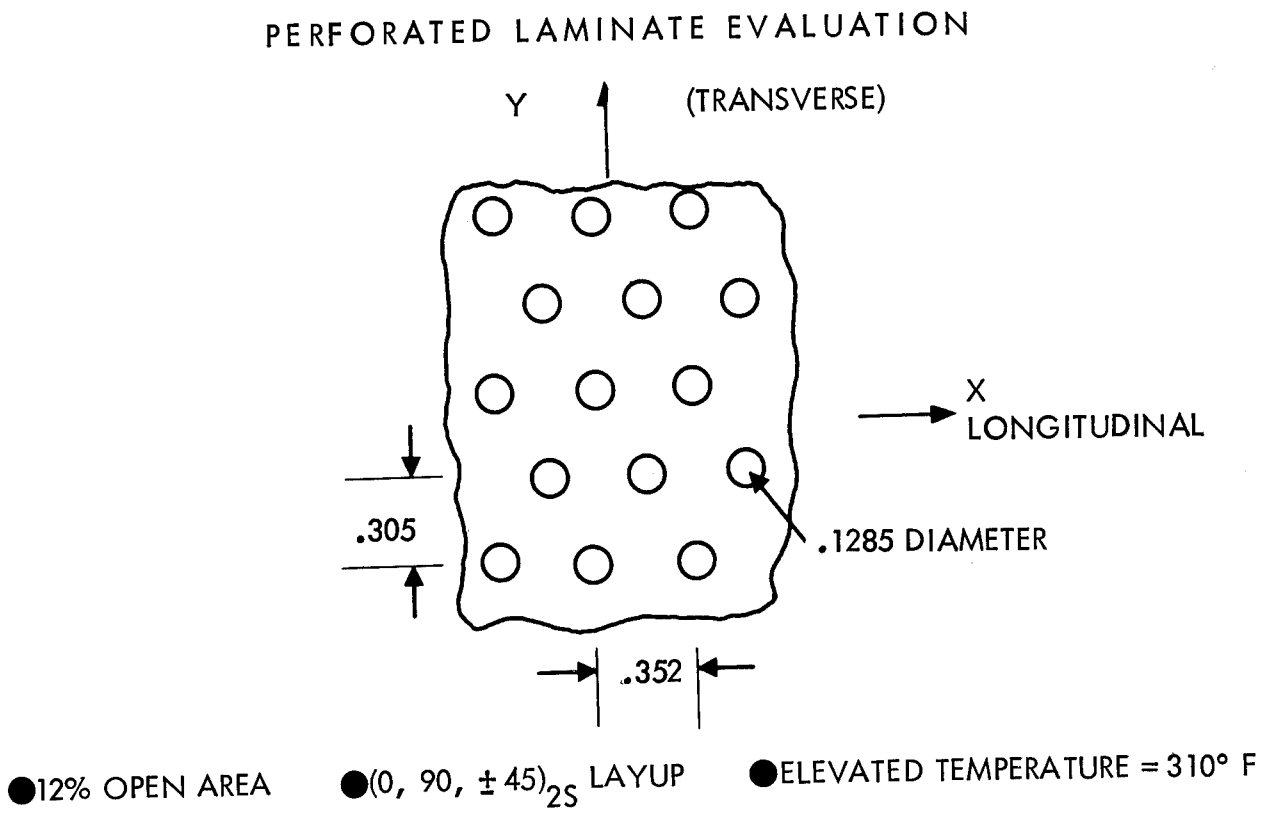

Figure 7.- Perforated laminate evaluation.

H-3 HELICOPTER COMPOSITE MAIN ROTOR BLADE

DEVELOPMENT PROGRAM

D. J. Ianniello
Sikorsky Aircraft

and

J. B. Sainsbury-Carter
Reliable Manufacturing Inc.

ABSTRACT

In May 1973 Sikorsky Aircraft was awarded a contract (N00019-73-C-0319) by the Naval Air Systems Command to develop a main rotor blade for the H-3 helicopter utilizing advanced composite materials.

The objectives of the program are to demonstrate the helicopter rotor performance improvements attainable through optimum application of advanced composite materials in the design and construction of main rotor blades, and to make available a rotor blade system which will not be a limiting factor in achieving future helicopter performance growth. Major benefits anticipated from this program are:

- Superior performance associated with the use of advanced blade geometry made possible through the use of composites; notably advanced airfoil contour and high rate of twist. To build blades with such geometry from metallic materials is difficult and costly.

- Superior performance associated with operating helicopter rotors at higher forward speed due to the improved fatigue capability of advanced composite materials.

- Reduced life cycle costs of composite blades as compared to all metallic blades as a result of reduced maintenance costs, unlimited fatigue life, and improved corrosion resistance.

A unique feature of the blade lies in its fabrication concept. The blade is made in two separate halves, in steel clamshell molds, and is bonded together along its chord plane. This assures near perfect airfoil fidelity of the blade contour.

Both the preliminary design and detail design phases and most of the full scale ground fatigue tests have, thus far, been completed. The current phase of the program is now blade fabrication. Whirl and flight testing will be accomplished in early 1976 using a SH-3D helicopter as a test vehicle for the blades.

In addition to a detailed discussion of the blade design and unique construction concept, this paper will review both the very important tooling concepts and fabrication procedures.

INTRODUCTION

The helicopter rotor presents a major challenge to the design engineer, primarily due to the wide range of adverse operating conditions under which the rotor blades must operate. Achieving a proper balance between the sometimes conflicting requirements associated with these operating conditions will determine the success of a given blade design.

The principle objectives of this development program include demonstration of the rotor performance improvements attainable and the cost saving potential that can be realized through the use of advanced composite materials in the design of helicopter main rotor blades, Figure 1. An additional objective is the establishment of a technical base sufficient for the development of composite rotor blades for military and commercial helicopters.

A three phase program is currently in progress to meet the above objectives. Progress to date, including material and full scale specimen testing has been reported in detail, in interim technical reports, references 1-4.

Phase I was a fourteen month preliminary design effort which includes establishment of aerodynamic, aeroelastic and structural design concepts. Small specimen static and fatigue testing was used to evaluate effects of environmental exposure and impact damage on composite materials and in addition, full scale root end attachment and outboard blade section fatigue testing was conducted to establish confidence in the design and manufacturing concepts.

Once a satisfactory design had been selected, a sixteen month detail design and blade fabrication effort began which has, as an end product, the fabrication of nine full size H-3 composite rotor blades for subsequent flight and ground testing.

The testing phase of this effort will include full scale fatigue testing, 30 hours of whirl test and a 14 hour flight program to demonstrate performance, stability, and handling characteristics.

DESCRIPTION OF THE BLADE DESIGN

The H-3 composite blade, Figure 2, was conceived to fulfill certain requirements of future rotor blades. These include:

1. Higher fatigue strain allowables required because of high vibratory loads due to increased twist, higher speeds, higher rotor loadings and cambered airfoils.

2. Ease of manufacture of the variable geometry structure in order to reduce costs.

3. Ability to achieve accurate fidelity of the airfoil contour to fulfill the aerodynamic requirements.

Figure 3 is an exploded and sectioned view of the blade design. The basic outboard structure shown on the right of Figure 3 consists of a C-spar made from graphite and fiberglass epoxy laminates. The aft end of the C-spar is closed off with an effective web of aluminum honeycomb to maximize the torsional efficiency of the structure and correctly position the section shear center. Inboard, the C-spar gradually transitions into a closed single cell elliptical section.

The root end retention consists of a bolted connection between the elliptical spar section and an outside forked cuff. Other types of root attachments were investigated before this simple, conventional four bolt attachment was selected on the basis of inspectability, weight, and fabrication cost.

A skin of fiberglass covers the entire outside of the airfoil and forms the aft airfoil fairing. This fairing is filled with light Nomex honeycomb to transfer the shear to the C-spar.

A trailing edge strip of unidirectional graphite epoxy, oriented spanwise, helps provide the chordwise stiffness required to reduce the chordwise stress, and to increase the natural frequency of the blade's first bending mode further from the frequency of the aerodynamic exciting force to minimize vibration.

To provide the required chordwise balance axis of the basic sections, a leading edge weight of lead rods in a fiberglass base is molded inside the nose of the C-spar. The weight is located between 70 and 90 percent radius to achieve the benefits of centrifugal relief on reducing bending moments.

The tip end of the blade is swept aft at a 20 degree angle outboard of 95 percent radius. The purpose of the sweep is to reduce the tip mach number and provide an effective torsional stiffening to reduce the undesirable effects of twist at high forward speeds, (Reference 5).

A unique concept for an adjustable tip weight fitting is provided to compensate for blade to blade mass properties variations. This concept makes use of composite materials to provide a simple, reliable weight retention system. Special emphasis was given to minimize the aerodynamic surface which must be removed to adjust the balance weights so that the weight adjustment operation will result in minimum possible change to the aerodynamic characteristics. A further description of this concept will be presented in the discussion of the fabrication process.

A replaceable abrasion strip of electroformed nickel covers the leading edge of the blade outboard of 70 percent radius. A replaceable tip cap is also provided to permit repair of damage in the tip area.

The most important feature of the design concept takes full advantage of the use of composite materials, Figure 4. Here the blade is layed up in two halves so that the upper and lower surfaces can be cured against hard tooling insuring excellent fidelity of airfoil contour and maximum compaction of the laminates. In addition, the build-up of tolerances on each half is machined off along the chord plane. This permits the relaxation of dimensional control of the components which results in low fabrication costs. The two halves can then be joined by adhesive bonding along the chordplane. Next, a composite leading edge structural splice cap and a nickel abrasion strip are bonded to the completed blade assembly.

In order to assess the adequacy of both the design concepts and the manufacturing approach, eight full scale fatigue specimens were fabricated and subjected to static and fatigue testing, Figure 5. In addition, one of the root attachment fatigue specimens was fatigue tested after a severe notch was cut into the highly stressed bolt attachment area. All specimens survived the fatigue tests at load levels several times higher than maximum flight loads and confirmed the validity of the design and fabrication techniques to provide an infinite life blade. The related test data is reported in detail in references 1 - 4.

DESCRIPTION OF THE BLADE FABRICATION PROCESS

The primary fabrication feature consists of the blade being constructed in two halves separated at the chordplane. This provides extreme ease of manufacture and inspectability. The entire fabrication process up to and including bonding of the two half blade assemblies is carried out in steel clamshell tooling, Figure 6. The exacting tolerances required of a high performance airfoil contour and the requirement for thermal compatability between the tooling and the composite materials dictated the selection of steel for these molds. These tools also incorporate a vacuum porting system for vacuum chucking of the blade skins into the tooling for machining of the blade chord plane.

The blade fabrication begins by laying up the individual plies of graphite and fiberglass epoxy into the clamshell molds, Figure 7. Broadgood material is used in varying widths (5" to 12") and the lay-up sequence selected to produce a balanced laminate.

The C-spar laminate increases in thickness from twenty plies at the blade tip up to eighty-five plies at the root end. Approximately 70 lbs. of graphite and 60 lbs. of fiberglass are used in each blade. Due to the large variation in laminate thickness, the cure cycle and resin gel characteristics of the graphite material, (RAC 6350), were tailored by the material supplier to produce a high quality laminate over the entire thickness range while minimizing the possibility of experiencing an exothermic reaction in the thick laminate. Intermediate compaction, using a vacuum bag, was necessary after every twenty-five plies were layed into the clamshell mold to insure proper nesting of the material in the tool. The completed lay-up is cured in an autoclave at 350°F. Laminate distortion and the variation in part weight from skin to skin has been minimal.

The second step in the fabrication process is to bond phenolic spacer blocks in the blade root attachment area. These blocks are used to react the bolt pre-load for the cuff attachment. In addition, a fiberglass build-up, Figure 8, which will be later machined to contain balance weights, is layed-up at the blade tip. Finally, the graphite trailing edge wedge used to tune the blade chordwise stiffness is bonded to the cured skin/spar during this operation.

In order to insure a proper fit up of the aluminum honeycomb core which closes the graphite C-spar, the aluminum core is pre-cut to contour on a tracer planer, which uses as a model, a cast plastic impression of the tapered transition between the graphite spar and the basic three ply fiberglass skin, Figure 9. Positioning of this core in the laminate assembly is accomplished by a locating fence which is mounted directly to the clamshell mold, Figure 10.

Lightweight Nomex honeycomb which is purchased as rectangular block is then positioned against the aluminum core to fill the balance of the blade skin/spar. No pre-machining of the Nomex honeycomb is required since the core has enough flexibility to take the shape of the skin contour. The entire core is then bonded to the skin/spar using a 250°F adhesive system.

Up to this stage of fabrication, all components have been layed up, cured, and bonded in the steel clamshell molds without regard to the dimensional tolerances of each of the pieces. This leads to a low cost fabrication approach since a single machining operation eliminated all the tolerances at the chordplane.

For this development program, machining of the chord plane is accomplished using a commercial router with valve stem type cutters.

Since the chordplane twists along the span of the blade, a system was designed which would permit the router to accurately traverse this twisting plane. This was accomplished by means of a bridge system which is mounted directly on the clamshell model and rides along the mold faces which have been machined parallel to the twisted chordplane of the blade, Figure 11.

The router bridge is essentially a linkage mechanism which will permit itself to rack as it moves along the twisted plane and maintains the cutter parallel to the chordplane.

The cutting of the chordplane, using this system, is achieved within an accuracy of $\pm$ .004" which can then be absorbed within the glue line of the chord splice.

Prior to assembling the two half blade sections together, a fiberglass chord splice is bonded to the lower half blade. This splice serves two important functions. First, it provides some additional torsional rigidity to the half blade section which must be removed from its clamshell mold and transferred for assembly on to the other half blade for bonding, and secondly, it assures that during the bonding operation, the bonding pressure does not cause the cell walls of abutting sections of honeycomb core to cut into each other due to the applied bonding pressure. The chord splice material is a low temperature epoxy pre-preg system which is co-cured to the half blade.

Since weight and weight moment control play a critical role in the fabrication of helicopter rotor blades, each half of the blade assembly is weighed and balanced to a specific value of spanwise and chordwise weight moment. This is very conveniently accomplished at this point in the fabrication process by placing each half blade assembly on a balance scale system and adding more counterweight at the leading edge of the blade or applying additional layers of adhesive in the trailing edge region of the chord plane.

In order to verify part fit-up of the two half-blade assemblies, a preliminary chord plane bond check is performed by temporarily assembling the blade half with a layer of adhesive which is sandwiched between very thin layers of mylar film. The assembly is then bagged and held under vacuum for a minimum of thirty minutes. The parts are then disassembled and the adhesive is inspected for a honeycomb core imprint. Permissible bond void size has been established on the basis of investigations conducted on the test specimens fabricated under phase one of this program. In non-critical areas of the chordplane, localized void areas may be filled by applying an additional layer of adhesive on final assembly.

The two half blades are then assembled in one of the clamshell molds, Figure 12. A plastic caul plate is used on the airfoil surface away from the mold to prevent bag wrinkles or other distortions from being transferred into the surface of the airfoil. After vacuum bagging, the blade assembly

is cured at 250°F with an additional 10 psi of positive pressure. Following inspection of the bonded assembly, the blade is then prepared for the lay-up of the leading edge splice cap.

The splice cap material is a low temperature (250°F) fiberglass pre-preg system which is layed up at ± 45°F directly on to the blade. This approach of applying the wet pre-preg to a cured leading edge surface leads to achieving the critical fit of the splice to the blade. A semi-rigid fiberglass caul plate with provisions to accept the nickle and polyurethane errosion protection serves as a female mold to shape the outside surface of the splice cap to the aerodynamic contour. The blade holding fixture, Figure 13, uses a mechanical force system which is augmented by autoclave pressure to apply load to the fiberglass splice during curing.

The final assembly operations required to complete the blade fabrication include the root end machining for joining the cuff fitting to the blade, and the machining of the tip block for the housings which retain the tip balancing system.

At the blade root attachment, steel bushings are bonded into the root attachment holes in the blade. Small specimen fatigue testing of bolted attachment in graphite epoxy indicated that improved fatigue strengths were achieved with metallic bushings. Once the bushings have been bonded in place, the cuff is assembled to the blade and the holes in both the cuff and the blade itself are drilled and line reamed, Figure 14. The bolts are installed with an interference fit to prevent fretting of mating surfaces in the joint.

At the blade tip, the fiberglass block which was layed up and cured inside the blade C-spar section to form a solid composite structure, is now machined to accept three cylindrical steel containers which are bonded into the block. Tip weights consisting of disks of steel and tungsten are installed within these containers to provide the capability of balancing each blade statically and dynamically. A light weight cover provides a seal for each of these containers within the aerodynamic contour of the blade surface.

The completed blade assembly, Figure 15, is both statically and dynamically balanced prior to installation.

CONCLUSION

The structural and dynamic capability of composite rotor blades has been previously demonstrated for a variety of helicopters both in the United States and abroad.

The H-3 composite blade described in this paper represents a further advancement in this technology since the design flexibility afforded to the rotor blade designer by composite materials has been coupled with a very

simple fabrication concept to produce a composite rotor blade of high reliability at relatively low cost.

REFERENCES

1. Interim Engineering Report H-3 Composite Main Rotor Blade Development Contract No. N00019-73-C-0319, August, 1973

2. Interim Engineering Report H-3 Composite Main Rotor Blade Development Contract No. N00019-73-C-0319, November, 1973

3. Interim Engineering Report H-3 Composite Main Rotor Blade Development Contract No. N00019-73-C-0319, May, 1974

4. Interim Engineering Report H-3 Composite Main Rotor Blade Development Contract No. N00019-73-C-0319, February, 1975

5. Arcidiacono, P. and Zincone, R., "Titanium UTTAS Main Rotor Blade", 31st Annual National Forum of the American Helicopter Society, May, 1975

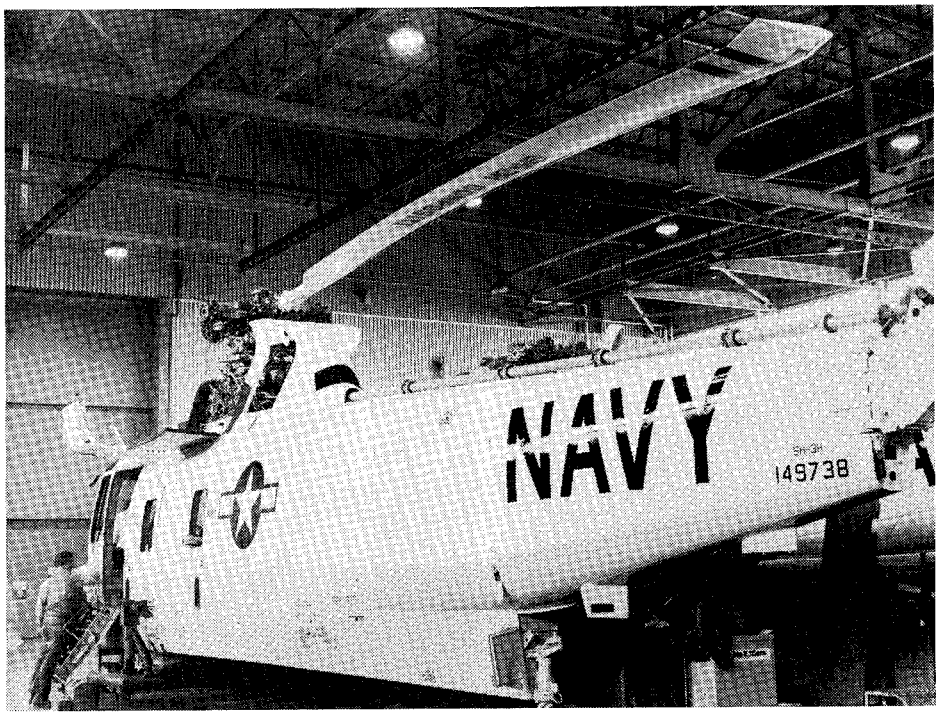

Figure 1.- Composite blade installed on SH-3H helicopter.

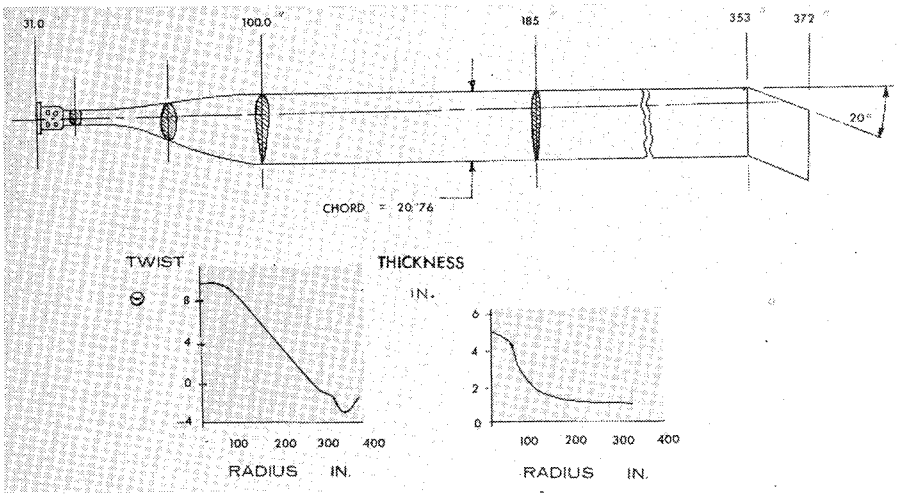

Figure 2.- Aerodynamic configuration H-3 composite blade.

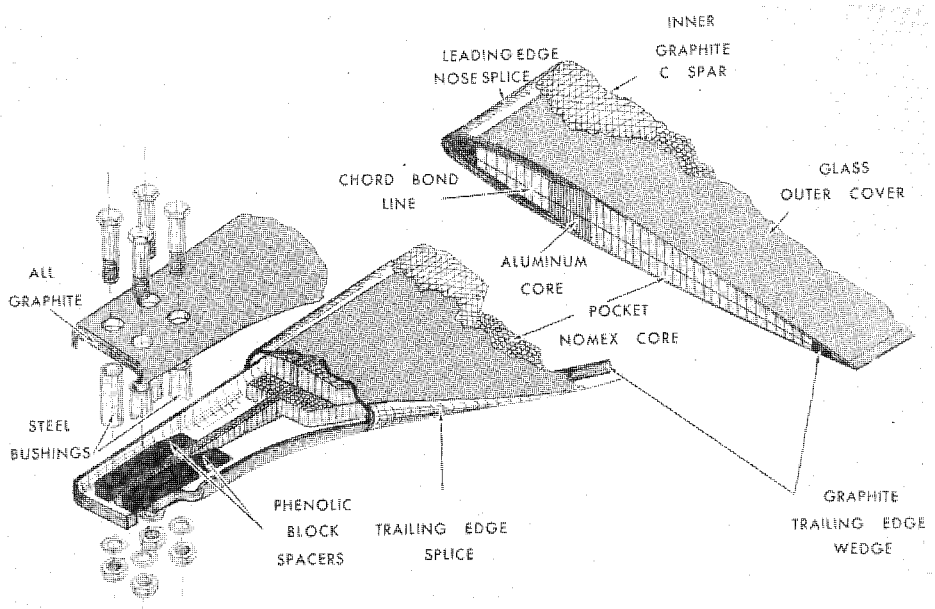

Figure 3.- Exploded and sectioned view of blade.

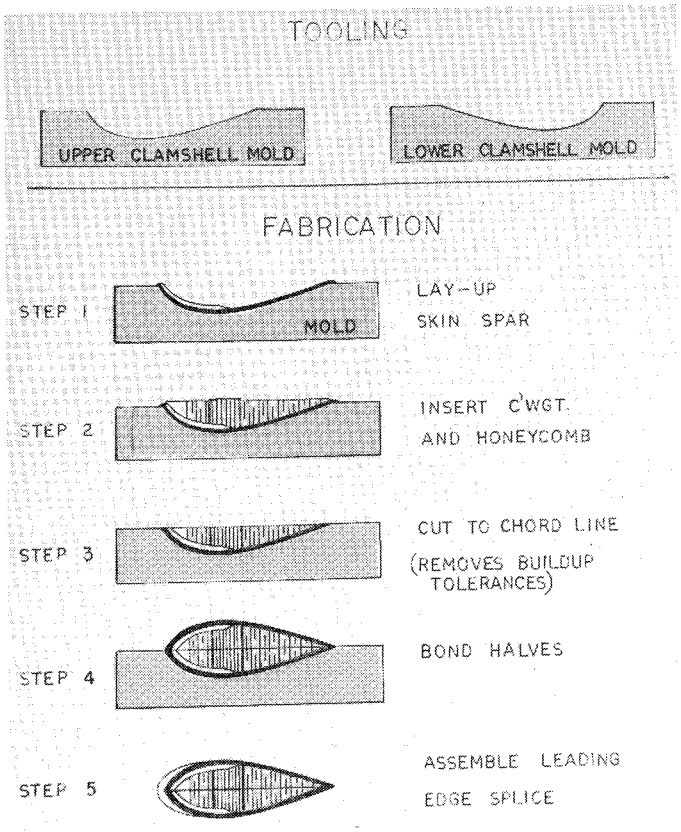

Figure 4.- Unique two-piece fabrication concept.

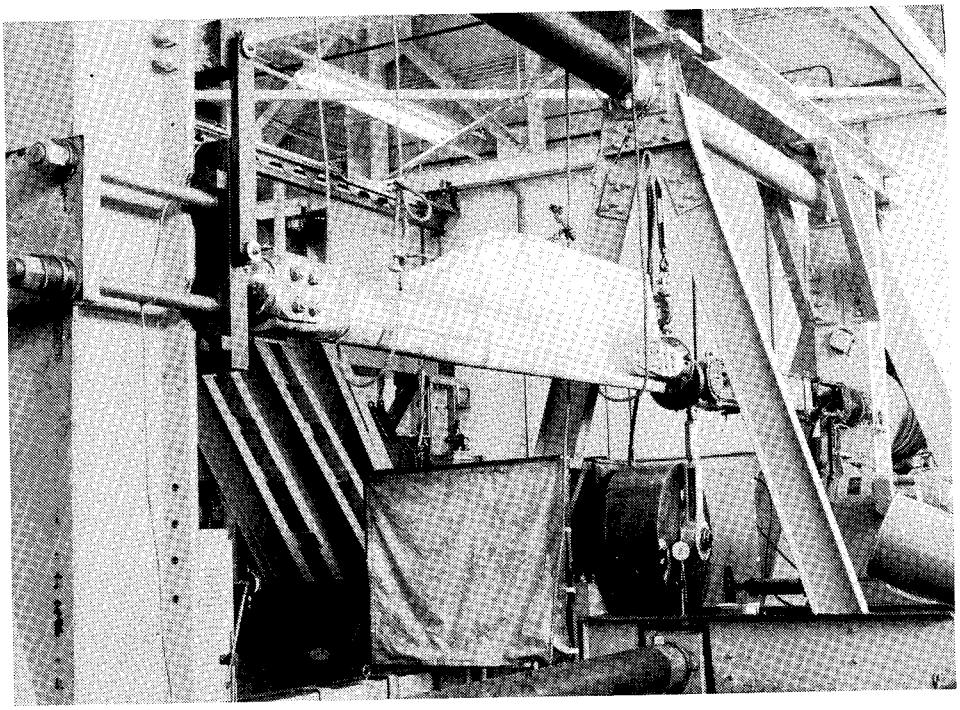

Figure 5.- Fatigue specimen in test.

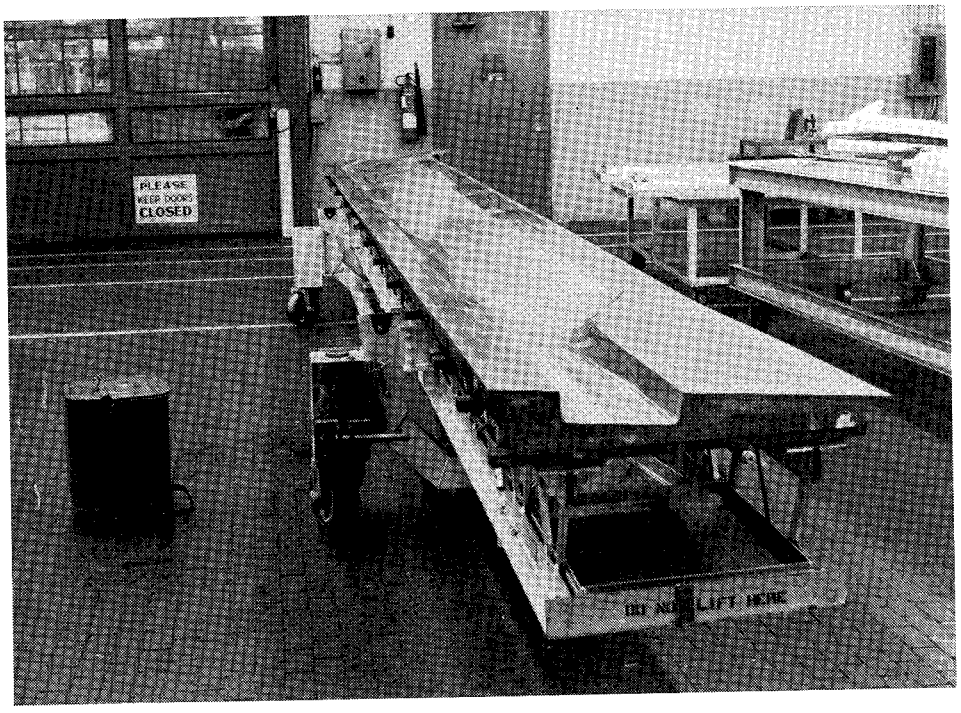

Figure 6.- Steel clamshell tool.

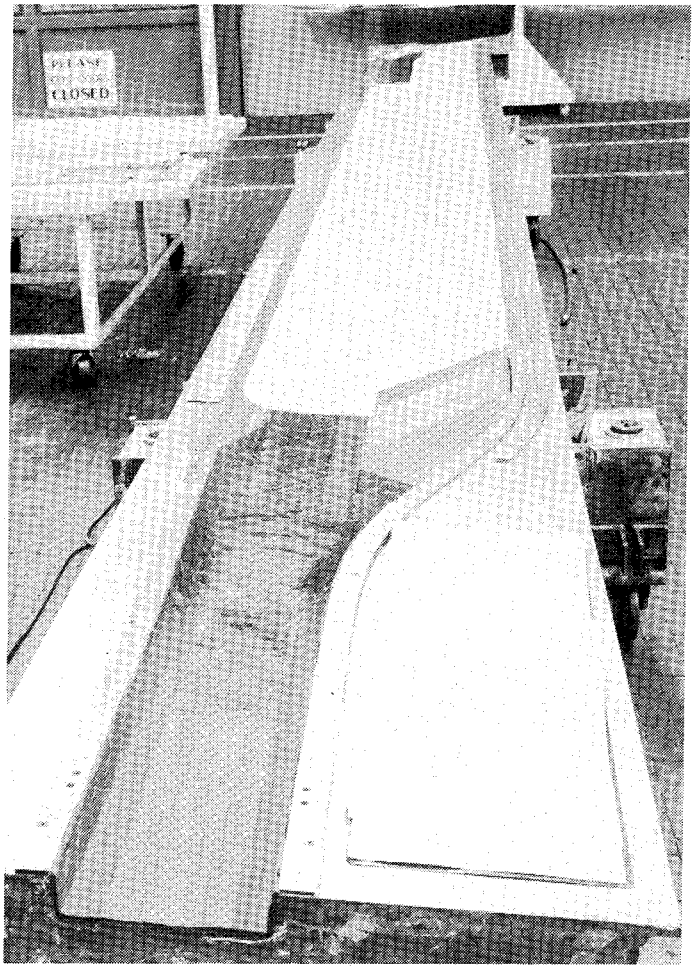

Figure 7.- Layup of skin/spar.

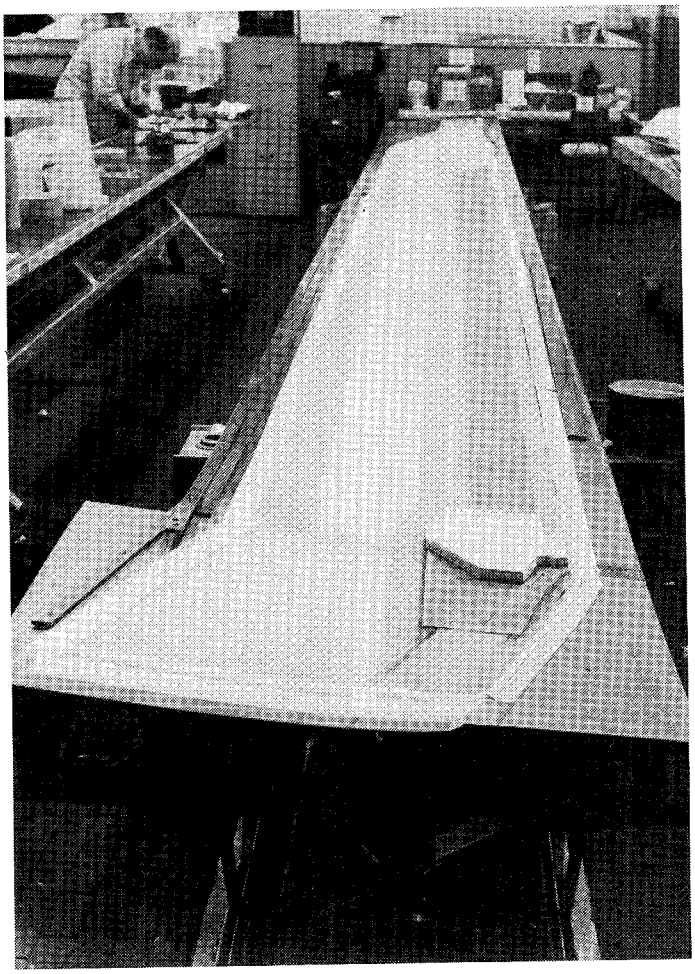

Figure 8.- Tip weight retaining block.

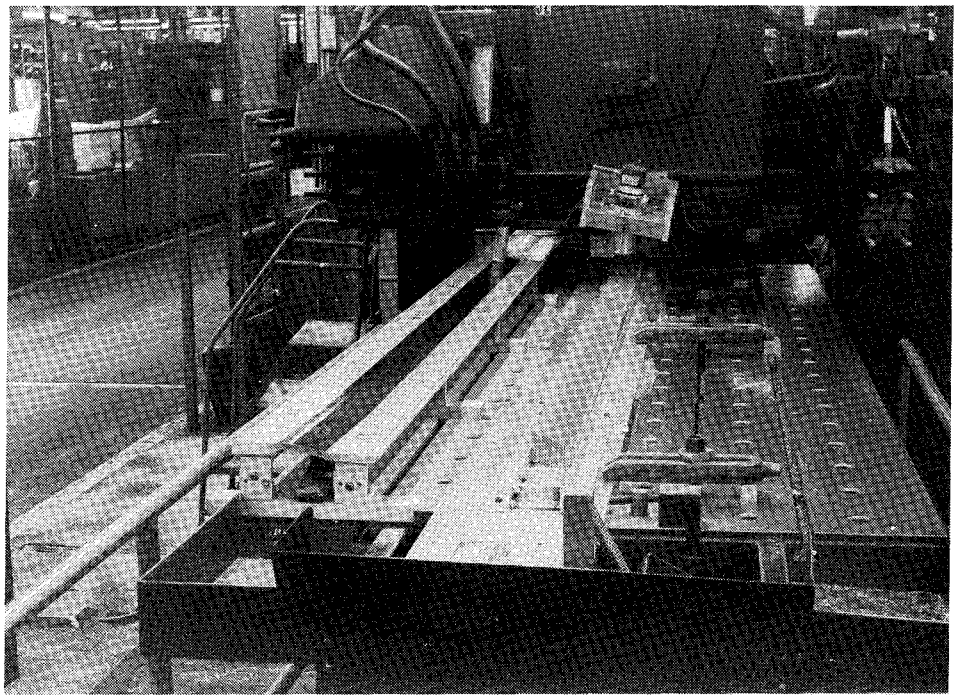

Figure 9.- Contour machining of aluminum core.

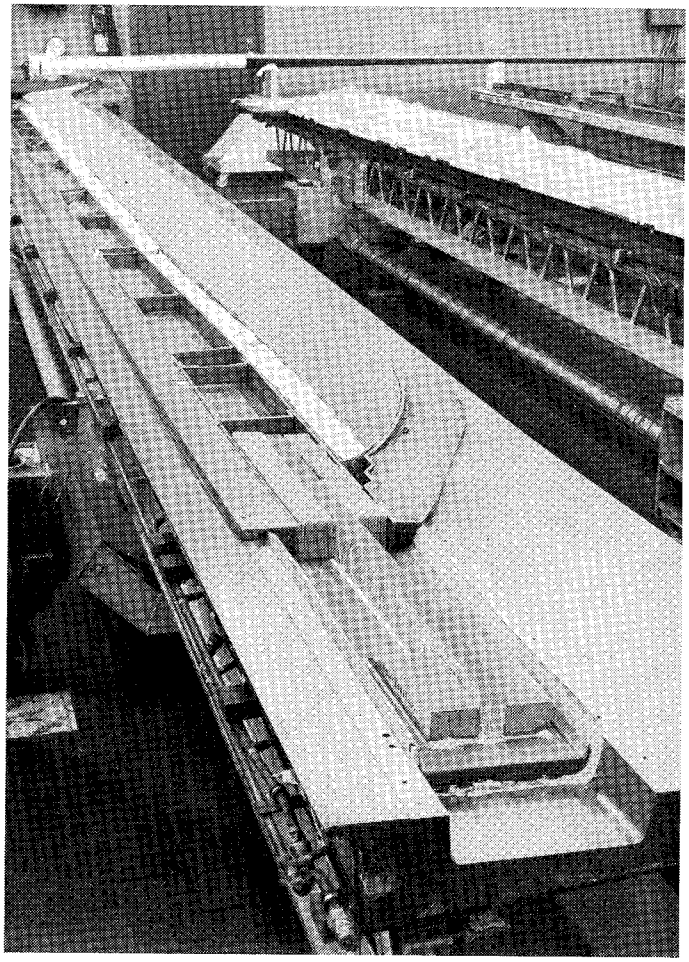

Figure 10.- Location of honeycomb core.

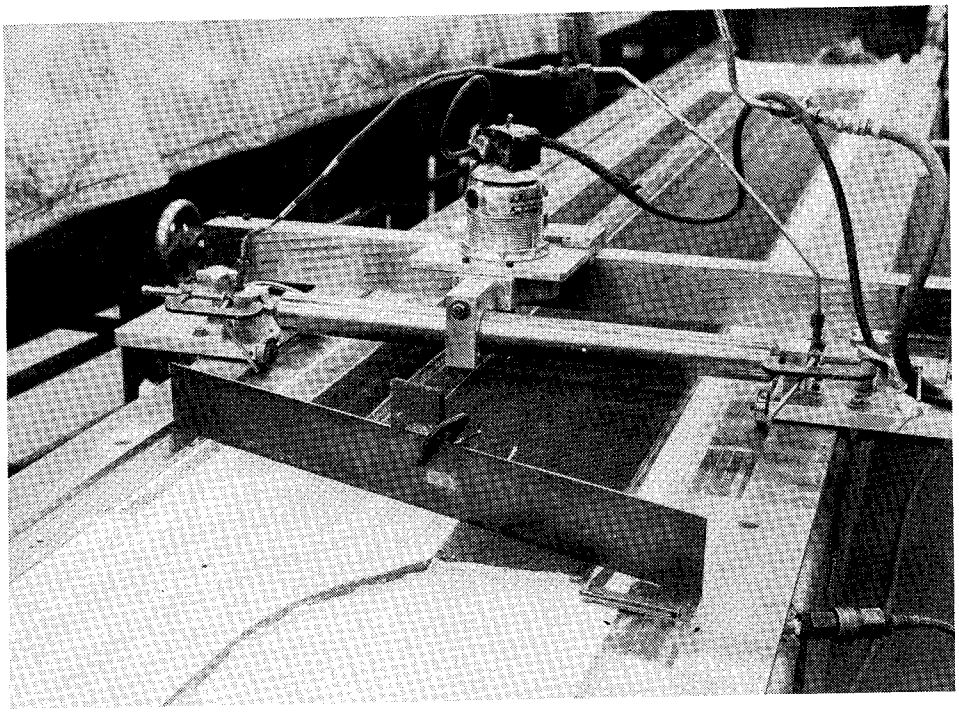

Figure 11.- Routing of chordplane.

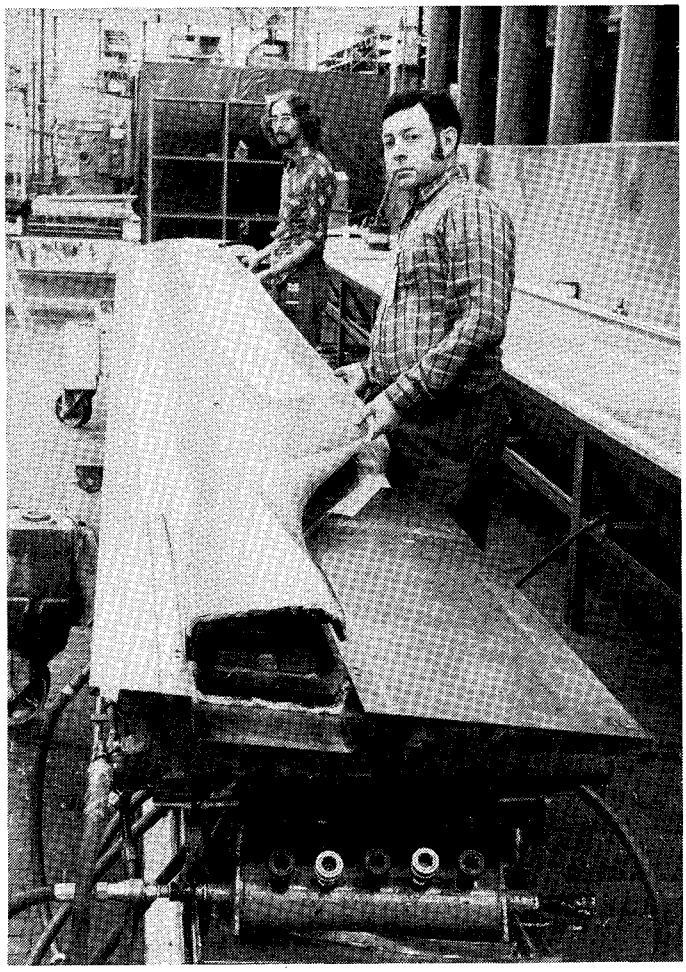

Figure 12.- Assembly of two blade halves for bonding.

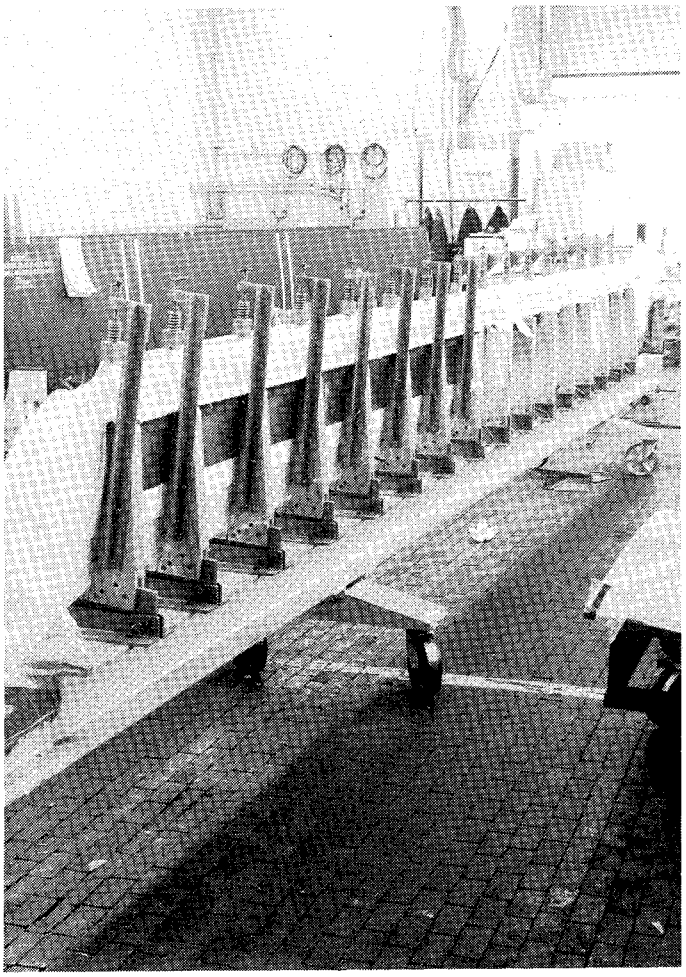

Figure 13.- Holding fixture for layup and cure of leading edge splice cap.

Figure 14.- Drill and line ream root end.

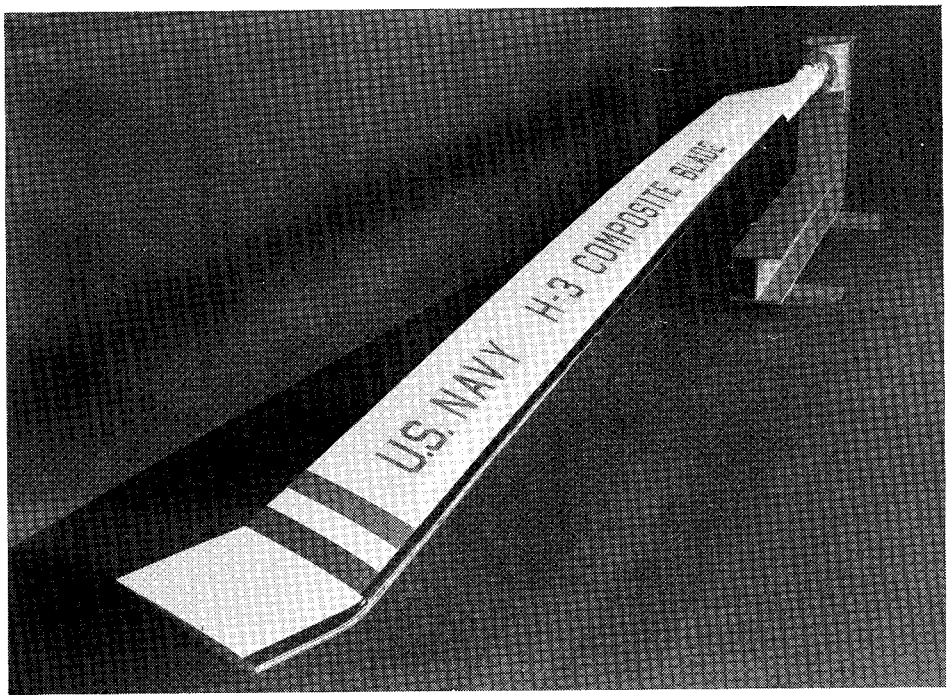

Figure 15.- Completed assembly.

TIME-TEMPERATURE-STRESS CAPABILITIES OF COMPOSITE MATERIALS FOR ADVANCED SUPERSONIC TECHNOLOGY APPLICATIONS

J. Haskins and J. Kerr

General Dynamics

SUMMARY

Time-temperature-stress characteristics of four classes of high temperature composite materials are established to assess their suitability for advanced supersonic technology considerations. The tests discussed include: thermal aging, ambient aging, fatigue, tensile, shear, fracture and flight simulation with some results being available for 10,000 hours exposure. The results are presented with emphasis on their influence on design of flight vehicles.

INTRODUCTION

Composite materials have the potential of significantly reducing weight of future supersonic cruise aircraft structures. However, implementation of these materials into vehicle usage is contingent upon demonstrating their airworthiness when exposed to a long time supersonic flight environment. The objectives of this research are to establish the time-temperature-stress characteristics and capabilities of five classes of high temperature composite materials to determine their suitability for supersonic cruise aircraft consideration. The changes in baseline tensile, notched tensile, shear, fatigue and fracture properties that occur over long periods of time are being measured for ambient and thermal aging conditions, as well as random cyclic loading with cyclic temperature variations. Figure 1 summarizes the work. The graph at the left shows what one might expect over 50,000 hours for a typical advanced composite, and how the strength might decrease as exposure time increases under different conditions. A brief summary of the test environments, materials studied, types of tests, analysis used and data comparisons is given at the right of Figure 1.

In order to predict the effects of realistic load and temperature cycling on material properties, we have simulated the supersonic cruise aircraft environment. This simulation consists of 25,000 two-hour flights, or

50,000 hours of testing. The key element of the program is random load spectrum testing, and the application of a wear-out model to predict the effects of random loading and temperature cycling on the material properties; then to be able in real time to measure the actual changes in properties, and to use thermal aging and constant amplitude fatigue data to analyze the significant factors in life prediction. This will, hopefully, enable one to accelerate testing in order to predict the useful life of a composite material.

As the program is a lengthy one (complete results will not be available until approximately 1981), this paper attempts to present an introduction to the study and to indicate the status of the various experimental portions currently in progress. The following sections describe the materials and test procedures and briefly discuss some of the significant results obtained thus far.

MATERIALS

Of the multitude of advanced composite material systems that have been developed and evaluated, five have generally been accepted as the most promising for aerospace structural design applications: boron/epoxy (B/E), graphite/epoxy (G/E), boron/polyimide (B/PI), graphite/polyimide (G/PI), and boron/aluminum (B/Al). Within each of these five classes there are several types of matrix materials and different types of filaments. Table I lists the specific advanced composite systems evaluated in this program. The selection of these particular composite systems was based on cost, current availability and manufacturing maturity, existing data base, fabrication history, good thermomechanical and physical properties, and material suppliers' continuing interest in producing a particular system.

The organic matrix composites were fabricated by Convair from vendor supplied prepreg material using conventional autoclave processing methods. The B/Al, which was purchased in the form of finished sheet material, was fabricated by diffusion bonding at approximately 800°K (975°F) using a single-step hot pressing technique. Both unidirectional and $[0° \pm 45°]$ laminates were evaluated for each system. Six ply laminates were used for all tests except flexure, short beam shear, transverse tensile, and R = -1 fatigue for which 12 ply panels were required. Diamond impregnated saws were used for specimen cutting, and all holes and notches were prepared by rotary ultrasonic drilling, electrical discharge machining, or ultrasonic impact grinding. Quality assurance testing was conducted on the epoxy and polyimide prepregs and on all fabricated panels of all materials. These

acceptance tests included ultrasonic C-scans, volume percentage determinations, mechanical property testing, and for the organic matrix composites flexural testing before and after 24-hour water boil. Specimen configurations selected for the program generally followed those called out in the Advanced Composites Design Guide (reference 1).

While all five materials passed the acceptance tests, one, B/PI, was later dropped from the program because of extensive thermal degradation observed during thermal aging and short term flight simulation testing at 505K (450F). Later tests by the resin producer, Ciba Geigy, substantiated Convair's data and reinforced the conclusion that the resin was not suitable for this application.

BASELINE TESTING

The purpose of the baseline tests is threefold. First, these data will serve to characterize the composite materials and add to any existing data bases. Second, the baseline tests will provide the scale and shape parameters necessary to define the statistical distribution of the ultimate tensile strengths for each of the material systems. These, in turn, are used to set the loads for the short term tests, and with the short term results, are used in a wear out analysis model to relate static and fatigue strengths. Finally, the baseline tests will provide a rational starting point against which the various environmental effects may be measured.

Tests that were conducted included: ultimate tensile, tensile modulus, Poisson's ratio, notched tensile (K_t = 3), transverse tensile (unidirectional laminates only), shear, and fracture. Testing was performed over the temperature range from 218°K (-67°F) to 450°K (350°F) for the epoxy specimens, to 616°K (650°F) for the polyimide specimens, and to 700°K (800°F) for the boron aluminum specimens. Customary units rather than the International System of Units (SI) were used as the working units of measurement for all tests.

Some typical results are shown in Table II for A-S/3501 graphite epoxy. The data are limited to those obtained from tensile testing as the shear and fracture tests have not yet been completed. The values are averages of from 3 to 10 specimens per test condition. From room temperature up to 450°K (350°F) temperature had little influence on unnotched or notched tensile strength, modulus or Poisson's ratio for either unidirectional or crossplied material tested in the fiber direction. For unidirectional material, there

was a substantial loss in the transverse strength at 450°K (350°F). Moderate to large strength decreases were also found at 218°K (-67°F) for both layups. The effect of the notch, 0.64 cm (0.25 in.) diameter hole in 2.5 cm (1 in.) wide specimen, was to reduce the net section strength by approximately 10 percent for the unidirectional material, and 20 percent for the crossplied material. Again, these reductions were independent of temperature for tests from 297°K (75°F) to 450°K (350°F).

MOISTURE AND WEATHER TESTING

Most of the data generated to date on advanced composite materials have been initial strength data without regard to environmental conditions. The small amount that is available is generally for only relatively short periods of exposure compared to the lifetime of a commercial airliner. This portion of the program was intended to evaluate the composite systems as a function of exposure to moisture, ambient aging, and atmospheric contaminants over relatively long periods of time.

For the resin matrix composites, 24-hour water boil, 6-week humidity, and 20-week and 52-week ambient aging tests have been conducted as accelerated means of simulating long-term ambient exposure. Residual strength testing (flexure) of these specimens has been completed, and the results in percent retention of flexural strength are listed in Table III. In order of increasing effect on mechanical properties, the various exposures are ranked as one might predict, i.e., 20-week ambient, 52-week ambient, and either 6-week humidity or 24-hour water boil. The results are typical of those obtained by others (references 2 and 3).

For epoxy systems, crossplied laminates traditionally have shown better 450°K (350°F) strength retention after exposure than unidirectional laminates. No definite theory has been advanced to explain this, but contributing factors might include specimen configuration, built-in thermal stresses from curing, compression mode of failure after exposure, etc. An examination of the epoxy flexural strength data (not shown in Table III) shows that after long term aging, the failure strengths for both unidirectional and crossplied laminates are nearly the same. This would be anticipated for a matrix dominated failure mode. The room temperature flexural strengths were nearly unaffected by any of these exposures, while those at 450°K (350°F) were, in general, severely degraded; the only exceptions being the crossplied B/E material after the 20 and 52-week ambient age. The unidirectional specimens were particularly affected with losses in the 450°K (350°F) flexural strength of from 77 to 41 percent depending on the type of exposure.

The effects of the moisture exposures on the polyimide specimens were generally less damaging than for the epoxy systems. Some decreases in flexural strength of the crossplied material were observed at 450°K (350°F) after the 24-hour water boil and 6-week humidity tests, but both of these exposures are quite severe. For the 20 and 52-week ambient ages no significant effects were observed.

Absorption of moisture appears to be the primary cause for the deterioration in high temperature properties. One commonly accepted theory is that water plasticizes the resin, which could act to destroy secondary bonding forces--either hydrogen bonding between functional groups, or electrostatic forces. Destruction of these secondary bonding forces would lower both the glass transition and the heat distortion temperatures and, thereby, decrease the high temperature resistance.

Another environmental study is being conducted to determine the effects of corrosion and atmospheric contaminants on the four composite systems. Tensile specimens of the epoxy and polyimide systems and tensile and shear specimens of coated and bare B/Al have been placed in an outdoor industrial-seacoast atmosphere corrosion test facility maintained by Convair in San Diego, California. A high temperature coating with a maximum use temperature of about 589°K (600°F) was applied to one-half of the B/Al specimens. The coating consisted of a chemical conversion coating followed by an epoxy primer and a polyimide topcoat. No coatings were used on any of the organic matrix composites. The specimens are tested after 10,000 and 50,000 hours of exposure for the B/Al and 50,000 hours for the epoxy and polyimide specimens.

To date, the 10,000 hour B/Al exposure tests have been completed. No change was observed in the coated specimens, but the uncoated specimens all showed evidence of surface corrosion. The results of post exposure tensile and shear testing, given in percent retention, are presented in Table IV. No effects to either tensile or shear properties were observed for the coated samples. For the uncoated specimens, significant decreases were found in the transverse tensile strength and the shear strength, while the longitudinal tensile strength was unaffected by the 10,000 hour exposure. A surface effect such as corrosion of the bare aluminum would be expected to decrease the matrix controlled properties, i.e., transverse tensile and shear, but have little effect on longitudinal tensile, a fiber controlled property.

To check the extent and nature of the surface corrosion, a metallographic examination of bare and coated specimens was performed. No change in appearance was found for the coated specimen after the 10,000 hour exposure as the coating had provided complete protection. Examination of the uncoated specimen, on the other hand, revealed extensive intergranular attack at the surface which extended to a depth of approximately 0.07 mm (0.003 in.). An example of these corrosion crack regions is shown in Figure 2. Some surface disruption has also occurred near one of the boron filaments.

The uncoated shear specimens had been prepared prior to placing in the test facility so that the machined edges as well as the surfaces were exposed to the atmosphere. These specimens showed a decrease in shear strength of approximately one third. Later, a second set of shear specimens was prepared by re-machining one-half of each of the three failed specimens. For these specimens, only the surface of the test area had been exposed and subjected to corrosive attack. The shear strength of these specimens, Table II, was only slightly lower than the unexposed material. The configuration of the shear specimen used for these tests is one in which stress concentrations build up at the machined surfaces at either end of the shearing regions. If these surfaces are exposed to a corrosive environment, the subsequent corrosion cracks can initiate failures at loads substantially lower than those obtained from undamaged specimens. It is this phenomenon which is believed to have been responsible for the significant effect on shear strength of machining the notch before or after exposure.

THERMAL AGING

All of the composite materials are being thermally aged for periods up to 50,000 hours. At various times during the 50,000 hours, specimens are removed for determination of residual tensile strength and for B/Al also residual shear strength. Both unidirectional and $[0 \pm 45]$ crossply materials are included. The aging temperatures are: epoxy, 394°K (250°F) and 450°K (350°F); polyimide, 505°K (450°F) and 561°K (550°F); and B/Al, 450°K (350°F), 561°K (550°F), and 700°K (800°F). The organic matrix composites are aged at one atmosphere (101 kN/m^2) and at a reduced pressure of 13.8 kN/m^2 (2 psi) to simulate high altitude flight conditions. Previous work has shown a direct correlation of thermal aging and oxygen pressure on residual strength of resin matrix composites (reference 4). The B/Al system is aged at atmospheric pressure only.

Exposures are conducted in specially constructed resistance heated aging furnaces. The reduced pressure specimens are enclosed in sealed containers with a vacuum pump simultaneously pumping on one side of each container. A constant fresh supply of air to all specimens is assured by bleeding air through a valve into the other side of each container to maintain 13.8 kN/m^2 (2 psi). Temperatures are maintained by controllers to $\pm$ 2°K ($\pm$ 5°F) with infrequent excursions to a maximum of $\pm$ 6°K ($\pm$ 10°F).

Tests are currently in progress for all materials with data available out to at least 5,000 hours for all systems, and to 10,000 hours for the epoxy specimens and some of the B/Al specimens. Strength versus aging time curves are shown in Figure 3 for G/E, Figure 4 for G/PI, and Figure 5 for B/Al. These curves are only for specimens which were aged at one atmosphere.

The results shown in Figure 4 for G/E are typical of both the epoxy systems. At 394°K (250°F) no degradation has occurred during the first 10,000 hours. At 450°K (350°F), however, a fall off in strength began after approximately 1,000 hours. At 10,000 hours significant loses in strength, particularly in the $[0° \pm 45°]$ crossplied material, were found. The specimens aged at a reduced pressure of 13.8 kN/m^2 (2 psi) and a temperature of 450°K (350°F) showed almost no effects after 10,000 hours. Only the crossplied B/E, which suffered a loss in strength of approximately 30 percent, was affected. All other specimens (crossplied and unidirectional layups) retained 100 percent of their unexposed tensile strength.

The G/PI data, Figure 5, are similar in that no decrease in strength occurred in 5,000 hours at the lower aging temperature, 505°K (450°F), while significant loses were found at the higher temperature, 561°K (550°F). The 505°K (450°F) specimens actually showed an increase in tensile strength after the 5,000 hours age. In like manner to the epoxy specimens, where decreases in strength occurred, the crossplied material was, percentagewise, affected more than the unidirectional material. Reduced pressure exposures were conducted at both test temperatures for unidirectional specimens. Those aged at 505°K (450°F) showed no effect after 5,000 hours, while those aged at 561°K (550°F) decreased in strength approximately 10 percent.

Residual strength data for B/Al aged 10,000 hours at 450°K (350°F) and 5,000 hours at 561°K (550°F) are presented in Figure 5. Significant decreases in the room temperature tensile strengths in the 0° directions of both the unidirectional and $[0° \pm 45°]$ crossplied layups were found after aging at 561°K (550°F). These decreases were approximately 40 and 50

percent, respectively. Decreases were also observed at 450°K (350°F), although not as large. Smaller effects were found in the transverse tensile strengths, while the longitudinal shear properties were nearly unchanged. The data indicate the decrease in properties to be primarily fiber related, rather than to a degradation of the aluminum matrix. Apparently the boron filaments become weakened and embrittled as a result of diffusion to the filament-matrix interface during thermal exposure. An excellent review of interfacial effects on tensile properties of B/Al after thermal exposure can be found in reference 5.

FATIGUE

Constant-amplitude fatigue tests will be conducted before and after the flight simulation environmental exposures. The bulk of these tests and the ones that serve as the baseline for later comparisons are performed on the unexposed composite materials. It is these tests that are discussed in this section.

Test parameters that were considered include: (1) orientation - unidirectional and $[0 \pm 45]$ crossply; (2) specimen configuration - flawed and unflawed; (3) temperature - room and one elevated temperature; and (4) stress ratio - R = 0.1 and R = -1. The flawed specimens (K_T = 3) contained a center hole having a diameter equal to one-fourth of the specimen width.

All tests were performed on Sonntag SF1U and SF10U fatigue machines at a constant frequency of 30 Hz. For elevated temperature tests, clamshell and ring furnaces were used. Temperature was monitored by a thermocouple attached to the specimen at the center of the gage section. A total of nine specimens were used for obtaining an S-N curve at any given set of conditions.

While fatigue testing has not been completed as yet, considerable data have been obtained. Results for unidirectional and $[0° \pm 45°]$ crossplied G/E are shown in Figures 6 through 9. Individual data points are included in Figure 6, but have been omitted for clarity from the other figures. Figures 6 and 7 compare the results of axial fatigue testing at room temperature and stress ratios of R = 0.1 and R = -1 for both unnotched and notched specimens. These data show the fatigue life for a stress ratio of R = -1 to be much lower than for R = 0.1. For both stress ratios, the fatigue life for notched specimens is less than for unnotched specimens except the unidirectional material tested at R = -1 where no notch effect was observed. Similar data are presented in Figures 8 and 9 for testing at

450°K (350°F). Again the fatigue strength is greatly reduced for the R = -1 tests compared to those conducted at a stress ratio of R = 0.1. The presence of a notch is shown to reduce the fatigue strength for the R = 0.1 tests, but not for the R = -1 tests. Further, the unidirectional notched specimens performed better than those which were unnotched. The reason for this behavior is not clearly understood at this time, but is believed to be related to the phenomenon of crack blunting brought on by the combination of high compression loading and a matrix softened because of elevated temperature exposure. Additional studies of this effect are needed.

FLIGHT SIMULATION TESTING

During flight simulation testing, we are simulating both temperature and load on the test specimens. Figure 10 illustrates a typical load and temperature profile used during testing. This evaluation is based on three equally important series of tests: baseline tests (BT), described previously, short term tests (STT), and long term tests (LTT). An attempt is made here to describe each of the test types and their relationships.

It is assumed that at any time in the life of a specimen the strength is dependent upon flaw field status. For the purpose of data analysis, the flaw field growth is dependent upon the instantaneous state of the field and a measure of work input to the system. The state of the system is monitored by residual strength measurements. The assumption is made that the initial state is random which yields a distribution in both life and residual strength. The test program is designed to yield data with respect to the character of the distributions.

The use of the Wiebull distribution as a material behavior model has been described in references 6, 7, 8 and 9. References 7, 8 and 9 also include background information concerning the concepts of wear-out and endurance which are used freely here.

The baseline tests (BT) and existing test data are intended to provide the Weibull scale parameter and the shape parameter for the ultimate tensile strengths for each of the material systems. It is assumed that the fatigue failures to be obtained in subsequent tests result from time dependent flaw growth and strength degradation to the point that the specimens will not sustain the expected service loads in tension. As such, the baseline tests provide the strength measure for the specimens at zero time under fatigue

loading. The data reduction scheme currently rests upon the use of the Halpin-Waddoups wear-out model (references 7, 8, 9 and 10) to relate the static and fatigue strengths.

The short term tests (STT) were intended to provide the data necessary to set reasonable load levels for the long term tests. A complete STT run was made for 100 and 200 test hours, respectively. Since the number of loads imposed in those time periods must be maximized for them to have any relation to the LTT, the load spectrum for the STT is accelerated to 1 flight per minute. During the STT, the specimens were exposed to the maximum use temperature.

The loads for the 100 hour tests were set to try to induce some fatigue failures. The fatigue life and residual strength data were then used with the static data to fit a preliminary wear-out model. The model was used to set loads for the 200 hour tests. The results of the 200 hour tests were used to refine the wear-out model, and this refined model was used to set the loads for the long term tests.

Figure 11 is used to demonstrate the features of the data produced by the short term tests. The boron epoxy notched data is used to present the distributions in both life and residual strength mentioned earlier.

The peak load which will occur during the random load spectrum has been adjusted so that in Figure 11, 80 percent of the specimens will survive one lifetime of random load testing. The peak load is represented by the horizontal line at 0.78. The Weibull strength distribution shown vertically on the ordinate line represents the baseline data. It is plotted at 10^{-2} lifetimes for convenience, but really represents the distribution of strength for notched boron/epoxy before any cyclic loads were applied. The distribution curves for one-fourth and one-half lifetimes are also shown. These are given by the 100 and 200 hour short term tests. The three curves intersecting the distribution curves are survival curves for .9, .8 and .5. These curves give the fraction of the population that will survive a given load after being subjected to random loading for a number of lifetimes. Note then that after one lifetime of testing, 80 percent of the population will survive a load of 0.78, while only 50 percent will survive a load of 1.25.

The horizontal distribution curve drawn from the peak load line for convenience represents the distribution of fatigue failures expected during the course of random load testing for the peak load of 0.78.

The data shown in Figure 11 are typical of the manner in which the wear-out model and short term test (STT) were used to set load levels for the various composites for the long term test (LTT). The loads are adjusted in each case so that 80 percent of the specimens being tested will survive 50,000 hours, or one lifetime of random loading and temperature cycling. The 50,000 hours is composed of 25,000 flight simulations similar to the one shown in Figure 10. The flight simulation portion of the program is in progress, but no results will be available until the first 10,000 hours has been completed.

CONCLUSIONS

The studies presented in this paper are directed toward characterizing the properties of several types of advanced composite systems and a determination of the effects of long time supersonic flight simulation. These studies are still in progress, and the conclusions to be drawn at this time are limited. There have been, however, several interesting observations resulting from the tests which have been completed. These are summarized briefly below.

1. Absorption of moisture by the epoxy systems evaluated on this program can cause a significant decrease in short time elevated temperature strength. The results point out the need for a moisture-proof coating when these materials are subjected to long periods in ambient environments. Moisture effects were generally less damaging for the G/PI system, particularly for the ambient environment exposures.

2. Uncoated B/Al is subject to pitting and subsequent intergranular corrosion cracking when exposed for long periods in an industrial-seacoast environment. These corrosion cracks can seriously degrade the matrix controlled properties by acting as crack starters.

3. The B/E and G/E systems exhibit good resistance to thermal aging in one atmosphere air at 394°K (250°F) for 10,000 hours, but show significant losses in strength after 10,000 hours at 450°K (350°F). At a reduced pressure of 13.8 kN/m^2 (2 psi), the 450°K (350°F) exposure has almost no effect after 10,000 hours. Similar results were obtained for G/PI with good strength retention after 5,000 hours at 505°K (450°F), but significant losses after 5,000 hours at 561°K (550°F), both at one atmosphere. Low pressure exposures at 561°K (550°F) resulted in only minor strength losses after 5,000 hours. Tests on B/Al revealed serious strength losses after 5,000

hours at 561°K (550°F). Smaller decreases were also observed after 10,000 hours at 450°K (350°F). The data indicated the decrease in strength to be primarily fiber related, rather than to a degradation of the aluminum matrix.

4. Fatigue strength of G/E at room and elevated temperature was found to be very dependent on the stress ratio used in testing. Results for tension-compression loading (R = -1) were considerably lower than those obtained for tension-tension loading (R = 0.1). The addition of a notch (circular hole) further reduced the fatigue strength for specimens tested at an R value of 0.1. For notched specimens tested at R = -1, the fatigue strengths were lowered, raised, or unaffected depending on the test temperature and laminate orientation. The reason for this behavior is thought to be related to the phenomenon of crack blunting brought on by the combination of high compression loading and a matrix softened by elevated temperature exposure.

ACKNOWLEDGEMENT

The work in progress described herein is sponsored by the National Aeronautics and Space Administration, Langley Research Center, Hampton, Virginia, under Contract NAS1-12308, monitored by Mr. Bland Stein.

REFERENCES

1. Advanced Composites Design Guide, Volume 1, Material Characterization, January 1971.

2. Hertz, J., Investigation into the High-Temperature Strength Degradation of Fiber-Reinforced Resin Composite During Ambient Aging, Report No. GDCA-DBG73-005, Contract NAS8-27435, NASA-Marshall Space Flight Center, Huntsville, Alabama 1973.

3. Scheck, W. G., Development of Design Data for Graphite Reinforced Epoxy and Polyimide Composites, Report No. GDC-DBG70-005, Contract NAS8-26198, NASA-Marshall Space Flight Center, Huntsville, Alabama 1974.

4. Chase, V. and Beeler, D., Manufacturing Methods for Large High-Temperature Sandwich Structures, Technical Report AFML-TR-70-211, Air Force Materials Laboratory, Dayton, Ohio 1970.

5. Metcalfe, A. G., ed.: Interfaces in Metal Matrix Composites, Academic Press, New York 1974.

6. Lemon, G. H., Statistical Considerations for Structural Reliability Analysis, Proceedings of the Colloquium on Structural Reliability, Pittsburgh, Pa., 9-12 October 1972.

7. Wolff, R. V. and Lemon, G. H., Reliability Prediction for Adhesive Bonds, AFML-TR-72-121, March 1972.

8. Manning, S. D., Lemon, G. H and Waddoups, M. E., Composite Wing for Transonic Improvement, Volume III, Structural Reliability Studies, AFFDL-TR-71-24, March 1971.

9. Waddoups, M. E., Wolff, R. V. and Wilkins, D. J., Reliability of Complex Large Scale Composite Structure-Proof of Concept, AFML-TR-73-160, July 1973.

10. Halpin, J. C., Waddoups, M. E. and Johnson, T. A., Kinetic Fracture Models and Structural Reliability, International Journal of Fracture Mechanics, Volume 8, 1972, pp 465-468.

TABLE I

LIST OF ADVANCED COMPOSITE SYSTEMS

MATERIAL SYSTEM	TYPE	VENDOR	NOMINAL FIBER VOLUME (%)	SPECIFIC GRAVITY
BORON/EPOXY	RIGIDITE 5505 4.0-MIL BORON	Avco	58	2.0
GRAPHITE/EPOXY	A-S/3501	HERCULES	60	1.6
BORON/POLYIMIDE	B/P105AC 4.0-MIL BORON	Avco	50	2.0
GRAPHITE/POLYIMIDE	HT-S/710	HERCULES	63	1.5
BORON/ALUMINUM	DIFFUSION BONDED 5.6-MIL BORON; 6061 ALUMINUM	Avco	50	2.6

TABLE II

SUMMARY OF BASELINE TENSILE PROPERTIES OF A-S/3501 GRAPHITE/EPOXY

	TEMPERATURE, DEG K (DEG F)						
	218 (-67)	297 (75)	394 (250)	408 (275)	422 (300)	436 (325)	450 (350)
TENSILE STRENGTH, MN/m^2 (ksi)							
[0]	882 (128)	1,540 (224)	1,510 (219)	1,670 (242)	1,500 (218)	1,610 (234)	1,590 (230)
[0±45]	449 (65.2)	496 (71.9)	525 (76.2)	484 (70.2)	509 (73.8)	502 (72.8)	500 (72.5)
[90]	–	59 (8.6)	–	–	–	–	37 (5.4)
TENSILE MODULUS, GN/m^2 (Msi)							
[0]	–	141 (20.4)	146 (21.2)	166 (24.0)	139 (20.2)	139 (20.1)	150 (21.8)
[0±45]	48 (6.9)	57 (8.3)	56 (8.1)	54 (7.8)	51 (7.4)	53 (7.7)	58 (8.4)
POISSON'S RATIO							
[0]	–	0.33	0.34	–	0.35	–	–
[0±45]	–	0.70	–	–	–	–	–
NOTCHED TENSILE STRENGTH, MN/m^2 (ksi)							
[0]	1,030 (150)	1,380 (200)	1,390 (202)	1,620 (235)	1,450 (210)	1,410 (204)	1,350 (196)
[0±45]	312 (45.3)	412 (59.7)	401 (58.2)	398 (57.7)	394 (57.1)	429 (62.3)	416 (60.3)

TABLE III

SUMMARY OF EFFECTS OF MOISTURE & AMBIENT AGING ON RESIN-MATRIX COMPOSITES

RETENTION OF FLEXURAL STRENGTH (PERCENT) AFTER INDICATED EXPOSURE*

ORIENT	TEMP DEG K (DEG F)	24 HOUR H_2O BOIL	6 WEEK HUMIDITY	20 WEEK AMBIENT	52 WEEK AMBIENT
B/5505 BORON/EPOXY					
[0]	297 (75)	94	103	105	110
[0]	450(350)	23	39	59	53
[0 ± 45]	450(350)	63	74	102	94
A-S/3501 GRAPHITE/EPOXY					
[0]	297 (75)	100	100	110	96
[0]	450(350)	34	30	54	46
[0 ± 45]	450(350)	54	41	81	57
HT-S/710 GRAPHITE/POLYIMIDE					
[0]	297(75)	85	85	103	100
[0]	450(350)	105	106	85	107
[0 ± 45]	450(350)	75	81	111	93

*AVERAGE OF 3 TESTS

TABLE IV

TENSILE & SHEAR DATA FOR BARE & COATED BORON/ALUMINUM AFTER 10,000-HOUR ATMOSPHERIC CONTAMINANTS EXPOSURE

SPECIMEN TYPE	CONDITION	RETENTION OF STRENGTH, (%)[a]
90 TENSILE	BARE	76
90 TENSILE	COATED	100
0 TENSILE	BARE	100
0 TENSILE	COATED	100
0 SHEAR	BARE, MACHINED BEFORE EXPOSURE	69
0 SHEAR	BARE, MACHINED AFTER EXPOSURE	94
0 SHEAR	COATED	100

[a]AVERAGE OF 3 TESTS

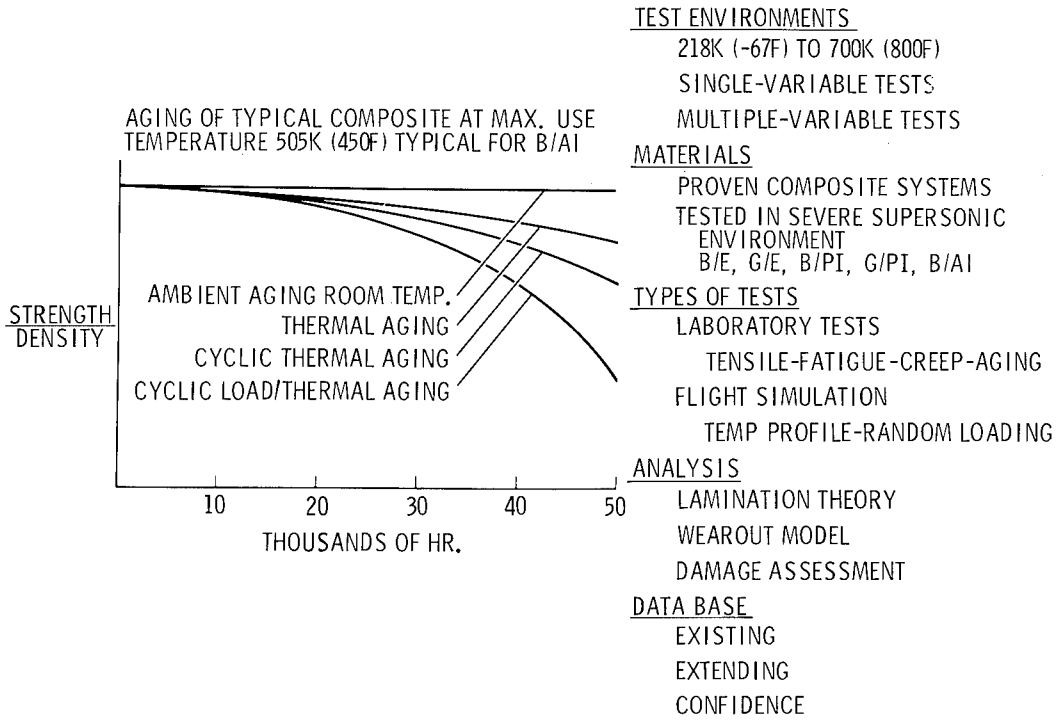

Figure 1.- Characterization of composite material for up to 50,000 hours of supersonic cruise aircraft environment.

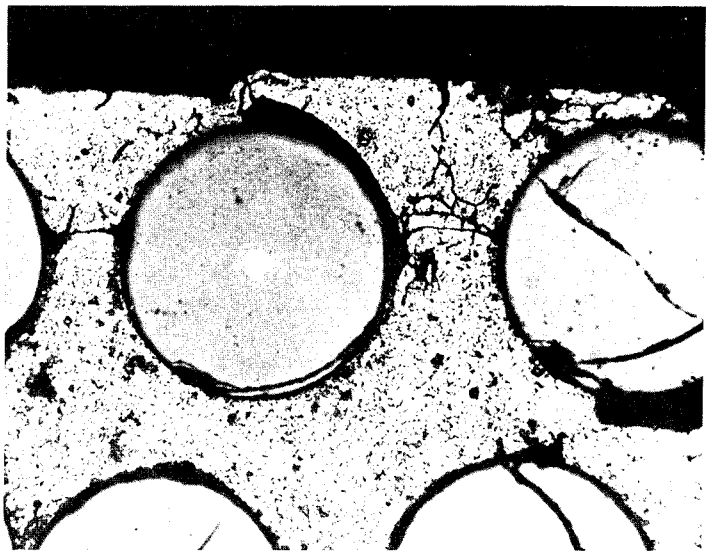

Figure 2.- Intergranular corrosion cracks in unidirectional boron/aluminum after 10,000 hours of atmospheric contaminants exposure in industrial-seacoast environment.

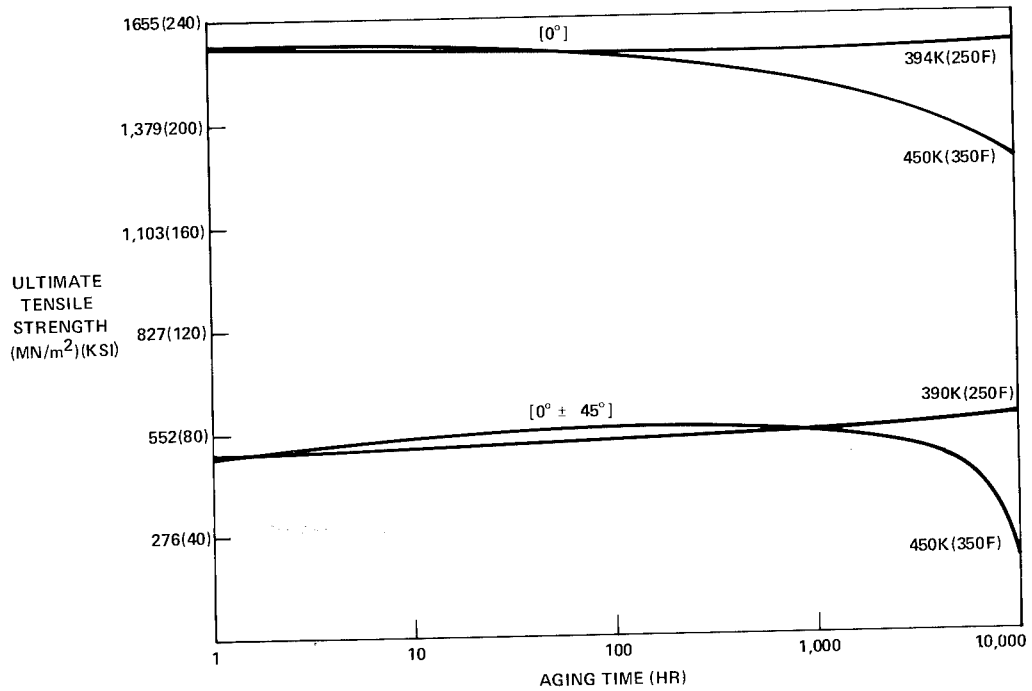

Figure 3.- Tensile strength of AS/3501 graphite epoxy at 450K (350F) after thermal aging at indicated temperature.

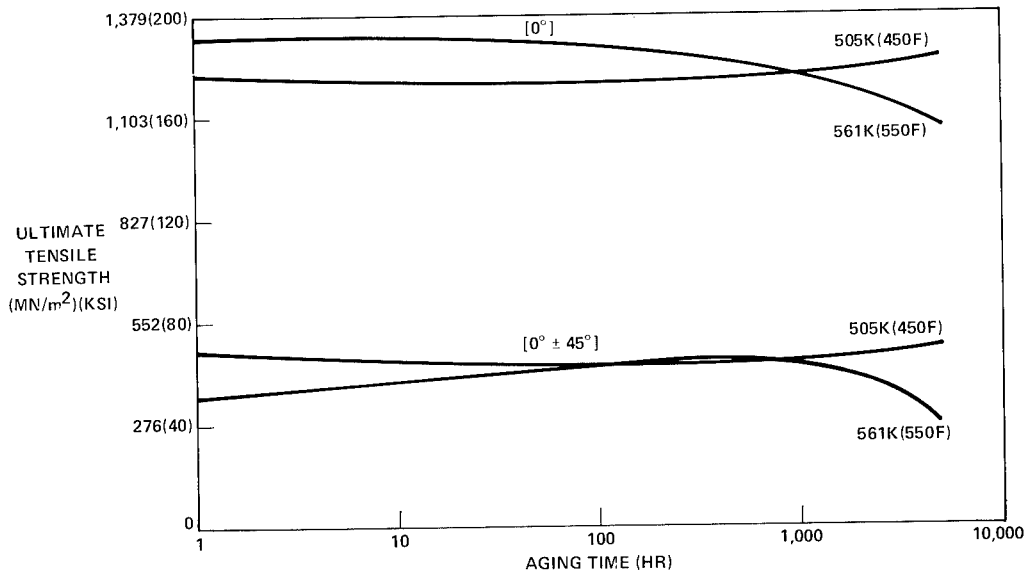

Figure 4.- Tensile strength of HT-S/710 graphite/polyimide at 505K (450F) and 561K (550F) after thermal aging at the same temperatures.

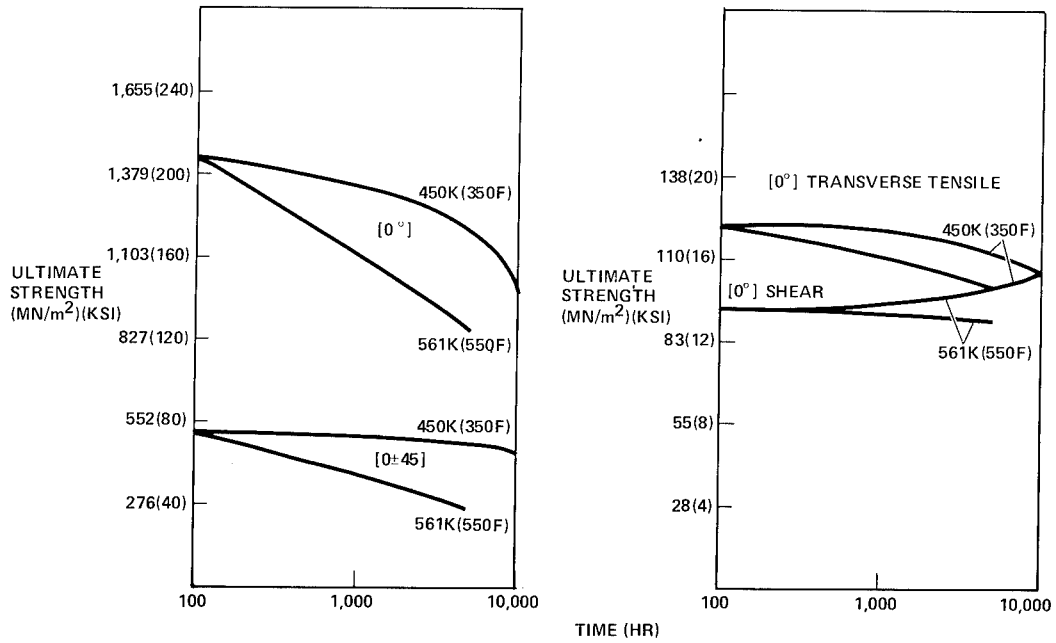

Figure 5.- Tensile and shear strength of diffusion-bonded boron/aluminum 297K (75F) after thermal aging at indicated temperature.

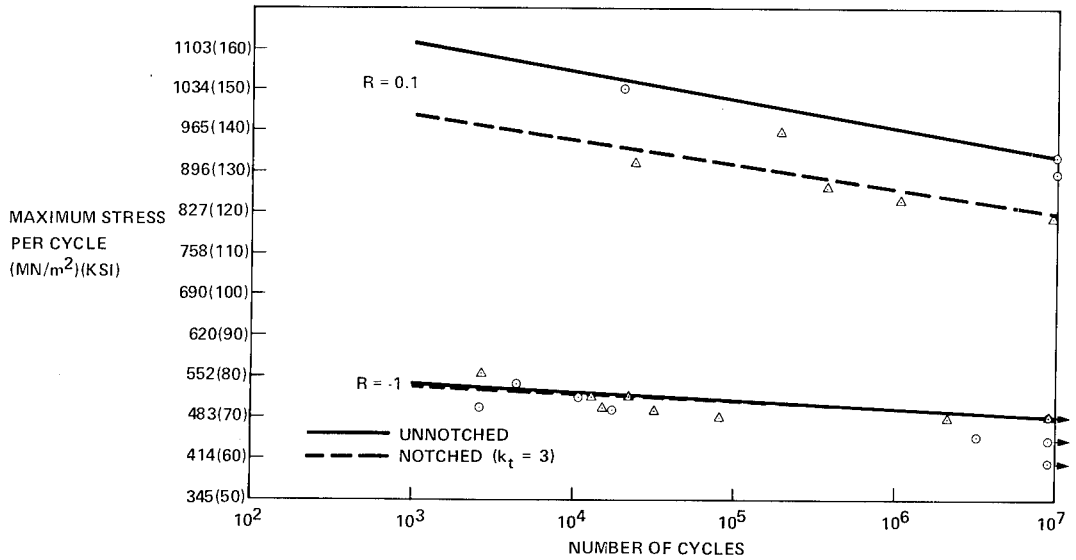

Figure 6.- Fatigue properties of [0°] graphite/epoxy composite at 297K (75F).

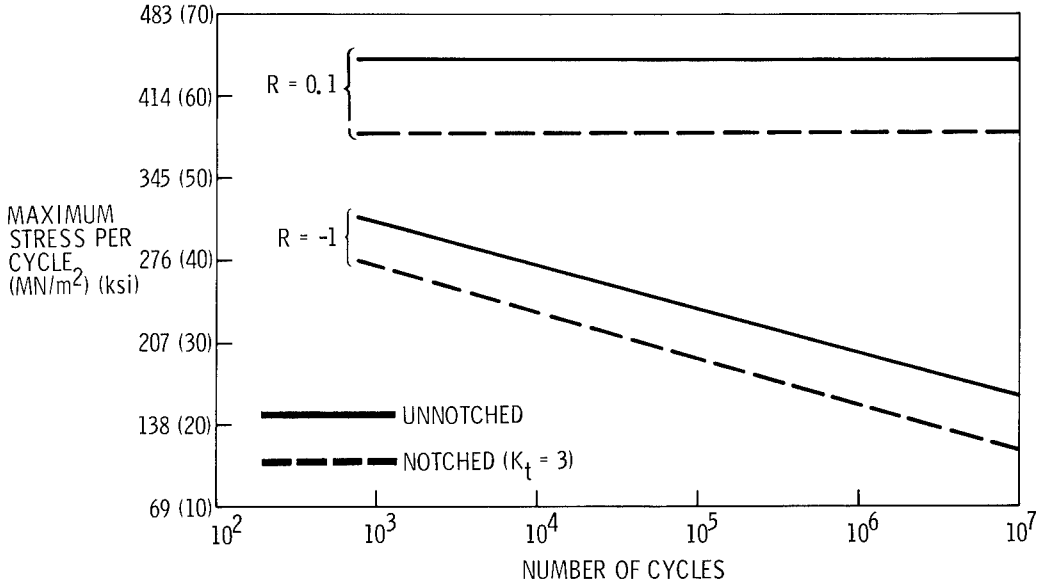

Figure 7.- Axial fatigue properties of $[0 \pm 45]_s$ graphite/epoxy composite at 297K (75F).

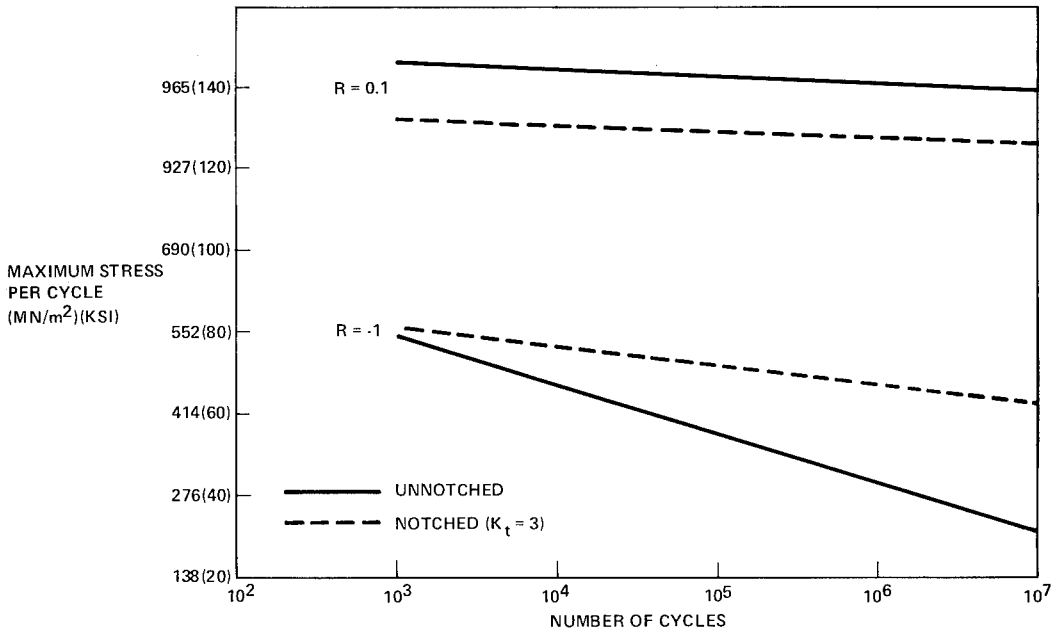

Figure 8.- Fatigue properties of [0°] graphite/epoxy composite at 450K (350F).

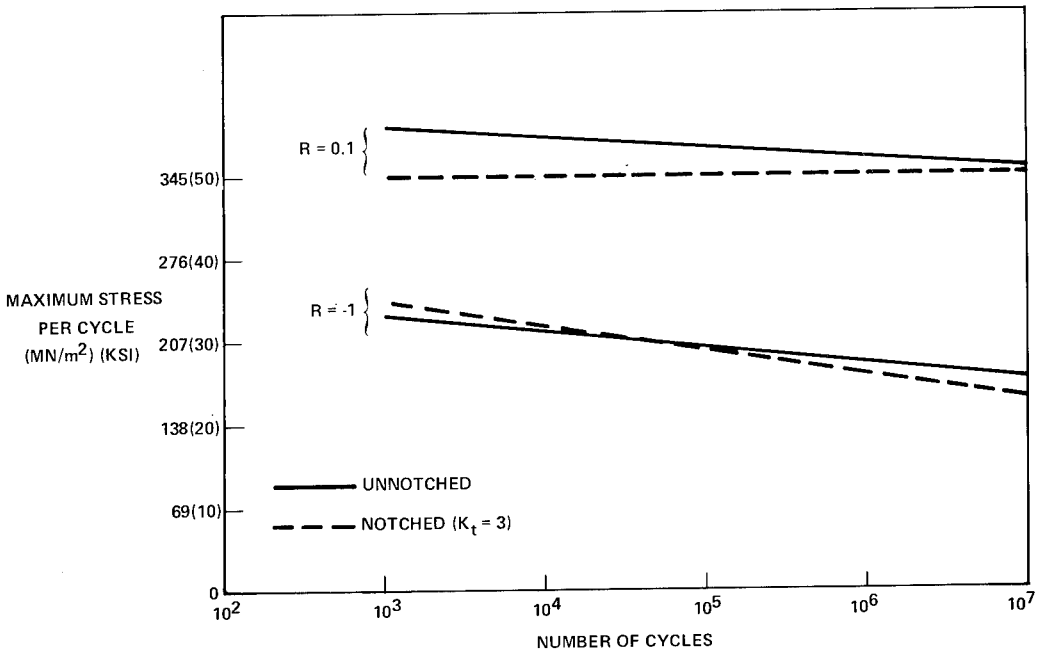

Figure 9.- Fatigue properties of $[0 \pm 45^{\circ}]$ graphite/epoxy composite at 450K (350F).

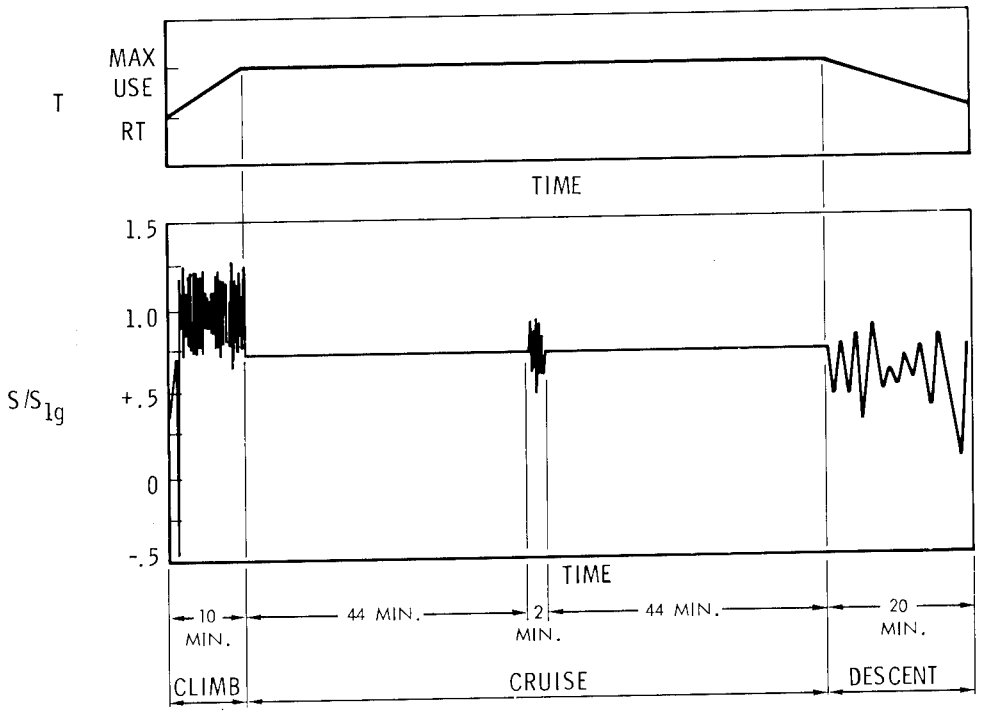

Figure 10.- Typical flight simulation load & temperature profile.

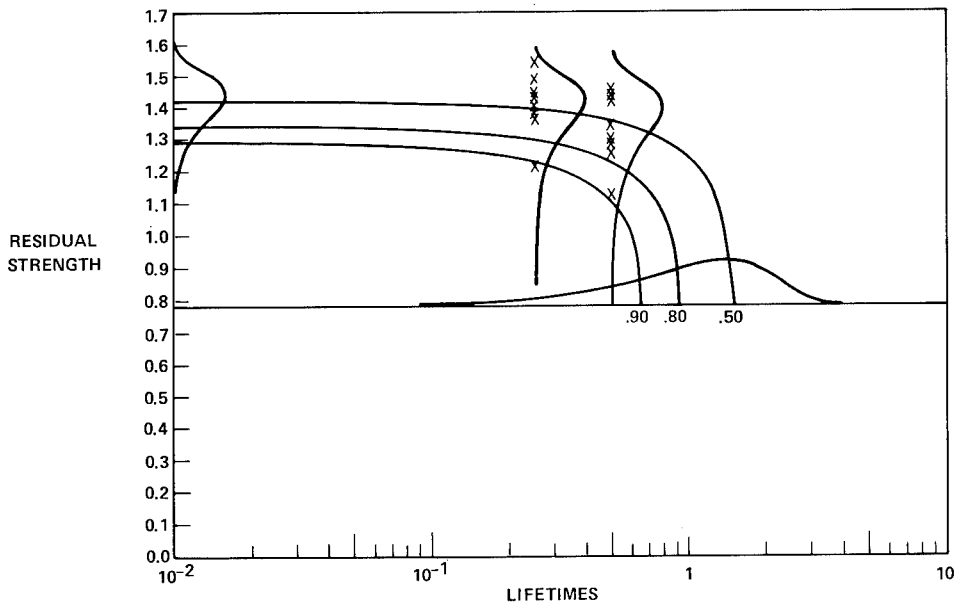

Figure 11.- Boron-epoxy notched short term tests.

MOISTURE - AN ASSESSMENT OF ITS IMPACT ON THE DESIGN OF RESIN BASED ADVANCED COMPOSITES

By Charles D Shirrell, John C Halpin,
Air Force Flight Dynamics Laboratory

and Charles E Browning
Air Force Materials Laboratory

SUMMARY

Epoxy resin based matrix and adhesive systems absorb water. A primary consequence of water absorption is a dilatational strain impairing the matrix strain allowables and a reduction in the heat distortion temperature of the resin. The magnitude of these defects, the rate of moisture absorption, and its distribution within a solid object are sensitive to the specific chemical details of the resin system.

The Air Force Flight Dynamics Laboratory and the Air Force Materials Laboratory recently sponsored a workshop which examined the environmental durability of resin matrix composites. This workshop was held at Battelle's Columbus Laboratories on September 30 and October 1-2, 1975. The purpose of this paper is to discuss the data base presented at this conference, the conclusions of the Materials and Processing Panel, and the recommendations of this panel for further study.

INTRODUCTION

Advanced polymeric matrix composite materials have emerged as strong candidates for production airframe construction. Current and projected activities involve an increasing commitment of advanced composites in strength critical, primary, safety-of-flight structures. Occurring simultaneously with these pioneering efforts is the implementation of new structural integrity policies by the USAF which reemphasize the need for proven life-cycle durability prior to the acceptance of production aircraft.

Recent developments in the application of polymeric matrix composites to aircraft structures have revealed significant changes in the mechanical properties and dimensional shapes of these materials due to the effects of combined moisture and thermal environments. If these properties are significantly diminished, then service life and reliability of polymeric matrix composites may be compromised unless these effects are accounted for in design.

Therefore, it is important that the rates and extent of moisture absorption, the induced swelling of the matrix, and any loss in elevated temperature properties of the composite be thoroughly understood. Knowledge of these factors will guide the structural engineer in the conditioning of environmental test specimens and then enable the aerospace designer to eliminate any environmentally induced weakness in a composite structure. These topics were discussed by the Materials and Processing Panel of the AFFDL/AFML sponsored workshop on the Environmental Durability of Resin Matrix Composites.

The objectives of this panel were:

1. To assess the significance of environmental exposure, particularly moisture absorption, on the performance of advanced resinous composites;

2. To review the current understanding of the mechanisms that cause property changes in the composites; and,

3. To evaluate the capability to predict the extent of degradation which should be anticipated as a result of service exposure.

The conclusions of the panel are summarized in Table I and the panel's recommendations for areas that need to be studied further are given in Table II.

The effect of moisture exposure on advanced composites is considered to be a reversible, physical phenomenon which acts mainly on the resinous matrix. Graphite and Boron fibers are not considered to be moisture sensitive. Chemical degradation of epoxy matrices has not been conclusively demonstrated and while further work is required in this area, it is not considered responsible for the composite property degradation observed to date.

MOISTURE ABSORPTION/DESORPTION

Water penetration in advanced resinous composites takes place by the following mechanisms:

1. Through the fiber-matrix interface (capillary);

2. Through cracks and voids in the composite; and,

3. Through the resin (diffusional).

In composite articles with large edges, capillary action along the fiber-resin interface would play a significant role in moisture penetration. Also, as a composite article undergoes cyclic loading and ultraviolet light induced surface crazing, the formation of cracks and voids in the composite becomes an increasingly important mechanism for moisture penetration. However, the primary mechanism of water penetration in large well-fabricated composite articles is rapid surface absorption followed by diffusion of the water through the resin.

In its simplest form, diffusion in isotropic materials is based on the hypothesis that the rate of transfer, F, of diffusing matter through unit area of a section is proportional to the concentration gradient measured normal to the section:

$$F = -D\ \partial c/\partial x\ , \tag{1}$$

and

$$q = DA \int_o^t (dc/dx)dt\ , \tag{2}$$

where:

q - The amount of diffusing substance passing through surface area, A;

t - The length of time of exposure;

c - The concentration of diffusing matter;

x - The space coordinate measured normal to the diffusing section; and,

D - The diffusivity or sometimes called the diffusion coefficient.

Equation 1 is known as Fick's first law of diffusion.

A more general diffusion equation, known as Fick's second law and valid for one-dimensional diffusion, reads:

$$\partial c/\partial t = D\ \partial^2 c/\partial x^2\ , \tag{3}$$

or for three-dimensional diffusion:

$$\partial c/\partial t = D\left[\frac{\partial^2 c}{\partial x^2} + \frac{\partial^2 c}{\partial y^2} + \frac{\partial^2 c}{\partial z^2}\right]. \tag{4}$$

Analysis of hygrothermal absorption data for epoxy composites shows that the moisture content asymptotically approaches an equilibrium moisture level, Figure 1. This equilibrium moisture content is determined solely by the relative humidity to which the sample is exposed (Figure 2). The rate at which the sample reaches the equilibrium moisture content is determined by the thickness, Figure 3, and by the exposure temperature, Figure 4. For a well cured laminate, the equilibrium moisture content and the rate of moisture absorption was found to be insensitive to the degree of curing, Figure 5. Desorption is also a non-linear process and Figure 6 shows that the moisture content asymptotically approaches zero from its initial value.

In principle any problem concerning concentration-independent diffusion can be solved by using equations 1 and 3 with appropriate boundary conditions. Usually the solution is either a series of Bessel functions, a series of error functions, a series of trigonometric functions, or a numerical methods technique (Ref 1).

An empirical relationship for the non-linear water absorption behavior of epoxy composites has been developed by McKague, Reynolds, and Halkias (Ref 2):

$$M_t = M_i + (A*RH-M_i)\tanh\left[(4/\ell)\ \{(D_o\exp(-E_d/RT))(t/\pi)\}^{\frac{1}{2}}\right] \quad (5)$$

where:

M_t - The moisture content at time t, % by weight;

M_i - The initial moisture content, % by weight;

A - The absorptivity coefficient;

RH - The relative humidity;

ℓ - The laminate thickness, cm;

D_o - The permeability index, cm^2/sec;

E_d - The energy of activation for diffusion, cal/mole;

R - The universal gas law constant, 1.986 cal/mole-^oK;

T - The exposure temperature, ^oK; and,

t - The exposure time, sec.

The material parameters - A, D, and E - necessary for utilization of equation 5 are given in Table 3. Preliminary evidence indicates that equation 5 may overestimate M_t by 10-20% for transient conditions. However, for hygrothermal conditions equation 5 gives excellent results.

The diffusion coefficient of water vapor in most polymers differs from that of many other gases in that it is concentration-dependent. This is generally caused by a swelling of the resin matrix by the diffusing water molecules, leading to a loosening of the resin matrix chemical structure which facilitates the movement of additional water molecules (Ref 3). The most general treatment of such diffusion should be based on the equation:

$$\frac{\partial c}{\partial t} = \frac{\partial (D \partial c/\partial x)}{\partial t} + \frac{\partial (D \partial c/\partial y)}{\partial t} + \frac{\partial (D \partial c/\partial z)}{\partial t} \qquad (6)$$

A rapid method for establishing whether diffusivity is concentration-dependent or not is the determination of both absorption and desorption time curves. The absorption and desorption for a T300/5208 graphite/epoxy composite are given in Figure 7. These curves would coincide for a constant diffusion coefficient but differ for a concentration-dependent one. Unfortunately, the specific mathematical relationship between diffusivity and moisture concentration is not known at this time for resinous composites and thus it is impossible to obtain an exact solution to equation 6.

Solution of equation 4 or equation 6 allows the calculation of the moisture distribution in the composite. Figure 8 shows the concentration gradients at all points in a sheet exposed on both sides (Ref 4). Upon drying, the outer plies of the composite go to zero moisture content and the moisture content in the middle of the laminate increases. For transient conditions such as those composite components on aircraft might see, the moisture distribution in a laminate could be very complex.

Normalization of the equilibrium moisture content using the following relationship:

$$M(\infty)_M = \frac{\rho_{comp}}{\rho_M X_M} M(\infty)_\ell \qquad (7)$$

where:

$M(\infty)_M$ - The equilibrium moisture content in the composite matrix;

ρ_{comp} - The density of the composite laminate;

ρ_M - The density of the composite matrix;

X_M - The volume fraction of the composite matrix; and,

$M(\infty)_\ell$ - The equilibrium moisture content in the composite laminate.

indicates that the equilibrium moisture content for the resin systems in use today appears to be very similar. Figure 9 illustrates the relationship between relative humidity and the percent water in the composite matrix.

CONSEQUENCES OF MOISTURE ABSORPTION

The mechanical effect of moisture absorption in resinous composites is the result of the effect of moisture on the fiber, the resinous matrix, and the interfacial region. The boron and graphite fibers used in advanced composites are essentially unaffected by moisture. Thus, the degrading effects of water on advanced composites are primarily a result of changes in properties of the resinous matrix and the interfacial region. The contribution of each of these regions to the total change in mechanical properties of a laminate is a function of the applied stress relative to the fiber orientation. In longitudinal stress the fibers are the predominate factor and only slight losses in mechanical properties are observed with moisture absorption. However, in shear, compression, and transverse stress the interfacial and matrix regions dominate the composite properties and significant mechanical property changes are observed with moisture absorption.

The effect of absorbed water on advanced composites is threefold: (1) the resin undergoes swelling which induces internal stresses; (2) the stiffness of the resin is reduced; and, (3) the adhesion of the fiber to the resin is reduced. As moisture is absorbed by an epoxy resin, the water molecules become mixed with the epoxy polymer molecules. The addition of these water molecules to the epoxy resin induces a swelling of the resin. Assuming additivity of volumes and a homogeneous moisture distribution, it is possible to compute the volume change due to moisture absorption using the following relationship:

$$\frac{\Delta V(t)}{V_o} = \rho_R M(t) \overline{V}_{H_2O} \qquad (8)$$

where:

$\Delta V(t)$ - The change in volume at time t;

V_o - The initial volume;

ρ_R - The density of the resin;

$M(t)$ - The moisture content at time t; and,

$\overline{V}_{H_2O}$ - The specific volume of water.

For an anisotropic cube of resin, it is possible to compute the dilatational strain using the following argument:

$$e_1 + e_2 + e_3 = \frac{\Delta V(t)}{V_o} \tag{9}$$

$$e_1 = e_2 = e_3 = \frac{1}{3}\frac{\Delta V(t)}{V_o}$$

$\therefore$

$$e = \frac{1}{3}\rho_R M(t)\overline{V}_{H_2O} \tag{10}$$

where:

e - The resin dilatational strain;

ρ_R - The density of the resin, $\sim$1.25 gm/cm^3 (for epoxies);

$M(t)$ - The moisture content at time t; and,

$\overline{V}_{H_2O}$ - The specific volume of water, $\sim$1.00 cm^3/gm.

Figure 10 illustrates the computed values of the resin dilatational strain plotted with experimental data for a series of epoxy-novalic resins (Ref 5). Initially the moisture is not homogeneously distributed throughout the resin laminate, as in Figure 8, and the resin dilatational strain is larger than that predicted from equation 10. As the equilibrium moisture content is approached and the moisture distribution becomes homogeneous, equation 10 gives excellent results. Moisture gradients, as in Figure 8, and the corresponding nonhomogeneous swelling of the resin could lead to the formation of microcracks and delaminations.

In addition to this phenomenon, the swelling of the resin by water leads to a volumetric dilatation of the resin which results in a softening of the resin. Classically as any polymer is heated it undergoes a characteristic rate of thermal expansion. Across a 10-15°F range, this rate of thermal expansion changes dramatically and approaches the rate of thermal expansion of a liquid. The temperature at which this break in the rate of thermal expansion occurs is known as the glass transition temperature and it is the point at which a hard rigid polymer turns into a soft rubbery polymer. If

a diluent, such as water, is added to a polymer, the glass transition temperature of the polymer will be reduced (Figure 11). Kelley and Buecke (Ref 6) have examined this phenomena and application of equation 11 enables the prediction of the glass transition temperature with moisture absorption:

$$T_g = \frac{\alpha_R T_{gR} + \alpha_D T_{gD} V_D}{\alpha_R V_R + \alpha_D V_D} \qquad (11)$$

where:

V_R - The volume fraction of the resin;

V_D - The volume fraction of the diluent;

T_{gR} - The glass transition temperature of the resin;

T_{gD} - The glass transition temperature of the diluent;

α_R - The differential coefficient of thermal expansion of the resin; and,

α_D - The differential coefficient of thermal expansion of the diluent.

Assuming a homogeneous moisture distribution in the resin matrix, it is possible to compute the suppressed glass transition temperature of an epoxy resin absorbing water. Using the following relationship:

$$V_R = \frac{1}{1 + \rho_R M_R \bar{V}_{H_2O}}$$

where:

ρ_R - The density of the resin, $\sim$1.25 gm/cm^3;

M_R - The moisture content of the resin;

$\bar{V}_{H_2O}$ - The specific volume of water, $\sim$1.00 cm^3/gm;

thus,

$$V_R = \frac{1}{1 + 1.25\, M_R} \text{ ; and}$$

$V_D = 1 - V_R$;

$T_{gR} = 216^{o}C$;

$T_{gD} = 3.98^{o}C$;

$\alpha_R = 3.75 \times 10^{-4}/^{o}C$ (Ref 7); and,

$\alpha_D = 3.839 \times 10^{-3}/^{o}C$.

the glass transition temperature as a function of the moisture content is plotted in Figure 12 along with experimental data. The glass transition temperature of water was taken to be that temperature at which water goes through its densest state. This is in analogy with the classical definition of glass transition temperature for polymers.

The relationship between modulus and temperature for both a wet and dry laminate is illustrated in Figure 13. For room temperature the difference between the modulus for wet and dry laminates is very small. However, at elevated temperatures the difference between the modulus for wet and for dry laminates becomes significant. The actual loss in properties of the epoxy resin depends not only on the moisture content but to some extent on the distribution of moisture in the resin. When the water is desorbed, the bulk resin returns to initial dry property level.

A unidirectional laminate saturated with water and loaded in tension while at elevated temperature would show only a slight loss in tensile strength over a dry laminate. This would be expected since the fibers dominate the composite tensile strength. However, if the loading is reversed and compression strength is measured, then the situation is entirely different. In compression the resin matrix serves as the "glue" holding the fibers together and not allowing them to buckle under load. Thus any phenomenon that would reduce the strength of the matrix would have a direct effect on the compression strength of a unidirectional laminate. Figures 14 and 15 illustrate this phenomenon and its relationship with the wet and dry glass transition temperature of the resin matrix. Figure 16 indicates that the relationship between the matrix shear stiffness and the composite shear stiffness is also affected by moisture absorption.

Up to this point this presentation has centered on the loss of mechanical properties due to a change in bulk resin properties. However, the interfacial region of advanced composites also plays a significant role in the environmental stability of composite structures. The basic assumption in strength analysis of composites is good fiber-matrix bonding. To date, there is no conclusive theory regarding the chemical and physical

nature of these interfaces (Ref 8). Kaelble and his coworkers (Refs 9 and 10) have developed an ingenious thermodynamical method of analyzing and predicting the water sensitivity of the fiber-matrix interface. Their results indicate that moisture degradation of interfaces in graphite-epoxy composites is essentially irreversible.

REFERENCES

1. Crank, J.: The Mathematics of Diffusion. Clarendon Press, Oxford, 1956.

2. McKague, E.L., Reynolds, J.D., and Halkias, J.E.: Life Assurance of Composite Structures. vol 1, AFML-TR-75-51, 1975.

3. Van Amerongen, G.J.: Diffusion in Elastomers. Rubb. Chem. Technol., vol 37, p1065, 1964.

4. Carpenter, J.F.: Moisture Sensitivity of Epoxy Composites and Structural Adhesives. MDC Report A2640, December 1973.

5. Hertz, J.: Investigation into the High-Temperature Strength Degradation of Fiber-Reinforced Resin Composite During Ambient Aging. NAS8-27435, 1973.

6. Kelley, F.N., and Bueche, F.: Viscosity and Glass Temperature Relations for Polymer-Diluent Systems. J. Poly. Scien., vol 1, p549, 1961.

7. Jones, W.B., Kaelble, D.H., and Knauss, W.G.: Investigation of Fatigue and Crack Propagation Behavior of Adhesives. Part I, AFML-TR-72-218, 1972.

8. Ishai, O.: Environmental Effects on Deformation, Strength, and Degradation of Unidirectional Glass Fiber Reinforced Plastics, I Survey. Poly. Eng. and Scien., vol 15, #7, 1975.

9. Kaelble, D.H., Dynes, P.J., Crane, L.W., and Maus, L.: Interfacial Mechanisms of Moisture Degradation in Graphite-Epoxy Composites. J. Adhesion, vol 7, p25, 1974.

10. Kaelble, D.H., Dynes, J. and Cirlin, E.H.: Interfacial Bonding and Environmental Stability of Polymer Matrix Composites. J. Adhesion, vol 6, p23, 1974.

TABLE 1

DURABILITY WORKSHOP

MATERIALS AND PROCESSING PANEL

CONCLUSIONS

1. All epoxy resin systems are essentially equally susceptible to water absorption.

2. There is a reasonable model which can be used to predict the rate and extent of water absorption.

3. Water absorption does not appear to produce irreversible chemical changes.

4. Water absorption does produce reversible polymer plasticization.

5. The moisture induced reduction in resin glass transition temperature is the mechanism for the mechanical property changes associated with moisture and temperature.

6. There is little optimism that practical water barrier coatings can be applied to real composite structures.

TABLE 2

DURABILITY WORKSHOP

MATERIALS AND PROCESSING PANEL

RECOMMENDATIONS

1. The mechanical effects resulting from cyclic exposure of temperature, moisture gradients, and stress to composite laminates should be studied.

2. A simple field applicable NDI method for measuring water content of composite laminates should be developed.

3. The effect of processing variables on the durability of composite laminates should be systematically studied.

4. The validity of the water diffusion model and applicability of Fick's law should be reexamined.

5. Resin systems with low water absorption should be developed and/or characterized.

6. Test methods and data to assess the effects of environmental degradation of composites must be developed and standardized.

7. Chemical Q/C procedures should be developed and applied to composite prepreg resin and adhesive formulations to assure product consistency and long term performance.

TABLE 3

MATERIAL PARAMETERS

MATERIAL	D_o (cm^2/sec)	E_d (cal/mole)	A
BR/5505			
ABSORPTION	2.52×10^{-4}	7,839	.0194
DESORPTION	6.82×10^{-2}	10,541	
T300/5208			
ABSORPTION	3.49×10^{-4}	7,525	.0146
DESORPTION*	1.248×10^{-1}	11,147	
AS/3501-5			
ABSORPTION*	1.464×10^{3}	17,681	.0191
DESORPTION*	1.132×10^{-1}	11,545	

*BASED ON LIMITED DATA

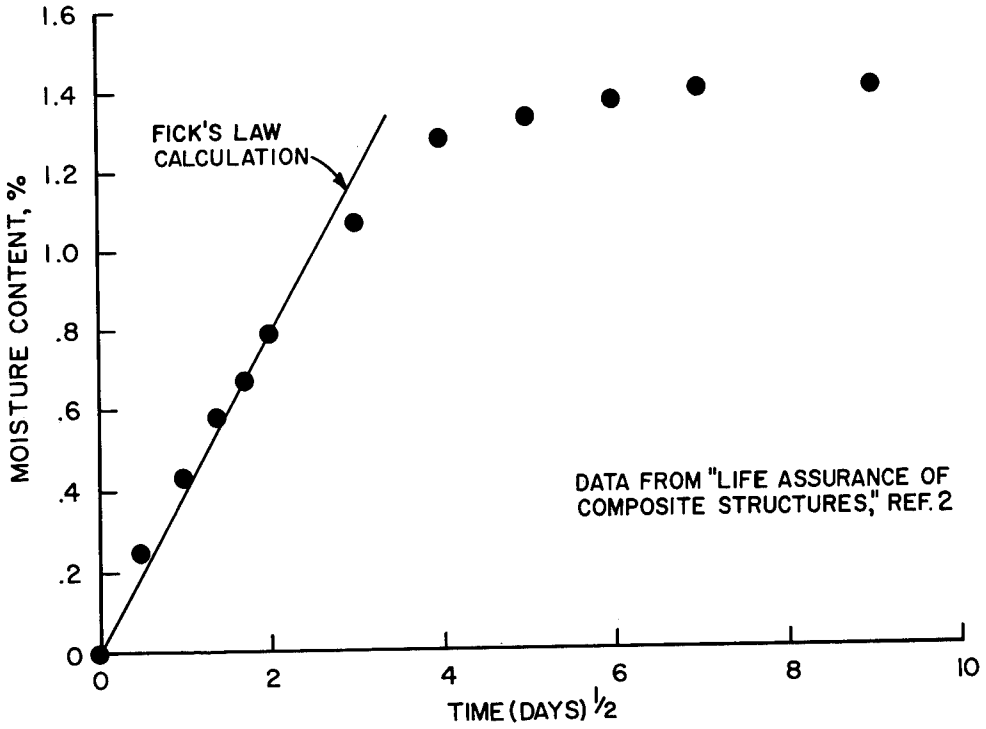

Figure 1.- Absorption behavior of epoxy composites (T300/5208-4 ply laminate at 75°F and 97% RH).

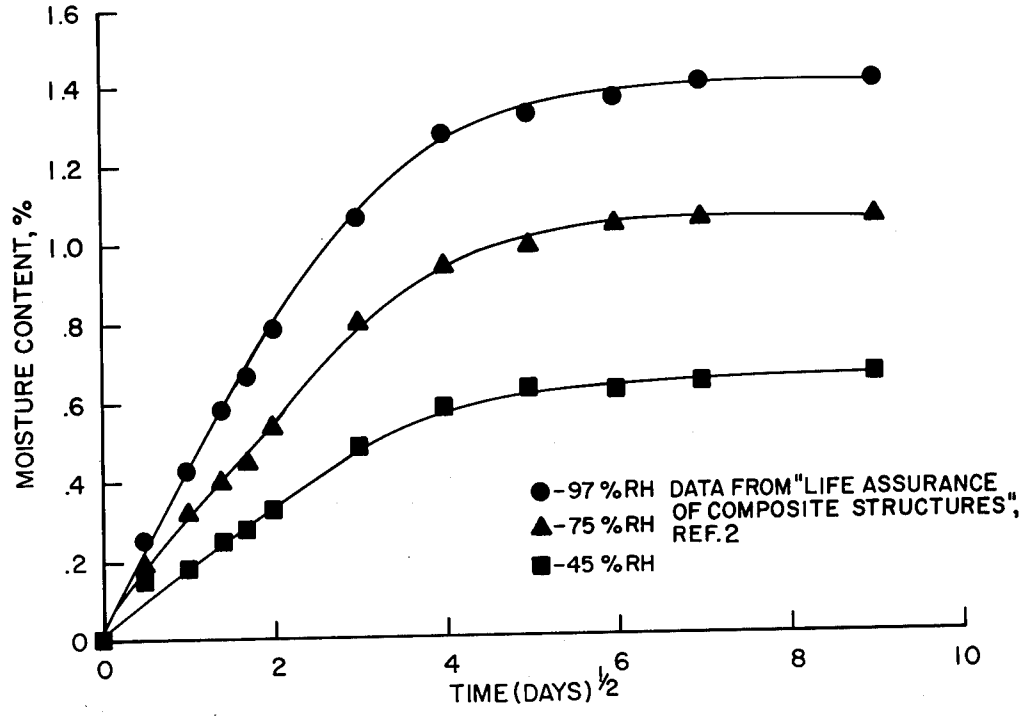

Figure 2.- Equilibrium saturation varies with humidity (T300/5208-4 ply laminate at 75°F).

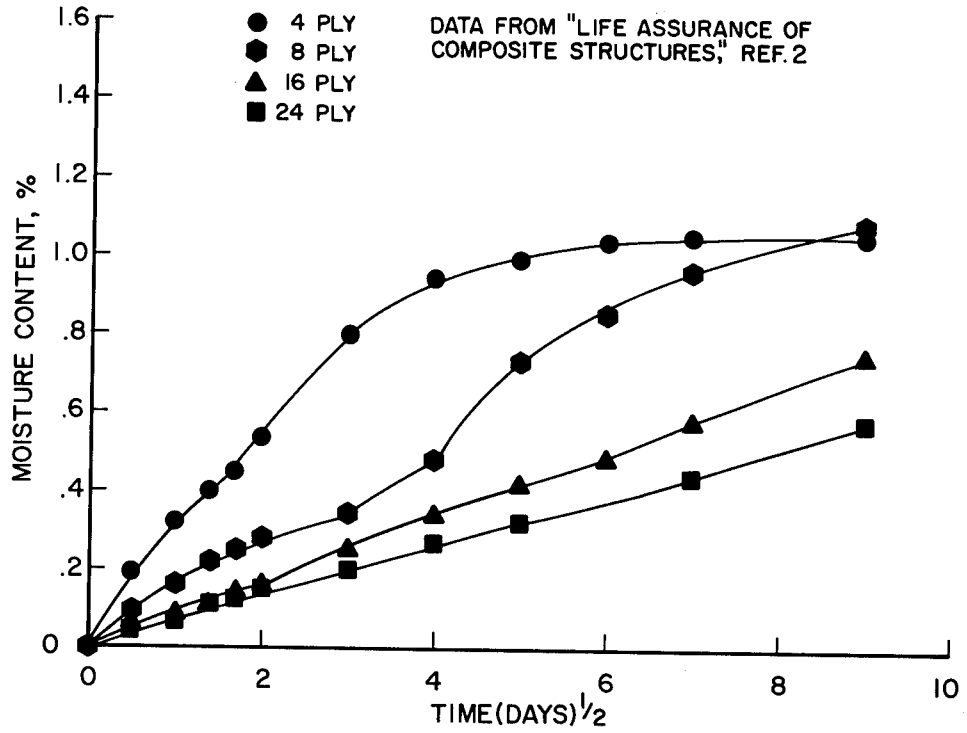

Figure 3.- Moisture absorption varies with thickness (T300/5208-75°F and 75% RH).

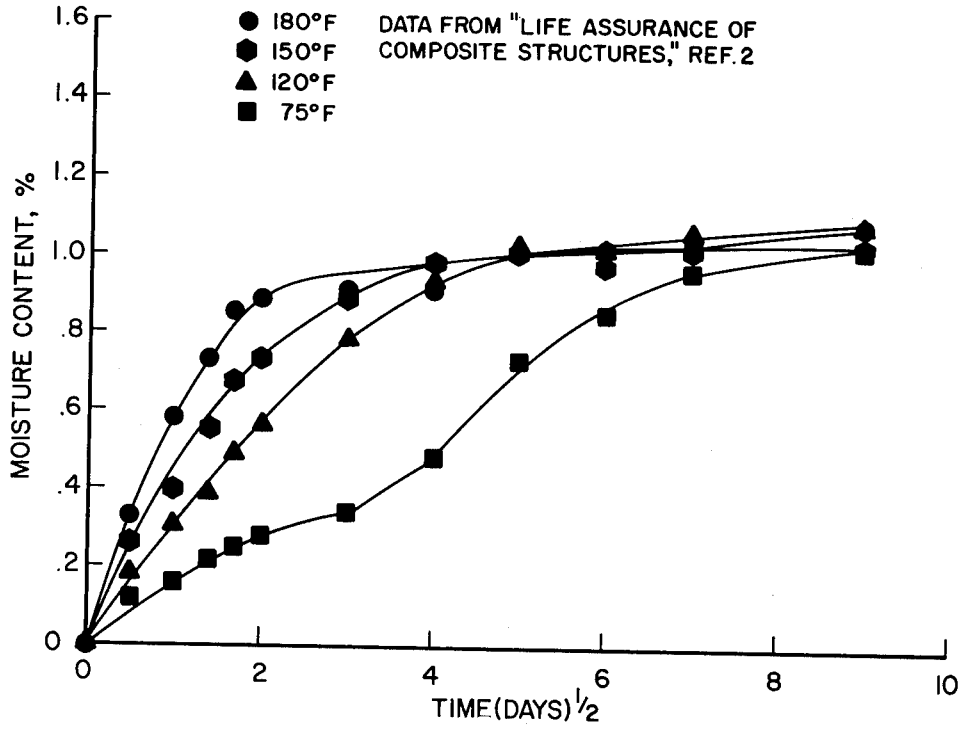

Figure 4.- Temperature accelerates the approach to saturation (T300/5208-8 ply laminate at 95% RH).

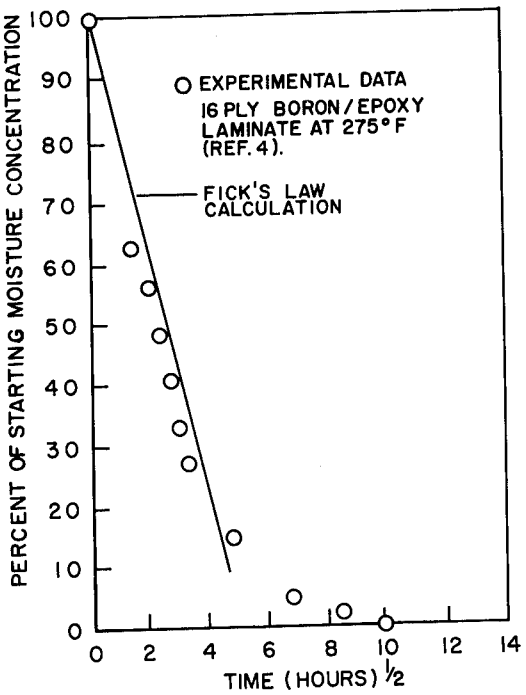

Figure 5.- Moisture absorption is insensitive to the degree of cure for well cured composites.

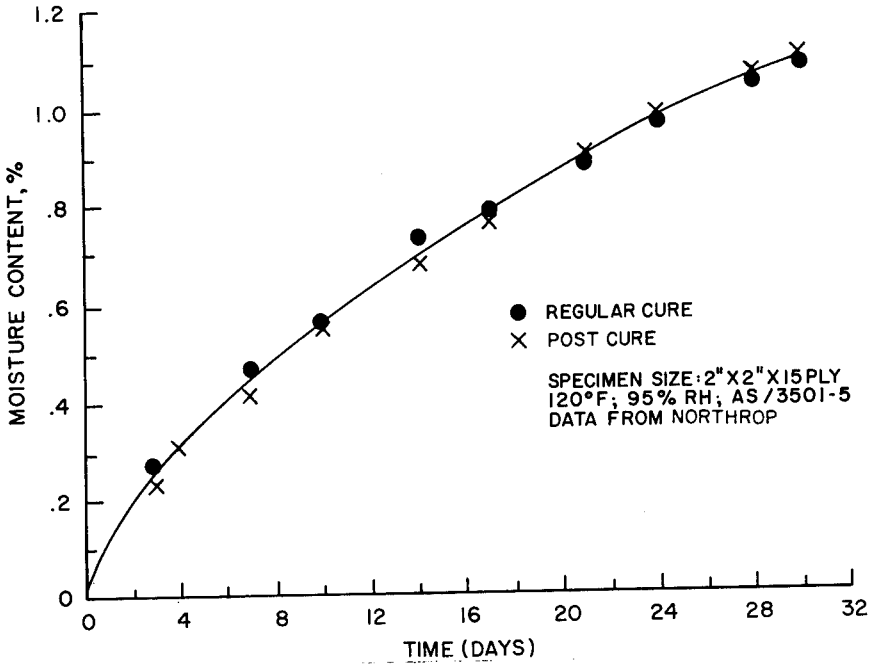

Figure 6.- Desorption behavior of epoxy composites.

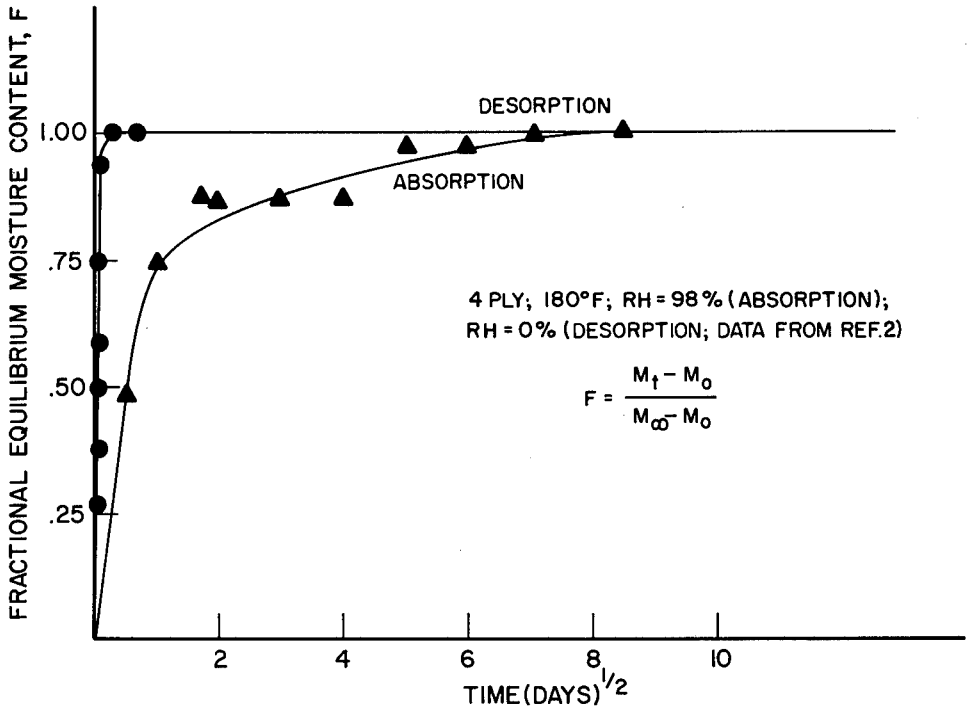

Figure 7.- Absorption and desorption as a function of the square root of time.

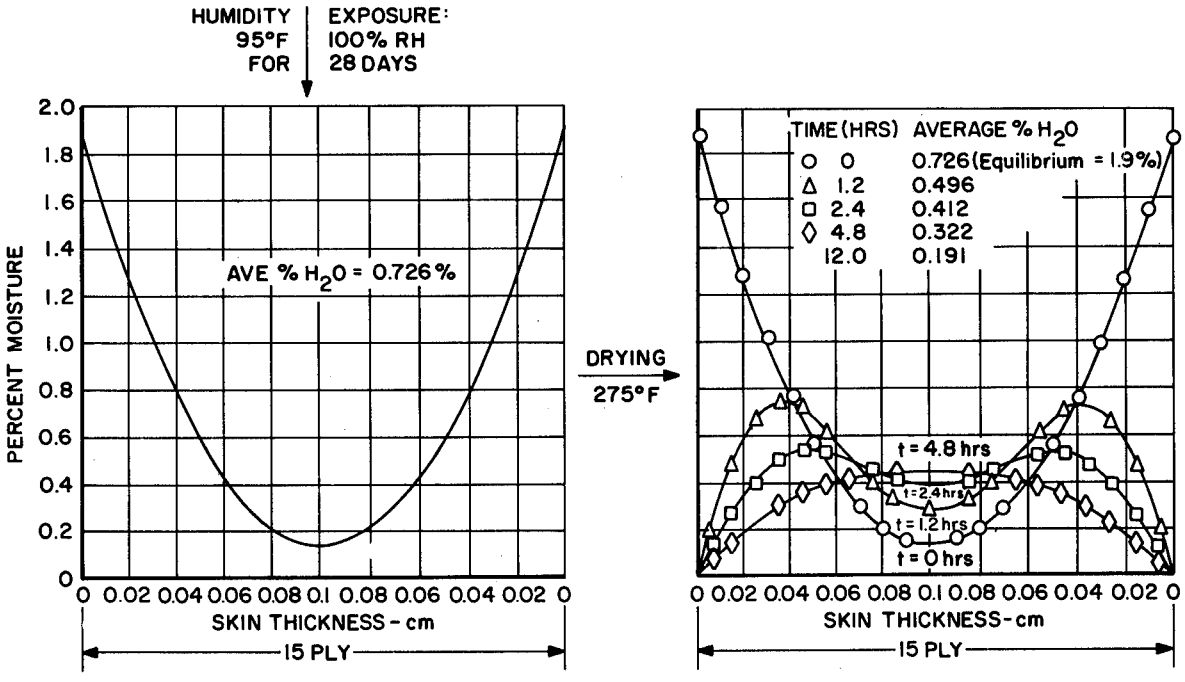

Figure 8.- Moisture profile for boron/epoxy laminate, 15 ply, dried at 275°F (starting moisture: 0.726% H_2O or 38% of saturation).

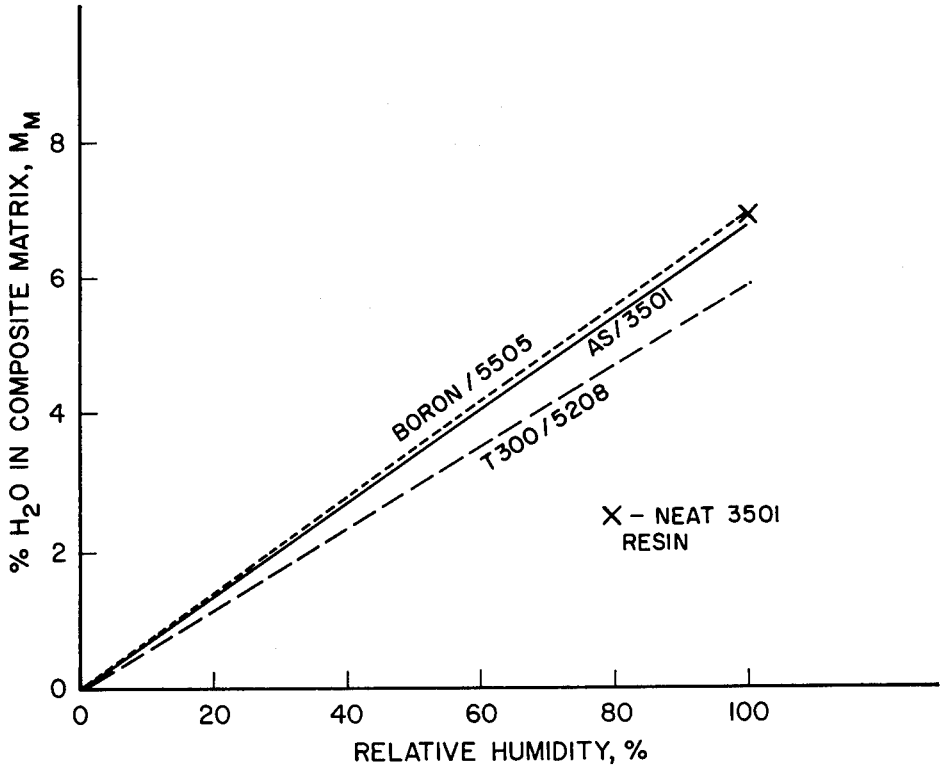

Figure 9.- Moisture content in the matrix normalized from the moisture content in the composite.

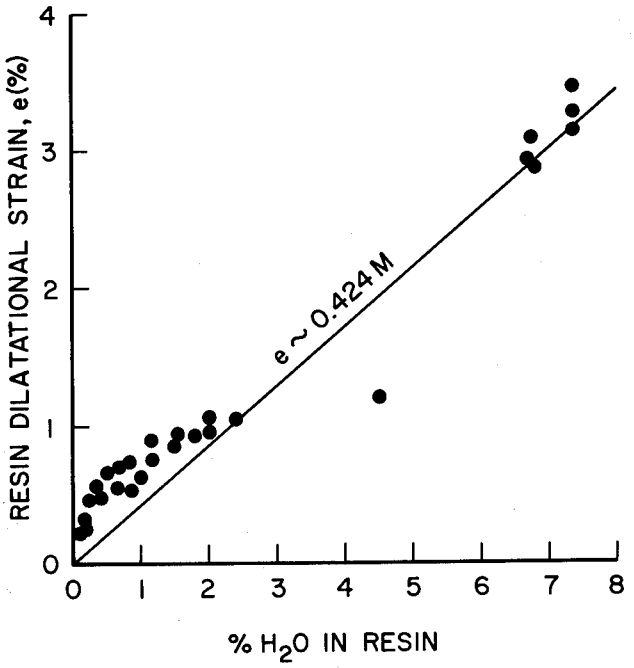

Figure 10.- Swelling behavior for epoxy - novalic systems.

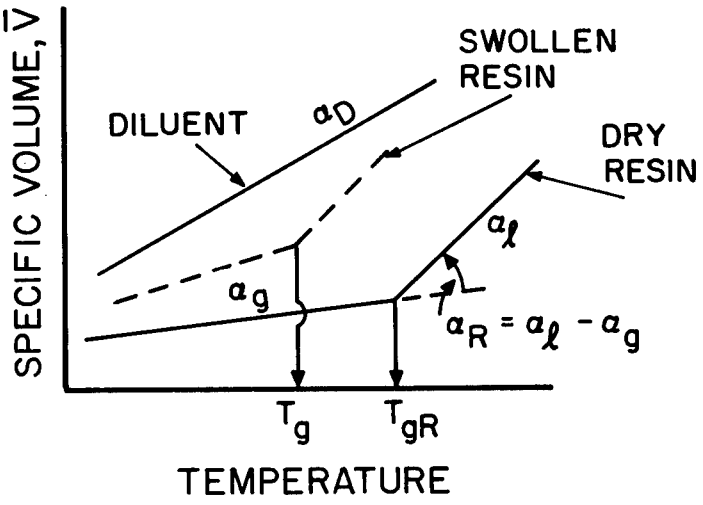

Figure 11.- Moisture plasticizes resins.

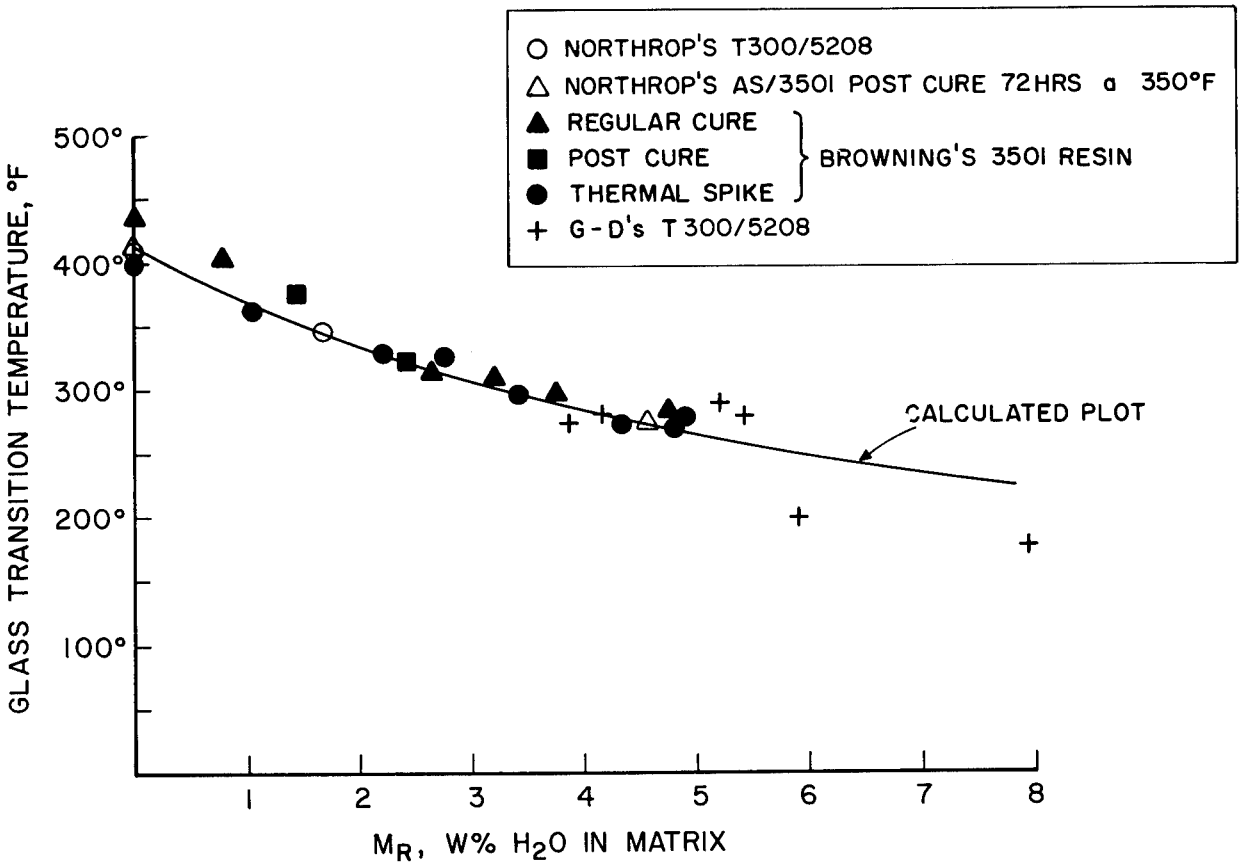

Figure 12.- Plasticization of epoxy resins and composites by water.

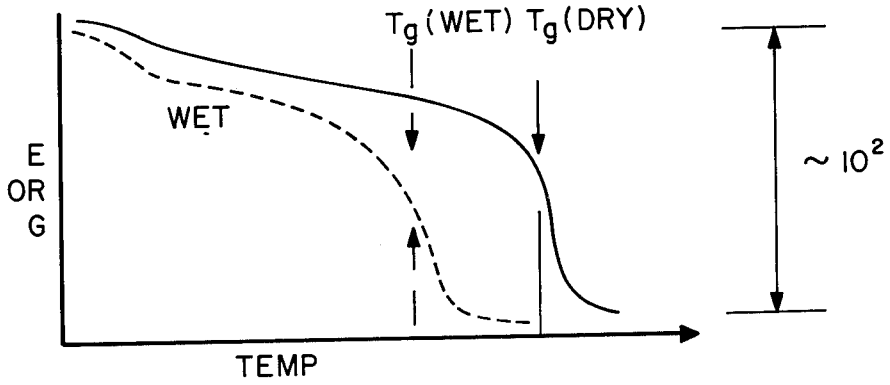

Figure 13.- Moisture effects in bulk resin.

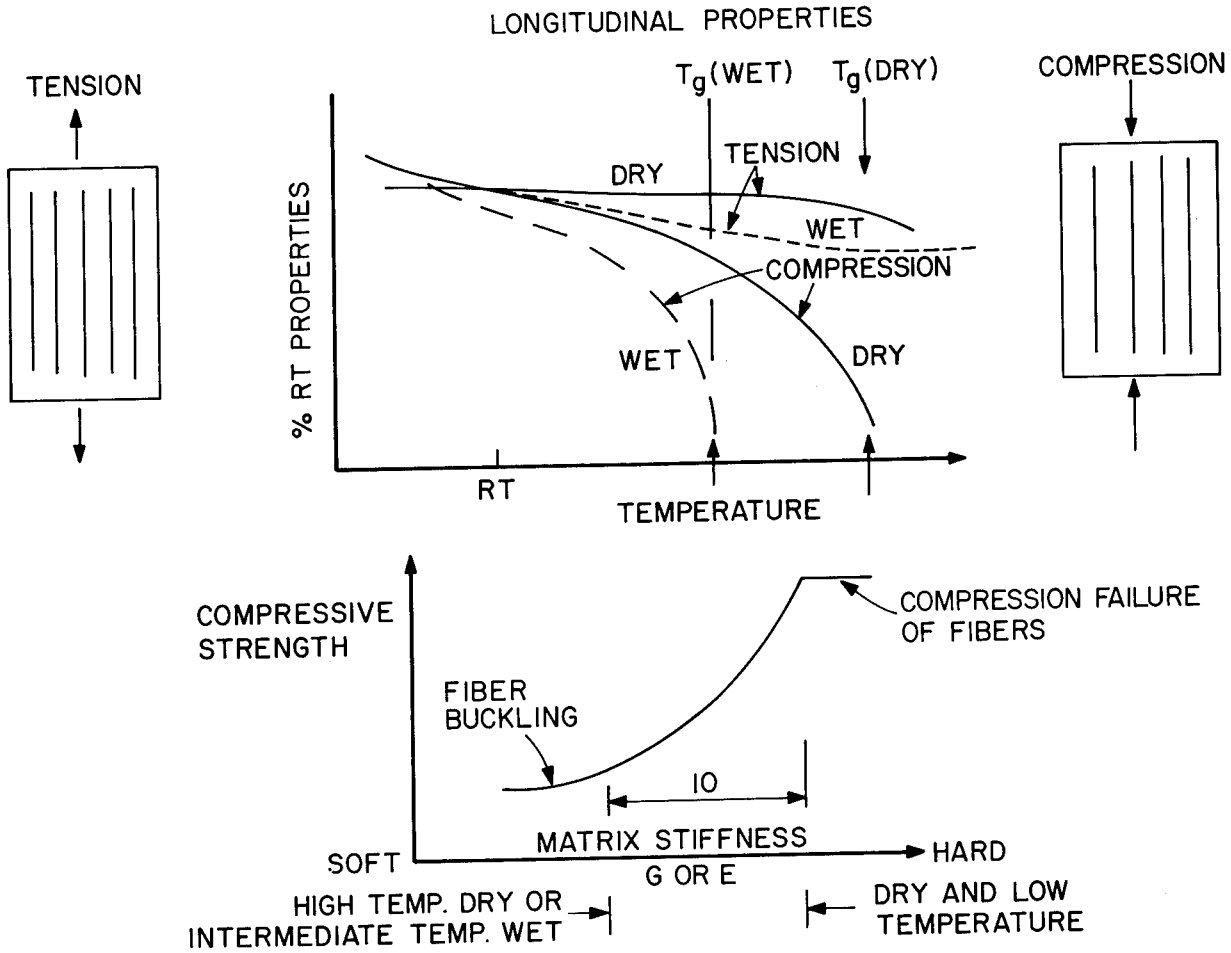

Figure 14.- Absorbed water effects matrix sensitive composite properties.

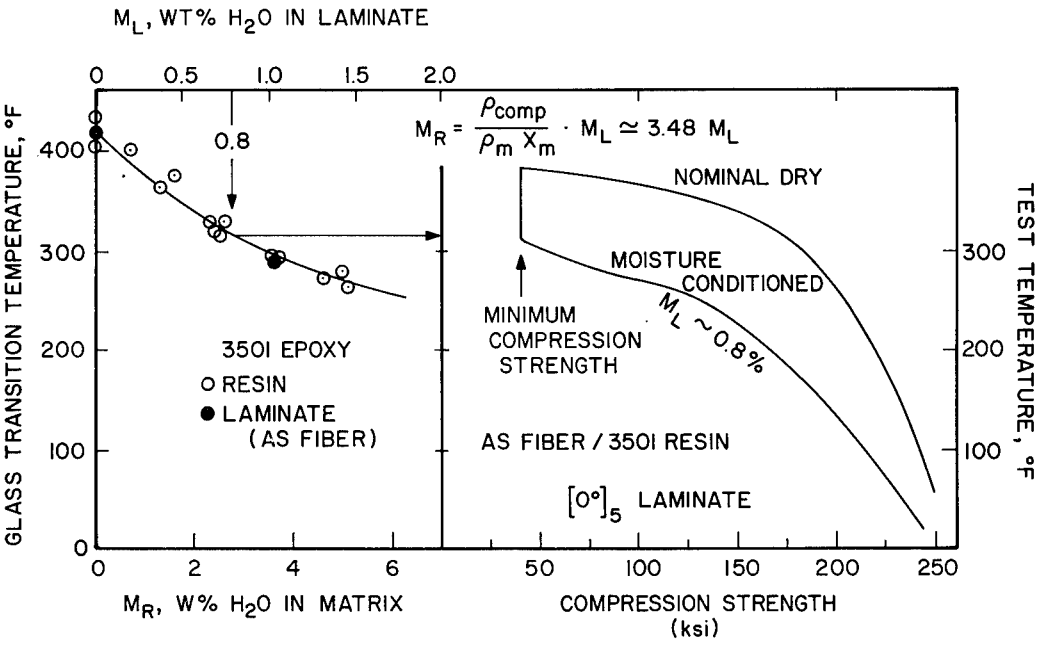

Figure 15.- A mechanical consequence of matrix softening.

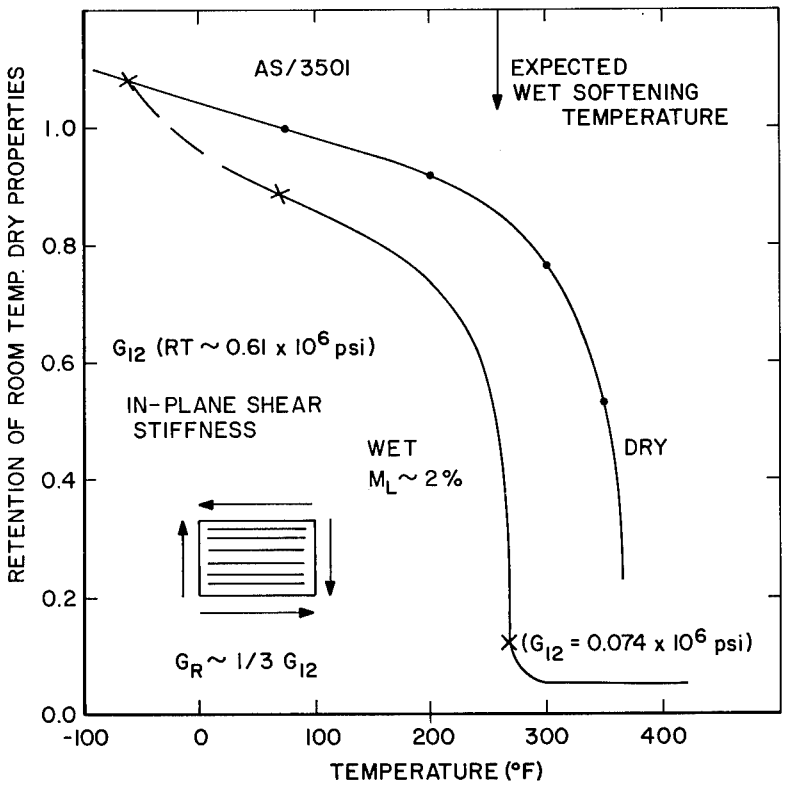

Figure 16.- Matrix shear stiffness dominates composite shear stiffness.

FLIGHT SERVICE EVALUATION OF KEVLAR-49/EPOXY COMPOSITE PANELS IN WIDE-BODIED COMMERCIAL TRANSPORT AIRCRAFT

By Robert H. Stone
Lockheed-California Co.

and H. Benson Dexter
NASA Langley Research Center

SUMMARY

Kevlar-49 fairing panels were installed on three production L-1011s in early 1973 for five years flight service evaluation. These panels include sandwich and solid laminate wing-body fairings and a 300°F service aft engine fairing. Participating airlines are Eastern, Air Canada, and TWA. The Kevlar-49 was directly substituted for fiberglass with no tooling or production changes required, except for machining. Two annual flight service inspections have been conducted. After 6000 hours service no major damage or defects have been noted requiring corrective action by airline Maintenance. Minor impact damage, delamination, and fastener hole fraying and elongation have been observed.

INTRODUCTION

The Kevlar-49 flight service program is being performed by Lockheed-California Co. under contract to NASA Langley to evaluate the environmental and flight service capabilities of Kevlar-49 compared to baseline fiberglass parts. Three fiberglass fairings on the L-1011 were selected for the program. (Figure 1). These parts include:

1) A large (60 x 67 inch approximately) sandwich wing-body fairing panel with Nomex core and a .020 inch exterior Kevlar-49 skin (1 ply 181 fabric, 2 plies 120 fabric) and a .015 inch interior Kevlar-49 skin (3 plies 120 fabric). (Figure 2)

2) A small (9 x 33 inch approximately) solid laminate wing-body fillet panel. This part averages .090 inch thickness with 9 plies 181 fabric. (Figure 3).

3) An aft engine sandwich fairing (30 x 72 inch approximately) with Nomex core and .020 inch Kevlar-49 skins (1 ply 181 fabric, 2 plies 120 fabric). (Figure 4).

A left hand and right hand set of each of the three parts were installed on each of three L-1011s for a total of 18 parts. The L-1011s include one each for Eastern, Air Canada, and TWA to provide a variety of flight service environments.

INITIAL DEVELOPMENT AND FABRICATION

The fairing panels selected for the program were all fiberglass production components in which Kevlar-49 fabric was substituted for the fiberglass on a ply-for-ply basis using the same epoxy resin as the production parts. For the wing-body fairings and fillets, a 250°F curing, 160°F service epoxy (Hexcel's F-155) was used; for the aft engine fairings, a 350°F curing, 300°F service epoxy (Hexcel's F-161) was used. The Kevlar-49 fabrics used were identical in thickness per ply and comparable in weave style to the fiberglass fabrics being replaced, and are identified by the same designations (181 and 120). Kevlar-49 fiber density is 43% less than fiberglass, and the Kevlar-49 fabrics were designed to provide the same proportional reduction in weight compared to the equivalent fiberglass fabrics. This weight savings translates into a predicted 30-35% weight savings on solid laminate parts, and 18-28% on sandwich parts depending on core type and thickness.

The Kevlar-49 fairings were fabricated by Heath-Tecna Corp., subcontractors for the production fiberglass fairings. Standard production tooling and production procedures for lay-up, cure, finishing, and co-cure of flame spray and moisture barrier film, were used on the Kevlar-49 parts. The only modifications required were pre-preg trimming, where fewer plies could be trimmed at one time; and ply indexing which was more difficult than with the transparent fiberglass. Machining of the cured Kevlar-49 required an extensive development task; and special tools were developed for trimming, drilling, and countersinking. These tools were all designed to operate either in a shearing action, or in a manner so that the Kevlar-49 fibers are drawn downward or inward as they are cut. These procedures and tools are described in detail in Ref. 1.

The structural capability of Kevlar-49 for the fairing applications was demonstrated by a structural proof test of the wing-body fairing. A full scale fairing was subjected to internal and external pressurization representing design ultimate aerodynamic loads. (1.2 psi and 2.4 psi respectively). The part exceeded design requirements under both test conditions, and was taken to failure under external pressurization.

The average weight savings achieved by substitution of Kevlar-49 for fiberglass on three ship sets was 26%. Kevlar-49 material costs were, of course, significantly higher than fiberglass. The added costs were significantly greater for the aft engine fairings because of the much higher scrap rate associated with the part's irregular shape. Production costs were 15% higher for the Kevlar-49 fairings, principally because of the special machining procedures required. These added costs, while significant, were considered justifiable for the weight savings achieved, except on the aft engine parts. Since these parts were fabricated, Kevlar-49 fiber and fabric costs have been reduced; and the lower cost heavy denier Kevlar-49 fabrics, which incorporate larger yarn bundles into the fabric, have been developed. A prototype wing-body fairing, which incorporates the lower cost but equivalent 281 fabric in place of 181 fabric, has been fabricated and proof tested under a separate Lockheed program.

FLIGHT SERVICE EVALUATION

The Kevlar-49 fairings have experienced nearly 15,000 flight hours of service since their installation in early 1973. As of October 1975, the Eastern panels have 7104 flight hours; and the Air Canada panels have 5420 flight hours. The TWA panels were removed from the aircraft due to special circumstances in April 1974, after one years' service and 2408 flight hours.

The flight service evaluation activities in this program consist of annual inspections which are normally scheduled during major maintenance checks of the aircraft at the airlines' maintenance bases. The first annual inspection of the Eastern panels was conducted by Eastern Maintenance personnel at Miami in early 1974. The panels had experienced 3539 flight hours at that time. Eastern reported no major damage or defects, or any condition differing significantly from comparable fiberglass parts.

The remainder of the inspections have taken place with the participation of Lockheed Engineering. In April 1974, after one year's service, the Air Canada panels were inspected at Lockheed's Burbank facility during aircraft modification. The TWA panels were also inspected at Burbank in April 1974 after their removal from the aircraft. Results of these inspections are

given in Ref. 2. The Eastern and Air Canada panels were inspected in April and May of 1975 after two years' service, at the airline maintenance bases in Miami and Montreal respectively, with a Lockheed Engineering representative present. Results of these two inspections are given in Ref. 3.

The Air Canada panels inspected at Lockheed in 1974 had accumulated 2360 flight hours at that time. No major defects or damage was noted. A crack, approximately 1 1/4" long was observed on the exterior surface of the left-hand wing-body fairing (Figure 5). This part was removed for more thorough inspection. There was no evidence of delaminations, and a weight check showed no significant weight gain after one years' service. Some fasteners were removed from the wing-body fillet panels for inspection of hole conditions, and no evidence of hole deformation was noted. The right-hand aft engine fairing had poor paint adhesion and was removed and repainted. The absence of this problem on any of the other Kevlar-49 parts indicates the problem was not associated with the Kevlar-49. The right-hand aft engine fairing also had fiberglass repair patches on two of the corners. No records of this repair could be obtained from Lockheed or Air Canada records.

The TWA panels, when removed and returned to Lockheed, had 2404 flight hours. No major defects or damage was noted. A very small crack was observed on the right-hand wing-body fairing exterior. Several elongated holes were noted on the right-hand wing-body fillet (Figure 6). This is a condition typically noted on fiberglass parts. The absence of hole elongation on the left-hand part indicates this condition may be related to poor indexing of the part holes to the aircraft hole pattern, and the part may have been forced into place to some extent. The right-hand aft engine fairing had a slight delamination of the outer ply along one edge (Figure 7). A small amount of sealing compound adhered to the part at that location indicating that the delamination was caused by adhesion of the sealant during part removal. The occurrence of this with the 350°F curing Kevlar-49/epoxy is significant. The higher temperature systems generally provide poorer skin-core adhesion than the 250°F curing epoxy as even though a supplementary co-curing adhesive film was used with the 350°F curing system.

The second annual inspection of Eastern panels, performed at Miami in April 1974, provided a more thorough inspection of these panels, with the three left-hand parts removed for inspection of the inner surface and fastener holes. The parts had accumulated 6061 flight hours at that time. As in the previous years' inspection, no major damage or defects were noted which required corrective action in the opinion of Eastern Maintenance personnel. The exterior skin of the left-hand wing-body fairing had been given a temporary repair consisting of an aluminum speed tape patch about 1 1/4 inch by 1 3/4 inch covered with a conductive metal filled coating. (Figure 8). The

cause of the damage could not be determined, and Eastern had no record of when or where the repair was made. A void, about 1/2 inch diameter, was noted on the inner skin with a 6 inch long delaminated strip extending from the void. Slight fraying of the Kevlar-49 fibers was noted around the fastener holes, and a slight convex deformation were noted along the line of fasteners on the lower edge of the inner skin. The fraying of fastener holes occurred to a greater extent on the left-hand aft engine fairing. (Figure 9), with most of the holes having this condition. Some of the holes were surrounded by a slight delaminated area, 1/4 inch diameter maximum. This fraying is the only condition noted which is not typical of fiberglass parts, and is related to the non-brittle characteristics of the Kevlar-49 fiber. No other damage was noted on the three left-hand panels, but considerable grime and oily residue was noted on both interior and exterior surfaces. (Figures 10 and 11). The oily residue was determined not to be hydraulic oil, but the wing-body parts are located adjacent to hydraulic lines so this is a potential problem. The right-hand wing-body fairing was inspected in-place and two small cracks, 5/16 and 1/8 inch long were noted. This part is particularly prone to impact damage because of its proximity to galley and cargo loading areas.

The second inspection of the Air Canada panels at Montreal in May 1975 provided an opportunity for comparison of the previous years' results. The parts had 4324 flight hours at the time of inspection. The crack noted the previous year on the left-hand wing-body fairing exterior was observed again (Figure 12), and had not propagated. The crack had not been repaired in the intervening year which illustrates the opinion of airline Maintenance that these are minor defects not requiring corrective action. A smaller crack, 1/4 inch long, was also noted on the panel exterior. The right-hand wing-body fillet was noted to have a slight outward bulge along the lower edge, and some of the fasteners were severely bent out of line. This part was removed for further inspection, and several fastener holes were noted to be significantly elongated. As discussed above, this condition appears related to panel, installation procedures. The only other damage noted was a small crack 1/4 inch long on the right-hand wing-body fairing exterior. The appearance of the Air Canada panels was similar to the Eastern panels with an oily residue noted, which was not hydraulic fluid.

RE-INSTALLATION OF TWA FAIRINGS

The TWA panels, as previously mentioned,were removed from service in April 1974. The parts were re-installed on a second TWA aircraft in Feb. 1975 for continuation of flight service evaluation. This re-installation, which is reported in Ref. 3, required considerable re-work. The crack and delaminated area previously described were repaired using standard fiberglass repair procedures and materials. The greatest amount of rewofk was re-

quired for re-location of fastener holes to fit the aircraft hole pattern. The four wing-body panels had a total of only six holes requiring relocation. The holes were filled with a glass filled 160°F service epoxy which was cured at 135°F. The new holes were drilled and countersunk using the procedures described in Ref. 1. The aft engine fairings presented a greater problem as all fastener holes had to be relocated. The existing holes were filled with a glass filled 300°F service epoxy which was cured at 335°F. Reinforcing strips of 120 glass fabric, impregnated with the same resin were applied to both surfaces. (Figure 13). The resin was cured for 2 hours at 335°F after a dwell at 180°F. After cure, a skin-core delamination was noted in the inner surfaces of the left-hand panel, and the Tedlar film was disbonded in patches. A wet lay-up fiberglass patch was used to replace the de-bonded Kevlar-49, and the resin was cured at 335°F under a vacuum bag, with longer dwell times at intermediate temperature and more carefully controlled heat-up rates. This prevented further part damage. The Tedlar film was sanded off, and a 10 mil vapor barrier coating was applied (Figure 13). Due to a shop error, the aluminum flame spray was sanded off the left-hand panel. This required re-application of flame spray (Figure 14). Application of flame spray to a cured part results in a more porous appearance and somewhat reduced adhesion than the original flame spray, but this process is acceptable for repair.

After re-work, the Kevlar-49 parts were painted and installed. This activity provided an unexpected opportunity to demonstrate the feasibility of using standard fiberglass repair techniques on Kevlar-49 parts, and the continuing flight service will serve to verify these procedures.

CONCLUSIONS

After two years and up to 6000 hours of flight service, no major defects or damages requiring corrective action by airline Maintenance were found. Minor defects observed include small exterior cracks caused by impact damage, small delaminations and skin-cure disbonds, and fastener hole fraying and elongation apparently related to installation problems. These defects are generally typical of in-service fiberglass part conditions. Repair and rework of Kevlar-49 parts can be successfully accomplished using standard fiberglass repair materials and procedures.

The above factors indicate that Kevlar-49 can provide serviceability and environmental resistance equivalent to fiberglass for up to 6000 hours of service.

REFERENCES

1. Wooley, J. H., et al.: "Flight Service Evaluation of PRD-49/Epoxy Composite Panels in Wide-Bodied Commercial Transport Aircraft - Final Report". NASA CR-112250, March 1973

2. Wooley, J. H., : "Flight Service Evaluation of PRD-49/Epoxy Composite Panels in Wide-Bodied Commercial Transport Aircraft - First Annual Flight Service Report", NASA CR-132647, July 1974

3. Stone, R. H., : "Flight Service Evaluation of Kevlar-49/Epoxy Composite Panels in Wide-Bodied Commercial Transport Aircraft - Second Annual Flight Service Report", NASA CR-132733, October 1975

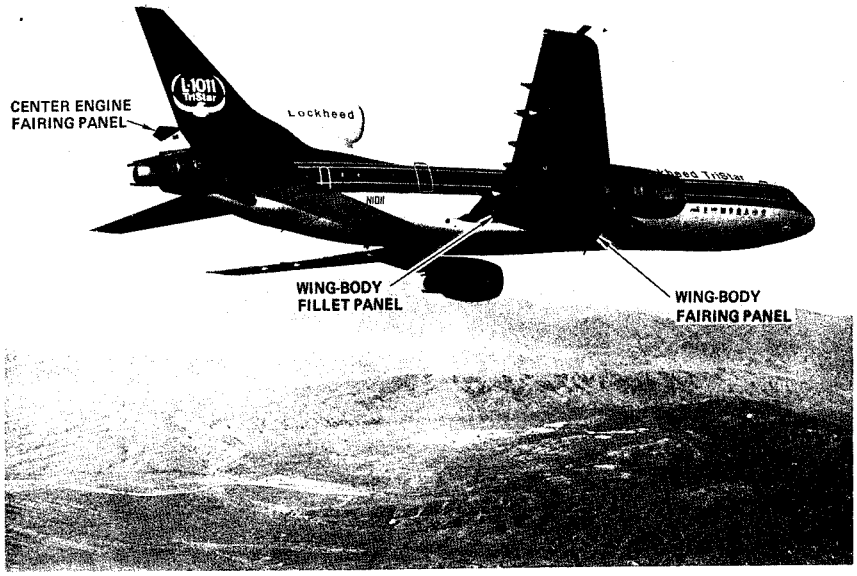

Figure 1 - Lockheed L-1011 with Kevlar-49 Fairings

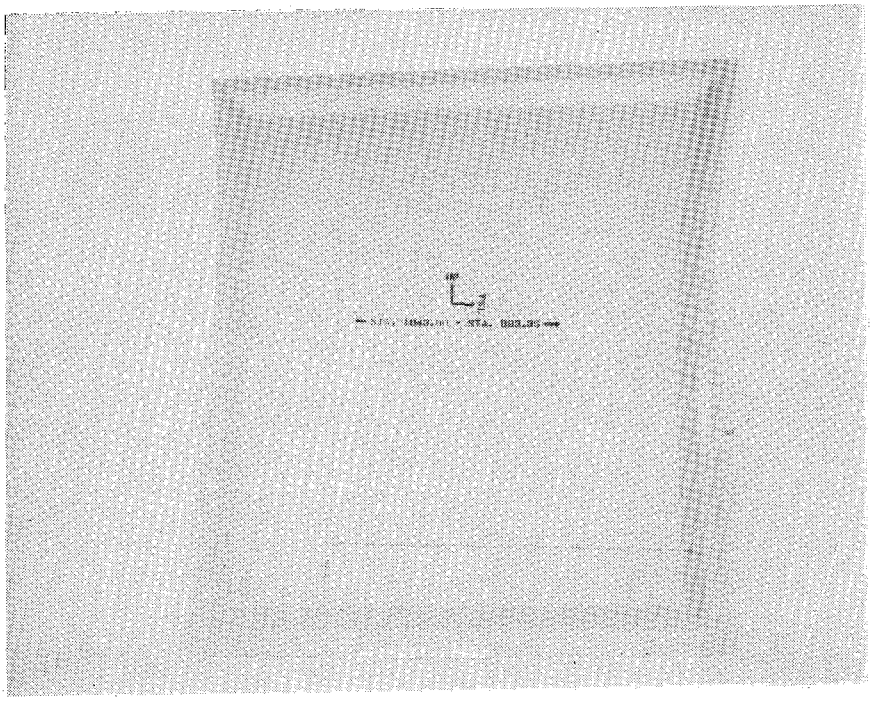

Figure 2 - Kevlar-49 Wing-Body Fairing

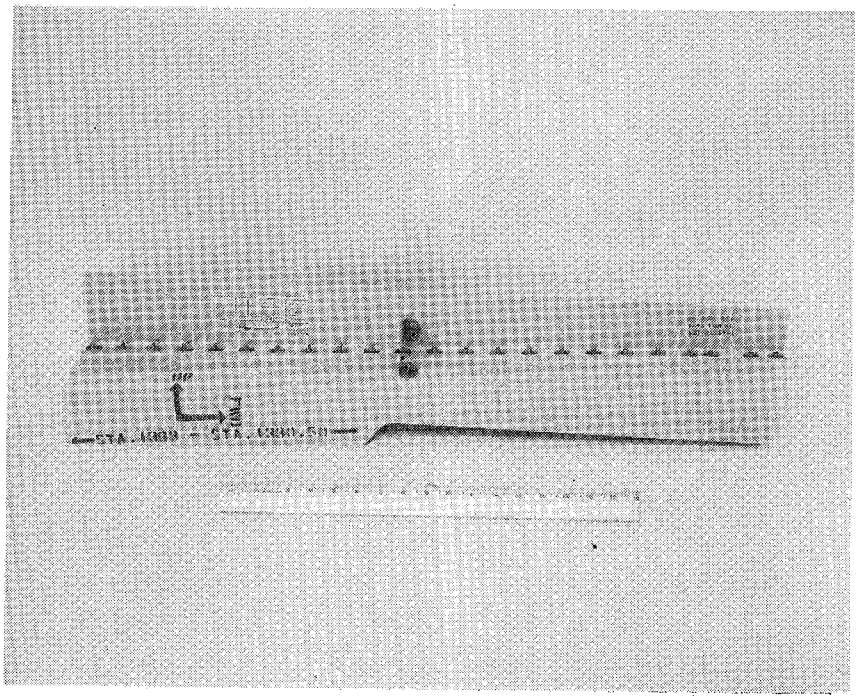

Figure 3 - Kevlar-49 Wing-Body Fillet

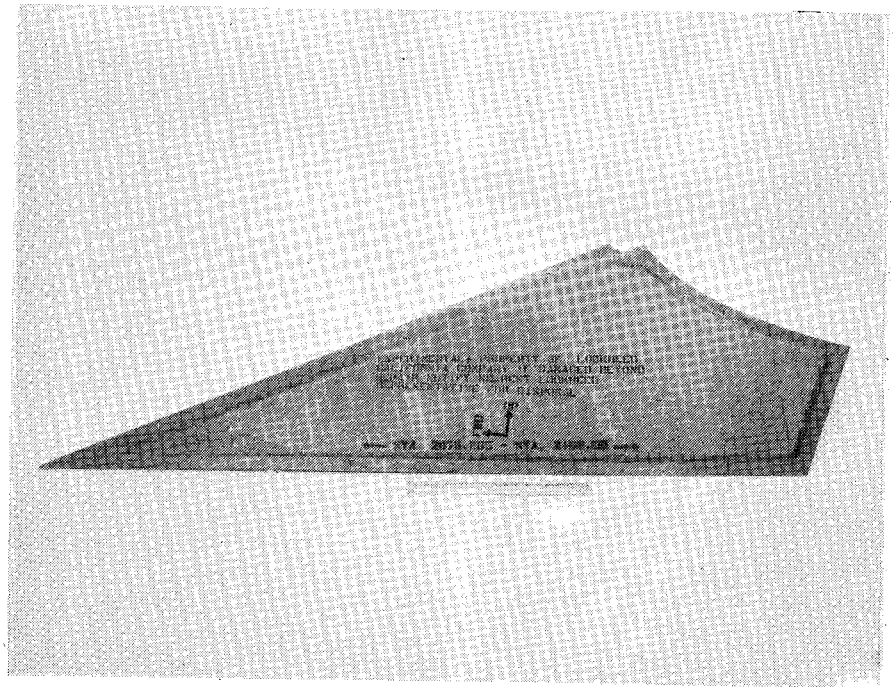

Figure 4 - Kevlar-49 Aft Engine Fairing

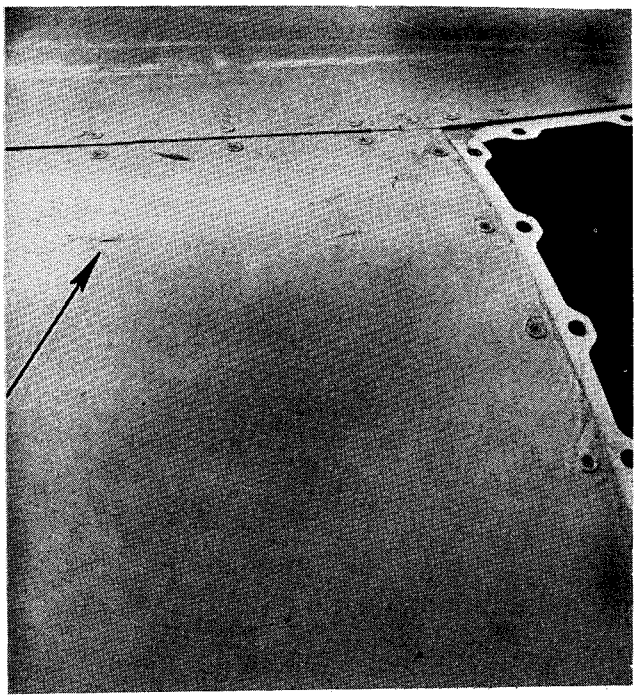

Figure 5 - Crack - Exterior Fairing Surface 1974 Inspection

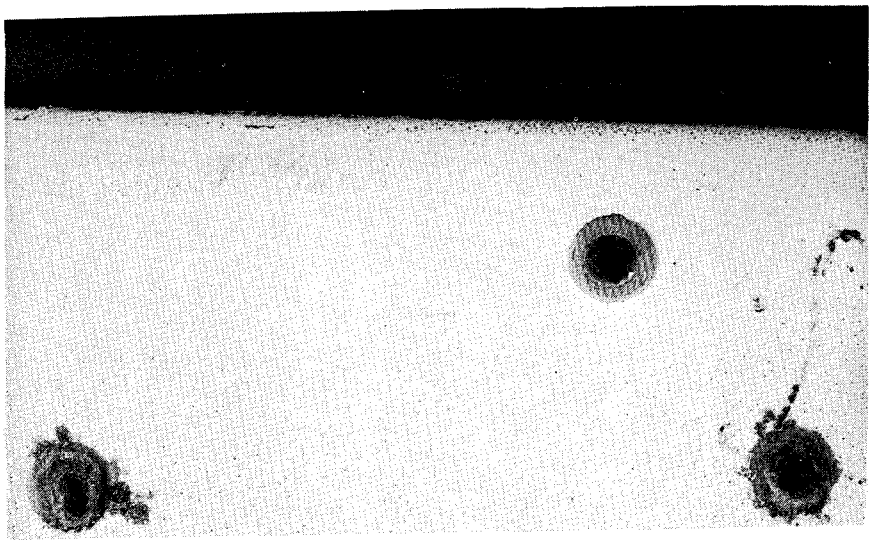

Figure 6 - Wing-Body Fillet with Elongated Holes

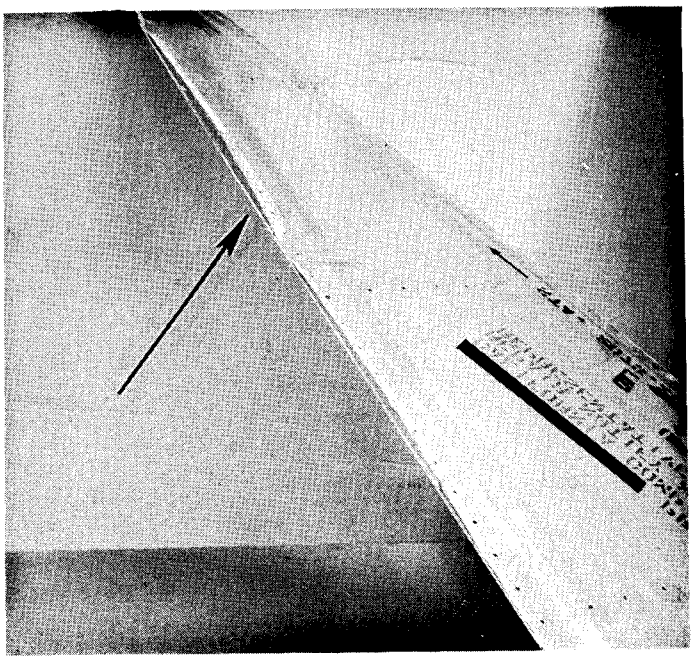

Figure 7 - Delamination on Aft Engine Fairing

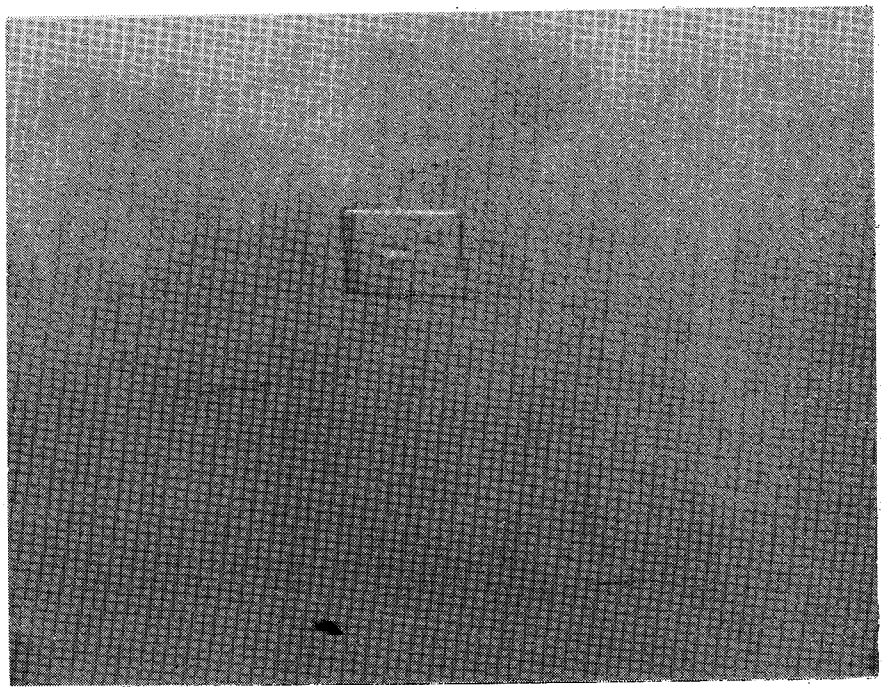

Figure 8 - Temporary Patch - Fairing Exterior Surface

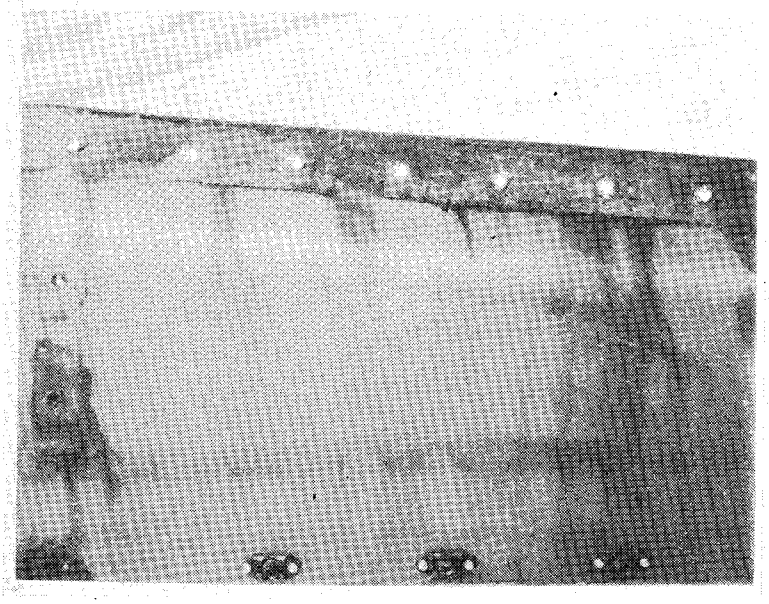

Figure 9 - Aft Engine Fairing with Frayed Holes

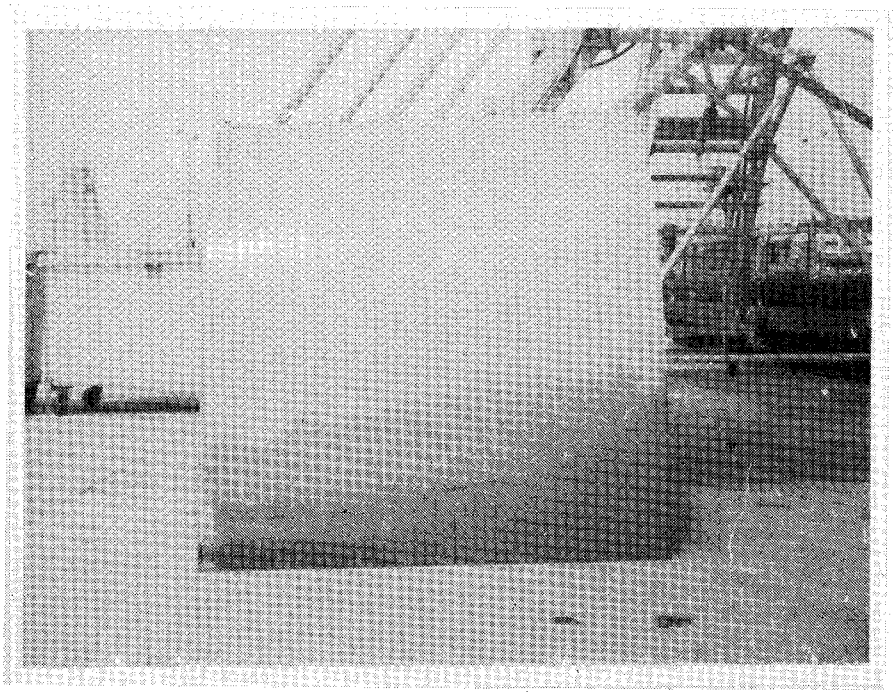

Figure 10 - Wing-Body Fairing - Exterior Surface Condition

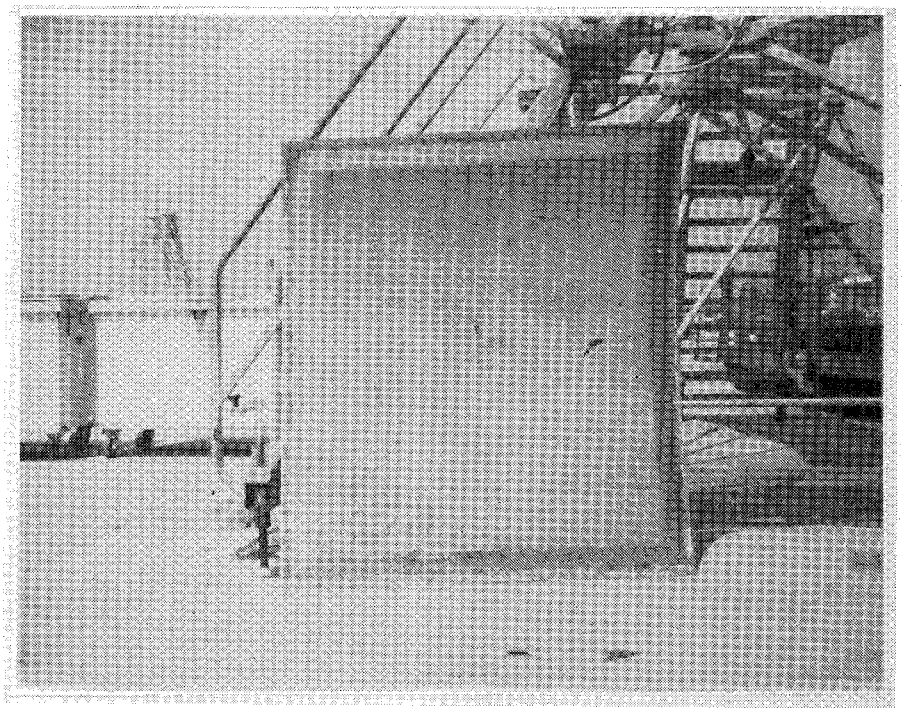

Figure 11 - Wing-Body Fairing - Interior Surface Condition

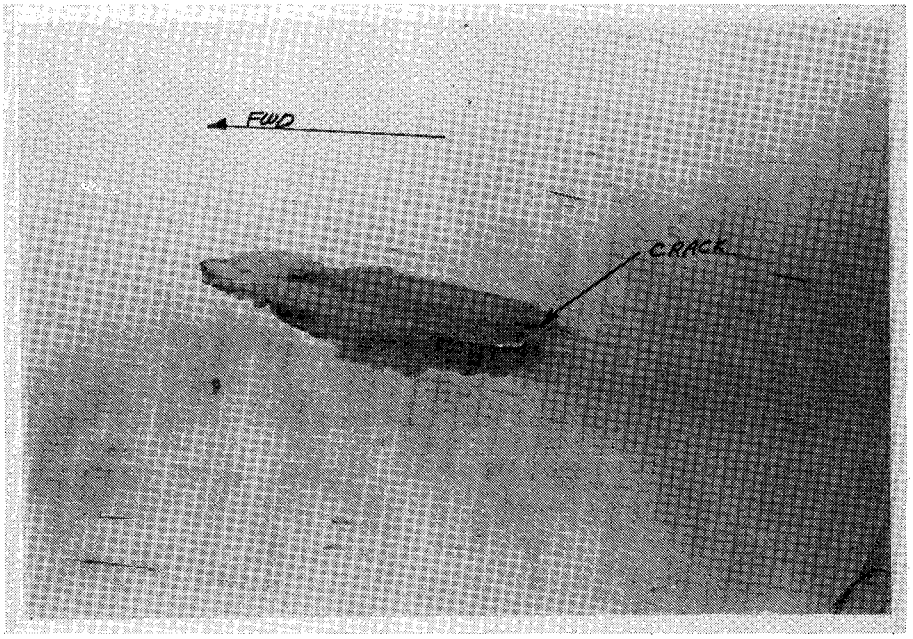

Figure 12 - Crack - Exterior Fairing Surfaces - 1975 Inspection

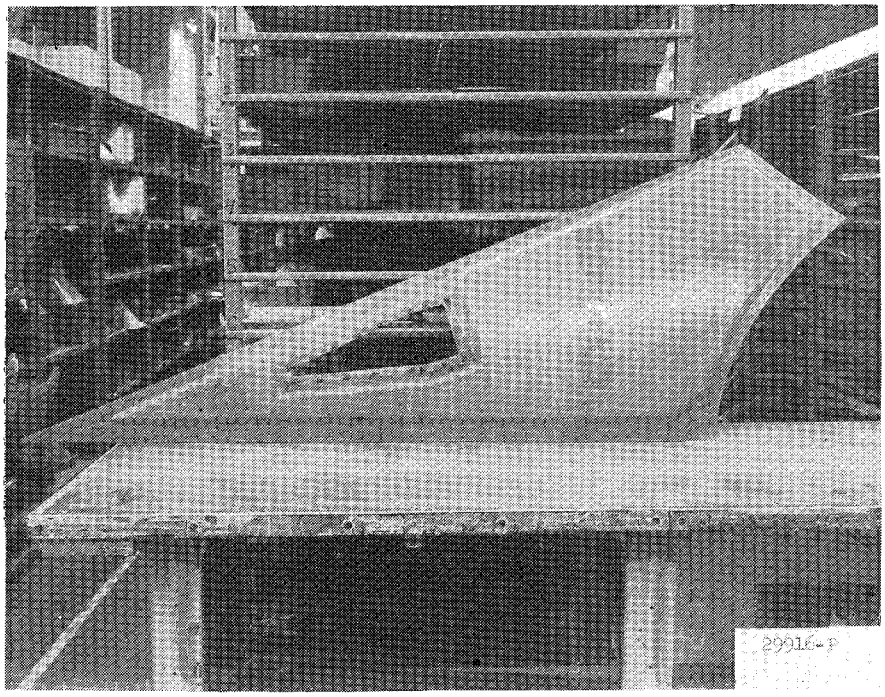

Figure 13 - TWA Aft Engine Fairing - Showing Vapor Barrier Coating and Reinforcing Strips

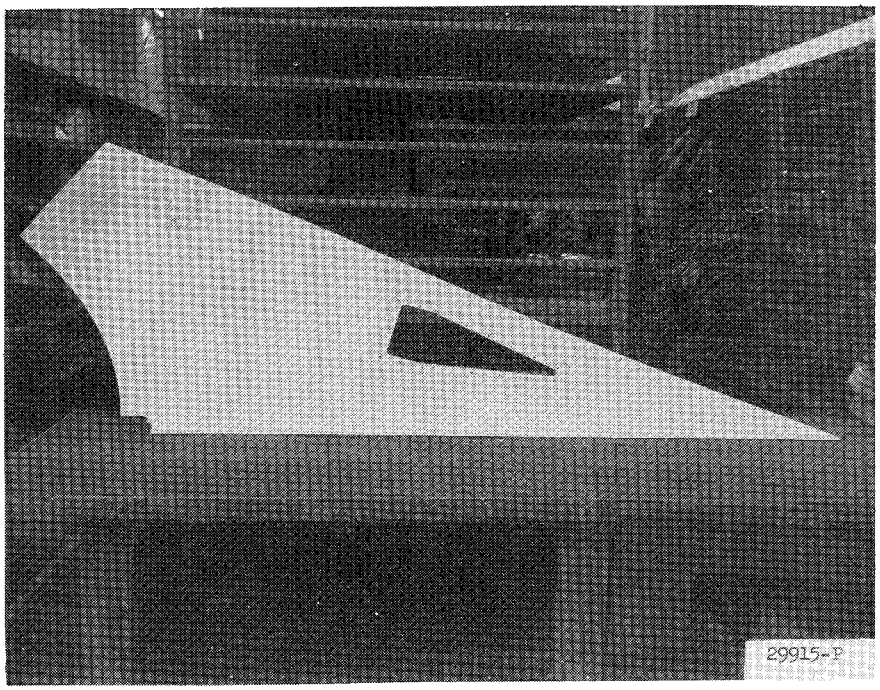

Figure 14 - TWA Aft Engine Fairing with Flame Spray

PROGRESS REPORT ON THE NASA GRAPHITE SPOILER FLIGHT SERVICE PROGRAM

By Robert L. Stoecklin
Boeing Commercial Airplane Company

and Richard A. Pride
NASA Langley Research Center

SUMMARY

One hundred fourteen Boeing 737 graphite composite flight spoilers were fabricated in a production environment, certified, and 108 of these were installed for commercial service. Flight times and load cycle data are presented for the entire fleet of spoilers. Maintenance experience and repair data are included as well as test data from selected spoilers removed from commercial service. Airline acceptance of and responses to the program have been excellent.

PROGRAM REPORT

It has long been recognized by both NASA and industry that "real-life" usage data is essential to expanded structural applications of graphite composite materials. In 1972 Boeing ofeered to NASA a plan to produce and service-test 737 graphite flight spoilers in conjunction with several airlines operating 737 aircraft. Since the spoiler design had already been engineered, tested, and in service with Western Airlines (Figure 1), the offer satisfied NASA's requirements, and the program rapidly took form.

The spoiler (Figure 2) is of full-depth honeycomb design, adhesively bonded, and approximately 8 square feet in area. It incorporates four supports on the hinge line and is operated by a single hydraulic actuator attached at the spoiler centerline. The composite design utilizes precured graphite-epoxy skins over an aluminum honeycomb core, with production aluminum details along the hinge line. The end ribs are fiberglass.

For this program the precured skins were fabricated from 3 different material systems in order to evaluate this variable.

- **UNION CARBIDE 2544/T300 (350F CURE)**
- **NARMCO 5209/T300 (250F CURE)**
- **HERCULES 3501/AS (350F CURE)**

The selection of the spoiler was particularly appropriate. It is a secondary structural component, and its multiple usage on the aircraft precludes it from being critical to flight safety. It is of convenient physical dimensions and is readily adaptable to production.

The fabrication process was planned to permit the manufacturing environment to resemble, as closely as possible, a genuine production environment. The graphite skins were laid up and precured on a production tool, 4 skins at a time. The assembly was performed in two stages, with the skins being bonded to the frame assembly as the second stage. All units produced were ultransonically inspected, with permanent records retained for future reference. Three spoilers were static tested to destruction and the test results became the basis for securing type certification from the FAA. All spoilers were completed to airline standards of appearance as well as "fit-and-function". The installations were accomplished at the airline's facilities utilizing airline maintenance personnel. Boeing's Customer Service network was brought onboard to assist in tracking spoiler performance and operation. In addition to customer service support, each spoiler is physically examined annually by program personnel. Each of the three spoiler variations carries an FAA type certificate, the same as a regular production component. Full compliance with FAR 25 was required of each spoiler type, plus the demonstrated ability of not compromising the flight characteristics of the 737 aircraft.

The required number of spoilers were fabricated, tested, certified, and installed on 737 aircraft of five widely-dispersed airlines. The installations began in July 1973 and the 108th and final spoiler was installed in August, 1974. A sixth airline, VASP, headquartered in San Paulo, Brazil, was added to the program when PSA sold 4 of their participating aircraft to VASP in May, 1974. As shown in Figure 3, the participating airlines operate in a wide variety of climatic conditions. This distribution was deliberately sought as the widest possible combination of environmental variables, since a key element of this program is "environmental exposure". We were also fortunate in obtaining the unqualified cooperation of these airlines, without which the program could not succeed. NASA-Langley is included here but their participation is limited to the ground exposure portion of the program. Ground exposure racks are deployed at all airline headquarters with the exception of Piedmont.

Figure 4 summarizes the total flight activity on the program. This data is cumulative through July 31, 1975, the latest month for which data was available for inclusion in this report. Incidentally, a "spoiler hour" is one spoiler flying for one hour, making each spoiler an individual data point of service experience, both hours and landings. Because of the large (108) number of identical units being evaluated, the total experience expected to be achieved during the course of this program is over a million flight hours and projected total landings is 1.8 million. The plot of accumulated experience to date (Figure 5) illustrates how linear the data accumulation actually is, and how relatively insensitive the program is to having several units temporarily "on the sidelines" in the repair or evaluation process.

The program required the removal of a total of 6 spoilers per year for evaluation and testing (Figure 6), with each of the three different material systems represented by two spoilers. Each spoiler removed was ultrasonically inspected, and the records compared to the original production inspection records. One spoiler from each of the three material systems was then selected for assignment to static test, while the other three were returned to service. This annual sampling procedure will continue for the duration of the program.

One of the most interesting results to date is the experience associated with "unscheduled removals" (Figure 7). As is true with most research and exploration, unforeseen developments occur which were not a part of the original planning. A total of 28 spoilers are included in the "unscheduled removal" category as of September 30. Of this number, only 3 spoilers or 11% are classified as maintenance or handling damage, while 25 spoilers or 89% must be classified as "design-related" damage. Only one unit has been removed as a result of a failure of the laminate, and that one (S/N 0014) can be attributed to a deficiency in an "in-process" repair prior to original installation. This "in-process" repair technique has been subsequently altered and improved. The three maintenance-damaged spoilers have all been attributed to "human-error" situations and do not reflect any shortcomings of the laminates. The 25 design-related damage instances relate to a physical interference occurrence which has minimal effect on the ductile aluminum spoiler but a more severe effect on the graphite skin laminates.

The problem of blisters relates specifically to that portion of the spoiler near the actuator rod-end attachment. The design of the rod end was modified for the production airplane to increase its strength by increasing the cross-section of the housing (Figure 8). In theory this could be accomplished without interference to the underside of the upper surface skin. However, there is no constraint to prevent the actuator piston rod from rotating about its own longitudinal axis, which, when it occurs, permits an interference between the outer corner of the rod end and the inside of the upper skin. This forced deflection causes minimal damage to an aluminum skin but precipitates an interlaminar shear failure in the high-modulus graphite skin laminate. This shear failure manifests itself as a blister on the spoiler upper surface immediately above the actuator attachment lugs. It is this type of failure which is expressed by the 89% of unscheduled removals. The significant observation to be made at this point in the program is the lack of what I will term "significant" operation problems. If one ignores the "self-imposed" interference problem, then the cumulative failure rate is less than 3%, and that entirely due to external causes. The net result is a failure rate on the composite laminates in this program of zero.

One significant feature of the program is the requirement to static test part of the spoilers removed from service on a pre-determined schedule. The schedule calls for static-testing to failure 3 of the 6 scheduled removals each year. The ultrasonic inspections search for defects or anomalies not present at the time of fabrication, while the destruction testing monitors changes in physical strength characteristics as a function of time. The first year evaluations have been completed with the tabulated results as shown in Figure 9. The data yields approximately 10% reduction in strength

levels compared to the original static test results, remembering that two of the three test specimens had either a defect or a repair built in. The 10% figure is generally compatible with material property data obtained from exposure rack data which is a companion part of this program. Subsequent tests will establish the accuracy of this trend.

Since we have seen the occurrence of some delaminations and damage, one must necessarily address the subject of repair, which is a real-life operational problem. The need for repair first arose in the fabrication process, where a number of composite skin defects were detected either visually or through the ultrasonic inspection process. Since repair of a structural component is an operational must, whether in original fabrication or operational use, the problem could not be ignored. Also, the opportunity to demonstrate the environmental resistance of repaired laminates was welcomed. Since there exists no generally accepted repair criteria for graphite composite laminates, it was necessary to generate repairs compatible to this program (Figure 10). The approach was to restore the original strength, with replacement of the fibers and fiber orientations removed. In addition, the replaced laminates should be cured in the same manner as the original laminate. However, since the adhesive system is cured at 250°F, curing a 350°F laminate repair could seriously impair the laminate-to-core adhesive. Therefore, all repairs were successfully made with 250°F curing prepreg, and reinserted in the second stage bonding tool for dimensional control, with autoclave pressure limited to the 35 psi used for adhesive cure. Initially, repairs were accomplished with wet layup prepreg and relied on the resin to achieve the interlaminar bond. However, experience with unit S/N 0014 showed that resin bond alone is insufficient, necessitating a modification of the repair process to include bonding adhesive on the ply steps, and co-curing the adhesive with the repair prepreg. The resulting bonds are more clearly defined on the ultrasonic color scans and no adverse reports have been registered since the process was modified.

Corrosion experience on this program is one of the more pleasant subjects. In one brief sentence, we've had very little. One instance of external aluminum corrosion on one spoiler has been observed, and this has been traced to improper anodizing of the corroding doublers. Physical dissection of the three static test spoilers has yielded absolutely no evidence of corrosion in the spoiler interiors. A skin sample cut from the static test spoiler 0053 (in service with New Zealand's National Airways) showed a .82% weight loss when baked in a 170°F oven for 24 hours to drive off moisture. Two other New Zealand spoilers (0087 and 0088) showed no detectable weight loss when subjected to a similar drying cycle. Additional evidence of moisture absorption will be sought from pending scheduled spoiler removals.

In conclusion, the performance achieved in the flight service program has been excellent. The favorable experience achieved should provide a significant "building block" for graphite composite usage on commercial aircraft in the 1980's by both manufacturers and operators.

FIGURE 1 - GRAPHITE EPOXY SPOILER IN SERVICE DEMONSTRATION

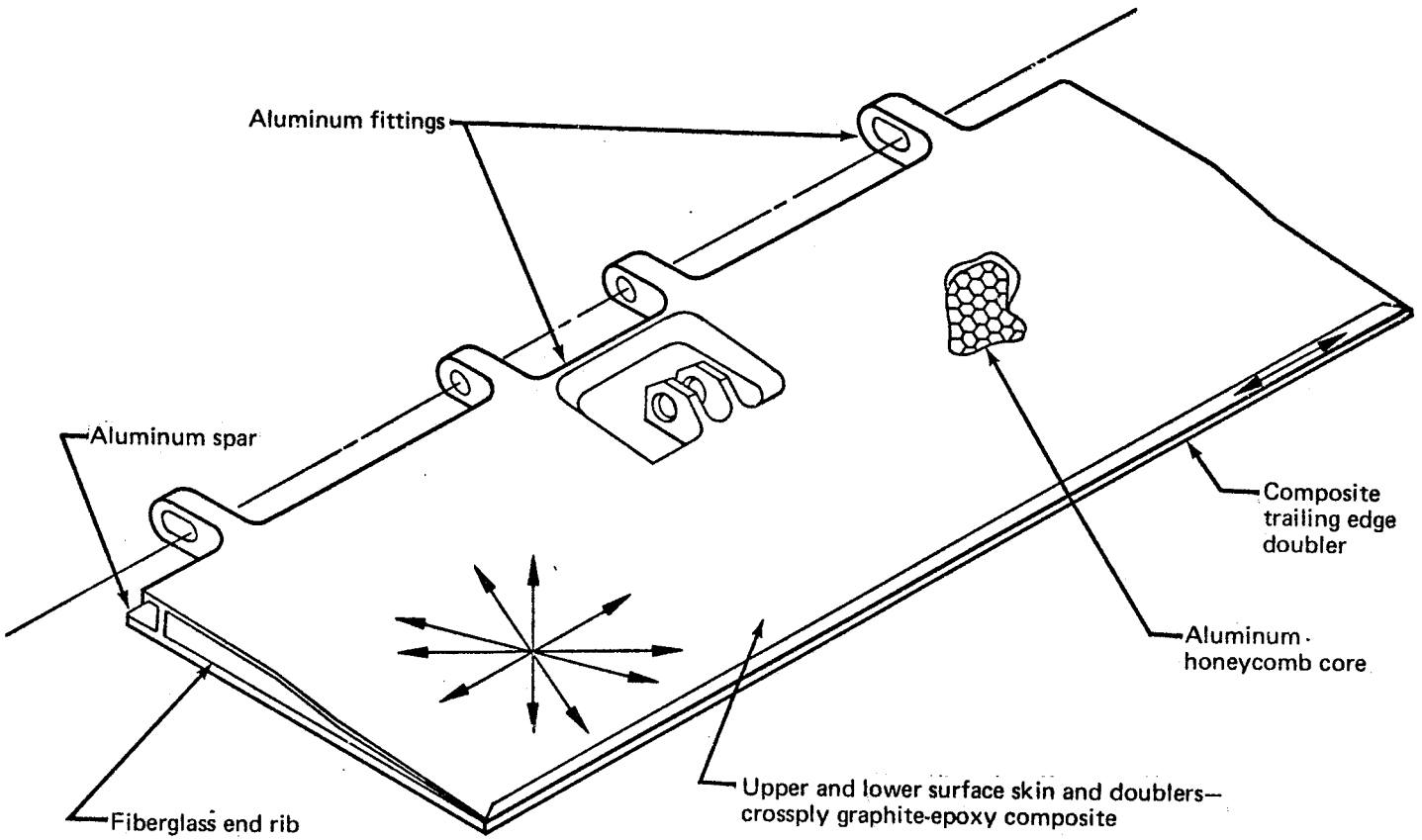

Note: All structure is adhesively bonded

FIGURE 2 - 737 GRAPHITE-EPOXY FLIGHT SPOILER

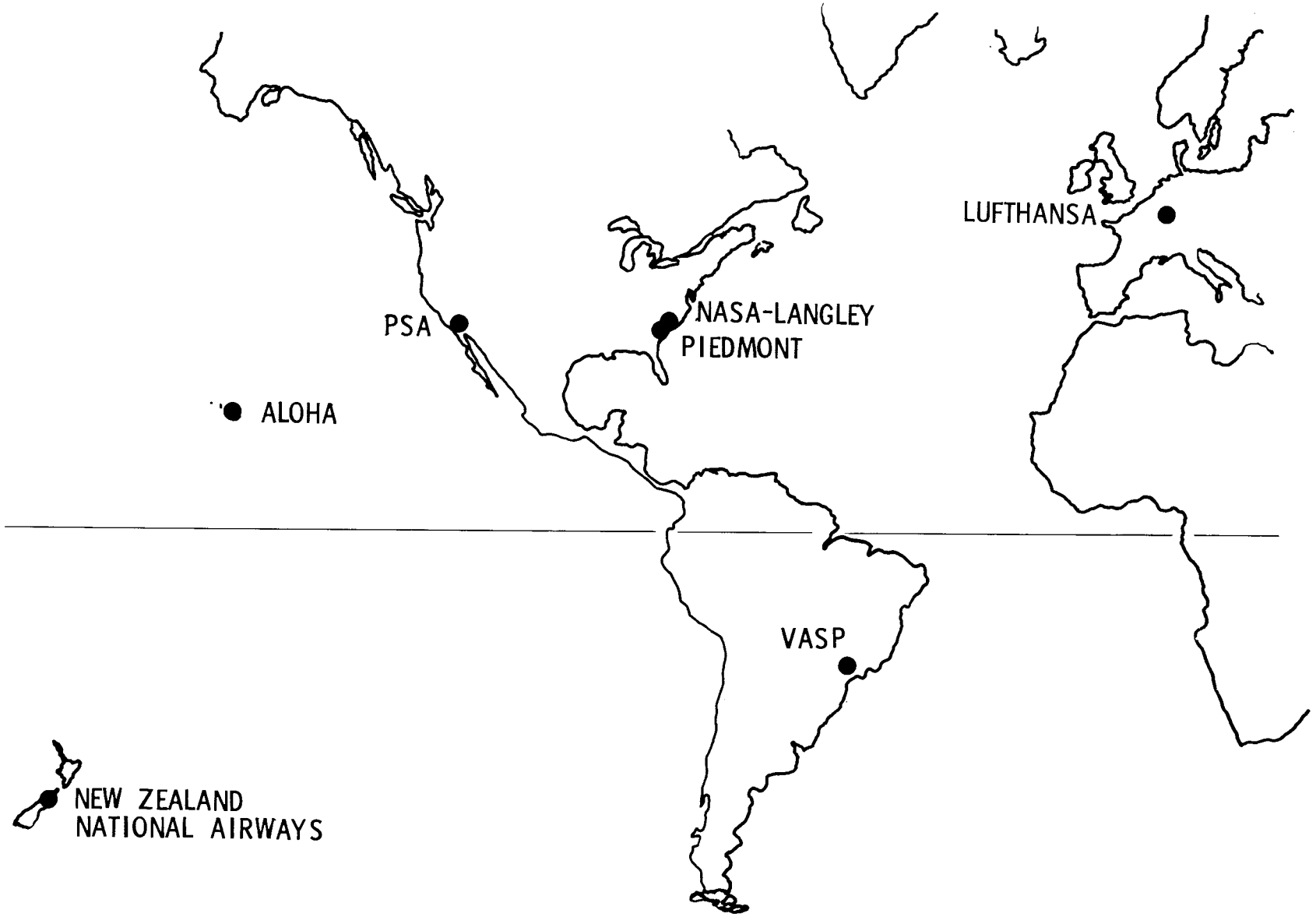

FIGURE 3 - GEOGRAPHIC DEPLOYMENT OF PARTICIPATING AIRLINES

Airline	TOTAL SPOILER HOURS	TOTAL SPOILER LANDINGS	SPOILER COUNT			
			Currently in Service	Out for Repair	Out for Evaluation	Destroyed in Static Test
PSA	28,595	49,475	3	0	1	0
Aloha	51,176	136,002	15	2	0	1
New Zealand	62,237	83,601	13	2	0	1
Lufthansa	94,088	122,103	19	4	0	1
Piedmont	101,540	154,349	28	3	1	0
VASP	40,668	48,689	11	5	0	0
TOTALS	378,304	594,219	89	16	2	3

HIGH TIME SPOILER : 0011 & 0013 ON D-ABEN (LH) - 4348 HOURS

HIGH LANDING SPOILER : 0023 & 0025 ON N73711 (ALOHA) - 9934 LDGS.

FIGURE 4 - FLIGHT SERVICE DATA SUMMARY (as of July 31, 1975)

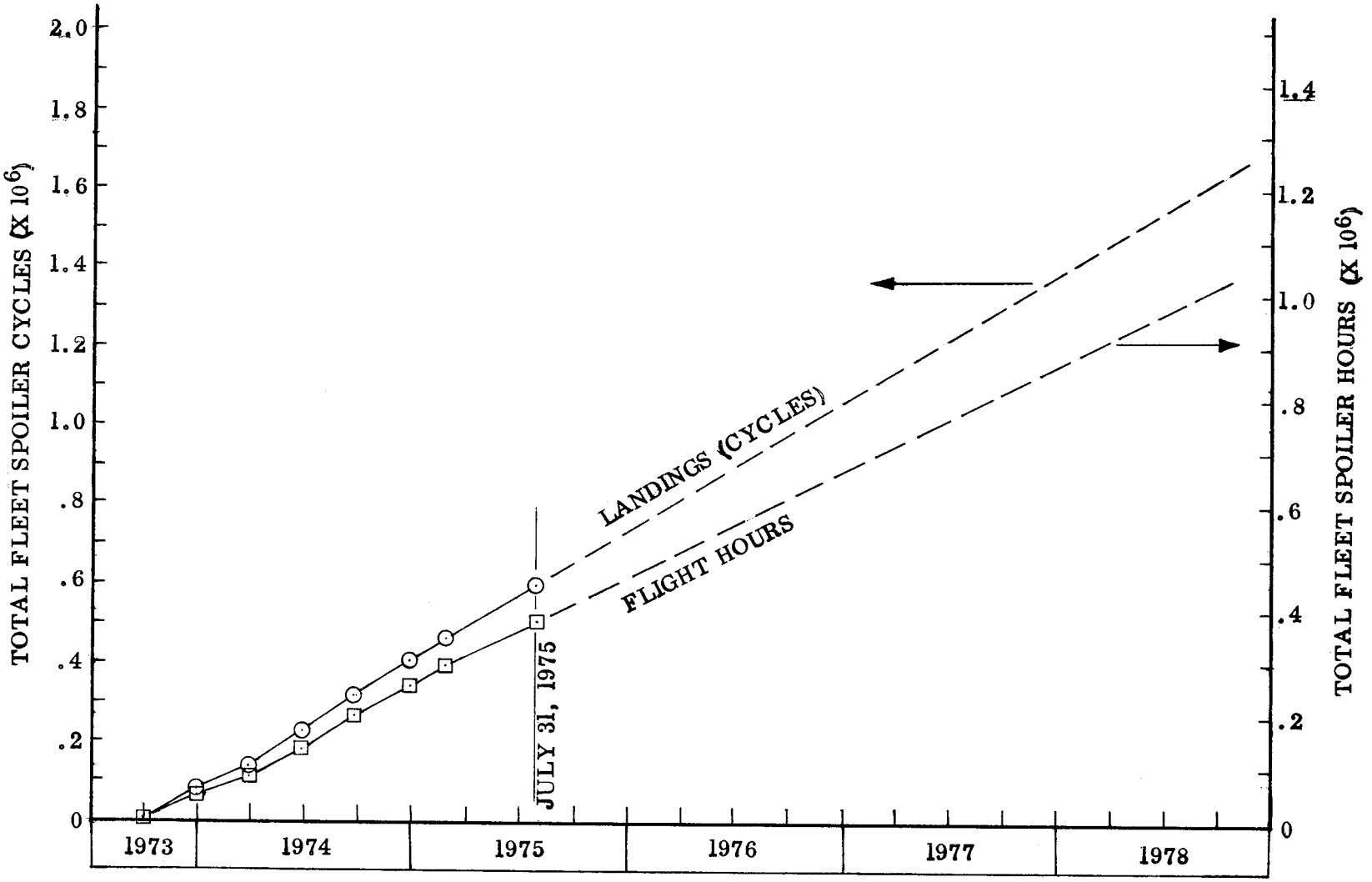

FIGURE 5 CUMULATIVE FLEET FLIGHT-HOURS AND LANDINGS

	SPOILER S/N	AIRLINE	FLIGHT HOURS AT REMOVAL	NDT INSPECTION RESULTS	VISUAL INSPECTION RESULTS	DISPOSITION
1st YEAR	0014	LH	2055	IN-PROCESS REPAIR DELAMINATION VISIBLE	IN-PROCESS REPAIR DELAMINATING ALONG PERIMETER	STATIC-TESTED
	0028	PI	2640	NO DEFECTS NOTED	NO DEFECTS	RETURNED TO SERVICE
	0045	PSA	1902	NO DEFECTS NOTED	NO DEFECTS	STORAGE
	0053	NZ	2599	NO DEFECTS NOTED	NO DEFECTS	STATIC-TESTED
	0094	PI	2582	NO DEFECTS NOTED	NO DEFECTS	RETURNED TO SERVICE
	0104	Aloha	2096	UPR SURF. BLISTER NO REPAIR EFFECTED	BLISTER VISIBLE	STATIC-TESTED
2nd YEAR	0025	Aloha	3757	NO DEFECTS NOTED	NO DEFECTS	HOLD FOR STATIC TEST
	0057	LH	N/A	NO DEFECTS NOTED	NO DEFECTS	HOLD FOR STATIC TEST
	0085	LH	N/A	NO DEFECTS NOTED	NO DEFECTS	HOLD FOR STATIC TEST

FIGURE 6 - SCHEDULED REMOVAL EXPERIENCE

	SPOILER S/N	AIRLINE	FLIGHT HOURS @ REMOVAL	REASON FOR REMOVAL	DISPOSITION
65-76327-3	0083	LH	3726	SURF. PUNCTURE	REPAIR
	0089	NZ	1685	T.E. DAMAGE	REPAIR; RET. TO SERVICE
	0112	LH	3592	SURF. PUNCTURE	REPAIR

UPPER SURFACE BLISTER REPAIR

	SPOILER S/N	AIRLINE	FLIGHT HOURS @ REMOVAL	DISPOSITION
65-76327-1	0012	LH	3420	REPAIR; RET. TO SERVICE
	0015	VP	3037	REPAIR
	0018	VP	3037	REPAIR
	0021	LH	3453	REPAIR; RET. TO SERVICE
	0024	ALOHA	1767	
	0026	ALOHA	2864	
	0032	PI	2082	
	0035	PI	1992	
	0036	PI	1982	
65-76327-2	0048	ALOHA	2655	
	0052	NZ	3518	REPAIR; RET. TO SERVICE
	0059	VP	2424	REPAIR
	0066	NZ	3397	REPAIR; RET. TO SERVICE
	0078	ALOHA	1997	REPAIR; RET. TO SERVICE
65-76327-3	0084	LH	3726	REPAIR
	0087	NZ	3929	REPAIR
	0088	NZ	3929	REPAIR
	0090	ALOHA	1165	REPAIR; RET. TO SERVICE
	0091	ALOHA	2664	REPAIR; RET. TO SERVICE
	0093	PI	2582	REPAIR; RET. TO SERVICE
	0104	ALOHA	2096	REPAIR; STATIC-TESTED
	0105	ALOHA	99	REPAIR; RET. TO SERVICE
	0105	ALOHA	1371	REPAIR
	0109	VP	3553	REPAIR
	0111	VP	3553	REPAIR
	0114	LH	3014	REPAIR; RET. TO SERVICE

FIGURE 7 - UNSCHEDULED REMOVAL EXPERIENCE

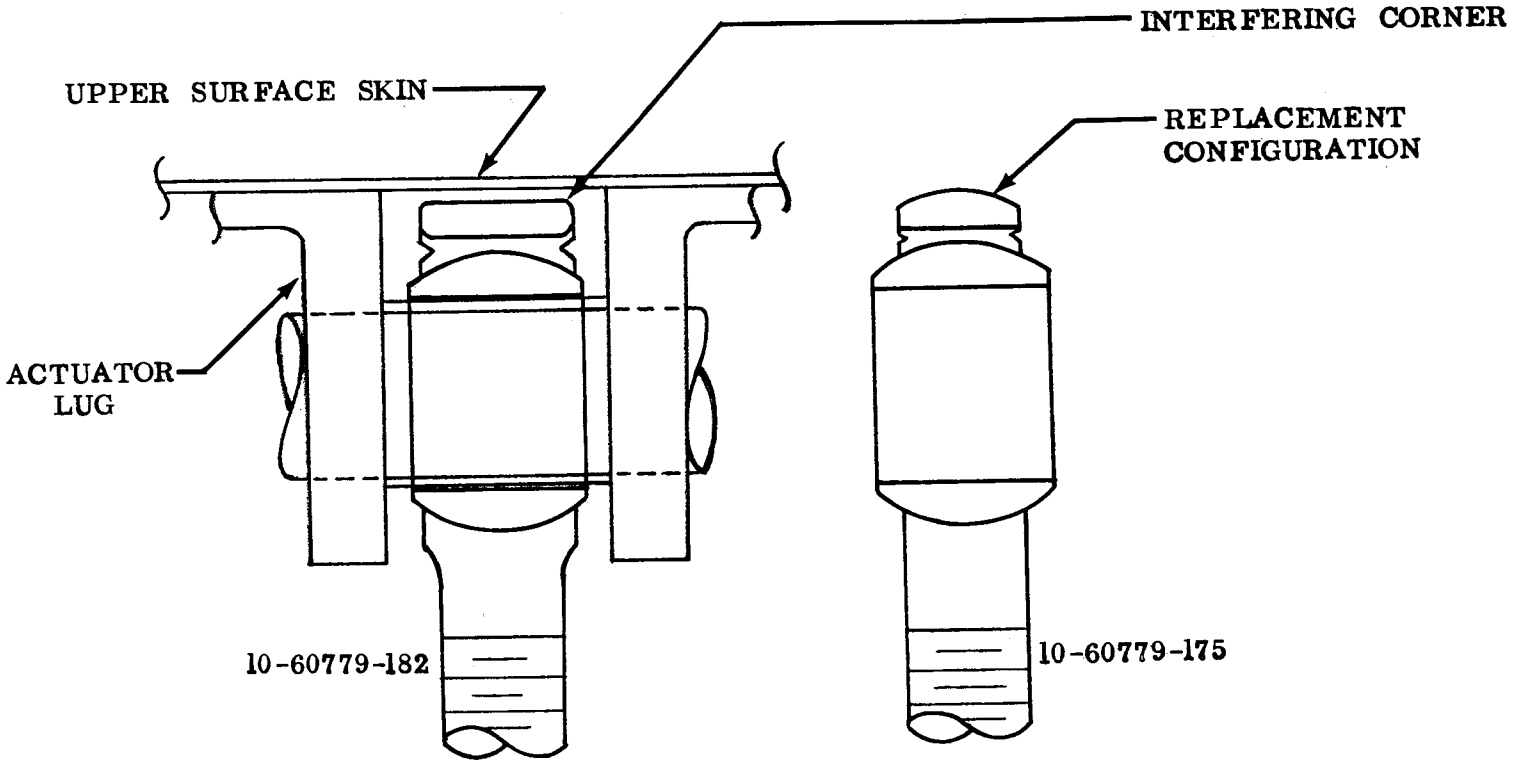

FIGURE 8 - ACTUATOR ROD END GEOMETRY

SPOILER S/N	AIR LINE	NDT RESULTS	STATIC TEST RESULTS		TIME IN SERVICE	FLIGHT HOURS
			% CHANGE STRENGTH	% CHANGE STIFFNESS		
0014 (-1)	LH	UPPER SURF. SKIN REPAIR DELAMINATION	-15%	-10%	11 MOS. 3 DAYS	2055
0028 (-1)	PI	CLEAR	NOT TESTED		11 MOS. 26 DAYS	2640
0045 (-2)	PSA	CLEAR	NOT TESTED		11 MOS. 19 DAYS	1902
0053 (-2)	NZ	CLEAR	-14%	-10%	14 MOS. 1 DAY	2599
0094 (-3)	PI	CLEAR	NOT TESTED		12 MOS. 12 DAYS	2582
0104 (-3)	ALOHA	UPPER SURF. BLISTER	-10%	-16%	13 MOS. 0 DAYS	2096

FIGURE 9 - TESTING OF REMOVED SPOILERS

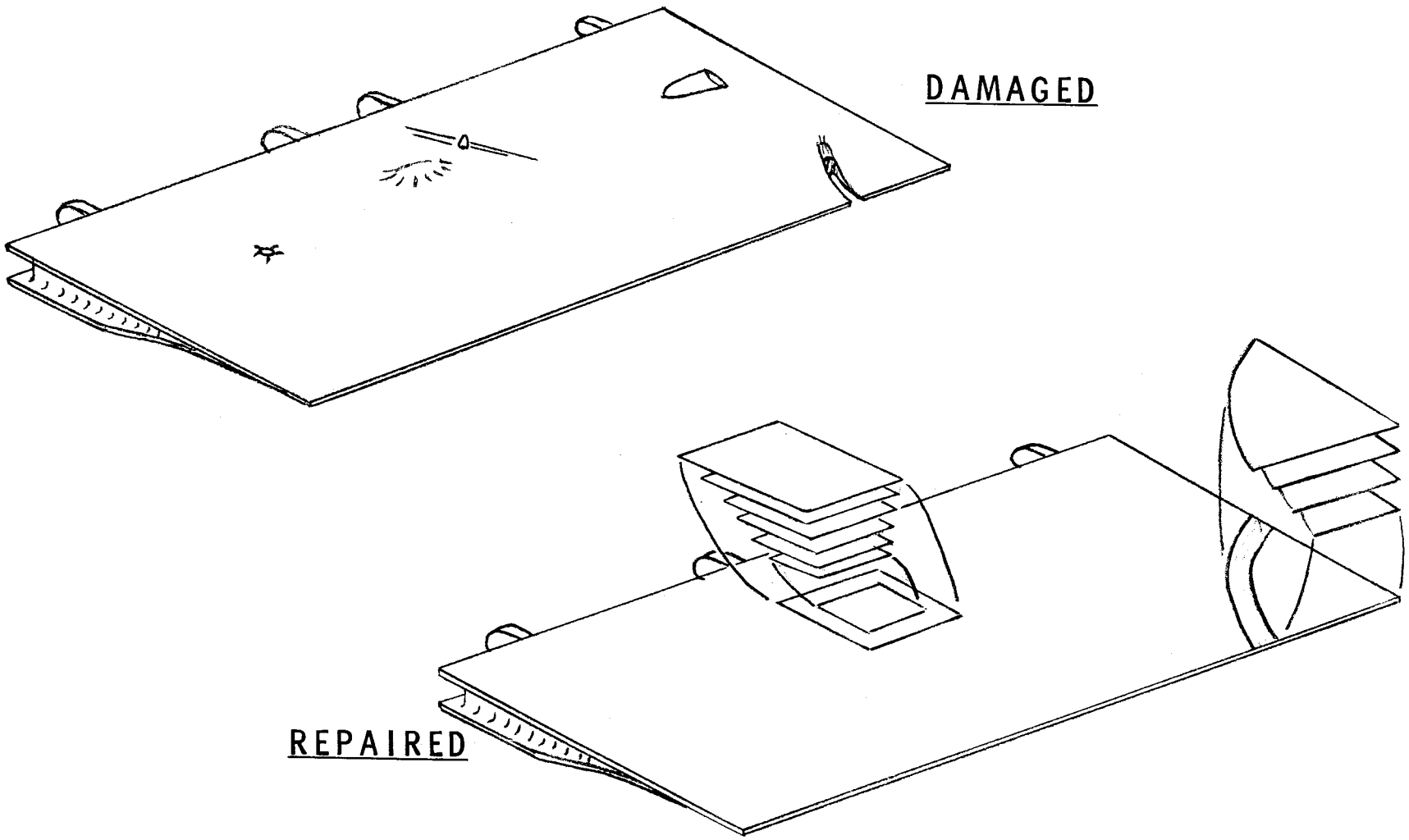

FIGURE 10 - REPAIR TECHNIQUES

ENVIRONMENTAL EXPOSURES OF ADVANCED COMPOSITES FOR AIRCRAFT APPLICATIONS

By Richard A. Pride and Marvin B. Dow
NASA Langley Research Center

SUMMARY

An interim report on results of a number of flight service evaluations and ground-based environmental exposures for several advanced composite materials sponsored by the NASA Langley Research Center is presented. The airlines flying the composite components have been selected so as to provide a worldwide range of environmental conditions. Flight service has exceeded 2 years for many of the components with over half a million component flight hours satisfactorily accumulated to date.

Concurrent with the flight service evaluations, specimens of the same composite materials are being subjected to long-term environmental exposures at the main terminals of many of the participating airlines and at the Langley Research Center. After the first year of environmental exposure, specimens of three graphite/epoxy materials and two Kevlar 49/epoxy materials have been removed from the exposure racks and have been tested for residual strength in flexure, short beam shear, and compression. Test results indicate generally less than 10-percent change in mechanical properties and an average moisture pickup of less than 2 percent of the epoxy-matrix weight. No useful correlation has been found between the amount of moisture picked up and the residual strength of individual specimens.

In addition, results of several related research programs are reviewed. Outdoor exposure on unstressed, epoxy-matrix controlled composite specimens for times in excess of 4 years has resulted in less than 10-percent change in residual room-temperature strength. Cyclic and continuous exposures in fuel-tank environments of both stressed and unstressed angle-ply tensile specimens have also resulted in less than 10-percent change in residual strength for times up to 1 year. The combined effects of sustained loading and outdoor environment on interlaminar shear strength of epoxy-matrix composites have produced a 30-percent reduction in creep-rupture strength at high stress levels, but the data can be extrapolated to a greater than 20-year service life for 1 g operating stress levels.

An overall conclusion that may be drawn from these interim test results is that there has been a minimal effect of the environment to date on composites for subsonic commercial-aircraft applications.

INTRODUCTION

The improved structural efficiency and weight savings that can be achieved by the use of advanced composite materials in aircraft structural components

have been amply demonstrated in numerous test programs in recent years. However, two barriers to extensive production commitments continue to exist: uncertainty that a production environment can produce cost-effective components and uncertainty concerning the long-term durability of composites. Continual increases in the utilization of composite materials in a wide variety of applications and reductions in manufacturing costs are expected to bring composite-hardware cost into a competitive position with metals for aircraft applications at some time in the future. But even then, widespread use in airframes will not occur unless both the manufacturers and the airlines have developed a strong confidence in the projected durability of the composite hardware for times up to 20 years.

Recent concerns with the influence of moisture on residual strengths and stiffnesses of epoxy-matrix composites, particularly at elevated temperatures, came to a focal point during the Air Force sponsored Durability Workshop at the Battelle Columbus Laboratories on September 30 to October 2, 1975. Almost all data presented were based on artificially accelerated environmental aging. However, until the proper correlation can be established with accelerated environmental parameters, the only sure manner in which to determine environmental effects is to expose composite materials in the real world in real time.

In order to develop user confidence in composite durability, the Langley Research Center (LaRC) several years ago started conducting flight service evaluations of advanced composite structural components for commercial aircraft. The airlines flying the composite components have been selected so as to provide a world-wide range of environmental conditions. Concurrent with the flight service evaluations, specimens of the same composite materials are being subjected to long-term environmental exposures at the main terminals of many of the participating airlines and at the LaRC. Periodic tests of the exposure specimens are performed to determine if the material properties are being degraded from the exposure. The full range of the LaRC program on environmental exposures of advanced composites includes programs for long-term exposures in aircraft fuels and hydraulic fluids, thermal cycling, and outdoor exposure combined with stress, in addition to flight service programs and their related ground-based exposure of the flight materials. Interim test results available to date are presented herein.

ENVIRONMENTAL EXPOSURE PROGRAMS

The LaRC flight service evaluation programs to develop user confidence in the durability of composite structural components are shown in figure 1. The various types of aircraft on which these composite components are installed are shown. The development of each of these programs is described in a number of reports presented elsewhere in the present publication with the exception of the CH-54B helicopter fuselage (ref. 1) and the DC-10 aft pylon skin (ref. 2). Installation of these components on full-time service aircraft provides the most direct and realistic exposure to all the environmental elements. In addition, flat laminates of each of the composite materials in the flight components were manufactured at the same time as the flight components and subsequently were cut into numerous replicate flexure, interlaminar shear, compression, and tension

specimens to be placed in appropriate ground-based exposure racks as a first step in simulating the aircraft environmental exposure.

The service experience generated through September 30, 1975 for these flight components is listed in table I. The 132 components in the seven programs include two boron/epoxies, two Kevlar 49/epoxies, four graphite/epoxies, and one boron/aluminum as composite materials. All these are continuing to perform satisfactorily in their respective flight environments from the $3\frac{1}{2}$ years of the calendar time for the helicopter through the more than 7000 flight hours on the high-time aircraft to the more than 400 000 component flight hours on the spoilers. The accumulated flight service currently exceeds half a million component flight hours of experience with 12 operators.

As indicated previously, concurrent with the flight service evaluations, specimens of the same composite materials have been placed in exposure racks for long-term environmental exposure at many of the main terminals of the participating airlines. Rack locations are shown in figure 2, along with typical installations on roof tops of racks designed to hold unloaded specimens and racks holding loaded specimens. The unloaded specimen racks contain specimens from three programs but are located at terminals of the participants in the Boeing 737 spoiler program. The loaded specimen racks contain only tensile specimens from the DC-10 rudder program and are located only at San Francisco and the LaRC. Roof-top locations at airports were selected in order to obtain a close match to the ground environment that the aircraft experiences for about two-thirds of its lifetime, yet keep the rack safe from damage or pilferage.

The rack for unloaded specimens is designed with five replicate panels, one of which is shown in figure 3. Interlaminar shear, flexure, and compression specimens of several composite materials are held in the panel in a manner that provides a maximum exposure to sunlight on one surface but allows free circulation of air around the specimen. At the end of the designated exposure period, the panel is removed from the rack and is shipped with specimens still in place to the LaRC for residual strength testing. Currently, there are over 2100 unstressed specimens in the environmental exposure program, and removals are scheduled to occur after 1, 3, 5, 7, and 10 years.

Similar exposures are underway with stressed tensile specimens, but on a more limited schedule. A closeup photograph of one of the constant tensile-load fixtures is shown in figure 4. Because of the size and complexity of the fixture, only 20 replicates are placed in an exposure rack and only two racks with stressed specimens have been installed: one at San Francisco and one at the LaRC. The loading spring is preset in a laboratory testing machine to a load level which produces a tensile stress equal to 40 percent of the average tensile ultimate stress in the specimen. An equal number of unstressed tensile specimens are placed in the same rack for comparative exposure. Removals are scheduled for 1, 3, 5, 7, and 10 years. First removals of stressed specimens were scheduled for November 1975; no test data are available.

Results of room temperature tests of the composite materials removed from six unloaded specimen racks after 1 year of outdoor ground-based exposure are shown in figures 5, 6, and 7 for flexure, interlaminar shear, and compres-

sion strength, respectively. Strength values are presented in ratio form as the average retained strength (based on three replicate tests after exposure of each material) divided by an average initial baseline strength (based on five replicate tests of each material after fabrication). The three graphite/epoxy material systems, Thornel 300/5209, Thornel 300/2544, and AS/3501, are the same three materials used in the initial phase of the 737 spoiler flight service evaluation. Detailed test data for these graphite/epoxy systems are tabulated in reference 3. The two Kevlar 49/epoxy materials, F-155 and F-161, are the same materials used in the L-1011 fuselage fairing panel flight service evaluation. Two other material systems have been added to the unloaded specimen racks since the ground exposure program began, but 1-year data are not yet available. The residual strength values shown are generally less than 10 percent different from the initial baseline values, and no particular trend is observed to rank one exposure site as more severe than any other. Also, the more fiber dominated flexure strengths do not appear to be affected any less than the matrix dominated interlaminar shear and compression strengths. An overall average change in residual strength after 1 year of exposure is less than 5-percent decrease from the initial baseline.

All material specimens were weighed after removal from the exposure racks. The weights were compared with initial values to determine the extent of weight change, which for these specimens is assumed to be primarily due to moisture absorption from the air at the exposure sites. Detailed data are tabulated in reference 3 for the three graphite/epoxy systems; and, although there is considerable scatter, the average moisture pickup is less than 2 percent of the epoxy-matrix weight. Attempts to correlate changes in residual strength with moisture pickup generally indicate no particular trend. An example is the plot shown in figure 8 which relates individual specimen weight gain to the flexure strength retained after 1-year outdoor exposure for the AS/3501 graphite/epoxy material. An observation can be made that specimens with the most weight gain were the strongest; but the trend is not a strong one, and the logic is counter to the anticipated degradation due to moisture. The only reasonable conclusion is that the data exhibit considerable scatter. Similar results were obtained for the other materials in other types of tests.

Although the ground-based environmental exposure sites are widely dispersed at principal terminals of the participating airlines in the spoiler flight service program, it is of interest to note that all except for Frankfurt, Germany are located at or near sea coasts. According to weather data collected by the Air Force Weather Service over the past 20 years, the average annual environmental conditions for these exposure sites tabulated as follows:

	Temperature		Relative humidity,
	K	°F	percent
Hampton, Virginia	289	60	72
San Diego, California	290	62	75
Frankfurt, Germany	282	49	78
Honolulu, Hawaii	297	76	75
Sao Paulo, Brazil	291	65	79
Wellington, New Zealand	288	59	72

Average temperature ranges from a low of 282 K (49° F) at Frankfurt to a high of 297 K (76° F) at Honolulu, Hawaii. Average relative humidity varies even less from a low of 72 percent in Hampton, Virginia and Wellington, New Zealand to a high of 79 percent in Sao Paulo, Brazil. Thus the equilibrium moisture content of epoxy-matrix composites exposed at these sites will probably reach levels of 3 to 4 percent of the matrix weight, but it may take several years to approach equilibrium at these temperatures.

Of greater significance in the long duration exposures than average temperatures and relative humidity may be the cyclic variations that occur daily, weekly, and monthly. Typical cyclic variations in these environmental factors are shown in figure 9 for weather data during 1974-1975 at Hampton, Virginia. Extremes in relative humidity range from a low of around 30 percent and a high of around 100 percent. These values are reached several times in almost every month of the year so that there does not appear to be a seasonal variation. However, with temperature, the daily spread between high and low remains essentially constant at about 15 K (27° F) throughout the year. The average temperature is high in the summer and low in the winter, with a seasonal variation of about 22 K (40° F). On a daily scale, both temperature and humidity go through a cyclic variation of up to the same magnitudes as given previously, with the humidity reaching its high values generally when the temperature is low during the day. Obviously, daily variations may not be regular if weather fronts are passing through the area. Accounting for daily cyclic variations may be very difficult, but these cyclic effects may have considerable influence on the mechanical behavior of matrix controlled composite laminates. There is no clear indication of this in currently available strength data.

Another form of cyclic variation in environment occurs for composite components that are in flight service and therefore cycle between ground conditions and high-altitude flight conditions where both the temperature and the absolute moisture content generally are quite low. There are some data available from the spoiler program. As indicated in reference 4, a number of spoilers have been taken out of flight service and returned to The Boeing Commerical Airplane Company for inspection and repair if needed. These have been cleaned and weighed upon receipt from 30 to 60 days after removal from an aircraft. Weight changes are shown in figure 10 for the spoilers on which determinations have been made. The weight changes are plotted as a function of number of flights for the spoilers ranging from 3000 to 8000 flights. No particular trend is observed, and no trend was observed either when the variable was flight hours or calendar service time. These spoilers have been in service from 12 to 24 months so that weight gains up to 4 or 5 percent of the matrix weight may not be unreasonable, based on similar ground-based exposures. The large amount of scatter is undoubtedly due in part to the sensitivity of the weight determination. Spoiler weights are determined to the nearest 0.01 pound on a 13-pound component (0.004 kilogram on a 6-kilogram component), but only about 1 pound (0.45 kilogram) of that component is epoxy matrix. Even with the scatter, it is apparent that flight components absorb about the same amount of moisture as comparable ground-based specimens.

Consider next some data obtained from several research programs related to the overall environmental effects study for composites. Interim results from

another long-term outdoor investigation of matrix controlled composite strength are presented in figure 11. Interlaminar shear strength values retained for times in excess of 4 years in an early development graphite/epoxy material system continue to lie within the ±10-percent scatter band established with the initial data up to times in excess of 4 years. These data are for unstressed short-beam shear specimens. By way of comparison, two points are shown for angle-ply tensile specimens which were stressed during the exposure at 25 percent of their average ultimate strength. Their retained strength ratio lies in the middle of the unstressed data, suggesting that for outdoor exposure times up to 1 year there is no difference between stressed and unstressed specimens at the 25-percent level.

The long-term effects of continuous and cyclic exposures to JP-4 jet fuel and Skydrol hydraulic fluid on several epoxy-based composite materials are being investigated by The Boeing Commercial Airplane Company under contract to NASA Langley (NAS1-12428). Results to date for ±45° tensile specimens of Thornel 300/5209 graphite/epoxy after various exposures are compared with initial tensile strength values in figure 12. The initial strength value is based on the average of 10 tests while all subsequent values after exposure are the average of two replicates. Both unstressed exposures and stressed-to-25-percent-of-ultimate-strength exposures are being conducted continuously in ambient air as a control, in JP-4, in Skydrol, and in a mixture of JP-4 and water and are being conducted cyclically in JP-4 and air. The mixture of fuel and water exposure has specimens immersed but located at the interface of the mixture. The fuel and air cycling alternately immerses specimens in fuel for 24 hours and then in air above the fuel for 24 hours. Specimens have been removed from each of the fluids after 3, 6, and 12 months exposure and tested at room temperature. The only noticeable reduction in tensile strength occurred after exposure in the fuel and water mixture, but none of the values have been changed by more than 10 percent. Also, no particular difference has been observed between stressed and unstressed exposures. This exposure program will be continued for another 4 years under the present contract.

Another environmental effect that is being investigated at the LaRC is thermal cycling of bonded joints between boron/epoxy composite and aluminum. Double-lap tensile-shear specimens have been fabricated with the composite adherends secondarily bonded to the aluminum with AF 127-3 film adhesive cured at 386 K (235° F). These particular specimens are representative of the bonded composite reinforcement in the C-130 center wing box and thermal cycles were selected for average service environment between 255 K and 344 K (0° F and 160° F). After cycling in a laboratory chamber, specimens were removed and tested for residual strength. The results, shown in figure 13, indicate up to a 25-percent reduction in initial shear strength of the adhesive after 7500 thermal cycles which correspond approximately with one design lifetime for the airplane.

The combined effects of sustained loading and outdoor environmental exposure on interlaminar shear strength of boron/epoxy composite material are shown in figure 14. Special-design equipment at the LaRC provides for sustained flexure loads to be applied to short-beam shear specimens and to be maintained until creep rupture occurs. Similar tests are conducted indoors in a controlled laboratory environment and outdoors at the LaRC at stress levels of 60 to 80 percent of the static shear strength. Creep-rupture lifetimes up to half a year

have been obtained to date with the influence of the outdoor environment reducing the observed lifetime at a given high stress level by a factor of more than 10. Comparisons of creep-rupture data with residual-strength data of unstressed outdoor exposures at a given lifetime show that the applied stress has a much greater influence on residual properties than does the outdoor environment. Extrapolation of the outdoor rupture data indicates a greater than 20-year service life at 1 g operating stress levels of up to 30 percent of ultimate strength. Similar data are being determined for graphite/epoxy material as well.

CONCLUDING REMARKS

An interim report on progress achieved with a number of ongoing long-term environmental exposure programs on advanced composite materials has been presented.

Composite components are being flown on airlines that have been selected to provide a world-wide range of environmental conditions. Flight service has exceeded 2 years for many of the components with over half a million component flight hours satisfactorily accumulated to date, in spite of nearly a 5-percent moisture pickup based on the epoxy weight. Ground-based exposures of the same materials for more than 1 year have indicated an average strength change of about 5-percent decrease and an average moisture pickup of about 2 percent of the epoxy weight.

Other environmental exposures included the cyclic and continuous exposures in fuel-tank environments, and the data have shown less than 10-percent reduction in strength. Also included were effects of sustained stresses combined with outdoor environment in which the high sustained stresses have had a much greater influence than has the outdoor environment, but for which a greater than 20-year life is projected at operating stress levels.

Overall, there has been, to date, a minimal effect of environment on composites for subsonic commercial-aircraft applications.

REFERENCES

1. Welge, R. T.: Application of Boron/Epoxy Reinforced Aluminum Stringers and Boron/Epoxy Skid Gear for the CH54B Helicopter Tail Cone. Phase II: Fabrication, Inspection and Flight Test. NASA CR-112101, 1972.

2. Elliott, S. Y.: Boron/Aluminum Skins for the DC-10 Aft Pylon. NASA CR-132645, 1975.

3. Stoecklin, Robert L.: 737 Graphite Composite Flight Spoiler Flight Service Evaluation. NASA CR-132663, 1975.

4. Stoecklin, Robert L.; and Pride, Richard A.: Progress Report on the NASA Graphite Spoiler Flight Service Program. Third Conference on Fibrous Composites in Flight Vehicle Design - Part I, NASA TM X-3377, 1976, pp. 441-454.

TABLE I.- LANGLEY FLIGHT SERVICE PROGRAMS FOR ADVANCED COMPOSITES

[Projected summary as of Sept. 30, 1975]

Program			Number of aircraft	Number of components	Aircraft operator	Start of flight service	Cumulative flight hours		
Aircraft	Component	Material					High-time aircraft	Total aircraft	Total component
CH-54B	Tail cone	Boron/epoxy reinforced aluminum	1	1	U.S. Army	March 1972	621	621	621
L-1011	Fairing panels	Kevlar 49/epoxy	3	18	Eastern, Air Canada, TWA	January 1973	7189	15 434	92 604
737	Spoiler	Graphite/epoxy	27	108	Aloha, PSA Piedmont, Lufthansa, New Zealand, VASP	July 1973	4720	103 083	412 333
C-130	Center wing box	Boron/epoxy reinforced aluminum	2	2	USAF	October 1974	775	1 428	1 428
DC-10	Aft pylon skin	Boron/aluminum	3	3	United	August 1975	580	1 120	1 120
DC-10	Upper aft rudder	Graphite/epoxy	10	10	----------	April 1976	----	-------	-------
L-1011	Vertical fin	Graphite/epoxy	2	2	----------	January 1979	----	-------	-------
Total:			48	144				121 686	508 106

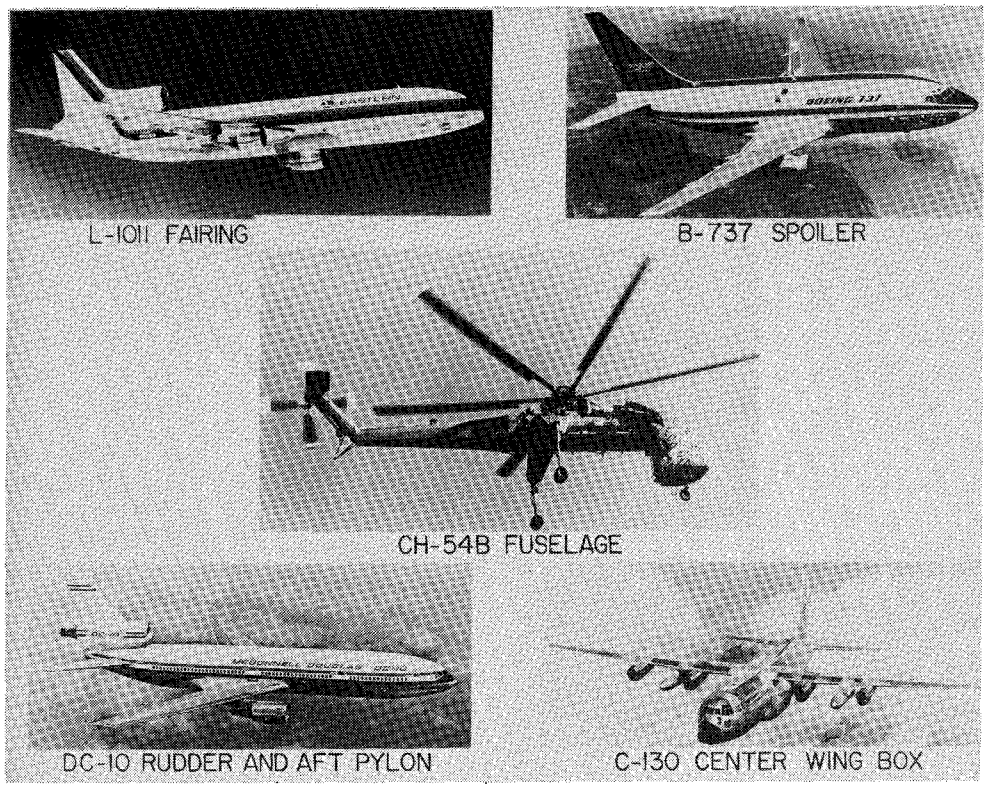

Figure 1.- Composite structural components and aircraft types participating in the Langley flight service evaluation programs.

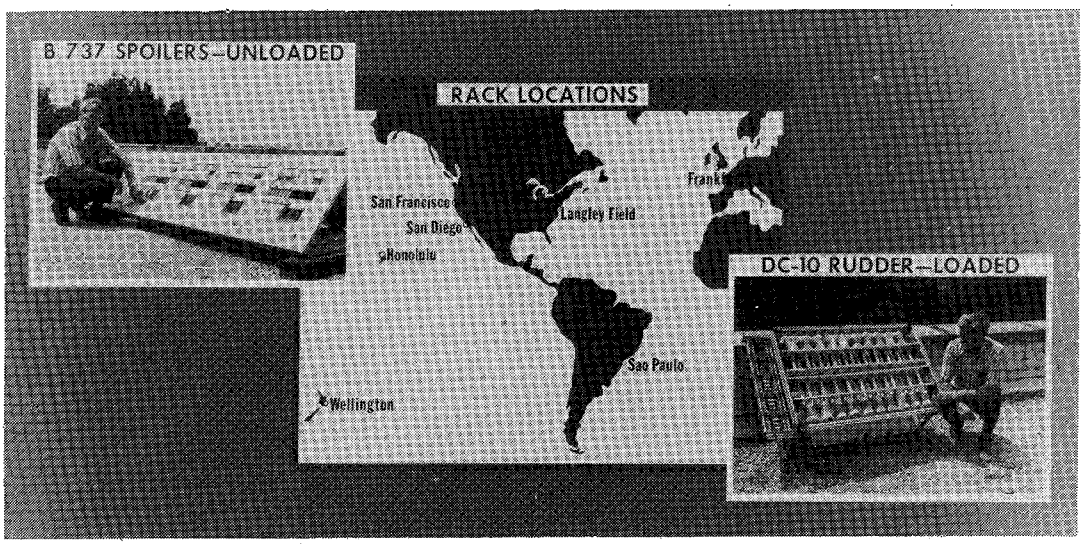

Figure 2.- Ground-based environmental exposure of composite materials used in flight service programs.

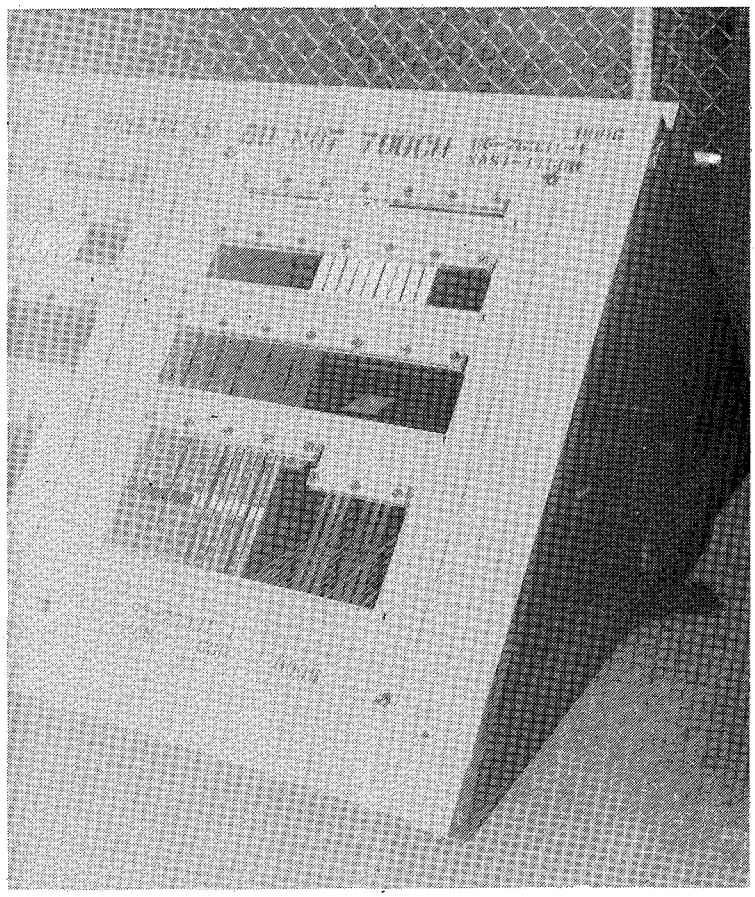

Figure 3.- Panel holder for one set of unstressed composite specimens.

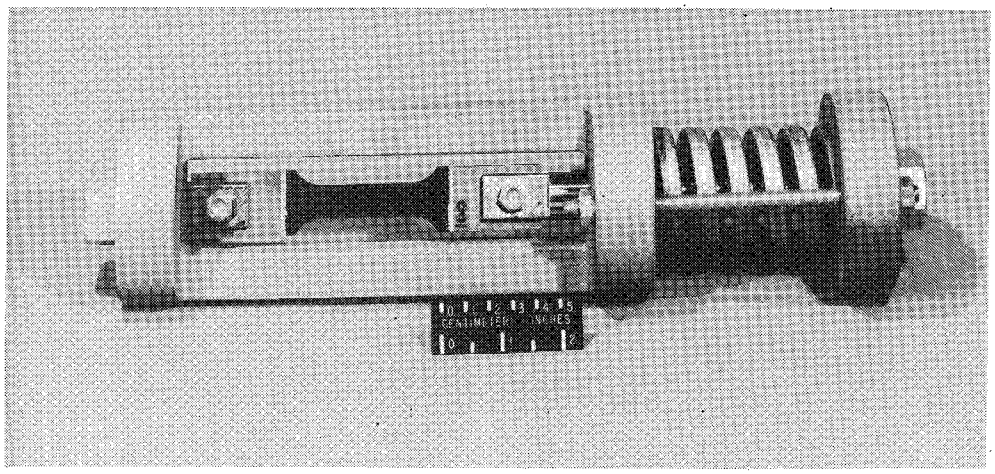

Figure 4.- Constant tensile load fixture for composite specimens.

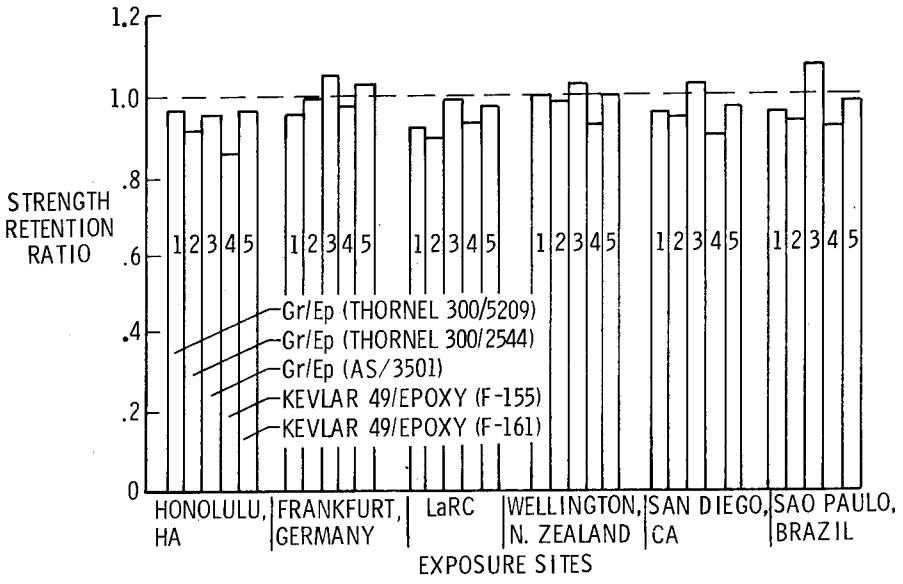

Figure 5.- Flexure strength of composite materials after 1 year of outdoor, ground-based exposure.

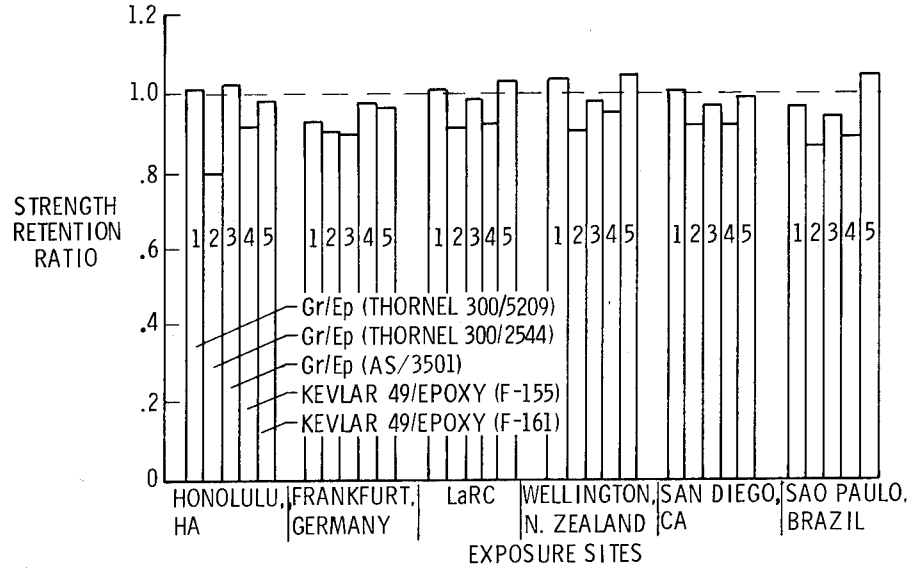

Figure 6.- Interlaminar shear strength of composite materials after 1 year of outdoor, ground-based exposure.

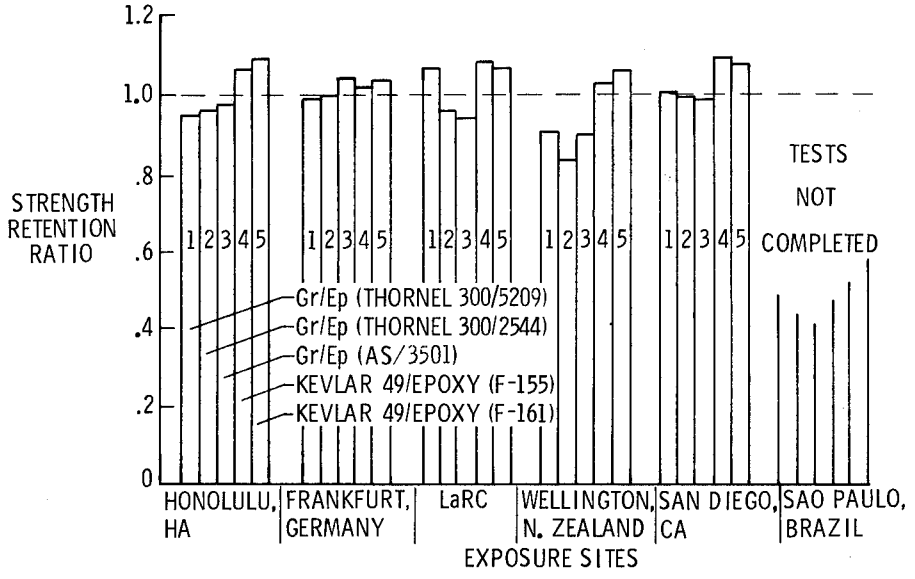

Figure 7.- Compression strength of composite materials after 1 year of outdoor, ground-based exposure.

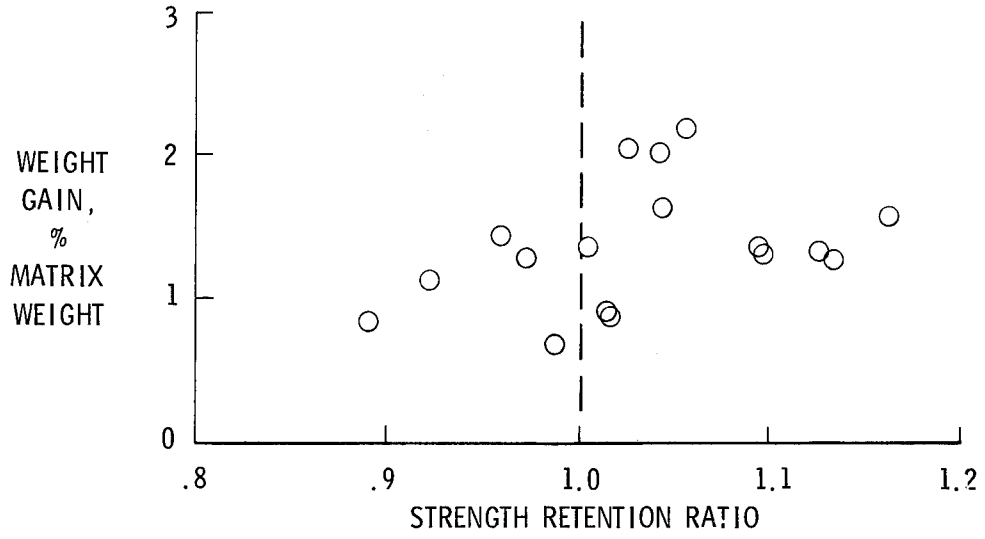

Figure 8.- Correlation between weight gain and retained flexure strength after 1 year of outdoor, ground-based exposure for AS/3501 graphite/epoxy material.

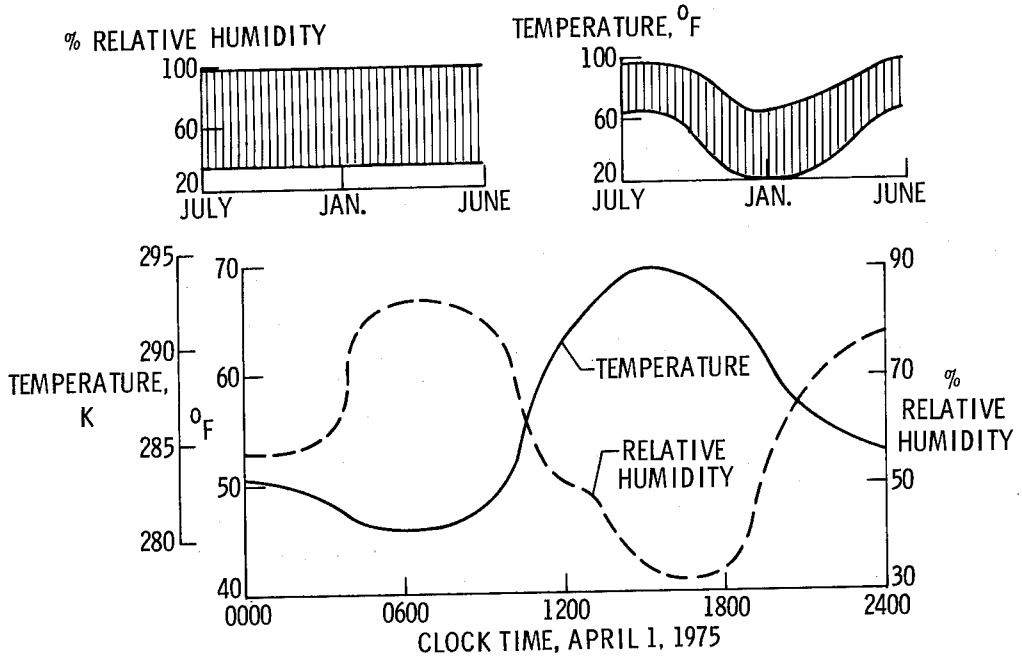

Figure 9.- Typical variations of environmental factors in daily, weekly, and monthly cycles at Hampton, Virginia, exposure site.

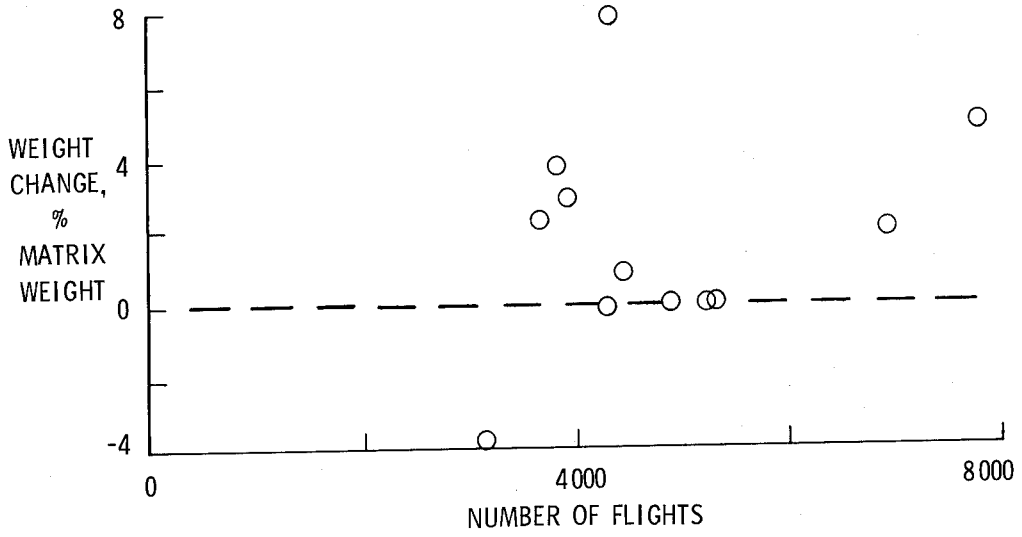

Figure 10.- Weight changes observed after removal from flight service for graphite/epoxy spoilers on 737 transport aircraft.

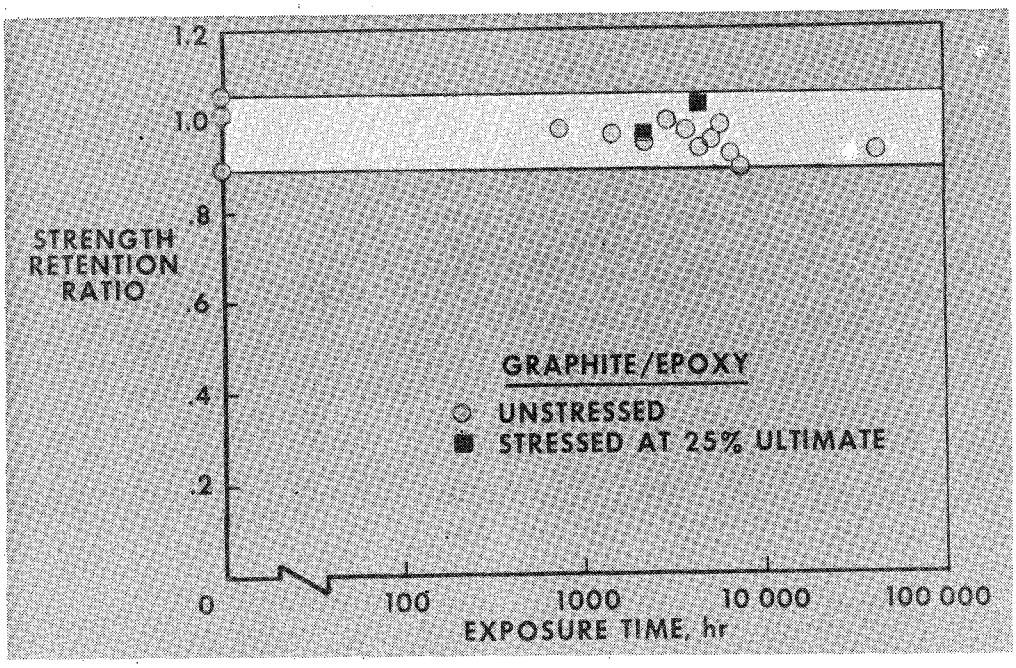

Figure 11.- Strength retained after outdoor, ground-based exposure of composite specimens designed to fail in matrix-controlled modes.

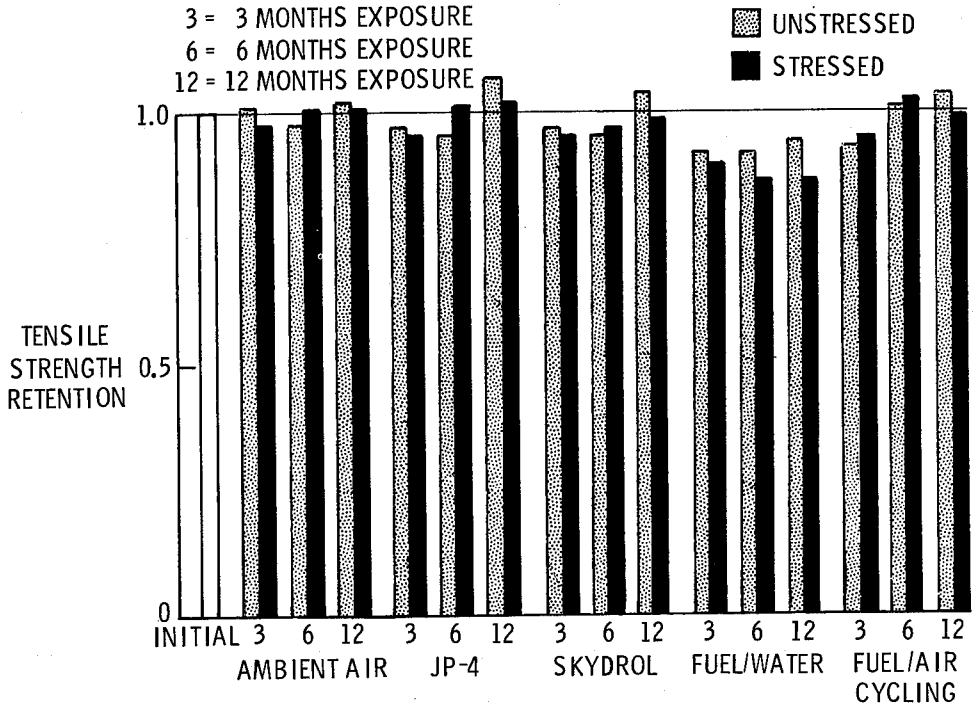

Figure 12.- Tensile strength of ±45° laminated, T-300/5209 graphite/epoxy specimens after exposures in aircraft fuels and hydraulic fluids for times up to 1 year. (Half the specimens were exposed, as fabricated, and half were exposed with a constant stress equal to 25 percent of the average initial failure stress.)

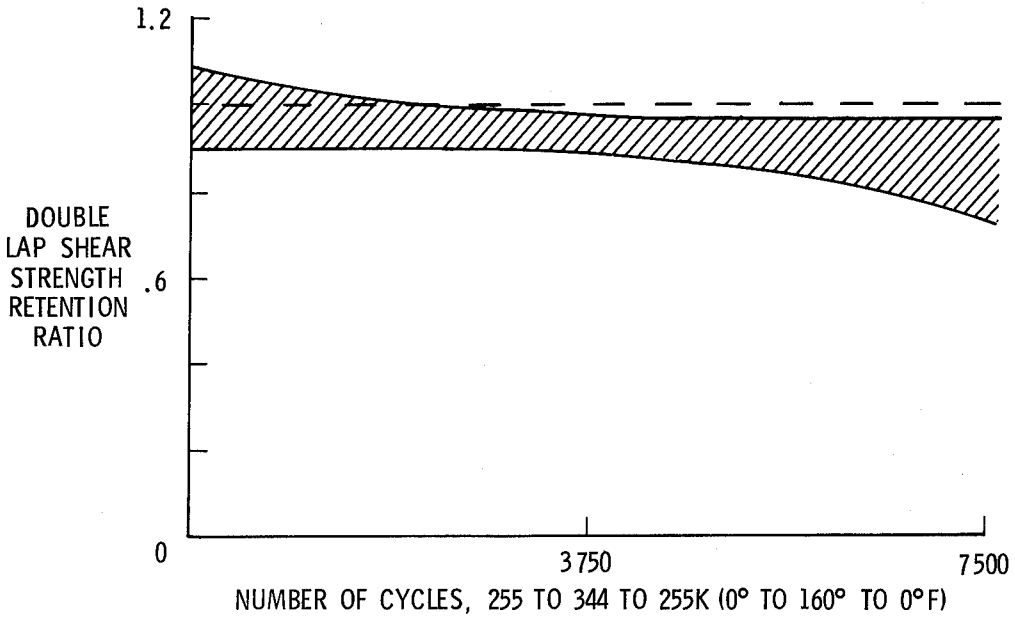

Figure 13.- Effects of thermal cycling on the shear strength of adhesively bonded joints between boron/epoxy composite and aluminum alloy.

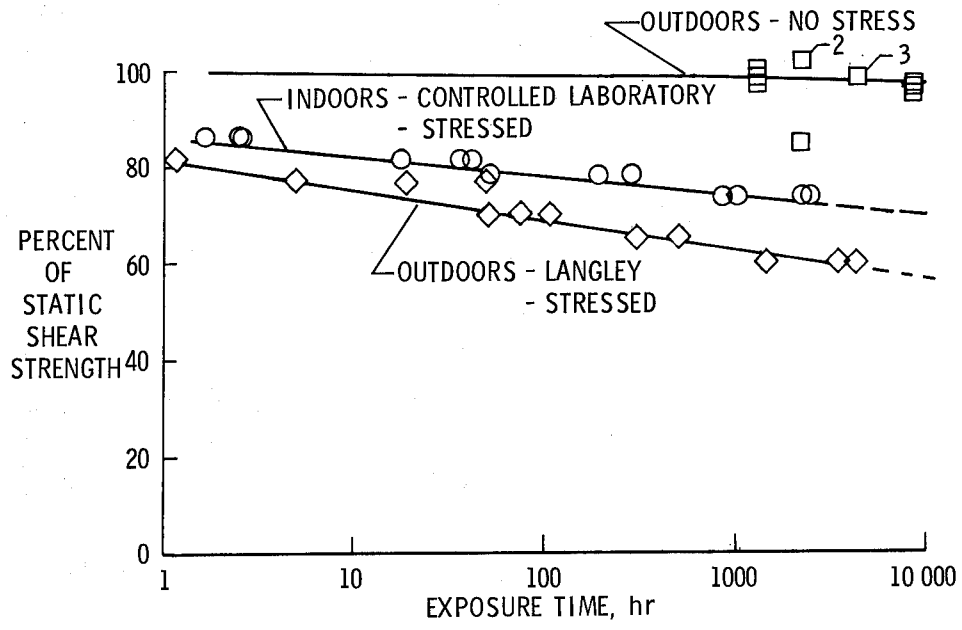

Figure 14.- Comparison of indoor and outdoor environmental exposure for sustained-load creep-rupture tests on short-beam, interlaminar shear specimens of boron/epoxy.

THE AIR FORCE IN-SERVICE ADVANCED COMPOSITE EVALUATION PROGRAM

By T. Bennett
Aeronautical Systems Division

Paper not available for publication

ADVANCED COMPOSITE FAN BLADE FLIGHT EVALUATION PROGRAM

Matthew H. Chopin*

Wright-Patterson AFB, Ohio

SUMMARY

A brief program background and the preparation for and conduct of the first flight evaluation by the U.S. Air Force of a turbine engine fan stage fabricated of advanced composite materials is discussed. Composite material properties and basic design philosophy is presented along with preliminary flight evaluation results. This is the first application of filamentary reinforced metal matrix composites to a flight turbine engine structural component.

INTRODUCTION

The audience is well aware that the U.S. Air Force has sponsored extensive development of advanced filamentary composite materials since the potentials of these very lightweight and high-strength materials were first recognized in the early 1960's. During this period, the use of advanced composite materials in aircraft turbine engines was investigated, and rig and ground testing of primary structural parts made of these materials was accomplished; with some highly promising results.

However, no aircraft turbine engine primary structural parts had been flown in the U.S. until recently when on 4 August 1975 an F-111D aircraft equipped with a TF30-P-9 augmented turbofan engine($66\text{-}88 \times 10^3$ Newtons (15 - 20,000 lb) thrust class) flew for the first time at Edwards AFB, California. One of the TF30 engines powering the F-111 was modified to incorporate advanced composite 3rd stage fan blades which were manufactured by Pratt & Whitney Aircraft, Division of United Technology Corp. The program is under sponsorship of the Aeronautical Systems Division (ASD) of the Air Force Systems Command. The Logo for this flight program is presented in Figure 1, with Figure 2 illustrating the right hand installation in the F-111 aircraft. The location of the composite fan in the TF30-P-9 is provided by Figure 3.

This event marked the first U.S. flight of a rotating structural engine component fabricated of a metal matrix filamentary composite material. It simultaneously initiated the ASD sponsored flight evaluation of this new material application which will be conducted over a multi-year time period.

---

* Aerospace Engineer, Directorate of Propulsion & Power Engineering, Aeronautical Systems Division

Of prime significance is the fact that the composite fan being evaluated is 40 percent lighter than the conventional 3rd stage TF30 titanium fan which it replaced. Studies have indicated that an optimum application of composites throughout an engine could reduce the overall weight by as much as 15 to 20 percent. This weight reduction can be translated into overall mission improvements for the aircraft such as increased pay load, or extended range, etc.

CONSTRUCTION DETAILS

The blades are fabricated of 50 Volume percent .0107 cm (4.2 mil) BORSIC* filaments and a plasma sprayed 6061 aluminum alloy matrix forming 152.4 cm X 38.1 cm (5 ft X 15 in) BORSICAL* tapes. These tapes are roll cut into 43 different ply shapes to provide proper fiber orientation as illustrated in Figure 4. The plys are than properly stacked and are diffusion bonded in a closed die at approximately 565°C (1050°F), under a ram pressure of 3.447 X 10^7 Pa (5000 psi), and under a vacuum of 1.333 X 10^{-5} Pa (10^{-4} Torr). The final product is a high quality solid diffusion bonded blade of complex shape requiring a minimum of finish machining.

A comparison of the composite and titanium blades is provided by Figure 5. Note the absence of the mid span shroud on the composite BORSIC/Aluminum blade. Figure 6 illustrates the root retention and the airfoil ply lay-up for this composite "core-shell" design wherein the core (uni-directional fibers) satisfies the bending and radial load requirements while the torsional stiffness and creep requirements are taken care of by the shell (fibers at $\pm$ 45°). A titanium dovetail is simultaneously diffusion bonded to the airfoil for holding the blade in the disc while an aluminum wedge splays the fibers to assist in retaining the airfoil in the dovetail. The airfoil incorporates an electro-deposited nickel cobalt leading edge extending from the blade tip to near the root to protect against sand and dust erosion, rain, and Foreign Object Damage (FOD).

The set of 36 composite blades weighs 7.43 Kg (16.38 lbs) as compared to 12.22 Kg (26.95 lbs) for the conventional titanium blades, thus resulting in a weight decrease of 4.79 Kg (10.57 lbs). A breakout of total stage weights is provided by Table 1 below.

---

* BORSIC and BORSICAL are registered trademarks of the Hamilton Standard Division of United Technologies Corporation for the fiber and tape, respectively.

Part (Quantity)	THIRD STAGE INSTALLATION WEIGHT COMPARISON Titanium Kg (lbs)	Composite Kg (lbs)	± Kg (lbs)
Blades (36)	12.22 (26.95)	7.43 (16.38)	-4.79 (10.57)
Disc (1)	8.66 (19.10)	7.89 (17.40)	- .77 (1.70)
Air Seal (1)	.76 (1.68)	.91 (2.00)	+ .15 (0.32)
Blade Locks (36)	- -	.08 (0.18)	+ .08 (0.18)
2nd Stator Assy	- -	.06 (0.13)	+ .06 (0.13)
		Total Decrease	-5.27 (11.64)

Table 1

Changing the material from the conventional titanium alloy to the composite permitted the removal of the TF30 mid span shroud due to the increased stiffness of the BORSIC fibers. The presence of mid span shrouds on titanium blades results in a performance loss which of course would not occur on a shroudless composite blade. No performance increase or decrease was detected during ground engine tests of the composite 3rd stage equipped TF30, although some benefit should be realized and detectable if all three of the shrouded fan stages were replaced with unshrouded composite blades.

A density comparison of BORSIC/Aluminum and representative aircraft turbine engine fan/compressor blade materials is provided by Table 2. It is apparent that the density of BORSIC/Aluminum is considerably less than that of stainless steel or titanium 6-4, thus offering a significant weight reduction over the other materials.

Density Comparisons		
Material	Density Kg/m^3	$(\#/in^3)$
Stainless Steel	7944.16	(0.287)
Titanium 6-4	4622.56	(0.167)
BORSIC/Aluminum	2768.0	(0.10)

Table 2

The disc used during this program was the standard TF30 3rd stage which was originally sized to support titanium blade loads. The only difference was in machining of the composite dovetail slots in the disc rim. If, however, the disc were sized using the composite blade loads, which are approximately half of the titanium loads, it is estimated that another 2.268 Kg (5 lbs), or 20 percent weight savings, could be realized by removing excess disc bore material.

Thus, composite fan stage weight reduction can be accomplished in three ways by: (1) the elimination of the mid span shrouds, (2) a significant material density reduction, and (3) a lighter disc through proper design and resizing for the lighter composite blade loads.

From a construction viewpoint, certain properties of BORSIC/Aluminum are superior to those of titanium which is currently favored for jet engine structural use where the operating temperature is below 425.0°C (800°F). It is expected that composite materials will replace titanium in future engine designs as more experience is gained with composites.

QUALITY ASSURANCE ASPECTS

Quality assurance was continuously addressed throughout the composite fan program with the objective being component flight worthiness. We wanted the blades to be qualified to fly.

The quality assurance program consisted of developing material acceptance standards, process standards and NDI methods, plus conducting extensive bench tests, foreign object damage (FOD) evaluations, and ground engine qualification tests to substantiate flight quality. A brief overview of pertinent quality aspects is discussed below.

Tape quality assurance tests used were those indicated in Figure 7 while NDI procedures used are indicated in Figure 8. Note that NDI methods and procedures vary depending upon the final use with (1) in process, (2) finished blade, (3) post engine test, and (4) post flight tests. Table 3 provides NDI results for the total number of blades fabricated during the program.

SUMMARY OF INSPECTION RESULTS
(In-Process and Finished Blades)

Total Number of Blades Fabricated	246
Number Accepted	227
Acceptance Rate	92.3%
Number Rejected	19
Cause of Rejection	
Inadequate Natural Frequency	4
Poor Bond (C-Scan Detected)	8
Cracks (X-Ray Detected)	1
Processing Errors	6

Table 3

Basic bench testing consisted of salt corrosion, bending fatigue, thermal fatigue, combined stress fatigue, spin pit, and ballistic impact testing as indicated in Figure 9. A Goodman diagram was generated using spin pit (steady), bending fatigue (vibratory) and combined stress fatigue tests, both at room temperature and 232°C (450°F). Stresses from instrumented engine test blades were compared to these Goodman allowables to assure an adequate margin existed within the operating range of the engine.

An extensive FOD program was conducted to verify that the blades could sustain impact damage which consisted of the items listed in Figure 10. It should be noted that for this third stage fan application the susceptibility to large FOD is not as great as a 1st stage application. The concern is for small, hard objects such as rivets, bolts, sand, etc., which might make its way to the 3rd stage. A large portion of the FOD evaluation was carried out back-to-back with composite and titanium blades in a spin pit to obtain comparison data to standard titanium blades. Results indicated the composite blades to be slightly less FOD tolerant than titanium blades.

A 50 hour engine test segment was intentionally conducted with a composite blade leading edge "damaged and blended out" to the maximum limit permitted for a titanium blade. No problem was encountered. Additionally, a severe blade tip to engine case rub was experienced during engine testing, and considerable hours were accumulated before the damage was discovered. The entire third stage fan set was then inspected radiographically and seven blades were replaced due to crack indications. The engine tests were then completed as scheduled without any further problems.

FLIGHT HARDWARE CERTIFICATION

The basic fan design was flight qualified by 550 hours of extensive engine testing consisting of stress surveys, performance calibrations, distortion surveys, and endurance cycles at both sea level and altitude, subsonic and supersonic conditions. The endurance test schedule was the same as that used for the TF30-P-9 engine qualification.

Engine testing was conducted on two separate blade sets. Blade set #1 was used for the subsonic engine test program and accumulated 350 hours of operation under conditions indicated in Figure 11 while blade set #2 accumulated 200 hours of operation at supersonic sea level and altitude conditions as depicted in Figure 12. These two tests encompassed the maximum F-111 flight conditions of RPM, temperature, and dynamic pressure which are illustrated in Figure 13. Flight certification requirements were reviewed independently by both contractor and USAF personnel for overall adequacy, such that following completion of the tests, the blade design would be flight qualified.

A special Quality Plan was developed for fabricating the composite flight blades since they would be a limited production run. Flight evaluation parts were to be manufactured to contractor "Production Delivery" standards meaning that all finished parts would be subjected to quality control procedures equivalent to those employed for production items. Briefly, this entails release of all materials by the Materials Control Laboratory, and Quality Control would approve the procedures and equipment used, witness the testing, and provide standard Quality Control documentation. Any significant deviations must be noted in a Laboratory Deviation or Waiver which must be jointly released by Design, Materials Engineering, Production Engineering, and the Procuring Agency (or its representative).

Two new flight evaluation blade sets were planned to be fabricated to this qualified design in accordance with the contractor developed Quality Plan discussed above. However, when tape for flight blade fabrication was received from the vendor, a serious quality problem was discovered, i.e., low acceptance tensile strength. Approximately this same time, a very restrictive aircraft availability schedule was imposed by HQ AFSC limiting the evaluation to a very tight schedule and a narrow flight window (this aircraft availability restriction was subsequently relieved).

A major decision was therefore made to flight evaluate those blades which had recently completed the ground engine tests. Selection of one flight set of 36 blades (plus five spares) was made from the 72 blades of test sets 1 and 2 after being inspected for quality by the contractor in accordance with criteria previously established in the program and detailed in the Quality Plan. The blades were subsequently marked with P&WA's experimental inspection acceptance symbol to indicate the limited flight evaluation use intended. The blades were assembled into the modified 3rd stage disk, dynamically balanced by the contractor, and shipped to the USAF for installation at Edwards AFB. It is noteworthy that the blades now flying have accumulated between 140 to 350 hours of prior ground engine test time, depending upon which test set they were selected from.

The second flight evaluation set is only partially fabricated at this time. Its completion is contingent upon solution of the tape quality problem and availability of any additional funds which may be required as a result of this problem.

FLIGHT EVALUATION PROGRAM

The flight evaluation is being conducted "piggy-back" on Air Force Flight Test Center (AFFTC) aircraft supporting the USAF B-1 flight test program. Actual hardware implementation was accomplished by authority of Air Force Systems Command Regulation 80-33, "Class II Modification of Aerospace Vehicles". Class II modifications are considered "changes or alterations to the standard configuration of aerospace vehicles, subsystems,

components, etc., which are essential to approved RDT&E programs in compliance with pertinent Air Force regulations and directives." The modifications were performed by flight test center machine shop and turbine engine maintenance personnel and basically consisted of a swap-out of the assembled and prebalanced 36-blade third stage composite fan assembly with the standard titanium fan assembly. These two assemblies are illustrated in Figures 14a and b.

Examples of special documentation required for the flight evaluation are as follows: (1) Environmental Impact Study, (2) Safety/Hazard Analysis Report, (3) Technical Order Changes, (4) Inspection Requirements and Removal Criteria, (5) Field Trim Balance Procedures following fan swap-out (should this become necessary), and (6) Reporting Forms. Photographic documentation is also being provided.

Borescope ports were installed in the fan case to facilitate periodic on-the-wing visual inspection of the blades; thus, two borescope ports, one on each side of the engine, were required to allow for either a right or left hand aircraft installation. Figure 15 illustrates the location of these fan case borescope ports with respect to the third stage inlet guide vanes. The port is accessible either through the fire extinguisher access door, or by dropping the fuselage bay door as illustrated in Figure 16. During inspection, the borescope probe penetrates the case between two vanes and provides good visibility of the blade leading edge and platform transition area. Inspection requirements were conservatively set at (1) visual post flight for first 10 flights, increasing to (2) visual following each 25 hour flight period and finally (3) radiographic on-the-bench after 200 hours.

Table 4 provides the allowable damage and repair limits for seven different blade areas indicated in Figure 17. These areas define the maximum blend and repair limits permitted for damage such as nicks, cracks, scratches, etc. These limits were prepared based upon the extensive component, bench, and engine testing performed during conduct of the program, and will be used routinely throughout the evaluation by test center maintenance personnel. They represent a "first approximation" at what can realistically be allowed for these types of composite blades and may be expanded later as more experience is obtained.

Maximum Allowable Blended Crack or Nick Limits

Blade Area		Stage 3	
	A	5/16" R	
	B	1/32" RB	
	C	5/32" D	
	D	1/8" D	
	E	1/8" D	
	F	Nick - 1/16" D	Crack - None
	G	Nick - 1/32" RB	Crack - None
	H	1/32" RB	

R - Radius
D - Depth
RB - Round Bottom

Table 4

FINDINGS

As of 1 October 1975, the composite blades had accumulated 7 hours of normal flight operation in the F-111D at altitudes ranging from sea level to 15,240M (50,000 + feet) and speeds from subsonic to Mach 2.2. No particular problems have been experienced, nor has the composite fan contributed to any mission aborts.

No maintenance problems were anticipated in swapping out the composite fan, and none were encountered. To date, there has been only limited handling of the blades by maintenance personnel, and no removals or repairs have been required due to operational use. The repair limits therefore have not been validated, however, we expect them to be used in the future.

CONCLUSIONS

The program to validate the use of advanced composite materials in aircraft turbine engines has been very successful thus far. I would like to re-emphasize that this is the first time that a metal matrix filamentary advanced composite has been flown in a turbine engine as a rotating structural component and the evaluation has only just begun. We still have several years of flying ahead of us. This program admittedly will not start an avalanche of turbine engine designs using composites but it is expected to add significantly to the experience base so vitally needed to develop confidence in the material applications so that composites will seriously be considered in the next generation of aircraft turbine engines.

REFERENCES

1. Boll, K. G., Advanced Composite Engine Development Program, AFML TR-72-108, Parts I, II, III, Wright-Patterson AFB, Ohio, July 1972.

2. Randall, David G., Final Report for TF30 Third Stage Composite Fan Blade Service Program, (Draft PWA-5141, 15 October 1974). Final Report to be issued by Aeronautical Systems Division, Wright-Patterson AFB, Ohio.

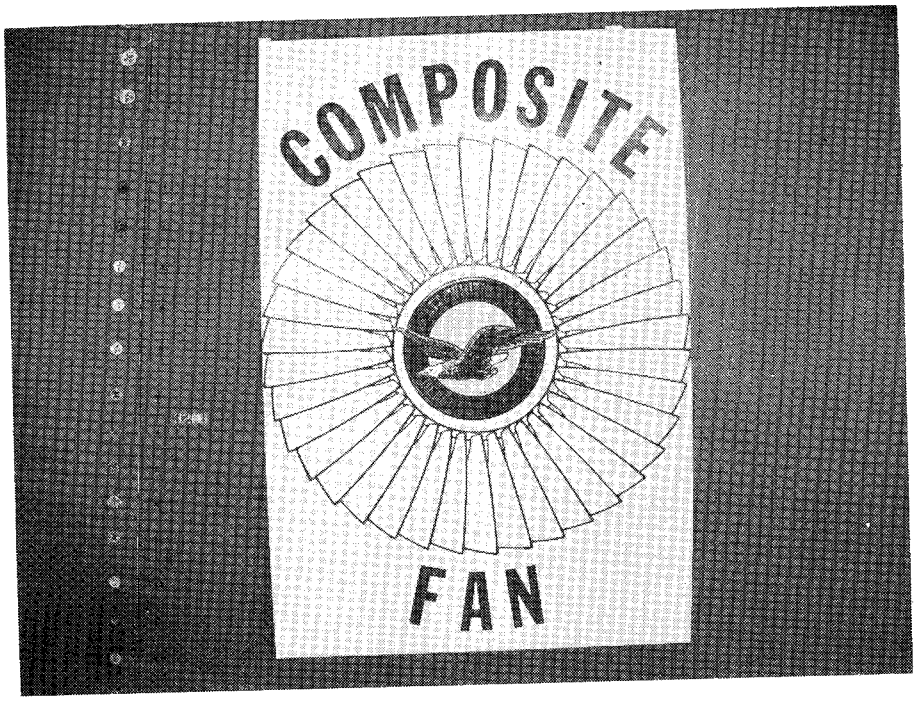

Figure 1.- Logo for composite fan program.

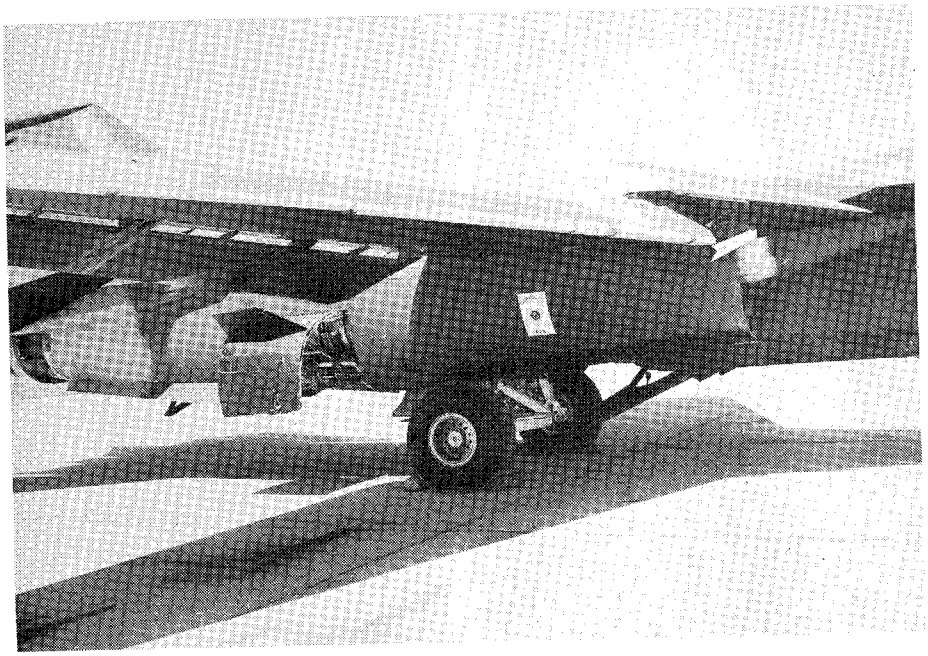

Figure 2.- Right hand engine installation in F-111D.

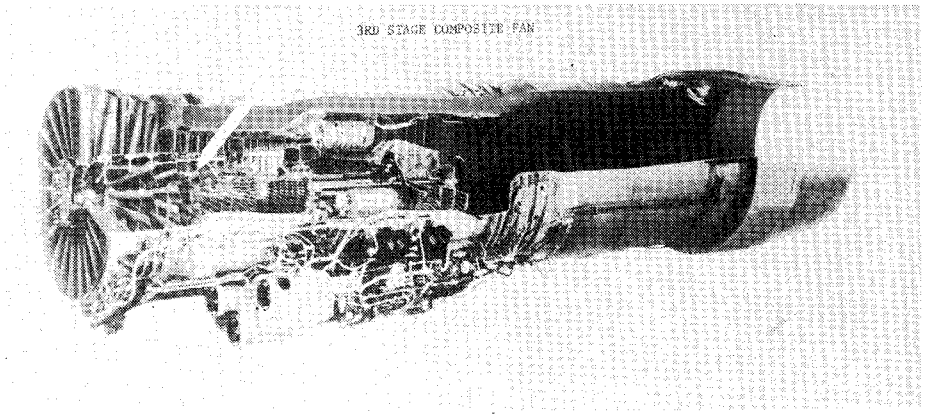

Figure 3.- Location of composite fan in TF30 P-9 engine.

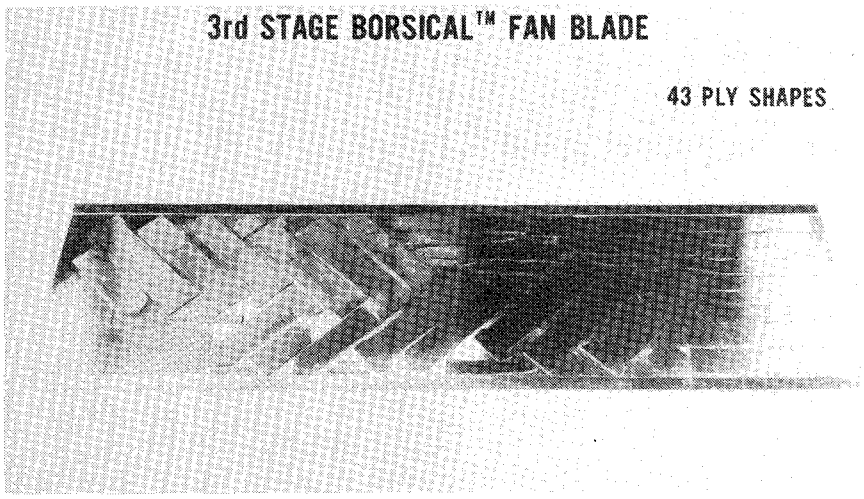

Figure 4.- Roll-cutting templates for TF30 P-9 composite blade.

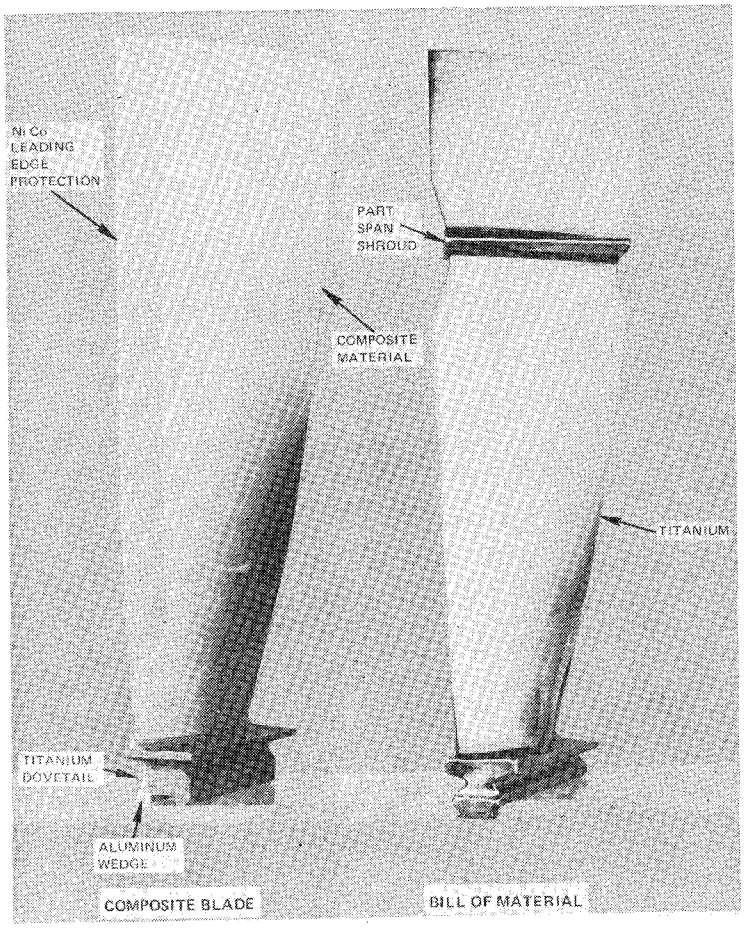

Figure 5.- Comparison of composite and titanium TF30 3rd stage fan blades.

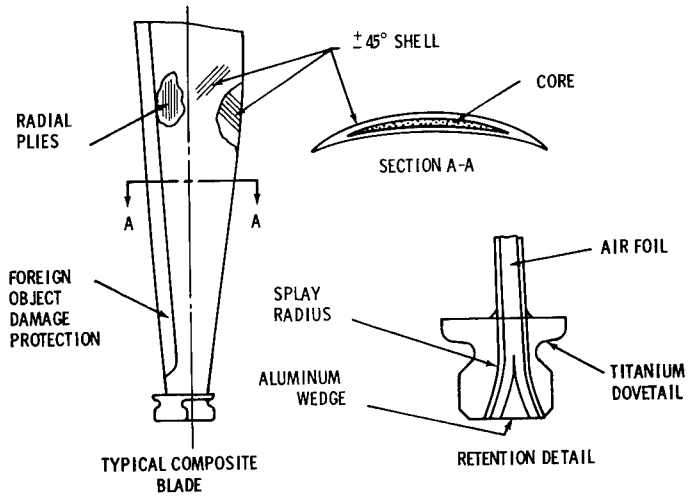

Figure 6.- Composite blade construction details.

- o VISUAL INSPECTION
- o AREAL WEIGHT
- o FIBER V/O
- o NO. FIBERS/INCH
- o FIBER DIAMETER
- o ELASTIC MODULUS
- o TAPE TENSILE STRENGTH
- o PANEL TENSILE STRENGTH

Figure 7.- Tape quality assurance tests.

IN-PROCESS	FINISHED BLADE	POST-TEST	POST-FLIGHT
o VISUAL	o VISUAL	o VISUAL	o VISUAL
o DENSITY	o FREQUENCY	o FREQUENCY	o X-RAY
	o X-RAY	o X-RAY	
	o FPI	o FPI	
	o DIMENSIONAL	o DIMENSIONAL	
	o PROOF SPIN	o EDDY CURRENT	

Figure 8.- Blade inspection methods.

- o SPIN PIT TESTING
- o BENDING FATIGUE
- o COMBINED STRESS FATIGUE
- o THERMAL FATIGUE
- o SALT CORROSION
- o BALLISTIC IMPACT
- o DROP-WEIGHT TEST
- o FOREIGN OBJECT DAMAGE (FOD)

Figure 9.- Bench test program.

- o SPIN PIT (FOD) SINGLE BLADE TESTS (BORSIC & TI)
  - 1" ICE BALLS
  - RTV BIRDS
  - STARLINGS
  - SAND/GRAVEL
  - RIVETS
- o 50 HRS ENGINE OPERATION WITH DAMAGED BLADE
- o BALLISTIC IMPACT EVALUATION
- o SUSTAINED SEVERE TIP RUB

Figure 10.- Damage tests.

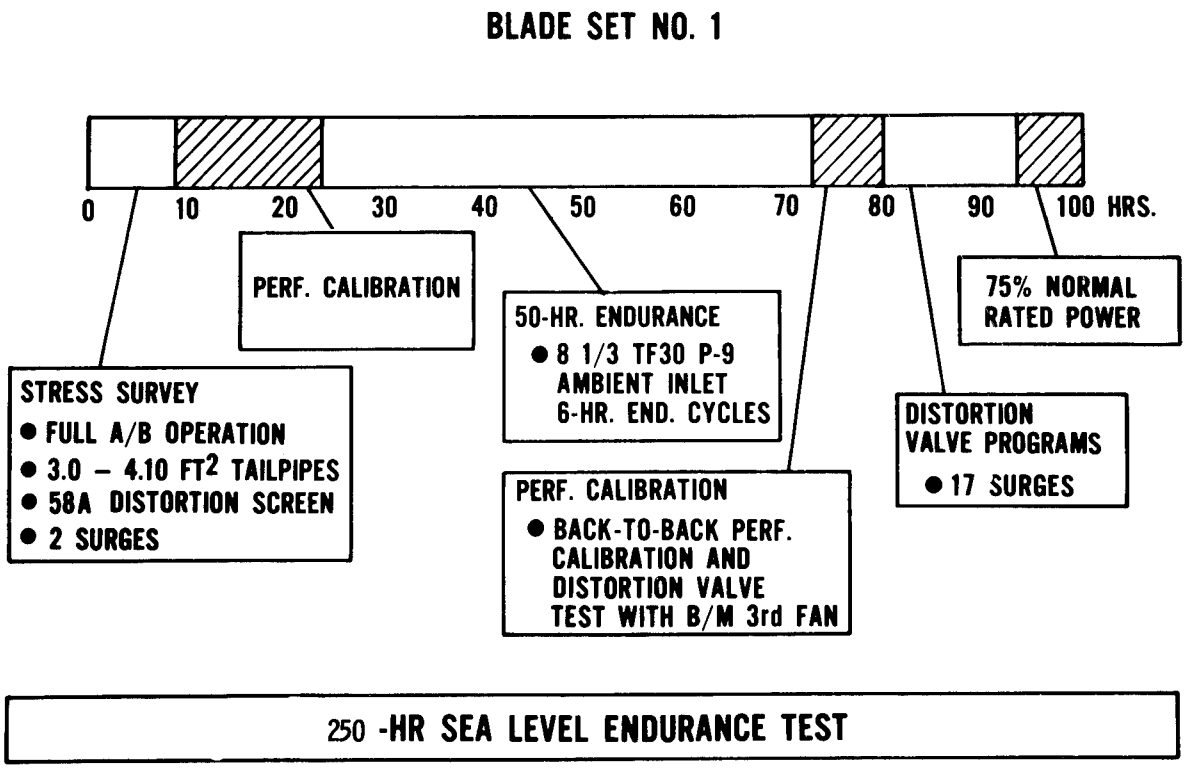

Figure 11.- Subsonic engine test program.

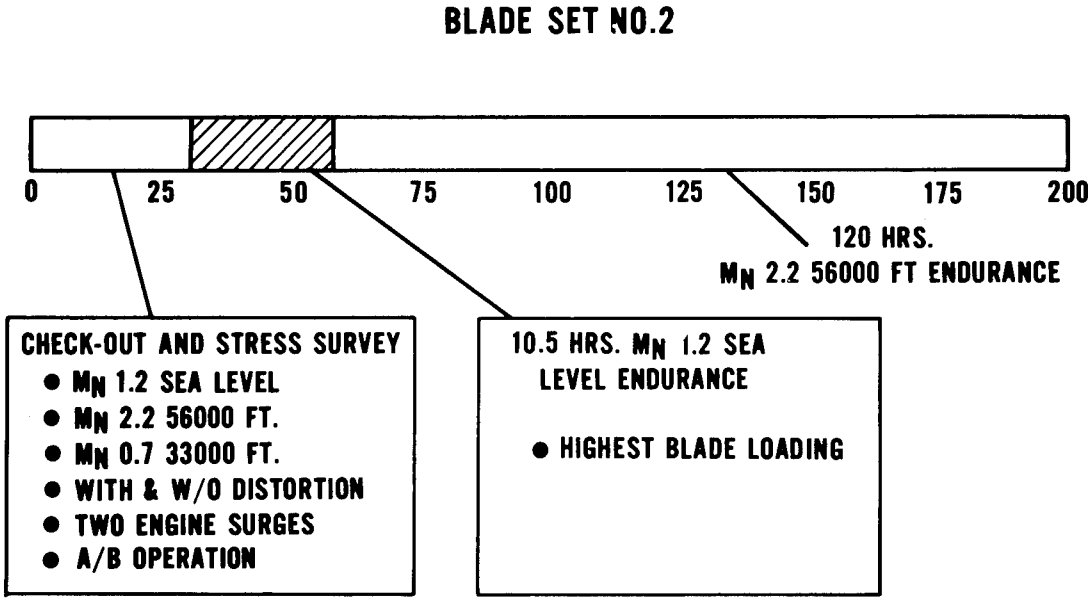

Figure 12.- Supersonic engine test program.

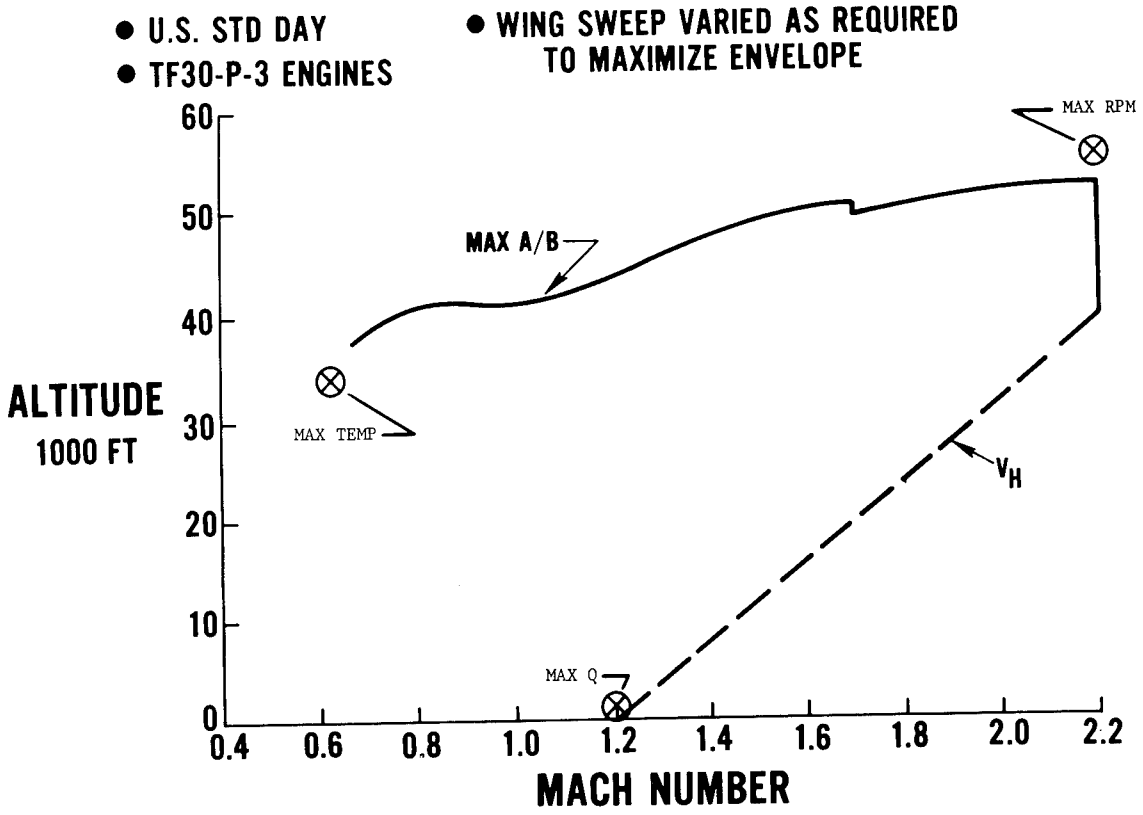

Figure 13.- Typical F-111 flight envelope.

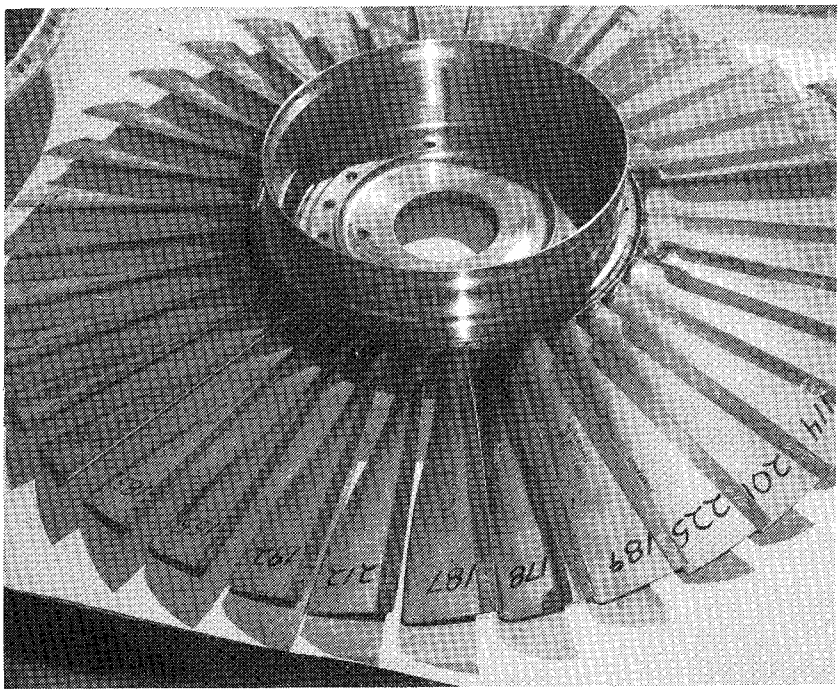

(a) Composite.

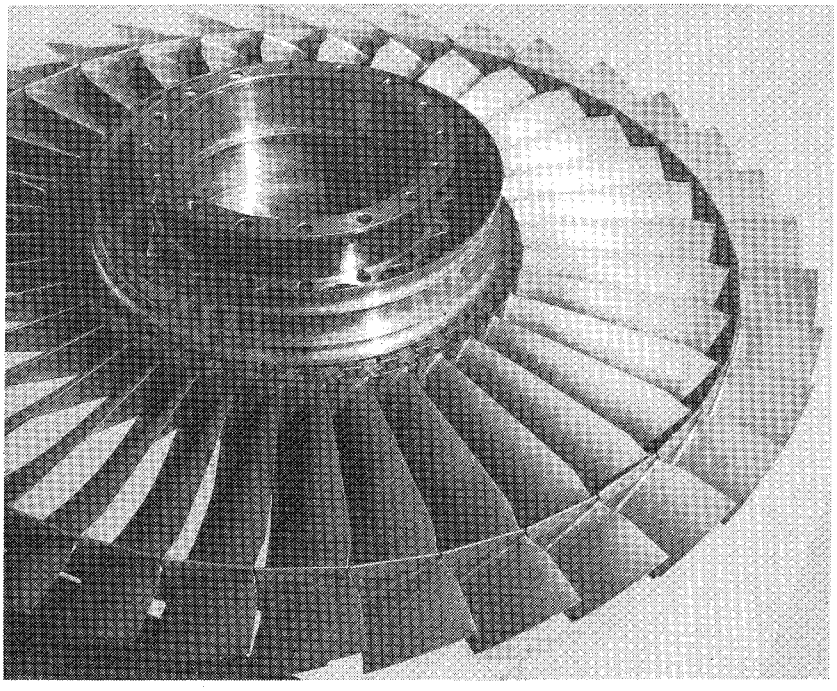

(b) Titanium.

Figure 14.- Fan assembly.

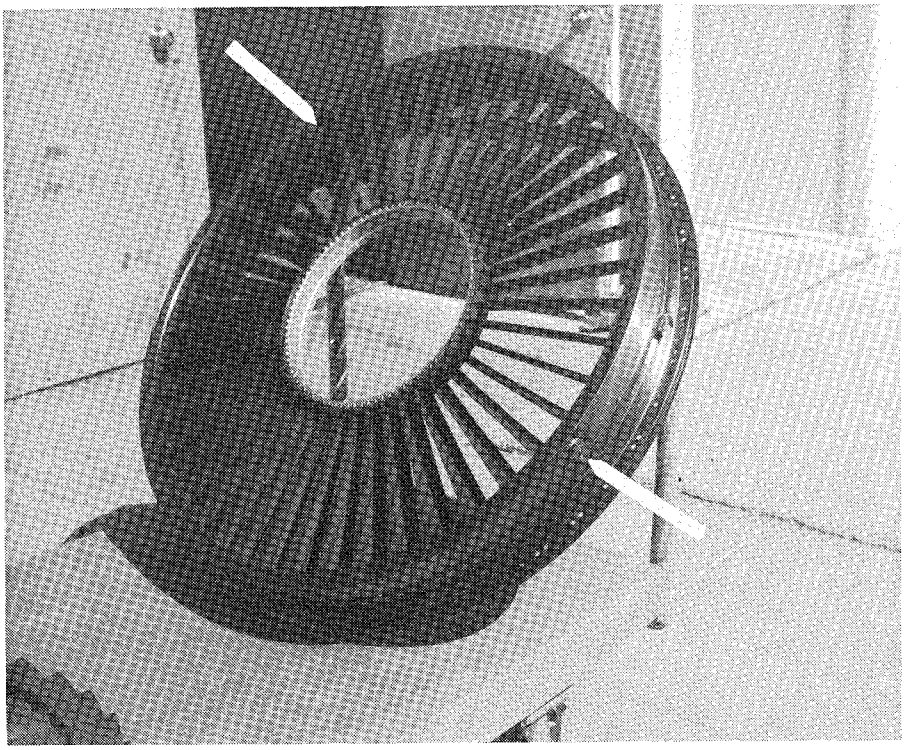

Figure 15.- Fan case borescope port.

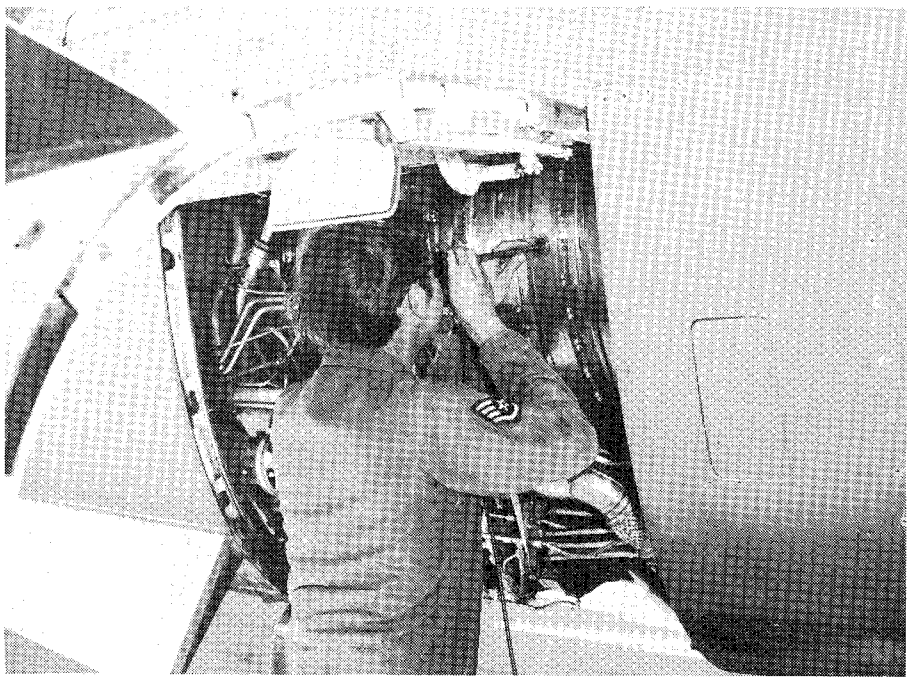

Figure 16.- Performing borescope inspection.

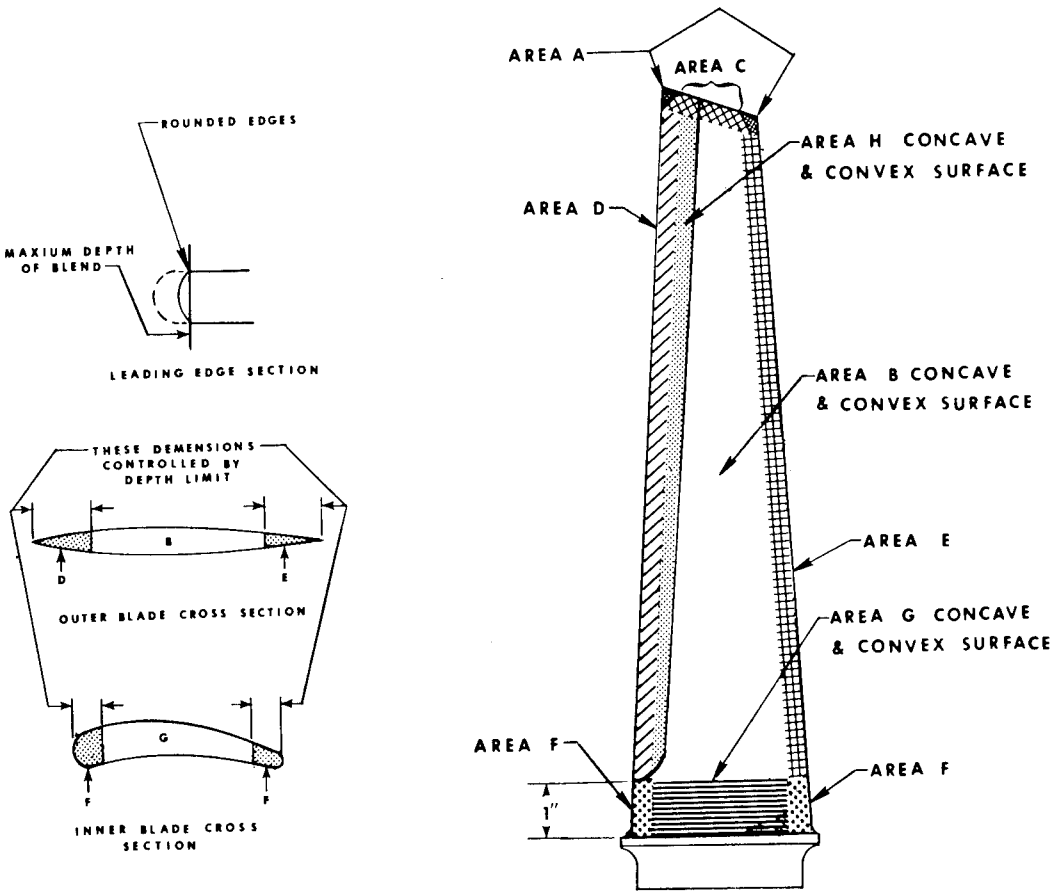

Figure 17.- Composite blade damage zones.